PHOTOGRAPH THIS SHEET

DTIC FILE COPY

LEVEL

INVENTORY 1

AD-A203 181

DTIC ACCESSION NUMBER

CHEMISTRY AND PHYSICS OF ELECTRIFIED INTERFACES

DOCUMENT IDENTIFICATION

29 AUG - 2 SEPT 1988 EXTENDED ABSTRACTS AND PROGRAMME

This document has been approved for public release and sale; its distribution is unlimited.

DISTRIBUTION STATEMENT

ACCESSION FOR	
NTIS GRA&I	X
DTIC TAB	☐
UNANNOUNCED	☐
JUSTIFICATION per form 50	
BY	
DISTRIBUTION /	
AVAILABILITY CODES	
DIST	AVAIL AND/OR SPECIAL
A-1	

QUALITY INSPECTED

DISTRIBUTION STAMP

DTIC ELECTE S 1 JAN 1989 D E

DATE ACCESSIONED

DATE RETURNED

89 1 27 020

DATE RECEIVED IN DTIC

REGISTERED OR CERTIFIED NO.

PHOTOGRAPH THIS SHEET AND RETURN TO DTIC-FDAC

DTIC FORM 70A MAR 86

DOCUMENT PROCESSING SHEET

PREVIOUS EDITION MAY BE USED UNTIL STOCK IS EXHAUSTED.

AD-A203 181

Divisione di Elettrochimica della Società Chimica Italiana
and
International Society of Electrochemistry (ISE)
Bioelectrochemical Society (BES)

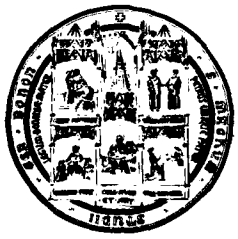
International Conference

Chemistry and Physics of Electrified Interfaces

solid/electrolyte and biological systems

EXTENDED ABSTRACTS

US ARMY RESEARCH, DEVELOPMENT & STANDARDIZATION GROUP (UK)
BOX 65
FPO NY 09510-1500



MCM

Alma Mater Studiorum
Sæcularia Nona

BOLOGNA

29 August - 2 September 1988

89 1 27 030

Divisione di Elettrochimica della Società Chimica Italiana
and
International Society of Electrochemistry (ISE)
Bioelectrochemical Society (BES)

International Conference

Chemistry and Physics of Electrified Interfaces

solid/electrolyte and biological systems

PROGRAMME

US ARMY RESEARCH, DEVELOPMENT & STANDARDIZATION GROUP (UK)
BOX 65
FPO NY 09510 1500



M·CM·LXXXVIII
Alma Mater Studiorum
Sæcularia Nona

89OLOGNA1 27 020

29 August - 2 September 1988

Divisione di Elettrochimica della Società Chimica Italiana
and
International Society of Electrochemistry (ISE)
Bioelectrochemical Society (BES)

International Conference

CHEMISTRY AND PHYSICS OF ELECTRIFIED INTERFACES

Solid/Electrolyte and Biological Systems

Organized on occasion of the celebration of the 900 years of the University of Bologna

PROGRAMME

BOLOGNA

29 August - 2 September 1988

Palazzo dei Congressi

ORGANIZING COMMITTEE

S. TRASATTI *(Chairman)*	*(University of Milan)*
E. VECCHI *(Secretary)*	*(University of Bologna)*
A. DE BATTISTI	*(University of Ferrara)*
F. DI QUARTO	*(University of Palermo)*
L. FORNARO	*(University of Milan)*
R. GUIDELLI	*(University of Florence)*
B. A. MELANDRI	*(University of Bologna)*
G. PIAZZA	*(University of Bologna)*
M. P. TOSI	*(University of Trieste)*

LOCAL ORGANIZERS
(University of Bologna)

G. PIAZZA *(Chairman)*
P. FETTO
B. A. MELANDRI
F. SCAGNOLARI
E. VECCHI

INTERNATIONAL ADVISORY BOARD

R. R. ADZIC	*Belgrade* (YUG)
W. J. ALBERY	*London* (GBR)
A. J. BARD	*Austin* (TX, USA)
G. F. BASSANI	*Pisa* (ITA)
G. CHIAROTTI	*Rome* (ITA)
Y. A. CHIZMADZHEV	*Moscow* (USSR)
B. E. CONWAY	*Ottawa* (CAN)
M. COSTA	*Paris* (FRA)
E. A. DAVIS	*Leicester* (GBR)
M. FLEISCHMANN	*Southampton* (GBR)
H. GERISCHER	*Berlin* (FRG)
D. HENDERSON	*San Jose* (CA, USA)
H. D. HURWITZ	*Bruxelles* (BEL)
V. E. KAZARINOV	*Moscow* (USSR)
L. KESZTHELYI	*Szeged* (HUN)
D. M. KOLB	*Berlin* (FRG)
Ya. M. KOLOTYRKIN	*Moscow* (USSR)
A. A. KORNYSHEV	*Moscow* (USSR)
W. LORENZ	*Leipzig* (GDR)
S. McLAUGHLIN	*Stony* Brook (NY, USA)
S. MOTOO	*Takeda* (JAP)
R. PARSONS	*Southampton* (GBR)
P. N. ROSS	*Berkeley* (CA, USA)
J. SOBKOWSKI	*Warsaw* (POL)
J. ULSTRUP	*Lyngby* (DEN)
H. T. WITT	*Berlin* (FRG)
E. B. YEAGER	*Cleveland* (OH, USA)

ACKNOWLEDGEMENTS

Thanks are due to the following Institutions for their support to the Conference

Accademia delle Scienze dell'Istituto di Bologna
Banca Operaia di Bologna, Bologna
Banco di Sicilia, Bologna
COFID, Bologna
Comune di Bologna
Consiglio Nazionale delle Ricerche
Elettrochimica M. Ginatta S.p.A., Torino
Ente Nazionale per l'Energia Elettrica
FIAMM S.p.A., Vicenza
Gruppo Nazionale di Struttura della Materia (GNSM-CISM)
Istituto Bancario Italiano, Bologna
Istituto Donegani, Novara
Ministero della Pubblica Istruzione
Montedison S.p.A., Milano
O. De Nora Impianti Elettrochimici S.p.A., Milano
Presidenza del Consiglio dei Ministri (proposta MRST)
Provincia di Bologna
Regione Emilia-Romagna
Società Chimica Italiana (SCI)
Società Italiana di Fisica
U.S. Army Research Office
Università di Bologna

PROGRAMME

Monday 29 August

9.00 *Opening Session*
Presentation of the "Luigi Galvani Medal" to Prof. H. Gerischer

(1) Experimental Approaches

Chairman: H. Gerischer *(Fritz-Haber-Institut, Berlin, FRG)*

9.30 In situ Scanning Tunneling Microscopy — L1
D. M. Kolb *(Fritz-Haber-Institut, Berlin, FRG)*

10.15 Surface Electronic Structure from Ellipsometry — L2
F. Chao*, M. Costa, J. Lecoeur, J. P. Bellier, V. Russier
(CNRS, Meudon, FRA)

11.00 Poster Session

Chairman: J. Lipkowski *(University of Guelph, CAN)*

12.15 Single-Crystal Electrochemistry: Experimental Challenges to Current Theory — L3
P. N. Ross *(Lawrence Berkeley Lab, Berkeley, CA, USA)*

13.00 *Pause*

Chairman: W. J. Plieth *(Free University, Berlin, FRG)*

14.30 Non-linear Optical Probes of Electrochemical Interfaces — L4
G. Richmond *(University of Oregon, Eugene, OR, USA)*

15.15 In situ Surface Extended X-ray Absorption Fine Structure Spectroscopy and X-ray Diffraction of Monolayers Adsorbed at Electrochemical Interfaces — L5
O. R. Melroy *(IBM, San Jose, CA, USA))*

16.00 Poster Session

17.00 Poster Discussion. *Leaders:*
R. R. Adzic *(University of Belgrade, YUG)*
V. E. Kazarinov *(Academy of Sciences, Moscow, USSR)*
E. B. Yeager *(Case Western Reserve Univ., Cleveland, OH, USA)*

18.00 *Adjournment*

Tuesday 30 August

(2) Semiconductors, Photoeffects and Modified Electrodes

Chairman: U. Stimming *(Columbia University, New York, NY, USA)*

9.00 **Electrochemistry of Semiconductors in Non-aqueous Solvents** L6
A. Kumar, S. R. Lunt, P. G. Santangelo, B. J. Tufts, N. S. Lewis*
(Stanford University, CA, USA)

9.45 **Electronic Properties of Amorphous Silicon Surface Barriers and Junctions** L7
W. E. Spear*, S. H. Baker *(University of Dundee, GBR)*

10.30 Poster Session

Chairman: L. Peraldo Bicelli *(Polytechnic of Milan, ITA)*

11.45 **Picosecond Time-resolved Photogeneration of Charge Carriers at Electrode Interfaces** L8
F. Willig *(Fritz-Haber-Institut, Berlin, FRG)*

12.30 *Pause*

Chairman: K. Doblhofer *(Fritz-Haber-Institut, Berlin, FRG)*

14.00 **New Materials and Techniques in Photoelectrocatalysis** L9
H. Tributsch *(Hahn-Meitner-Institut, Berlin, FRG)*

14.45 **Structure and Dynamics in Modified Electrodes** L10
L. R. Faulkner *(University of Illinois, Urbana, IL, USA)*

15.30 Poster Session

16.30 Poster Discussion. *Leaders:*
H. Gerischer *(Fritz-Haber-Institut, Berlin, FRG)*
R. Memming *(Inst. Solarenenergieforschung, Hannover, FRG)*
J. W. Schultze *(University of Düsseldorf, FRG)*

17.30 *Adjournment*

Wednesday 31 August

(3) Microscopic Aspects

Chairman: J. K. Sass *(Fritz-Haber-Institut, Berlin, FRG)*

8.45 **Quantum Chem. Modeling of the Properties of Isolated Adsorbates** L11
A. B. Anderson *(Case Western Reserve Univ., Cleveland, OH, USA)*

9.25 **The Adsorption of Water on Surfaces: Basic Aspects** L12
T. E. Madey *(Nat. Bur. Stand., Gaithersburg, MD, USA)*

10.05 The Interaction of Dipoles with Metal Surfaces: Beyond the Arrowed Circle? L13
S. Holloway *(University of Liverpool, GBR)*

10.45 *Break*

Chairman: M. Costa *(CNRS, Meudon, FRA)*

11.10 Individual Ionic Hydration Properties in Relation to Ion Adsorption at Electrodes and the Transition from "Molten Salt" to "Hydrated-ion" Behaviour at Interfaces L14
B. E. Conway *(University of Ottawa, CAN)*

11.50 Optical Properties of Rough Metal Surfaces L15
M. I. Urbakh *(Academy of Sciences, Moscow, USSR)*

12.30 *Adjournment*

Thursday 1 September

(4) Biological Systems

Chairman: H. D. Hurwitz *(Free University, Brussels, BEL)*

9.00 Experimental Tests on the Gouy-Chapman Theory Using Phospholipid Bilayers L16
S. McLaughlin*, M. Langner, R. McDaniel *(State University, Stony Brooks, NY, USA)*

9.45 Structural Rearrangements in Biomembrane Electric Fields L17
E. Neumann*, K. Tsuji *(University of Bielefeld, FRG)*

10.30 Poster Session

Chairman: J. Teissié *(CNRS, Toulouse, FRA)*

11.45 Bioelectrochemistry at Conducting Organic Salt Electrodes L18
W. J. Albery *(Imperial College, London, GBR)*

12.30 *Pause*

15.00 Poster Session

Chairman: A. Gliozzi *(University of Genoa, ITA)*

16.00 The Motive Power of Molecular Hydration L19
V. A. Parsegian *(Nat. Inst. of Health, Bethesda, MD, USA)*

16.45 The Application of the Laser Induced Proton Pulse for Measuring Charge Translocation Across Biomembranes L20
M. Gutman*, E. Nachliel *(Univ. of Tel-Aviv, ISR)*

17.30 Poster Discussion. *Leaders:*
M. Blank *(Columbia University, New York, NY, USA)*
Yu. A. Chizmadzhev *(Academy of Sciences, Moscow, USSR)*
L. Kesztheiyi *(Academy of Sciences, Szeged, HUN)*

18.30 *Adjournment*

Friday 2 September

(5) Double Layer Structure: Theory and Modeling

Chairman: M. Sluyters-Rehbach *(University of Utrecht, HOL)*

9.00 Fractal Aspects of Electrode/Electrolyte Interfaces L21
S. H. Liu *(Oak Ridge National Laboratory, TN, USA)*

9.45 Effects of Ion Pair Correlations in Electric Double Layers L22
S. Marcelja *(Australian National University, Canberra, AUS)*

10.30 Poster Session

Chairman: M. L. Rosinberg *(Univ. P. et M. Curie, Paris, FRA)*

11.15 Molecular Dynamics Simulation of Water at Interfaces L23
K. Heinzinger*, E. Spohr *(Max-Planck-Institut, Mainz, FRG)*

12.00 Water Adsorption. Quantum Chemical Approach L24
An. M. Kuznetsov*, R. R. Nazmutdinov, M. S. Shapnik
(University of Kazan, USSR)

12.45 *Pause*

Chairman: P. Nikitas *(Aristotelian Univ., Thessaloniki, GRE)*

14.15 Metal Electrons in the Double Layer Modeling L25
A. A. Kornyshev *(Academy of Sciences, Moscow, USSR)*

15.00 Molecular Models of Water and Neutral Solutes Against a Charged Wall L26
R. Guidelli*, G. Aloisi *(University of Florence, ITA)*

15.45 Poster Session

16.45 Poster Discussion. *Leaders:*
F. Forstmann *(Free University, Berlin, FRG)*
D. Henderson *(IBM, San Jose, CA, USA)*
W. Schmickler *(University of Bonn, FRG)*

17.45 *Closing Session*

POSTERS

TOPIC 1 ***(Experimental Approaches)***

1 Electrode impedance of cobalt in concentrated nitric acid
E. Stupnisek-Lisac, H. Takenouti

2 LEED-AES study of electrodes following electrochemistry
R. Durand, R. Faure, D. Aberdam, S. Traore

3 Adsorption of organic molecules onto a metal surface, studied using surface plasmon-polaritons
S. Cowen, J. R. Sambles

4 Investigation of CO_2 reduction in aprotic media by in situ FTIR spectroscopy
J. Desilvestro, S. Pons

5 Surface tension measurement: toward higher accuracy
S. Bordi, M. Carlà, R. Cecchini

6 Iron behaviour in HF solutions
A. Frignani, C. Monticelli, G. Brunoro, M. Tassinari, G. Trabanelli

7 In situ STM of electrode surfaces with atomic scale resolution
T. Twomey, J. Wiechers, R. J. Behm, D. M. Kolb

8 In situ FTIR studies of the reduction of adsorbed CoPc in the presence of CO_2
P. A. Christensen, A. Hamnett, A. V. G. Muir

9 XPS and LEED study of underpotentially deposited copper on Pd(100)
T. Solomun

10 Aluminum electrocrystallization from metal-organic electrolytes
V. Kautek, S. Birkle

11 Electrocatalytic properties of well defined Pt surfaces modified by irreversibly adsorbed adatoms
A. Fernández-Vega, J. M. Feliu, A. Aldaz, J. Clavilier

12 Morphological and electrocatalytic properties of gold deposits on NaY zeolite
O. Enea

13 Electrochemical and ellipsometric study of the reduction processes of hydrated platinum oxide
J. O. Zerbino, C. L. Perdriel, A. J. Arvia

14 Correlation between SERS and electrochemical results in measurements of pyrrole adsorption on Ag electrode
J. Bukowska, K. Jaszczynski, K. Jackowska

15 Electrocatalytic oxidation of ethanol on platinum single crystal electrodes
M.-C. Morin, J.-M. Leger, C. Lamy, J.-L. Vasquez, A. Aldaz

16 An EMIRS study of the adsorption of ethanol on platinum electrodes in acid medium
B. Beden, J.-M. Leger, C. Lamy, J.-M. Perez, A. Aldaz

17 Electrocatalysis of oxygen on single crystal stepped surfaces of gold
S. Strbac, N. Anastasijevic, R. Adzic

18 Electrosorption properties of platinum single crystal stepped surfaces
N. M. Markovic, N. S. Marinkovic, R. R. Adzic

19 Reduction of p-benzoquinone dioxime on Pt/M(upd) modified electrodes in $HClO_4$ solutions: a reaction model for the ECECE mechanism
G. Kokkinidis, G. Papanastasiou

20 The influence of specific adsorption on the electronic surface states of Ag(111) and Ag(100)
C. Franke, G. Piazza, D. M. Kolb

21 Electrochemical investigation on chlorophyll A. Different aggregates in water-acetone mixtures
A. Agostiano, M. Caselli, M. Della Monica, F. K. Fong

22 Kinetics of the $Fe(CN_6)^{3-}/Fe(CN_6)^{4-}$ couple at passive titanium electrodes
T. Hurlen, V. Wilhelmsen

23 Optical properties of Hg-Electrode interface studied by surface plasmon technique
A. Tadjeddine, A. Rahmani, G. Piazza, M. Costa

24 Surface structural changes of evaporated thin silver film electrodes during the adsorption of chloride ion. A capacitance and resistance study
R. I. Tucceri, D. Posadas

25 Surface conductivity changes and differential capacity studies of thin silver films during the adsorption of PF_6^-, F^- and Cl^- ions
R. I. Tucceri, F. M. Romeo, D. Posadas

26 Mediation of interfacial reactions by low levels of in-situ generated hydroxy species
L. D. Burke, K. J. O'Dwyer, W. A. O'Leary

27 A study on spectroelectrochemistry of the redox reaction of hemoglobin
S. Song, S. Dong

28 Raman spectroscopy at metal electrodes
B. Pettinger, U. Tiedemann

29 Formation of a monolayer of oxide at Au single crystal face electrodes in sulphamic acid solutions
F. Silva, C. Moura, A. Hamelin

30 SERS investigations of Cu-Phthalocyanine chemisorption layers on Ag electrodes. The excitation profile
R. Castillo, W. Plieth

31 Permittivity studies on suspensions
J. Liszi

32 Electromodulation of surface plasmon dispersion relation and adsorption of anions at the electrochemical interface
P. G. Dzhavakhidze, A. A. Kornyshev, A. Tadjeddine, M. I. Urbakh

33 Investigation of adsorption inhomogenity of polycrystalline platinum by optical methods
V.E. Kazarinov, A. M. Funtikov, G. A. Tsirlina

34 Evaluation of the adsorption parameters of organic molecules from ellipsometric measurements on electrodes
U. Palm, T. Silk, T. Raud

35 Scanning tunneling microscopy of interfaces relevant to electrochemistry
M. H. Dean, D. Liebeskind, U. Stimming

36 Potential relaxation of metal electrodes immersed into aqueous electrolytes
J. K. Sass, U. Stimming, K. Tellefsen

37 Vibrational electron energy loss spectroscopy of H_2O adsorbed on Cu(110) with inverted orientation induced by coadsorbed cesium
J. Schott, D. Lackey, J. K. Sass

TOPIC 2 *(Semiconductors, Photoeffects and Modified Electrodes)*

1 Electrolyte electroreflectance and photoelectrochemical topological investigation of semiconducting electrodes by scanning light-spot optical microscopy
G. Razzini, L. Peraldo Bicelli

2 Electrochemical and photoelectrochemical study of vacuum evaporated films of thiophene oligomers
D. Fichou, G. Horowitz, Y. Nishikitani, F. Garnier

3 The semiconductor properties of passive tin electrodes in slightly alkaline solutions
M. Seruga, M. Metikos-Hukovic, S. Ferina

4 Photothermal beam deflection and photoacoustic experiments in photo-electrochemistry
F. Decker, M. Fracastoro-Decker, M. Cella, H. Vargas

5 Semiconductor electrode modification: influence on the state distribution at the interfaces
P. Allongue, J. Souteyrand

6 Effect of water on the formation of GaAs/electrolyte interfaces
S. Blonkowski, P. Allongue, H. Cachet

7 Photoelectrochemical preparation of Lewis acido basic electrocatalyser on passive iron materials
T. Mouhandess, J. F. Nowak, G. Picq, F. Rouina, P. Vennereau

8 Study of etching mechanisms of gallium phosphide by means of (photo-)electrochemical methods
H. Goossens, F. Vanden Kerchove, V. P. Gomes

9 Charge carriers in layer of silver/silver oxide
T. Grozdic

10 Study of the impedance of a galena electrode effect of a collector for sulphide flotation
D. Schuhmann, P. Vanel, E. Idzebet

11 The comparability of redox reactions at n- and p-type electrodes
R. Reineke, R. Memming

12 Molecular catalysts in photoelectrochemical cells: study of an efficient system for the selective photoelectroreduction of CO_2: p-GaP or p-GaAs / Ni(cyclam)$^{2+}$, aqueous medium.
J-P. Petit, P. Chartier, M. Beley, J-P. Deville

13 Electrochemical study of phosphorus doped cadmium telluride
P. Lemasson

14 In-situ vibrational study of the n-Si/electrolyte interface using Fourier-transform electrochemically modulated IR spectroscopy
F. Ozanam, J.-N. Chazalviel

15 Local photocurrent and high power density investigations on oxide films of valve metals with a focussed laser beam
J. Thietke, K. Bade, J. W. Schultze

16 Profile of the electrical potential in an electrolyte-insulator-semiconductor system
M. Grattarola, A. Morro, F. Conzi, A. Cambiaso, M. Parodi

17 Multilayer/multijunction photoelectrodes
V.M. Ayers

18 Reduction of $V(OH)_4^+$ on passive titanium
W. Wilhelmsen

19 The role of redox-ion migration in electrochemical processes on polymer-modified electrodes
K. Doblhofer, J. Ye

20 The electrochemistry of graphite and modified graphite surfaces
S. Hossain, D. Tryk, E. Yeager

21 Photoluminescence and molecular orbital theory in anodic oxides films formed on Al_2O_3
B. Jovanic, Lj. D. Zekovic, V. V. Urosevic, B. Radenkovic

22 Photoelectrochemically synthesized interfacial oxides on silicon: composition and electronic properties
J. Stumper, C. Pettenkofer, R. Greef, H. J. Lewerenz

23 Study of the anodic decomposition of III-V semiconductor electrodes induced by hole injection
D. Vanmaekelbergh, J. J. Kelly

24 Semiconducting metal oxide photoanodes - Their characteristics and implications (XXI)
S. K. Bahador

25 Study of the ionic adsorption on EOS structures by coupling electroreflectance, photocurrent and capacitance measurements
M. Jaffrezic-Renault, H. Perrot, C. Nguyen van Houng

26 $La_{0.17}WO_3$-Perowskite: chemical characterization of the single crystal (111)/aqueous solution interface by XPS/UPS
H. Kohler, V. Neu, K.-D. Kreuer, D. Schmeisser, W. Göpel

27 In vitro photoelectrochemical model of the Z scheme in plant photosynthesis
A. Agostiano, M. Della Monica, F. K. Fong

28 Photoanodic behaviour of cuprous oxide layers on copper electrodes in aqueous electrolytes
A. Aruchamy, A. Fujishima

29 Photocatalytic deposition of Uranyl ions onto semiconductor suspensions
R. Amadelli, A. Maldotti, V. Carassiti

30 Direct measurements of semiconductor bands unpinning under illumination by electrolyte electroreflectance
D. Tafalla, M. Pujadas, P. Salvador

31 Electrochemical behaviour of the cell $Pb/PEO_n.Pb(ClO_4)_2/Pb$
A. K. Saraswat, A. Magistris, G. Chiodelli, P. Ferloni

32 Entrapment of enzymes in electrochemically polymerized organic films
Ph. N. Bartlett, R. G. Whitaker

33 Chemico-physical characterization of amorphous anodic films on niobium by photocurrent spectroscopy.
F. Di Quarto, S. Piazza, R. D'Agostino, C. Sunseri

34 Electrochemical and photoelectrochemical study of passivated Ti and Nb electrodes in nitric acid solutions
W. A. Badawy, A. Felske, W. J. Plieth

35 An impedance study of polyaniline and polypyrrole films in non aqueous solutions
G. Pistoia, S. Panero, B. Scrosati

36 pH effects on the photooxidation of d-sorbitol at TiO_2 surfaces
O. Enea, J. P. Ango, D. Duprez

37 Indium(III)-Hexacyanoferrate(II,III) as a novel polynuclear mixed-valent inorganic material for modification of electrode surfaces
P. J. Kulesza, M. Krzowska

38 On the capacity behaviour of inhomogeneous and amorphous semiconductor electrodes
M. H. Dean, U. Stimming

39 Use of semiconductor electrochemistry techniques for the characterization of anticorrosive coatings
L. Giorgi

40 Oxidation behaviour of chevrel type oxygen reduction catalysts
W. Jaegermann, C. Pettenkofer, B. Schubert, M. Alonso-Vante, E. Gocke, H. Tributsch

41 Site specific surface interaction of I_2 on $CuInSe_2$ (112) in relation to photoelectrochemical phase transformation
M. Sander, W. Jaegermann, H. J. Lewerenz

42 Incorporation of electroactive species in self-assembling monolayers on gold electrodes
K. A. Bunding Lee

43 Photoelectrochemical microscopy of thin TiO_2 films
M. R. Kozlowski, C.-H. Paik, P. S. Tyler, W. H. Smyrl, R. T. Atanasoski

44 Impedance response of pyrite photoanode/redox electrolyte interface
M. Alonso Vante, X.-P. Li, H. Tributsch

45 Morphology and reactivity of semiconductor electrode surfaces studied by laser spot scanning technique
P. Carlsson, B. Holmström, K. Uosaki, H. Kita

TOPIC 4 (Biological Systems)

1 A gradient of the electrochemical potential of the proton, driving force and modulator of proton transfer at the biological membrane/water interface
R. Naumann

2 Photo induced transmembrane electron transfer in model systems for photosynthesis
P. Seta, E. Bienvenue, T. A. Moore, A. Moore, D. Gust

3 The Helmholtz formula and the membrane potential
D. Schuhmann

4 Phase transitions induced by an electric field in black lipid membranes
M. Robello, A. Gliozzi

5 Some problems in electroarteriography
C. G. Anton, J. L. Vasquez, J. Medrano, J. M. Feliu, A. Aldaz

6 Lateral proton conduction along lipid monolayers at the air/water interface
M. Prats, J. F. Tocanne, J. Teissié

7 The electric state of ion-exchange membrane surfaces emersed from electrolytes
M. Cappadonia, K. Doblhofer

8 Some electrochemical behaviour of bilayer lipid membranes modified with porphirynes
P. Krysinski

9 Bioelectrochemical activity at the surface of inert metal electrodes implanted into the brain tissue
T. B. Shvets-Teneta-Guriy, A. G. Dubinin

10 Dynamics of lateral charge transport in amphiphilic monolayer and bilayer assemblies
C. A. Widrig, M. Majda

11 Oscillations in iron-bromate systems
F. D'Alba, S. Di Lorenzo, C. Lucarini

12 Dynamic changes of bacteriorhodopsin reconstituted in DMPC-bilayers during proton pumping
A. Böttcher, M. Denker, R. Groll, F. Meyer, J. F. Holzwarth

13 Charge injection via light-induced picosecond charge separation in an artificial molecular membrane
R. Eichberger, F. Willig, V. Storck, V. S. Durfee

14 Microelectrophoretic investigations of lipophilic anions transport kinetics across the mebrane of human erythrocytes in vitro
S. Kalinowski, P. Krysinski, S. Minc

15 Composite films of Co tetra/p-tolyl/porphyrin immobilized in zeolitic Ru oxide/cyanoruthenate microstructures as cytochrome P450-like models for anodic electrocatalysis
P. J. Kulesza, T. Mlodnicka, J. Haber

16 Liquid junction potentials between pH buffer solutions
M. J. F. Rebelo

17 The effect of transmembrane electrical fields on the kinetics of electron transfer reactions
G. Venturoli, M. T. Scupoli, B. A. Melandri

TOPIC 5 *(Double Layer Structure: Theory and Modeling)*

1 Contribution of the metal to the silver-water interfacial capacitance
G. Valette

2 Adsorption from dilute solutions of solvents with asymmetric molecules
P. Nikitas, A. Pappa-Louisi

3 Poisson-Boltzmann equation for highly charges polyelectrolyte systems
F. Bordi, C. Cametti, A. Di Biasio

4 A variational calculation of the static image plane position at a charged jellium surface
M. L. Rosinberg, V. Russier

5 Improvements in the two-parallel-condenser model of the double layer in the presence of organic adsorption
D. Schuhmann

6 Determination of the distance of closest approach for solvent molecules to a metal surface
V. Russier, S. Amokrane, J. P. Badiali

7 Electrical double layer interactions between ionized inverted micelles in microemulsions
D. Bratko, A. Luzar, S. H. Chen

8 Electrical response of fractal and porous electrodes
J.-N. Chazalviel, B. Sapoval, J. Peyrière

9 What can be inferred about the structure of the metal solution interface from the electrochemical experiment
J. Stafiej, Z. Borkowska

10 Electrochemical work function approach to the kinetics along simple rate-determining steps: example of oxygen reduction at platinum electrodes
A. Damjanovic

11 Underpotential deposition of jellium on jellium
E. Leiva, W. Schmickler

12 Pair correlation functions and the structure of the electric double layer
M. Plischke, D. Henderson

13 The differences of surface potentials between water and some organic solvents
Z. Koczorowski, I. Zagórska, A. Kalinska

14 U.H.V. simulation of the double-layer structure at the Au(100)-(5×20)/CH_3-CN and β-CN interfaces
T. Solomun, K. Christmann, H. Baumgärtel

15 Influence of surface crystallography on molecular adsorption at the gold-solution interface.
J. Richer, A. Iannelli, L. Stolberg, D. E. Irish, J. Lipkowski

16 Adsorption of β-cyclodextrin on the mercury electrode from water and water + ethanol mixture
J. Taraszewska, J. Siedzik

17 Local interactions in the double layer and orientation of adsorbate molecules
A. Daghetti, S. Trasatti, G. Rocchini, I. Zagórska, Z. Koczorowski

18 Diffusion kinetics at fractal interfaces
L. Nyikos, T. Pajkossy

19 Analysis of concentration, electric potential and charge density profiles in interfacial region of an aqueous electrolyte near a charged surface.
V. S. Vaidhyanathan,

20 The fractal structure of surface inhomogeneity as the origin of CPE-behaviour in the faradaic and non-faradaic region
W. H. Mulder, M. Sluyters-Rehbach, J. H. Sluyters

21 Adiabatic charge transfer across the charged metal/electrolyte interface.
A. V. Gorodyskii, A. I. Karasevskii, D. V. Matyushov

22 Self-organization phenomenon in multistage metal electroreduction processes. Theory and experiment.
I. N. Karnaukhov, A. I. Karasevskii, N. D. Ivanova, Y. I. Boldyrev

23 Determination of the composition of electrochemically active ions on an electrode
V. S. Kublanovskii, A. V. Gorodyskii

24 Theoretical considerations on the adsorption isotherm for ionic systems at electrode interphases
R. Gonzales, F. Sanz

25 The proton discharge reaction on gold and silver
U. Frese, W. Schmickler

26 Adsorption behaviour of 2-propanol and of hexafluoro-2-propanol
M. R. Moncelli, R. Guidelli

27 Adsorption of aromatic aminoacids and related compounds in relation to calculated molecular structural indexes
C. Fontanesi, A. Barbieri, R. Andreoli, L. Benedetti, G. Gavioli

28 Polycrystalline effects in the double layer structure and adsorption on solid electrodes
U. Palm, E. Lust, K. Lust, M. Salve

29 Study of electrochemical kinetics using the "FREECE" technique
U. Stimming, J. K. Sass, J. Schott

30 Surface potential at liquid/liquid interface calculated on the basis of potential Volta differences method
V. I. Parfenyuk, G. A. Krestov

31 Adsorption of organic substances at the mercury/ethylene glycol interface and air/ethylene glycol interface: lauronitrile in 0.5 M $NaClO_4$
G. Borghesani, A. De Battisti, J. I. Japaridze, S. Trasatti

32 Electrical double layer between mercury and aliphatic diols
G. Borghesani, A. De Battisti, C. Locatelli, J. I. Japaridze, S. Trasatti

33 Electrochemical intercalation into graphite seen as an electrocapillary process
A. Metrot, A. Harrach

34 Specific adsorption of halides on Ag(110): surface science model studies of the inner layer structure
B. Straehler, J. K. Sass, K. Bange, J. Schott

Divisione di Elettrochimica della Società Chimica Italiana
and
International Society of Electrochemistry (ISE)
Bioelectrochemical Society (BES)

International Conference

CHEMISTRY AND PHYSICS OF ELECTRIFIED INTERFACES

Solid/Electrolyte and Biological Systems

Organized on occasion of the celebration of the 900 years of the University of Bologna

EXTENDED ABSTRACTS

BOLOGNA

29 August - 2 September 1988

Palazzo dei Congressi

ORGANIZING COMMITTEE

S. TRASATTI (Chairman)	(University of Milan)
E. VECCHI (Secretary)	(University of Bologna)
A. DE BATTISTI	(University of Ferrara)
F. DI QUARTO	(University of Palermo)
L. FORMARO	(University of Milan)
R. GUIDELLI	(University of Florence)
B. A. MELANDRI	(University of Bologna)
G. PIAZZA	(University of Bologna)
M. P. TOSI	(University of Trieste)

LOCAL ORGANIZERS
(University of Bologna)

G. PIAZZA *(Chairman)*
P. FETTO
B. A. MELANDRI
F. SCAGNOLARI
E. VECCHI

ACKNOWLEDGEMENTS

Thanks are due to the following Institutions for their support to the Conference

Accademia delle Scienze dell'Istituto di Bologna
Banca Operaia di Bologna, Bologna
Banco di Sicilia, Bologna
COFID, Bologna
Comune di Bologna
Consiglio Nazionale delle Ricerche
Elettrochimica M. Ginatta S.p.A., Torino
Ente Nazionale per l'Energia Elettrica
FIAMM S.p.A., Vicenza
Gruppo Nazionale di Struttura della Materia (GNSM-CISM)
Istituto Bancario Italiano, Bologna
Istituto Donegani, Novara
Ministero della Pubblica Istruzione
Montedison S.p.A., Milano
O. De Nora Impianti Elettrochimici S.p.A., Milano
Presidenza del Consiglio dei Ministri (proposta MRST)
Provincia di Bologna
Regione Emilia-Romagna
Società Chimica Italiana (SCI)
Società Italiana di Fisica
U.S. Army Research Office
Università di Bologna

FOREWORD

Contributions have been grouped according to the five topics in which the Conference has been articulated, with lectures coming first in each goup. In the Index of Contributions, lectures are denoted by "L" followed by a number from 1 to 26. Posters are labelled with a progressive number starting with 1 in each group. Numbers are in both cases those appearing in the final Programme.

In the Author Index, contributions are indicated by a code of two numbers separated by a dash: the first denotes the topic, while the other refers to the sequential order described above. In particular, in the case of posters the complete code identifies the poster board.

The Proceedings of the Conference will be published in a special issue of Electrochimica Acta planned for 1989.

The Organizing Committee is indebted to the members of the Advisory Board for their invaluable advice: R. R. Adzic, W. J. Albery, A. J. Bard, G. F. Bassani, G. Chiarotti, Y. A. Chizmadzhev, B. E. Conway, M. Costa, E. A. Davis, M. Fleischmann, H. Gerischer, D. Henderson, H. D. Hurwitz, V. E. Kazarinov, L. Keszthelyi, D. M. Kolb, Ya. M. Kolotyrkin, A. A. Kornyshev, W. Lorenz, S. McLaughlin, S. Motoo, R. Parsons, P. N. Ross, J. Sobkowski, J. Ulstrup, H. T. Witt, E. B. Yeager.

July 1988

Sergio Trasatti

Table of Contents

INDEX OF CONTRIBUTIONS

TOPIC 1 (Experimental Approaches)

L2 *Surface Electronic Structure from Ellipsometry.*
Chao F., Costa M., Lecoeur J., Bellier J. P., Russier V. 1

L3 *Single-Crystal Electrochemistry: Experimental Challenges to Current Theory.*
Ross P. N. 4

L4 *Nonlinear Optical Probes of Electrochemical Interfaces.*
Richmond G. L. 7

L5 *In situ Surface Extended X-Ray Adsorption Fine Structure Spectroscopy and X-Ray Diffraction of Monolayers Adsorbed at Electrochemical Interfaces.*
Melroy O. R. 10

1 *Electrode Impedance of Cobalt in Concentrated Nitric Acid.*
Stupnisek-Lisac E., Takenouti H. 11

2 *LEED AES Study of Electrodes Following Electrochemistry.*
Durand R., Faure R., Aberdam D., Traore S. 14

3 *Adsorption of Organic Molecules onto a Metal Surface, Studied Using Surface Plasmon-Polaritons.*
Cowen S., Sambles J. R. 17

4 *Investigation of CO_2 Reduction in Aprotic Media by in-situ FTIR Spectroscopy.*
Desilvestro J., Pons S. 18

5 *Surface Tension Measurements: Toward Higher Accuracy.*
Bordi S., Carlà M., Cecchini R. 21

6 *Iron Behaviour in HF Solutions.*
Frignani A., Monticelli C., Brunoro G., Tassinari M., Trabanelli G. 24

7 *In-situ Scanning Tunneling Microscopy of Electrode Surfaces with Atomic Scale Resolution.*
Twomey T., Wiechers J., Behm R. J., Kolb D. M. 27

8 *In-situ FTIR Studies of the Reduction of Adsorbed CoPc in the Presence of CO_2.*
Christensen P. A., Hamnett A., Muir A. V. G. 30

9 *XPS and LEED Study of Underpotentially Deposited Copper on Pd(100).*
Solomun T. 33

10 *Aluminum Electrocrystallization from Metal-Organic Electrolytes.*
Kautek W., Birkle S. 36

11 *Electrocatalytic Properties of Well Defined Pt Surfaces Modified by Irreversibly Adsorbed Adatoms.*
Fernández-Vega A., Feliu J. M., Aldaz A., Clavilier J. 39

12 *Morphological and Electrocatalytic Properties of Gold Deposits on NaY Zeolite.*
Enea O. 42

13 *Electrochemical and Ellipsometric Study of the Reduction Processes of Hydrated Platinum Oxide.*
Zerbino J. O., Perdriel C. L., Arvia A. J. 45

14 *Correlation Between SERS and Electrochemical Results in Measurements of Pyrrole Adsorption on Ag Electrode.*
Bukowska J., Jaszczynski K., Jackowska K. 48
15 *Electrocatalytic Oxidation of Ethanol on Platinum Single Crystal Electrodes.*
Morin M. -C., Leger J. -M., Lamy C., Vazquez J. -L., Aldaz A. 51
16 *An EMIRS Study of the Adsorption of Ethanol on Platinum Electrodes in Acid Medium.*
Beden B., Leger J. -M., Lamy C., Perez J. -M., Aldaz A. 54
17 *Electrocatalysis of Oxygen on Single Crystal Stepped Surfaces of Gold.*
Strbac S., Anastasijević M., Adžić R. R. 57
18 *Electrosorption Properties of Platinum Single Crystal Stepped Surfaces.*
Marković M. M., Marinković M. S., Adžić R. R. 60
19 *Reduction of p-Benzoquinone Dioxime on Pt/M(upd) Modified Electrodes in $HClO_4$ Solutions: a Reaction Model for the ECECE Mechanism.*
Kokkinidis G., Papanastasiou G. 63
20 *The Influence of Specific Adsorption on the Electronic Surface States of Ag(111) and Ag(100).*
Franke C., Piazza G., Kolb D. M. 66
21 *Electrochemical Investigation on Chlorophyll A Different Aggregates in Water-Acetone Mixtures.*
Agostiano A., Caselli M., Della Monica M., Fong F. K. 70
22 *Kinetics of the Hexacyanoferrate(II)/(III) Couple at Passive Titanium Electrodes.*
Hurlen T., Wilhelmsen W. 72
23 *Optical Properties of Hg-Electrode Studied by Surface Plasmon Technique.*
Tadjeddine A., Rahmani A., Piazza G., Costa M. 75
24 *Surface Structural Changes of Evaporated Thin Silver Film Electrodes During the Adsorption of Chloride Ion. A Capacitance and Resistance Study.*
Tucceri R. I., Posadas D. 78
25 *Surface Conductivity Changes and Differential Capacity Studies of Thin Silver Films During The Adsorption of PF_6^-, F^- and Cl^- Ions.*
Tucceri R. I., Romeo F. M., Posadas D. 80
26 *Mediation of Interfacial Reactions by Low Levels of In-situ.Generated Hydroxy Species.*
Burke L. D., O'Dwyer K. J., O'Leary W. A. 83
27 *A Study on Spectroelectrochemistry of the Redox Reaction of Hemoglobin.*
Song S., Dong S. 86
28 *Raman Spectroscopy at Metal Electrodes.*
Pettinger B., Tiedemann U. 88
29 *Formation of a Monolayer of Oxide at Gold Single Crystal Face Electrodes in Sulphamic Acid Solutions.*
Silva F., Moura C., Hamelin A. 89
30 *SERS Investigations of Cu-Phthalocyanine Chemisorption Layers on Silver Electrodes. The Excitation Profile.*
Castillo R., Plieth W. J. 93
31 *Permittivity Studies on Suspensions.*
Liszi J. 96

32 *Electromodulation of Surface Plasmon Dispersion Relation and Adsoprption of Anions at the Electrochemical Interface.*
Dzhavakhidze P. G., Kornyshev A. A., Tadjeddine A., Urbakh M. I. 97
33 *Investigation of Adsorption Inhomogenity of Polycristalline Platinum by Optical Methods.*
Kazarinov V. E., Funtikov A. M., Tsirlina G. A. 101
34 *Evaluation of the Adsorption Parameters of Organic Molecules from Ellipsometric Measurements on Electrodes.*
Palm U., Silk T., Raud T. 103
35 *Scanning Tunneling Microscopy of Interfaces Relevant to Electrochemistry.*
Dean M. H., Liebeskind D., Stimming U. 106
36 *Potential Relaxation of Metal Electrodes Immersed into Aqueous Solutions.*
Sass J. K., Stimming U., Tellefsen K. 107
37 *Vibrational Electron Energy Loss Spectroscopy of H_2O Adsorbed on Cu(110) with Inverted Orientation Induced by Coadsorbed Cesium.*
Schott J., Lackey D., Sass J. K. 110

TOPIC 2 (Semiconductors, Photoeffects and Modified Electrodes)

L6 *Electrochemistry of Semiconductors in Non-Aqueous Solvents.*
Kumar A., Lunt S. R., Santangelo P. G., Tufts B. J., Lewis N. S. 113
L7 *Electronic Properties of Amorphous Silicon Surface Barriers and Junctions.*
Spear W. E., Baker S. H. 115
L8 *Picosecond Time-Resolved Photo-Generation of Charge Carriers at Electrode Interfaces.*
Willig F. 116
L9 *New Materials and Techniques in Photoelectrocatalysis.*
Tributsch H. 118
L10 *Structure and Dynamics in Modified Electrodes.*
Faulkner L. R. 120
1 *Electrolyte Electroreflectance and Photoelectrochemical Topological Investigation of Semiconductor Electrodes by Scanning Light-Spot Optical Microscopy.*
Razzini G., Perzldo Bicelli L. 122
2 *Electrochemical and Photoelectrochemical Study of Vacuum Evaporated Films of Thiophene Oligomers.*
Fichou D., Horowitz G., Nishikitani Y., Garnier F. 125
3 *The Semiconducting Properties of Passive Tin Electrodes in Slightly Alkaline Solutions.*
Šeruga M., Metikoš-Huković M., Ferina S. 128
4 *Photothermal Beam Deflection and Photoacoustic Experiments in Photoelectrochemistry.*
Decker F., Fracastoro-Decker M., Cella M., Vargas H. 131
5 *Semiconductor Electrode Modification: Influence on the State Distribution at the Interface.*
Allongue P., Souteyrand E. 134
6 *Effect of Water on the Formation of GaAs/Electrolyte Interfaces.*
Blonkowski S., Allongue P., Cachet H. 136

7 *Photoelectrochemical Preparation of Lewis Acido Basic Electrolyser on Passive Iron Materials.*
Houhandess T., Nowak J. F., Picq G., Rouina F., Vennereau P. 138
8 *Study of Etching Mechanisms of Gallium Phosphide by Means of (Photo-)Electrochemical Methods.*
Goossens H., Vanden Kerchove F., Gomes W. P. 141
9 *Charge Carriers in Layer of Silver/Silver Oxide.*
Grozdić T. 144
10 *Study of the Impedance of a Galena Electrode. Effect of a Collector for Sulphide Flotation.*
Schuhmann D., Vanel P., Hdzebet K. 147
11 *The Comparability of Redox Reactions at n- and p-Type Electrodes.*
Reineke R., Hemming R. 150
12 *Molecular Catalysts in Photoelectrochemical Cells: Study of an Efficient System for the Selective Photoelectroreduction of CO_2: p-GaP or n-GaAs/Ni(cyclam)$_2^+$, Aqueous Medium.*
Petit J.-P., Chartier P., Beley M., Deville J.-P. 153
13 *Electrochemical Study of Phosphorus Doped Cadmium Telluride.*
Lemasson P. 156
14 *In-situ Vibrational Study of the n-Si/Electrolyte Interface using Fourier-Transform Electrochemically Modulated IR Spectroscopy.*
Ozanam F., Chazalviel J. -N. 159
15 *Local Photocurrent and High Power Density Investigations on Oxide Films of Valve Metals with a Focussed Laser Beam.*
Thietke J., Bade K., Schultze J. W. 162
16 *Profile of the Electrical Potential in an Electrolyte - Insulator - Semiconductor System.*
Grattarola M., Morro A., Conzi F., Cambiaso A., Parodi M. 165
17 *Multilayer-Multijunction Photoelectrodes.*
Ayers W. M. 168
18 *Reduction of $V(OH)_4^+$ on Passive Titanium.*
Wilhelmsen W. 172
19 *The Role of Redox-Ion Migration in Electrochemical Processes on Polymer-Coated Electrodes.*
Doblhofer K., Ye J. 175
20 *The Electrochemistry of Graphite and Modified Graphite Surfaces.*
Hossain S., Tryk D., Yeager E. 178
21 *Photoluminescence and Molecular Orbital Theory in Anodic Oxides Films Formed on Al_2O_3.*
Jovanić B. R., Zeković Lj. D., Urošević V. V., Radenkovic B. 181
22 *Photoelectrochemically Synthesized Interfacial Oxides on Silicon: Composition and Electronic Properties.*
Stumper J., Pettenkofer C., Greef R., Lewerenz H. J. 184
23 *Study of the Anodic Decomposition of III - V Semiconductor Electrodes Induced by Hole Injection.*
Vanmaekelbergh D., Kelly J. J. 187

24 *Semiconducting Metal Oxide Photoanodes - Their Characteristics and Implications (XXI).*
Bahador S. K. 190
25 *Study of the Ionic Adsorption on EOS Structures by Coupling Electroreflectance, Photocurrent and Capacitance Measurements.*
Jaffrezic-Renault N., Perrot H., Nguyen van Huong C. 193
26 *$La_{0.175}WO_3$ - Perowskite: Chemical Characterisation of the Single Crystal (111)/Aqueous Solution Interface by XPS/UPS.*
Kohler H., Neu W., Kreuer K. -D., Schmeisser D., Göpel W. 196
27 *In vitro Photoelectrochemical Model of the Z Scheme in Plant Photosynthesis.*
Agostiano A., Della Monica M., Fong F. K. 199
28 *Photoanodic Behaviour of Cuprous Oxide Layers on Copper Electrodes in Aqueous Electrolytes.*
Aruchamy A., Fujishima A. 201
29 *Photocatalytic Deposition of Uranyl onto Semiconductor Suspensions.*
Amadelli R., Maldotti A., Carassiti V. 204
30 *Direct Measurements of Semiconductor Bands Unpinning under Illumination by Electrolyte Electroreflectance.*
Tafalla D., Pujadas M., Salvador P. 207
31 *Electrochemical Behaviour of the Cell $Pb/PEO_n.Pb(ClO_4)_2/Pb$.*
Saraswat A. K., Magistris A., Chiodelli G., Ferloni P. 210
32 *Entrapment of Enzymes in Electrochemically Polymerized Organic Films.*
Bartlett Ph. N., Whitaker R. G. 213
33 *Chemico-Physical Characterization of Amorphous Anodic Films on Niobium by Photocurrent Spectroscopy.*
Di Quarto F., Piazza S., D'Agostino R., Sunseri C. 215
34 *Electrochemical and Photoelectrochemical Study of Passivated Ti and Nb Electrodes in Nitric Acid Solutions.*
Badawy W. A., Felske A., Plieth W. J. 218
35 *An Impedance Study of Polyaniline and Polypyrrole Films in Non Aqueous Solutions.*
Pistoia G., Panero S., Scrosati B. 221
36 *pH Effects on the Photooxidation of D-Sorbitol at TiO_2 Surfaces.*
Enea O., Ango J. P., Duprez D. 224
37 *Indium(III)-Hexacyanoferrate(II, III) as a Novel Polynuclear Mixed-Valent Inorganic Material for Modification of Electrode Surfaces.*
Kulesza P. J., Krzowska M. 227
38 *On the Capacity Behavior of Inhomogeneous and Amorphous Semiconductor Electrodes.*
Dean M. H., Stimming U. 230
39 *Use of Semiconductor Electrochemistry Techniques for the Characterization of Anticorrosive Coatings.*
Giorgi L. 233
40 *Oxidation Behaviour of Chevrel Type Oxygen Reduction Catalysts.*
Jaegermanr W., Pettenkofer C., Schubert B., Alonso-Vante N., Gocke E., Tributsch H. 238

41 *Site Specific Surface Interaction of I_2 on $CuInSe_2$(112) in Relation to Photoelectrochemical Phase Transformation.*
Sander M., Jaegermann W., Lewerenz H. J. 241
42 *Incorporation of Electroactive Species in Self-Assembling Monolayers on Gold Electrodes.*
Bunding Lee K. A. 244
43 *Photoelectrochemical Microscopy of Thin TiO_2 Films.*
Kozlowski M. R., Paik C. -H., Tyler P. S., Smyrl W. H., Atanasoski R. T. 247
44 *Impedance Response of Pyrite Photoanode/Redox Electrolyte Interface.*
Alonso-Vante M., Li X. -P., Tributsch H. 249
45 *Morphology and Reactivity of Semiconductor Electrode Surfaces Studied by Laser Spot Scanning Technique.*
Carlsson P., Holmström B., Uosaki K., Kita H. 252

TOPIC 3 (Microscopic Aspects)

L12 *The Adsorption of Water on Surfaces: Basic Aspects.*
Madey Th. E. 257
L13 *The Interaction of Dipoles with Metal Surfaces: Beyond the Arrowed Circle ?.*
Holloway S. 259
L14 *Individual Ionic Hydration Properties in Relation to Ion Adsorption at Electrodes and the Transition from "Molten-Salt" to "Hydrated-Ion" Behaviour at Interfaces.*
Conway B. E. 260
L15 *Optical Properties of Rough Metal Surfaces.*
Urbakh M. I. 262

TOPIC 4 (Biological Systems)

L16 *Experimental Tests on the Gouy-Chapman Theory Using Phospholipid Bilayers.*
McLaughlin S., Langner M., McDaniel R. 265
L17 *Structural Rearrangements in Biomembrane Electric Fields.*
Neumann E., Tsuji K. 268
L20 *The Application of the Laser Induced Proton Pulse for Measuring Charge Translocation Across Biomembranes.*
Gutman M., Nachliel E. 271
1 *A Gradient of the Electrochemical Potential of the Proton, Driving Force and Modulator of Proton Transfer at the Biological Membrane/Water Interface.*
Naumann R. 274
2 *Photo Induced Transmembrane Electron Transfer in Model Systems for Photosynthesis.*
Seta P., Bienvenue E., Moore T. A., Moore A., Gust D. 275
3 *The Helmholtz Formula and the Membrane Potential.*
Schuhmann D. 278
4 *Phase Transitions Induced by an Electric Field in Black Lipid Membranes.*
Robello M., Gliozzi A. 281
5 *Some Problems in Electroarteriography.*
Anton C. G., Vazquez J. -L., Medrano J., Feliu J. M., Aldaz A. 283

6 *Lateral Proton Conduction Along Lipid Monolayers at the Air/Water Interface.*
Prats M., Tocanne J. F., Teissié J. 286
7 *The Electric State of Ion-Exchange Membrane Surfaces Emersed from Electrolytes.*
Cappadonia M., Dobihofer K. 289
8 *Some Electrochemical Behaviour of Bilayer Lipid Membranes Modified with Porphirynes.*
Krysiński P. 292
9 *Bioelectrochemical Activity on the Surface of Inert Metals Electrodes Implanted into the Brain Tissue.*
Shvets-Teneta-Guriy T. B., Dubinin A. G. 295
10 *Dynamics of Lateral Charge Transport in Amphiphilic Monolayer and Bilayer Assemblies.*
Widrig C. A., Majda M. 297
11 *Oscillations in Iron-Bromate Systems.*
D'Alba F., Di Lorenzo S., Lucarini C. 298
12 *Dynamic Changes of Bacteriorhodopsin Reconstituted in DMPC-Bilayers during Proton Pumping.*
Böttcher A., Denker H., Groll R., Meyer F., Holzwarth J. F. 300
13 *Charge Injection via Light-Induced Picosecond Charge Separation in an Artificial Molecular Membrane.*
Eichberger R., Willig F., Storck W., Durfee W. S. 303
14 *Microelectrophoretic Investigations of Lipophilic Anions Transport Kinetics Across the Membrane of Human Erythrocytes In-vitro.*
Kalinowski S., Krysiński P., Hinc S. 305
15 *Composite Films of Co Tetra/p-Tolyl/Porphyrin Immobilized in Zeolitic Ru-Oxide/Cyanoruthenate Microstructures as Cytochrome P_{450}-Like Models for Anodic Electrocatalysis.*
Kulesza P. J., Miodnicka T., Haber J. 308
16 *Liquid Junction Potentials Between pH Buffer Solutions.*
Rebelo M. J. F. 310
17 *The Effect of Transmembrane Electrical Fields on the Kinetics of Electron Transfer Reactions.*
Venturoli G., Scupoli M. T., Melandri B. A. 312

TOPIC 5 (Double Layer Structure: Theories and Modeling)

L22 *Effects of Ion Pair Correlations in Electric Double Layers.*
Marcelja S. 317
L23 *Molecular Dynamics Simulation of Water at Interface.*
Heinzinger K., Spohr E. 319
L24 *Water Adsorption. Quantum Chemical Approach.*
Kuznetsov An. M., Nazmutdinov R. R., Shapnik M. S. 322
L25 *Metal Electrons in the Double Layer Modeling.*
Kornyshev A. A. 325
L26 *Molecular Models of Water and Neutral Solutes Against a Charged Wall.*
Guidelli R., Aloisi G. 328
1 *Contribution of the Metal to the Silver-Water Interfacial Capacitance.*
Valette G. 329

2 *Adsorption from Dilute Solutions of Solvents with Asymmetric Molecules.*
Nikitas P., Pappa-Louisi A. 332
3 *Poisson-Boltzmann Equation for Highly Charged Polyelectrolyte Systems.*
Bordi F., Cametti C., Di Biasio A. 335
4 *A Variational Calculation of the Static Image Plane Position at a Charged Jellium Surface.*
Rosinberg M. L., Russier V. 338
5 *Improvements in the Two-Parallel-Condenser Model of the Double Layer in the Presence of Organic Adsorption.*
Schuhmann D. 341
6 *Determination of the Distance of Closest Approach for Solvent Molecules to a Metal Surface.*
Russier V., Amokrane S., Badiali J. P. 344
7 *Electrical Double Layer Interactions Between Ionized Inverted Micelles in Microemulsions.*
Bratko D., Luzar A., Chen S. H. 347
8 *Electrical Response of Fractal and Porous Electrodes.*
Chazalviel J. -N., Sapoval B., Peyrière J. 348
9 *What Can Be Inferred About the Structure of the Metal Solution Interface from the Electrochemical Experiment.*
Stafiej J., Borkowska Z. 351
10 *Electrochemical Work Function Approach to the Kinetics Along Simple Rate-Determining Steps: Example of Oxygen Reduction at Platinum Electrodes.*
Damjanovic A. 354
11 *Underpotential Deposition of Jellium on Jellium.*
Leiva E., Schmickler W. 357
12 *Pair Correlation Functions and the Structure of the Electric Double Layer.*
Plischke M., Henderson D. 359
13 *The Differences of Surface Potentials Between Water and Some Organic Solvents.*
Koczorowski Z., Zagórska I., Kalińska A. 362
14 *U. H. V. Simulation of the Double-layer Structure at the Au(100)-(5x20)/CH_3-CN and Ó-CN Interfaces.*
Solomun T., Christmann K., Baumgärtel H. 365
15 *Influence of Surface Crystallography on Molecular Adsorption at the Gold-Solution Interface.*
Richer J., Iannelli A., Stolberg L., Irish D. E., Lipkowski J. 369
16 *Adsorption of β-Cyclodextrin on the Mercury Electrode from Water and Water + Ethanol Mixture.*
Taraszewska J., Siedzik J. 370
17 *Local Interactions in the Double Layer and Orientation of Adsorbate Molecules.*
Daghetti A., Trasatti S., Rocchini G., Zagórska I., Koczorowski Z. 373
18 *Diffusion Kinetics at Fractal Interfaces.*
Nyikos L., Pajkossy T. 375
19 *Analysis of Concentration, Electric Potential and Charge Density Profiles in Interfacial Region of an Aqueous Electrolyte, Near a Charged Surface.*
Vaidhyanathan V. S. 377

20 *The Fractal Structure of Surface Inhomogeneity as the Origin of CPE-Behaviour in the Faradaic and Non-Faradaic Region.*
Mulder W. H., Sluyters-Rehbach M., Sluyters J. H. 360
21 *Adiabatic Charge Transfer Across the Charged Metal/Electrolyte Interface.*
Gorodyskii A. V., Karasevskii A. I., Matyushov D. V. 383
22 *Self-Organization Phenomenon in Multistage Metal Electroreduction Process. Theory and Experiment.*
Karnaukhov I. M., Karasevskii A. I., Ivanova M. D., Boldyrev V. I. 384
23 *Determination of the Composition of Electrochemically Active Ions on an Electrode.*
Kublanovskii V. S., Gorodyskii A. V. 386
24 *Theoretical Considerations on the Adsorption Isotherm for Ionic Systems at Electrode Interphases.*
Gonzalez R., Sanz F. 387
25 *The Proton Discharge Reaction on Gold and Silver.*
Frese U., Schmickler W. 390
26 *Adsorption Behaviour of 2-Propanol and of Hexafluoro-2-Propanol.*
Moncelli M. R., Guidelli R. 393
27 *Adsorption of Aromatic Aminoacids and Related Compounds in Relation to Calculated Molecular Structural Indexes.*
Fontanesi C., Barbieri A., Andreoli R., Benedetti L., Gavioli G. 394
28 *Polycrystalline Effects in the Double Layer Structure and Adsorption on Solid Electrodes.*
Palm U., Lust E., Lust K., Salve M. 397
29 *Study of Electrochemical Kinetics using the "FREECE" Technique.*
Stimming U., Sass J. K., Schott J. 401
30 *Surface Potential at Liquid-Liquid Interface Calculated on the Basis of Potential Volta Differences Method.*
Parfenyuk V. I., Krestov G. A. 402
31 *Adsorption of Organic Substances at the Mercury/Ethylene Glycol Interface and Air/Ethylenglycol Interface: Lauronitryle in 0.5M $NaClO_4$.*
Borghesani G., De Battisti A., Japaridze J. I., Trasatti S. 404
32 *Electrical Double Layer Between Mercury and Aliphatic Diols.*
Borghesani G., De Battisti A., Locatelli C., Japaridze J. I., Trasatti S. 407
33 *Electrochemical Intercalation into Graphite Seen as an Electrocapillary Process.*
Metrot A., Harrach A. 410
34 *Specific Adsorption of Halides on Ag(110): Surface Science Model Studies of the Inner Layer Structure.*
Staehler B., Sass J. K., Bange K., Schott J. 413

Author Index 415

1. Experimental Approaches

SURFACE ELECTRONIC STRUCTURE FROM ELLIPSOMETRY

F. CHAO, M. COSTA, J. LECOEUR, J.P. BELLIER, V. RUSSIER
L.E.I. du C.N.R.S., 1, Pl. A. Briand - 92195 Meudon Principal Cédex, France

There were several theoretical atteapts to calculate the electronic density profiles at a metal-electrolyte interface [see for example 1-4]. One of the purposes was to determine the metal surface dipole properties with a view to separate the metal contribution from the solution contribution in the capacitive response to the electric field. In the well known TRASATTI equation [5]

$$E = \frac{\vartheta_M}{e} + \delta\chi^M_{(S)} - g^S_{(M)}\,(\text{dipoles}) + g^M_S\,(\text{ions}) + \text{cte} \qquad (1)$$

the matter was to separate the variations against potential of $\delta\chi^M_{(S)}$, the metal dipole from $[-g^S_{(M)}\,(dipole) + g^M_S\,(ions)]$, the solution contribution.
To support the theory, there is a lot of excellent capacitance measurements, on well defined single cristal surfaces, with pure electrolytes, under electrochemical conditions avoiding any specific adsorption or contamination, or under well-controlled adsorption conditions (see for example [6]). The ionic structure of the metal surface was shown to have a strong effect on the capacity value but the theories are based on a jellium model for the metal which does not account for this parameter.
Optics can be another way of studying the microscopic properties of the electrochemical interface, if accurate measurements are carried out in the same severe conditions defined above. Our previous attempts in this field [7] were analysed with a model which neglect the non-local dielectric properties of the surface.
The purpose of this work is :
1/ to give some experimental results of ellipsometry on Au(111), Au(100), Au(110), Au(210), and Ag(111), Ag(100), for several wavelengths,in a potential range avoiding any specific adsorption ;
2/ to briefly summarize the existing theories concerning the interaction of light with a noble metal surface (generally in vacuum,see for example [8,9]) and to underline what modification has to be introduced to account for the metal-electrolyte interface ;
3/ to separate in the total optical response, what is due to the metal and what is due to the solution;
4/ to comment what we can expect from the extrapolation of the optical measurements to the zero frequency state defined in the equation (1).

Experiments

They are well described elsewhere [6,7]. The electrodes are disks cut from a single crystal rod (99,999%). The crystallographic orientation (better than ± 15') was determined by X-ray. The surface was mechanically mirror-like polished and then electrochemically polished. After rinsing with pure water and drying with pure nitrogen, the surface was tested in a UHV chamber by its Auger spectrum and LEED pattern. Then the sample was moved in a special transfer chamber from UHV to a glove box with a permanently purified N_2 atmosphere and set first in an electrochemical cell for the capacitance measurements, then in an electro-optical cell for ellipsometry. A special electrode support avoid any stress on the working surface. The dipping technique was used for the capacitance measurements. The electrolyte was 0.01 M NaF in "Suprapur" water (glassy carbon counter electrode and MSE reference electrode).
The electrooptical cell was designed to resist to oxygen diffusion from the ambient. The ellipsometer with Δ and Ψ modulation [7] is well adapted to detect very small variations of Δ and Ψ from a steady state situation (The reference state was E_{pzc} for each surface). On the fig.1 are represented the experimental results for the Au(111) and Au(110) samples.

The model : The interface is schematized on fig.2 where the ε_i are the optical permittivities and the distances are referred to the metal edge in the jellium model. Whatever the model [7-9] to describe the interface/light interaction, it can be demonstrated that the ellipsometric response can be written under the following form:

$$\frac{2\delta\Psi}{\sin 2\Psi_o} - j\delta\Delta = j\frac{K}{\lambda}\left[(\varepsilon_M-\varepsilon_o)x(\sigma,\omega)+(\varepsilon_C-\varepsilon_M)\frac{\sigma}{n_o}\right] + j\frac{K}{\lambda}\left[d_1(\sigma)(1+\varepsilon_o\varepsilon_M)+(d_2-d_1)\left(\varepsilon_I+\frac{\varepsilon_o\varepsilon_M}{\varepsilon_I}\right)+d_D\left(\varepsilon_D+\frac{\varepsilon_o\varepsilon_M}{\varepsilon_I}\right)\right] \quad (2)$$

$$\text{with } K = \frac{4\pi\varepsilon_o^{1/2}\cos\Psi_o\sin^2\Psi_o}{\left(\varepsilon_M-\varepsilon_o\right)\left(\varepsilon_o\sin^2\Psi_o-\varepsilon_M\cos^2\Psi_o\right)} \quad (3)$$

$$\varepsilon_M = \varepsilon_C - \frac{\omega_p}{\omega(\omega+i\sigma)} \quad (4)$$

$$x(\sigma,\omega) = \int_{-\infty}^{+\infty} z\rho(z)dz \quad (5)$$

In the right hand side of the equation (2) the first term represents the contribution of the metal surface perturbed by the solution, and the second term represents the contribution of the solution side. The difference between the models is in the expression of $x(\sigma,\omega)$. ε_C is the metal core permittivity, $\rho(z)$ the induced charge at the metal surface, $x(\sigma,\omega)$ the centre of mass of the charge, d_1 the closest distance of the water molecules of the inner layer to the jellium surface. The parameters which vary significantly with the charge in our experimental conditions are $x(\sigma,\omega)$ and $d_I(\sigma)$. (ε_M, ε_C, K are experimentally determined for each sample; $\varepsilon_o = 1.777$; $\varphi_0 = 70°$; 425 nm < λ < 750 nm). As an example, for Au-111:

$$[\delta\delta\Delta]_0^{\sigma} = 0.183[d_1(\sigma)-d_1(0)]+0.081[\mathrm{Re}x(\sigma,\omega)-\mathrm{Re}x(0,\omega)] \quad (6)$$

$$[\delta\delta\Psi]_0^{\sigma} = -0.081\,[\mathrm{Im}x(\sigma,\omega)-\mathrm{Im}x(0,\omega)] \quad (7)$$

Then Δ varies with both $d_1(\sigma)$ and $\mathrm{Re}x(\sigma,\omega)$ while Ψ only varies with $\mathrm{Im}x(\sigma,\omega)$. All the other terms are negligeable.
We shall compare the variations of Δ and Ψ with the results predicted by the theoretical models for d_1 and $x(\sigma,\omega)$.

As preliminary conclusions we can say that:
1) Theory does not account for the non variation of Δ and Ψ with a negative charge.
2) Δ and Ψ variations are the reverse of these predicted by metal surface/vacuum theories [8,9]. The reason is that the spilled-out electrons have not the same distribution profile that in metal/electrolyte interface.
3) A strong effect of the single crystal orientation is observed in the optical response, which is not accounted by any theory.

Bibliography

1. V.I. Feldman, A.A. Kornyshev, M.B. Partenskii, Solid State Com. 53, 1985,p.157.
2. V. Schmickler, J. Electroanal. Chem. 150, 1983, p.19.
3. J.P. Badiali, M.L. Rosinberg, F. Vericat, L. Blum, J. Electroanal. Chem. 158, 1983, p. 253.
4. V. Russier, Thèse, Paris 1986.
5. S. Trasatti in "Advances in Electrochemistry" 10 1977 p.213.
6. J.P. Bellier, J. Lecoeur, A. Rousseau, J. Electroanal. Chem. 200, 1985, 55.

7. F. Chao, M. Costa, R. Cherrak, J. Lecoeur, J.P. Bellier, J.Electroanal. Chem. 222, 1987, p.19.
8. P. Gies, R.R. Gerhardts, Europhysics Letters 1 (10), 1986, p. 515.
9. A.A. Kornyshev, LCI Internal Report 1986.

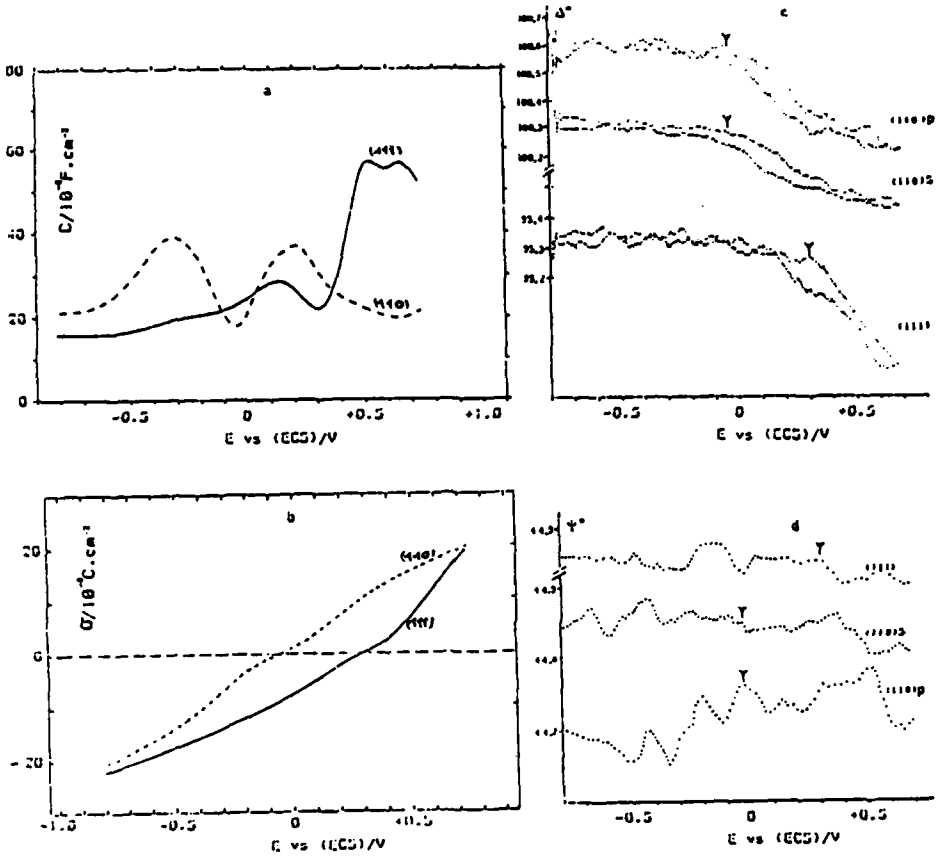


Fig.1-Au/NaF 0,01M;λ = 650nm; a:C(E); b:σ(E); c:δΔ(E); d:δΨ(E); $\Upsilon E_{p/c}$

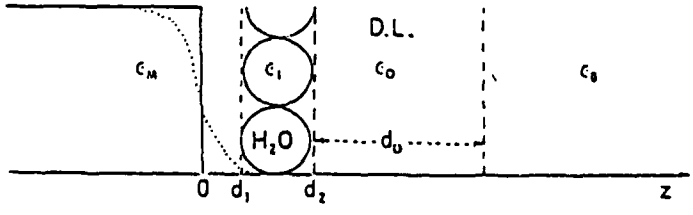


Fig.2-Scheme of the metal/electrolyte interface

SINGLE-CRYSTAL ELECTROCHEMISTRY: EXPERIMENTAL CHALLENGES TO CURRENT THEORY

Philip N. Ross
Materials and Chemical Sciences Div.
Lawrence Berkeley Laboratory
Berkeley, CA 94720

Within the last decade, a number of electrochemical research groups have developed a new type of research apparatus uniting UHV surface analytical systems with electroanalytical cells [1-4]. At the same time, Clavilier and co-workers[5] developed what we now call the "bead method" for preparing clean, well-ordered surfaces of the low-index planes of platinum and gold by laboratory techniques (not requiring UHV systems and the usual methods of ion-bombardment and thermal annealing). The development of the bead method has enabled a larger spectrum of electrochemists (not having or wanting UHV systems) to contribute in a meaningful way to single-crystal electrochemistry. Together, the combined progress produced by these developments in experimental techniques has made possible definitive determination of the relation between the atomic structure of the metal surface and the type of electrochemistry which takes place on these surfaces in different electrolytes. The growth in the number of such studies has been so rapid that it is not possible to review them all here without doing injustice to some important areas. Instead, I will emphasize new results from the study of electrode processes on the low-index surfaces of platinum that are extraordinary, and cannot be explained by current theory.

When a metal ion is either partially or completely discharged at the surface of a dissimilar metal, it is often the case that the free energy of formation of the adatom state is more negative than the free energy of formation of the bulk phase of that metal. In such cases, the discharge occurs at a potential "under" , i.e. cathodic to, the potential for the deposition of the bulk phase, giving rise to the terminology underpotential deposition (UPD). Electrochemists have long been interested in the details of this process both because of its possible technological importance in electrocatalysis and metal deposition but also because it is interesting surface chemistry in and of itself. The early studies of UPD employed polycrystalline metal electrodes from which one usually observed multiple states, leading to the reasonable supposition that the multiple states were related to structural heterogeneity in the surface. However, modern studies employing single-crystal electrodes have shown that the multiplicity of states on polycrystalline surfaces is not simply related to surface heterogeneity. In general, comparison of single-crystal with polycrystalline UPD reveals the following characteristics: i.) multiple states are observed even on structurally homogeneous surfaces; ii.) the isotherm for a given state often has a narrower than Langmuirian distributon function; iii.) assuming complete discharge of the ion, the coverage by adatoms at potentials approaching bulk deposition is often much less than a monolayer. Consider, in particular, the voltammetry results for copper UPD on the low index surfaces of platinum[6,7]. While current theory for UPD processes can explain peaks somewhat narrower than Langmuirian by use of

nearest-neighbor interaction, the occurence of peaks with a FWHM of only 15 mV and coverages less than half a monolayer cannot be accounted for with such models. In addition, the strong dependence of the FWHM on the size of atomically flat regions of the surface suggests long-range interactions among the forces acting parallel to the surface are surprisingly important to these electrode processes (and probably others as well).

Using the then controversial bead method for producing single-crystal surfaces, Clavilier[4] produced voltammetry curves for Pt(111) electrodes in dilute acid solutions that showed anomalous features never before reported for any platinum surface. These features, which occur in the scans in the potential range 600-850 mV (vs RHE), are anomalous in the sense that they had never before been observed, and they occur in a potential region which from thermodynamic considerations indicates the features are unlikely to be either adsorbed hydrogen or adsorbed oxygen. Since the reports by Clavilier and co-workers, there has been a period of intense activity at several laboratories, especially those with the aforementioned UHV surface analytical systems, to understand these anomalous features. A summary of the characteristics of the anomalous features is given in a recent paper[5]. The anomalous features are observed on well-ordered surfaces in a variety of electrolytes over a wide range of pH (0-11), but the potentials at which they appear and the detailed shapes of voltammetry change considerably. It has been reasonably well established that adventitious impurities are not responsible for the features, i.e. the only species participating are protons, water and anions of the solute . The use of (111) single crystals with varying degrees of ordering in the surface, as determined independently with LEED, has shown that the anomalous voltammetry is unique to a (111) surface consituted from structurally perfect domains containing at least 50 Pt atoms (i.e. minimum characteristic diameter of 5-8 Pt atoms). There is a critical condition in the relation between the range of perfection in the surface and the occurance in the anomalous features in the voltammetry, i.e. with the introduction of a critical number of defects the features disappear entirely. The critical size of atomically flat regions exceeds the characteristic dimension of any single species potentially involved in the process(es). This has suggested to us[6] that hydrogen-bonded ice-like networks form on the regions of critical flatness, and thus serve to transmit structural phase information parallel to the surface over greater-than-molecule distances. In a recent review paper on this topic[6], I have suggested some specific structural models for the double-layer at Pt(111), and ascribe all aspects of the anomalous features to capacitive processes involving ordered phases in the double-layer. These proposed structural models are, however, quantitively different from the classical models, and may be unacceptable in terms of current theory.

The metal UPD processes and the anomalous processes on Pt(111) share a common feature of extreme sensitivity to long-range order in the surface. Current theory for the structure of the double-layer at metals, and on electrosorption phenomena at metals, is derived directly from classical models developed from studies with mercury. By its very nature as a liquid metal, there is no long-range order in the mercury

surface, and models need only be concerned with structure in the direction normal to the surface. It is not surprising, then, that these models could be used successfully with polycrystalline metals, whose surface structure could in a sense be said to have "liquid-like" randomness in the coordination parallel to the surface. However, the modern work with single crystals has shown the need to include lateral bonding (ordering) forces parallel to the surface in addition the binding forces perpendicular to the surface. Some theorists have already anticipated the importance of lateral interactions in the double-layer at metals, in particular, Guidelli[10]. Guidelli's treatment anticipates the formation of superlattice structures and the existance phenomena (superlattice phase transitions) that are similar to those I suggested for the anomalous processes on Pt(111). Although fully three-dimensional theories of the double-layer will obviously be computationally formidable, the recent results from single-crystals indicate that this additional degree of sophistication in the models is required for an accurate description of the metal-solution interface.

References

1.) A. Hubbard, Acc. Chem. Res. 13(1980)177

2.) E. Yeager, A. Hoss, B. Cahan, and D. Scherson, J. Vac. Sci. Technol. 20(1982)128

3.) P. Ross and F. Wagner, in Advances in Electrochemistry and Electrochemical Engineering, H. Gerischer and C. Tobias eds., Wiley, New York (1984), pp 64ff

4.) D. Aberdam, R. Durand, R. Faure, and F. El-Omar, Surf. Sci. 17(1986)303

5.) J. Clavilier, J. Electroanal. Chem. 107(1980)205

6.) P. Ross and P. Andricacos, J. Electroanal. Chem. 167(1984)301

7.) D. Kolb, K. Al Jaaf-Golze and M. Zei, "Untersuchungen zur Struktur von Metalladsorbaten" in Grundlagen von Elektrodenreaktionen, GdCH-Monographie, 1985, pp 99ff

8.) F. Wagner and P. Ross, J. Electroanal. Chem. in press

9.) P. Ross, "Long-Range Structural Effects in the Anomalous Voltammetry of Pt(111)", in Molecular Phenomena at Electrode Surfaces, M. Soriaga ed., ACS Symposium Series, The American Chemical Society, Washington DC, in press

10.) R. Guidelli, J. Electroanal. Chem. 123(1981)59; 197(1986)77

NONLINEAR OPTICAL PROBES OF ELECTROCHEMICAL INTERFACES

G. L. Richmond
Chemical Physics Institute, University of Oregon
Eugene, OR 97403

Over the past five years, research in this laboratory has focussed on the use of optical second harmonic generation (SHG) in probing interactions at the solid/liquid interface. The SH studies have provided valuable information about the sensitivity of SHG to such phenomena as molecular and ionic adsorption at smooth electrode surfaces, oxidative film formation, underpotential deposition processes, oxide formation and the dynamics of adsorption and thin film growth processes.[1] More recently, our studies have focussed on the use of SHG to probe electrode surface structure and symmetry by rotational anisotropy in the SH response from crystalline electrode surfaces.[2] This talk will focus on our more recent results in this area for single crystals of Ag, Cu, Au and Si studied in aqueous solutions. Both static and time-resolved measurements will be discussed as they relate to potential induced effects including thin film growth processes.

It is generally recognized that electrode surface morphology can significantly influence the chemistry that takes place at the surface. Unfortunately, direct correlations between surface structure and chemical mechanisms are difficult to make as a consequence of the lack of in situ electrode surface characterization methods. For this reason, the rotationally anisotropic nonlinear response from immersed electrode surface has been the focus of our investigations. The goals of the studies reported here have been to determine the microscopic origins of the observed anisotropy in the surface nonlinearity, and to apply the technique to the study of the surface structure under various conditions. The results on native electrode surfaces will be presented first and will be followed by a summary of the investigations on surfaces modified by electrodeposited metal overlayers.

The observation of rotational anisotropy in the SH intensity from the solid/liquid interface was first reported by this laboratory for single crystal silver electrodes in simple aqueous electrolytes. Figure 1(a) and (b) show the variation in the p- and s-polarized SH intensity as a Ag(111) electrode in Na_2SO_4 is rotated about its surface normal. Analysis was made by p-polarized 1.06 μm radiation impinging on the surface at 10^o relative to the surface normal. The patterns shown in figure 1 are consistent with the 3m symmetry of a Ag(111) surface. Furthermore the results fit the theoretical description for the p-polarized and s-polarized output given respectively as:[3]

$$I^{(2\omega)}(\parallel,\parallel) \propto a_{\parallel,\parallel} + c^{(3)}_{\parallel,\parallel}\cos(3\phi) \qquad (1)$$

and

$$I^{(2\omega)}(\parallel,\perp) \propto b^{(3)}_{\parallel,\perp}\sin(3\phi) \qquad (2)$$

In this expression ($\parallel,\perp$) refers to (fundamental, second harmonic) beam polarizations for s($\perp$) and p($\parallel$) polarized light relative to the incident plane. ϕ is the angle through which the crystal surface is rotated. The coefficients $a_{\parallel,\parallel}$; $c^{(3)}_{\parallel,\parallel}$; and $b^{(3)}_{\parallel,\perp}$ contain the bulk isotropic and anisotropic material parameters as well as the surface isotropic and anisotropic tensor elements.

The observed anisotropy clearly indicates that the surface has a high degree of crystallinity in solution. The question of whether this is truly a surface effect rather than a bulk one has been investigated in several studies and has been confirmed in particular for the p-polarized output case. The significance of this observation to our understanding of the microscopic origin of the SH response is that silver, which is considered to be a free-electron metal, would be expected to give an isotropic SH

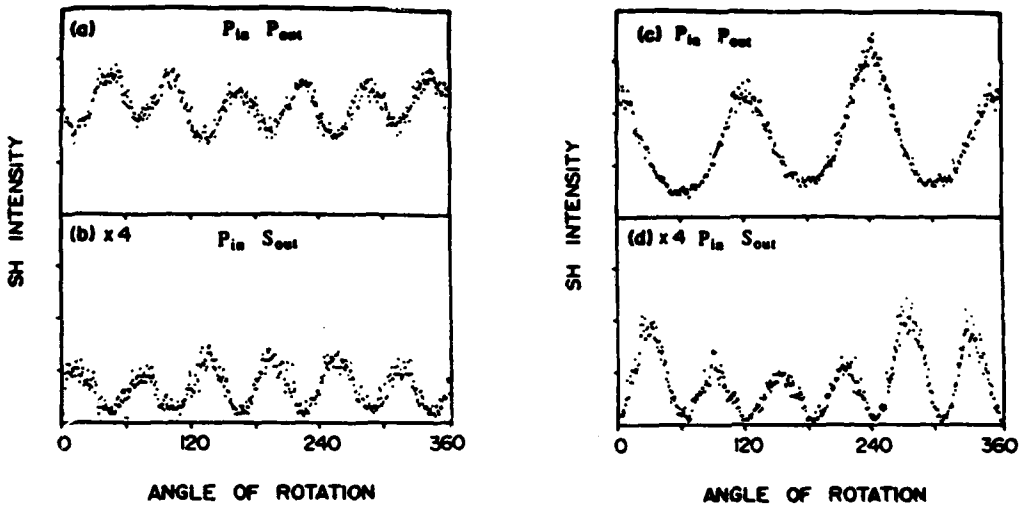


Figure 1. SH intensity as a function of angle of rotation for (a) Ag(111) electrode immersed in 0.1M $NaClO_4$ at -0.19V vs Ag/AgCl; p-polarized SH light; (b) Same as (a) with s-polarized SH light. (c) Cu(111) in 0.1M Na_2SO_4 at -0.3V; p-polarized SH light; (d) same as (c) with s-polarized SH light.

response with respect to the azimuthal rotation. Although the contribution of interband transitions to the nonlinear polarizability has been recognized since the early work of Bloembergen, the fundamental and second harmonic wavelengths (1.17 eV and 2.34 eV) used in the experiments cited above are well below the energy of silver interband transitions (3.8 eV). The origin of this anisotropy will be discussed in more detail in the presentation.

It is interesting to compare the results for Ag(111) to those of Cu(111) and Au(111) in solution. The results for the later in 0.25M Na_2SO_4 are shown in Figure 1(c) and 1(d). The observed patterns are identical to those obtained for Cu(111) in UHV but are quite different than those for silver for the p-polarized case. Gold gives a similar response to copper with three maxima and minima. The conclusion drawn from the studies is that this observed difference between Ag, and, Cu and Au is a consequence of the resonance in the latter two cases between 2ω and the interband transitions. This would lead to a larger contribution from the $c^{(3)}_{\perp,\parallel}$ term in equation 1 and hence the observed pattern.

We have extended these studies to the examination of the structure of thin films deposited on the Ag, Cu and Au surfaces by under potential deposition. An example of these results are shown in Figure 2 and 3 for Tl deposited on Ag(111). Coulometric measurements suggest that thallium deposits on the (111) face of silver in three steps to form a monolayer. A second full monolayer subsequently deposits prior to bulk deposition. Shown if figure 2 is the cyclic voltammetry for this system with arrows indication the points where the SH measurements were made. Figure 3 shows the p-polarized SH intensity as a function of angle of rotation for fractional (a,b), full (c), and two (d) monolayer coverages. The solid lines are theoretical curves generated by fitting the data to equation (1). The positions of the maxima and minima in both the p-polarized and s-polarized (not shown) anisotropy do not change as a function of coverage. This indicates that the overlayer structure has the same symmetry elements as the substrate surface, since the SH signal is thought to arise from the substrate/overlayer interface. For even a fractional monolayer coverage of Tl, the pattern for the p-polarized SH intensity as a function of angle of rotation changes dramatically. How the

interfacial electronic and structural properties are related to changes in the magnitude of each of the $a_{\perp,\parallel}$ and $c^{(3)}_{\perp,\parallel}$ coefficients of the tensor elements will be discussed in the presentation. As an example, the large change in $c^{(3)}_{\perp,\parallel}$ which is observed at 2 monolayers confirms the presence of epitaxial growth. The results will be compared with deposition on the other metal surfaces.

In the final portion of the talk, results for time-resolved measurements of thin film growth will be given. In these experiments the transient SH response from a mode-locked picosecond laser is used to monitor the UPD growth process after a fast potential step to a bias where selective degrees of reduction occur. The results indicate behavior at the surface which is not possible to obtain from simple current transient analysis.

1. G.L. Richmond, H. M. Rojhantalab, J. M. Robinson, and V. L. Shannon, J. Opt. Soc. Am. B 4, 228 (1987).
2. V. L. Shannon, D. A. Koos, and G. L. Richmond, J. Chem. Phys., 87, 1440 (1987).
3. J. E. Sipe, D. J. Moss, and H. M. Van Driel, Phys Rev. B, 35, 1129 (1987).

Support from NSF CHE 8513008 is gratefully acknowledged.

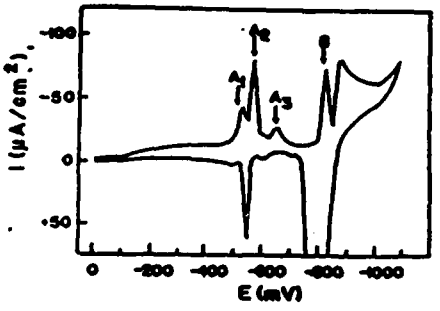


Figure 2. CV for thallium deposition on a Ag(111) electrode from 1.0 mM Tl_2SO_4 / 0.25 M Na_2SO_4 / pH = 3.0. 10 mV/s.

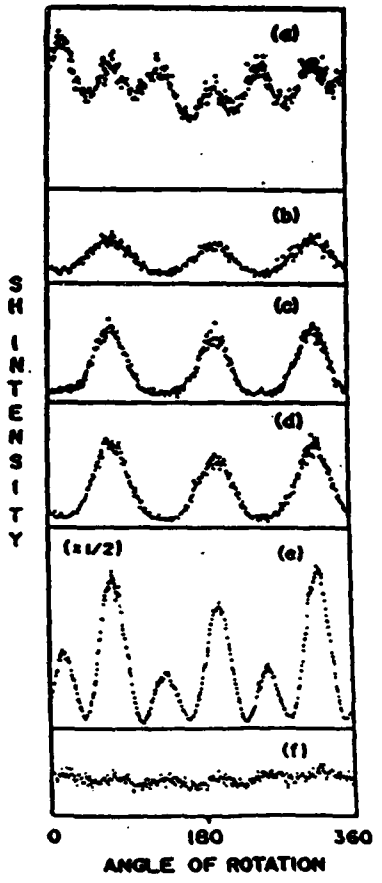


Figure 3. Dependence on Tl coverage of the p-polarized SH intensity as a function of angle of rotation for the solution in figure 2 at: (a) 0.00V (b) -0.52V (c) -0.57V (d) -0.67V (e) -0.85V (f)-0.90V.

IN SITU SURFACE EXTENDED X-RAY ABSORPTION FINE STRUCTURE SPECTROSCOPY AND X-RAY DIFFRACTION OF MONOLAYERS ADSORBED AT ELECTROCHEMICAL INTERFACES

Owen R. Melroy
IBM Almaden Research Center
650 Harry Road, San Jose, CA 95120

The availability of synchrotron radiation with its high flux (5 orders of magnitude more intense than conventional x-ray sources), and high degree of collimation has allowed x-ray spectroscopies to be used to probe surface structure. These spectroscopies, most commonly used in vacuum, are also ideally suited for probing the structure of electrochemical interfaces. X-rays with energies above 5 keV have significant penetration depth in liquids and because of their wavelength provide direct, crystallographic information. This talk will focus on two spectroscopies, surface extended x-ray absorption fine structure (SEXAFS) and grazing incidence x-ray scattering, which we have used to elucidate the structure of mono-atomic adlayers at electrochemical interfaces. All measurements were made in situ with the electrode under potential control.

The Surface Extended X-Ray Absorption Fine Structure (SEXAFS) spectrum of an electrochemically deposited ad-layer of copper on a gold (111) electrode immersed in solution and under potential control was obtained by employing fluorescence detection and grazing incidence geometry. With the x-rays polarized parallel to the plane of the gold surface, two peaks were observed in the radial distribution function, indicating two different near neighbors for copper. The near neighbors were determined to be gold at 2.58 ± 0.03Å and copper at 2.92 ± 0.03Å. The copper-copper distance is identical to the gold-gold lattice spacing showing that at full coverage, the copper ad-layer forms a 1 x 1 commensurate layer on the gold (111) substrate. With the x-rays polarized perpendicular to the surface, no backscattering from copper atoms was observed which indicates that all of the copper atoms lie in the plane of the surface. Scattering was observed for gold and oxygen. The EXAFS experiment can not distinguish whether the oxygen scattering is from adsorbed water or the sulfate electrolyte. The intensity of the gold-copper scattering relative to the copper-copper in the two orientations suggests the copper atoms sit in 3 fold hollow sites.

X-ray scattering was used to study the structure of electrochemically deposited monolayers of lead on silver (111) and gold (111) electrodes. When deposited on silver, the lead orders in a hexagonal closed packed (*hcp*) geometry with the lead lattice compressed 1.2% relative to bulk lead. A rotational epitaxy angle of 4.4° was observed. From the width of the first order diffraction peak, the domain size was determined to be > 300 Å indicating that even immersed in solution, the lead forms a well ordered two dimensional solid. Between monolayer formation and bulk deposition, the near neighbor distance of the lead monolayer decreases linearly with applied potential. Since the lead monolayer is in equilibrium with the lead in solution, the isothermal compressibility of the monolayer can be calculated and is 0.98 $Å^2$/eV. This is in good agreement with that of a two dimensional, free electron gas. On a gold (111) substrate, the lead monolayer was again found to order into a *hcp* geometry, incommensurate with the gold. The lead layer was compressed 0.7% relative to bulk lead, with a domain size > 200 Å.

ELECTRODE IMPEDANCE OF COBALT IN CONCENTRATED NITRIC ACID

E. Stupnisek-Lisac* and H. Takenouti**

* Institut of Physical Chemistry, Technological Dept., University of Zagreb, ZAGREB, YOUGOSLAVIA

** LP 15 du CNRS "Physique des Liquides et Electrochimie", Université P. et M. Curie, tour 22, 4 place Jussieu, 75252 PARIS Cédex 05, FRANCE.

INTRODUCTION

In our previous work (1-2), it was shown that the cobalt does not passivate spontaneously even in a fumic nitric acid though its anodic behaviour is strongly dependent on acid concentrations. This dependence is mainly due to the hydration number of cobalt, nitrate salt covering the electrode surface : hexa-hydrate for low (C < 11 M), tetra-hydrate for medium (12 < C < 19 M) and bi-hydrate salt for high acid concentrations. Corresponding to this salt layer, the open-circuit corrosion potential measured with respect to acid concentration exhibits three distinct domains. At the threshold concentration a steep potential change or a large potential oscillation is observed.

The polarization curve showed in general monotoneous curve. The anodic current is limited by the convective diffusion through the salt layer. However, at the vicinity of these two critical concentrations an anodic current maximum and an cathodic current minimum are to be seen. The present work aimed at to understand this peculiar feature by means of the electrode impedance techniques in 11M-HNO_3 solution.

EXPERIMENTALS

The solution was prepared of an analytical grade concentrated acid and ion-exchanged water. The electrode was Co cylinder rod (Johnson-Matthey), the diameter of which was 5 mm. Only the cross section of the rod was allowed to come in contact with electrolyte hence forming an disk electrode. The remaining surface was covered by polyethylene thermofitting sheath. The electrode was stationnary and its surface faced upwards. The regulating device was a home made potentiostat coupled with a Transfer Function Analyser (Solartron 1250). Between the working electrode and the earth, an electronic circuit giving a negative resistance was inserted (3). The potential was measured between the reference electrode (saturated calomel) and the working electrode. Potentials were referred to the normal hydrogen scale (nhe) by adding .25 V to the measured value. No correction for ohmic drop was made.

RESULTS AND DISCUSSION

The figure 1 depicts the polarisation curve obtained under potentiostatic regulation. The open-circuit potential, marked A, corresponds to that measured in a solution of low concentration. At 0.42 V a steep current decrease reaching to the cathodic value was observed. At 0.53 V, the overall current is nul, and this potential corresponds to the open-circuit potential observed for a solution of medium concentration. At a higher potential range, a current plateau of 40 mA/cm^2 was observed. This limiting current is eight times smaller than the maximum current observed at 0.42 V which indicates a deep change in the convective diffusion process. By decreasing potential a steep current increase from cathodic to anodic value was observed. Hence

the polarisation curve reveals a large hysteresis cycle under a potentiostatic regulation.

If a negative resistance circuit was inserted, the broken-line part of the polarisation curve was to be yielded. This curve indicates that the transition between one branch to another can take place progressively and reversibly. Even if the ohmic drop was corrected by using the value of electrolyte resistance from the impedance measurements, this overhanging part remained positive near zero overall current. That is to say, the multiplicity of the steady-states is not solely due to the solution resistance. The electrode process itself might imply an autocatalytic reaction.

The electrode impedance was measured at the steady-state polarisation marked by A to D on the figure 1. The diagram A shows an usual feature of corroding electrode. From the high frequency capacitive loop, one evaluates a parallel capacitance close to 150 $\mu F/cm^2$ and a resistance to 1 $ohm.cm^2$. The capacitance is reasonably attributed to the double layer and the resistance to the charge transfer one. The small resistance value indicates that a fast corrosion process is taking place at the electrode. The diagrams B and C are similar in feature. The capacitive loop observed in a high frequency range ($f > 1$ kHz) can be related to the double layer capacitance and the charge transfer resistance as in the case of the corroding electrode. Another capacitive loop centred around 100 Hz may be related to the surface relaxation of a reaction intermediate. For lower frequencies, the diagram bends to left corresponding to the passivation process. For lower frequencies, the impedance comes back to a positive value through a large inductive loop. A similar diagram observed during the transpassive dissolution of nickel (4) was explained by an autocatalytic process.

If the electrolyte resistance, high frequency limit of the impedance, at different polarisation points are compared, one can see that this resistance is particularly small in the diagram C. That is, the electrolyte at the very vicinity of the electrode is substentially different from other cases.

In a previous work (1-2) it was concluded that the cathodic process observed in the potential range of 0.4 to 0.53 V is due to the reduction reaction of nitrous ion. The change form one polarisation characteristics to another is attributed in the change of the hydration number of salt layer. A small electrolyte resistance observed on diagram C is in agreement with the release of free-water due to the change in the hydration number.

CONCLUSION

The polarisation curve obtained with a negative resistance circuit exhibited a progressive and reversible change of two distinct I-E characteristics. This change is due to the hydration number of salt layer formed upon the electrode surface : Its changes from six to four. The autocatalytic nature of electrode reaction, likely the reduction reaction of nitrous ion, is verified as well by the polarisation curve experiments and by the impedance measurements.

REFERENCES

(1) E. STUPNISEK-LISAC, Surface and Coating Technology, 30 (1987) 355.
(2) E. STUPNISEK-LISAC and H. TAKENOUTI, 39th Meeting of I.S.E., Extended Abstracts, Vilnius 1986.
(3) I. EPELBOIN, C. GABRIELLI, M. KEDDAM, J.C. LESTRADE and H. TAKENOUTI, J. Electrochem. Soc., 119 (1972) 1632.
(4) M. KEDDAM, H. TAKENOUTI and N. YU, J. Electrochem. Soc., 132 (1985)2561.

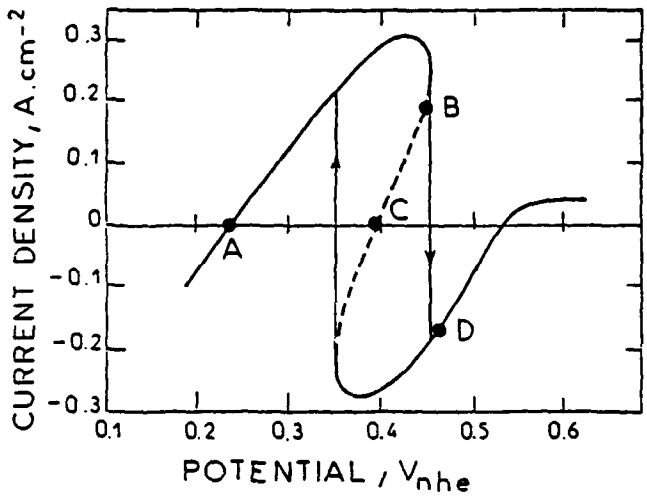


Figure 1 : Polarisation curve. Co in 11M-HNO_3. Broken line, that obtained with a negative resistance.

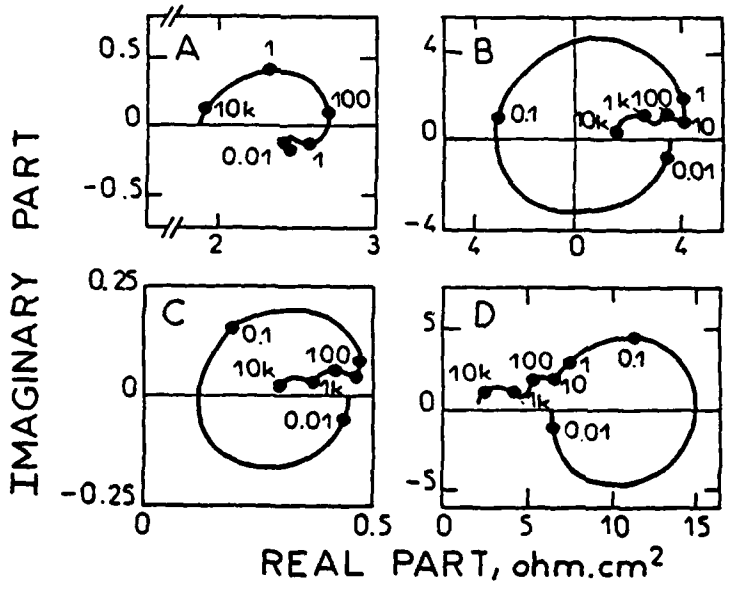


Figure 2 : Impedance diagram. A to D corresponds the point marked on Fig. 1 by the same letter.

R. DURAND, R FAURE
CREM-GP associé au CNRS, (UA 1212), INP GRENOBLE
BP 75, F 38402 Saint Martin d'Hères

D. ABERDAM, S. TRAORE
LSP associé au CNRS (UA 8) Université Joseph Fourier (USTMG)
BP 87, F 38402 Saint Martin d'hères

LEED AES STUDY OF ELECTRODES FOLLOWING ELECTROCHEMISTRY.

INTRODUCTION

As long as Grazing X-Ray Diffraction and Tunneling Microscopy will not reach a sufficient degree of development, the study of electrode structure and composition,- before and following an electrochemical experiment-, will be dependent on ex-situ ultra-high-vacuum techniques, such that Low Energy Electron Diffraction (LEED), Auger Electron Spectroscopy (AES), X-Ray Photoelectron Spectroscopy (XPS). Amongst people having worked on electrode transfer from a cell to an UHV chamber, (1-3), Hansen and Kolb have introduced the concept of emersed electrode. They have shown that, under some conditions, a gold electrode keeps it double layer unperturbed after transfer into UHV : electrode potential, electric charge,and coverages remain constant.

We present here a work on underpotential deposition on Platinum single-crystal electrodes. After a brief description of the experimental set-up and procedures, we focus on the results and their thermodynamic interpretation.

EXPERIMENTAL SET-UP

The apparatus is a combination of a UHV chamber, equipped with LEED, AES, with a reaction chamber in which an electrochemical cell is introduced to perform voltammetric experiments sheltered from atmospheric air. The transfer of the electrode from one part to the other is performed under UHV, using a magnetically actuated transfer rod. The sample holder must fit requirements from UHV techniques (ion bombarding, sample annealing, temperature measurement) and from electrochemical experiments (immersion in acid solution). The electrochemical cell is suited for the dipping geometry, the active surface being the diametral plane of the hemispherical sample. The cell is put at the top of a glass piston which allows us to introduce the cell in the reaction chamber.

PROCEDURES OF EMERSION AND TRANSFER BACK TO THE UHV.

The aim is to keep the structure and composition of the electrode surface as they were just before emersion, and to eliminate the electrolyte attached to the surface after emersion, in order to avoid deposition of species during evaporation in vacuum. This is easier with the use of a supporting electrolyte (0.1 M to 1 M acid solution) and of a moderate metallic cation concentration (10^{-3} M). This corresponds to well defined thermodynamical conditions for the electrosorption process. In contrast with the behaviour of gold electrodes which are hydrophobe, the electrolyte stays on platinum after emersion, and we describe four steps :

1. Emersion (breaking the liquid column).

At this stage no transient electric current is mesurable and it is very likely that the thermodynamic charge of the electode is conserved. A relatively big droplet of electrolyte remains on the electrode surface.

2. Phenomena at the droplet-electrode interface.

Between *emersion* -1- and elimination of the droplet -3-,a few seconds evolve, necessary to move the electrode. During this time, what happens with electrode potential and surface coverages ? One may write the following equations :

$$dQ = C\,dE - F \sum n_j\, d\Gamma_j \qquad [1]$$
$$d\mu_j = F\, n_j\, dE + \sum (\delta\mu_j/\delta\Gamma_i)_E\, d\Gamma_i \qquad [2,3,...]$$

Now, $dQ = 0$ (isolated electrode) and all $d\mu_i = 0$ (the amount of species i is much greater in the droplet than on the surface). As a consequence, $dE = 0$ and $d\Gamma_i = 0$. This reasoning is not allowed in the cases where :

* a faradaic reaction can take place (additional term in equation [1]),
* the electrosorption of one of the species has not reached equilibrium (equation [2] incorrect).

3. Elimination of the droplet.

We eliminate the droplet by blowing it with the help of a strong flow of very pure argon gas, normal to the surface of the electrode. The thickness of the residual electrolyte is estimated using AES of anion elements. It is found less than 1 nm. Therefore, redeposition of cations is negligible. No contamination by the argon gas has been detected.

4. Pumping down and Surface analysis.

A turbomolecular pump is used to pump-down the system instead of a ion pump to avoid gas reactions at the titanium metal. LEED immediately shows whether some change occurred relative to surface structure, such that presence of defects, or of a superstructure...

AES allows us to check the amount of metal atoms adsorbed on the surface. AES also allows us to correlate the amount of anion elements on the surface to what is expected from the double layer charge at emersion potential. In addition, some chemistry can take place at the surface, particularly with sulfate ions. Sulfur is initially detected in an oxidised form, together with a large amount of oxygen. After some hours, the oxygen desorbs, and elemental sulfur is detected.

EXAMPLES.

1. Experiments in perchloric solutions.

We find that the ratio of superficial concentrations of Chlorine and Oxygen, measured by AES, corresponds roughly to the composition of ClO_4^- anions. The amount of perchlorate ions depends little on the concentration of the perchloric solution, but strongly on the emersion potential. It is close to what is expected in the outer Helmholtz plane and the

upper limit of the thickness of the liquid film left on the surface after blowing the droplet is therefore of the order of 1 nm.

2. Pt(111) electrode.

On this surface, a few cycles of electroadsorption desorption of oxygen change dramatically the voltammograms relative to the electrosorption of hydrogen or metals. We have shown by LEED (4) that this change is related with the formation of monoatomic steps resulting from the coalescence of point defects created by a place exchange mechanism between platinum and oxygen atoms.

3. UPD of Copper on Pt(110).

The electrosorption of Copper takes place in a range of potential where no or little co-electrosorption of other species occurs. In this simple case, quantitative AES using calibration with pure platinum and copper samples correlates well with electric charge measurements, assuming a electrosorption valency n_i=2 for copper (5).

4. UPD of Lead on Pt(100).

We observe, in voltammetry, a sharp UPD peak. Electric charge measurements indicate a coverage of 1 Pb atom for 2 Pt atoms.

In our early experiments, we found no lead by AES. Due to a small amount of molecular oxygen dissolved into the solution, which allowed the faradaic reaction : $1/2\ O_2+2H^++2e^- \rightarrow H_2O$ adsorbed. Pb atoms dissolved back in the droplet after emersion. After vacuum degasing the solutions, AES and electric charge measurements agree very well. The LEED pattern then shows a c(2x2) superstructure of the lead overlayer (6).

5. Surface alloying of Silver on Pt(100).

Two UPD peaks of silver are observed on Pt(100) corresponding to the adsorption of a first and second layer of silver. Cycles of adsorption desorption of silver including the UPD peak relative to the second layer deposition give rise to superficial alloying. This is demonstrated by AES, using excitation at variable angle of incidence. But the phenomenon is complicated by an overlap between the adsorption of silver with the ill reversible adsorption reaction : $H_2O \rightarrow OH_{ads}+H^++e^-$. So Changes of Γ_{Ag} and Γ_{OH} are possible in the droplet after emersion at constant electric charge. In fact, AES frequently shows silver in excess with respect to the amount expected from electric charge measurements.

REFERENCES.

1. A.T HUBBARD, R.M.ISHIKAWA, J.KATEKARU, **J. Electroanal. Chem. 86** (1978) 271.
2. F.T WAGNER, P.N.ROSS, **J. Electroanal. Chem. 150** (1983) 141
3. D.M.KOLB, **Z. Phys. Chem. N.F. 154**,(1986),179.
4. D.ABERDAM, R.DURAND, R.FAURE, F.El-OMAR, **Surface Sci. 162** (1985) 782.
5. D.ABERDAM, R.DURAND, R.FAURE, F.El-OMAR, **Surface Sci. 171** (1986) 303.
6. D.ABERDAM, S.TRAORE, R.DURAND, R.FAURE, **Surface Sci. 180** (1987) 319.

ADSORPTION OF ORGANIC MOLECULES ONTO A METAL SURFACE, STUDIED USING SURFACE PLASMON-POLARITONS

S COWEN AND J R SAMBLES

Thin Film and Interface Group
Department of Physics
University of Exeter
Stocker Road
Exeter EX4 4QL
United Kingdom

ABSTRACT

Optical excitation of surface plasmon-polaritons (SPP)at the interface between a metal film and an electrolyte using the attenuated total reflection technique is employed to study the change in the interface with both potential and adsorbates.

The SPP is highly localised in a direction normal to the interface. Thus with carefully chosen metal film thickness giving a deep reflective minimum when the incident radiation is at the correct angle to couple to the SPP momentum, small changes in the structure of the interfaces are detected as significant changes in the reflectance against angle data.

The changes, which are in the position of the SPP minimum, its depth and its width, are functions of the applied potential, the specific adsorbates etc. In the current experiment, the system gold/perchloric acid plus 4,4 - bipyridyl ethene (BPE) is examined.

Potentials are chosen to vary from the region of the potential of zero charge up to values close to where oxidation of the gold normally occurs.

INVESTIGATION OF CO_2 REDUCTION IN APROTIC MEDIA BY IN SITU FTIR SPECTROSCOPY

Johann Desilvestro* and Stanley Pons+

*Paul Scherrer Institut
CH-5303 Würenlingen
SWITZERLAND
and
+Department of Chemistry
University of Utah
Salt Lake City, Utah 84112
U.S.A.

Introduction: The electrochemical reduction of CO_2 has attracted considerable interest over more than 100 years (1). Reaction products, such as formic acid, methanol, CH_4, CO and carbonate, oxalate, glycolate, etc., depend critically on solvent, electrode material, and current density. Little is known about the CO_2 reduction mechanism. Based on cyclic voltammetry (2) and in situ UV/VIS (3) and FTIR (4) reflectance spectroscopy, CO_2^- has been suggested as an intermediate.

In situ IR spectroelectrochemistry appears to be a very powerful tool for the elucidation of electrochemical reaction mechanisms since it is a highly specific molecular probe, applicable to a practically unlimited number of electrode/electrolyte combinations (5). Thus we applied FTIR spectroscopy to the electrochemical CO_2 reduction in aprotic solvents on various electrode materials. In this work, we will present and discuss FTIR reflectance spectra in the range of 4000-500 cm^{-1} as a function of electrode (Pt) potential during CO_2 reduction in actonitrile.

Experimental: All measurements were performed in 0.1 M tetra-n-butylammonium tetrafluoroborate (TBAF)/acetonitrile as electrolyte. Electrode potentials were measured and are reported vs. Ag/0.01 M $AgNO_3$ in acetonitrile/0.1 M TBAF. Tetrabutylammonium oxalate (TBAOX) was prepared by neutralizing a concentrated aqueous solution of oxalic acid with aqueous tetrabutylammonium hydroxide. After evaporation of H_2O and drying under vacuum, a white and very hygroscopic solid was obtained. TBAOX/acetonitrile solutions were slightly turbid.

Cells for IR spectroelectrochemical experiments were equipped with a flat ZnSe window. The 1 cm diameter Pt disk was positioned close to the cell window. Infrared reflectance spectra were obtained with a Bruker FT-98 vacuum spectrometer modified for surface studies. The average of up to 500 spectra at a given potential was ratioed with the same number of spectra at the reference potential.

Results and Discussion: At -1.5 V, significant cathodic currents started to flow in CO_2 saturated CH_3CN/TBAF solutions. Only a small and very broad oxidation wave at $E \approx 0.2$ V was observed when the potential was cycled between +0.75 and -2.5 V. In situ FTIR spectra showed the appearance of a species with an absorption band at 1690 cm^{-1} at potentials as positive as -1.0 V. At more negative potentials (cf. Figs. 1a-d), CO_2 is reduced as evidenced by the positive (upwards) going CO_2 bands at 2347/2336 cm^{-1} (asymmetric stretching mode, line narrowing) and 659 cm^{-1} (degenerate bending mode). At the same time, IR absorption bands at 1687, 1647, 1387-1304, 978, and 840 cm^{-1} become more intense. The positive going peaks at 1096-1029 cm^{-1} are due to solvated BF_4^- (loss of T_d symmetry) disappearing from the thin electrolyte layer between Pt and cell window in order to keep electroneutrality. The much weaker spectral features at 1479 and 888 cm^{-1} can be assigned to vibrations of the less mobile TBA^+ ions. All spectral changes reversed when the electrode potential was readjusted to 0.4 V, which documents the quasi-reversibility of electrochemical CO_2 reduction in acetonitrile.

Chandrasekaran et al. (4) observed a weak spectral feature at 1680 cm^{-1} due to a surface species originating from CO_2 reduction at Pt in CH_3CN. They assigned this band to adsorbed CO_2^-. However, our IR peaks are much stronger and correspond mainly to bulk solution species. We believe that the bands at 1687/1647 cm^{-1} ($\nu_{C=O}$), 1387-1304 (ν_{C-O}), and 840 cm^{-1} (δ_{OCO}) are due to formation of solvated oxalate. This view is further supported by in situ spectra obtained for the quasi-reversible oxidation of TBAOX (cf. Fig 2, peaks at 1685, 1651, 1355, and 837 cm^{-1}). The much stronger peaks at 1557, 1290, and 746 cm^{-1} however, seem to correspond to oxalate which is not or only partly solvated by CH_3CN.

We conclude that electrochemical CO_2 reduction in CH_3CN yields mainly solvated $C_2O_4^{2-}$. Solid TBAOX on the other hand, dissolves in acetonitrile in the form of aggregates such as ion pairs, giving rise to IR spectra shifted towards lower wavenumbers.

References

(1) a) B. Vassiliev, V.S. Bagotzky, N.V. Osetrova, O.A. Khazova, and N.A. Mayorova, J. Electroanal. Chem., *189*, 271 (1985); b) ibid., *189*, 295 (1985); c) ibid., *189*, 311 (1985).

(2) E. Lamy, L. Nadjo and J.M. Saveant, J. Electroanal. Chem., *78*, 403 (1977).

(3) A.W.B. Aylmer-Kelly, A. Bewick, P.R. Cantrill, and A.M. Tuxford, Disc. Faraday Soc., *56*, 96 (1973).

(4) K. Chandrasekaran and J.O'M. Bockris, Surface Science, *185*, 495 (1987).

(5) J.K. Foley, C. Korzeniewski, J.L. Daschbach, and S. Pons, in "Electroanalytical Chemistry", A.J. Bard, ed., *Vol. 14*, Marcel Dekker, Inc., New York, p. 309 (1986).

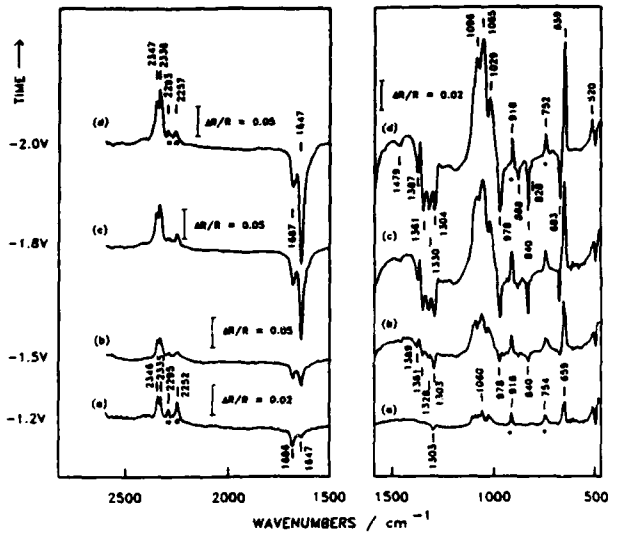


Figure 1: Steady-state FTIR reflectance spectra for CO_2 reduction in CO_2 saturated CH_3CN/0.1 M TBAF as a function of electrode (Pt) potential. The reference spectrum for (a)-(d) was obtained at 0.4 V. Stars indicate the positions of strong CH_3CN bands.

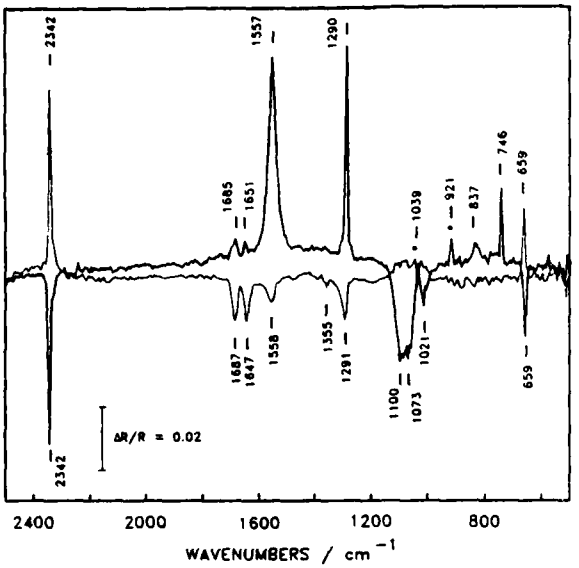


Figure 2: In situ FTIR reflectance spectra for the oxidation of TBAOX (0.01 M) in CH_3CN/0.1 M TBAF at Pt/0.1 V (thick curve). The reference spectrum was obtained at -1.5 V. Re-reduction of the TBAOX oxidation product (CO_2 at Pt/-1.8 V (thin curve). The reference spectrum was collected at 0.1 V. Stars indicate the positions of strong CH_3 bands.

Surface tension measurements: toward higher accuracy

S. Bordi
Dipartimento di Chimica
Università degli Studi di Firenze, Italy

M. Carlà and R. Cecchini
Dipartimento di Fisica
Università degli Studi di Firenze, Italy

Interfacial tension (γ) remains the most significant experimental quantity to describe the thermodynamic behaviour of the polarized liquid–liquid interface.

Several experimental techniques were devised to measure it, but only those based on a sessile or hanging drop yield absolute data and are free of any contact angle problems, that heavily trouble most other methods.

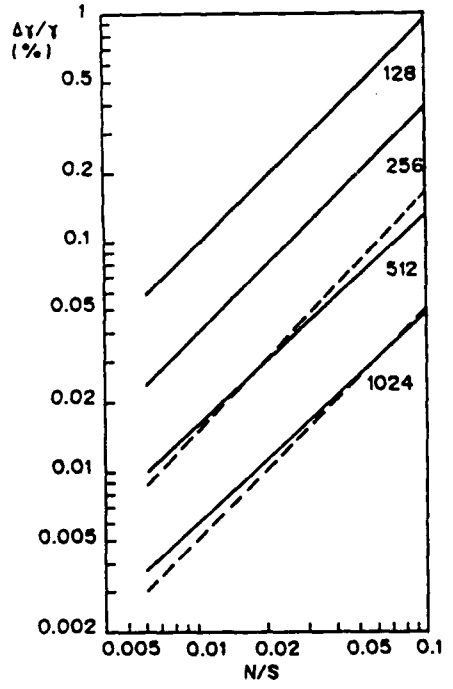


Fig. 1. *'Single shot' accuracy in interfacial tension vs noise to signal ratio for a camera resolution from* 128 × 128 *to* 1024 × 1024 *pixel and a shape factor* $\beta = 5$.

Despite these favourable characteristics, these techniques have found a limited application for a very long time, because of the cumbersome work required to get and process even a single set of experimental data. Recently they gained a new attention owing to the latest technological developments in digital image acquisition and processing. See, e.g., [1,2,3,4] for image digitization and processing and [5,6,7] for the online connection of a video camera to a computer.

In this last application it is mandatory the use of a solid state video camera, as the poor linearity of vidicons makes it impossible to get accurate drop shape data. The poor resolution of the camera, if compared with that of a good traveling microscope, can be largely counterbalanced by the great number of profile data points that can be taken and processed.

Fig. 1 shows the results of the computer simulation we used to study the accuracy obtainable in an interfacial tension measurement with a sessile drop apparatus and a solid state video camera. The flow chart of the simulation program is reported in fig. 2.

The relevant input parameters were the drop shape factor β [8], the scale factor, the camera resolution and noise level, and the shape of the diffraction band. The geometric profile was generated by a Runge–Kutta integration method and then scaled to bring the

drop equator to about 85% the frame size. The illuminance of each pixel was calculated taking into account the diffraction effects; the whole frame was blurred with noise in a variable amount before extracting the drop profile and fitting by least squares to get back the drop parameters. The drop profile was cut on either side at an angle $\varphi = 135°$, as it is common practice in real measurements, because the bottom of the drop may be distorted by the electrode edge. To evaluate the error in the γ value due to the image acquisition process,the procedure was repeatedly executed with several sets of the initial parameters.

The results in fig. 1 (for a typical drop shape factor $\beta = 5$) have been obtained for a camera resolution from 128×128 to 1024×1024 pixel and for a noise to signal ratio in the range $0.006 \div 0.1$. Solid lines refer to data obtained without any diffraction effect and slotted lines to data obtained with a two pixel wide diffraction band. It is apparent that a camera with a resolution better or equal to 512×512 pixel is required to replicate the single measure accuracy of 0.01% offered by other techniques [9,10].

Fig. 3 shows the performance of a 512×512 pixel system as a function of the shape factor β. Accuracy is poor for very low β values ($\beta < 1$), which correspond to an almost spherical drop. Values of β in the range $1 \div 5$ offer the best compromise. In fact, no improvement in accuracy is obtained for $\beta > 5$ and values of β over 5 are not advisable as the drop height decrease may bring into play disturbance from the drop supporting surface. All these data refer only to the random errors that affect the 'smoothness' of the electrocapillary curves.

Systematic errors introduced by a misalignment between the vertical axis of the drop and the camera vertical were computed using the same program, by rotating a small angle the drop profile in the plane before generating the frame. Results are shown in fig. 4. A misalignment up to $2 \cdot 10^{-3}$ rad can be tolerated before introducing an error greater than 0.01%. It is possible to get and maintain in the mechanical assembly of a sessile drop apparatus an alignment sensibly better than this value, hence it seems useless to burden the fit program with the calculation of the drop axis rotation.

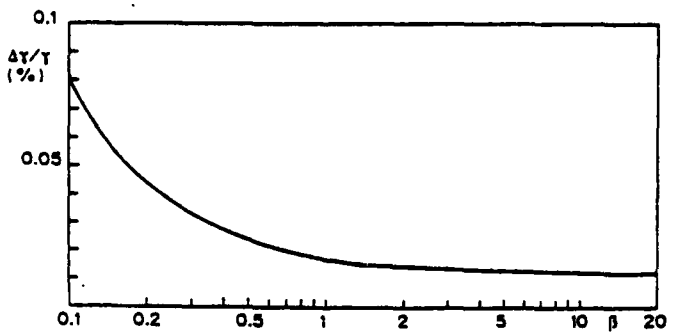


Fig. 3. *'Single shot' accuracy vs β value (camera resolution 512x512 pixel, N/S ratio = 0.01).*

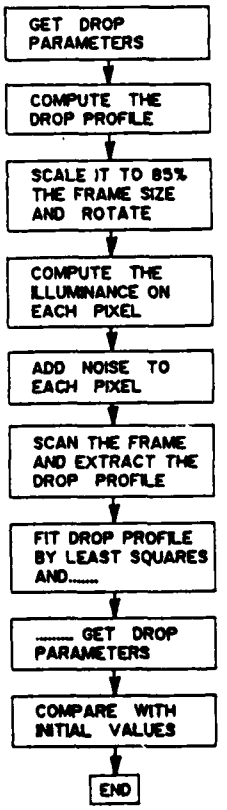


Fig. 2. *Flow chart of the simulation program.*

The most important source of systematic errors remains the magnification factor m of the optics, whose effect can readily be calculated to be: $\Delta\gamma/\gamma = 2\,\Delta m/m$.

On the basis of these results, we are currently assembling a sessile drop apparatus employing a CID camera GE TN2250 equipped with a 512×512 pixel sensor, selected because of its highly regular pixel geometry, and a macro-zoom objective Zeiss Tessovar. Full details on the apparatus construction will be given in a forthcoming paper.

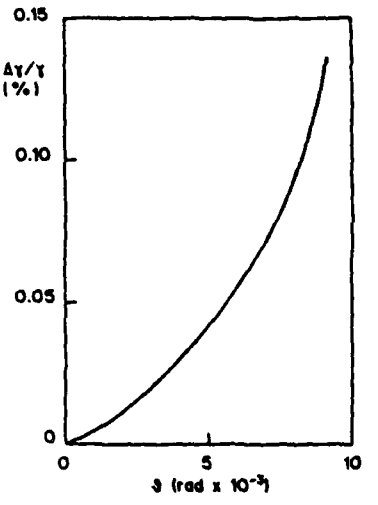


Fig. 4. *Systematic error in γ due to misalignement of the camera vertical axis.*

References

[1] D. S. Ambwani and T. Fort Jr., *Surface and Colloid Science* (R. J. Good and R. R. Stromberg eds.) Vol II, pp. 93-119 (Wiley, New York, 1979).

[2] H. Vos and J. M. Los, *J. Colloid Interface Sci.* **74**, 360 (1980).

[3] R. E. Patterson and S. Ross, *Surface Sci.* **81**, 451 (1979).

[4] J. N. Butler and B. H. Bloom, *Surface Sci.* **4**, 1 (1966).

[5] H. H. Girault, D. J. Schiffrin and B. D. Smith, *J. Electroanal. Chem.* **137**, 207 (1982).

[6] H. H. Girault, D. J. Schiffrin and B. D. Smith, *J. Colloid Interface Sci.* **101**, 257 (1984).

[7] S. H. Anastasiadis, J.-K. Chen, J. T. Koberstein, A. F. Siegel, J. E. Sohn and J. A. Emerson, *J. Colloid Interface Sci.* **119**, 55 (1987).

[8] F. Bashforth and J. C. Adams, *An Attempt to Test the Theories of Capillary Action*, (Cambridge University Press, Cambridge, 1883).

[9] D. M. Mohilner and T. Kakiuchi, *J. Electrochem. Soc.* **128**, 350 (1981).

[10] M. Carlà, G. Aloisi, G. Papeschi and S. Bordi, *J. Electrochem. Soc.* **130**, 1859 (1983).

IRON BEHAVIOUR IN HF SOLUTIONS

A. Frignani, C. Monticelli, G. Brunoro, M. Tassinari & G. Trabanelli

Corrosion Study Centre "A. Daccò" - Chemistry Department,
University of Ferrara, 46 L. Borsari, 44100 Ferrara - ITALY

Formerly (1), the behaviour of Armco iron was studied in various acid solutions at 60 °C (1.7 N HF; 1.4 N HCl; 1.5 N $HClO_4$ and 1.5 N H_2SO_4). Notwithstanding its higher pH value (≅ 2.3), HF exerted a very high aggressiveness towards iron, similar to that exerted by strong acids. The high dissolution rate of Armco iron in 1.7 N HF was related to the high current densities for the cathodic reaction of hydrogen evolution, close to those obtained in the solutions of strong acids (pH ≅ 0), although the influence exerted on the anodic reaction of metal dissolution by fluoride anions (or by undissociated HF) cannot be neglected.

To fully understand the iron dissolution mechanism in HF, it was considered interesting to investigate the cathodic reaction of hydrogen evolution on Armco iron in different acid solutions, and to compare it with the results obtained on a bright platinum electrode.

Some dilute solutions of strong acids (HCl; H_2SO_4) and weak acids (CH_3COOH; HCOOH; HF) were tested. HCOOH was particularly suitable as comparative acid because it has about the same pK_a as HF. As supporting electrolyte 0.1 N $NaClO_4$ was used .

Armco iron cylinders and bright platinum disc were used as electrodes, both in stationary and in rotating conditions (0 - 4500 r.p.m.) The cathodic curves of hydrogen evolution reaction were recorded, and the limiting currents (i_L) were measured.

Results

With rotating cylindrical Armco iron electrode, dilute solutions (0.001 N) of weak acids (CH_3COOH; HCOOH; HF) behave like dilute solutions (0.001 N) of strong acids . (The pH of all solutions but acetic is ≅ 3). In fact the values of limiting current densities (i_L) for the hydrogen evolution reaction are close and increase linearly as a function of the square root (SR) of the rotation speed (RS) of the electrode (Fig. 1). On the contrary, with more concentrated solutions (0.1 N) of weak acid the values of i_L are almost indipendent of the RS. The i_L values in HF solution are higher than those in the other two acids (Fig. 2) .

The hydrogen evolution reaction on Armco iron electrode was investigated in HF solutions of increasing concentrations, from 0.001 N to 1 N (Fig. 3). The pH values of these solutions are very close to 3.

While the lowest concentration (0.001 N) i_L increases linearly as a function of the SR, at 0.01 N i_L increases linearly only up to 250 r.p.m., and then remains more or less constant . If the HF concentration is increased to 0.1 N , i_L is always indipendent RS. Finally, at the highest concentration (1 N) i_L tends to decrease as a function of the RS.

A quite different behaviour was experienced with a bright platinum rotating disk (Fig. 4). In fact, in 0.1 N HF (pH $\cong$ 3) i_L increases linearly as a function of the SR of RS of the electrode.

This behaviour was also experienced in dilute solutions (0.001 N) of strong acids at the same pH of 0.1 N HF.

Conclusions

H^+ discharge reaction in dilute (0.001 N) solutions of weak acids on Armco iron follows the same reaction path as in dilute solutions of strong acids, and this discharge involves the solvated H^+ ions.

A very different behaviour is observed in more concentrated solutions of weak acids, where probably the undissociated acid molecule carries the H^+ ions to be consumed (3). Moreover, despite the close pK_a values of HCOOH and HF, $i_{L(\omega=0)}$ value of HF is about twice that of HCOOH.

These results show that, as assumed in (3), weak acid solutions may become more aggressive than strong acid solutions when the former are predominantly in the undissociated form.

The marked different behaviour of Armco iron (Fig. 2) from bright platinum (Fig. 4) in 0.1 N HF solutions shows that a strong interaction has to be considered between HF molecule and iron surface.

References

1) A. Frignani, G. Brunoro, M. Zucchini & G. Trabanelli, ASMI, Atti I° Convegno Nazionale, Milano 26-27 settembre 1983, p.311, Pitagora Editrice, Bologna

2) A. Frignani, C. Monticelli & G. Brunoro, Br. Corros. J., 22, 190 (1987)

3) H. Kaesche, "Metallic Corrosion" (English translation), p.90, N.A.C.E., Houston, Tx, 1985

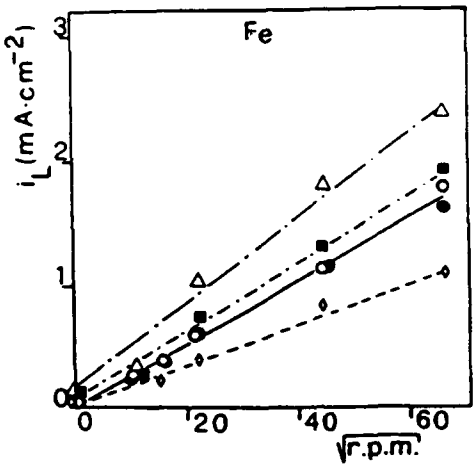


Fig. 1 - i_L for the h.e.r. on Armco iron in 0.001 N acid solutions as a function of the rotation speed (r.p.m.)

△ HF; ■ HCOOH; ● $HClO_4$; ○ HCl
◇ CH_3COOH

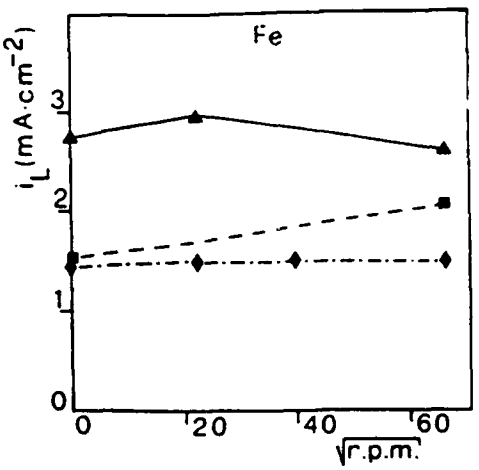


Fig. 2 - i_L in 0.1 N solutions of weak acids : ▲ HF; ■ HCOOH
◆ CH_3COOH

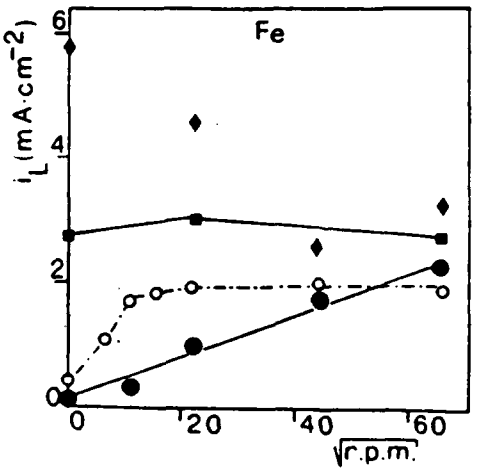


Fig. 3 - i_L for the h.e.r. in various solutions of HF, on Armco iron :

◆ 1N ; ■ 0.1 N; ○ 0.01 N
● 0.001 N

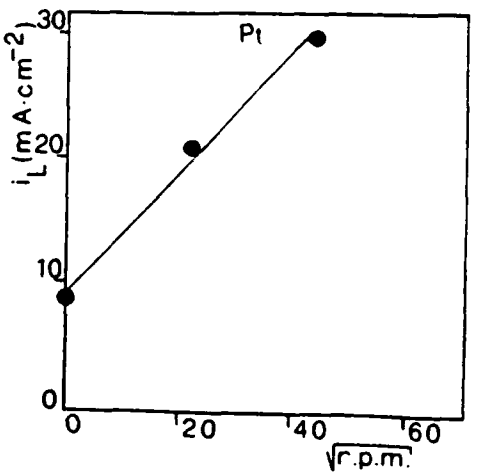


Fig. 4 - i_L for the h.e.r. in 0.1 N HF on bright platinum disk as a function of the rotation speed (r.p.m.)

In-situ Scanning Tunneling Microscopy of Electrode Surfaces with Atomic Scale Resolution

T. Twomey, J. Wiechers, R. J. Behm and D. M. Kolb*

Fritz-Haber-Institut der Max-Planck-Gesellschaft,
Faradayweg 4-6, D-1000 Berlin 33, F. R. G.

A Scanning Tunneling Microscope has been developed which allows electrode surfaces to be studied in situ, under potentiostatic control. The microscope itself is a modified version of the 'standard' pocket-size STM, decoupled from its surroundings by a stack of copper plates and viton spacers and uses an electrochemically etched tungsten wire as a tunneling tip. Insulation of all except the foremost 10^{-4} - 10^{-5} cm^2 of the tungsten surface and judicious choice of tip potential enable one to reduce unwanted electrochemical currents to practically zero. Resolution of better than 3 Å in a direction normal to the surface, (z), and of 10 - 20 Å laterally, (x,y directions) is achieved using this set-up.

First results of investigations of the topography of a flame-treated Au(111) surface are presented here, demonstrating that steps of monoatomic height may be clearly resolved (Fig. 1). A projected top view of this image illustrates the three-fold symmetry of the (111) surface.

It has also prooved possible to follow the topographical changes occuring during simple electrochemical processes with this technique.

A sequence of images, for example, monitoring the adsorption and desorption of Cl^- ions on the surface will be presented. Quite considerable changes in the surface structures occur in particular at step sites, simply as a result of this process (1).

Even more remarkable are the morphological changes caused by oxidation-reduction cycles. Fig. 2 illustrates the effect of one such cycle on a clean, freshly tempered Au(111) surface. The attack on the terrace in the centre of the image is clearly seen.

(1) J. Wiechers, T. Twomey, D. M. Kolb and R. J. Behm, J. Electroanal. Chem. submitted.

* Institut für Kristallographie, Universität München, Theresienstr. 41, D-8000 München 2, F. R. G.

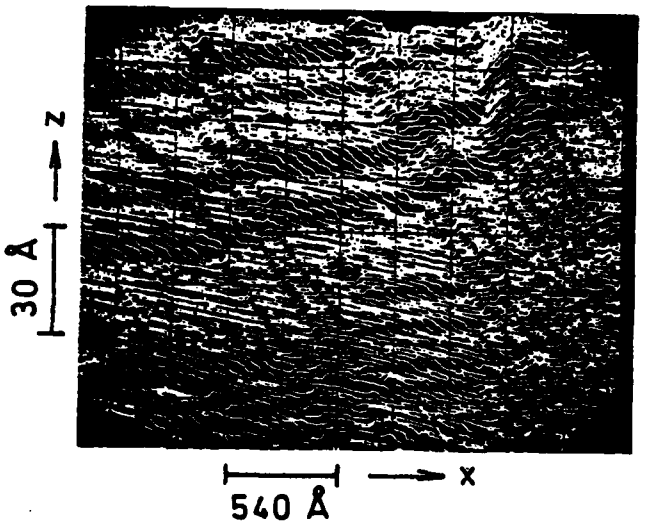
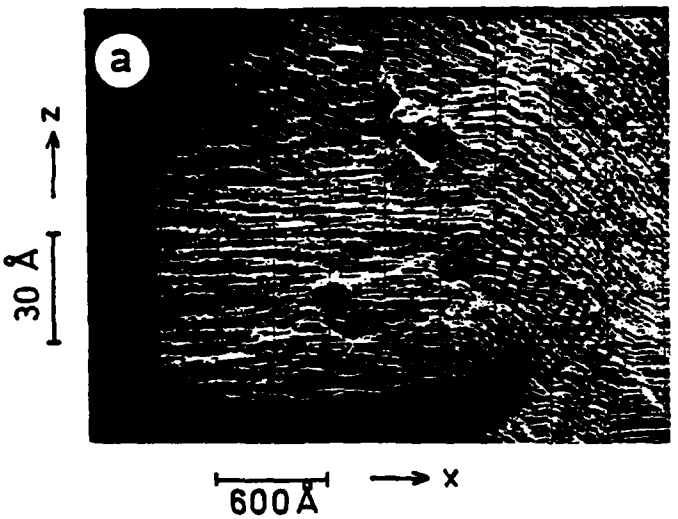


Fig. 1: STM image (2700 Å x 2700 Å) of a freshly prepared Au(111) in 0.05 M H_2SO_4 at rest potential. Vertical scale as indicated.



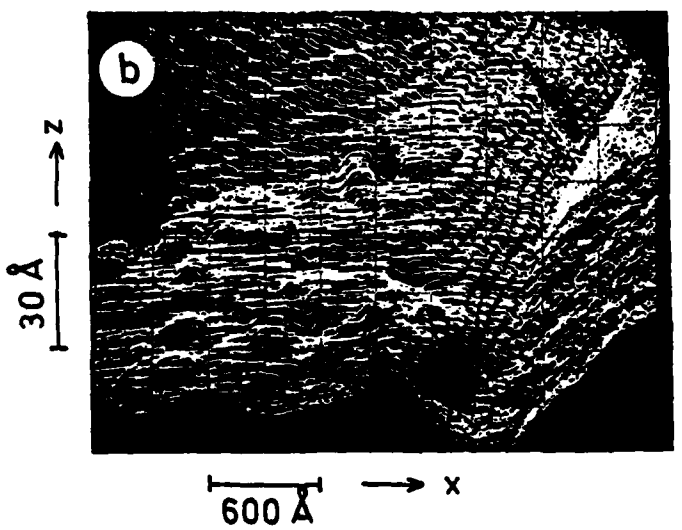


Fig. 2: (a) STM image (2700 Å x 2700 Å) of a clean, freshly flame-treated Au(111) surface at rest potential in 0.05 M H_2SO_4.
(b) STM image of the above region, again at rest potential in the same solution, having cycled the electrode once to 1.5 V(Pd-H) and back, at 10 mV s^{-1}.

IN-SITU FTIR STUDIES OF THE REDUCTION OF ADSORBED CoPc IN THE PRESENCE OF CO_2.

P. A. CHRISTENSEN, A. HAMNETT AND A. V. G. MUIR

The Inorganic Chemistry Laboratory, South Parks Road, Oxford OX1 3QR

CoPc has been reported[1]-[3] to be one of the most active phthalocyanines for CO_2 reduction. The mechanism of the reduction in aqueous solution is thought to involve cobalt hydride intermediates[2],[4],[5], but little evidence exists for such species. There are differing reports concerning the reduction products[3],[5], and it was hoped that the relatively new SNIFTIRS[6] technique would shed some light upon the problem.

EXPERIMENTAL

A. Electrochemical Methods.

Cobalt[II] phthalocyanine (CoPc) was prepared in high yield by refluxing stoichiometric quantities of anhydrous cobalt[II] acetate (East Anglia Chemicals) and phthalonitrile in quinoline for 4 hours. The crude product was filtered off and purified by two sublimations at 450°C and 10^{-3} Torr.

Thin layers of CoPc were deposited onto the edge graphite electrodes by adsorption for two minutes from its solution in pyridine (Aldrich Gold Label) or THF (M & B Laboratory Chemical)[7][8]. Electrodes were washed with copious amounts of double distilled water prior to insertion into the cell.

All electrochemical experiments were performed in 0.1M potassium hydrogen phosphate/ 0.1M sodium hydroxide (pH 7.2) buffer made up with ultrapure water. Solutions were purged with N_2 (cryogenic boil-off) or saturated with CO_2.

Cyclic voltammetry experiments were carried out in a 3-electrode single-compartment cell with a calomel reference electrode and Pt gauze counter electrode.

B. Spectroelectrochemical Methods.

The spectroelectrochemical cell and the SNIFTIRS technique have been described elsewhere[9].

Spectra were collected at 8 cm^{-1} resolution. The single-step or "staircase"[6] spectra consisted of 69 scans at each potential. The results are presented as S_n/S_1, where S_1 is the spectrum collected at the base potential E_1 *vs* SCE and S_n is the spectrum collected at potential E_n.

RESULTS AND DISCUSSION

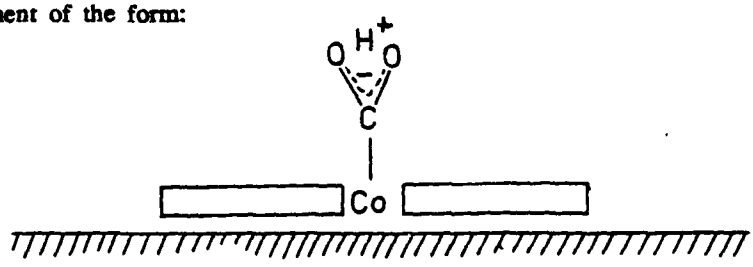
Cyclic voltammograms of a CoPc-coated edge graphite electrode immersed in N_2-purged buffer at pH 8.4 show three waves in the potential region 0 to

-1.3V *vs* SCE. The waves at -0.5V and -1.0V can be attibuted to the one- and two- electron reductions of the CoPc[5]. A third wave is observed at about -1.25V, probably corresponding to the reduction of protons. None of these waves is observed in the absence of CoPc.

A reference spectrum for the CoPc-modified electrode was then collected at the base potential of 0V *vs* SCE and the potential stepped to -1.2V. Spectra were collected at regular intervals up to 32 minutes after the potential step. The modified electrode slowly deprotonated the buffer at -1.2V, supporting its role as a catalyst in the reduction of protons at this potential, though no H_2 evolution was observed. Loss features due to $H_2PO_4^-$ were observed at 1230 cm^{-1} (s,sh), 1159 cm^{-1} (vs) and 1078 cm^{-1} (vs); with gain features due initially to HPO_4^{2-} at 2950 cm^{-1} (m), 2400 cm^{-1} (w) and 1076 cm^{-1} (vs) and 990 cm^{-1} (m); and then to PO_4^{3-}, 2800 cm^{-1} (s,br) 2280 cm^{-1} (vw) and 1007 cm^{-1} (vs)[12].

Even in the presence of CO_2, the buffer was deprotonated to HPO_4^{2-} at potentials <-0.9V; in this case with the concommittant loss of CO_2 from solution (feature at 2340 cm^{-1}). Only in the absence of CO_2 and at potentials <1.1V *vs* SCE was the buffer converted to PO_4^{3-}. No features were observed in the SNIFTIRS spectra of the electrode unless the opotential was cathodic of the second reduction; only this reduction results in the deprotonation of the $H_2PO_4^-$. It is possible that the first electron may go on the ring or on the metal. If the latter, then we must conclude that Co^I, which has a d^8 configuration, is unwilling to increase its coordination number. The second electron transfer is accompanied by proton abstraction from solution. In principle, the hydrogen might coordinate either to ring or metal but the subsequent chemistry suggests the *metal* is the more likely site; after two electron transfer we then have, formally, $[Co^{II}(H)Pc]^-$.

At potentials E, -1.2V < E < -0.9V, CO_2 is lost from solution and a product feature appears at 1294 cm^{-1}. The intensity of this feature suggests a surface species. Some of the CO_2 loss can also be attributed to dissolution to HCO_3^- (weak feature at 1350 cm^{-1}). Further product features may be hidden under the strong phospate bands. The band at 1294 cm^{-1} may originate from the symmetric stretch of an electron-rich Co-CO_2^- fragment of the form:



The absorptions due to this species would then be expected to be lower in frequency than those for formate, *e.g.* 1640 cm^{-1} (HCO_2^- asymmetric stretch) and 1340 cm^{-1} (HCO_2^- symmetric stretch)[17]. A consideration of the surface selection rule[10] suggests that the observation of the symmetric, as opposed to asymmetric, stretch of species A favours an orientation in which

the phthalocyanine ring of A lies flat on the electrode surface, as shown above.

At potentials < -1.1V appreciable dissolution of the CO_2 occurs as evinced by the appearance of a gain feature at 1400 cm^{-1} attributed to CO_3^{2-}. It was shown that *CoPc is inactive towards the reduction of* CO_3^{2-}.

If the potential is *stepped* from 0.0 to -1.05V and the spectrum gathered at -1.05V is compared to successive spectra obtained by stepping the potential *up*, it is observed that about 30% of the CO_2 lost from solution during the cathodic step is slowly returned. In addition some reprotonation of the HPO_4^{2-} takes place. However, the product feature at 1294 cm^{-1} is retained, as indeed was the solution HCO_3^- peak at 1350 cm^{-1}. Potential dependent acid/base equilibria have been observed on edge graphite, and we conclude that surface-bound HCO_3^- may form at cathodic potentials, which, if flat, would be invisible to our probe.

At no time was H_2 evolution observed in the above experiments. However, if pyridine was replaced by THF, hydrogen evolution occurred at potentials < -1.0V, indicating that the electrochemical behaviour of the CoPc is critically dependent upon the solvent used in the solution from which it was deposited on the electrode

References

1. S. Meshitsuka, M. Ichikawa and K. Tamaru, J. C. S. Chem. Comm., 1974, 158.
2. H. Tanabe and K. Ohno, Electrochimica Acta, **32**(1987), 1121.
3. S. Kapusta and N. Hackerman, J. Electrochem. Soc., **131**(1984), 1511.
4. K. Kusuda, R. Ishihara, H. Yamaguchi and I. Izumi, Electrochimica Acta, **31**(1986), 657.
5. C. M. Lieber and N. S. Lewis, J. Am. Chem. Soc., **106**(1984), 5033.
6. A. Bewick and S. Pons, in "Advances in Infrared and Raman Spectroscopy" Vol. 12 (1985) p1, R. J. H. Clark and R. E. Hester (Eds.), Wiley Heyden, (London).
7. A. Elzing, A. Van der Putten, W. Visscher and E. Barendrecht, J. Electroanal. Chem., **200**(1986), 313.
8. A. Elzing, A. Van der Putten, W. Visscher and E. Barendrecht, J. Electroanal. Chem., **233**(1987), 99.
9. P. A. Christensen, A. Hamnett and P. R. Trevellick, J. Electroanal. Chem., **242**(1988), 23.
10. A. C. Chapman and L. E. Thirwell, Spectrochimica Acta, **20**(1964), 937.
11. G. Socrates, "Infrared Characteristic Group Frequencies", Wiley-Interscience, 1980.
12. R. G. Greenler, J. Chem. Phys., **44**(1966), 310.

XPS AND LEED STUDY OF UNDERPOTENTIALLY DEPOSITED COPPER ON Pd (100)

T. Solomun

Fritz-Haber Institut der Max-Planck Gesellschaft,
Faradayweg 4 - 6, 1000 Berlin 33, West Germany.

Present address: Institut für Physikalische und Theoretische Chemie,
Takustraße 3, 1000 Berlin 33, West Germany

Though submonolayer deposits of metals on metals have a clear catalytic significance there exist only a few studies of undepotental metal electrodeposition on palladium, a transition metal of surpassing importance in electrocatalysis. Indeed, this is the first report were a single-crystal Pd surface was utilised in this context. In an early work of Szabo/1/, it has been demonstrated that alloying occurs upon undepotential electrodeposition of copper on a poly-crystalline palladium electrode. For the Cu/Pd system, solid solutions with any concentration between pure copper and pure palladium can be obtained. The phase diagram contains stable ordered structures based on the stoichiometric compositions $PdCu_3$ and PdCu.

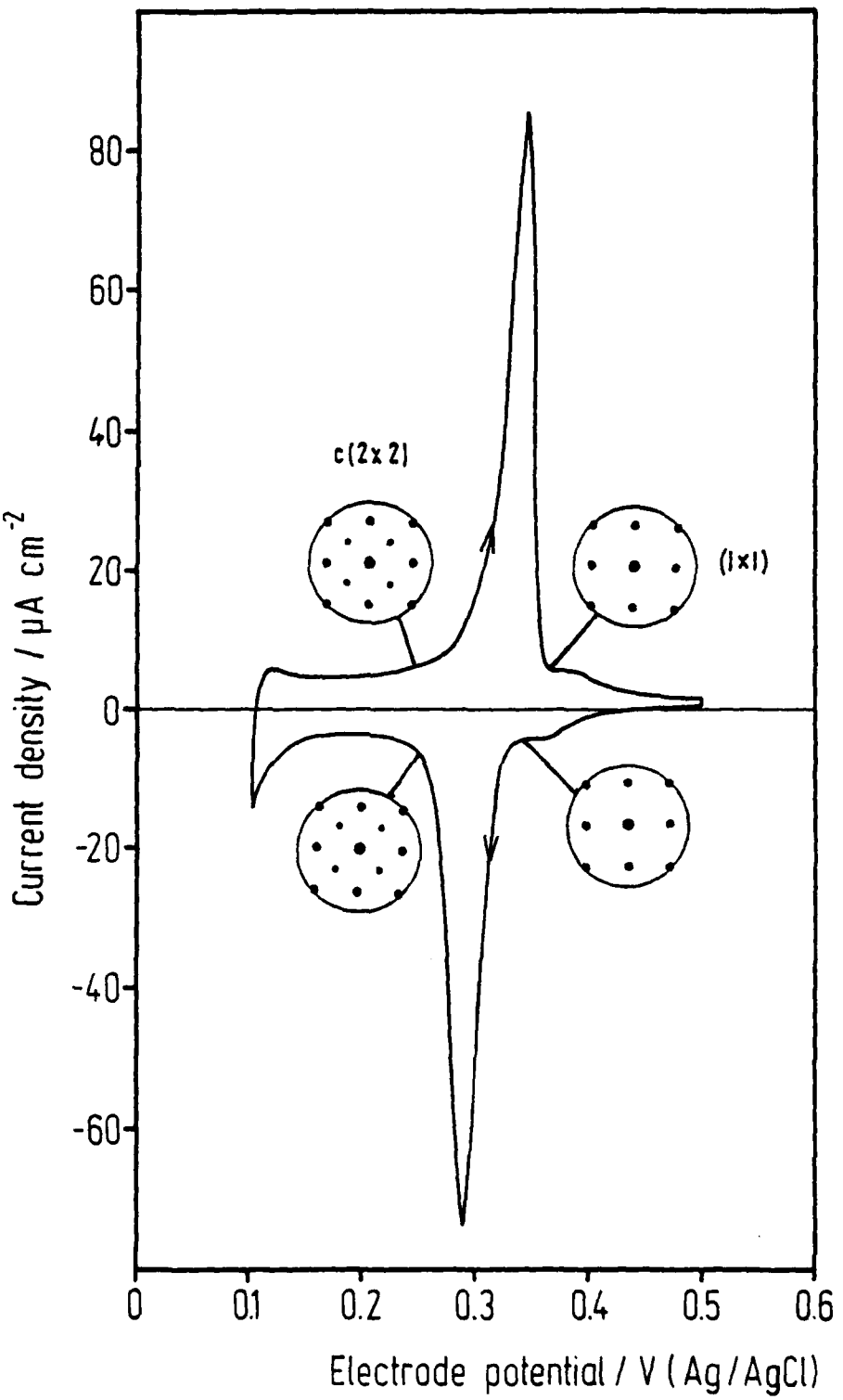
We present here results concerning undepotential deposition of copper on a well-characterized Pd (100) surface. They were obtained on an apparatus which permitted surface analyses by LEED and XPS, and subsequent transfer (back-transfer) of the surface to an electrochemical cell under the experimental conditions where contamination of the surface can be considered negligable. Under conditions of negative linear potential scan, about 8/10 of a nominal copper monolayer is deposited in a reversible maner at 0.28 V (vs.Ag/AgCl) over a rather narrow potential range (Fig. 1), resulting in a c- (2 x 2) LEED pattern. The metallic nature of the deposit was established on the basis of Cu- ($2p_{3/2}$) and Cu-$L_3M_{4,5}M_{4,5}$ transitions /2/. Indeed, a negative chemical shift of about 1eV of the

Cu-($2p_{3/2}$) core-level (on the binding energy scale with respect to the pure metal transition) was observed after potentiostatic emersion at 0.25V. This would correspond to a reascnable value for a Pd/Cu alloy /3/. It is worth noting that for palladium deposition on a Cu (100) surface under UHV conditions, the formation of the c- (2x2) LEED pattern was found to be thermally activated at temperatures just below 300 K with the best c- (2x2) patern corresponding to a Pd coverage higher than half a monolayer ($\theta_{Pd} \approx 0.8$) /4/. ISS measurements /4/ have indicated that the surface is bimetallic, with approximately equal numbers of Cu and Pd atoms, implying a certain amount of Pd atoms in the second layer. On the basis of that we assign the electrodeposit formed at 0.28 V to a precursor state of a bulk alloy, formation of which (under the experimental conditions of this study) takes place below O.1V.

---

1. S. Szabo, I. Electroanal. Chem., 77 (1977) 193.
2 G. Schön, Surf.Sci., 35 (1973) 96.
3. N. Martensson, R. Nyholm, H. Calen, I. Hedman and B. Johansson, Phys. Rev. B, 24 (1981) 1725.
4. G. W. Graham, Surf. Sci., 171 (1986) L432.

Fig. 1: Cyclic voltammogram for the Pd (100) electrode in 10^{-3}M $CuSO_4$/10^{-2}M H_2SO_4 electrolyte at a sweep rate of 10 mVs^{-1}.


80
60
40
20
0
-20
-40
-60
c(2x2)
(1x1)
Current density / µA cm^{-2}
0
0.1
0.2
0.3
0.4
0.5
0.6
Electrode potential / V (Ag/AgCl)

ALUMINUM ELECTROCRYSTALLIZATION FROM METAL-ORGANIC ELECTROLYTES

W. Kautek[+] and S. Birkle

Research Center, Siemens AG
D-8520 Erlangen
Federal Republic of Germany

Abstract.
The aluminum electrodeposition from aprotic solutions of the organic complex $KF{\cdot}2Al(C_2H_5)_3$ on polycrystalline aluminum and vitrous carbon is described for potentiostatic and voltage pulse conditions. Below currents of about -3 mA/cm², electron transfer controls the deposition rate. At stationary polarizations above 0.1 V, a slow chemical process characterized by a reaction current of 5 mA/cm² precedes charge transfer. On a foreign substrate, i.e. vitreous carbon, peripheral kinetically controlled growth of instantaneously formed two-dimensional plates takes place on top of plates so as to produce three-dimensional nuclei which then grow by a transport limited mechanism.

1. Introduction

The interest in the preparation of aluminum deposits has steadily increased during the last decades as the excellent corrosion resistance of aluminum /1/ permits the solution of many engineering problems. Several procedures can be employed for the deposition on various metals such as metal spraying, hot-dipping, vacuum deposition, cladding etc. These techniques are rather expensive and often impracticable because of possible damage of the specimen at high temperatures employed. The problem of electrodeposition at moderate temperatures attracted vivid attention. Organo-aluminum baths of the type $MeX{\cdot}2AlR_3$ have been suggested /2/ where Me was preferentially sodium and X equal fluorine. A development to a technical deposition process has been conducted /3/, recently, leading to the so-called SIGAL®-process.
The object of this work was a systematic understanding of the electrochemical processes involved. We investigated the deposition both on polycrystalline aluminum and on vitreous carbon paying attention to the early stages of the reaction.

2. Experimental

Electrolytes were prepared by heating an analytical grade toluene solution of $Al(C_2H_5)_3$ (Schering) with a stoichiometric amount of analytical grade potassium fluoride at about 100°C under argon to give a dilution of four mole toluene to one mole KF. The electrochemical cell could be kept under solvent saturated dry argon gas, and was thermostated at 103 ± 3 °C.

+ Laboratory of Chemical Surface Technologies,
Federal Institute for Material Research and Testing
Unter den Eichen 87, D-1000 Berlin 45
Federal Republic of Germany

A conventional potentiostatic three-electrode configuration with IR-compensation was employed. The substrate disks were fitted into cylinders of Macor®-glass ceramics to form rotating disk electrodes. As reference and counter electrode served aluminum rods. Fast current transients were recorded by a digital storage oscilloscope to produce hard copies on a x-y recorder.

3. Results and Discussion

In the electrodeposition of aluminum from $KF \cdot 2Al(C_2H_5)_3$ onto conducting substrates, several rate limiting mechanisms could be detected. Diffusional rate control was eliminated to uncover the reaction current (j_r) employing a rotating disk electrode and extrapolating the extended "mixed-control"-Levich-equation

(Equ. 1) $$1/j = 1/j_r + 1/A \cdot m^{-0.5}$$

where A contains diffusional parameters and m is the rotational speed. At extremely low overvoltages near equilibrium of the aluminum electrode, the transfer of three electrons to an Al-complex species determines the rate. The exchange current of about 0.4 mA/cm² is comparable to an aqueous galvanic bath, e.g. of zinc. Above overvoltages of -0.1 V, however, a chemical dissociation process preceding charge transfer becomes the slowest step. A reaction current (j_r) is limited to a value around -5 mA/cm² ("A" in Fig. 1). In the range of -0.3 V up to -0.7 V another deposition mechanism occurs in form of a flat kinetic current wave below c. -20 mA/cm² ("B"). Unusual kinetic Tafel parameters point onto possible slow chemical reactions and/or surface diffusion, i.e. crystallization. Negative of -0.7 V co-deposition of aluminum and alkalimetal takes place /4/.

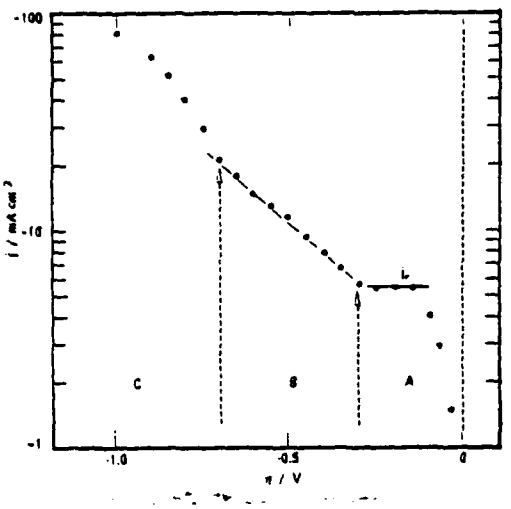


Fig.1 Tafel plot

The voltage pulse deposition of Al on a foreign substrate, here vitreous carbon, gave a detailed insight into the initial steps of electrocrystallization which are nucleation and growth. The number of two-dimensional nuclei (N) renders itself the potential dependent term because the reversible work of nucleation is a function of η, the overvoltage. The nucleation peak current in the ms-time domain (Fig. 2) is directly proportional to the number of two-dimensional nuclei formed, i.e. $j \propto N$:

(Equ. 2) $$\log j = \log zFN_o - (\pi^2 \bar{A}/zFkT) \cdot /\eta/^{-1}$$

The slope of this straight line is determined by the ratio of the molar area covered by one mole in a monolayer, $\bar{A}$, and the charge z. In the domain $/\eta/ > 0.6$ V, where an alloy of Al (z=3) and K (z=1) is deposited, this ratio, i.e. the negative slope, is about 2.6 times greater than for pure Al at $/\eta/ < 0.6$ V.

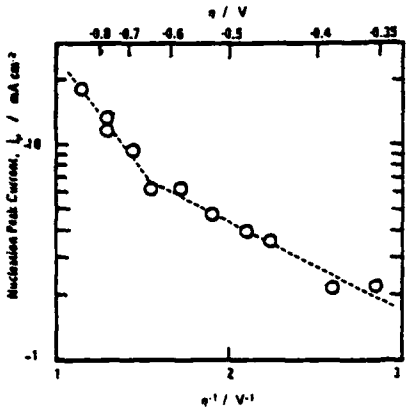


Fig.2 Nucleation peak current vs. η^{-1}. Potential dependence of 2D-nucleation.

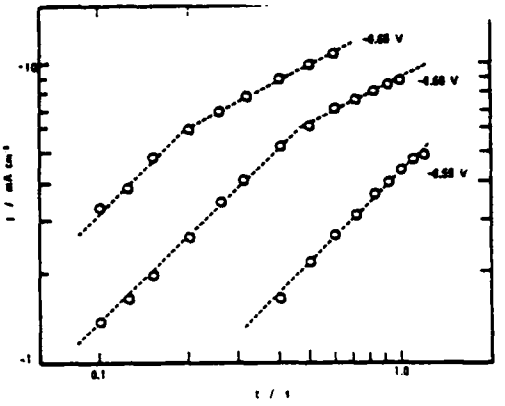


Fig.3 log j - log t plot for the growth of Al-nuclei. Slopes are 1 and 0.5.

Though $\bar{A}$ of potassium is larger than of aluminum, the charge z obviously controls the slopes. The intercept at $\eta^{-1}=0$ represents a measure of the maximum number of nucleation sites N_o characteristic of a certain substrate surface. N_o turns out to be of practical relevance for the adherence and the roughness of a deposit.

In Fig. 3 we observe a peripheral growth of instantaneously formed two-dimensional plates, at short pulse times and low overvoltage, according to a rate law of

(Equ. 3) $$j = (2zF\pi Mk^2/d)N \cdot t$$

on top of plates so as to produce three-dimensional nuclei at longer pulse durations and higher overvoltages which then grow by a transport limited mechanism according to

(Equ. 4) $$j = [(8zFM^2D^{1.5}c^3)/(d^2\pi^{0.5})]N \cdot t^{0.5}$$

k represents the growth rate, h the height of two-dimensional growth centers, M the molecular weight, d the density, and N the instantaneous number of nuclei.

References

/1/ W. Kautek, Corros. Sci. 28, 173 (1988); C.A. Boose and R.J.A. Blankers, TNO Report 85M/016089BLA/AKU, Apeldoorn, The Netherlands (1984).

/2/ K. Ziegler and H. Lehmkuhl, Z. Anorg. Allg. Chem. 283, 414, (1956); DBP Pat. 1,047.450 (1954).

/3/ R. Dötzer, Chem. Ing. Technik 45, 653 (1973); S. Birkle, J. Gehring, K. Stöger, and H. de Vries, Metall 36, 673 (1982); S. Birkle, Metalloberfläche 40, 249 (1984).

/4/ W. Kautek, to be published; E. Bonitz, Angew. Chem. 67, 525 (1955).

ELECTROCATALYTIC PROPERTIES OF WELL DEFINED Pt SURFACES MODIFIED BY IRREVERSIBLY ADSORBED ADATOMS

Fernández-Vega A., Feliu J.M., Aldaz A., Clavilier J.*

Departamento de Química Física, Universidad de Alicante, Apartado 99, 03080 Alicante (SPAIN); * Laboratoire d'Electrochimie Interfaciale, 1 P. Aristide Briand, 92195 Meudon Principal Cedex (FRANCE).

The electrooxidation of formic acid on Pt is a model for a structure sensitive reaction (1). There are significant differences in the surface reactivity, as it can be seen from the voltammetric behaviour of this reaction on the three basal platinum orientations. A well-known, dual path, mechanism has been proposed for this oxidation according to the general scheme:

$$\text{HCOOH/Pt} \begin{cases} \xrightarrow{1} \text{active intermediate} \xrightarrow{E1} CO_2 + H_2O \\ \xrightarrow{2} \text{blocking intermediate} \xrightarrow{E2} CO_2 \end{cases}$$

with potential E1 < E2, both paths being structure sensitive. Among the three basal orientations, Pt(111) electrode surface is the one which undergoes the lowest effect of self-poisoning, but its activity for the reaction path 1 is the lowest, too. Conversely, Pt(100) sites are very efficient for both site-demanding reactions.

Foreign adatoms have been widely used in order to increase the selectivity of the electrocatalyst for reaction path 1 by avoiding the formation of the blocking species through path 2. Moreover, by means of well selected adspecies an enhancement of the catalytic activity for the reaction path 1 could be achieved.

It has been shown that there is an irreversible, structure sensitive, adsorption step (2) of some of the classical adatoms which leads to the formation of stable adspecies coverage on platinum surfaces. This behaviour avoids the presence of the adsorbing heteroatom as a cation into the desired fuel containing solution. Moreover, in this way the surface composition of the electrode surface can be kept constant in a wide potential range where also the oxidation of formic acid takes place.

The electrode surfaces used in this work are single crystal Pt(111) or Pt (100) ones, modified by adsorption of the previously chosen adspecies at different controlled coverages (2). The initial state of the electrode surface, which enables us to measure the hydrogen and/or adspecies coverage, was defined voltammetrically (Figure 1) from the data obtained in a cell containing the test electrolyte alone, 0.5M sulphuric acid.

These controlled electrode surfaces were introduced into the formic acid solution at a controlled potential value, in which no oxidation of the organic compound takes place. After that, an electrochemical experiment can then start in a conventional way (Figure 2). The complete experimental procedure can be repeated as times as desired in order to obtain differently covered surfaces.

The systems described in this work, Pt(111)/Bi and Pt(100)/Sb, have a common characteristic feature: the oxidation and reduction processes of the irreversibly adsorbed heteroatom take place at a potential range lower than the corresponding to the oxidation of the isolated poison (3). Moreover, the catalytic enhancement of the formic acid oxidation reaction takes place at the potential range corresponding to the adspecies reduced state.

In both cases, the formic acid oxidation peak current densities versus the different adspecies coverage show a maximum electrocatalytic activity at relatively high adspecies coverage (Figure 3). So, for the Pt(111)/Bi system, a coverage range between 0.7 and 0.8 for the adsorbed heteroatom leads to more than 40 mA/sq.cm.. For the Pt(100)/Sb system, a narrow range of coverage, around 0.9, leads to near 30 mA/sq.cm.. In both cases, the electrocatalytic activity of the starting platinum surface has been greatly increased.

Also, a separate set of experiments can be planned in order to isolate the poison, adsorbed from the formic acid solution used in this work. This was possible by applying the dissociative adsorption technique (3) to the differently covered electrode surfaces, i.e. surfaces as shown in Fig. 1. For the Pt(111)/Bi system it has not been possible to detect a significant amount of the adsorbed poison, even with low bismuth coverages. For the Pt(100)/Sb system poison was absent at antimony coverages higher than 0.9, the amount of adsorbed poison being lower as antimony adspecies coverage increases from the bare surface to this coverage value,0.9. In this system the charge involved in the oxidation of the adsorbed poison leads to the same result as in the bare Pt(100) surface: two electrons by occupied hydrogen site.

REFERENCES

1. J. Clavilier, R. Parsons, R. Durand, C. Lamy, J.M. Leger, J. Electroanal. Chem. 124(1981)321.
2. J. Clavilier, J.M. Feliu, A. Aldaz, J. Electroanal. Chem. 243(1988)419.
3. J. Clavilier, S.G. Sun, J. Electroanal. Chem. 199(1986)471.

LEGENDS FOR FIGURES

Figure 1.- (a) Bi covered Pt(111) surface (adspecies coverage 0.82) in the test solution, 0.5M sulphuric acid. 50 mV/s.
(b) Sb covered Pt(100) surface (adspecies coverage 0.86).

Figure 2.- (a) and (b): oxidation of 0.25M HCOOH in 0.5M sulphuric acid solution, first sweep, on the corresponding surfaces shown in Figure 1.

Figure 3.- Summary plots of HCOOH oxidation current densities versus the adspecies coverage for (a) Pt(111)/Bi system and (b) Pt(100)/Sb system.

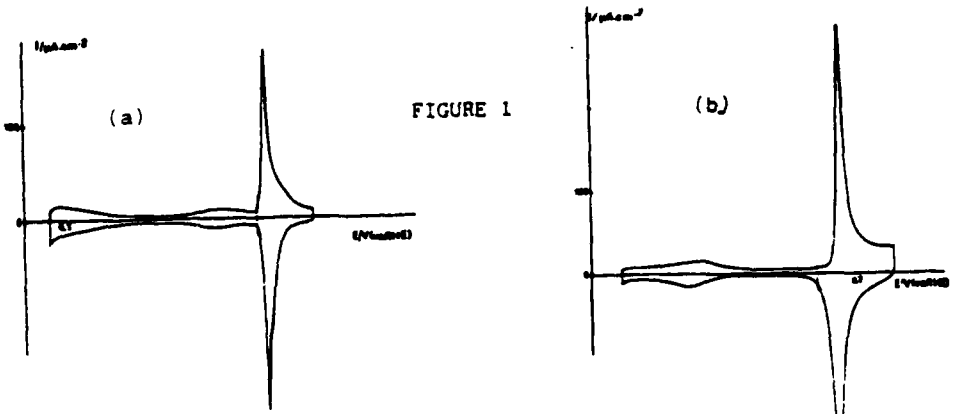


FIGURE 1

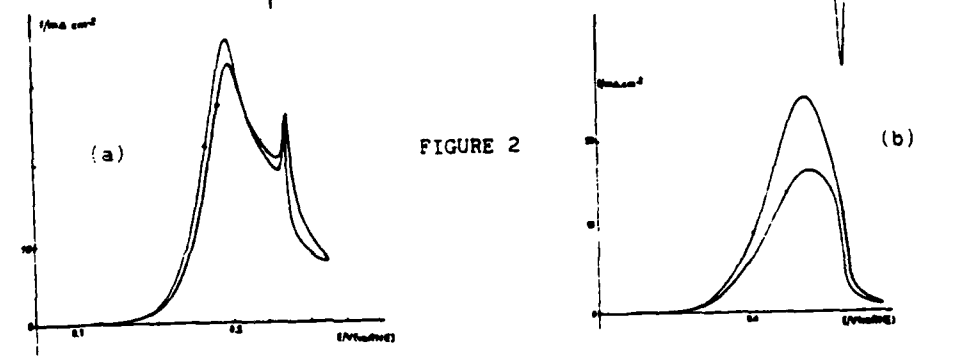


FIGURE 2

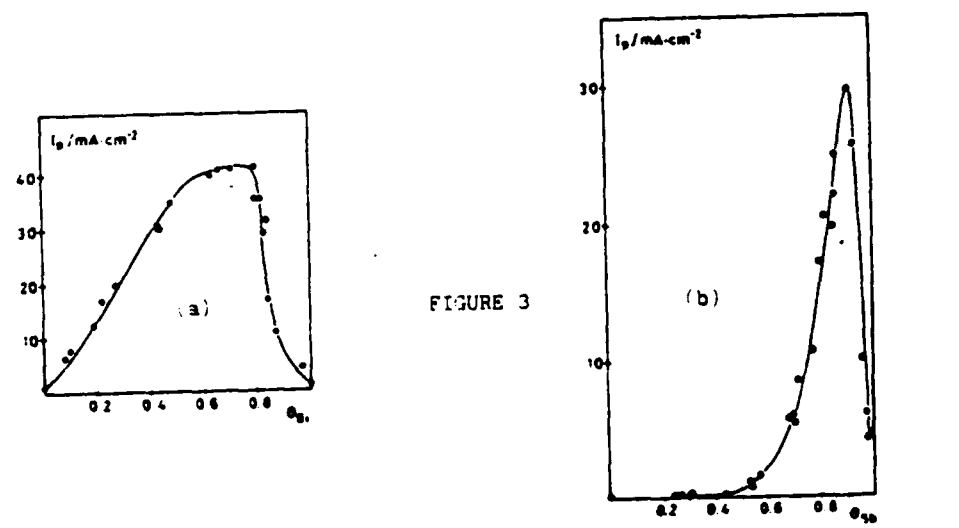


FIGURE 3

MORPHOLOGICAL AND ELECTROCATALYTIC PROPERTIES OF GOLD DEPOSITS ON NaY ZEOLITE

O. ENEA

UA au CNRS n° 350, Université de POITIERS
40, avenue du Recteur Pineau, 86022 POITIERS, France

INTRODUCTION

Gold deposits on Nafion membranes were recently found to be very efficient anodes for the electrocatalytic oxidation of CO [1] and of alcohol vapors [2], [3] . Such activity is principally due to the high roughness of the metallic film and to the proton pumping through the membrane, both properties being allowed by the use of a solid polymer electrolyte (SPE) as support for gold particles.

In addition, Nafion membranes display good electrical conductivity, long term chemical stability and valuable mechanical properties. Unfortunately, Nafion is quite expensive, its use limited at temperatures lower than 200°C and some of its properties may change with the swelling produced by organic solvents. Such disadvantages might be avoided by using inorganic membranes as supports for the metallic deposits.

In this study, the morphology of gold particles deposited on NaY zeolite is described and their electrocatalytic properties are examined for the first time in relation with their use as anodes for the oxidation of some organic (ethanol) or inorganic (ammonia) compounds in the gas phase.

EXPERIMENTAL

Electrolyte solutions were prepared from NaOH (Merck "suprapur") dissolved in deionized "Milipore Q" quality water.

Ethanol vapors were obtained as previously [3] from pure ethanol (pro analysi, Merck) by using an evaporator-condenser system kept at convenient temperatures and flushed with prepurified nitrogen. Ammonia vapors were produced by flushing the prepurified nitrogen through the aqueous NH_4OH solutions, the NH_3 content of which was chosen to obtain the required partial pressure of ammonia vapors.

Small discs (14 mm in diameter, 0.3 to 0.7 mm thick) were prepared by pressing 0.1 to 0.2 g zeolite Y powder ($Na_{56}Al_{56}Si_{136}O_{384}$, 240 H_2O , 7.4 Å diameter of channels) in sodium form.

Each disc of NaY zeolite was mounted at the bottom of a half cell in which an alkaline solution (1M NaOH) of 0.1% wt. sodium borohydride was further introduced. The other side of the disc faced a solution containing 0.1 % wt. of $HAuCl_4$. Gold ions were reduced at room temperature during ca. 80 minutes and then, the metallic film (1 µm to 5 µm thick) was washed, dried, and the second half cell sealed.

All the voltammetric experiments were carried out in a two-compartment cell thermostated at 25°C, the gold film exposed facing the gas compartment being used as working electrode. In the electrolyte compartment, a mercurous sulphate electrode (MSE) connected through a Luggin capillary was the reference electrode, while a C ribbon (Carbon Lorraine) was the counter one.

In a typical experiment, each compartment of the cell was filled with 1M NaOH, pure N_2 bubbled and the "true" surface of Au-NaY zeolite electrode determined with respect to that of an auxiliary working electrode (0.035 cm^2) by comparing their voltammograms. The gas compartment was

further filled, washed, dried and flushed with pure N_2 during 30 minutes before the potential cycling. After the recording of I - E profiles for Au-NaY zeolite electrode under N_2 flow, ethanol or ammonia vapors were introduced and their concentration tested by gas chromatography.

Cyclic voltammetric measurements carried out in the same experimental conditions (50 mV s^{-1} sweep rate, -1.2 to 0.3 V/MSE potential limits, 25°C, 1M NaOH in the liquid compartment), were performed with a conventional electronic equipment. The morphological features of the Au-NaY zeolite electrodes were observed by SEM with a JEOL - 35 CF instrument.

RESULTS AND DISCUSSION

The metal layer exclusively formed on one side of the zeolite disc, appears to consist of small Au particles (diameter > 100 nm) densely packed in a porous film 1 µm to 5 µm thick. The roughness factor (r.f.), calculated as the ratio of the "true" surface (6.47 cm^2 or 5.10 cm^2), stabilized after an appropriate electrochemical treatment, and the geometrical "apparent" surface (1.31 cm^2), was 5.72 and 4.51, respectively, for two of the Au-NaY zeolite electrodes mostly used in this study.

The voltammogram recorded with the gold film facing pure N_2 (curve 1, Fig. 1) is very similar to that obtained when the gas compartment was filled with 1M NaOH, but noticeably modified when ethanol (curve 2, Fig. 1) or ammonia vapors were introduced. An important oxidation peak (A) occurs on the positive scan (curve 2, Fig. 1) in the potential range where the presence of hydroxyl species adsorbed on the surface of gold is seen on the voltammogram recorded under the nitrogen flow (curve 1, Fig. 1).

In the range of relatively low vapor pressures (up to 35 Torr for ethanol and up to 126 Torr for ammonia), $\log i_{max}$ increases linearly with $\log p$ for ethanol as well as for ammonia vapors (Fig. 2).

However, ethanol or ammonia solutions introduced in the gas compartment are almost not oxidized. The use of gaseous reactants enhances the whole electrochemical process because hydration effects and mass-transfer problems are less important.

Au-NaY zeolite electrodes display a number of similar features with Au-Nafion electrodes, do not present swelling problems and can be used at temperatures higher than 200°C, but their chemical and mechanical stability must be improved.

ACKNOWLEDGEMENTS

The author is grateful to Professor M. GUISNET (Université de Poitiers) for enlightening discussions, to Dr. S. GNEP for assistance in the preparation of zeolite discs, to Dr. E. GARNIER for X-ray characterisation of Au-NaY zeolite electrodes, and to Mrs. C. BESSE for the electron microscopy examinations.

REFERENCES

1) H. KITA and H. NAKAJIMA, Electrochim. Acta, 31, 193 (1986).
2) O. ENEA, J. Electroanal. Chem., 235, 393 (1987).
3) O. ENEA, J. Electrochem. Soc., in press.

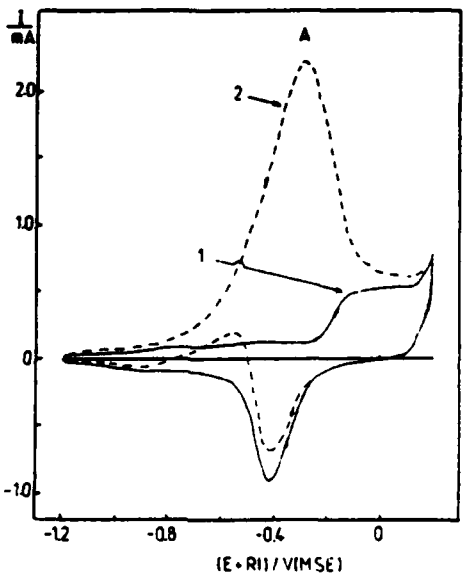


Figure 1 Voltammograms of Au-NaY zeolite electrode.
1) N_2 flow, 2) ethanol vapors, p 11.5 Torr.
Surface area : geometrical 1.31 cm^2, "true" 6.47 cm^2.
Sweep rate 50 mV s^{-1}, 1M NaOH, 25°C.

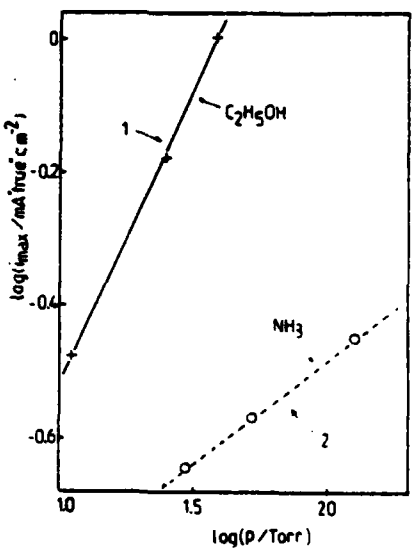


Figure 2 Dependence of i_{max} on the partial pressure p :
1) ethanol vapors from 11.5 to 37.5 Torr (r.f. 5.72);
2) ammonia vapors from 30 to 126 Torr (r.f. 4.50).
Sweep rate 50 mV s^{-1}, 1M NaOH, 25°C.

ELECTROCHEMICAL AND ELLIPSOMETRIC STUDY OF THE REDUCTION PROCESSES OF HYDRATED PLATINUM OXIDE

J.O. Zerbino, C.L. Perdriel and A.J. Arvia

Instituto de Investigaciones Fisicoquímicas Teóricas y Aplicadas (INIFTA). Facultad de Ciencias Exactas, Universidad Nacional de La Plata. Casilla de correo 16, Suc. 4, 1900 La Plata, Argentina

INTRODUCTION: The electrochemical formation of the thick hydroxide platinum layers was investigated using potentiodynamic techniques, X-ray diffractograms and scanning electron microscopy [1].The influence of the characteristics of the square-wave potential perturbation used to grow the hydrous oxide layer and to electroreduce it to platinum overlayer have also been investigated under different experimental conditions [2]. Despite these results the structure of this type of oxide layers is still poorly known. The present work provides a new insight about the structure of this type of oxide layers through the study of its ellipsometric and electrochemical response as well as the study of the electroreduced platinum overlayers resulting from these oxide layers.

EXPERIMENTAL: A cell similar to that reported in previous work was employed [3]. A Rudolph Research type 43702-200E ellipsometer in the null mode was used. The angle of incidence of light was 69° and the angle of the compensator was set at 135°. Measurements were made at 405, 450, 492, 546, 580, and 671 nm, by filtering the light beam before impinging the electrode.

The electrode was a polycrystalline platinum disk of 1.1 cm diameter, which was polished with increasingly finer alumina, ending with 0.05 μm, and further ultrasonic cleaning for 2 min. The supporting electrolyte 1 M H_2SO_4 was prepared from H_2SO_4 (Merck p.a.) and Milli Q (Millipore) water. Solutions were free from oxygen by bubbling purified nitrogen.

RESULTS AND INTERPRETATION: Two types of results are reported, namely, those for the hydrous platinum oxide layer accumulated through a square wave perturbing potential (RSWPS) treatment at 3.12 kHz between 2.4 V and 0.0 V (vs. RHE), during the time t ($5s \leq t \leq 240$ s), and those for the platinum overlayer resulting from the hydrous oxide layer electroreduction.

The ellipsometric parameters (Δ and ψ) were firstly obtained for the original metal surface at 0.06 V and, then, those of the accumulated hydrous oxide layer were measured at 1.5 V, at six wavelength values. The values of Δ and ψ are time dependent, their shift corresponding to a decrease in the oxide layer thickness, although this decrease was always less than 10% for 30 min at 1.5 V. Experimental data shown in Fig. 1 were corrected in order to refer them to a 10 min potential holding at 1.5 V. The correlation of Δ and ψ values for the different t and λ was made on the basis of a single film model approximation. From these correlation the following optical data was obtained in the 405-671 nm range: $1.615 \geq n \geq 1.567$; $0.0138 \leq k \leq 0.0261$. The electroreduction charge density, q/mC cm^{-2}, is related to the ellipsometric film thickness, d_{ox}/Å by the equation: $q = 6.67 \times d_{ox}^{0.557}$.

In the entire spectral range the fitting of results can be satisfactorily made on the basis of a common set of n and k values for any hydrous oxide thickness. From these results one can conclude that the oxide layer is transparent, and it contains a relatively large amount of water. The dashed lines in Fig. 1 correspond to constant thickness values.

The ellipsometric parameters resulting for the electroreduced platinum overlayer (Fig. 2) can be fitted with the same approach used for the case of the hydrous platinum oxide layer in Fig. 1. Data for the electroreduced

platinum overlayer can be grouped into two correlations depending on whether the electroreduction scan rate is in the order of 2 mV s^{-1} or 100 mV s^{-1}, independently of the value of λ. Ellipsometric data (n,k) has been plotted as a function of λ in Fig. 3. The optical indices for 2 mV s^{-1} reveal that the electrodispersed platinum surface is less compact than that resulting at 100 mV s^{-1}. This fact agrees with the electrode roughness measured through the H-adatom electrosorption charge [2].

Finally the correlation between the thickness of the oxide layer (d_{ox}) and that of the electroreduced platinum overlayer (d_r) resulting from ellipsometric data (Fig. 4) exhibits again two linear behaviours depending on the electroreduction conditions of the hydrous oxide layer.

In conclusion, ellipsometric data supports the high water content of the hydrous platinum oxide layers produced through fast periodic perturbing potentials. These layers exhibit n and k values which are practically independent of the layer thickness. Ageing effects associated with the decrease in thickness can be detected through ellipsometry. The electroreduction of the oxide layer furnishes a platinum overlayer with a roughness (compactness and thickness) dependent on the electroreduction conditions.

REFERENCES

[1] A.C. Chialvo, W.E. Triaca and A.J. Arvia, J.Electroanal.Chem., 146, 93 (1983).

[2] A.E. Bolzan, A.M. Castro Luna, A. Visintin, R.C. Salvarezza and A.J. Arvia, Electrochim.Acta (submitted).

[3] M. López Teijelo, J.O. Zerbino, J.R. Vilche and A.J. Arvia, Electrochim. Acta, 29, 939 (1984).

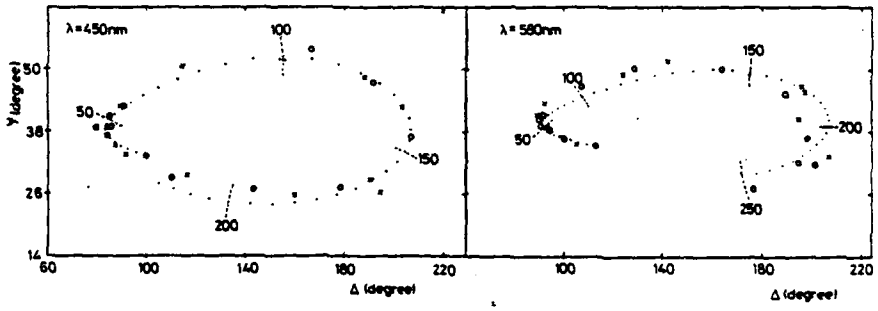


Fig. 1.- Ellipsometric data (Δ-ψ plots) at two different wavelengths corresponding to hydrous platinum oxide layers obtained through RSWPS at 3.12 kHz. The numbers indicate the film thickness in nm.

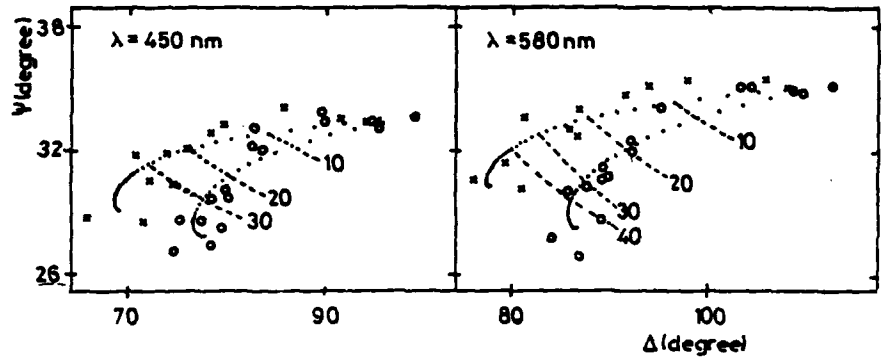


Fig. 2.- Ellipsometric data (Δ-ψ plots) at two wavelengths corresponding to the electroreduced platinum overlayers under different conditions, (x) v = 2 mV s^{-1}, (o) v = 100 mV s^{-1}. The numbers indicate the film thickness in nm.

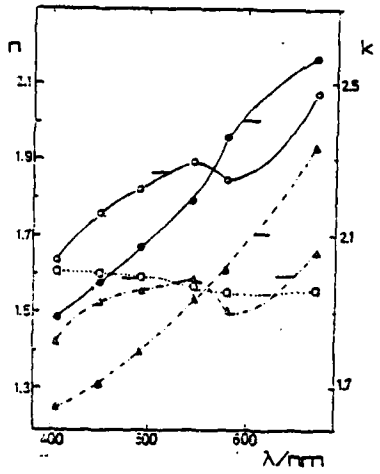


Fig. 3.- n-λ and k-λ plots electroreduced platinum overlayers. (o,● v = 100 mV s^{-1}), (Δ,▲ v = 2 mV s^{-1}). hydrous platinum oxide layer.

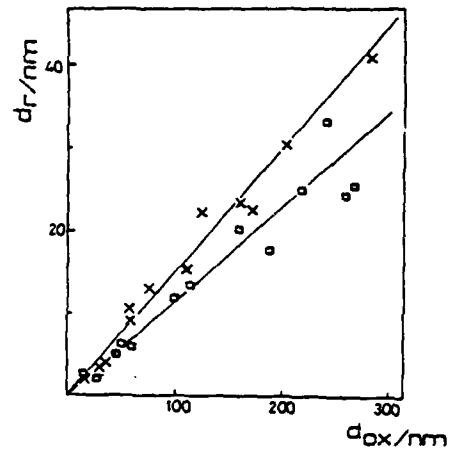


Fig. 4.- d_r vs. d_{ox} plot. (x) v = 2 mV s^{-1}; (□) v = 100 mV s^{-1}.

CORRELATION BETWEEN SERS AND ELECTROCHEMICAL RESULTS IN MEASUREMENTS OF PYRROLE ADSORPTION ON Ag ELECTRODE

J.Bukowska *, K.Jaszczynski and K.Jackowska **
* Laboratory of Intermolecular Interaction
** Laboratory of Electrochemistry, Department of Chemistry,
Pasteura 1, University of Warsaw , 02-093 Warszawa, Poland

This work concerns the results of SERS and impedance measurements of pyrrole adsorption from aqueous solution at pH 6 containing 0.1 M $LiClO_4$ or 0.1 M KCl as supporting electrolyte on roughened, activated by ORC (oxidation - reduction cycling) polycrystalline silver electrode.

The impedance measurements were carried out potentiostatically at potentials changing from -0.3 to -1.2 V and in frequency range from 720 to 0.5 Hz. From that measurements, the capacitance values were determined assuming the series equivalent RC circuit, with accuracy not worse than 5%. The Raman Spectrometer (Cary 82) with Ar^+ ion laser of Spectra Physics operating at 514.5 nm was used for SERS studies.

The comparison of the normal Raman spectrum of 0.05 M pyrrole solution in H_2O with SERS spectrum of roughened Ag electrode immersed in 0.005 M pyrrole solution in 0.1 M KCl/H_2O at -0.9 V vs SCE (Fig.1) shows that:
- the relative intensities of the band in SERS spectrum are changed in comparison to normal Raman Spectrum,
- the band frequencies of $\nu_{C=C}$, ν_{C-N}, ν_1 (ring breathing) pyrrole vibrations at the electrode surface are lower than that in the normal Raman spectrum of pyrrole solution,
- the band frequencies are potential dependent, increasing with cathodic polarization.

Such changes can indicate that the pyrrole molecules are oriented parallely to the electrode surface.

The influence of the electrode potential and of pyrrole concentration on the Raman intensity (I) of the ring breathing mode band ν_1 in 0.1 M $LiClO_4$ (Fig.2a) and 0.1 M KCl solutions (Fig.2b) suggested that in the presence of ClO_4^- ions pyrrole is adsorbed in wider potential range than in the presence of chloride ions.

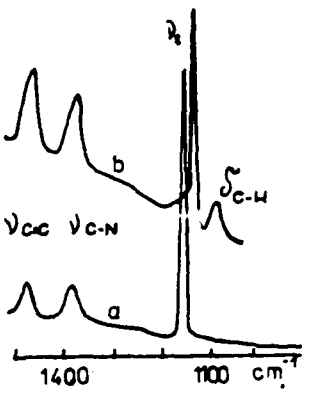


Fig.1

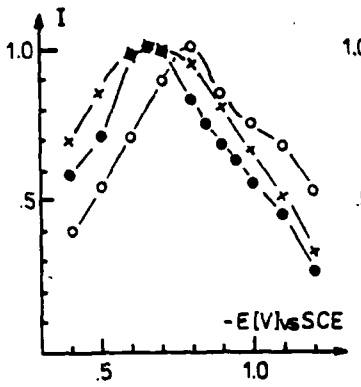


Fig.2a

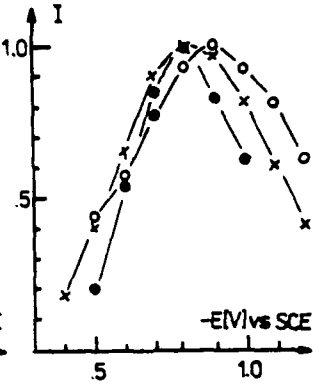


Fig.2b

Fig.1 Comparison between normal Raman spectrum of 0.1 M pyrrole/H_2O (a) and SERS spectrum of 0.1 M KCl + 0.005 M pyrrole (b). E = -0.9 V vs SCE.

Fig.2 Dependence of Raman intensity (SERS spectrum) on the electrode potential of roughened silver electrode in:
a) 0.1 M KCl + (-e-) 0.0005 M pyrrole;
(-x-) 0.005 M pyrrole; (-o-) 0.05 M pyrrole,
b) 0.1 M $LiClO_4$ + (-e-) 0.0005 M pyrrole;
(-x-) 0.005 M pyrrole; (-o-) 0.05 M pyrrole
Intensity I in arbitrary units.

Fig.3 shows the correlation between SERS and differential capacitance (Cs) results obtained on roughened silver electrode in 0.1 $LiClO_4$ + 0.005 M pyrrole (Fig.3a) and in 0.1 M KCl + 0.005 M pyrrole solutions (Fig.3b). As may be seen, the Cs(E) values in 0.1 M KCl blank solution are much higher than those in 0.1 M $LiClO_4$. In both blank solutions the capacitance hump appears at potentials more positive than pzc (accepted to be in the range -0.9 ÷ -1.0 V vs SCE) resulting from the weak specific adsorption of ClO_4^- in 0.1 M $LiClO_4$ and from the strong specific adsorption of Cl- ions in 0.1 M KCl. After addition of pyrrole the Cs values decrease and the hump disappears.

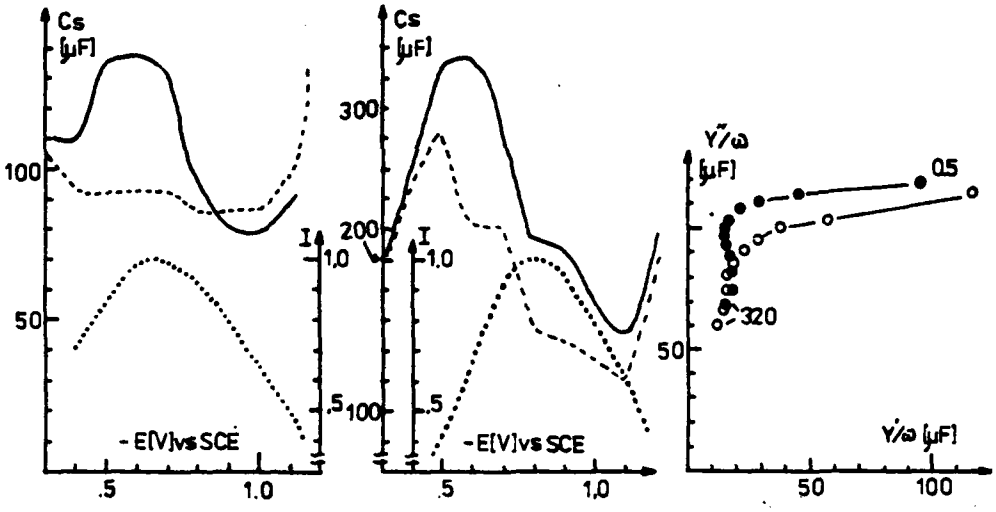


Fig.3a Fig.3b Fig.4

Fig.3 Comparison between capacitance results (Cs in 0.05 Hz) and Raman intensity plotted vs the electrode potential of roughened silver electrode
a) —— 0.1 M $LiClO_4$; --- 0.1 M $LiClO_4$ + 0.005 M pyrrole
... SERS 0.1 M $LiClO_4$ + 0.005 M pyrrole,
b) —— 0.1 KCl ; --- 0.1 M KCl + 0.005 M pyrrole;
... SERS 0.1 M KCl + 0.005 M pyrrole.
Intensity I in arbitrary units.

Fig.4 Plots of Y/ω function for roughened silver electrode in (-e-) 0.1 M KCl + 0.005 M pyrrole and (-o-) 0.1 M $LiClO_4$ + 0.005 M pyrrole. E = -1.2V vs SCE. Electrolyte resistance subtracted. Frequency in Hz.

In the positive range of potentials with respect to pzc, where the specific adsorption of Cl- ions is strong, the Raman spectrum shows lower intensity. In the perchlorate medium, the Raman spectrum can be observed at lower negative potentials, the I vs E curves become wider and are shifted to more positive potentials as compared to the chloride containing solutions. The increase of Cs values at lower frequencies and more negative potentials than -1.0 V vs SCE is caused by the current increase. It is illustrated by the frequency normalized admittance Y/ω (Fig.4).

The result of more complete analysis of impedance and admittance plots as well as the results of cyclic voltammetry are also presented and compared with SERS results.

ELECTROCATALYTIC OXIDATION OF ETHANOL ON PLATINUM SINGLE CRYSTAL ELECTRODES.

M-C. MORIN, J-M. LEGER and C. LAMY,
Laboratoire de Chimie I, Electrochimie et Interactions, U.A. au CNRS n°350, Université de Poitiers, 40, avenue du Recteur Pineau, 86022 - POITIERS , France,
J-L. VAZQUEZ and A. ALDAZ,
Departamento de Quimica Fisica, Universidad de Alicante, Apartado 99, 03080 - ALICANTE, Spain.

INTRODUCTION

The study of the electrooxidation of ethanol on platinum single crystal electrodes is very useful for the understanding of the reaction mechanism. In this way, single crystal electrodes may allow to separate the different reactions involving the adsorbed intermediates. Structural effects of the electrode surface have been previously described with other organic molecules such as methanol (1),formic acid (2) or ethylene-glycol (3).

In this work, the electrocatalytic oxidation of ethanol is studied both in alkaline and acid medium on the three low index Pt single crystal planes, (100), (110) and (111).

EXPERIMENTAL

The single crystal planes were prepared and thermally pretreated according to the technique previously described by Clavilier et al (4). The electrolyte solutions (0.1 M CH_3CH_2OH in 0.15 M NaOH or 0.1 M $HClO_4$) were prepared from Millipore "Milli Q" water and Merck "Suprapur" compounds. Voltammograms were recorded at room temperature and at 50 $mV.s^{-1}$, with a mercurous sulphate reference electrode, but the potentials are quoted vs.the reversible hydrogen electrode (RHE). The upper potential limit was limited to avoid oxygen adsorption. This latter point is important, because oxygen adsorption may lead to surface re-arrangements in particular with the (111) orientation.

RESULTS

The oxidation of ethanol on platinum single crystal electrodes in perchloric medium is shown in Fig 1 for the three planes studied. An important structural effect is observed. The Pt(100) plane exhibits a caracteristic sharp peak (2.1 mA cm^{-2} at 0.75 V/RHE) during the positive sweep similarly to the case of methanol (1). The reverse sweep shows only a wide peak and a slow decrease of the current appears during continuous cycling. The curve corresponding to the Pt(110) plane is different with a peak at 0.72 V/RHE (1.8 mA cm^{-2}) for the positive sweep, and a greatest current density for the reverse with 2.7 mA cm^{-2} at 0.78 V/RHE when the upper limit is fixed at 0.9 V/RHE. An important decrease of these current densities is observed during continuous cycling. The Pt(111) plane exhibits the smallest current densities, but at lower potential (0.5 mA cm^{-2} at 0.55 V/RHE for the positive sweep). On this plane, the curves recorded during the sweeps are superimposed for the lower potential showing a weak poisoning effect.

In order to detect strongly adsorbed species, ethanol was adsorbed at open circuit before the electrode was transfered in the supporting electrolyte. A voltammogram was then recorded in order to oxidize the adsorbed species (5). The curves obtained (Fig 2) show sharp oxidation peaks especially on the Pt(100) plane. Such results prove the formation of strongly adsorbed species, i.e. poisoning species, on the electrode surface and also confirm structural effects. On the other hand, these results in acid medium are very similar to those obtained with methanol (5), showing likely the presence of the same poisoning species.

The voltammograms obtained in alkaline medium for the oxidation of ethanol on Pt(hkl) are shown in Fig 3.

For the Pt(100) plane, a single peak is observed at 0.72 V/RHE during the positive sweep with a current densitie of 4.9 mA cm^{-2}. The broad peak observed during the reverse sweep display two maximum with current densities of 3.5 mA cm^{-2}. For the Pt(110) plane, the peak during the positive sweep is observed at the same potential than for the Pt(100) plane with i= 7.9 mA cm^{-2}. The reverse sweep is caracterized by a main peak at 0.68 V with a shoulder at higher potentials. Concerning these two orientations, an important shift is observed between the two sweeps. This phenomena can be related to poisoning effects.

The results obtained with the Pt(111) plane show the greatest current densities, respectively of 16.8 and 17 mA cm^{-2} around 0.78 V/RHE for the two sweeps.

The electrooxidation of the species resulting from ethanol previously adsorbed at open circuit, according to a method described in (5), is shown in Fig. 4 in the case of the three planes. The oxidation peaks obtained are very weak comparatively to what obtained in acid medium showing a small amount of poisoning species at the surface of the three planes.

REFERENCES

(1) J. CLAVILIER, C. LAMY and J-M. LEGER, J. Electroanal. Chem., 125(1981)249.

(2) J. CLAVILIER, R. PARSONS, R. DURAND, C. LAMY and J-M. LEGER, J. Electroanal. Chem., 124(1981)321.

(3) A. FERNANDEZ-VEGA, J-M. FELIU, J-L. VASQUEZ, A. ALDAZ and J. CLAVILIER, 38th ISE Meeting, Maastricht (The Netherlands), 1987, Abstract 5.4.

(4) J. CLAVILIER, R. FAURE, G. GUINET and R. DURAND, J. Electroanal. Chem., 107(1980)205.

(5) S.G. SUN, Ph. D. Thesis, PARIS(1986)

LEGEND OF THE FIGURES.

Fig.1: Voltammograms of Pt(hkl) in 0.1 M $HClO_4$ + 0.1M C_2H_5OH; 50 mV s^{-1}; 25° C
(---) Pt(100); (——) Pt(110); (·-·) Pt(111)

Fig.2: Oxidation of previously adsorbed ethanol; 50 mV s^{-1}; 25° C; 0.1 M $HClO_4$. (···) without adsorbed species.

Fig.3: As in Fig.1, but in 0.1 M NaOH

Fig.4: As in Fig.2, but in 0.1 M NaOH

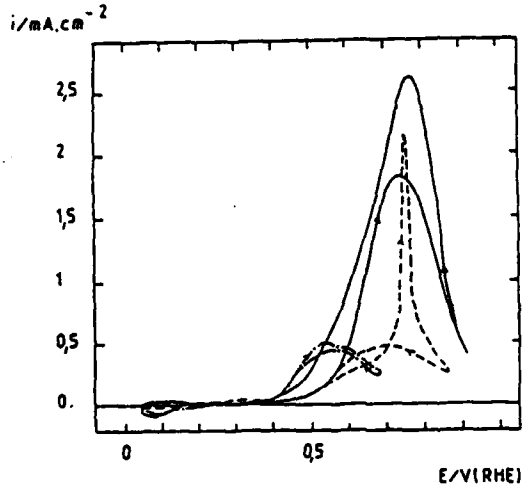


Figure 1

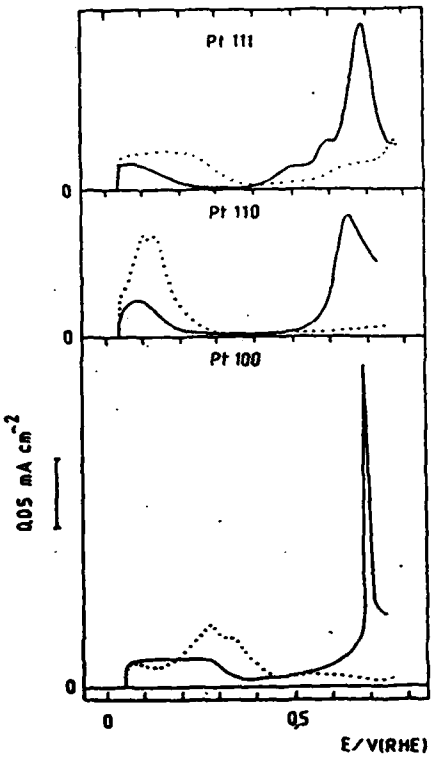


Figure 2

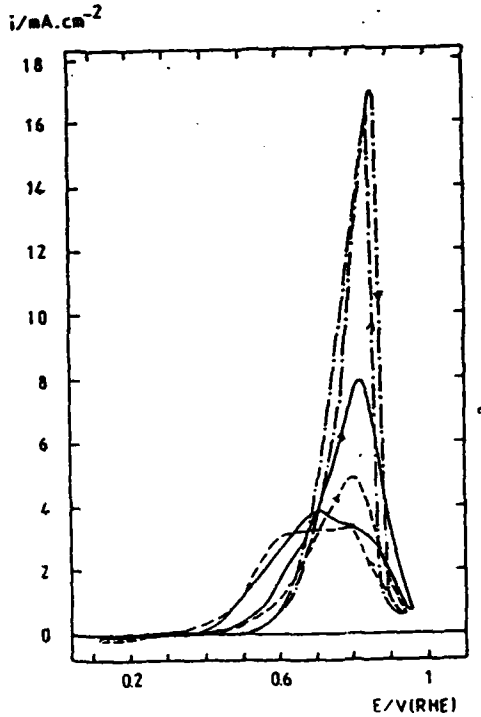


Figure 3

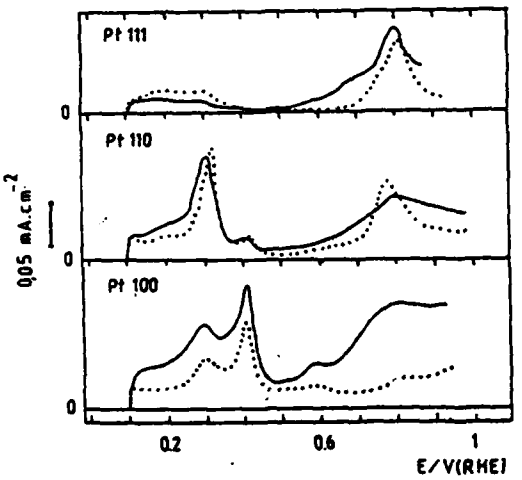


Figure 4

AN EMIRS STUDY OF THE ADSORPTION OF ETHANOL ON PLATINUM ELECTRODES IN ACID MEDIUM

B. BEDEN, J.M. LEGER and C. LAMY,
Laboratoire de Chimie I, U.A. CNRS 350, Université de Poitiers, 40 avenue du recteur Pineau, 86022 Poitiers (France).
J.M. PEREZ and A. ALDAZ,
Departamento de Quimica Fisica, Universidad de Alicante, Apartado 99, 03080 Alicante (Spain).

INTRODUCTION

The study of the adsorption and electrooxidation of ethanol on catalytic surfaces is of great interest, because of its possible use in fuel cells (it is easy to produce it from biomass), and, from a more fundamental point of view, because it is the first term of the series of the aliphatic alcohols having a C-C bond. Although the electrooxidation of ethanol on platinum has been the subject of numerous electrochemical investigation (1), there is still a lot of uncertainties concerning the nature of the adsorbed intermediates. On the other hand, it was not until the late 1970's that "in situ" spectroscopic methods could be developed and applied to the study of electrode-aqueous solution interface, thus leading to detailed information on the nature of the adsorbed intermediates resulting from the chemisorption of various organic molecules, CO, HCOOH, CH_3OH,... (2).

The aim of the present work is to investigate the electrooxidation of ethanol on platinum in acid medium, using EMIRS (Electrochemically Modulated Reflectance Infrared Spectroscopy), a technique developed recently (3) (4).

EXPERIMENTAL

EMIRS experiments were realized with an EMIRS III (Hi-Tek Instruments) grating spectrometer. In short, the principle of the technique is to analyze the infrared beam after a single reflection upon the electrode surface on which the electrochemical oxidation occurs. Modulating the electrode potential (typically with square pulses of 400 mV amplitude, at a frequency of 13.6 Hz), and making a lock-in detection of the infrared signal, allows us to extract the only information coming from the electrode surface. The three-electrode spectroelectro-chemical cell is of a special design to allow the reflection of the infrared beam (through a CaF_2 window) after passing through a thin layer of electrolyte (a few microns thick), in order to minimize the strong absorption of the infrared beam by water.

RESULTS

Typical voltammograms showing the electrocatalytic oxidation of ethanol on polycrystalline platinum are given in Figs. 1a for 10^{-3} M ethanol, and 1b for 1 M ethanol, in 0.5 M $HClO_4$. Oxidation of ethanol obviously starts at potentials more positive than 0.4 V/RHE, allowing thus to modulate the electrode potential between 0 and 0.4 V/RHE, during the spectral accumulation.

Using EMIRS, it was possible to detect numerous absorption bands in the wavenumber range investigated (700-3000 cm^{-1}),

depending both on the electrode potential and on the bulk concentration of ethanol. Most of the bands appeared as pseudo-derivatives, due to the modulation technique (Fig.2).

In agreement with previous results (5) the following attributions, in the range 1600-3000 cm^{-1}, are likely :

2950-3000	(strong)	C-H stretches (from CH_3)
2600-2800	(weak)	C-H (softened C-H stretching modes)
2340	(strong)	weakly adsorbed CO_2 (slightly downshifted)
2040-2060	(strong)	linearly adsorbed CO (resulting from dissociative chemisorption)
1820-1870	(weak)	bridge-bonded CO (resulting from chemisorption
1670-1710	(medium)	complex band, including the contribution of a carbonyl, engaged in an acid or acetyl-like functional group.

The most interesting point is that the relative intensities of the bands vary with the concentration of ethanol in the bulk (fig.3) and averaging times, therefore suggesting that competitive adsorption does occur.

Other characteristic absorption bands were detected in the range 900-1300 cm^{-1}, and discussed in the light of several structural models for possible adsorbed intermediates.

REFERENCES

(1) K.D. SNELL and A.G. KEENAN, Electrochim. Acta, 27 (1982) 1683.

(2) C. LAMY, Electrochim. Acta, 29 (1984) 1581.

(3) A. BEWICK and B.S. PONS, in R.J.H. CLARK and R.E. HESTER (Eds.), Advances in infrared and Raman Spectroscopy, vol.12, Wiley Heyden, London, (1985) chap.1.

(4) B. BEDEN and C. LAMY, in R.J. GALE (Ed.), Spectroelectrochemistry, Theory and Practice, Plenum Press, New York, (1988) in press.

(5) B. BEDEN, M.C. MORIN, F. HAHN and C. LAMY, J. Electroanal. Chem., 229 (1987) 353.

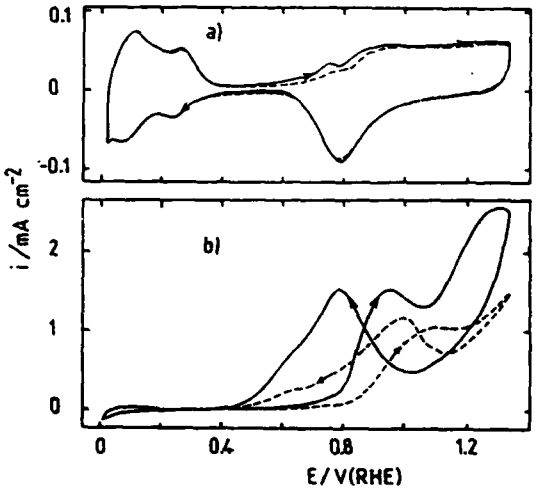


Fig.1 :

Voltammograms of a Pt electrode, showing the oxidation of a) 10^{-3} M C_2H_5OH, b) 1 M C_2H_5OH in 0.5 M $HClO_4$; 25°C, v = 50 mV/s.
(-----) electrode in the bulk electrolyte,
(- - - -) electrode close to the infrared window

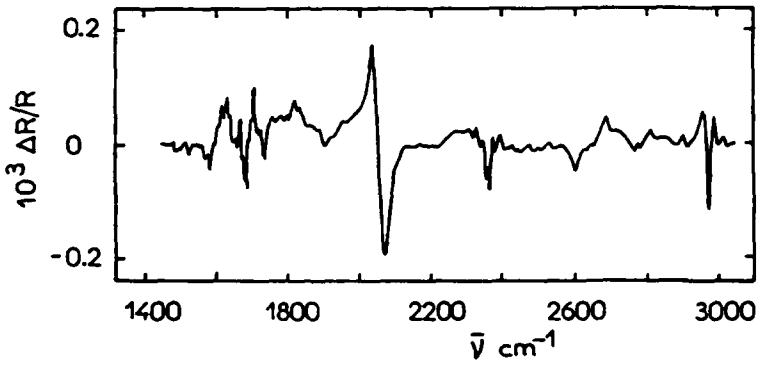


Fig.2 : EMIRS spectrum of the species resulting from the chemisorption of 10^{-3} M C_2H_5OH in 0.5 M $HClO_4$ at a Pt polycrystalline electrode (modulation amplitude 400 mV, mean potential 0.2 V/RHE, f = 13.6 Hz, room temperature, 35 averaged scans).

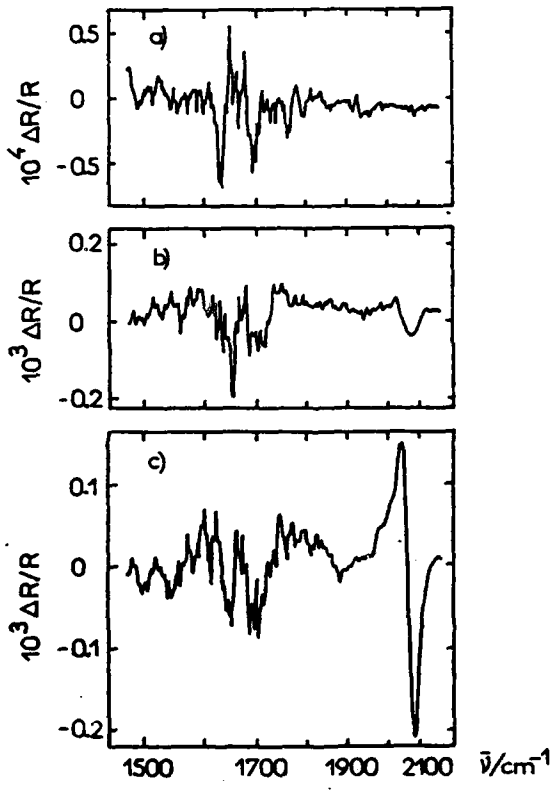


Fig.3 :

EMIRS spectra showing the influence of the bulk concentration of ethanol Same conditions as Fig.2, except for the concentration of C_2H_5OH and the number of averaged scans.
a) 10^{-4} M C_2H_5OH, 25 scans
b) 10^{-2} M C_2H_5OH, 6 scans
c) 1 M C_2H_5OH, 15 scans

ELECTROCATALYSIS OF OXYGEN ON SINGLE CRYSTAL STEPPED SURFACES OF GOLD

S.Štrbac, N.Anastasijević and R.Adžić

Institute of Electrochemistry ICTM and Center for Multidisciplinary Studies, University of Belgrade, Belgrade, Yugoslavia

Electrochemical reactivity of gold towards oxygen has been investigated through oxide formation and oxygen reduction reactions on single crystal electrode surfaces of various orientations.

A pronounced structural sensitivity of both reactions has been found. Oxide formation and oxygen reduction show sensitivity to the discrete structure of the surface, i.e. to the surface orientation, presence of steps, their density and orientation. In alkaline solutions not only kinetic but also the mechanism of O_2 reduction is structure dependent, involving a 2e- reduction on most surfaces and 4e- reduction on Au(100) and only a few vicinal surfaces.

An effort has been made to explane this sensitivity by taking into account some static physical properties (surface energy and work function) and electrochemical (pzc) features of gold single crystals, reflecting the average state of the surface itself. The approach proved only partially suitable and required modifications to account for a sensitivity to a discrete surface structure.

Anodic part of cyclic voltammetry curves for oxide formation on Au(hkl) for the faces investigated in 0.05M H_2SO_4 are given in Fig. 1.

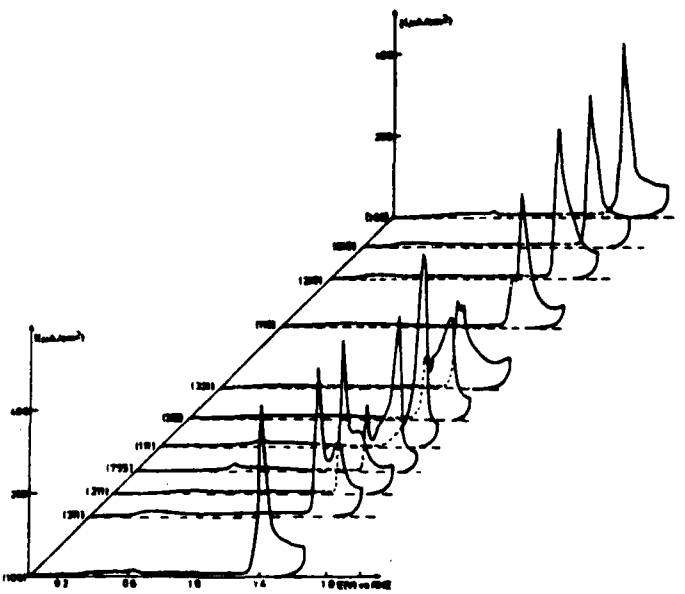


Fig. 1. Oxide formation on Au(hkl) in 0.05M H_2SO_4; sweep rate 50 mVs^{-1}.

Initial stages of oxidation can be correlated with calculated relative surface energy $\gamma(hkl)/\gamma(210)$ (Fig. 2). Adsorbed anions (HSO_4^-, SO_4^{2-}) exert a pronounced effect on this reaction.

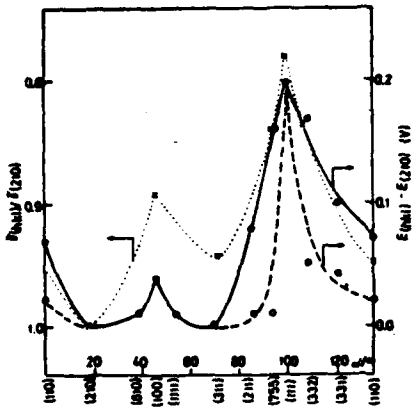
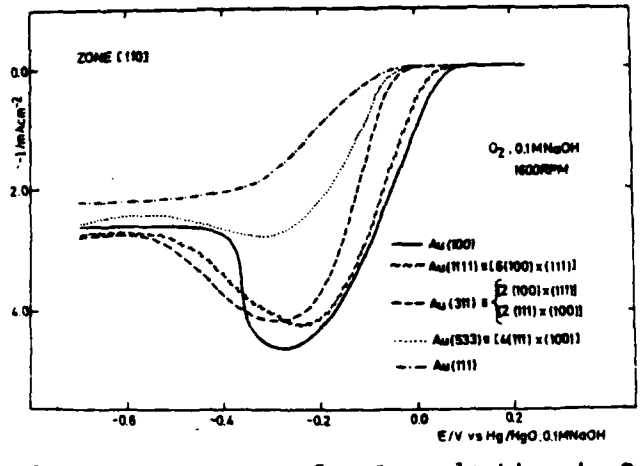


Fig.2. Correlation between $\gamma(hkl)/\gamma(210)$ and E(hkl)--E(210) and E_{av} - E(210) in the dependence of crystallographic orientation.

Oxygen reduction on Au(hkl) in 0.05M H_2SO_4 proceeds as a 2e- process on all faces but with different half-vawe potentials. Taken as a measure of the electrocatalytic activity of Au(hkl) they have been found to be in correlation with the surface energy. The correlation breaks down only for Au(100) face. This suggests that the activation barier of the process is modified by the average energy state of the surface itself. In the case of Au(100) the symmetry factor responsible for its higher activity outweights the electronic factor. No such correlation was found for alcaline solutions.

Both kinetics and mechanism of O_2 reduction on Au(hkl) in alkaline solutions are dependent on crystallographic orientation (Fig. 3). Introduction of steps of the (111) orientation into



Fif.3. Polarisation curves for O_2 reduction in 0.1M NaOH for the faces investigated from the zone [110]. Sweep rate 50 mVs^{-1}; 2500 rpm.

the Au(100) surface causes that the overall number of electrons exchanged gradually decreases from 4 on Au(100) to 2 on the "flat" (111) face.

Rotating disk-ring measurements show no hydrogen peroxide generation on Au(100) in the region of a 4e-reduction (Fig. 4) which coincides with the presence of almost neutral $AuOH^{-(1-\lambda)}$ on the surface. This makes it the most active electrocatalyst for oxygen reduction in alkaline solutions.

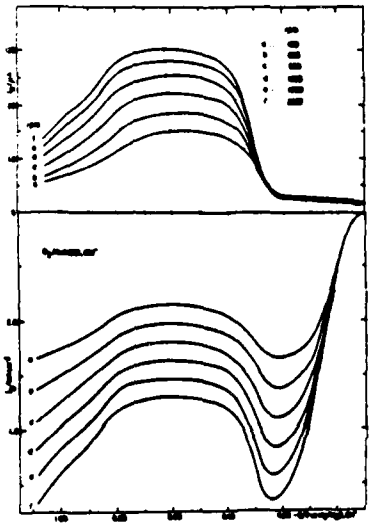


Fig.4. Rotating Au(100) –disk - Pt(poly) ring measurements of O_2 reduction in 0.1M NaOH. Sweep rate 50 mV s^{-1}.

The Au(311)≡[2(100)x(111)] plane also shows a high activity in the region of the $AuOH^{-(1-\lambda)}$ present on the surface but with HO_2^- detected on the ring, which indicates a different mechanism in comparison with Au(100). The reaction goes through a "true parallel" pathway as previously reported by the same authors. For Au(111) kinetic analysis of disk-ring results gives a 2e-serial pathway operating in that potential region but without catalytic decomposition of HO_2^- .

Data for both reactions clearly demonstrate that each crystallographic orientation gives electrode surface with distinct electrochemical properties.

ELECTROSORPTION PROPERTIES OF PLATINUM SINGLE CRYSTAL STEPPED SURFACES

N.M.Marković, N.S.Marinković and R.R.Adžić

Institute of Electrochemistry, ICTM and Center for Multidisciplinary Studies, Belgrade, Yugoslavia, P.O.B. 815.

Hydrogen adsorption and the effects of anion adsorption on that process have been investigated on single crystal platinum stepped surfaces with 15 orientations. The preparation of well-ordered surfaces involved a flame annealing followed by cooling in hydrogen and protection by a drop of water during the transfer into the electrochemical cell. The structure of some stepped surfaces has been verified by LEED.

Local geometry of sites completely determines the adsorption behaviour of hydrogen. No evidence of induced heterogeneity was found. Except for the Pt(111) and some vicinal surfaces, the adsorbate-adsorbate interaction seems negligible. For these surfaces, some lateral repulsion of partially discharged hydrogen adatoms seems operative. Voltammetry shows the effects of terrace orientation, step orientation and step density for all stepped surfaces investigated. It is proposed that, once verified by LEED, these voltammetry curves could be used as a fingerprint for identification of surface structures of platinum electrodes.

Anions exert a pronounced effect on hydrogen adsorption. They are exceptionally strongly held in steps and hydrogen adsorption is concurrent with their desorption. Fig. 1 shows the effects of four different anions on hydrogen adsorption on Pt(100). The shapes of voltammetry curves in $HClO_4$ and H_2SO_4 have been recently discussed in some detail (1). A shoulder at E=-0.04 V in $HClO_4$ and a small peak at E=-0.02 V in H_2SO_4 have been ascribed to the surface imperfections, a small concentration of steps on that plane. It seems difficult to obtain by the above method a well-ordered surface structure with Pt(100). The effect of this feature is seen on curve in HCl as a small peak at E=-0.15 V. A strongly adsorbed chlorides cause adsorption of hydrogen to occur in a narrow potential region upon their desorption.

Further evidence of the presence of some steps on thought to be a well ordered Pt(100) is seen in Fig. 2. It shows that for the stepped surfaces Pt(11,1,1)=6(100)-(111) and Pt(610)=6(100)-(100) the peak appears at the same potential as in Fig. 1. The main peak is smaller than on "flat" Pt(100) as expected and shifted to more negative potentials due to a strong adsorption of chlorides in steps.

Stepped surfaces give also information on the "anomalous" cathodic spike in the anodic going sweep for Pt(100) in HNO_3 (Fig. 1 ad 3). Its nature is not yet well

understood. Fig. 3 shows that the spike for vicinal surfaces is only a half or less than half of that on Pt(100), which strongly suggests that the process requires a two-dimensional order. The six-atoms wide terrace of Pt(11,1,1) and Pt(610) is barely wide enough for such a process to occur.

Vicinals of Pt(111) show a quite different behaviour produced only by a step of different orientations viz., Pt(755)=6(111)-(100) and Pt(332)=6(111)-(111), Fig. 4. The (111)-(111) terrace-step combination gives the sites of the (110) geometry which results in a strong peak at about -0.22 V as for Pt(110). On the other hand, Pt(755) is not active for this reaction, similarly to Pt(111).

Further details of the investigations of the effects of anions on hydrogen adsorption on stepped surfaces will be given and the adsorption isotherms analyzed. The data seems to offer a wealth of information on various adsorption processes on polycrystalline Pt surfaces and a better understanding of the low-index planes.

REFERENCE:

1. N.M.Marković, N.S.Marinković and R.R.Adžić, J.Electroanal.Chem., 241 (1988) 309.

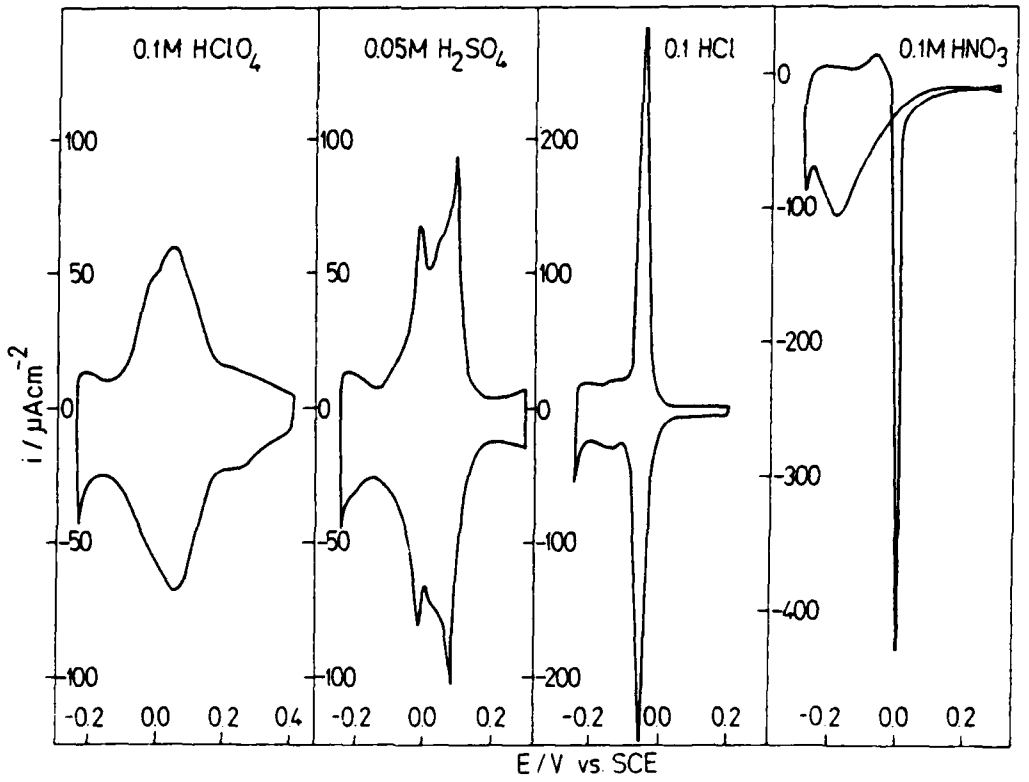


Fig. 1. Cyclic voltammetry for Pt(100) in four different electrolytes. Sweep rate 50 mV/s.

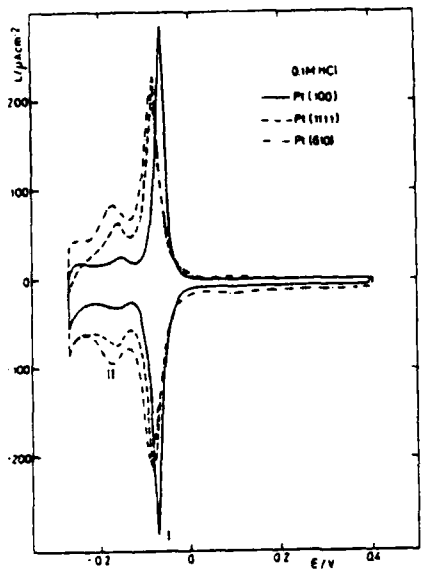


Fig.2. Comparison of the voltametry curves for Pt(100), Pt(11, 1, 1) and Pt(610) in 0,1M HCl. Sweep rate 50 mV/s.

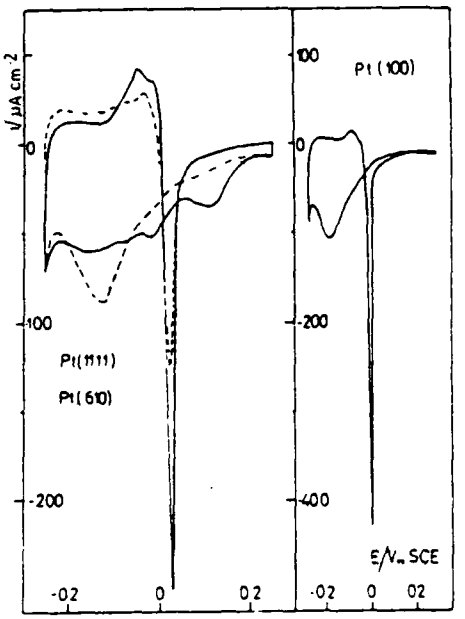


Fig.3. Cyclic voltamograms for Pt(100), Pt(11,1,1) and Pt(610) in 0,1M HNO_3. Sweep rate 50 mV/s.

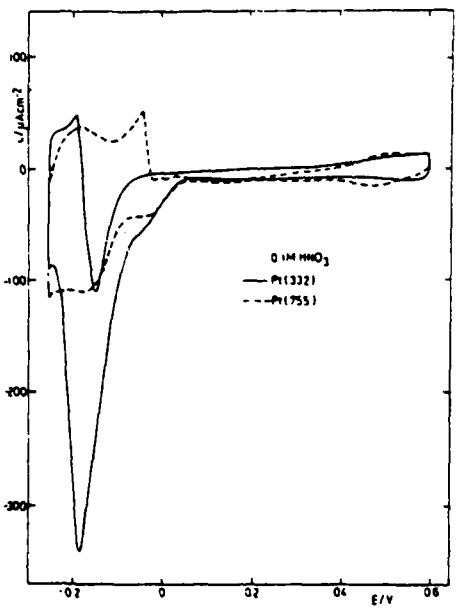


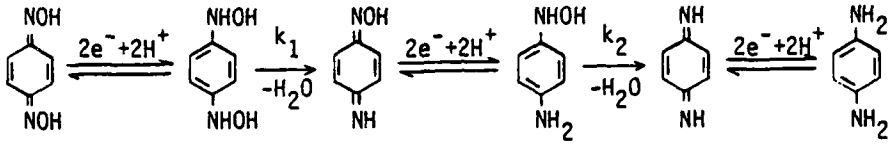
Fig. 4. Cyclic voltammograms for Pt(755) and Pt (332) in 0,1M HNO_3. Sweep rate 50 mV/s.

REDUCTION OF p-BENZOQUINONE DIOXIME ON Pt/M(upd) MODIFIED ELECTRODES IN $HClO_4$ SOLUTIONS: A REACTION MODEL FOR THE ECECE MECHANISM.

G. Kokkinidis and G. Papanastasiou

Laboratory of Physical Chemistry, Department of Chemistry, University of Thessaloniki, 54006 Thessaloniki (Greece).

Introduction: In the study of chemical reactions coupled to electron transfer processes, the ECECE mechanism, where three charge-transfer steps are separated by two chemical reactions, has received little attention. An example of such scheme is the reduction of p-benzoquinone dioxime on Pt/M(upd) electrodes in aqueous acid solutions.



(1)

The chemical steps are dehydration reactions of intermediate hydroxylamines. The electroactive intemediates, generated by the slow chemical reactions, are more easily reducible than the original reactant, thus leading to kinetically-controlled limiting currents.

Chronoamperometric treatment for the ECECE mechanism: Schematically the ECECE process can be presented as follows:

$$A \xrightarrow{n_1 e} B \underset{k_{1b}}{\overset{k_1}{\rightleftharpoons}} C \xrightarrow{n_2 e} D \underset{k_{2b}}{\overset{k_2}{\rightleftharpoons}} E \xrightarrow{n_3 e} F \qquad (2)$$

In the theoretical treatment of the above mechanism it is considered that the experiment is performed at a plane electrode under potentiostatic conditions.

Starting with Fick's second law coupled with suitable kinetic parameters and taking into account the initial and boundary conditions, the Laplace transform method leads to the following final expression for the current as a function of the time t:

$$\frac{i}{F A D^{1/2} C_A^b} = \left[n_1 + n_2 \Phi_1(t) + n_3 \Phi_2(t)\right] \frac{1}{\sqrt{\pi t}} \qquad (3)$$

where

$$\Phi_1(t) = 1 - e^{-k_1 t} \qquad (4)$$

$$\Phi_2(t) = 1 - e^{-k_1 t} - \frac{\sqrt{t}}{2} \exp\left[-\frac{k_1 + k_2}{2} t\right] X(t) \qquad (5)$$

and

$$X(t) = \int_0^t \frac{(1-e^{-k_1 y}) \exp\left(\frac{k_1 + k_2}{2} y\right)}{y^{3/2}} I_o\left[\frac{k_1 - k_2}{2} (t-y)\right] dy \qquad (6)$$

I_o being the modified Bessel function of zero order.

Equation 13 could be applied for studing the kinetics of the chemical reactions involved in the ECECE mechanism of p-benzoquinone dioxime reduction on Pt/M(upd) electrodes. But, because of the non-linear form of equation 13, it seems to be very difficult to determine the values of the rate constants of the chemical steps from chronoamperometric j(t) curves by applying a statistical method. Alternative methods, described below, were chosen for the determination of the rate constants.

Determination of k_1 from ring-disc measurenents: Considering the first two steps involved in the reaction mechanism (reaction 1) of p-benzoquinone dioxime, the rate constant k_1 of the dehydration of the dihydroxylamine intermediate can be determined by means of the equation [1]:

$$\frac{N}{N_k} = 1 + 1.28 \left(\frac{\nu}{D}\right)^{1/3} \frac{k_1}{\omega} \qquad (7)$$

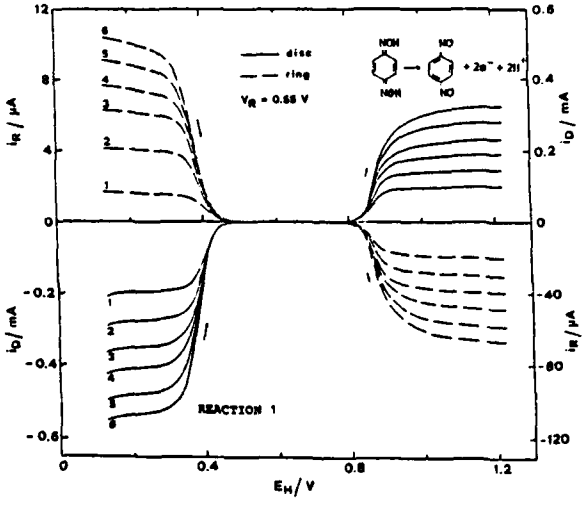


Fig. 1. Ring-disc measurements for p-benzoquinone dioxime (10^{-3} M) reduction and oxidation on Pt in 0.5 M $HClO_4$ in the presence of 2.5×10^{-4} M $Bi(ClO_4)_3$. $|dE/dt| = 10$ mV s^{-1}. Rotation frequency f Hz: (1) 8.33; (2) 18.33; (3) 33.33; (4) 50; (5) 75; (6) 100.

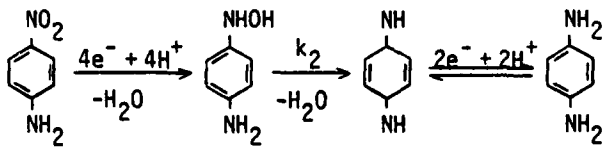
where N_k is the kinetic and N the ordinary collection efficiency of the ring-disc electrode.

The kinetic collection efficiency for the chemical reaction can be determined as a function of the rotation frequency from the ring-disc experiments on Pt/Bi(upd) presented in Fig. 1. At $V_{ring} = 0.55$ V only the p-phenylenedihydroxylamine intermediate is oxidized back to p-benzoquinone dio-

xime when the disc potential is on the plateau of the reduction wave, since the other reaction products or intermediates are oxidized at more positive potentials. The kinetic collection efficiency will be $N_k = I_R/I_D$. I_R is the ring current when the disc potential is on the plateau of the reduction wave. I_D should be the disc current corresponding to the first two-electron step reduction of p-benzoquinone dioxime to p-phenylenedihydroxylamine. Direct measurement of this is not possible, but it is obvious that it should be similar to that corresponding to the two-electron oxidation of p-benzoquinone dioxime to p-dinitrosobenzene on the disc electrode.

From the slope $d(1/N_k)/d(1/\omega) = 2.979$ the value of k_1 at T = 298 K was determined; $k_1 = 44 \pm 5\ s^{-1}$. For this determination values $\nu = 8.929 \times 10^{-3}\ cm^2\ s^{-1}$, $D = 6.56 \times 10^{-6}\ cm^2\ s^{-1}$ and $N = 0.21$ have been used. The ordinary collection efficiency of the ring-disc electrode was evaluated from the ring-disc data of the system p-benzoquinone dioxime/p-dinitrosobenzene, which is free from chemical complications.

Determination of k_2 from disc measurements of p-nitroaniline: The reduction of p-nitroaniline proceeds through an ECE mechanism, where the slowest step is the dehydration of the p-hydroxylaminoaniline intermediate.



(8)

p-Nitroaniline gives well formed reduction wave on a Pt/Pb(upd) rotating disc electrode in the range between the reversible potentials of hydrogen and lead. Accurate values of n_{app} at different rotation frequencies were obtained after correction of the limiting current densities with respect to hydrogen evolution. The data were analysed according to the equation proposed by Filinovskii [2].

$$\frac{n_{app}}{n_1} = 0.94 \left[1 + \frac{n_2}{n_1} \left(1 - \frac{(1 + \delta^2 k/1.9D)^{1/2}}{1 + \delta^2 k/D} \right) \right] \qquad (9)$$

where $n_1 = 4$, $n_2 = 2$ and $\delta = D^{1/3} \nu^{1/6} \omega^{1/2}$. The mean value of k_2 at T = 298 K was found; $k_2 = 13.8 \pm 0.8\ s^{-1}$.

References

1) W.J.Albery and S.Bruckenstein, Trans. Faraday Soc., 62, 1946 (1966).
2) V.Yu.Filinovskii, Elektrokhimiya, 5, 635 (1969).

THE INFLUENCE OF SPECIFIC ADSORPTION ON THE ELECTRONIC SURFACE STATES OF Ag(111) AND Ag(100)

C. Franke, G. Piazza and D. M. Kolb*

Fritz-Haber-Institut der Max-Planck-Gesellschaft,
Faradayweg 4-6, D-1000 Berlin 33, FRG

Surface states are electronic states which are strongly localized at the surface of a solid. They are a consequence of lattice termination, and exist in energy gaps of the two-dimensional (surface) band structure (so-called crystal-induced surface states /1/). They are an intrinsic property of the clean surface and are usually quenched by adsorption processes /2/. The surface band structures of Ag(111) and Ag(100) with surface states A and B are shown in Fig. 1 /3-5/.

The existence of surface states at the metal-electrolyte interface has been demonstrated in the past for all three low-index faces of Ag and Au /3-6/. It was shown that surface states are readily detected by potential-modulation experiments, such as electroreflectance (ER) spectroscopy, because the electrode potential shifts the energetic position of the surface states with respect to that of the bulk states. Hence, optical transitions between occupied bulk states and empty surface states become potential-dependent in their energy; the transitions shift to higher photon energies with increasing positive electrode potential. Such a dependence contains information about the potential difference between metal surface and the position of maximum density of the surface state, which is believed to be about 0.1 nm outside the metal; i.e., in the double layer region/5/.

In Fig. 2 are shown the ER spectra of Ag(100) in 0.5 M $NaClO_4$ for various bias potentials. The pronounced minimum in $-\Delta R/R$, which shifts markedly with electrode potential, is caused by the optical transition from bulk states about 1 eV below the Fermi level into surface state A at $\bar{X}$ of the surface Brillouin zone /3,5/. As has been pointed out earlier /3-5/, the shift in transition energy with potential is surprisingly large in the case of Ag; it is 0.9 eV/V for this transition in KPF_6 solution and increases with specific adsorption.

In order to establish the influence of specifically adsorbing ions on the surface states, a systematic study was performed for Ag(111) and Ag(100) in electrolytes containing PF_6^-, ClO_4^-, SO_4^{2-}, Cl^-, Br^- or I^- /7/. In Fig. 3, as an example, the effect for Ag(111) of increasing chloride concentration is demonstrated: the transition energy is shifted towards lower wavelengths (corresponding to an increase of positive charge on the metal) and simultaneously the surface state feature is attenuated and finally disappears. A similar behaviour is observed for surface state A of Ag(100).

The energetic position for the optical transition into surface state A of either Ag(111) or Ag(100) is such that the low-coverage region of chloride adsorption is readily tested. For the very positive electrode potentials, which would be required to achieve maximum Cl^- coverage, the optical transition is shifted in the case of Ag(111) out of the accessible wavelength range (i.e., $\lambda < 250$ nm) or in the case of Ag(100) into the interband transition ($\lambda < 320$ nm). For detection of surface state B of Ag(100), however, very positive potentials are needed in order to move the optical transition from very low energies into the near-IR region, where the transition is no longer masked by water absorption /4/. The result for Cl^- adsorption from a 0.1 M KCl solution is shown in Fig. 4, where the ER-effect is

plotted as a function of potential for various wavelengths. Under such high-coverage conditions, surface states are expected to be completely quenched by the Cl^- adlayer. Yet, two derivative-like features in $-\Delta R/R$ are clearly seen, which markedly shift with wavelength (this is equivalent to a shift in transition energy with potential). Furthermore, both features are located in energy symmetrically around that surface state feature observed in the absence of specific adsorption (see insert). We ascribe the two spectral features in the ER-spectrum, Fig. 4, to optical transitions within a silver-halide surface-complex, the energetic levels of which are affected by the electrode potential. The close similarity in transition energies for surface state B and the two features in Fig. 4 suggests that surface state B is involved in bond formation between Ag(100) and the chloride ion.

The main results of this study can be summarized as follows. The surface states of Ag(hkl) are neither quenched by water nor by weakly adsorbing species such as perchlorate or sulfate ions. The large shift with electrode potential of the surface states relative to the bulk states, which is observed in KPF_6, suggests a strongly non-linear potential drop across the electric double layer even in the absence of specific adsorption. The initial stages of halide adsorption cause the attenuation of the surface states, often accompanied by an energy shift, while at high coverages new spectral features appear which are tentatively assigned to optical transitions within a surface complex. Surface states A and B of Ag(100), which have s- and p-character, respectively, react quite differently with one and the same adsorbate.

References

/1/ A. Goldmann, V. Dose and G. Borstel, Phys. Rev. B32 (1985) 1971.
/2/ B. Reihl, K. H. Frank and R. R. Schlittler, Phys. Rev. B30 (1984) 7328.
/3/ D. M. Kolb, W. Boeck, K. M. Ho and S. H. Liu, Phys. Rev. Lett. 47 (1981) 1921.
/4/ W. Boeck and D. M. Kolb, Surface Sci. 118 (1982) 613.
/5/ K. M. Ho, C. L. Fu, S. H. Liu, D. M. Kolb and G. Piazza, J. Electroanal. Chem.150 (1983) 235.
/6/ S. H. Liu, C. Hinnen, C. N. v. Huong, N. R. DeTacconi and K. M. Ho, J. Electroanal. Chem. 176 (1984) 325.
/7/ C. Franke, G. Piazza and D. M. Kolb, Electrochim. Acta (Telavi issue) in press.

*Permanent address: Chemistry Department, University of Bologna, I-40126 Bologna.

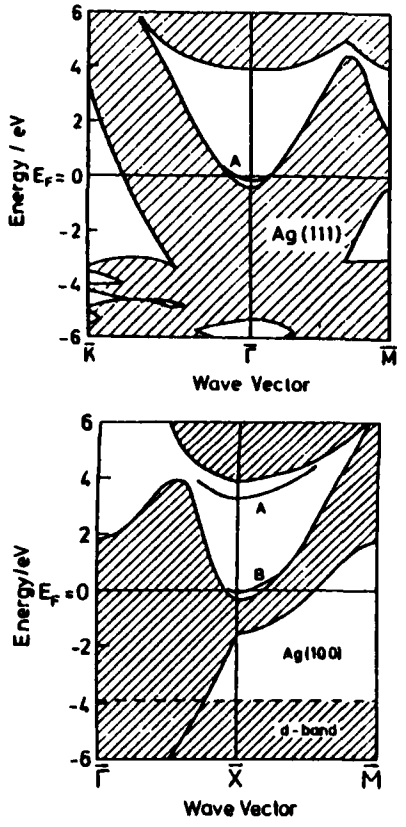


Fig. 1: Surface band structures of Ag(111) and Ag(100). A, B: surface states.

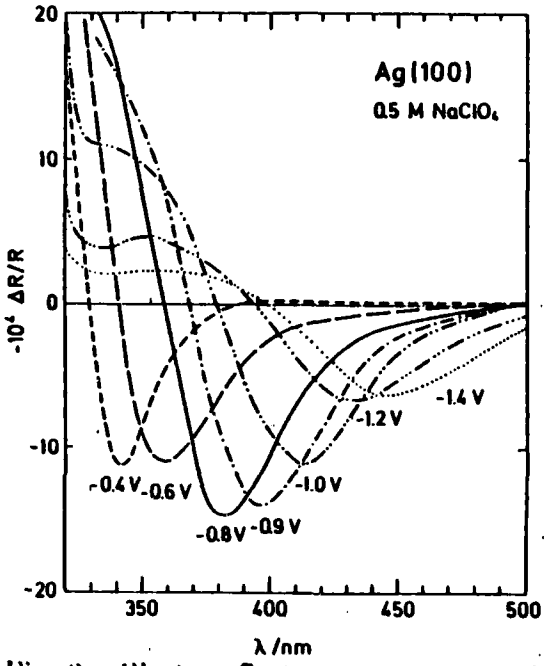


Fig. 2: Electroreflectance spectra of Ag(100) in 0.5 M $NaClO_4$ for various bias potentials. The dip in $-\Delta R/R$, which shifts in wavelength with electrode potential, is caused by an optical transition into an empty surface state (A). p-polarisation. $\Upsilon_1 = 45°$. $\Delta U_{pp} = 100$ mV.

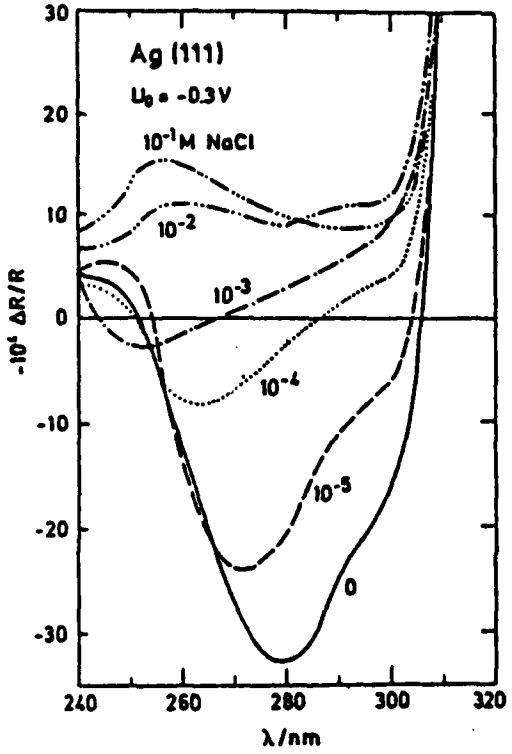


Fig. 3: Influence of chloride adsorption on the surface state feature of Ag(111) in 0.5 M $NaClO_4$ with different amounts of NaCl added. p-polarisation.
$\vartheta_1 = 45°$. $U_0 = -0.3$ V vs. SCE.
$\Delta U_{pp} = 100$ mV.

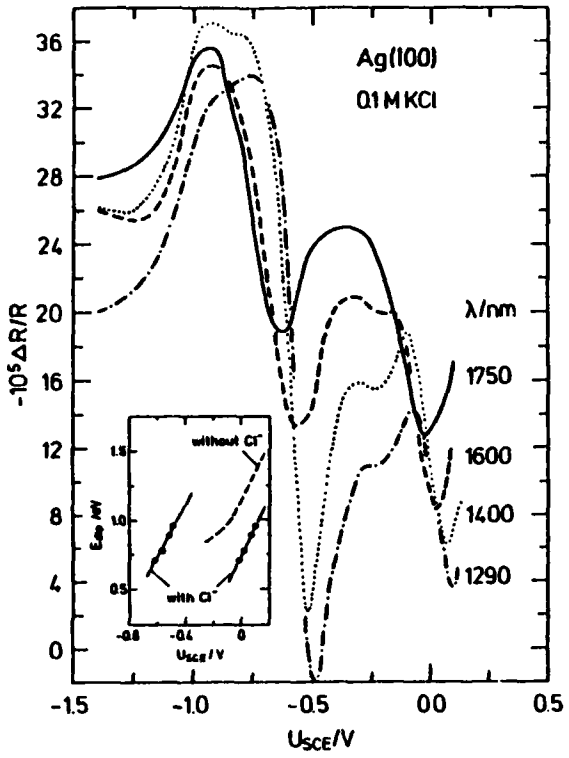


Fig. 4: Electroreflectance effect of Ag(100) in 0.1 M KCl as a function of electrode potential for various wavelengths. Normal incidence.
$\Delta U_{pp} = 100$ mV. The insert shows the change in transition energy E_{dip} with electrode potential for 0.5 M NaF /4/ and for 0.1 M KCl.

ELECTROCHEMICAL INVESTIGATION ON CHLOROPHYLL A DIFFERENT AGGREGATES IN WATER-ACETONE MIXTURES

A. Agostiano, M. Caselli, *M. Della Monica, **F.K. Fong.

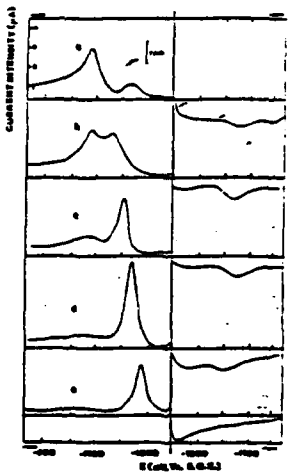
* Dipartimento di Chimica- Università di Bari
**Chemistry Department- Purdue University, West Lafayette (USA)

The oxidation and reduction of water photocatalized in vitro by Chlorophyll is a matter of great interest. Photooxydation has been observed when the chlorophyll is deposed on a metallic surface or at the interface between non-mixable liquids.

The characterization of the photocatalytic chlorophyll has focused the efforts of several research groups. The action spectra of the photooxidation of water in presence of chlorophyll a (Chl a) on a metallic surface was shown to follow closely the absorption spectra of the dihydrated oligomers (Chl a. $2H_2O)n$.[1] The dihidrate dymer (Chl a.$2H_2O)_2$ absorbing at 678 nm was proposed as a model for the reaction center of PS II in green plant photosynthesis.[2] Recently the interest on Chl a aggregation and photochemistry has turned to Chl a solutions in water-acetone mixtures. By spectroscopic measurements was showed that the dihydrated dymer exists in the bulk solution only in a minor exent in the presence of the monomer form up to a 40:60 water-acetone composition.[3]The equilibrium is given by

Chl a.Ac (662 nm) $+4H_2O$ - (Chl a.$2H_2O)_2$

This equilibrium can be investigated by polarographyc and related tecniques(Fig.1).



[1]M. J. Showell, F.K.Fong, J.A.C.S. 104,277,(1984)
[2]F.K.Fong, light reaction patu of photosynthesys, Vol.35 p.277-329 (1982)
[3]A.Agostiano, K.A.Butcher, A.J.Gotch, F.K.Fong, Chem. Phys. Lett. 137, 37 (1987)

Two well defined peaks are recorded when a fast triangular sweep is imposed on a fixed mercury electrode mantained for a given time at a fixed potential. An increase of the water content is accompanied by an increase of the intensity of the peak at more negative potential relatively to that at the less negative potential. For the Chl a in 50:50 water-acetone mixture a single peak at -1270 mV was observed

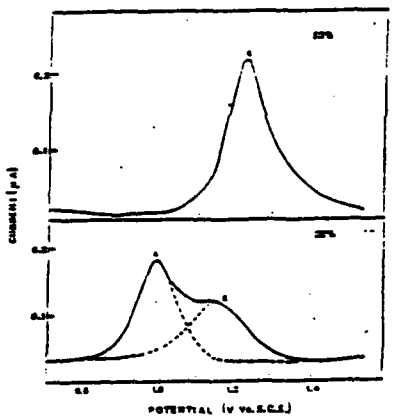
A dependence of the peak potential on the solvent composition was also noted.

The relative intensity of the two peaks depends on the accumulation time.

A third polarographic peak at -1424 mV is observed in 50:50 water-acetone mixtures when the Chl a concentration exceeds 1 X 10^{-5}M. Thi peak can be attributed to the oligomer of the Chl a dihydrate.

From the electicity amount,a coverage area of 259 and 587 A^2 can be calculated for the Chl a.Ac and the dihydrate dymer respectively.

These results are confirmed by differential pulse measurements(Fig.2).



This tecnique can be used in order to determine the differently solvated species of Chl a in water-acetone mixtures.The results can be interpreted by employing the relationship thet rule the adsorption of an electroactive species.

KINETICS OF THE HEXACYANOFERRATE(II)/(III) COUPLE AT PASSIVE TITANIUM ELECTRODES

T.Hurlen and W.Wilhelmsen
Department of Chemistry, University of Oslo,
P.O.Box 1033, Blindern, N-0315 Oslo 3, Norway

The $Fe(CN)_6^{4-}/Fe(CN)_6^{3-}$ reactions have been studied by stationary and transient polarization measurements on potentiostatically well stabilized (18–20 h) passive titanium electrodes at 25 °C. The reactions appear first-order in reactant dependence, provided an extra half-order non-reactant inhibiting effect of $Fe(CN)_6^{4-}$ is built into the rate constants. They further depend on the electrode potential, the solution pH, the passive film thickness and the way of forming the passive film. The results support that the electron exchange mainly occurs with the metal through thin passive films (< 45 Å) and with the conduction band (or an impurity band) in the oxide of thicker films [1–3]. The work builds on previous work of ours on the passive behaviour of titanium [4,5].

Stationary data

When $Fe(CN)_6^{3-}$ and/or $Fe(CN)_6^{4-}$ was added to a cell in which a galvanostatically formed (with $j = j_f$ till $U = U'$) and potentiostatically stabilized (at U' for 18–20 h) passive titanium electrode was held at its stabilization potential (U'), the current density on the electrode changed by $\Delta j'$ from its mostly negligible quasi-steady passive current ($j_p \approx 10^{-6} Acm^{-2}$). This change was found to depend not only on U' and the concentrations (ox) and (red) of the redox components, but also on j_f and the pH of the cell solution.

In Fig.1, data are presented for $\Delta j'$ *vs* U' at given pH, j_f, (ox) and (red). Also a scale for the passive film thickness (δ) is provided, since δ here is a known linear function of U' [4]. With higher j_f or at higher pH, analogous results were obtained, but with lower values for $\Delta j'$.

In Fig.2, effects of (ox) and (red) on $\Delta j'$ at given j_f, pH and U' are exemplified. Altogether, such results of the present work fit with the following suggestively written rate equations:

$$j'_+ \approx \Delta j' = F[k_+(red)^{-\frac{1}{2}}](red) \qquad U' > U_{rev} \tag{1}$$

$$-j'_- \approx -\Delta j' = F[k_-(red)^{-\frac{1}{2}}](ox) \qquad U' < U_{rev} \tag{2}$$

where k_+ and k_- are rate constants which depend on U' (or δ), j_f and pH, and the expressions in brackets may be considered first-order rate constants depending also on (red). The two lines in Fig.2 have been drawn with slopes of $\frac{1}{2}$ or 1 in accordance with the equations (1) and (2), respectively. Positive test results directly on the (red) dependence in (2) also have been obtained.

Transient data

Initial polarization data have been determined from potentiostatic transients following square single-pulse potential excursions away from a stationary state obtained as described above. Such data generally obey the Tafel law with slope depending on the state from which excursions are made. Also, corresponding anodic and cathodic Tafel lines (applying to the same starting state for the potential steps) generally were found to intersect each other at the reversible redox potential, yielding a common value for the exchange current (j_o) of the redox couple under the conditions applying.

In Fig.3, exchange current and Tafel slope data thus obtained are presented as functions of U' or δ. The anodic (α_+) and cathodic (α_-) symmetry factors are defined by writing $b = 2.303 \times \frac{RT}{\alpha F}$ for the numerical Tafel slope. With increasing U' or δ, j_o falls exponentially to a value roughly maintained for $U' > 0.2$ V(sce) or $\delta > 45$ Å, and a change in symmetry occurs by α_+ decreasing and α_- increasing. A rather strange asymmetry appears with the thinnest passive films studied.

The results of Fig.3 largely agree with expectations for the electron exchange mainly occuring with the metal through sufficiently thin passive films (possibly by resonance tunneling) and with the conduction band (or an impurity band) in the semiconducting oxide of thicker films [1-3]. Support for this is given also by the stationary data of Fig.1.

In Fig.4, data are presented for j_o *vs* c under conditions of $c = (\mathrm{ox}) = (\mathrm{red})$ and $\delta \approx 57$ Å. These results, which illustrate effects also of pH and j_f, yield:

$$j_o = Fkc^{\frac{1}{2}} = F[k(red)^{-\frac{1}{2}}]c \qquad (3)$$

in accordance with equations (1) and (2). The lines in Fig.4 have all been drawn with slope of $\frac{1}{2}$.

The suggested non-reactant inhibiting effect of $Fe(CN)_6^{4-}$ has much in common with the pH effect and may perhaps have a related explanation through adsorption and surface charge effects. We have not yet any detailed explanation for it.

REFERENCES

1. K.E.Heusler and K.S.Yun, *Electrochim. Acta* **22**, 977 (1977).
2. S.R.Morrison, *Electrochemistry at Semiconductor and Oxidized Metal Electrodes*. Plenum, New York (1980).
3. W.Schmickler and J.W.Schultze, in *Modern Aspects of Electrochemistry*(Edited by J.O'M.Bockris, B.E.Conway and R.E.White), No.17, Chapter 5. Plenum, New York and London (1986).
4. T.Hurlen and W.Wilhelmsen, *Electrochim. Acta* **31**, 1139 (1986).
5. W.Wilhelmsen and T.Hurlen, *Electrochim. Acta* **32**, 85 (1987).

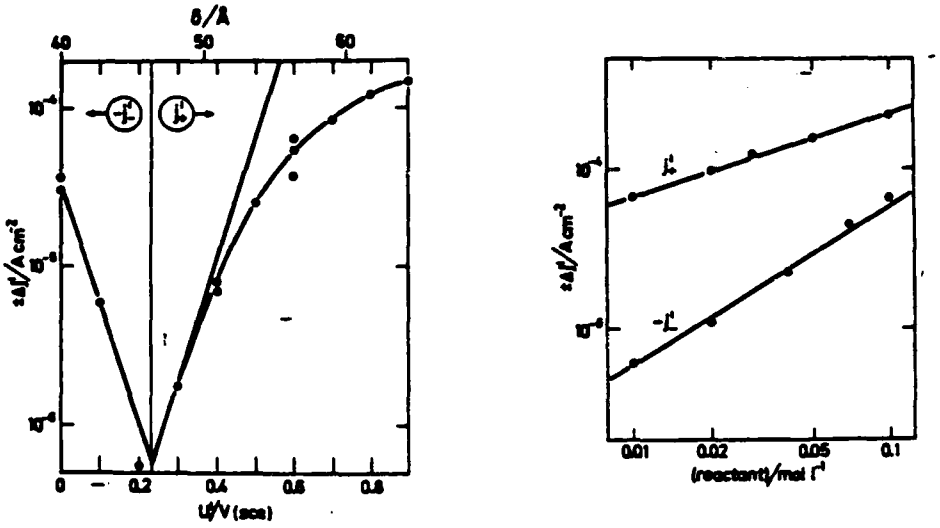


Fig.1. Stationary Tafel data (pH = 3.0, $j_f = 2\ \mu Acm^{-2}$, (ox) = (red) = 0.01 M and quasi-steady passive film thickness at each potential as noted by top scale).

Fig.2. Stationary rate vs reactant concentration at 0.01 M product concentration (pH = 3.0, $j_f = 2\ \mu Acm^{-2}$, U' = 0.6 and 0.1 V(sce) for j'_+ and j'_-, respectively).

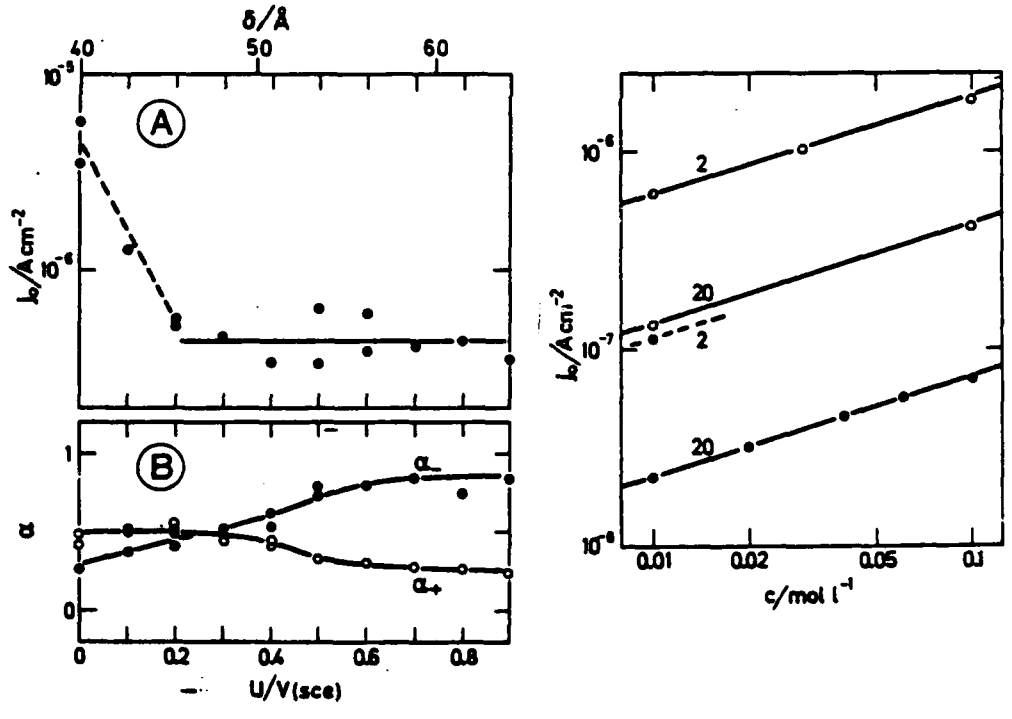


Fig.3. Exchange current (A) and symmetry factors (B) from initial Tafel data for various U' or δ (pH = 3.0, $j_f = 2\ \mu Acm^{-2}$, (ox) = (red) = 0.01 M).

Fig.4. Exchange current vs c = (ox) = (red) for $\delta \approx 57$ Å and $j_f/\mu Acm^{-2}$ as given at the curves. (o) pH = 3.0, U' = 0.6 V(sce). (•) pH = 4.7, U' = 0.5 V(sce).

OPTICAL PROPERTIES OF Hg-ELECTRODE STUDIED BY SURFACE PLASMON TECHNIQUE

A. TADJEDDINE, A. RAHMANI, G. PIAZZA* and M. COSTA

Laboratoire d'Electrochimie Interfaciale du CNRS
1, Pl.A. Briand F-92195 MEUDON PRINCIPAL CEDEX

The rôle of mercury in interfacial electrochemistry has been centered mainly on the description of the structure of the electric double layer at the contact between the metal and the electrolytic solution. The surface electronic structure of mercury has been so far the concern of physicists and results are still discussed. One has been confronted to the difficulty that, depending on the measurement technique employed, the bulk dielectric function in the optical frequencies range may either be in good agreement with or exhibits significant deviation from the classical Drude formula [1-5]. Our aim is the study of the optical properties of mercury in contact with electrolytic solutions under electrical polarization. We present here the first step of our investigation. It deals with the preparation of mercury films supported on platinum base which can be used as vertical electrode in our experimental set-up and their characterization by means of surface plasmon excitation technique.

PREPARATION OF THE SAMPLES

The present optical scheme of our apparatus cannot allow the use of an horizontal mercury surface. This difficulty has been overcome by means of a layer of Hg supported on an optically polished Pt base which could be easily kept in vertical position. Several methods of preparation of such layered systems are described in the electroanalytical literature. Studies have been done in order to characterize their behaviour, particularly in relation to alloy and intermetallic compounds formation [6,7]. We have employed the method proposed by Hartley et al. [8] to eliminate the small drops of mercury formed on the base Pt during the electrochemical deposition of the metal from a mercurous nitrate solution. The homogeneous distribution of the liquid metal on the surface was achieved by energetic evolution of hydrogen at highly cathodic potential in 0.1N $HClO_4$ solutions.

SP excitation has been performed using attenuated total reflection (ATR) in Otto configuration with focused light. Details on the experimental set-up and procedure can be found in previous papers [9,11].

* Permanent address: Istituto Chimica Ciamician Via Zamboni, 40126 Bologna, Italy.

RESULTS AND DISCUSSION

Fig. 1 presents the reflectivity of p-polarized light as a function of the angle of incidence for various λ recorded for a 1.5 μm thick mercury film in contact with water. All of them display a well-defined minimum indicative of the occurence of the SP resonance which allows us to reach the SP dispersion curve presented fig.2. For such thick film we observe a normal dispersion indicative of Hg behaviour in good agreement with the electrochemical behavior of the film (fig. 2b). Thinner films display an anormal SP dispersion curve (fig.3) which has been observed for silver and aluminium based alloy [11-12] and can be assigned to the optical behaviour of dilute Hg based platinum compounds observed electrochemically for such films (fig.3b).

REFERENCES

[1] S.A. RICE, D. GUIDOTTI, H.L. LEMBERG, W.C. MURPHY and A.N. BLOCH in "Aspects of the study of surfaces", I. Prigogine and S.A. Rice, Wiley 27 (1974) 543.

[2] D. GUIDOTTI and S.A. RICE, Phys. Rev., B15 (1977) 3796.

[3] T. INAGAKI, E.T. ARAKAWA and M.W. WILLIAMS, Phys. Rev. B23 (1981) 5246.

[4] W.L. SCHAICH, submitted.

[5] A. TADJEDDINE, G. PIAZZA and M. COSTA, Europhys. Lett. 5 (1988) 87.

[6] T.M. FLORENCE, J. Electroanal. Chem. 27 (1970) 273.

[7] M.Z. HASSAN, D.F. UNTEREKER and S. BRUCKENSTEIN, J. Electroanal. Chem. 42 (1973) 161.

[8] A.M. HARTLEY, A.G. HIEBERT and J.A. COX, J. Electroanal. Chem. 17 (1968) 81.

[9] A. TADJEDDINE, S. CHIALI and M. COSTA, J. Chem.. Phys. (France) 80 (1983) 1977.

[10] M. ABRAHAM and A. TADJEDDINE, J. Phys. (France) 48 (1987) 267.

[11] A. TADJEDDINE, A.F. BENHABIB, A. ZEGHIB and J. Le BAS, J. Phys. (France) 48 (1987) 1715.

[12] A. HADJADJ, A. TADJEDDINE and G. HINCELIN, J.Electroanal. Chem. 228 (1987) 251.

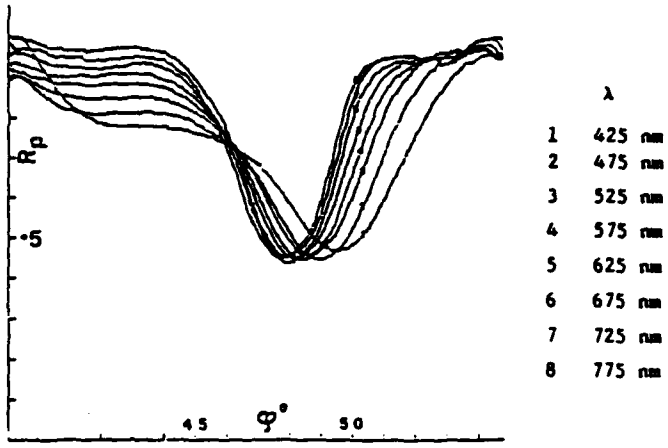


Fig.1 : R_p as a function of the angle of incidence for various λ : Hg film (1.5 µm)/ water.

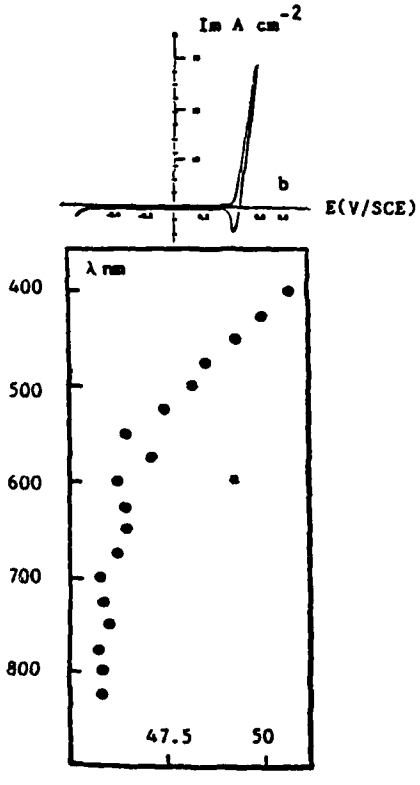


Fig.2 : a - SP dispersion curve of thick Hg film (1-5 µm)
b - i(E) curve of this film in $HClO_4$ 0.1M.

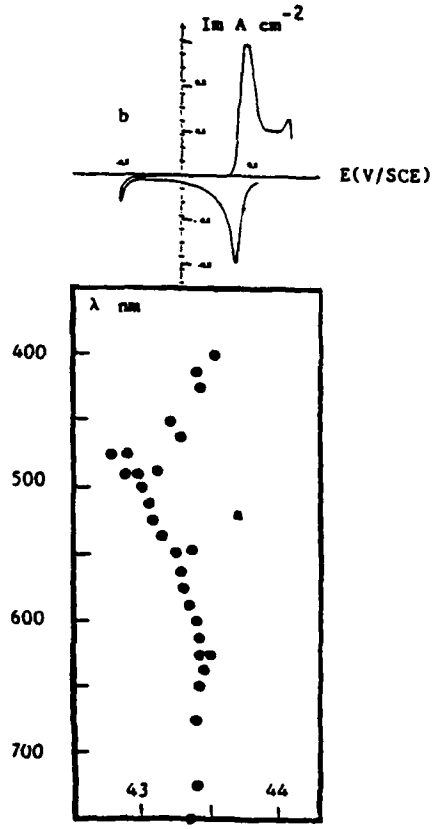


Fig.3 : a - SP dispersion curve of thin Hg film (0.5 µm)
b - i(E) curve of this film in $HClO_4$ 0.1M

SURFACE STRUCTURAL CHANGES OF EVAPORATED THIN SILVER FILM ELECTRODES DURING THE ADSORPTION OF CHLORIDE ION. A CAPACITANCE AND RESISTANCE STUDY

R.I. Tucceri and D. Posadas

Instituto de Investigaciones Fisicoquímicas Teóricas y Aplicadas (INIFTA), Facultad de Ciencias Exactas, Universidad Nacional de La Plata, Sucursal 4, Casilla de Correo 16
1900 La Plata, Argentina

INTRODUCTION

The capacitance vs. potential curve of single silver crystals in chloride solutions [1] shows a narrow peak in the potential range between -0.5 V and 0.0 V vs. SCE depending on the crystallographic orientation. Apparently this peak does not appear in polycrystalline and evaporated thin films [2-4]. The peak has been attributed to a partial charge transfer and latter to a rearrangement of the adsorbed surface layer by Valette et al. [1,5] and to a reconstruction of the silver surface layer by Fleishmann et al. [6].

In this work we will show that the appearance of this peak is connected with profound changes of the capacitive response of evaporated thin film silver electrodes.

EXPERIMENTAL

The capacitance and electrode resistance were measured in the way described before [7], care was taken to minimize the drift of the resistance measuring circuitry. The ΔR change due to drift at open circuit was of about 10^{-4} Ω.

Silver thin film electrodes of about 25 nm were obtained by high vacuum evaporation onto acrylic substrates optically polished. The initial resistance of the films were about 10.00 Ω.

RESULTS AND DISCUSSION

Despite the fact that evaporated thin silver films have a random orientation or at most a <111> facetting [8,9] their capacity vs. potential response, in different potassium halide solutions when compared with previous work with single crystals, is much alike to that of the (110) orientation, except by the absence of the extreme anodic peak in chloride solutions.

In 0.04 M KCl solutions, while the potential is cycled between -1.3 V and -0.3 V vs. SCE no changes are observed in the C vs. E response. However, as the anodic limit is increased to 0.0 V, changes in the capacitive curves are observed with the number of potential cycles (Fig. 1): (i) the characteristic peak at -0.2 V is developed and (ii) the shape of the C vs. E curve changes becoming progressively similar to that observed by previous workers [2,6] with polycrystalline silver in chloride containing electrolytes, and (iii) the values of C at the cathodic limit slightly increases with the number of cycles. This could mean that a slight increase on the roughness factor has also occurred. After about eight cycles these features remain constant with the number of cycles.

The change of resistance of the electrode with potential cycling indicates that the electrode dissolution is at most 20% of a silver atom layer.

On the basis of the present findings we conclude that the observed change in the C vs. E response during the potential cycling must be due to a reestructuration of the silver surface atoms assisted by the submonolayer formation of AgCl in agreement with many suggestions made previously.

REFERENCES

[1] G. Valette, A. Hamelin and R. Parsons, Z.Phys.Chem., N.F., 113 (1978) 71.
[2] D. Larkin, K.L. Guyer, J.T. Hupp and M.J. Weaver, J.Electroanal.Chem., 138 (1982) 401.
[3] A.V. Shlepakov and E.S. Sevastyanov, Elektrokhimiya, 14 (1978) 287.
[4] R.I. Tucceri and D. Posadas, to be published.
[5] G. Valette and R. Parsons, J.Electroanal.Chem., 204 (1986) 291.
[6] M. Fleishmann, M. Robinson and R. Waser, J.Electroanal.Chem., 117 (1981) 257.
[7] R.I. Tucceri and D. Posadas, J.Electroanal.Chem., 191 (1985) 387.
[8] T.M. Gardiner and M.H.B. Stiddard, Thin Solid Films, 77 (1981) 335.
[9] M.S. Zei, Y. Nakai, G. Lehmpfuhl and D.M. Kolb, J.Electroanal.Chem., 150 (1983) 201.

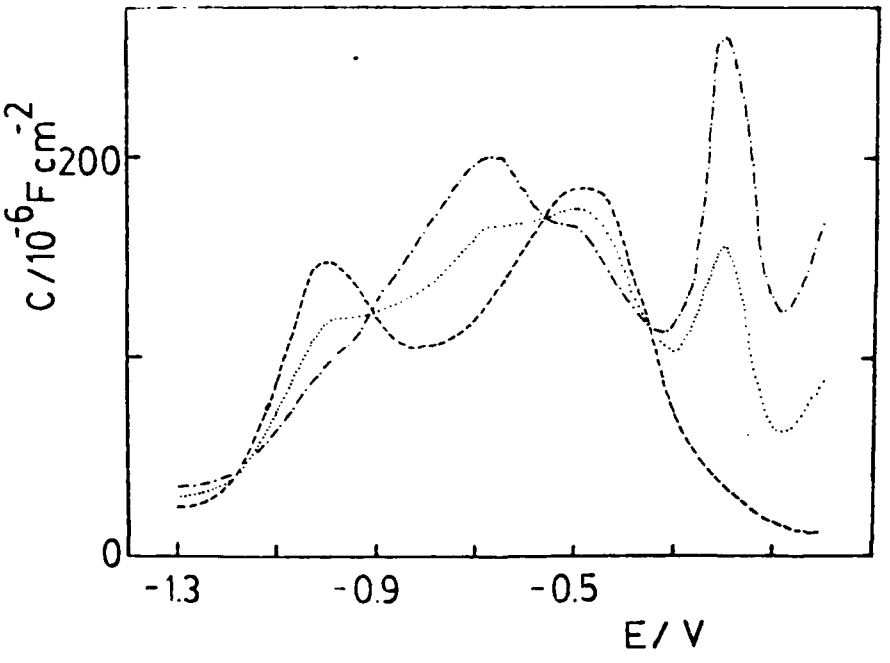


Fig. 1.- C vs. E response for thin silver film electrodes in 0.04 N KCl for different number of potential cycles the anodic limit was changed from -0.3 V to 0.0 V at the 4th cycle. (---) 1st cycle, (···) 6th cycle, (-·-) 12th cycle.

SURFACE CONDUCTIVITY CHANGES AND DIFFERENTIAL CAPACITY STUDIES OF THIN SILVER FILMS DURING THE ADSORPTION OF PF_6^-, F^- AND Cl^- IONS

R.I. Tucceri, F.M. Romeo* and D. Posadas

Instituto de Investigaciones Fisicoquímicas Teóricas y Aplicadas (INIFTA), Facultad de Ciencias Exactas, Universidad Nacional de La Plata, Sucursal 4, Casilla de Correo 16 1900 La Plata, Argentina

* Departamento de Química Física, Facultad de Ciencias Exactas y Naturales, Universidad de Buenos Aires

INTRODUCTION

Surface resistance changes, ΔR, of electrodes reflect how the metal electrons are influenced by the structure of the double layer. Systematic studies of the influence of the surface charge, σ, both in the absence and presence of specific adsorption on ΔR are very scarce. In this work we have studied the σ dependence on ΔR of thin silver films in solutions of different concentrations of very slight specifically adsorbed electrolytes and in mixtures of KF + KCl at constant ionic strength.

EXPERIMENTAL

Vacuum evaporated thin metal silver films of thickness $d \cong 25$ mm were used throughout. The circuitry and cell to measure the resistance and capacitance have been described previously [1,2]. Five single electrolyte solutions of KPF_6 ($0.005 < c < 0.1$ M) and seven of KF ($0.005 < c < 0.5$ M) and mixtures of the type xM KCl + $(1-x)M$ KF with $M = 0.04$ and $1.25 \times 10^{-3} < x < 0.04$ M were studied.

RESULTS AND DISCUSSION

The C vs. E curve was integrated in order to obtain the surface charge. The $\Delta R/R$ vs. σ plot is shown in Fig. 1 for KPF_6. In this case $\Delta R/R$ is independent of the concentration except for the small dip near $\sigma = 0$ which increases as c decreases. For KF, $\Delta R/R$ depends slightly on c. The minimum at $\sigma \cong 0$ also appears in this case. The anodic limiting value of $\Delta R/R$ for F^- is bigger than for PF_6^-.

We will assume that the major effect of the surface charge on the resistance is that due to the change of the surface electron distribution. The latter can be written as [3]

$$n(z) = n_+ \left[1 - \frac{\beta}{\alpha+\beta} e^{\alpha(z-z_o)}\right] \qquad z \leq z_o$$

$$n(z) = n_+ \frac{\alpha}{\alpha+\beta} e^{-\beta(z-z_o)} \qquad z > z_o$$

where n_+ is the ion density in bulk metal, $z_o = \alpha^{-1} - \beta^{-1} - \sigma/n_+$ is the inflexion point on the abcissa in the electron profile and α^{-1} and β^{-1} are the charge dependents attenuation lengths in the metal and solution side respectively. Within this scheme R results proportional to z_o. Since ΔR increases markedly at

positive charges this indicates that z_o must be positive at $\sigma=0$.

In the case of mixtures of KCl+KF the specifically adsorbed charge σ'_{Cl^-} was obtained following the usual procedures [4]. Plotting $\Delta R/R$ vs. σ at constant σ'_{Cl^-} allowed to obtain the coefficients $[\partial(\Delta R/R)/\partial\sigma]_{\sigma'_{Cl^-}}$ as a function of σ'_{Cl^-} (Fig. 3) and $[\partial(\Delta R/R)/\partial\sigma'_{Cl^-}]_{\sigma}$ as a function of σ.

Fig. 3 shows that in the presence of adsorbed chloride $[\partial(\Delta R/R)/\partial\sigma]_{\sigma'_{Cl^-}}$ increases with σ'_{Cl^-} up to an adsorbed charge of about $\sigma'_{Cl^-} \cong 60\ \mu C\ cm^{-2}$. From there on it decreases with σ'_{Cl^-}. The maximum in $\partial(\Delta R/R)/\partial\sigma$ corresponds to a surface structure of the adsorbed chloride of c(2x2) [5].

A possible explanation for this effect is that at low surface concentrations electrostatic interactions lead to an increase of the attenuation length within the metal. Involving partial charge transfer beyond $\sigma'_{Cl^-} \cong 60\ \mu C\ cm^{-2}$ would allow to explain the decrease of $\partial(\Delta R/R)/\partial\sigma_m$ with σ'_{Cl^-}.

REFERENCES

[1] R.I. Tucceri and D. Posadas, J.Electrochem.Soc., 128 (1981) 1478; 130 (1983) 104.

[2] R.I. Tucceri and D. Posadas, J.Electroanal.Chem., 191 (1985) 387.

[3] J.P. Badiali, M.L. Rosimberg and J. Goodisman, J.Electroanal. Chem., 130 (1981) 31; 143 (1983) 79; 150 (1983) 25.

[4] G. Valette, A. Hamelin and R. Parsons, Z.Phys.Chem., 113 (1978) 71.

[5] G. Valette and R. Parsons, J.Electroanal.Chem., 204 (1986) 291.

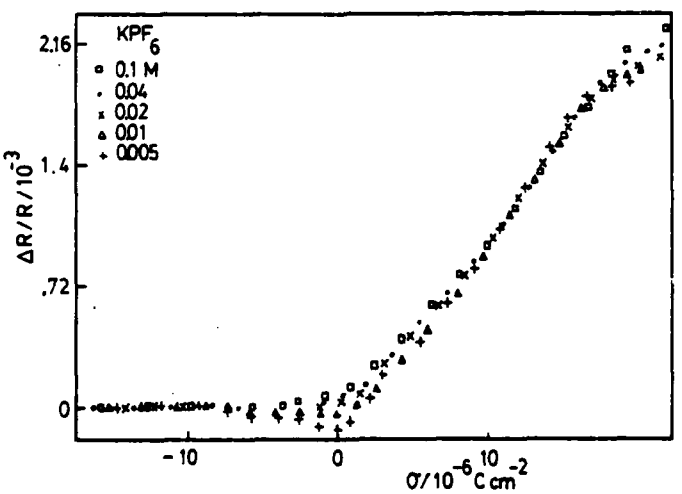


Fig. 1

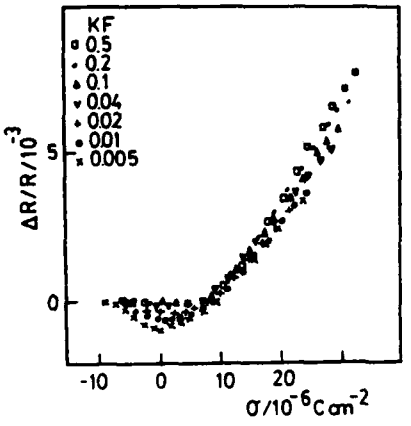

KF
0.5
0.2
0.1
0.04
0.02
0.01
0.005
ΔR/R/10^-3
5
0
-10
0
10
20
σ/10^-6 C cm^-2

Fig. 2

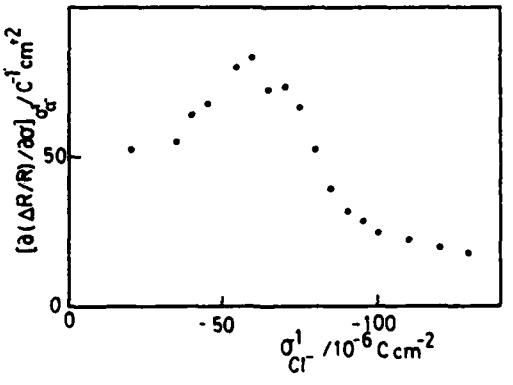

[∂(ΔR/R)/∂σ]σ→0 / C^-1 cm^2
50
0
0
-50
-100
σ Cl^- /10^-6 C cm^-2

Fig. 3

MEDIATION OF INTERFACIAL REACTIONS BY LOW LEVELS OF IN-SITU GENERATED HYDROXY SPECIES

L.D. BURKE, K.J. O'DWYER and W.A. O'LEARY

CHEMISTRY DEPARTMENT, UNIVERSITY COLLEGE CORK, CORK, IRELAND

The study of electrocatalytic processes is a topic of major interest at the present time, especially in connection with the development of certain types of fuel cells (e.g. methanol/air). In a review of this area Pletcher (1) has pointed out the unsatisfactory state of this field, electrocatalyst development being essentially empirical and a gulf existing between those who develop electrode materials and those who seek to understand the physical chemistry of electrocatalysis. We suggest that a novel proposal made recently in this laboratory in connection with gold (2), namely that low-level, or incipient, hydrous metal oxide (or hydroxide) species mediate many electroorganic oxidation processes, can rationalize many observations in this field.

In the traditional view of electrocatalysis (1,3) major stress is laid on activated chemisorption, i.e. the reactant molecules adsorb initially at metal atoms at the surface (which usually contain unfilled d-orbitals and unpaired electrons) in such a manner that bonds in the reactant are significantly weakened, if not cleaved - a process that is assumed to facilitate further reaction of organic species. Such a view appears to be valid for certain reactions, e.g. oxidation of molecular hydrogen. However, an additional factor that must be taken into account is that many organic reactions, e.g. methanol oxidation, viz.

$$CH_3OH + H_2O = CO_2 + 6H^+ + 6e^- \qquad [1]$$

involve an oxygen insertion step and this is where hydrous oxide species play a major role in electrocatalysis.

An extensive review of the electrochemical behaviour of hydrous oxides was published recently (4); the lack of attention to such species, especially in the field of electrocatalysis, seems to be due to the following reasons:-

(1) Hydrous oxide formation at noble metal surfaces under constant potential or single sweep conditions is confined largely to high energy, low coverage, adatom (M^*) sites, i.e. the response (voltammetric, spectroscopic, etc.) for the production of such species is usually quite low.

(2) An enhanced response is expected for such species if they mediate an electrooxidation process (2); however, such responses are often distorted by the formation of CO_{ads}-type deactivating species.

(3) Hydrous oxide formation in the case of Pt - usually the most active of the noble metals - in acid occurs in the region of hydrogen desorption; the current associate with the latter usually mask that due to the former process.

(4) In hydrous oxides there is an unusual interaction between acid/base and redox properties which has only recently received some clarification (4).

To explore the role of hydrous oxides in electrocatalysis at noble metal anodes in general the following four compounds were selected for investigation - hydrazine (an excellent model compound as the main product of oxidation in this case - N_2 gas - does not deactivate the surface), methanol, formaldehyde and formic acid (the latter are of interest in fuel cell work). In cyclic voltammetry experiments hydrazine oxidized on gold in both acid and base. As expected in terms of the interfacial cyclic redox (or hydrous oxide mediated) view of electrocatalysis the onset (anodic sweep) and termination (cathodic sweep) potential for oxidation coincided; however, this critical potential value dropped by ca. 0.38V (on the RHE scale) on changing from H_2SO_4 to NaOH (1.0 mol dm^{-3}, 25°C) solution - strong evidence for hydrous oxide participation (2,4).

Thick hydrous oxide films on Pt reduce in acid at ca. 0.2V(RHE) - a potential that coincides with the well known anomalous H_3 peak for the latter metal. We propose that the latter response is due to hydrous oxide formation at adatom (Pt^*) sites, viz.

$$Pt^* + 6H_2O = [Pt(OH)_6]^{2-} + 6H^+ + 4e^- \quad [2]$$

Support for this suggestion is provided by the fact that onset/termination potential for hydrazine oxidation on Pt in acid occurs (Fig.1) in the same region. Quite a wide variety of organic compounds (including those listed earlier) behave in the same manner providing precautions are taken to minimize deactivation, i.e. the oxidation currents must be recorded immediately following a potential step from a higher value, e.g. 1.3V(RHE). Complications occur with Pt in base as the metal/hydrous oxide transition is in the H_2 evolution region (4) and the onset potential for oxidation occurs only following removal of some surface hydrogen - this onset value for base, however, is again significantly lower than for acid. The electrocatalytic behaviour of palladium is similar to that of platinum; however, the activity is significantly lower presumably because the hydroxy species involved, $[Pd(OH)_6]^{2-}$, is more prone to dissolution (5), i.e. the surface coverage of the mediating species is low in the case of Pd.

The other noble metals investigated, Rh, Ru and Ir, behaved very poorly as electrocatalysts for the oxidations in question here. This may be due to one, or a combination, of the following factors;-

(a) Regular, compact, monolayer oxide formation usually has an inhibiting effect on the oxidation reactions in question here. Incomplete monolayer oxide reduction, including removal of subsurface oxygen, may be a source of inhibition with these three metals whose affinity for oxygen is much higher than that of Pt.

(b) The hydroxy complexes formed in the case of these three metals are also more stable than their Pt, Pd or Au analogues, i.e. they are a weaker source of OH species (obviously the latter may be involved in the oxidation process). Alternatively, if the oxidation involves inner-sphere coordination the organic molecule is less likely to displace OH species at coordination sites. Finally, the reduced form of the couple may play a role in these reactions. This, in the case of Pt,is the metal adatom; however, with the other metals, e.g. Ir, the hydrous oxide is quite difficult to reduce (4) below the Ir(III) state. According to the latter view the redox couple at the interface plays a dual role, the reduced form activates the reactant while the oxidized form converts it to products; it is possible that with alloy systems these two functions occur at different, neighbouring, sites. However, care is required in drawing

conclusions here as the superior performance of alloy systems for certain reactions may be due to suppression of poisoning effects.

In conclusion, the hydrous oxide mediation theory of electrocatalysis provides a logical explanation for the electrocatalytic behaviour of a wide range of both metals and active oxides, e.g. RuO_2 (6). There is obviously much scope for further fundamental and applied work in this area.

REFERENCES

1. D. Pletcher, J. Appl. Electrochem., 14 (1984) 403.
2. L.D. Burke and V.J. Cunnane, J. Electroanal. Chem., 210 (1986) 69.
3. G.P. Sakellaropoulos, Adv. in Catalysis, 30 (1981) 217-333.
4. L.D. Burke and M.E.G. Lyons, Modern Aspects of Electrochem., No. 18 (1986) 169-248.
5. L.D. Burke and M.B.C. Roche, J. Electroanal. Chem., 186 (1985) 139.
6. L.D. Burke and J.F. Healy, ibid., 124 (1981) 327.

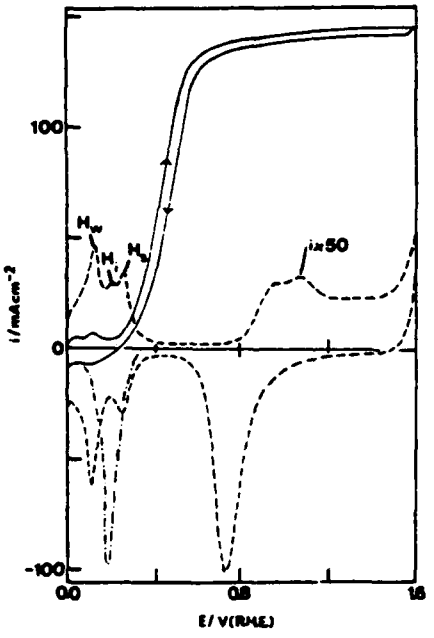


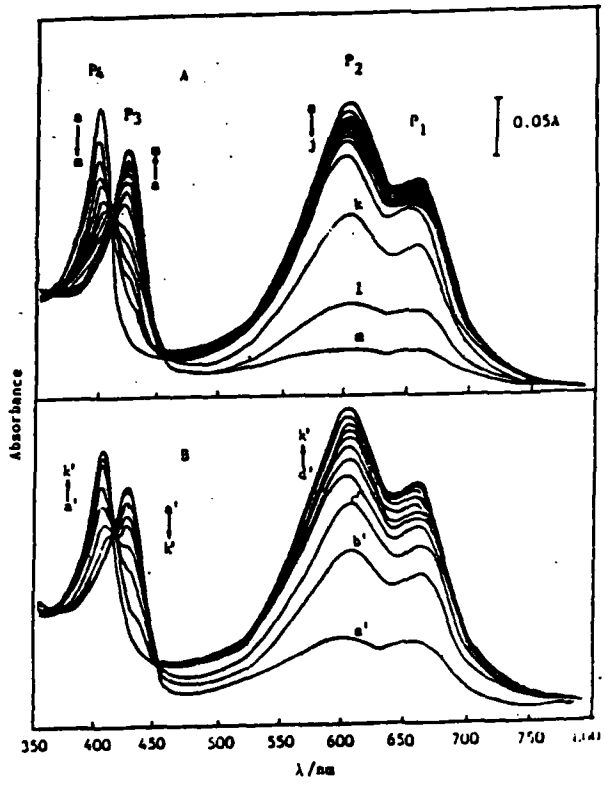
Fig.1: Cyclic voltammogram (---), 0-1.6V, 50 mV s^{-1}, for a platinized Pt electrode in 1.0M H_2SO_4, 25°C (the anomalous H peak is labelled here as H_1). A further scan (——) was recorded following addition of hydrazine, to a level of 0.1M, to the solution. A typical peak (-·-) for hydrous Pt oxide reduction (4) in 1.0M H_2SO_4 at 40 mV s^{-1} is also shown here.

A STUDY ON SPECTROELECTROCHEMISTRY OF THE REDOX REACTION OF HEMOGLOBIN*

Shihua SONG and Shaojun DONG**

Changchun Institute of Applied Chemistry, Chinese Academy of Sciences, Changchun, Jilin 130021, People's Republic of China

The electron transfer process of biomacromolecules at the electrode can be facilitated by using mediator. Certain organic compounds show their ability to mediate the electrode reaction of horse heart cytochrome c. Most of the previous papers reported the electrochemistry of hemoglobin(Hb) at mercury electrode while few at solid electrode. In this paper the electrode reaction of Hb at platinum electrode in the presence of methylene blue(MB) has been studied by in situ spectroelectrochemistry and ESR electrochemistry.



Hb undergoes very slow heterogeneous electron transfer at naked platinum electrode, resulting in no apparent reduction and oxidation peaks in cyclic voltammograms. When Hb was added to a solution containing MB, the electrode reaction of Hb becomes quite fast. This electrode process was carried out in an optically transparent thin-layer cell with platinum gauze as a working electrode at different applied potentials, as shown in Fig.1. It is assumed that MB does not form a complex with the heme iron in Hb as proved by no change of the spectra of MB upon the

Fig.1 Spectra of Hb at Pt electrode in $1 \cdot 10^{-4}$M MB
A: Reduction of Hb at potentials from 0 to -0.22V
B: Oxidation of Hb at potentials from -0.2 to 0V

* This project is supported by National Science Foundation of China
** To whom correspondance should be addressed

addition of Hb. In Fig.1A, the two peaks, P_1 and P_2, are the absorption bands corresponding to the monomer and dimer of MB, while P_3 and P_4 are of the reduced and oxidized states of Hb. The total reduced form of Hb, yielding P_3, is obtained during the potential shifts negatively to -0.16V. Simultaneously, MB is reduced to leucomethylene blue(LMB) indicated by the disappearance of absorption bands P_1 and P_2. At the reverse potential step (see Fig.1B), LMB begins to be reoxidized at -0.2V, while reduced Hb does so at the more positive potential of -0.14V. These results indicate that Hb takes part in a quasi-reversible redox reaction at platinum electrode in the presence of MB solution.

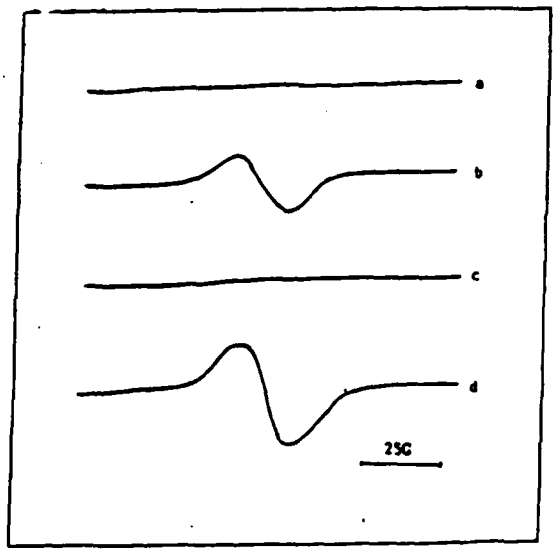


Fig. 2 ESR signals of $1 \cdot 10^{-3}$M MB during potential scan
a: start, b: scan from 0.2 to -0.13V, c: at -0.4V, d: reverse scan from -0.4 to -0.13V.

What's the reason that MB could mediate the electrode reaction of Hb? There was a hypothetic consideration for the formation of cation radical of MB or the charge transfer complex produced during electrolysis of MB but without any direct evidence. In order to clarify this phenomenon, MB in aqueous solution was monitored by in situ ESR electrochemistry in a thin-layer cell. The ESR signal produced electrochemically in MB solution was firstly observed, as shown in Fig.2. Curves a and c correspond to the total oxidized and reduced states of MB, curves b and d correspond to the potential scan negatively 0.2→ -0.13V and positively -0.4→ -0.13V. Obviously, the ESR signalcan only appear when both MB and LMB were existed. Since LMB is easily oxidized by MB, a cation radical of LMB^+ is produced by one electron transfer of the charge transfer complex intramolecule. MB is adsorbed favorably onto the platinum electrode surface, a charge transfer complex might be induced at the electrode surface in a solution containing MB which showing feature of semiconductive properties for mediation for Hb electrode reaction.

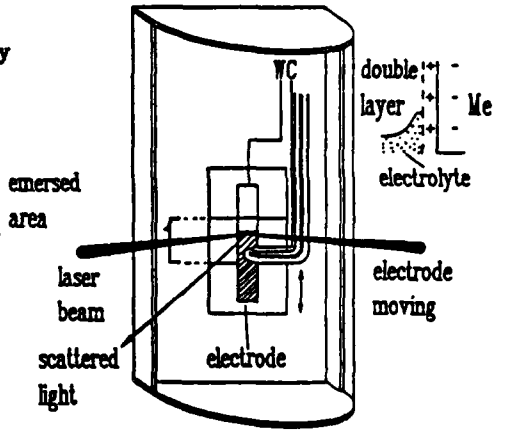
Raman Spectroscopy at Metal Electrodes

Bruno Pettinger and Ulrich Tiedemann

Fritz-Haber-Institut der Max-Planck-Gesellschaft
Faradayweg 4-6, D-1000 Berlin 33, West-Germany

A Pt-electrode exhibits, according to the current understanding, no surface enhancement for Raman scattering at electrodes. In fact, the observed Raman effects are very weak. In account of the low intensity level, the "emersion technique" has been further developed: A periodical immersion-emersion Raman cell has been constructed in order to combine electrochemical studies with surface Raman scattering at an arbitrary metal substrate [1]. As shown in fig. 1, it consists of a metal plate, a glass capillary and between them a drop of electrolyte. That means only a small part of the metal surface has contact with the electrolyte, because capillary forces hold the drop between the metal and the thin glass tube. The drop remains there even if the metal plate is slowly moved up and down. Thus, parts of the metal electrode allways will be immersed, the applied potential establish the electrical double layer and adsorption equillibrium, and this double layer then will be emersed. Since the emersed area contains only the electric double layer, but no bulk electrolyte, Raman spectroscopy on the emersed area monitors the interfacial area alone. The whole unit is placed into a chamber filled with inert gas having an optical window for spectroscopic studies.

Stationary and quasi-stationary Raman studies on dyes (rhodamine 6G and crystal violet) at (emersed) Pt electrodes revealed that absolute and relative Raman intensities are influenced by the electrode potential, anion coadsorption, temperature and surface roughness. Insofar Pt behaves like Ag surfaces. In the absence of a surface enhancement, an adsorbed dye should show a diminuished resonance Raman scattering, because a dipole resonantly induced in the molecule will transfer its energy to the metal electrons rather than emitting photons. Observed is, however, an apparently undiminuished resonance Raman process.



1) B. Pettinger and U. Tiedemann, J. Electroanal. Chem. 219, 228 (1987).

Formation of a monolayer of oxide at gold single crystal face electrodes in sulphamic acid solutions.

Fernando Silva and Cosme Moura
Departamento de Química
Faculdade de Ciências
Universidade do Porto
Portugal

A. Hamelin
Laboratoire de Electrochimie Interfaciale
CNRS-Bellevue
9650 Meudon Cedex
France.

The of oxidation of gold single crystal face electrodes has been the subject of several studies(1,2,3).

All studies have indicated pronounced structural sensitivity of anion adsorption on oxide formation. Trigonal simmetry of the anions has been proposed, by H. A. Kozlowska *et al* (3), to play an important role in the early stages of oxidation process of gold single crystal face electrodes.

Sulphamic acid is a strong acid (pK=1, 25 ^{o}C) and the suphamate anion has trigonal symmetry around the S atom. A comparison of the structure of sulphamate anion with that of sulphate anion indicates that the O atoms are drawn closer together in the plane of the S atom than in the case of sulphate(4)

Preliminary results obtained for four crystal faces of gold with crystallographic orientations (111), (110), (100) and (210) are reported here. They indicate the influence of crystallographic orientation in the adsorption of sulphamic acid. The different degrees of adsorption are reflected on the oxidation process of gold single crystal faces.

Results

The dependence of the differential capacity on the potential and solute concentration may be used to illustrate adsorption-desorption processes. On gold single crystal faces the crystallographic orientation (co) exerts a profound influence on C(E) either for weakly or strongly adsorbing anions (5). Figure 1 shows the influence of co on the differential capacity of gold single crystal face electrodes in sulphamic acid solutions. The strength of adsorption is higher for the face with lowest surface energy (111) and lower for the face of highest surface energy (210). Hysteris of both sweeps of C(E)

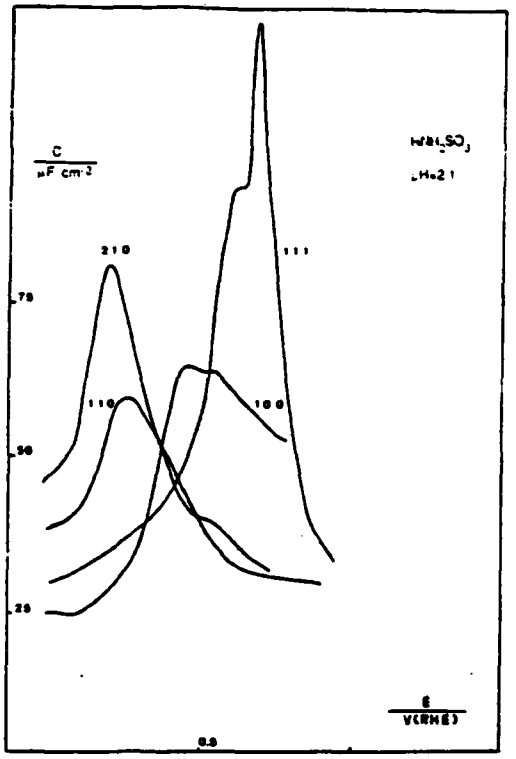


Figure 1- C(E) curves for the adsorption of sulphamate anion on Au(111), (110), (100) and (210)

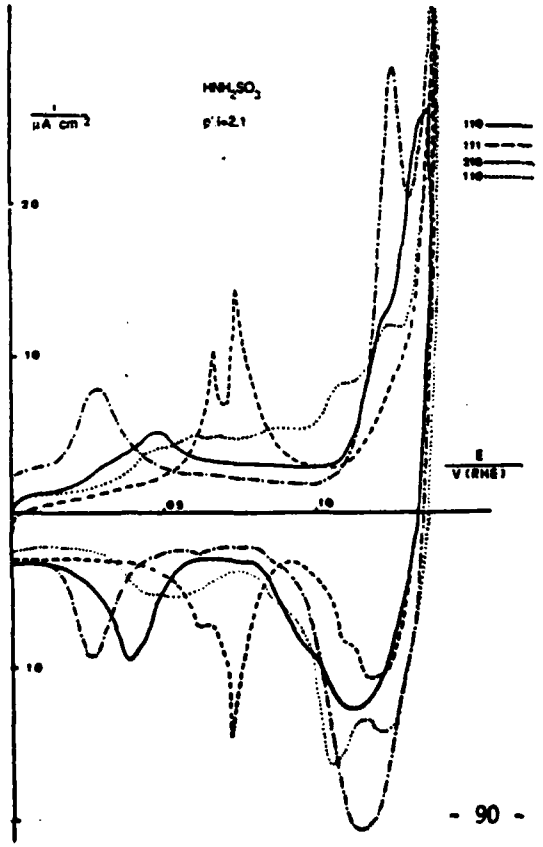


Figure 3-i-E profiles for the early oxidation of gold face electrodes in sulphamic acid solutions

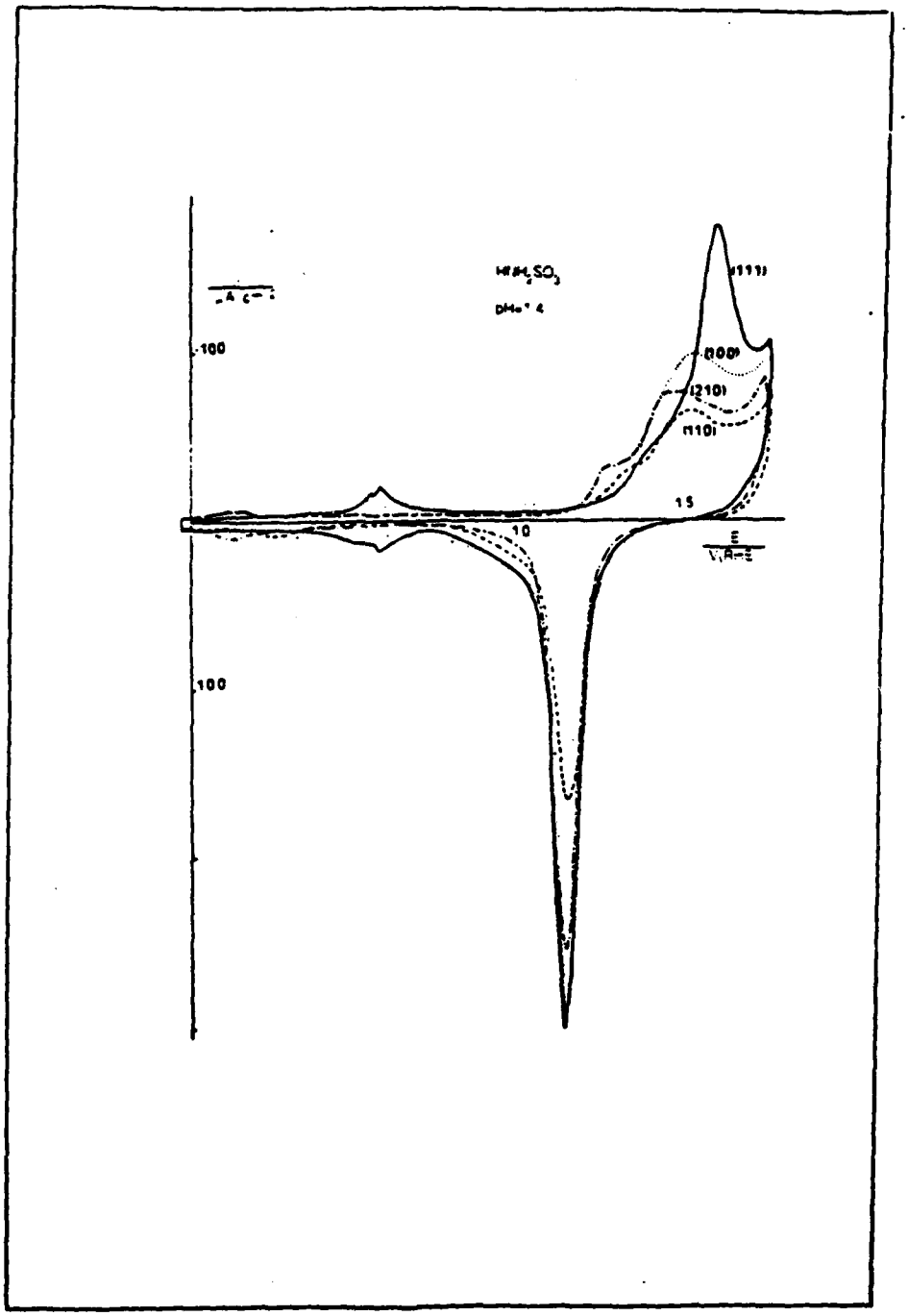


Figure 2- Cyclic voltammetry i-E profiles for Au single crystal face electrodes in sulphamic acid solutions recorded at 50 mVs^{-1} and 25°C

curves is not important for the (210) face. On the (111) face electrode a sharp peak on C(E) curves, (fig. 1), indicates that the adsorbed species are better ordered on this face. Such is made possible because the spacial distribution of the O atoms in the sulphamate anion matches the distribution of surface atoms on unreconstructed gold (111) surface.

The mismatch f the symmetry of the surface atoms with the spacial distribution of the O atoms reduce the strength of adsorption and the broad peak in C(E) for (210) suggests less ordered adsorbate.

Different degrees of adsorption of sulphamate anion occur on each face at each concentration, as detected from the C(E) curves. This is expected to have marked effects on the formation of a monolayer of oxidized compounds on each face.

The effect of the presence of sulphamate anion at the surface is shown by the alterations on the i-(E) profiles obtained in perchloric acid and sulphamic acid solutions with the same pH as shown in fig. 2. The potential of onset of oxidation is higher in sulphamic acid solutions and shifts to more positive values as the concentration increases. The assigment of the oxidation peaks to each of the processes proposed (3) is easier if the i-(E) curves are recorded in an expanded scale as shown in fig. 3.

The presence of sulphamate ion at the surface blocks, at least partially, the initial stages of oxidation of gold. Nevertheless, a certain degree of heterogeneity on the gold surface, which varies with co, is maintained. Detailed results of all low index faces will be presented and discussed according to the model proposed in reference 3.

References

1- D. Dicktermen and J. W. Schultze nad K. D. Vetter, J. Electroanal. Chem.., 55(1974)429.

2- M. Sotto, J. Electroanal. Chem., 69(1976),1229 ; 70(1976)1291, 72(1976)287.

3- H. A. Kozlowska B. Conway A Hamelin and L. Stoicoviciu, J. Electroanal. Chem.228(1987)429 and Electrochem. Acta, 3(1986)105.

4- F. A. Kanda and A. J. King, J. Amer. Chem. Soc., 73(1951)2315.

5- A. Hamelin, in Trends in Interfacial Electrochemistry, ed. A. Fernando Silva, Nato ASI Series C179, Reidel Publish. Company, Dordrecht, 1986.

Acknowledments: F. S. and C. M. gratefully acknowledge the finantial support of INIC-CIQ-L3 and F. Calouste Gulbenkian-Lisbon.

SERS Investigations of Cu-Phthalocyanine Chemisorption layers on Silver Electrodes. The Excitation Profile.

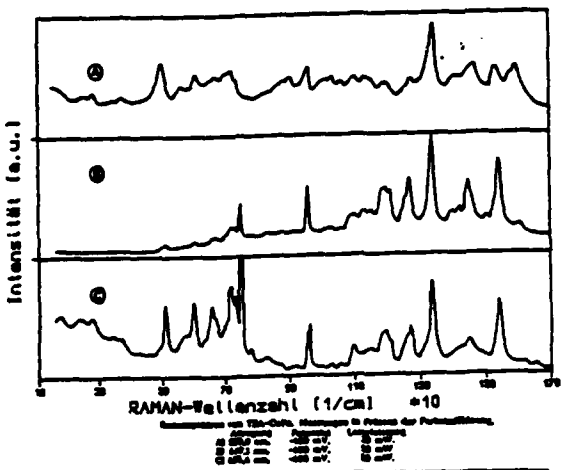
R. Castillo and W. Plieth
Institute of Physical Chemistry
Free University of Berlin, Berlin West (Germany).

Enhancement of Raman signals from adsorbates is known to occur on copper, gold and specially on silver, and can generally be achieved by adequately roughening the metal surface. In our case we have chosen the electrochemical method, which provides the posibility of influencing the adsorbed scattering molecules by means of the applied electrical field. A mechanically and chemically polished silver electrode immersed in a dilute aqueous solution of Cu-phthalocyanine with potassium sulphate as the supporting electrolyte was adequately polarized as to redeposit the anodically dissolved metal, leading to the appearance of a SERS spectrum. Cyclic voltammetry in the range up to 1 V (vs. Hg_2SO_4) showed no processes which could be attributable to anything else than silver itself or, if present, dissolved oxygen. This is in agreement with previous reports on the redox properties of Cu-phthalocyanine[1]. Cathodic excursions of a blank electrode into the hydrogen evolution region did not result in the apppearance of any Raman signal, dispite of claims for the contrary[2]. The obtained SERS spectrum consists of numerous, well defined Raman lines in the range from 400 to 1600 cm^{-1} (Fig. 1). The strong absorbing solution of the dye was rinsed out until a practically transparent electrolyte was obtained, avoiding thereby light absorption of both laser and scattered light. Using the numerous lines of an argon and krypton laser as well as the tunable output of a dye laser, detailed measurements over a wide spectral region were accomplished. Fig. 2 shows partial results as the normalized intensities of several Raman lines in the absorption region of the Cu-phthalocyanine. Besides the evident correlation with the absorption spectrum, the excitation profiles reveal the vibronic nature of a partially overlapped absorption band at about 610 nm. The stronger shoulder at 627 nm shows, on the contrary, no ramanspectroscopic relevance. A comparison of the excitation profiles in different spectral regions permits us to estimate the enhancement due exclusively to the absorption of the dye as three orders of magnitude. The existence of vibrational couppling brings about the regularity shown in Fig. 3, where the

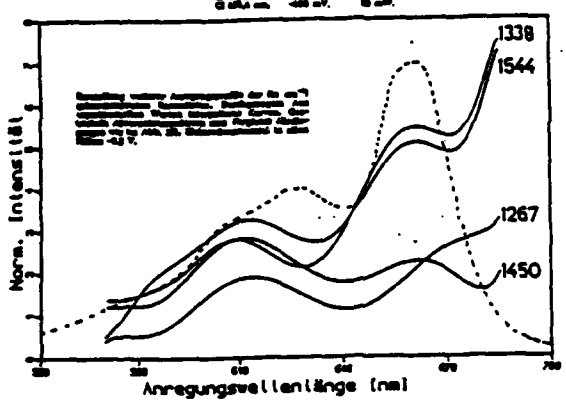
energy distance from the maximum in the excitation profile to the absorption band is plotted against the corresponding Raman shift for each line. Raman lines at 956 cm^{-1} (benzol breathing mode) and 506 cm^{-1} (benzol deformation) do not fit in this curve, confirming that the benzol rings do not belong to the chromophore part of the molecule. The excitation profiles can be rationalized as an unambiguous function of the dye absorption; no complex having special absorption properties can be found, as is usually postulated in the SERS literature. Although an absorption band belonging to the electronic plasma resonance of a colloid-like film on the silver electrode was clearly identified with reflexion measurements, no correlation could be established between this absorption band and the excitation profiles. Another interesting fact is the pronounced susceptibility of the excitation profiles to the electrode potential: they shift to higher wave numbers as the potential becomes more negative. The well known potential dependence of the Raman lines must so be asserted, at least in this case, as a potential modulated absorption shift of the adsorbate. An unshifted excitation profile, like that shown in Fig. 2, can actually be observed only at the rest potential.

By similarity with colloidal systems, where the absorption maximum strongly depends on the degree of association of the particles, and considering the instability of the SERS electrode and the results of the reflection measurements, one could envision the surface of a SERS electrode as a two dimensional colloid, in which the electrically charged particles are trapped between the irregularities of the massive metal and stabilized by specifically adsorbed anions and probably by the scattering molecules themselves. It seems then plausible to attribute the potential influence to a mechanical displacement of the charged particles in the electrostatic field of the electrode. Thus, a negative polarisation should attract the positive charged particles, bringing them closer together and causing an absorption shift in the same direction as in the case of true colloidal systems. Indeed, this seems the only way to explain the hysteresis observed in intensity/potential curves ("intrinsic time constant"). The total charge needed to "saturate" a SERS electrode corresponds to one monolayer of particles of 8 nm diameter.

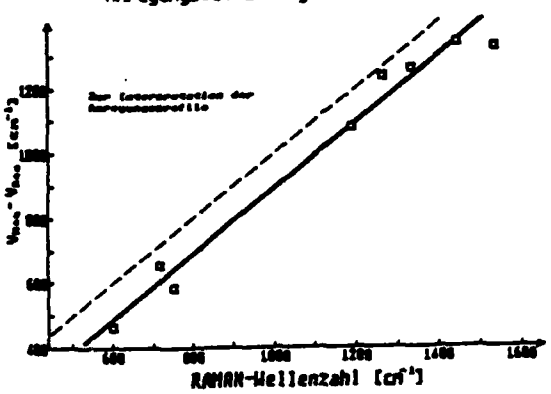
1) L. Rollmann, R. Iwamoto. J. Am. Chem. Soc. 90, 1435 (1968).
2) R. Kötz, E. Yeager. J. Electroanal. Chem. 113, 113 (1980).


Intensität (a.u.)
RAMAN-Wellenzahl (1/cm) *10

①


1338
1544
1267
1450
Norm. Intensität
Anregungswellenlänge (nm)

②


RAMAN-Wellenzahl (cm⁻¹)

③

PERMITTIVITY STUDIES ON SUSPENSIONS

János Liszi

University of Veszprém, Hungary

The permittivity of synthetic cation exchange resin--oil suspensions was studied as a function of the frequency and temperature. Frequency range studied: 50 Hz -- 12 MHz. Temperature range: -20 - +80 ^{o}C. In this way, two different dielectric relaxation ranges were found. The second relaxation of the systems for Na^{+}, K^{+} and Ca^{2+} forms of the resins, was observed completely in the radio-frequency range, while the first one was observed partially, only. Therefore, the investigations were limited only to this second effect.

Results

1. The suspension technique is a suitable method for the investigation of the permittivity of synthetic ion exchange resins. The experimental results are related to the suspension studied (resin-oil suspension).
2. The second relaxation effect has a Fuoss-Kirkwood distribution of relaxation times with β parameter values of about 0.4-0.8.
3. The relaxation time increases with the decreasing temperature. The values of Arrhenius-activation energies are in the order of 60-80 k Joule mol^{-1} which are higher than that of pure water: $\sim$ 20 k Joule mol^{-1}.
4. The water content plays a role as well. Higher water content in the resin matrix results in a lower relaxation time. The high activation energy values give proof of the motion of suspected molecules being in hindrance.
5. The behaviour of Na^{+}- and K^{+}-form resins is similar, while in the case of Ca^{2+} ions a longer relaxation time was experienced.

ELECTROMODULATION OF SURFACE PLASMON DISPERSION RELATION AND ADSORPTION OF ANIONS AT THE ELECTROCHEMICAL INTERFACE

P.G.Dzhavakhidze*+, A.A.Kornyshev+#, A.Tadjeddine#+ and M.I.Urbakh+

+ The A.N.Frumkin Institute of Electrochemistry of the Academy of Sciences of the USSR, Moscow, USSR

Laboratoire d'Electrochimie Interfaciale, CNRS, Meudon, France

* Department of General and Theoretical Physics, Georgian Polytechnic Institute, Tbilisi, USSR

Surface plasmon (SP) spectroscopy proved to be a powerful tool for the study of optical properties of metal surfaces, thin films and interfaces [1,2]. SP's are collective oscillations of conduction electrons confined to the interface between an SP-active medium and a dielectric. Their localization makes SP's resonance conditions very sensitive to the microscopic properties of the interfaces. SP's can be excited optically by attenuated total reflection or detected by reflectometry or ellipsometry. In electrochemistry this technique has been repeatedly applied to in situ studies of the metal/electrolyte interfaces.

Most of experimental studies of SP's dispersion relation $\omega_{sp}(k_{\parallel})$, have been done on Ag which is both a "good" ideally polarizable electrode (no chemical reactions in a wide potential range) and an SP-active material in the infra-red and visible spectral region. Measurements were performed on both polycrystalline [3] and single-crystal [4] electrodes. It was shown that the dependence of ω_{sp} (for a given $k_{\parallel}$) on the potential drop, φ, changes sharply in the vicinity of p.z.c. In the anodic range, ω_{sp} monotonously decreases with polarization (with almost constant derivative) while it is practically independent of cathodic polarization. It was also shown that the position of the bending point depends on the type of adsorbed ions and might not coincide exactly with p.z.c. [5]. (These data are reproduced in Fig.1)

Though more than a decade have passed since first results were obtained for $\omega_{sp}(k_{\parallel})$ dependence on the potential drop, no convincing explanation of these plots has yet been proposed. Noteworthy, similar dependences (viz. weak dependence of the signal in the cathodic range and sharp variation with the increase of anodic polarization) have been observed in electroreflectance, ellipsometry and second harmonic generation on silver electrodes [6]. Thus, this

asymmetry seems to be of general nature and its analysis might be crucial for understanding the microscopic properties of the interface Ag/electrolyte.

There is obviously no essential change of surface electronic structure of a pure metal near p.z.c. Hence, the asymmetry may be caused by some changes in the double layer. As independent electrochemical impedance measurements show [7], at $\varphi \lesssim \varphi_{p.z.c.}$ oxidation of silver and adsorption of anions start which must influence the electron density distribution near the interface and, thereby, affect the SP-dispersion.

In this paper we show that taking into account the effect of adsorption (or oxidation) on the free electron density distribution allows to explain naturally the observed plots of the electromodulation of SP frequency, $\omega_{sp}(k_{\parallel})$.

In so doing we -

1. Use a phenomenological theory which relates the SP dispersion law to the generalized nonlocal dielectric function of the metal/electrolyte system [8].
2. Suggest a microscopic model for the calculation of this dielectric function in the optical frequency region (an appropriate modification of the Aspnes and McIntyre model [9]).
3. Make the density functional calculations of the surface electronic profile in the presence of a layer of negative charge put on the edge of the semi-infinite positive jellium which simulates the metal skeleton (the layer models the anion adsorbate or primary oxidation film in analogy with the Lang "step"-model for a cation adsorbate film [10]).
4. Modelling the dependence of the negative charge density of the film on the electrode polarization, we study the character of the SP frequency electromodulation.

The essential feature of our results is that the curves characterized by different intensity of the polarization-induced adsorbtion or oxidation (which is poorly known) differ only in the electromodulation slope, $d\hbar\omega_{sp}(k_{\parallel})/d\varphi$, but all meet in one bending point; its position depends only on the critical charge at which the adsorbtion (or oxidation) starts (Fig.2).

We thus risk to conclude that the bending points in the $\omega_{sp}(k_{\parallel})$ versus potential plots determine critical polarizations of adsorption. Preliminary estimates show that this conclusion is in accordance with SP- and adsorbtion data obtained in a series of single-crystal faces and metals.

REFERENCES

1. F.Abeles, T. Lopez-Rios and A.Tadjeddine, Solid State Commun. 16 (1975) 843 .
2. D.M.Kolb In Modern Problems in Condensed Matter Sciences. Surface Polaritons (V.M.Agranovitch and D.L.Mills, eds.) Chapter 8; Amsterdam: North-Holland, 1982, p. 299.
3. R.Koetz, D.M.Kolb and J.K.Sass, Surf. Sci. 69 (1977) 359.
4. A.Tadjeddine, D.M.Kolb and R.Koetz, Surf. Sci. 101 (1980) 277.
5. A.Tadjeddine, J.Electroanal.Chem. 169 (1984) 129.
6. F.Chao and M.Costa, Surf. Sci. 135 (1983) 497; G.L.Richmond, Chem. Phys. Lett. 113 (1985) 359.
7. A.Hamelin, T.Vitanov, E.Sevastyanov and A.Popov, J.Electroanal. Chem. 145 (1983) 225.
8. A.M.Brodsky and M.I.Urbakh, Usp.Fiz.NauK 138 (1982) 413; Prog.Surf.Sci. 15 (1984) 121; J.Electroanal. Chem. 171 (1984) 1.
9. A.A.Kornyshev and M.I.Urbakh, J.Electroanal. Chem. 235 (1987) 11.
10. N.D.Lang, Phys.Rev.B 4 (1971) 4234.

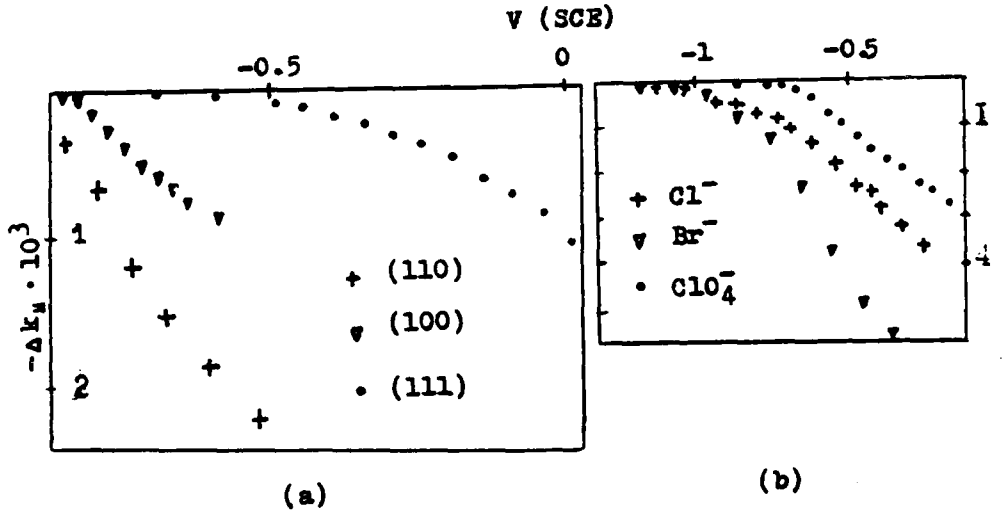


Fig.1 Potential dependence of the position of SP resonance [3-5] :(a) effect of surface orientation (Ag(hkl)-0.5 M $NaClO_4$); (b) effect of adsorption of anions (Ag polycrystalline). $\Delta k_{\parallel}$ in units ω/c .

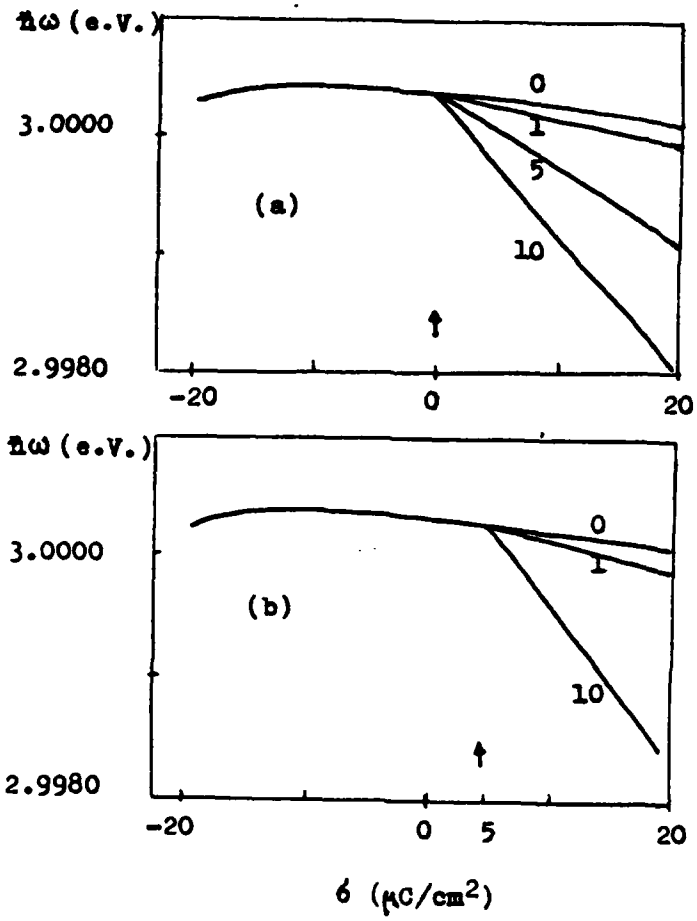


Fig.2 Calculated plots of SP frequency dependence on the electrode charge, σ, for different intensities of the field-induced adsorption, γ (charge density in the adsorption layer $n_a = \gamma(\sigma - \sigma_{cr})/d$ where d is the thickness of the layer). The critical charges at which adsorption starts - (a) zero, (b) 5 $\mu C/cm^2$ (Calculation for Ag, bulk electron density $8.7 \cdot 10^{-2}$ a.u., $d = 2$ a.u.)

INVESTIGATION OF ADSORBTION INHOMOGENITY OF POLYCRISTALLINE PLATINUM BY OPTICAL METHODS

V.E.KAZARINOV, A,M.FUNTIKOV, G.A.TSIRLINA

The A.N.Frumkin Institute of Electrochemistry, Academy of Sciences of the U.S.S.R, 117071, Moscow, Leninsky prospect, 31

The investigation of inhomogeneous adsorbtion of hydrogen and anions Cl^- and Br^- on the surface of polycristalline platinum by methods of impedance, electroreflectance (ER) and electroscattering (ES) of light as well as by method of electromodulation of reflectance phase (ERPh) was carried out. Recently developed method ES /1/ allows to investigate selectively the changes of dielectric permittivity of transition layer on the metal/solution interface which are inhomogeneous along the electrode surface and thus in the case of inhomogeneous adsorbtion this method supplements ER data. What about ERPh, one can measure in modulating conditions the capacity components connected with the adsorbtion of different type of particles (Γ_i) /2/.

It was shown that dependencies ER and ES on the potential E_r(RHE) of smooth polycristalline Pt in sulphuric and perchloric acids can differ substantially in accordance with preliminary treatments of electrode. In particular, anodic treatment in HCl with further purification from Cl^- by cathodic polarization allows to obtain the surface for wich on ER curves we can observe maximum of positive signal at the weakly bonded hydrogen region and on ES curves we can observe minimum of the negative signal at the potentials of strongly bonded hydrogen. The treatment of Pt by triangular pulses (100-500 V/s) at the range of E_r from 0,04 to 1,45 V results in a rapid growth of ES minimum and the appearance of the minimum of negative signal on the ER curves at the same potentials. ER signal at more negative E_r does not practically change. Pulse treatment does not result in substantial change of the curves of adsorption capacity that is why the growth of signal minimum can be connected only with the change of the character of inhomogeneous distribution of adsorbed hydrogen (H_{ad}).

The analysis of ER and ES data in surface inactive electrolytes on the basis of the approach developed in /3/ allows to introduce the idea about the existance of two forms of H_{ad} which are distributed inhomogeneously along the surface. The correlation length of this inhomogeneous distribution is about 1000 Å . In HCl and HBr solutions the signals ER and ES at the potentials of hydrogen and double layer regions have a negative mark and only one minimum at E_r of adsorbtion capacity maximum. It was discovered by ERPh method that $d\Gamma_{Cl^-}/dE$ and especially $d\Gamma_{Br^-}/dE$ contribute greately into capacity at the potentials of maximum of optical signals. The comparison of ER spectra measured in H_2SO_4 and in solutions of halogenhydrogen acids proves that in the last case the anion adsorbtion makes the main contribution to optical signals in a wide range of E_r. Considerable contribution of H_{ad} appeares only at minor E_r in HCl solutions.

Spectra of plasma ER of Pt calculated according to /4/ coincide well with experimental spectra of ER measured in HCl and HBr solutions at the potentials of double layer region. It allows to determine by the data of ER and ERPh the residual charge (q) on adatoms Cl_{ad} and Br_{ad}. The average value of q for Cl_{ad} is about 0,8, and differential q for both halogenides become more positive with E_r and reachs $-0,35\pm0,05$ when Γ_{Cl} and Γ_{Br} are high enough.

Correlation of ES signals in minimum in H_2SO_4, HCl and HBr solutions does not depend on the value of signals (i.e. on the character of primary treatment, on the value of correlation length). It shows the similar geometry of Pt inhomogeneous properties in relation of hydrogen and anions adsorbtion.

1.V.E.Kazarinov, A.M.Funtikov, G.A. Tsirlina.Elektrochimiya, 1988, in press.
2.A.M.Funtikov. Elektrochimiya, 1983, v.19, p.1378.
3.A.M.Brodsky, M.I.Urbakh . Progress Surface Sci.,1984,v.15, p.121. L.I.Daikhin,
4.A.M.Brodsky, M.I.Urbakh. J.Electroanal.Chem.,1984 ,v.171 , p. 1 .

EVALUATION OF THE ADSORPTION PARAMETERS OF ORGANIC MOLECULES FROM ELLIPSOMETRIC MEASUREMENTS ON ELECTRODES

U.Palm, T.Silk, T.Raud

Tartu State University, Laboratory of Electrochemistry
Tartu, 202400 Estonian S.S.R. (U.S.S.R.)

In recent years a considerable increase of the use of optical methods for the study of the electrical double layer structure and electrochemical kinetics is observed. Among these methods the most informative are ellipsometry , electroreflectance, surface plasmon spectroscopy etc.

Fundamentals of the ellipsometry is based on the Drude theory describing the change of the polarization characteristics of monochromatic light beam, due to the reflection , with the structure and properties of the reflecting system. The auto matized ellipsometrc method enables to observe relatively rapid changes in the system and due to the high sensitivity it is possible to carry out investigations in the submonomolecular range of surface coverage. However, the use of ellipsometry for the study of the adsorption of ions and molecules has found comparatively scarce attention of electrochemists /1/. Comparison of the results obtained simultaneously by the optical and impedance studies allows to estimate the limits of the applcability of the ellipsometric method and to elucidate directly the details of surface phenomena accompanied with the adsorption.

Aim of this paper is to make an attempt to determine the adsorption parameters of organic compounds from the simultaneous ellipsometric and impedance (differential capacitance C) measurements on the surface of bismuth single crystal electrodes.

The basic equation of ellipsometry can be expressed in the form $\tan\psi \exp(i\Delta) = R_p/R_s$, where Δ and ψ are ellipsometric angles determining the elliptical polarization state of light beam, and R_p , R_s are reflection coefficients. The value of angle Δ is highly sensitive to the presence of the adsorbed surface films even in the submonomolecular level. It can be

shown that at the surface coverage Θ between 0 and 1, if the thickness of the adsorbed layer is much smaller than the light wave length, the decrease of Δ in respect to the base substrate $\delta\Delta = \Delta_o - \Delta$ is proportional to the coverage Θ. Knowledge of the maximum value $\delta\Delta_m$ of $\delta\Delta$ at $\Theta = 1$, experimentally obtainable in the case of formation of the condensed two-dimensional surface film, allows to estimate Θ values at an arbitrary conditions by formula $\Theta = (\delta\Delta / \delta\Delta_m)_{E=const}$, where E is the electrode potential /2/.

The measurements were carried out in 0.1 M Na_2SO_4 solutions with the varying camphor concentrations c in the range from $5 \cdot 10^{-5}$ to $5 \cdot 10^{-3}$ M. The electrodes were prepared from the single crystal planes of bismuth with crystallographic indexes (111), $(01\bar{1})$ and $(2\bar{1}\bar{1})$. The optical parameters Δ and ψ were determined by automatized ellipsometer L-119 with a rotating analyzer L-118 RA controlled by microcomputer HP-85.The method used permitted to estimate the parameters with the mean error 0.01° and 0.005° for Δ and ψ, respectively. A source of monochromatic light was He-Ne laser with wave-length 632.8 nm.

Our results obtained in 0.005 - 0.5 M Na_2SO_4 solutions demonstrated that within the limits of experimental accuracy an electrolyte concentration had practically no influence on Δ,E-plots. In the potential region $E > E_{q=o}$ (zero charge potential) a flat maximum in the Δ - E plot was observed.

The simultaneous C,E- and Δ,E - measurements in the camphor solutions showed a good correlation between the results of the both sets of measurements. The comparison of the adsorption potentials of camphor indicated for a whole camphor concentration c_k interval a good coincidence of the adsorption-desorption potentials in the case of the all single crystal planes studied by the impedance and ellipsometric methods.

In order to get adsorption isotherm we have calculated the optical degrees of coverage Θ_Δ from Δ - E plots at different c_k and the linearized isotherms were obtained in coordinates $\ln[\Theta/(1-\Theta)c_x]_x$ vs. Θ. So, the camphor adsorption can be described by the Frumkin isotherm, but the limits of its validity depends to some extent upon the crystallography of the crystal face - the most wide applicability region was obtained for the plane $(01\bar{1})$. According to our results the at-

traction coefficient a is independent on E and has a value a ≈ 1.7 for all the crystal planes investigated. By use of the linearized Frumkin isotherm at various potentials an apparent equilibrium constant of adsorption B was determined. A parabolic dependence of B on E with a good correlation coefficients was established. The potential corresponding to the maximum of the parabola was almost equal to the potential of maximum adsorption.The calculated value of ln B were following for the planes studied: (111) - 6.6±0.2 , (01$\bar{1}$) - 7.2± 0.1 and ($\bar{2}\bar{1}\bar{1}$) - 6.8±0.1 . These values are in a qualitative agreement with the results found from the capacity data.

As a conclusion of this work it can be mentioned that an ellipsometric method can successfully be used for the quantitative study of organic compounds on the solid electrodes and a number of effects due to the crystallographic structure of the electrode surface can be distinguished.

References

1. W.K.Paik, M.A.Genshaw, J.O'M.Bockris, J.Phys. Chem., 74 (1970) 4266.
2. T.A.Raud, T.[illegible]Silk, U.V.Palm, Elektrokhimiya, 24 (1988) 394.

SCANNING TUNNELING MICROSCOPY OF INTERFACES RELEVANT TO ELECTROCHEMISTRY

M.H.Dean, D.Liebeskind and U.Stimming

Electrochemistry Laboratory
Department of Chemical Engineering and Applied Chemistry
Columbia University, New York, New York 10027

Scanning tunneling microscopy (STM) allows the study of interfaces with an unprecented high resolution. Materials of sufficient electronic conductivity (although it is currently not quite clear where the lower limit is) forming interfaces with vacuum, air and liquids, including electrolytes, can be investigated using STM. Results will be presented for two areas relevant to electrochemistry: (i) STM investigations of graphite in water and electrolytes and (ii) STM investigations of passive metals in air.

Graphite has been imaged using STM in air, water and electrolyte solutions. Imaging in air of graphite has become a standard procedure and easily yields atomic resolution. Imaging in conductive liquids requires a suppression and/or compensation of the dissipative electrochemical processes. The electrochemical reaction involves a much larger area than the one in the tunneling process which is usually only between two atoms. The area affected by the concurring electrochemical process has been estimated. The bias voltage between tunneling tip and sample at which the electrochemcial process was compensated was compared with the comparable condition of an external potentiostatic circuit. This comparison results in an estimate that about 0.1 to 1 $(\mu m)^2$ of the surface is affected by the electrochemical process. While it can be disanvantatgeous if such electrochemical processes occur when using STM as a probe which is supposed not to interfer with the sample, it can be desirable for small scale electrochemically induced modifications of the surface. For probing the surface with STM, attempts have been undertaken to use valve metals as tip materials. Valve metals are covered with an commonly inert oxide film which renders them electrochemically inactive. In particular, modified aluminum tips show good promise. Such tips can be useful for imaging in electrolytes or under electrochemically defined conditions.

In corrosion research, studies of the passive film which protects the underlying metal from dissolution is of great importance. STM images have been obtained for passive iron and valve metals. In all these cases it is necessary to increase the bias voltage considerably, in most cases up to several volts. This is obviously necessary to sufficiently modify the barrier for the electron transfer created by the oxide. It demonstrates, on the other hand, that materials important in corrosion research can be imaged using STM.

POTENTIAL RELAXATION OF METAL ELECTRODES IMMERSED INTO AQUEOUS SOLUTIONS

J.K. Sass

Fritz-Haber-Institute of the Max-Planck Society
D-1000 Berlin 33, W. Germany

U. Stimming and K. Tellefsen

Department of Chemical Engineering and Applied Chemistry
Columbia University, New York, NY 10027

Fundamental information about the double layer at the metal/solution interface, particularly for potentials near the potential of zero charge (p.z.c.), may be obtained by immersing a clean electrode into a solution and monitoring its open circuit potential as a function of time on a scale of micro seconds. Ideally, a clean electrode should attain a steady potential at or near its p.z.c. upon immersion into a pure solution, provided that no faradaic or adsorption process occurs at the electrode. However, this potential is not observed instantaneously under experimental conditions; moreover, the time required to establish this potential depends on the types of ions in solution and their concentration.

In our work, a polycrystalline Au electrode was immersed in $HClO_4$, H_2SO_4 and $NaClO_4$ solutions with concentrations between 1 and 10^{-5} M. Millipore Milli-Q water was used for all cleaning and solution preparation procedures. The solutions were deaerated with Ar, since any dissolved O_2 would affect the electrode potential achieved. The Au electrode was cleaned in a reducing flame and quenched in Ar. The potential of the Au electrode was measured against a Pd/H electrode or a Pd wire, the potential of which was monitored with a Hg/Hg_2SO_4 reference electrode and potentials are reported with respect to the hydrogen electrode. The potential of the electrode as a function of time within the first 10 to 500 μs upon immersion was measured using a Tektronix oscilloscope with a 7D20 programmable digitizer.

A typical immersion transient of potential vs. time is given in Fig. 1 for 0.01 M $HClO_4$. The initial portion of this transient is approximately linear, followed by decay to the rest potential. This may indicate a relatively rapid formation of the double layer followed by a slower process. The potentials attained at the end of the linear portions of the transients for immersions into $HClO_4$ solutions were between 0.2 and 0.35 V s.h.e., which is close to the value of the p.z.c. of polycrystalline Au reported in the literature/1/.

It was found that time elapsed during the linear portions of the immersion transients were inversely proportional to the square root of solution concentration, as is shown in Fig. 2 for t(linear) vs. $1/\sqrt{c}$ for $HClO_4$, H_2SO_4 and $NaClO_4$, with slopes of 1.15, 0.52 and 1.62 $(mol\ l^{-1})^{1/2}$ μs, respectively. In $HClO_4$ solutions, this relation between relaxation time and concentration was not found for concentrations less than 0.02 M; with these more concentrated solutions, relaxation times of about 2.5 us were found, independent of concentration. These observations suggest that the time elapsed during the linear portion of the transient is due to a process involving ion migration. Also, the average thickness of diffuse double layer into solution calculated by Gouy-Chapman theory also depends inversely upon the square root of concentration. This suggests that the motion of the ions towards or away from the electrode is velocitative in nature, under the influence of an electric field at the electrode surface.

These results indicate that the technique of measuring the open circuit potential of an electrode upon immersion into solution as a function of time on a micro second scale may give useful information concerning the nature of the double layer, in particular the time dependent processes involved before it is completely established.

References

/1/ A. Hamelin, T. Vitanov, E. Sevestyanov and A. Popov, J. Electroanal. Chem., 145 (1983) 225

Acknowledgement

This work was supported in part by the National Science Foundation.

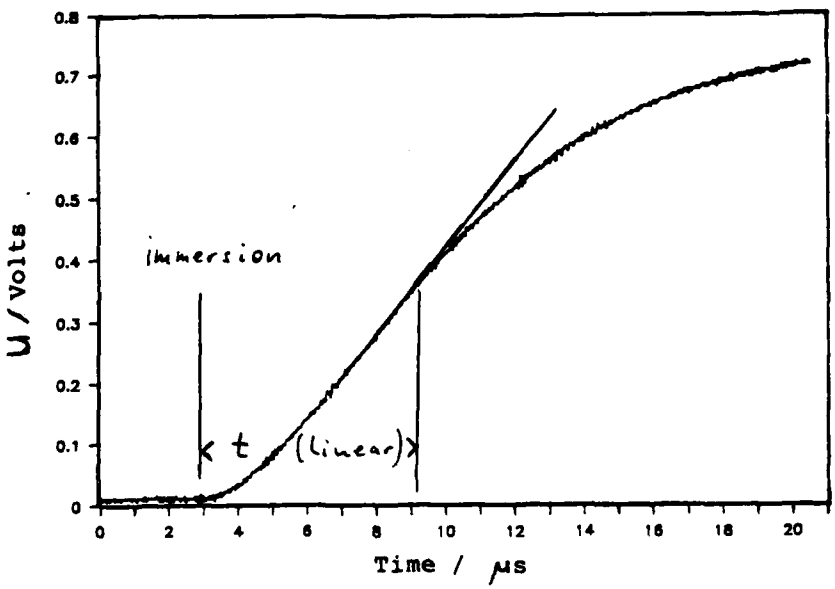


Figure 1 Potential vs. time immersion transient for Au into 0.01 M $HClO_4$ (potential w.r.t. internal Pd reference at 0.615 V against Hg/Hg_2SO_4).

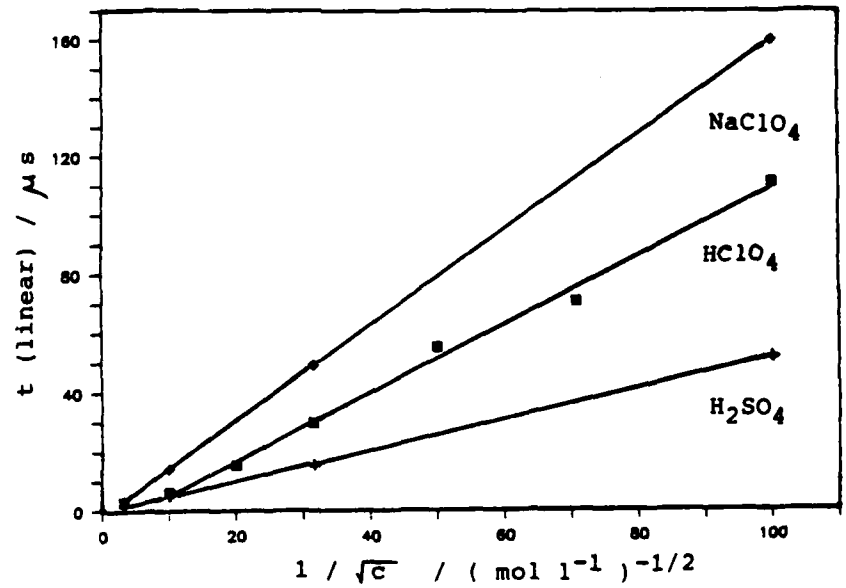


Figure 2 Time elapsed during the linear portion of the transients vs. $1/\sqrt{c}$ for immersion of Au into $HClO_4$, H_2SO_4 and $NaClO_4$ solutions.

Vibrational Electron Energy Loss Spectroscopy of H_2O Adsorbed on Cu(110) with Inverted Orientation Induced by Coadsorbed Cesium

I. Schott, D. Lackey and J.K. Sass

Fritz-Haber-Institut der Max-Planck-Gesellschaft
Faradayweg 4-6, D-1000 Berlin 33

Work function measurements have indicated that H_2O interacting with coadsorbed Cs on Ag(110) is oriented with the hydrogen towards the metal substrate /1/. In this study a similar behaviour for water on Cu(110) has been found and this interesting inverted orientation of a polar solvent molecule has been characterized by HREELS.

Compared to the vibrational properties of H_2O on the clean Cu(110) surface the presence of coadsorbed cesium induces a pronounced shift of the OH-stretch vibration to lower frequency which is accompanied by a substantial narrowing of the band. This finding is attributed to the hydrogen-down orientation of H_2O and a detailed discussion of the OH-stretch band with regards to frequency, line width and intensity will be given.

Thermal desorption experiments and work function measurements have been performed to a assist the vibrational characterization of the H_2O/Cs/Cu(110) system. Several cesium-induced water desorption states have been found and these states can be correlated with the vibrational spectrum of these H_2O molecules and with the work function changes induced by them. Electrochemical implications of our results, in particular those which are important for the use of infrared spectroscopy of interfacial water, will be examined in detail.

/1/ E.M.Stuve, K. Bange and J.K. Sass, Trends in Interfacial Electrochemistry, ed. A.F. Silva, D. Reidel Publishing Company, p. 255, 1986.

2. Semiconductors, Photoeffects and Modified Electrodes

Electrochemistry of Semiconductors in Non-Aqueous Solvents

Amit Kumar, Sharon R. Lunt, Patrick G. Santangelo
Bruce J. Tufts, and Nathan S. Lewis

Department of Chemistry,
Stanford University, Stanford, CA 94305

Our recent research has focused on three aspects of semiconductor electrochemistry: 1) the coordination chemistry of III-V surfaces, 2) the theory of cyclic voltammetry at semiconductor electrodes, and 3) the short wavelength spectral response properties of semiconductor junctions.

In the first area, we have developed procedures to modify the electrically active trap sites at certain semiconductor surfaces. We have demonstrated that adsorption of a family of transition metal ions onto single crystal and polycrystalline GaAs surfaces yields improved I-V response in the KOH-$Se^{-/2-}$ electrolyte. Mechanistic studies of this system implied that the primary effect of the adsorbate is to catalyze hole transfer into the electrolyte.

In order to understand the interfacial chemical reactions at these surfaces, we have performed extensive spectroscopic investigations of several metal ion/GaAs systems. Angle-resolved XPS experiments demonstrated that exposure of single crystal (100) n-GaAs surfaces to solutions of $Co^{III}(NH_3)_5X$ (X=NH_3, N_3^-, SCN^-, H_2O, Br^-, NO_2) yielded reduction to the Co^{II} state and oxidation of the GaAs. For this system, the structural environment of the Co has been determined from EXAFS studies. In these experiments, GaAs powders were exposed to labile Co ammine solutions ($Co^{III}(NH_3)_5OH_2$, $Co^{III}(NH_3)_5N_3$, $Co^{II}(H_2O)_6$ at pH>9). The edge adsorption position and structure for the cobalt ammine complexes were consistent with the XPS assignment of Co^{II}. When either $Co^{III}(NH_3)_5OH_2$ or $Co^{III}(NH_3)_5N_3$ were used, a best fit for the Co/GaAs system yielded 5 or 7 oxygen atoms at a distance of 2.11 or 2.08 Å. A second peak was fit by 6 Co atoms at 3.13 Å. At present, we cannot determine whether any of the second shell contains Ga or As because of the similar scattering properties for Co, Ga and As. However, the EXAFS for $Co^{III}(NH_3)_5OH_2$-treated GaAs powders was extremely similar to EXAFS data taken on bulk $Co(OH)_2$, suggesting that the cobalt species on the GaAs surface is very similar to $Co(OH)_2$.

We have also performed XPS and EXAFS studies on samples which were exposed to the KOH-$Se^{-/2-}$ electrolyte after chemisorption of metal ions. XPS data of this surface yielded a cobalt 2p XPS spectrum which was extremely close to that of $CoSe_2$. Also, EXAFS data on the GaAs treated sample yielded 6 Se atoms at 2.39 A from the Co scatterer.

In order make general statements about the mechanisms of metal ion adsorption on GaAs surfaces, other systems which exhibit improvements in photoanode behavior must be studied. We are currently investigating the properties of Ru ions adsorbed on GaAs. XPS of single crystal (100) n-GaAs and of GaAs powders exposed to $RuCl_3$ have determined the coverage of Ru to be 0.5 monolayer. In order to obtain the structural environment of the surface-bound Ru, we have performed EXAFS on GaAs powders. We are currently in the process of analyzing the EXAFS data, and will update our results at the conference.

The second area of research involves the cyclic voltammetry of semiconductors. The technique of cyclic voltammetry has been used extensively to probe the behavior of the semiconductor/liquid interface, but no quantitative analytical solutions for this experiment have been

reported to date. Initial work in our lab has concentrated on the theory for an ideal surface-attached electroactive species on a ideal semiconductor. To do this, we have developed the analysis using an equivalent circuit approach, with the semiconductor and diode elements placed in series as a working electrode for voltammetry.

Simulations have been performed under varying levels of illumination and for different values of the the diode barrier height, and the voltage scan rate. Chopped scans have also been simulated, where the diode is only illuminated during the forward scan while the reverse scan is performed in the dark. We have demonstrated that the key parameter that needs to be determined for all of these scenarios is the ratio of the open circuit impedance of the diode to the maximum faradaic impedance in the circuit. Use of this parameter has allowed us to generate a set of general working curves for the semiconductor electrode system of interest.

The general conclusions of this work are: 1) at sufficiently high light intensities, the difference in peak anodic potential between a metal/surface-confined redox couple system and the model semiconductor/electrode system is an excellent approximation to the open circuit voltage of the real semiconductor/surface-attached redox couple cell; 2) the limiting (high intensity, small scan rate) wave shape of an illuminated semiconductor electrode should resemble the shape at a metal electrode; 3) the chopped reverse cathodic scan of semiconductor voltammograms will often display a peak cathodic current at a potential more positive then then potential for the peak anodic current. These predictions are currently being compared with experiment on model diode/electrode and on real semiconductor photoelectrode circuits.

The third area of research utilizes short wavelength photons to study the interfacial kinetics of semiconductors. The short wavelength spectral response properties should be sensitive to the interface recombination events, and this response can therefore be used to elucidate the kinetics of majority carrier capture at semiconductor junctions. Using this method, we have shown that the interfacial properties of a freshly etched n-Si electrode in MeOH-$LiClO_4$-$MeFc^{+/0}$ are distinctly different (higher internal quantum efficiency) from that of a Schottky barrier device. With $MV^{2+,+}$ as the redox couple, smaller band bending is induced, yet the spectral response behavior is not affected. The analogous n-Si/Au Schottky barrier device showed a characteristic drop in quantum yield in the short wavelength region. This drop was quantitatively fit with an interfacial collection velocity of 10^7 cm/s, which is the value predicted when thermionic emission controls the interfacial kinetics. We also studied the properties of an MIS device that was fabricated by anodizing n-Si in the MeOH-$LiClO_4$-$MeFc^{+/0}$ system then evaporating gold to form the conducting overlayer. The spectral response behavior was intermediate between the Si/MeOH and Si/Au junctions, indicating a collection velocity that was higher than for the liquid systems but still reduced from the value for the semiconductor/metal Schottky barrier device.

We are currently extending this method to other semiconductor samples, including a-Si:H, GaAs, and InP. The a-Si:H system is especially interesting because the low mobility of carriers in this material makes is relatively sensitive to the interface kinetic properties. We expect that these systems will yield the first available data on the differences in collection velocity between Schottky, MIS, and liquid junctions. We will update our progress in this, and all other related areas, at the meeting.

Electronic Properties of Amorphous Silicon Surface Barriers and Junctions

W.E. Spear and S.H. Baker
Carnegie Laboratory of Physics, University of Dundee, Dundee, Scotland

The aim of this paper is to discuss some aspects of the electronic behaviour of the metal/a-semiconductor barrier and of the a-semiconductor junction, which are of relevance to the main subject of the Conference. The discussion will be confined to amorphous silicon (a-Si) prepared by the plasma decomposition of silane, which is of much current interest as an electronically viable and controllable thin film material. We shall begin with a brief survey of preparation and substitutional doping of a-Si and also consider the distribution and electronic nature of the states in a-semiconductors.

The main part of the paper will deal with the formation of the metal/a-Si barrier, the effect of interfacial states and with the barrier profile in the presence of the localised state distribution in the mobility gap of the a-material. We shall discuss recent experimental work using internal photoemission to investigate the barrier height on a-Si in relation to the metal workfunction. Analysis of the results leads to interfacial state densities of 10^{13} - $10^{14} cm^{-2} eV^{-1}$.

The final section of the paper will be concerned with some of the electronic properties of the a-Si p^+-i-n^+ junction. We shall draw attention to the injecting and blocking properties of the junction which are now widely used in fundamental studies on a-Si. The promising photovoltaic properties of the p^+-i-n^+ devices have led in recent years to world-wide industrial developments of large area a-Si devices for solar energy conversion.

Picosecond time-resolved photo-generation of charge carriers at electrode interfaces

F. Willig

Fritz-Haber-Institut der Max-Planck-Gesellschaft
Faradayweg 4-6, D-1000 Berlin 33, FRG

A great wealth of information has been collected over the years in stationary measurements at photoelectrochemical systems. Stationary photovoltages and photocurrents are interpreted with model concepts that contain implicit assumptions about the extremely fast charge carrier dynamics in the photo-electrochemical systems.

In the field of homogeneous photochemistry and in the field of solid state physics related light-induced processes have been studied since several years with direct time-resolved methods, i.e. with picosecond time resolution and recently also with sub-picosecond time resolution. It turns out that reliable experimental information on ultrafast processes can only be gained from direct time-resolved methods whereas the interpretation of stationary yield type measurements is more ambiguous.

Consequently in the last years several groups have taken up direct time-resolved methods for studying also the fast dynamical processes in photoelectrochemical systems. In particular nano- and recently picosecond time-resolved measurements of electron-hole pair separation have been carried out as laser-induced electrical response (LER) at insulator /1/ and semiconductor /2/ electrodes. We neglect here measurements of the trivial RC limited response of the circuit. Another direct picosecond time-resolved method involves fluorescence quenching of adsorbed molecules (FAM) that inject charge carriers into insulator /3,4/ and semiconductor electrodes /5/. Free carrier absorption has been utilized recently in transient grating experiments to study the discharge into the electrolytic solution from the surface of semiconductor electrodes /6/.

We will discuss in detail information that has been obtained on fast charge carrier dynamics at semiconductor and insulator electrodes, firstly from laser-induced electrical response (LER) measurements and secondly from fluorescence quenching of adsorbed molecules (FAM). The LER technique has been applied in

our laboratory with 70 ps rise time and a sensitivity limit in the range of μV. The FAM technique has been utilized with 10 ps time resolution for coverages down to 10^{-2} applying a synchroscan streak camera and with 40 ps apparent half width down to coverages of 10^{-4} applying time-resolved single photon counting. A more recent variation of the FAM method has been started in our laboratory in the form of time-resolved fluorescence decay in the individual subbands of superlattice structures in contact with an electrolyte. These signals contain direct time-resolved and energy-resolved information on charge carrier discharge into the electrolyte.

Finally we will give an outlook on the foreseeable progress in this new field of picosecond time-resolved measurements at photoelectrochemical and electrochemical systems.

/1/ M. Eichhorn, F. Willig, K.-P. Charlé, and K. Bitterling, J. Chem. Phys. 76 (1982) 4648

/2/ K. Bitterling and F. Willig, J. Electroanal. Chem. 204 (1986) 211; K. Bitterling, F. Willig and F. Decker, ibid, 228 (1987) 29

/3/ N. Nakashima, K. Yoshihara, and F. Willig, J. Chem. Phys. 73 (1980) 3553

/4/ K. Kemnitz, N. Nakashima, and K. Yoshihara, preprint

/5/ R. L. Crackel and W. S. Struve, Chem. Phys. Letters 120 (1985) 473

/6/ J. J. Kasinski, L. A. Gomez-Jahn, Sh. Gracewski, and R. J. D. Miller, preprint

NEW MATERIALS AND TECHNIQUES IN PHOTOELECTROCATALYSIS

Helmut Tributsch
Hahn-Meitner-Institut, Bereich Strahlenchemie
1000 Berlin 39, Fed. Rep. of Germany

Abstract:
Practically all materials which have proven to be useful for photoelectrocatalysis up to now have energy gaps which are too large to permit reasonably efficient energy conversion according to thermodynamics. It can be shown that this is due to the fact that the photogenerated overvoltage increases linearly with the energy gap (a consequence of properties of the quasi-Fermi level). The overvoltage dependent activation energy for electron transfer reactions can thus be reduced to much smaller values for large gap than for small gap semiconductors. In order to provide efficient photoelectrocatalysis with semiconductors of lower energy gap they have to provide electron transfer pathways across the electrode/electrolyte interface which are characterized by a low activation energy and a high interfacial minority carrier concentration. Semiconductor materials with more favourable interfacial properties for multi-electron transfer are needed as well as additional experimental techniques which provide informations about photogenerated charge carriers in interfaces and their reactivity in dependence of interfacial properties.

Photoelectrodes for interfacial coordination chemistry

Experimental evidence is presented which demonstrates that semiconducting transition metal chalcogenides with strong d-character (e.g. FeS_2) permit an efficient channelling of photogenerated holes via attached interfacial molecular bridges (e.g. -O-,CN-,-CO-) to redox species in the electrolyte, which is far more effective for electrode stabilization than electron transfer by tunnelling processes from redox species or conventional semiconductor surface modification/1/2/. Catalytical properties of d-band materials are drastically improving when electronic charge carriers are reacting via mixed transition metal clusters which serve as electron reservoirs (semiconducting cluster compounds of the type $Mo_4Ru_2Se_8$ /3/). The possibility of coupling photoelectronic processes of d-band materials to interfacial coordination chemistry may open interesting long term perspectives for electrochemical solar energy conversion: The semiconducting material could act like a large antenna for photons generating charge carriers which are safely transferred across the

semiconductor/electrolyte interface via transition metal bridges involving negligible activation energy and may be used for catalysis and energy conversion in chemically tailored groups attached to the bridges and protruding into the electrolyte.

Microwave interfacial and -photoelectrochemical techniques

Photogenerated charge carriers in interfaces can be determined by contact free measurements in time resolved, space resolved and stationary experiments/4/. Valuable information can not only be gained on recombination processes, charge separation and interfacial electron transfer reactions but also on photogenerated charge carriers which are lost due to side reactions and escape conventional photoelectrochemical detection/5/. Microwave photoelectrochemistry is becoming a very useful experimental technique for the characterization and optimization of photoactive interfaces and for tracking down mechanisms responsible for carrier losses. Examples of studies of semiconductor/electrolyte interfaces, of catalytic powders, the influence of surface morphology, chemical treatment and heterojunction formation of semiconductor interfaces with metal and polymer films will be provided .

A complementary technique aimed at improving the knowledge on the interrelation of surface structure and composition with photoactivity involves photoelectron spectroscopy (XPS) combined with in-situ determination of photovoltages.

These new tools may help to develope semiconductor interfaces towards higher photoelectrochemical and photocatalytic efficiencies.

References

/1/X.-P. Li, N. Alonso Vante and H. Tributsch, J. Electroanal. Chem. 242 (1988) 255
/2/ B. Schubert, N. Mgoduka and H. Tributsch, submitted
/3/ N. Alonso Vante and H. Tributsch, Nature 323 (1986) 431
/4/ M. Kunst and H. Tributsch, Chem. Phys. Lett. 105 (1984)
/5/ B. Messer and H. Tributsch, J. Electrochem. Soc. 133(1986) 2212

STRUCTURE AND DYNAMICS IN MODIFIED ELECTRODES

Larry R. Faulkner
Department of Chemistry
University of Illinois
1209 W. California St.
Urbana, Illinois 61801
USA

The placement of a modifying layer on the surface of an electrode is usually undertaken to alter the reactivity of the electrochemical interface. If the structure is thicker than a monolayer, the system normally has the effect of transforming the conventional two-dimensional reactive plane of the electrode into a three-dimensional reactive zone bounded by the electrode on one side and the solution phase on the other. This paper will concern systems in which the modifying structure is thicker than a few monolayers, but not so thick that the electrode effectively loses contact with the solution outside the structure. In practice, the thickness of the layer is 10-2500 nm.

If the modifying layer is to serve effectively as a three-dimensional reactive zone, it must permit efficient movement of the chemical species that are to react or evolve there. These species must be able to permeate the structure and to cross the boundary between the solution and the layer. Moreover, the layer must offer facile transport of electrons, because electrochemical reactivity throughout the layer depends on communication of charge between each reactive site and the electrode. This paper will deal with the relationship between the structure of the layer and the transport of molecules, ions, and electrons within it.

First, there will be a discussion of two limiting cases of film structure. New experimental results concerning quaternized poly(4-vinylpyridine) [QPVP] and poly(styrenesulfonate) [PSS] will be examined. Redox centers have been dispersed in QPVP by electrostatic binding of ferri/ferrocyanide and by coordination of $Ru(bpy)_2Cl^{1+/2+}$ moieties to free pendant pyridine groups. In PSS, $Ru(bpy)_3^{2+}$ and $Os(bpy)_3^{2+}$ were immobilized by ion-exchange. In addition, we studied the QPVP medium by binding $Re(CO)_3(phen)$ coordinatively to free pendant pyridine, an operation that fixed a luminescent rhenium complex within the film.

Observations by hydrodynamic voltammetry, infrared spectroscopy, and luminescence spectroscopy show that the QPVP-based networks are usually well solvated when they are exposed to aqueous working solutions and that they normally permit the rapid motion of mass by diffusion. However, the structure of the film is influenced strongly by the nature of the anion used in the supporting electrolyte. Perchlorate causes the film to collapse and become almost fully

unsolvated, so that the motion of mass is strongly retarded. The diffusion of electrons was characterized by steady-state and transient methods, and identical results were obtained. Measurements over a range of temperatures afforded activation parameters. The diffusion coefficient for electrons moving among ferri/ferrocyanide centers declines with increased loading of the iron complexes. This result and the magnitudes of the activation energies suggest that the diffusion of charge is governed by local, tethered motion of the redox centers, which seem to have to come in contact to exchange charge.

The PSS-based networks were studied in acetonitrile, and all evidence points to their being very compact and not very fully solvated. Electron diffusion coefficients were measure by several steady-state means and showed almost exponential rises with increased loading of the redox centers in the film. The results are consistent with a view of the electron motion as being controlled by the hopping of electrons among redox centers that are not necessarily in contact.

A model capable of predicting the concentration dependence of electron diffusion coefficients will be presented. The model is microscopic in character. It is based on a random walk by extended electron transfer among a random dispersion of hard spheres. Electron hopping is presumed to occur, on the average, across the mean nearest neighbor distance, which can be computed from the concentration of centers. The hopping time is the inverse of the first-order rate constant for "extended" electron transfer between redox centers not in contact. It is assumed to be an exponential function of the edge-to-edge separation between the redox centers. The model provides a basis for predicting the manner in which the electron diffusion coefficient will change as one modifies the size of the redox centers or the electronic properties of the centers or the intervening matrix.

The diffusion coefficients for the PSS-based systems fit the model to a promising degree.

Experimental and theoretical work in progress at the time of composition of this abstract may permit a discussion of the expected manner in which the electron diffusion coefficient depends on the local oxidation state of the network.

The paper will end with a discussion of implications for the design of modification layers that can permit the efficient transport of both mass and charge.

ELECTROLYTE ELECTROREFLECTANCE AND PHOTOELECTROCHEMICAL TOPOLOGICAL INVESTIGATION OF SEMICONDUCTOR ELECTRODES BY SCANNING LIGHT-SPOT OPTICAL MICROSCOPY

G. Razzini and L. Peraldo Bicelli

Centro di Studio sui Processi Elettrodici del CNR,
Dipartimento di Chimica Fisica Applicata del Politecnico,
Piazza L. da Vinci, 32, 20133 Milano, Italy

INTRODUCTION

In order to produce efficient photoelectrochemical (PEC) devices, optimization of the electrode properties seems to be necessary. For this purpose, the control of the semiconductor surface through light-spot tecniques may be important.

A "reflex microscope" provides an excellent optical system to observe the semiconductor electrode surface at the same time when "in situ" electrolyte electroreflectance (EER) and PEC experiments are performed. Such a system was employed to study the PEC behaviour of layered transition metal dichalcogenides and to analyse the EER and photocurrent signal of n-$CuInSe_2$ electrodes at different surface areas. This helped us to understand the influence of the semiconductor inhomogeneities on the PEC cell performance.

EER is a well-known non-destructive technique, particularly useful for the "in situ" study of the semiconductor-electrolyte interface if the surface chemistry of the semiconductor electrode is under control /1/. In fact, provided that stabilizing electrolytes and suitable potentials are used, it allows not only to measure the semiconductor direct band-gap energy and the flatband potential, but also to detect rapid shifts of the latter potential associated with chemical and/or PEC reactions occurring at the semiconductor-electrolyte interface.

Topological investigations using EER have already been reported with semiconductors inhomogeneously doped /2, 3/ and laser scanning techniques have been adapted to detect local variations in the quantum efficiency of semiconductor-electrolyte junctions /4/. With regard to these methods, the optical microscopy technique has the advantage of allowing the simultaneous observation of the electrode surface. This resulted to be very helpful to identify surface areas with different EER and PEC activity. Moreover, grain boundaries and localized defects were shown up very clearly on the surface of polycrystalline samples, so that it was easy to go back with the light beam to the same region though the electrode had to be removed from the cell in order to undergo different surface treatments.

EXPERIMENTAL

In principle, the experimental set-up for the "in situ" measurements is rather simple. A three-electrode PEC cell with the working electrode surface parallel to the optically transparent cell bottom is placed on the specimen supporting table of a reflex microscope and moved along the X and Y directions by means of micrometric screws. In this way, it is possible to explore the overall semiconductor surface while point by point EER and PEC measurements are performed.

RESULTS AND DISCUSSION

Photocatalytic behaviour of n-$MoSe_2$

Observation with our "in situ" technique of illuminated surface areas of $MoSe_2$ single crystals in contact with a 1M KI solution evidenced the formation of localized red spots due to iodine photoproduction /5/. The theoretically expected linear relationship between the photopotential and the logarithm of the light intensity was not followed on these "active" regions where much higher photopotentials (and thus higher efficiencies) were obtained than on the "inactive" areas. The cathodic reaction compensating the photocatalytic process was oxygen reduction as no iodine photoproduction was noticed in oxygen-free cells.

Hydriodic acid photodecomposition

Light induced HI decomposition in hydrogen and iodine was observed on the surface of platinized n-WSe_2 single-crystal electrodes /6/. Moreover, while the iodine production occurred on the smooth surface areas of the layer-type dichalcogenide, the hydrogen evolution process took only place on the microscopic surface steps possibly filmed with platinum.

Topological investigation of n-$CuInSe_2$ polycrystalline electrodes

$CuInSe_2$-based photovoltaic as well as PEC solar cells have shown impressive output stability and high conversion efficiency. Stable PEC cells can be made using polycrystalline n-$CuInSe_2$ photoanodes in contact with the aqueous polyiodide electrolyte and solar energy conversion efficiencies up to 12% have been obtained with these devices /7/.

Since n-$CuInSe_2$ polycrystalline electrodes are characterized by a very large grain size (up to some mm), donor concentration inhomogeneities as well as segregation phenomena at grain boundaries could easily be resolved by means of our optical techniques using radiation in the visible or in the near IR range /8/. Lead electrodeposition on the semiconductor surface was also performed and it was shown to occur preferentially on localized surface regions. The configuration of the electrodeposit resembled closely the EER map obtained from a systematic topological investigation. In fact, the intensity of the R/R signal was

higher in the regions where lead electrodeposition took place and viceversa. These results revealed that low-doped (high resistivity) domains exist on the surface of the n-type chalcogenide. Electroreduction of the semiconductor surface at potentials near flatband occurred at the less resistive area where bands unpinning was observed by EER. This was not the case for the low-doped domains of high resistivity where the band edges remained pinned. Light-spot PEC measurements with both monochromatic and white light illumination confirmed the electro-optical results.

CONCLUSIONS

The here reported results clearly evidence the importance of performing EER and PEC measurements on localized surface areas while simultaneously inspecting the semiconductor surface by optical microscopy. This particularly in view of producing well behaved electrodes for PEC cells.

REFERENCES

/1/ W.M. Shen, W. Siripala, M. Tomkiewicz and D. Cahen, J. Electrochemical Soc., 133, 107 (1986).

/2/ F.H. Pollak, C.E. Okeke, P.E. Vanier and P.M. Raccah, J. Appl. Phys., 49, 4216 (1978); 50, 5375 (1979).

/3/ J.L. Aubel, G. Pidick, U.K. Reddy and S. Sundaram, Rev. Sci. Instrum., 56, 268 (1985).

/4/ T.E. Furtak, D.C. Canfield and B.A. Parkinson, J. Appl. Phys., 51, 6018 (1978).

/5/ G. Razzini, J. Power Sources, 5, 263 (1980); L. Peraldo Bicelli and G. Razzini, Surf. Technol., 16, 37 (1982); 20, 383 (1983); 22, 115 (1984).

/6/ L. Peraldo Bicelli and G. Razzini, Surf. Technol, 20, 393 (1983).

/7/ G. Razzini, L. Peraldo Bicelli, B. Scrosati and L. Zanotti, J. Electrochem. Soc., 133, 351 (1986).

/8/ G. Razzini, L. Peraldo Bicelli, B. Scrosati, M. Pujadas, P. Salvador and F. Decker, J. Electrochem. Soc. (in press).

ELECTROCHEMICAL AND PHOTOELECTROCHEMICAL STUDY OF VACUUM EVAPORATED FILMS OF THIOPHENE OLIGOMERS

Denis FICHOU, Gilles HOROWITZ, Yoshinori NISHIKITANI and Francis GARNIER
Laboratoire de Photochimie Solaire, C N R S, 2 rue Henry Dunant, 94320 Thiais, France

INTRODUCTION

Polythiophene (PT) belongs to the class of the oragnic conducting polymers : its conductivity can be varied over several orders of magnitude by electrochemical or chemical doping and undoping. PT is electrochemically synthsized through the oxidation of the monomer in an organic solvent [1]. In its undoped state, PT behaves as a p-type semiconductor and has been reported as a possible electrode for photoelectrochemical (PEC) cells [2-5].

We have realized in our laboratory thin films of thiophene oligomers (nT) (n=4-8) by the technique of vacuum evaporation. Oligomers present the advantage over polymers of a well-defined structure, especially as far as the conjugation length, an important parameter controlling the properties of the material, is concerned. In this communication, the electrochemical doping and undoping of alpha-sexithienyl (6T) are studied. We also give results on the photoelectrochemical properties of this material

EXPERIMENTAL

Alpha-sexithienyl was synthesized from terthienyl (Fluka) according to the method proposed by Kagan and Arora [6]. 6T films were then evaporated on tin-oxide-coated glass slides at a pressure of 5×10^{-3} Pa by heating in a tungsten crucible. For PEC measurements, 6T was deposited on a nickel foil and all the parts of the foil not covered by the oligomer were isolated with parafin.

Electrochemical and photoelectrochemical measurements were carried out in a classical 3-electrode cell, with a Pt couter-electrode and a saturated calomel electrode (sce) reference. A PAR 173 potentiostat and 175 universal programmer were used.

Absorption spectra were recorded with a Cary 219 (Varian) spectrophotometer. The photocurrent action spectrum was obtained under chopped light with the help of a Jobin-Yvon HRS2 monochromator, and a PAR 128A lock-in amplifier.

RESULTS AND DISCUSSION

The electrochemical behavior of vaccum evaporated 6T on conducting SnO_2 in a 0.1 M

$LiClO_4$ acetonitrile solution is shown in Fig. 1. The cyclic voltammogram presents an irreversible oxidation peak at + 1.2 V/sce, and reversible oxidation and reduction peaks at 0.9 V/sce and 0.65 V/sce. These two last peaks correspond to the doping and undoping of the oligomer. The corresponding peaks on PT are located at 0.7 and 0.3 V/sce, respectively. The doping and undoping were verified by recording the absorption spectra of the oxidized and reduced form (Fig. 2). Also shown in Fig.2 is the absorption of the as-deposited film which shows several peaks, that can be ascribed to the different conformations of the oligomer [7]. The absorption edge occurs at about 600 nm (2 eV). Absorption at higher wavelengths than this edge is observed on the oxidized oligomer. This additional absorption reflects the appearence of states within the forbidden band, responsible for the increased conductivity of the material. The conductivity is $\simeq 10^{-8}$ S/cm for the undoped state, and 10^{-3} S/cm for the doped one. Importantly, the absorption spectrum of the reduced film does not coincide with that one of the as-deposited 6T. This is probably due to a change of the conformation of the oligomer, which could ascribe for the irreversible peak in the cyclic voltammogram.

The PEC behavior of 6T is shown in Fig. 3. It was obtained under illumination with a tungsten-halogen lamp in a water solution of 0.02 M $EuCl_3$. This salt was chosen because the redox potential of Eu^{2+}/Eu^{3+} (-0.59 V/sce) is more negative than the rest potential of the 6T-coated electrode. The same experiment with the Fe^{2+}/Fe^{3+} couple (+0.52 V/sce) resulted in the absence of a photocurrent.

The photocurrent action spectrum (Fig. 4) fairly follows the absorption spectrum. This means that 6T behaves as a p-type semiconductor with a band gap of 2.0 eV, and is thus very similar to PT in this respect.

REFERENCES

1. G. Tourillon and F. Garnier, *J. Electroanal. Chem.* **135** 173 (1982)
2. S. Glenis, G. Tourillon and F. Garnier, *Thin Solid Films* **122** (1984)
3. K. Kaneto, G. Ishii and S. Yoshino, *Jap. J. Appl. Phys.* **24** L320 (1985)
4. T. Kenmochi, E. Tsuchida, M. Kaneko and A. Yamada, *Electrocim. Acta* **30** 1405 (1985)
5. G. Zotti, G. Schiavon and G. Mengoli, *Mol. Cryst. Liq. Cryst.* **121** 341 (1985)
6. J. Kagan and S. K. Arora, *Macromolecules* **20** 1937 (1983)
7. D. Fichou, G. Horowitz, Y. Nishikitani and F. Garnier, submitted.

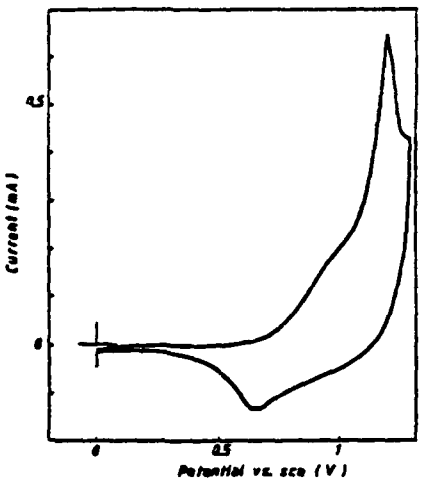


FIG. 1. Cyclic voltammogram of α-sexithienyl (6T) evaporated on SnO_2 glass, in 0.1 M $LiClO_4$ acetonitrile solution. Scan speed : 10 mV/s.

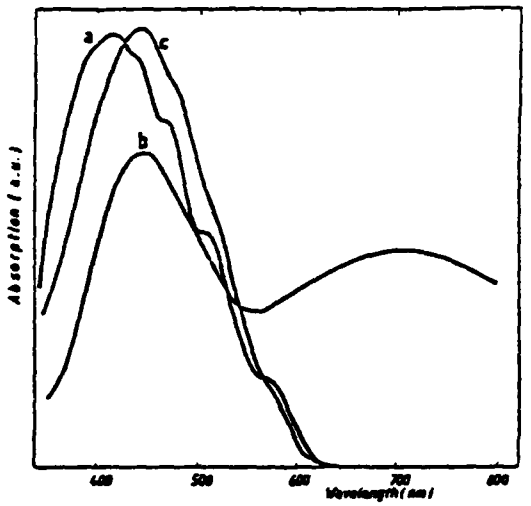


FIG. 2. Absorption spectra of 6T on SnO_2 glass. a : as deposited. b : after electrochemical oxidation. c : after electrochemical reduction.

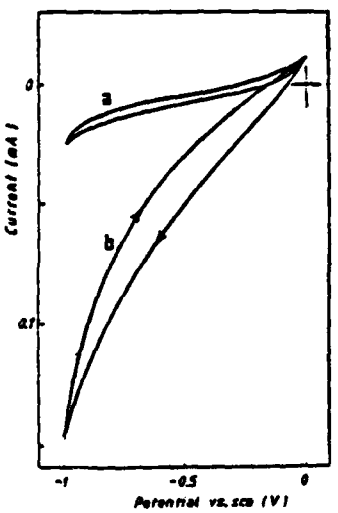


FIG. 3. Current-voltage plot of 6T in 0.02 M $EuCl_3$ water solution in the dark (a) and under white light illumination (b)

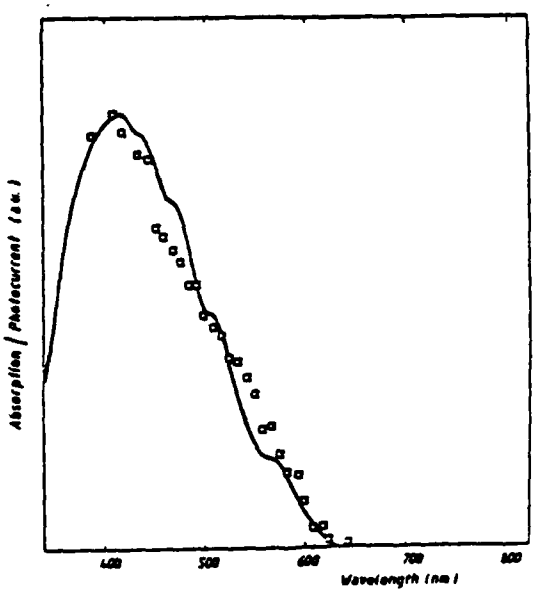


FIG. 4. Absorption spectrum (full line) and photocurrent action spectrum (squares) of 6T in 0.02 M $EuCl_3$ water solution at 0.4 V vs. sce.

THE SEMICONDUCTING PROPERTIES OF PASSIVE TIN ELECTRODES IN SLIGHTLY ALKALINE SOLUTIONS

M. Šeruga, M. Metikoš-Huković, S. Ferina
Institute of Electrochemistry, Faculty of Technology
University of Zagreb, Yugoslavia

INTRODUCTION

Electrochemical processes at metallic electrodes are often affected by the presence of a surface oxide film. Tin is a moderately corrosion resistant metal, that finds its most important applications in the tin - plate (food industry) and electronic industries. Its anodic behavior has been studied on several occasions[1,2,3]. Thin semiconducting SnO_2 films on glass substrates have frequently been used as working electrodes in electroanalytical and photoelectrochemical studies because of their good optical transparency, high electrical conductivity, high mechanical strenght and excellent chemical or corrosion resistance. In this work the formation, growth, reduction and solid state properties of passive film on tin in ammonium borate buffer solutions have been investigated.

EXPERIMENTAL

The electrodes were made from spectrocopically pure tin ($A=0.5cm^2$). The electrochemical cell was constructed in such a way that the electrode could be illuminated during the experiments. Investigations have been carried out at 25°C in 0.05M ammomium borate buffer solutions, pH=8.2 using cyclic voltammetry, a.c. impedance and photopolarization techniques in the potential range from -1.7 to +1.7V. The photopotential was measured by the light impulse in order of milliseconds. The reference electrode in all cases was saturated calomel electrode and all potentials are given with respect of this electrode.

RESULTS AND DISCUSSION

Figure 1 illustrates the general features of the passivation of a freshly polished tin electrode under a controlled potential scan. During the first anodic scan several poorly defined anodic current peaks are obtained. In the following successive scans the peak at +0.5V is removed, and the current plateau, formed just prior to oxygen evolution, better defined. Primary passivity is attained when the metal is covered with a monolayer of Sn(II) oxide. The formation of $Sn(OH)_2$ at more negative range of potentials (-1.15 to -0.78V) can be detected only by the a.c. capacitance measurements (Fig.1). The anodic current on this potentials is low, while the rate of H_2- evolution is high and the sum of these coupled reactions may result in the cathodic current. At more positive potentials the passive layer consists only of $Sn(OH)_4$ oxide which ensures more efficient passivation. Dehydration of $Sn(OH)_4$ to SnO_2 at +0.5V involves capacity and photopotential change as shown in Fig.1. The presence of two cathodic reduction peaks also indicates that Sn(IV) can exist in more species with different electrochemical stability (Fig.1). Capacitive and photopolarization measurements give significant information not only about the film formation process but also about the electronic structure of the film.

The semiconducting properties of the solid phase were studied under conditions where electronic conductivity prevailes (Fig.2). Passive films on tin show n-type semiconducting properties. Thin films followed a Mott-Schottky behavior; both flat band potential (E_{fb} = -1.3V) and donor concentrations have been estimated ($N_D = 0.2 \cdot 10^{16}$ cm^{-3}).

REFERENCES

1. A.M.Shams El Din, F.M.Abd El Wahab, Electrochim. Acta, 9 (1964)883
2. S.D.Kapusta, N.Hackerman, Electrochim. Acta, 25 (1980)1625
3.M.L.Varsanyi, J.Jaen, A.Vertes, L.Kiss,Electrochim.Acta,30(1985)529

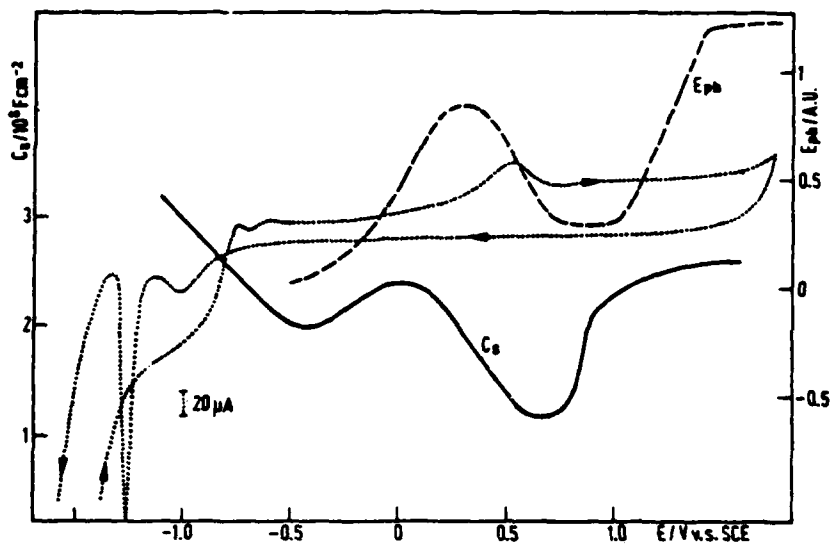


Fig.1. Capacitance, photopotential curves and cyclic voltammogram obtained at 10 mV/s, on freshly polished tin electrode in 0.05M borate buffer solutions, pH=8.2.

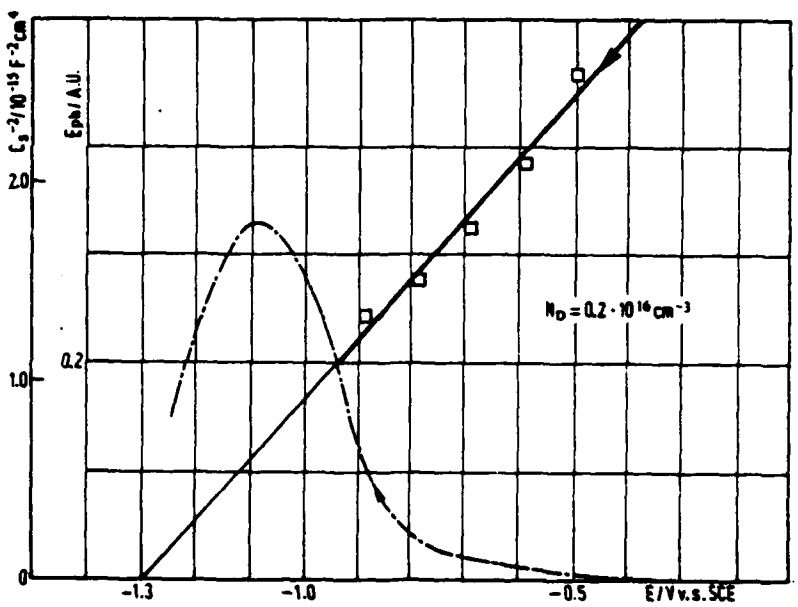


Fig.2. Photopotential-potential plot and the Mott-Schottky plot at 1000 Hz for an oxide covered tin electrode (n-type) in 0.05M borate buffer solutions, pH=8.2.

PHOTOTHERMAL BEAM DEFLECTION AND PHOTOACOUSTIC EXPERIMENTS IN PHOTOELECTROCHEMISTRY

F. Decker, M. Fracastoro-Decker, N. Cella and H. Vargas

Instituto de Física, Unicamp, 13081 Campinas, S.P., Brasil

Introduction

The knowledge of power dissipation mechanisms in photovoltaic and photoelectrochemical (PEC) cells provides an useful tool to determine their conversion efficiency and to design more efficient devices (1). Such mechanisms mainly result in heating of the fluid around the semiconducting element, and this heat transfer process can be detected by the deflection of a probe beam parallel to its illuminated surface (2), or by a pressure wave in an acoustic chamber (3) flush with the semiconductor back surface. We have demonstrated that, in the case of a PEC cell using a reactive electrolyte, the refractive index gradient close to the electrode surface can be due not only to a temperature variation, but also to a concentration change with distance from the electrode (4). Upon illumination with chopped light, thermal and ion concentration waves are generated at the electrode, which propagate with different diffusion coefficients into the electrolyte and contribute significantly to the deflection signal. We have shown, however, that in some cases these two contributions can be separated by a careful choice of the operation parameters of the cell. On the other hand, in the photoacoustic experiments the signal is mainly due to power dissipation within the electrode. It is then possible to investigate several possible dissipation mechanisms taking place within the semiconductor: hot carrier cooling, thermalization of charge carriers across a potential barrier, and contact effects.

Photothermal beam deflection experiments

We have performed experiments on metal and semiconducting electrodes with and without light and have observed that when the illuminated cell operates at open circuit, the thermal signal is predominant, whereas when a photocurrent is applied, both ionic and thermal effects contribute to the deflection of the probe beam. The observed signal, S, is proportional to the beam deflection, ψ, which is given by:

$$\psi = \frac{\ell}{n}\left(\frac{\partial n}{\partial c}\frac{\partial c}{\partial x} + \frac{\partial n}{\partial T}\frac{\partial T}{\partial x}\right)$$

ℓ being the interaction length, n the refractive index, c the concentration, T the temperature and x the distance between electrode and probe beam. From the above equation we deduced:

$$\ln S \propto \ln \psi = 0.5 \ln \left\{ C_1^2 \exp\left(-2\sqrt{\pi f/D_{ion}}\, x\right) + C_2^2 \exp\left(-2\sqrt{\pi f/D_{th}}\, x\right) - \right.$$

$$\left. - 2\, C_1 C_2 \exp\left[-\sqrt{\pi f}\, x \left(1/\sqrt{D_{ion}} + 1/\sqrt{D_{th}}\right)\right] \sin\sqrt{\pi f}\, x \left(1/\sqrt{D_{ion}} - 1/\sqrt{D_{th}}\right)\right.$$

By means of a fitting procedure of ln S vs. x or ln S vs. $\sqrt{f}$ curves the values of the thermal and ionic diffusion coefficients in the electrolyte, D_{th} and D_{ion}, can be calculated. D_{th} is almost three orders of magnitude larger than D_{ion}, and this makes the thermal signal predominant at high frequencies or large distances from the electrode, whereas at

low frequencies (below 1 Hz) or close to the electrode surface the ionic phenomenon strongly affects the total signal, although the thermal contribution is still present. When operating the cell with a modulated current in the dark, on the other hand, only the ionic effect is expected. However, experiments made without light on a Cu electrode in 1% H_2SO_4 have shown that also a thermal contribution is present, which we attribute to Peltier heat generated at the electrode/electrolyte interface rather than to Joule losses, due to the high conductivity of the metal and of the electrolyte used. We have also made beam deflection experiments in the dark on a semiconducting (n-GaAs) electrode and have noticed an even more significant thermal signal. In this case the thermal signal can be attributed not only to the Peltier heat, as in the case of a metal electrode, but also to the heat dissipated by the majority carriers at the semiconductor/liquid interface (due to the mismatch between redox potential and conduction band edge) and across other potential barriers in the solid (i.e., space-charge layer and ohmic contacts). Minority carrier injection (in the dark) and subsequent bulk recombination in the solid will depend mainly on the redox ions in the electrolyte, and can contribute to the thermal signal as well.

Photoacoustic experiments

Because the photoacoustic (PA) experiment is mainly a transmission experiment, i.e., the heat generated mainly at the semiconductor/electrolyte interface has to be transferred across the bulk substrate to the PA chamber in contact to the back surface of the electrode, this technique is less sensitive - in principle - to electrolyte effects and interfacial effects, than the Photothermal Beam Deflection one. We have therefore studied the PA signal of an illuminated $CdSe_xTe_{1-x}$ photoelectrode, at fixed chopper frequency, as a function of the potential applied by means of a potentiostat. In the reverse polarization, the PA signal usually varies linearly with the potential, as it was already observed with other photothermal techniques (5) and with PA (3). At forward bias, majority carrier injection into the electrolyte (see former section) can take place at the same time as minority carrier reaction at the electrode surface. At the cell open circuit potential (cell disconnected) the PA signal is the sum of the power dissipation of both effects (1). Furthermore, injected current-related distortion of the PA signal may occur if the illuminated area is less than the electrochemically active area of the electrode, in analogy to what observed in photovoltaic cells (6). At the electrode flat-band potential (zero photocurrent) the PA signal is only due to the photon flux and to the photon energy. From such signal and from the slope of the PA signal at reverse bias one can calculate the intrinsic quantum yield of the photocurrent (3). The power conversion efficiency and the power dissipation due to injection currents can also be calculated, according to a model analogous to that developped for photovoltaic cells (6).

Acknowledgements

The financial support of CNPq, FAPESP and FINEP is acknowledged. We thank Dr. David Cahen for many stimulating discussions.

References
1. D. Cahen, H. Flaisher and M. Wolf, "Photoacoustic and Photothermal Phenomena", Proc. 5th Int. Topic. Meeting, Heidelberg, 1987.
2. R.E. Wagner, V.K.T. Wong and A. Mandelis, Analyst 111, 299 (1986).
3. J. Rappich and J.K. Dohrmann, "Photoacoustic and Photothermal Phenomena", Proc. 5th Int. Topic. Meeting, Heidelberg, 1987.
4. F. Decker, R.T. Neuenschwander, C.L. Cesar and A.F.S. Penna, J. Electroanal. Chem. 228, 481 (1987).
5. A. Fujishima, Y. Maeda, K. Honda, G.H. Brilmyer and A.J. Bard, J. Electrochem. Soc. 127, 840 (1980).
6. D. Cahen, P.-E. Nordal and S.O. Kanstad, Appl. Phys. Lett. 49, 1351 (1986).

SEMICONDUCTOR ELECTRODE MODIFICATION : INFLUENCE ON THE STATE DISTRIBUTION AT THE INTERFACE

P. ALLONGUE, E. SOUTEYRAND

LP15 du CNRS "Physique des Liquides et Electrochimie"
Tour 22, 4 place Jussieu, 75252 Paris Cedex 05 - FRANCE

Surface modifications are currently a great deal of investigations for semiconductor electodes in view of improving or limiting some electrochemical reactions for example. Surface states are commonly invoked to explain the effect of such surface modifications upon the electrochemical properties of the modified surfaces. Nevertheless, most of the time direct physical characterizations of these interfacial states are not made.

The present work deals with surface modifications of semiconductor surfaces by electrodeposition of metal particules. We have experimentally established that this technique is able to long term stabilize n-GaAs in aqueous media provided that the particules present a critical size and a critical density <1>. We intend here to go deeper into the interpretation of this result in terms of interfacial state distribution (i) thanks to the photocapacitance technique, recently developed in a particular way which allows to determine the energy distribution of the state and to follow their (photo-)electrochemical behaviour <2> ; (ii) thanks to transmission electronic microscopy (TEM) observations of the surface which show that the spatial distribution of the metal particules depends on the surface preparation for a given metal. Our experimental results suggest that surface modifications should be regarded as a modification of both the energy distribution of the interface state and their spatial distribution.

Surface modifications :

n-GaAs (100) surfaces are coated with Pt and Ru microscopie particules (a few nm diameter) by electrodeposition from $(NH_4)_2PtCl_6$ and $RuCl_3$ solutions <3>. Three different surface preparations are used ; they consist in (i) a classical etching with a (H_2O, H_2O_2, H_2SO_4) mixture, (ii) a photocorrosion (PI) in 1M KOH (0.6mA/cm^2, for 10mn) and (iii) a chemical corrosion (CC) in $Fe(CN)_6^{3-/4-}$ pH=14 solution for 5mn. The surface topography as well as the film morphology (particule size and density, spatial distribution) are studied by TEM.

Photocapacitance (PC) results :

Fig.1 presents a PC spectrum for a surface coated with Ru and Fig.2 the state distribution <2>. There exist two types of states : (i) those which result from the GaAs-solvent interactions (the two band tails and the states E_1 and E_2 ; (ii) those which result from the GaAs-Ru interactions (the two induced states labelled "Ru"). The comparison between the spectrum of Fig.1 and that of the bare surface in the same conditions shows that Ru lowers the density of the state E_2 , in other words Ru passivates the state E_2 <2>. Pt exhibits a similar behaviour : it induces two surface states, but contrary to Ru it passivates the state E_1. A last PC results show that the density of the respective states E_1 and E_2 evolves differently during the surface preparation. Compared to the etched surface, photocorrosion only changes their relative spatial distribution (see below) while the chemical corrosion increases the density of the state E_2.

Surface observations :

The topography of the surface and the film morphology of a given metal depend on the preparation of the surface <2>. In the same way, for a given surface preparation the film morphology depends also on the metal. For instance, photocorrosion induces a surface with "waves" while the chemical

corrosion reveals a much less marked topography : Pt particules aggregate at the bottom of the "waves" for a photocorroded surface while they are almost uniformly distributed with an etched surface ; on a photocorroded surface Ru particules are completely uniformly distributed contrary to Pt ones (see above).

At first TEM observations confirm the PC results, which establish that Pt and Ru do not passivate the same state, because the film morphologies depend on the metal for a given surface preparation : there are two surface defects D_1 and D_2, related to the states E_1 and E_2 respectively (Fig.2), which spatial distributions depend on the surface preparation. As the Pt (Ru) induced states are spatially localized at the very metal particules, their spatial distribution must match that of D_1 (D_2) before deposition. As a consequence (i) by combining a surface preparation and a metal deposition we are able to change the energy distribution as well as the spatial distribution of the surface states ; (ii) we are able, by successive depositions of Pt and Ru, to obtain separated particules which should passivate both type of defects (D_1 and D_2).

As an application of these possibilities preliminary results that concern the stabilization of n-GaAs show that it can be effectively improved by just playing upon the surface preparation prior to deposition, whereas all the deposits present the critical density of state. These results will be discussed in terms of surface state distribution (energy + spatial) and transfer kinetics.

<1> P. ALLONGUE, E. SOUTEYRAND, L. ALLEMAND, H. CACHET
Proceeding of the 172nd Electrochemical Society Meeting
Honolulu (1987).

<2> P. ALLONGUE, Thesis, Paris (1988).

<3> P. ALLONGUE, E. SOUTEYRAND, J. Vac. Sci. Technol. B2, 1644 (1987).

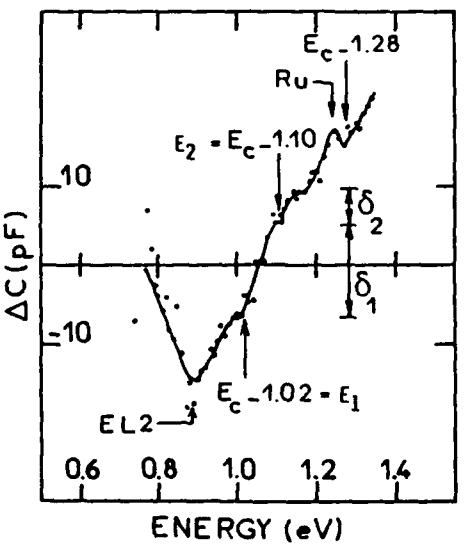


Figure 1 : PC spectrum corresponding to the junction n-GaAs/1M KOH modified by Ru electrodeposition. Surface preparation : etching.

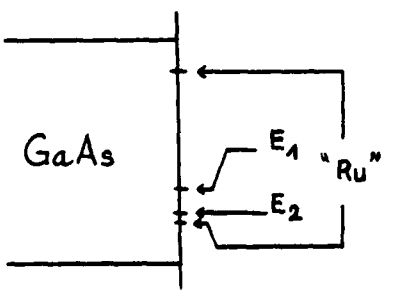


Figure 2 : Surface state distribution for the interface of Fig.1. The states E_1 and E_2 and those labelled "Ru" are due to interactions between GaAs and the solvent, GaAs and Ru respectively.

EFFECT OF WATER ON THE FORMATION OF GaAs/ELECTROLYTE INTERFACES

BLONKOWSKI S., ALLONGUE P., CACHET H.

LP 15 CNRS "Physique des Liquides et Electrochimie"
Université P. & M. Curie, tour 22
4, place Jussieu, 75252 PARIS Cédex 05, FRANCE

The potential barrier height V_b at a semiconductor-electrolyte (SC/EL) contact is usually defined as the difference between the flatband potential V_{fb} and the electrolyte redox level V_{redox} measured vs the same reference electrode. V_{fb} measurements we performed in various solvents show that the band-edge position is more or less dependent on V_{redox}, in the order acetonitrile (ACN), propylene carbonate (PC) and water (at a given pH) (1). For ACN, V_b is constant and equal to 1.05 V whatever V_{redox}. The apparent lack of Fermi level pinning (FLP) for PC and aqueous solutions is somewhat questionable because of the very existence of oxidizing water molecules (with respect to GaAs) in every cases.

Furthermore, analysis of V_{fb} measurements vs SC doping level (2) for GaAs and InP yields a rather surprising low value for the interfacial capacitance "C_H" ~ 1.5 $\mu F/cm^2$, as well as for aqueous or non-aqueous electrolytes. Such a value is to low to be satisfactorily explained by the contribution of a thin oxide film. On the other hand, analysis of photocapacitance data gives a direct estimation for $C_H \simeq 8 - 10\ \mu F/cm^2$, in agreement with the commonly accepted value for the Helmholtz capacitance (3). The discrepancy between these two "C_H" determinations suggests to re-examine the potential distribution accross the SC/EL interface and the actual effect of surface states.

To address this problem, it is noteworthy to look at semiconductor-metal (SC/M) interfaces. On the basis of various theoretical and experimental works, it is now considered that (i) the interface between a metal and a semiconductor is never abrupt : an interfacial zone exists with various properties and thickness ; (ii) the interface charge distribution due to electronic levels decreases in density towards the SC bulk, because of the spatial extension of wave functions associated to surface states. Lu, Barret, Neffati have recently proposed a model based upon the above considerations in order to explain the dependence of the Schottky barrier height upon the metal work function (4).

We have adapted this model to SC/EL interfaces by taking into account the electrical effects of the Helmholtz layer. For instance, Fig. 1 shows the profile of energy bands of a SC in contact with a redox electrolyte, in the case of a single acceptor-like surface state. This latter is characterized by its energy position, density and penetration depth. The profile is determined by solving the Poisson equation, assuming an exponential decrease of the state charge density (cm^{-3}). As a consequence, the barrier height is located inside the SC, at a distance which depends on the properties of surface states. Such a model is in principle able to explain the barrier height dependence on V_{redox} (FLP), in various electrolytes and to predict an additional capacitance (~ 1 $\mu F/cm^2$) in series with C_H.

The relevant question is to give the model parameters a physical meaning. For that purpose, electrochemical photocapacitance spectroscopy (EPS) seems very promising. EPS has been proved to get information about the surface state distribution in an original way. For GaAs, corrosion states

or states created by metal electrodeposition have been successfully localized and charge trapping processes revealed by analysing amplitude of phototransitions (3) (5). By means of EPS, we study the effects of electrolyte properties (redox level, water content ...) on the surface state response. These results will be correlated, through our model, with the available data on FLP.

REFERENCES

(1) N. GABOUZE, B. FOTOUHI, O. GOROCHOV, H. CACHET, N.A. YAO
J. Electroanal. Chem., 237, 289 (1987).
N.A. YAO, Thesis, University P. & M. Curie, Paris (1987).

(2) R. DEGRYSE, W.P. GOMES, F. CARDON and J. VENNIK, J. Electrochem. Soc., 122, 711 (1975).

(3) P. ALLONGUE, Thesis, University P. & M. Curie, Paris (1988).

(4) G.N. LU, C. BARRET et T. NEFFATI, Rev. Phys. Appl. 22, 1169 (1987).

(5) P. ALLONGUE, H. CACHET, Electrochim. Acta, 33, 79 (1988) and
Ber. Bunsenges. Phys. Chem., 91, 386 (1987), id. 92 (1988) to be published.

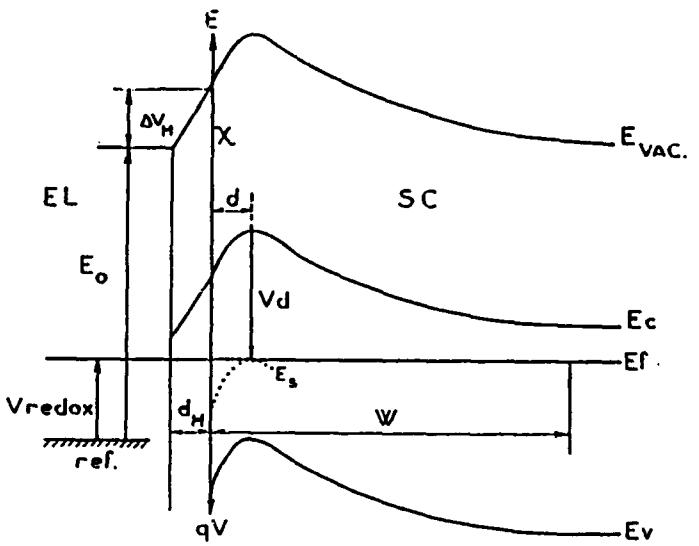


Fig. 1 : Energy diagram of a semiconductor/electrolyte junction in the case of a spatial distribution of interface states.

Example is given for a single acceptor state at the level E_s.
V_d, the barrier height, is defined as the maximum of the conduction band ; it is located at a distance d from the surface. d depends on the charge density and on the characteristic penetration length L (L < d) of the interface state.
d_H is the Helmholtz layer width (~ 3 Å) and ΔV_H the potential drop across this layer. W is the width of the space charge region inside the SC (W ≈ 1000 Å). χ is the electronic affinity ; E_{VAC}, E_c, E_f, E_v are respectively the vacuum, conduction band, Fermi and valence band levels. V_{redox} is the redox potential in the electrolyte.
E_o is the reference electrode energy level with respect to the vacuum level.

PHOTOELECTROCHEMICAL PREPARATION OF LEWIS ACIDO BASIC ELECTROLYSER ON PASSIVE IRON MATERIALS

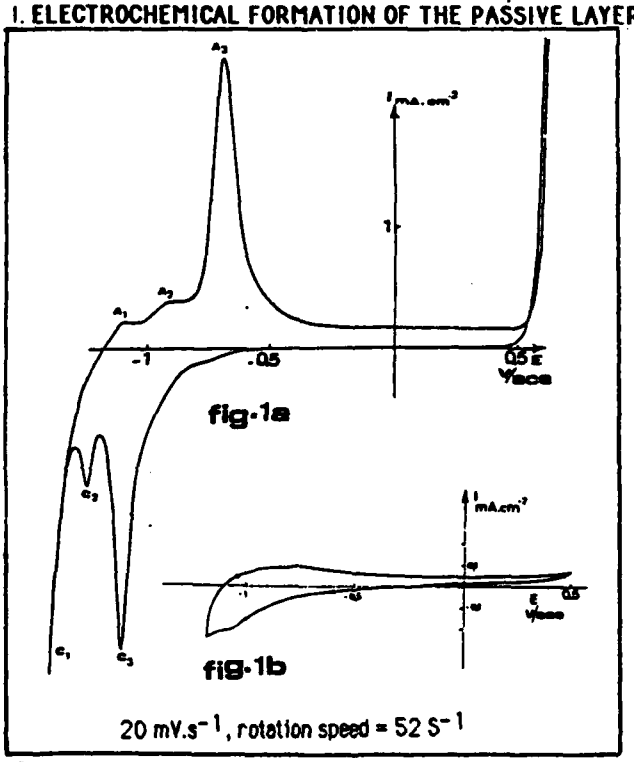
T. Mouhandess*, J.F. Nowak**, G. Picq*, F. Routine*, P. Vennereau*

The electrochemical reactivity of anodic oxide films on metals depends on the mode of conduction in the layers. The donor or acceptor character of the film determine the possibility to reduce or oxidize species on the surface, the rate of such a reaction depending on the population of majority carriers in dark conditions or on the population of photogenerated minority carriers.

The photoenergy creating the electron hole pairs can be decreased if the electronic structure of the layers corresponds to degenerated semi conductors.

This paper describes :
- condition of formation of passive oxide layer on industrial iron in KOH 1M solution ;
- the electrochemical behavior of the passive layer in dark conditions considering the $Fe(CN)_6^{3-}/Fe(CN)_6^{4-}$ system ;
- the photoelectrochemical reactivity of the passive layer.

I. ELECTROCHEMICAL FORMATION OF THE PASSIVE LAYER



20 mV.s^{-1}, rotation speed = 52 S^{-1}

Fig. 1a shows the well-known voltamogramm concerning the electrochemical behavior of Fe 2N in alkaline solution (rotating disc electrode). The protocole to form the oxide layer studied in this paper consists in multi cyclic polarisation in a domain of potential cathodically limited at -1.15V/SCE and anodically limited at 0V. The cathodic limit has been choosen between C_2 and C_3 to prevent the destruction of the inner layer of Fe^{2+} oxide.

* Centre de Recherches en Electrochimie Minérale et en Génie des Procédés (CREM.GP) (UA 1212 CNRS) B.P. 75 - 38400 Saint-Martin d'Hères (France)
** U.N.IR.E.C, Centre de Recherche B.P. 34 - 42701 Unieux (France)

Positive value is located in the passive domain. The curve obtained (Fig. 1b) does not vary after 20 cycles of polarisation. After [1-2] the layer formed may be constituted with oxide whose stoichiometry is between FeO and Fe_2O_3. After the oxide formation the shift of the positive limit of polarisation in the passive domain does not vary the voltamogram.

II. DARKNESS REACTIVITY OF THE $Fe(CN)_6$ SYSTEM

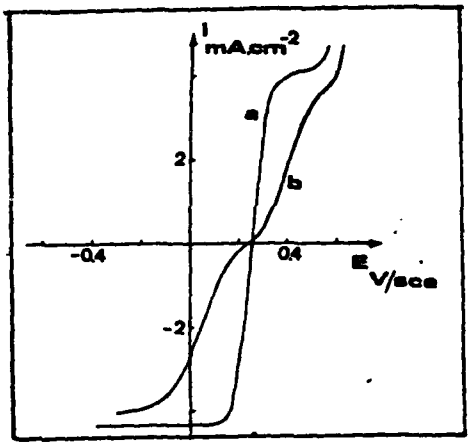


fig.2a

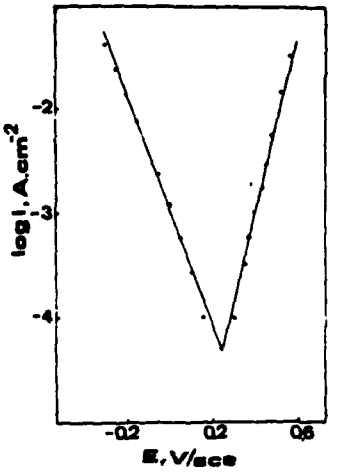


fig.2b

[red] = [OX] = 10^{-2}M, rotation speed = 78 S^{-1}

Fig. 2a presents stationary state i versus E curve. Curve a was obtained with the $Fe(CN)_6$ redox system on Au electrode and curve b on Fe electrode. The comparison between these curves shows that the rate of the redox reaction is lower on Fe electrode that on gold. The Tafel representation in Fig. 2b gives on apparent anodic transfer coefficient of 0.47 and a cathodic one of 0.35 after correction of diffusion process. These results have already been obtained in [3] in neutral solutions, on gold these values are well known to be each other close to unity.

The decrease of the apparent charge transfer coefficient on Fe compared to the gold electrode suggests that the passive layer on Fe electrode is semi conducting with a contribution of surface states in the optical gap [4].

III. PHOTOREACTIVITY OF THE PASSIVE LAYER

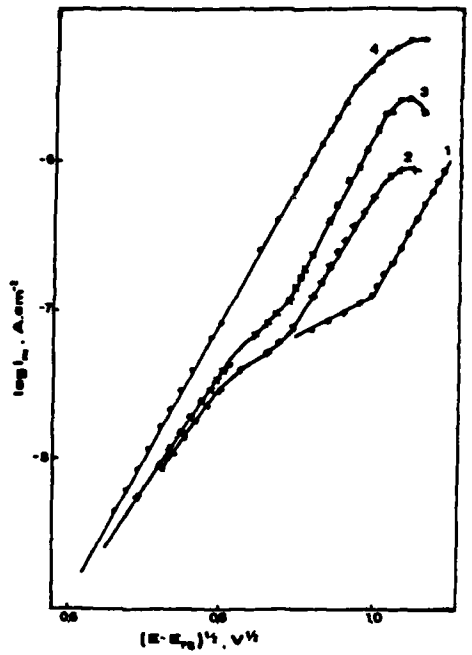


fig. 3

KOH 1M+ 1) Without $Fe(CN)_6^{4-}$; 2) 2.10^{-3} M 3) 4.10^{-3}M 4) $1.6\ 10^{-2}$M : $Fe(CN)_6^{4-}$

Fig. 3 exhibits the Poole Frenkel representation of the photocurrents [5] obtained in 1M KOH solutions (curve 1) in which increasing quantities of ferro cyanide have been added (curves 2,3,4). These curves confirm the high contribution of the surface states in the photo reactivity of the layer. The variation of the shape of the curves is due to the different widenesses of the distribution function of the reactive chemical species in solution (OH^- and ferro cyanide). The positive photocurrents correspond to a photo acceptor character of the surface states.

These results have been compared with those obtained with pure iron electrode (6N). The similirity of the results is consistant with the small contribution of impurities in the surface states distribution in the optical gap.

[1] C.V. D'ALKAINE, R. PEREIRO and D.J. SCHIFFRIN, 25th I.S.E. Meeting, Brighton, England (1974) Extended Abstracts, 727.
[2] A.M.T. OLMEDO, R. PEREIRO and D.J. SCHIFFRIN, J. Electroanal. Chem., 74 (1976), 19-36.
[3] R.V. MOSHTEV, Electrochimica Acta (1971),16, 2039-2048.
[4] A.J. APPLEBY in Comprehensive Treatise in Electrochemistry, 7, ch. IV; Ed. R.E. White...
[5] A.R. NEWMARK, U. STIMMING, J. Electroanal. Chem. 204 (1986), 197.

STUDY OF ETCHING MECHANISMS AT GALLIUM PHOSPHIDE BY MEANS OF (PHOTO-)ELECTROCHEMICAL METHODS.

H. Goossens, F. Vanden Kerchove and W.P. Gomes

Rijksuniversiteit Gent, Laboratorium voor Fysische Scheikunde, Krijgslaan 281, B-9000 Gent, Belgium.

It is well known that illumination may affect the etching rate of III-V semiconductors. The photoetching mechanism of GaAs by H_2O_2 or a mixture of CrO_3 + HF has been studied extensively[1-3]. It appears that the mechanisms are very complex, being composed of chemical, electrochemical and photoelectrochemical steps.

It is our aim to contribute to the fundamental study of the photo-etching mechanisms of III-V semiconductors by studying GaP, which has a larger band gap than GaAs, the valence band (VB) being situated 0.7 eV below the VB of GaAs. This low position of the VB is expected to prevent some complicating reactions.

The etching rates of monocrystalline samples of n-GaP were measured in different electrolyte solutions by using the following procedure. A perspex flow-through cell was constructed in order to obtain a very small volume (0.22 cm^3) of solution. A LKB Microperpex S peristaltic pump was used to deliver controlled flow rates between 50 and 0.5 cm^3/hr. A sample of 5 ml was necessary for the spectrophotometric determination of the dissolved Ga^{3+}, which was complexed by malachite green in a strong HCl solution and extracted with benzene [4]. The extinction was measured at 660 nm. The sensitivity of this analysis is 5 µmol/l.

The GaP single crystals were purchased from MCP (England). The thickness of the samples used was 1.5 mm, the diameter was 3 mm for flow-cell experiments and 5 or 6 mm for rotating electrode experiments. The face to be exposed to the electrolyte was polished in the usual way using Buehler Al_2O_3 powders (final polish: 0.3 µm).

The semiconductor sample was illuminated with a 150W mercury lamp. A glass fibre was used to introduce the light as close as possible to the electrode surface.

The results of the (photo-)etching rate measurements are summarized in Table 1. In columns 2 and 3, the etching rates at V_r (i.e. the rest potential) are given as they were measured in the flow-cell.

Table 1.

Dissolution rate ($r/10^{-10}$ $mol.cm^{-2}.s^{-1}$) of n-GaP at V_r in the flow-cell. Flow rate = 2.5 $cm^3.hr^{-1}$.

Electrolyte	Light	Dark
0.05 M H_2SO_4	1.4	<0.05
0.05 M H_2SO_4 + 0.01 M Br_2	1.4	<0.05
0.05 M H_2SO_4 + 0.01 M $K_2S_2O_8$	1.1	0.2
0.05 M H_2SO_4 + 0.01 M H_2O_2	1.7	0.5
0.1 M KOH	0.9	<0.05
0.1 M KOH + 0.01 M KOBr	6.1	0.6
0.1 M KOH + 0.01 M $K_2S_2O_8$	1.4	<0.05
0.1 M KOH + 0.01 M H_2O_2	0.5	0.1

In all these experiments the etching rate is considerably larger under illumination than in darkness. In darkness the etching rate, if any, is smaller than the detection limit in 4 of the 8 electrolytes considered. Hence, it can be concluded that in all solutions used a positive effect of light upon the etching rate exists.

In order to correlate the observed etching rates to the electrochemical properties of the semiconductor, current-voltage curves were measured. The electrochemical cell used contained the semiconductor electrode, a SCE reference electrode and a Pt counterelectrode. The potential and the current were monitored with a Tacussel Bipad Potentiostat. The applied potential was swept with a PAR 175 Universal Programmer. The current-potential curves were measured under chopped light at the (111) and ($\bar{1}\bar{1}\bar{1}$) faces of n-GaP in contact with aqueous electrolyte solutions. No significant differences were observed between the values obtained at (111) and ($\bar{1}\bar{1}\bar{1}$) face respectively. When e.g. for n-type a cathodic dark current I_d is observed at the potential V_r under illumination (where the current I_{ph} equals zero), then an anodic photoetching current I_{pe} should compensate for I_d:

$$I_{pe} = -I_d$$

Because of the small differences between I_d and I_{ph} and the observed influence of time on I_d and I_{ph} as well as on V_r, it was not yet possible to compare quantitatively I_{pe} to the photoetching rates of Table 1. Nevertheless, in all solutions, mentioned in Table 1, a positive I_{pe} resulted from the voltammograms. Hence, a positive qualitative correlation between photoetching rates and (photo-)electrochemical characteristics can be safely assumed.

In view of the foregoing results, it looked worthwhile to perform a more detailed examination of the current-voltage behaviour of the KOH + KOBr solution. This study should be separated into an anodic and a cathodic part. In KOH solutions, an influence of the OH^- concentration on the anodic current and on the dissolution rate of GaP was observed under certain circumstances. At a p-type GaP rotating disk electrode (RDE), the anodic dark current was directly proportional to the OH^- concentration and to $\sqrt{W}$, W being the rotation rate of the RDE. At n-type GaP, a clear change in the rate-determining step of the anodic photocurrent was observed when increasing the light intensity: at relatively low light intensities, the supply of holes to the surface is rate determining, whereas at relatively high light intensities, diffusion of OH^- ions from solution becomes the rate-determining step. This phenomenon was observed in the flow-cell as well as at the RDE. From the slope of the Levich plot it can be deduced that 11 OH^- ions and 6 holes are consumed per formula unit of GaP when the pH is ranging from 11 to 14, corresponding to the reaction equation[5]:

$$GaP + 6\ h^+ + 11\ OH^- \longrightarrow GaO_3^{3-} + HPO_3^{2-} + 5\ H_2O$$

At pH < 11, a positive deviation of the slope is observed, which can be ascribed either to a changed stoichiometry[5], i.e.

$$GaP + 6\ h^+ + 8\ OH^- \longrightarrow 1/2\ Ga_2O_3 + HPO_3^{2-} + 7/2\ H_2O$$

and/or to a noticeable participation of H_2O in the dissolution process.

Also in KOH solution, a transient anodic photocurrent was observed with n-GaP at relatively high light intensities. When the illumination was started, the photocurrent rose very fast, and afterwards it decreased slowly to a steady-state value. The transient photocurrents were registered by means of a memory oscilloscope. The peak values were directly

proportional to the light intensity; they were independent of W for the RDE and of the flow rate in the flow-cell. On the other hand, the steady-state values of the photocurrent were independent of the light intensity, but directly proportional to the diffusion rate of OH^-, as it is described by the Levich equation. At low light intensities, the photocurrent immediately rose to a constant value, which was proportional to the light intensity and independent of the diffusion rate of OH^-.

Capacitance measurements of n-GaP electrodes under the circumstances where a transient current was observed, revealed that the series capacitance increased drastically as a function of the light intensity, but eventually tended to a constant value, nearly corresponding to flat-band situation. Hence, no additional increase of the photocurrent could be produced by increasing the light intensity.

As Decker[6] pointed out for GaAs, the observed facts can be explained by the formation of an insoluble layer on the surface: certain surface intermediates (or products) cannot dissolve but by a reaction with OH^-. If the transport of OH^- is fast (i.e. it is not controlled by diffusion) then a steady state is established in which the dissolution rate is equal to the rate of formation of these intermediates or products, which depends on the light intensity. However, if the transport of the OH^- to the surface is too slow, undissolved intermediates or products will accumulate on the surface, where they form a resistive layer. As this layer is growing thicker, a decreasing fraction of the applied potential is extending across the space charge layer. As a consequence, the recombination of electrons and holes is favoured until eventually the growth of the resistive layer is slowed down to the dissolution rate under the influence of OH^-. At that moment, a steady-state photocurrent is obtained.

The study of the cathodic current-potential behaviour of KOH + KOBr is still in a preliminary phase and appears to be complicated by time-dependent effects which are presently under investigation.

References.

(1) J.J.Kelly and A.C. Reynders: Appl. Surf. Sci. 29, 149 (1987).
(2) J. van de Ven, J.E.A.M. van den Meerakker and J.J. Kelly: J. Electrochem. Soc. 132, 3020 (1985).
(3) J.J. Kelly, J. van de Ven and J.E.A.M. van den Meerakker: J. Electrochem. Soc. 132, 3026 (1985).
(4) A.M. Dymov and A.P. Savostin: Analytical Chemistry of Gallium, Ann Arbor Science Publishers, p. 116-117, London (1970).
(5) K.Uosaki and H. Kita: J. Electrochem. Soc. 128, 2153 (1981).
(6) F. Decker: Electrochim. Acta 30, 301 (1985).

CHARGE CARRIERS IN LAYER OF SILVER/SILVER OXIDE

T. Grozdić
Metalservis, Chemical Power Sources Institute, Belgrade

During anodic formation of silver oxide on silver, two oxides are formed-Ag_2O as semiconductor and AgO as a conductor.Oxide formation reaction occurs in liquid and solid state. If oxide layer is thick, rate determiring step in solid state becomes ion transport process, which may be determined by following ion as a charge carrier: Ag^+, O_2^- and O^o. This work is an attempt of indirect approval of Ag^+ as main charge carrier. The change of oxide conductivity or improvement of Ag^+ ion diffusion through silver oxide can be brought about in several ways:

a) introduction of impurities, i.e. by alloying with Tl, Pb and In,
b) irradiation of silver/silever oxide by γ-ray,
c) Photo-excitation of silver and silver alloys.

Galvanostatic discharge curves of silver alloy electrode show that capacity of electrode is higher than for pure silver electrode (1). On the contrary, intensity of photo-current alloyed electrode is lower then for pure silver, see Fig.1. It means that conductivity of silver aloy electrode is not increased by introduction of impurity. However, capacity of alloy electrode is almost for 150% increased by alloying silver. Pure silver electrode after two hour γ-ray irradiation rapidly increases capacity of electrode. Electrode has absorbed 2.10^4 Gy(see Fig.2.).

In porous layer of silver oxide or in the nonporous one the following mechanism of anodic formation of silver oxide is possible, see Fig.3. However, on the basis of presented results, the most probable main charge carrier is Ag^+.

Reference:
1. Grozdić, T., Wiesener, K., Mrha, J., Garche, J., 38 ISE, Maastricht, 1987, p. 459.

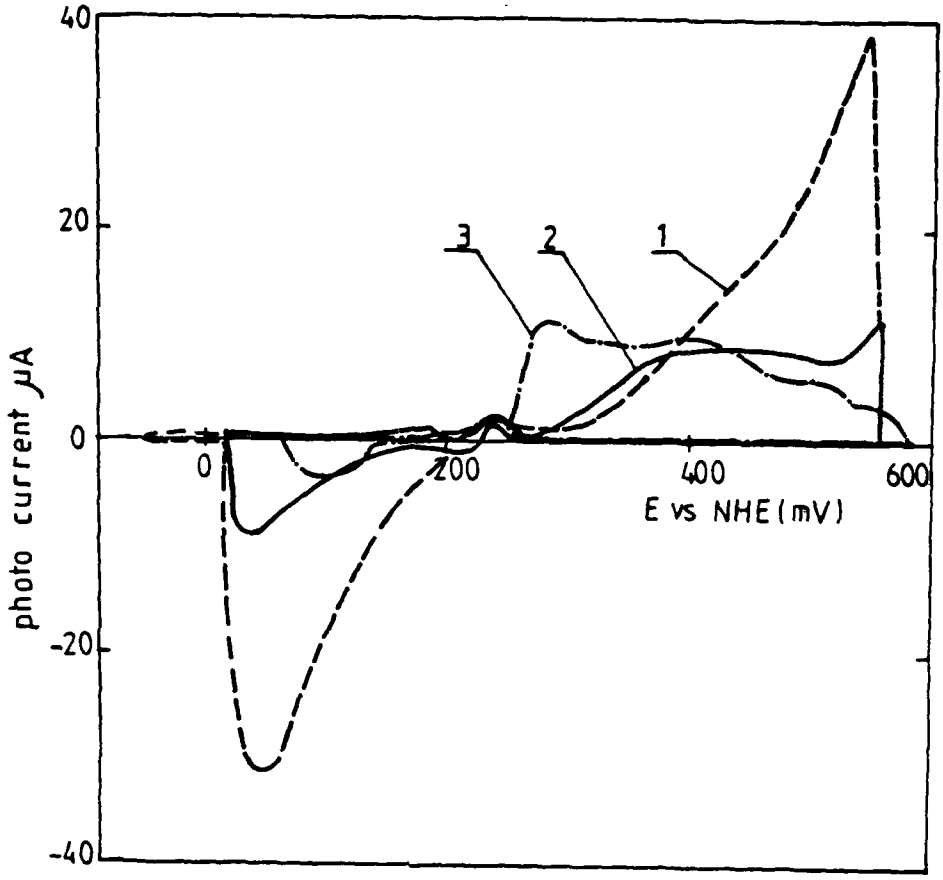


Fig.1.Photocurrent voltage curves. Curve for pure silver (1), Ag-0,44% Tl (2) and Ag-0,5% Pb (3). Wave lenght of incident photons is 400 nm and chopper frequency 2,1 cycle/s.Sweep rate 10 mV/s.Solution 1MKOH.

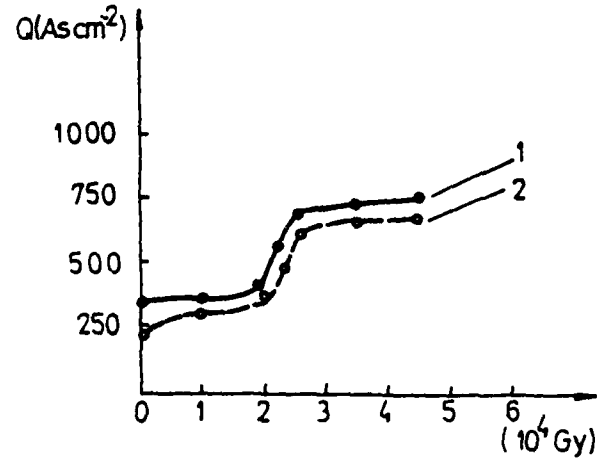


Fig.2.Charge and discharge capacity of pure silver electrode vs absorbed energy γ-ray. Solution 1MKOH.

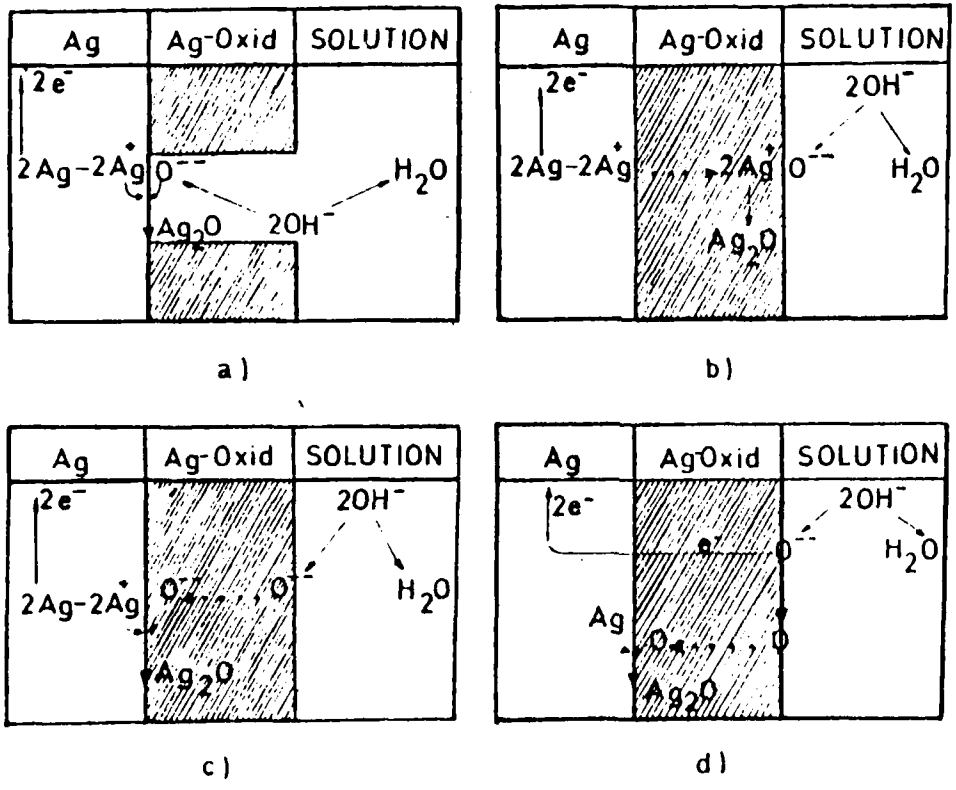


Fig.3.Schematic presentation of mechanism of anodic formation of silver oxide.

STUDY OF THE IMPEDANCE OF A GALENA ELECTRODE EFFECT OF A COLLECTOR FOR SULPHIDE FLOTATION

Daniel SCHUHMANN, P. VANEL and E. NDZEBET

Laboratoire de Physicochimie des Systèmes Polyphasés
UA 330 - Route de Mende - BP 5051 - 34033 Montpellier Cedex
France

Flotation is a mineral processing by which powdered mixed minerals in suspension are shared, some minerals being made hydrophobic by adsorption of a specific reactant (collector) while the hydrophilic minerals decant. Flotation of complex sulphides is usually carried out using alkyl-xanthates ($R\text{-}OCS_2^-$ or X^-) as collectors and air bubbling. It is now largely accepted that the flotation of galena with X^- involves electrochemical processes in which the dissolved oxygen is reduced while the X^- anions are oxidized, this couple leading to a mixed potential at the surface of the galena particles. These processes are complicated by the adsorption of the products and the mechanism is not yet elucidated. Studies by chronoamperometry (CA) [1,2] led to results contradictory with those obtained by chemical analysis. This was explained by stating that CA provides information on transient processes while those occuring after a long immersion would be different [3]. Impedance measurements were thus carried out with a natural galena crystal as electrode in the presence of a steady polarization simulating the mixed potential due to oxygen. Thus also allowed to investigate the influence of the semiconducting character of the mineral. Measurements without and with ethylxanthate were made with potassium borate (0.1 M) and sulfate (0.25 M) mixtures at pH 9.2 as in the flotation processing.

In a frequency ($f=\omega/2\pi$) range starting from 1 Hz, the spectra of the impedance Z could be fitted with the equivalent circuit of Fig. 1.a which is the low frequency approximation of circuits 1b and 1c. The diffusion impedance ($d/\sqrt{j\omega}$) for circuit 1a is represented by a W (in memory of Warburg). The circuits 1b or 1c (whose analytical expressions Z vs $j\omega$ are identical with different parameters) was verified by measurements up to 200 KHz. The interfacial impedance $Z_i = Z - R$ where R is the sum of the crystal and electrolyte resistances was plotted in the Cole-Cole plane $C^* = 1/(Z_i j\omega) = C' - jC''$. An example is plotted in Fig. 2. Dispersion of the low frequency capacity is observed below 1 KHz. The real part of its impedance may be empirically represented by $a + b/f$ [4]. Variations of C_0 and b with the steady potential are represented as Mott-Schottky plots in Fig. 3. The shift between the straight lines shows the presence of a noticeable capacity in series with the space charge capacity of a n-type semiconductor justifying the circuit 1c rather than 1b. From the above results and literature data in solid state physics, the donor concentration N_D could be evaluated ($4 \times 18\ cm^{-3}$).

These data allow to determine the electrostatic component $\Delta\Psi$ of the flat band potential E_{fb}, - 0.94 V. In contradiction with literature statements [5], it is thus shown that even if highly doped, natural galena cannot be considered as a degenerate semiconductor. As shown in Fig. 4, with or without X^-, the behaviour changes at potentials more anodic than that corresponding to the galena oxidation. E_{fb} is shifted of 0.9 to 1V showing that $\Delta\Psi$ is due to adsorption of OH^-, giving rise after oxidation to $Pb(OH)_2$. The effect of xanthate addition between -0.4 and -0.1 V may be explained by its physisorption in this range, changing $\Delta\Psi$. This new component also disappears when X^- is oxidized as a neutral product X_2 or PbX_2). This result supports the previous analysis of CA data [6].

d increasing with E, it seems that the diffusion impedance appearing at high frequencies is due to a cathodic process in the space charge region involving the minor carriers, i.e. holes h^+. The impedance in parallel on C_p in circuit 1c could be related to the reaction between h^+ and adsorbed radicals O_2^- formed from dissolved residual oxygen. This assumption is supported by measurements in the low frequency range down to 1 Hz. At high anodic potentials, a relaxation similar to that represented by circuit 1b is observed while at more cathodic potentials it becomes analogous to that predicted by the Randles model. The parameters are modified through oxygen bubbling. The low frequency impedance may thus be related to the formation of adsorbed O_2^- followed by further reduction processes leading to H_2O_2 or H_2O.

The present study allows to reconcile the mixed potential theory with earlier statements suggesting that the chemisorption of oxygen converted the particle surface from n type to p type semiconductor [7].

This is indeed possible with fine particles whose size is of the order of the space charge thickness. Sulphide flotation indeed seems to be the result of electrochemical processes but involving the semiconductor nature of these minerals.

REFERENCES

1 - R. Woods, J. Phys. Chem, 75, 354 (1971).

2 - O.H. Thi, M. Lamache and D. Bauer, Electrochim. Acta, 26, 33 (1981).

3 - A. Granville, N.P. Finkelstein and S. Allison, Inst. Min. Metall, Trans., 81, C1 (1972).

4 - E.C. Dutoit, R.L. Van Meirhaeghe, F. Cardon and W.P. Gomes, Ber. Bunsenges. Phys. Chem., 79, 1206 (1975).

5 - E.E. Maust, P.E. Richardson and G.R. Hyde, U.S. Department of Interior, Bureau of Mines, Report 8143 (1976).

6 - D. Schuhmann, A.M. Guinard-Baticle and M. Lamache,

Electrochim. Acta, 28, 79 (1983).

7 - I.N. Plaksin and R.L. Sh. Shafeev, Inst. Min. Metal. Trans., 72, 4715 (1963).

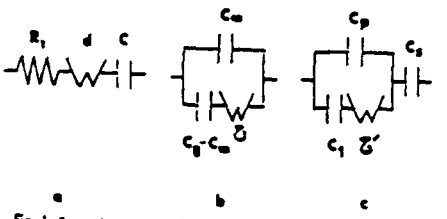


Fig. 1. Equivalent circuits for the impedance in the high frequency range.

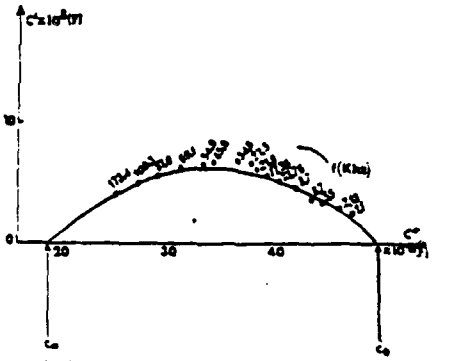


Fig. 2. Cole-Cole plot for the high frequency range; V = −0.4 V SCE; C(X⁻) = 0.

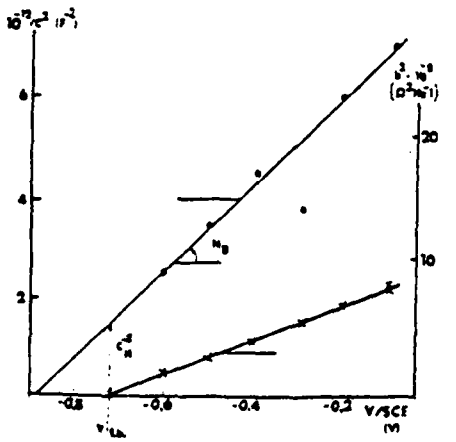


Fig. 3. Variations of (●) 1 C^2 /C is the high frequency value of the capacity) and (X) b^2 as a function of the steady potential V. No xanthate added.

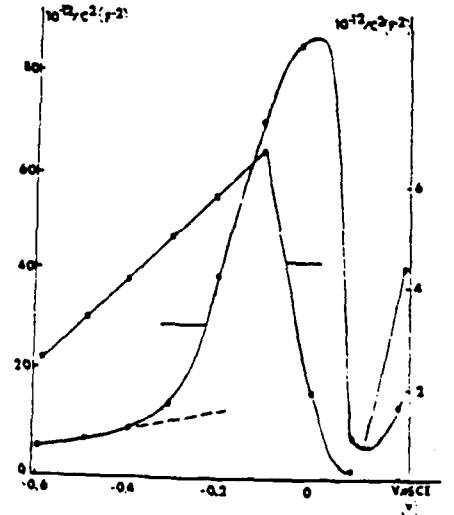


Fig. 4. Variations of 1 C^2 as a function of V (●) with and (■) without xanthate addition.

THE COMPARABILITY OF REDOX REACTIONS AT n- AND p-TYPE ELECTRODES

Rolf Reineke and Rüdiger Memming

Institut für Solarenergieforschung Hannover (ISFH)
Sokelantstr. 5 , D-3000 Hannover 1 , Fed. Rep. of Germany

The quantitative interpretation of photocurrents at n-type electrodes becomes possible by investigating the majority carrier currents at p-type electrodes (or vice visa). The reason is that the same reactions take place at both type of electrodes when the quasi-Fermi levels at both surfaces are identical. Under certain conditions it is directly accessible at the p-type electrode. Our interpretations are based on the following assumptions:

(i) In equilibrium the band positions are the same for the n- and the p-type electrode.

(ii) All reactions which take place (corrosion, different redox reactions, shift of flatband potential, formation of unsoluble layers) are only a function of the hole density p_s at the surface. These reactions may even be coupled.

(iii) For the p-type electrode the density of holes p_s at the surface is nearly in equilibrium with that in the bulk. Therefore the Fermi level of the majority carriers is constant. This is true for the total current being lower than that described by the thermionic emmission model :

$$|i| < A^* m^*/m_e * T^2 * \exp\left[(E_v - E_F - eU_{sc})/kT\right]$$

A is the Richardson constant of 120 $A*cm^{-2}*{}^{\circ}K^{-2}$, m^*/m_e the relative effective mass of the holes (majority carrier), U_{sc} the band bending, $E_v - E_F$ is the difference of the valence band and the Fermi level in the bulk of the semiconductor.

As an example we demonstrate that the stabilisation of n-GaAs against photocorrosion can be predicted quantitatively through investigation of majority carrier current at p-GaAs. In fig. 1 a semi logarithmic current potential (Tafel-) plot is shown for the oxidation reactions of rotating p-GaAs electrode in 1M HCl and 1.1 mM CuCl in the dark. Curve a) is the total current both of corrosion and Cu^+-oxidation. Curve b) is the fraction of the current caused by the oxidation of copper. This fraction of current is detected at a ring electrode. The difference of these currents is the amount of corrosion of p-GaAs (curve c). The latter one is also seen directly when no Cu^+ is present in the solution. In curve b) the deviation from the Tafel slope is due to the limited diffusion of Cu^+. From this plot we can see directly that about 75% of the total current (curve a) is due to Cu^+-oxidation (curve b) at low current densities. Starting at about 0.3 V (SCE) where the Cu^+-oxidation current reaches about 15% of its diffusion limit (i_{gr}) the proportion of corrosion increases significantly. Accordingly, a (photocurrent independent) 75% stabilisation is predicted from this data for n-GaAs. If the photocurrent density as controlled by the light intensity exceeds the critical value of 15% of i_{gr} the stabilisation decreases. Just this is seen from stabilisation measurements as obtained by light intensity controlled rotating ring-disc experiments (fig. 2). Furthermore it is shown in the poster that more complicated systems like the stabilisation by Fe^{2+} was frequently missinterpreted and can be easily understood by our method.

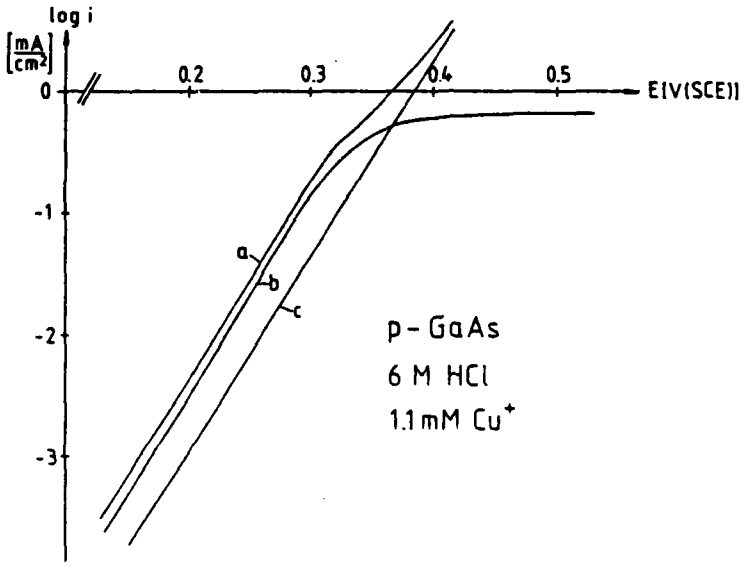


Fig. 1: Semi-logarithmic current potential plot of p-GaAs in a solution of 1 M HCl and 1.1 mM CuCl. Remarks see in the text.

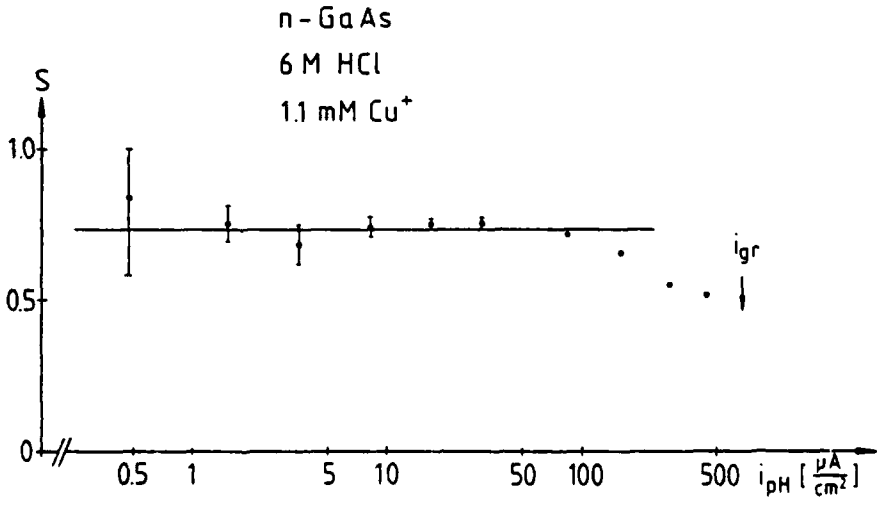


Fig. 2: Stabilisation of n-GaAs against photocorrosion at different light intensities in the same solution as in fig. 1.

MOLECULAR CATALYSTS IN PHOTOELECTROCHEMICAL CELLS: STUDY OF AN EFFICIENT SYSTEM FOR THE SELECTIVE PHOTOELECTROREDUCTION OF CO_2: p-GaP or p-GaAs / Ni(cyclam)$^{2+}$, aqueous medium

Jean-Pierre PETIT, Pierre CHARTIER,
Laboratoire d'Electrochimie et de Chimie Physique du Corps Solide,

Marc BELEY,
Laboratoire de Chimie Organo-Minérale,

Jean-Paul DEVILLE,
IPCMS - Groupe "Surfaces-Interfaces",

Université Louis Pasteur, 4, rue Blaise Pascal, F-67000 STRASBOURG

Some recent works have pointed out the interest in associating the semiconductor electrode with a molecular catalyst, in order to increase the yield and the selectivity of the CO_2 reduction in photoelectrochemical cells [1]. We report here about two systems:

p-GaAs / 0.1M $KClO_4$, H_2O, Ni(cyclam)$^{2+}$ (A)

p-GaP / 0.1M $NaClO_4$, H_2O, Ni(cyclam)$^{2+}$ (B)

(cyclam = 1, 4, 8, 11- tetra- azacyclotetradecane).

These systems have been shown to allow the selective photo-assisted reduction of CO_2 to CO in aqueous medium, Ni(cyclam)$^{2+}$ acting as a catalyst [2]. The faradaic yields in CO are good (more than 80% with system (B)) and the applied potentials (- 0.2 V/SHE in the case of p-GaP) are appreciably less negative than with systems previously reported in the literature (see Table 1).

Figure 1 illustrates how the photoelectrochemical cells (A) and (B) do act. In the proposed mechanism , the reduction of CO_2 to CO is initiated by that of Ni^{II}(cyclam)$^{2+}$ to Ni^{I}(cyclam)$^{+}$ by a photoelectron of the conduction band, this later being located at an appropriate potential with our experimental conditions, as indicated by Complex Impedance and LMIER [3] measurements.

The reduction of CO_2 in the aqueous systems (A) and (B) is of course in competition with the reduction of water to hydrogen. But Figure 2 clearly shows that the H_2 evolution can be nearly inhibited by using a sufficiently high concentration of catalyst.

It is also obvious from Figure 2 that the proposed systems are not stable in the course of time. Several studies have been carried out in order to determine the possible causes of such a loss in efficiency, by means of photoelectrochemical techniques (complex impedance measurements, I(V), I(t), I(ϑ), ...) and analytical methods (especially XPS surface analysis). The results of these experiments suggest that carbon atoms form on sites of the irradiated semiconductor surface which are not occupied by $Ni(cyclam)^{2+}$ and promote growth of carbon islets. The later gradually decrease the area of the active semiconductor surface, but increase the H_2 production and also possibly the formation of other CO_2 reduction products such as formic acid.

REFERENCES

1 See for example: Bradley, M.G.; Tysak, T.; Graves, D.J.; Vlachopoulos, N.A. J. Chem. Soc., Chem. Commun., (1983)349.

2 Beley, M.; Collin, J.-P.; Sauvage, J.-P.; Petit, J.-P.; Chartier, P. J. Electroanal. Chem. 206(1986)333.
Petit, J.-P.; Chartier, P.; Beley, M.; Sauvage, J.-P. N. J. Chem. 11(1987)751.

3 Petit, J.-P.; Alonso Vante, N.; Chartier, P. J. Electroanal. Chem. 157(1983)145.

p-SC	Applied potential / V vs SHE	Amount of catalyst / µmol	Irradiation time /hours	Charge passed / C	Amounts of products formed H_2 /µmol	CO /µmol	HCOOH+H_2CO /µmol	Faradaic yield in CO / %
GaAs	- 0.95	39	4.5	28	40	63	not anal.	47
GaP	- 0.20	8.5	2.5	3.7	3	16	not det.	83
GaP	- 0.75	600	15	53.5	23	234	10	85

Table 1 Some representative data about the photoelectroreduction of CO_2 to CO on p-GaAs and p-GaP in water catalyzed by $Ni(cyclam)^{2+}$.

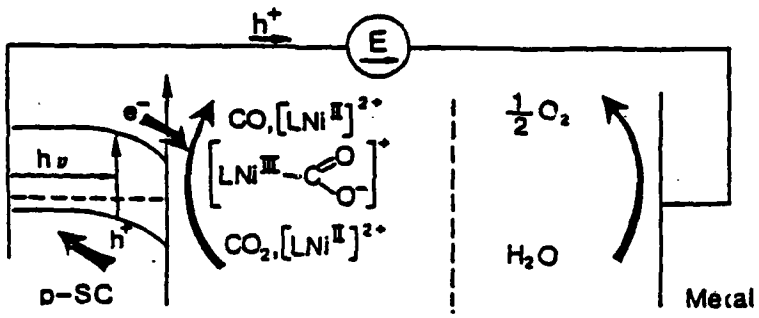


Figure 1 Principle of the photoelectrochemical cells (A) and (B).

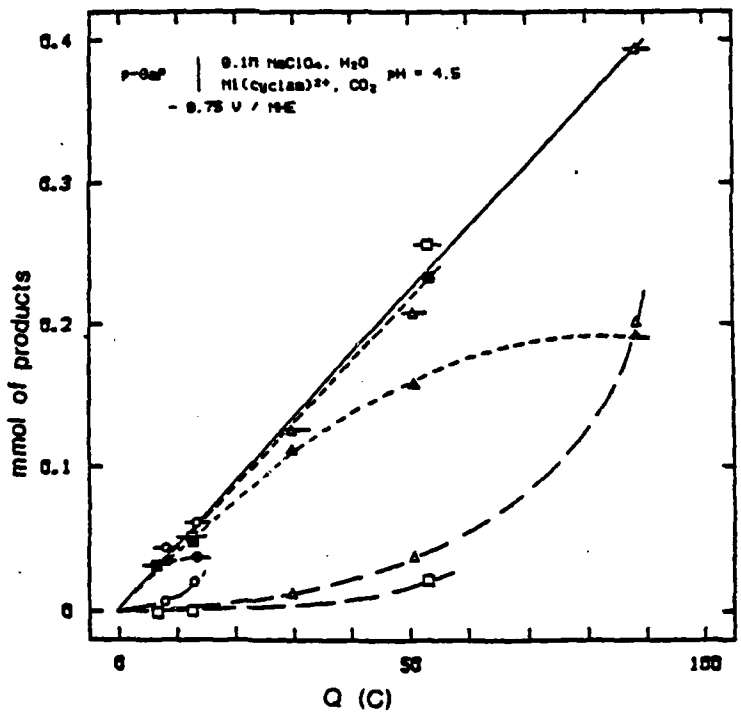


Figure 2 Plot of the quantities of CO and H_2 produced as electric charge passed through the semiconductor electrode:
—— CO + H_2 : —○— ; —☆— ; —○— (————)
CO : —■— ; —▲— ; —●— (– – – –)
H_2 : —□— ; —△— ; —○— (—— ——)
—— quantities of Ni(cyclam)2+:
—□— : 600 µmol; —△— : 70 µmol; —●— : 7 µmol

ELECTROCHEMICAL STUDY OF PHOSPHORUS DOPED CADMIUM TELLURIDE

P. Lemasson

Laboratoire de Photochimie Solaire - CNRS
2, rue Henry Dunant-94320 Thiais
FRANCE

INTRODUCTION

Cadmium telluride, a II-VI compound, presents different properties (energy gap ca. 1.5eV, direct fundamental transition, n- or p-type conductivity, large atomic numbers of the components,etc.) which make it attractive for applications as different as gamma and x-ray detectors or photovoltaic devices /1/. Further, its crystalline structure together with the value of its lattice parameter are ideally suited for the epitaxial growth of a material so important strategically as cadmium mercury telluride /2/. However, the practical use of this material is, up to now, limited mainly by the imperfections of the crystalline stucture both in the bulk and in surface. In order to induce specific optical and electrical properties of CdTe, different types of doping during the crystal growth have been used. Since the work of Selim and Kröger /3/, it is known that phosphorus may act either as an acceptor or as a donor depending on the annealing conditions, leading to p- or n-type conductivity respectively. Such samples are investigated electrochemically in the present work.

EXPERIMENTAL

The electrochemical set-up is classical. The reference electrode is a mercury-mercurous sulfate electrode denoted by MSE. Cadmium telluride wafers are cut from ingots grown by the travelling heater method (THM). The phosphorus concentration is 8×10^{19} atoms per cm^3, the mean conductivity is p-type and the mean free carrier concentration determined by Hall effect measurement is ca. $10^{15} cm^{-3}$. The samples are not annealed before experimental use. Prior to electrochemical operation, the electrodes are mechanically polished to a mirror finish and chemically etched in 1% bromine in methanol solution.

RESULTS AND DISCUSSION

In order to allow an easy comparison, classical current versus voltage characteristics obtained with n- and p-type cadmium telluride electrodes in basic electrolyte are presented in figs. 1 and 2 respectively.

For the n-type, a cathodic current develops at potentials negative of -1.2 V with a peak at ca. -1.6 V. Such a current can be correlated both with hydrogen evolution and cathodic decomposition according to

$$CdTe + 2\ e^- \rightarrow Cd + Te^{2-}$$

whose standard potential is

$$E_0 = -2.11 \text{ V vs. MSE}$$

On the anodic side, the dark current remains small up to + 1.0 V.

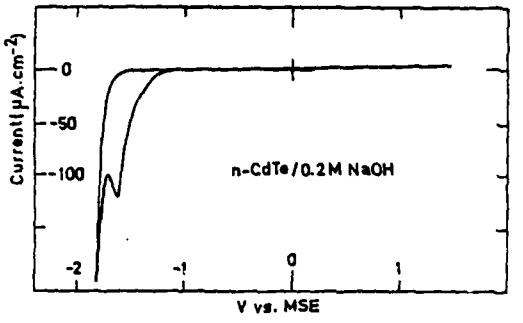


Fig. 1
Dark current versus potential characteristic of n-CdTe in basic electrolyte

For the p-type CdTe, an anodic current starts increasing at potentials positive of - 1.0 V. This current is mainly due to the anodic decomposition which can be written:

$$CdTe + 2\ OH^- + 2\ p^+ \rightarrow HCdO_2^- + H^+ + Te$$

whose standard potential is

$$E_0 = -0.97\ V \text{ vs. MSE}$$

On the cathodic side, the dark current remains negligibly small down to - 4.0 V.

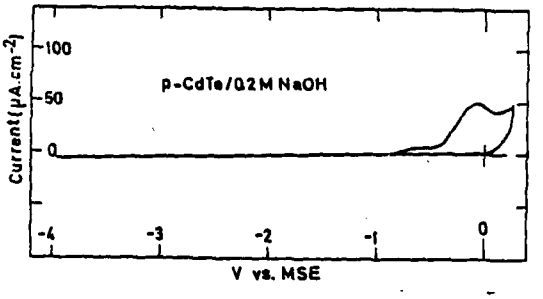


Fig. 2
Dark current versus potential characteristic of p-CdTe in basic electrolyte.

In fig.3 is presented the voltamogram obtained with a phosphorus doped sample. The anodic and cathodic currents which develop can be fairly compared to those existing both at n- and p-type electrodes.

By cycling ten times between -2 and = 1.0 V, the electrode surface is

modified. Two different zones appear clearly: a pretty smooth area and a rough one. The former can be attributed to the existence of a zone with n-type conductivity whereas the latter is due to a p-type conductivity of the corresponding area. The result is shown in fig. 4.

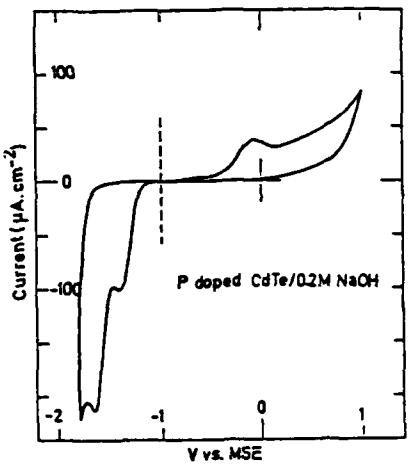


Fig. 3

Typical current vs. potential characteristic of a P-doped CdTe sample in basic electrolyte.

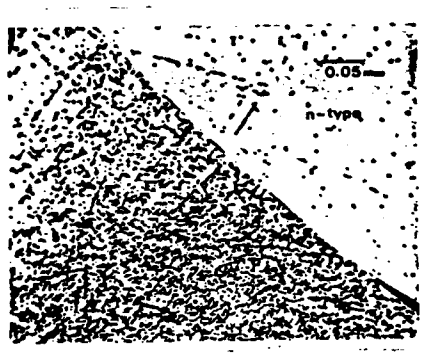


Fig. 4

Surface of the electrode presented in fig.3 after ten cycles between -2 and +1 V.

In such samples with high concentration of phosphorus atoms, the amphoteric character of the dopent is thus clearly demonstrated and p- and n-type conductivity may coexist in the same wafer.

REFERENCES

/1/ K. Zanio, "Cadmium telluride" in "Semiconductor and semimetals" Vol. 13, R.K. Willardson and A.C. Beer, Editors, Academic Press, New York (1978).

/2/ See e.g. "Cadmium mercury telluride" in "Semiconductors and semimetals", Vol. 18, R.K. Willardson and A.C. Beer, Editors, Academic Press New York (1981).

/3/ F.A. Selim and F.A. Kröger, J. Electrochem. Soc., 124, 401 (1977).

IN-SITU VIBRATIONAL STUDY OF THE n-Si/ELECTROLYTE INTERFACE USING FOURIER-TRANSFORM ELECTROCHEMICALLY MODULATED IR SPECTROSCOPY

F. Ozanam and J.-N. Chazalviel

Laboratoire de Physique de la Matière Condensée*, Ecole Polytechnique, F-91128 Palaiseau

In the last ten years the widespread interest for the semiconductor/electrolyte interface has stimulated the development of new techniques for the microscopic, *in-situ*, investigation of these systems [1]. Infrared vibrational spectroscopy is known to be a valuable probe for the electrochemical interface, as full surface selectivity may be obtained by using electrode potential modulation and lock-in detection of the optical signal (this technique is known as "EMIRS" [2]). The performance of the technique can be further improved in the case of semiconductor electrodes, because the electrode can then be shaped as a trapezoid and used as a multiple-total-internal- reflection prism, allowing for a sensitivity increased by the number of reflections. We have recently presented data obtained in the 1-5 μm wavelength range, at the n-Si/electrolyte interface, using a classical monochromator arrangement [3]. These data allowed to follow directly the oxidation of the,– initially hydrogenated –, silicon surface, by observing a decrease of the ν SiH band and an increase of the ν OH band, the latter being analyzed as a superimposition of adsorbed water and surface SiOH groups. It has also been shown that the electromodulated infrared spectroscopy technique can be made compatible with the Fourier-transform spectroscopy, by using an especially designed, slow-scanning-mirror Fourier-transform infrared spectrometer ("FTEMIRS" [4]).This results in an improvement in sensitivity by about one order of magnitude, which allows vibrational investigations down to lower vibrational frequencies. We report here on a new set of results on various n-Si/organic-electrolyte interfaces, using FTEMIRS together with a study as a function of light polarization, in the 900-4000 cm^{-1} frequency range. Details on the n-Si internal-reflection electrode and FTEMIRS spectrometer can be found in [4].

Results. Fig.1 shows a typical FTEMIRS spectrum (unpolarized light) and attribution of the various vibrational lines for an n-Si/acetonitrile + 0.1M TBAP interface. Lines such as ν CH, ν CN, δ CH_3 , ρ CH_3 and ν ClO, clearly arise from electrolyte species. They appear in the electromodulated spectra with the same shape as in standard IR transmission spectra, but with either sign. This effect results from a change in *population* of the solvent and ionic species near the interface upon electrode potential modulation [4]. These signals are minimized when the electromodulation potentials are chosen not too far from the flatband potential. More interesting are lines such as ν SiH, ν OH, δ OH_2 and ν SiO, which are clearly associated with interfacial chemical species. Here the electromodulation mechanism most probably arises from a Stark

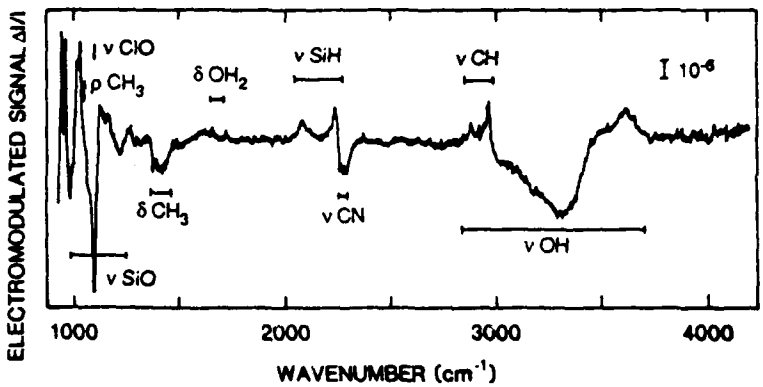


Fig.1. Typical electromodulated spectrum of a n-Si/acetonitrile + 0.1M tetrabutylammonium perchlorate interface. Electromodulation potentials V_1=-0.3V, V_2=+0.3V. Reference is Ag/Ag^+. Modulated charge 5×10^{-7} C/cm^2. Here the infrared beam is unpolarized.

effect: the species are essentially fixed on the surface whatever the electrode potential, but the modulated interface electric field may affect either the absorption intensity ("dipole strengthening") or the vibrational frequency ("Stark shift"), hence the appearance of derivative-shaped signals. The ν OH signal has been widely discussed earlier [3]. Hereafter we will mainly discuss the ν SiH, δ OH_2 and ν SiO signals, with special emphasis on the information that is brought by varying the polarization of the IR light.

ν SiH. Fig.2 shows the ν SiH signal as a function of the ageing time of the electrode in contact with the electrolyte, and with two different light polarizations: "s" (electric field parallel to the surface) and "p" (electric field parallel to the incidence plane). The decrease of the main line at 2070 cm^{-1} upon ageing has already been accounted for by the slow oxidation of the silicon surface, due to residual water (~ 10 ppm) present in the electrolyte, and the appearance of a second structure near 2270 cm^{-1} has been ascribed to Si-H groups backbonded to oxygen atoms [3], the absence of intermediate structures indicating that the oxidation is either absent or complete (oxide islands). Fig.2 further shows that the 2070 cm^{-1} signal is much stronger with p polarization than with s polarization. This gives evidence that the corresponding Si-H bonds are essentially perpendicular to the surface. On the other hand the 2270 cm^{-1} signal is only about a factor of two smaller with p than with s polarization. In view of the electromagnetic-field map in our experimental configuration, this is compatible with a random orientation of those SiH bonds backbonded to oxygen atoms.

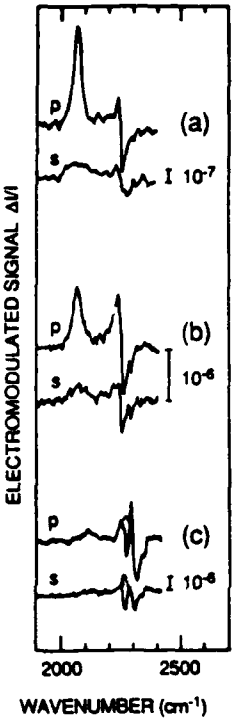


Fig.2. ν SiH spectrum for s and p polarizations. (a) 10h-aged interface; (b) 78h-aged; (c) anodically oxidized. Notice the different behaviors of the two ν SiH peaks upon changing the polarization. The 2270 cm^{-1} peak is superimposed with a sharp ν CN line. The dotted line in (c) is an attempt to remove the ν CN contribution. Electromodulated charges (a) 0.95,(b) 1.8,(c) 18 × 10^{-7} C/cm^2.

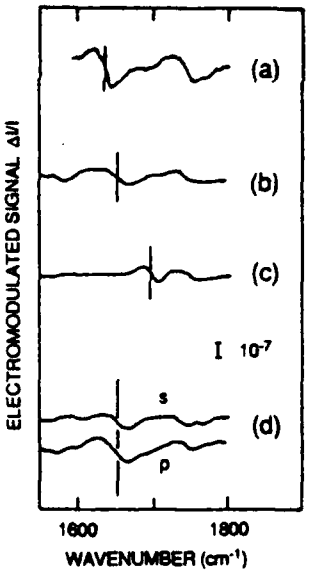


Fig.3. δ OH_2 spectrum for different solvents ((a) nitromethane, (b) acetonitrile, (c) dimethylsulfoxide) and light polarizations.((d) in acetonitrile). Notice the shifting upon changing the solvent. The feature near 1740 cm^{-1} may be ascribed to a surface contaminant.

δ OH_2. The small signal near 1650 cm^{-1} has been attributed to *the "scissor" mode of adsorbed* water (δ OH_2). This is confirmed by its slight shifting upon changing the solvent basicity (1635 cm^{-1} in nitromethane, 1650 cm^{-1} in acetonitrile, 1695 cm^{-1} in dimethylsulfoxide). This provides clearcut evidence for the presence of molecular adsorbed water at the interface, which had previously been inferred from a systematic study of the ν OH band [3]. The small effect observed upon changing the polarization of the light indicates a near-random orientation of these water molecules. A second line near 1740 cm^{-1} might be interpreted as due to another form of OH deformation (H_3O^+ or $SiOH_2^+$). The insensitivity of this line to solvent substitution rather favors its attribution to a surface contaminant (e.g., ν CO).

ν SiO. Fig.4 shows the ν SiO region as a function of ageing time and light polarization. The observed structures are rather complex. As a complementary information, the *direct* (i.e., *not* electromodulated) transmission spectrum of an anodically oxidized surface has been obtained by normalization to

the spectrum of the fresh surface. It is shown as Fig.4(f) and allows an easier attribution of these structures. The spectrum of the anodically grown layer consists in two lines at 1070 and 1230 cm^{-1}. The 1070 cm^{-1} line has about the same magnitude for s and p polarizations, whereas the 1230 cm^{-1} line disappears for s polarization; This shows that the 1070 cm^{-1} mode is coupled only with an electric field *parallel* to the surface, and the 1230 cm^{-1} mode with an electric field *perpendicular* to the surface. The 1070 (resp. 1230) cm^{-1} line therefore corresponds to ν SiO collective modes parallel (resp. perpendicular) to the surface, the 1070-1230cm^{-1} splitting being due to the electromagnetic interactions between the Si-O-Si vibrators in the layer. (In other words, 1070 (resp. 1230) cm^{-1} corresponds to a zero of Im(1/ε) (resp. of Im(ε)), ε being the complex dielectric constant of the oxide layer [5]).

Now, examination of the corresponding electromodulated spectrum (Fig.4(e)) allows to recognize the two (low-energy and high-energy) components corresponding to those in the direct spectra. The high-energy line essentially appears as the derivative of the direct spectrum (Stark shift) whereas the low-energy line appears as a W-shaped structure, which seems to indicate that the operating mode for the electromodulation here is rather a modulation of the linewidth [2]. Of course, the great advantage of the electromodulation technique is its superior sensitivity, which allows following the growth of the oxide from the very early steps. In Fig.4(a) there is only a single broad line appearing as a derivative shape. This may be understood as the spectrum of isolated, non-interacting Si-O-Si vibrators. As the density of vibrators increases, so do the interactions and the resulting splitting. The progressive shifting of the high-energy line from ~ 1170 to 1230 cm^{-1} is clear from Fig.4(b-e). Quantitative analysis of these data, together with those of the SiH spectrum, allows us to conclude that simple ageing of the surface leads to partial oxidation; i.e., after a few days about one half of the surface is still hydrogenated, the other half being covered with oxide islands of thickness ≈ 5 Å. After anodic oxidation, the whole surface is covered with an oxide layer (thickness ≈ 20 Å for an anodic oxidation such as shown in Fig.4(e-f)).

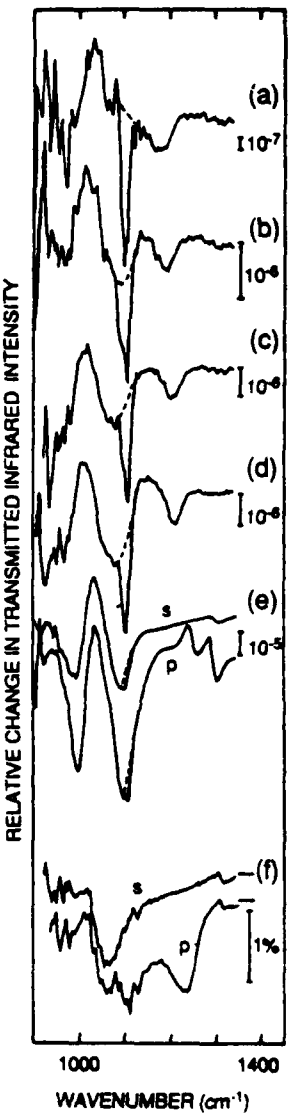


Fig.4. ν SiO spectrum for acetonitrile + TBAP electrolyte. (a) 8h-aged interface; (b) 26h-aged; (c) 80h-aged; (d) 144h-aged; (e) anodically oxidized (+5 V, ~ 100 μA/cm^2, 5 min.); (f) classical transmission spectrum of the oxidized surface (same as (e)) normalized to the initial surface. Electromodulated charges (a) 1.2, (b) 1.9, (c) 2.2, (d) 2.2, (e) 18 × 10^{-7} C/cm^2. The dashed lines have been drawn to remove the ν ClO peak due to the perchlorate ion.

References.

* URA 04 1254 du CNRS.

[1] J.-N. Chazalviel, Electrochim. Acta 33,461 (1988).

[2] A. Bewick and S. Pons, in *Advances in Infrared and Raman Spectroscopy*, Vol.12, R.J.H. Clark and R.E. Hester, eds. (Wiley Heyden, Chichester, 1985) pp. 1-63.

[3] A. Venkateswara Rao and J.-N. Chazalviel, J. Electrochem. Soc. 134, 2777 (1987).

[4] F. Ozanam and J.-N. Chazalviel, J. Electron Spec. 45,323 (1987).

[5] Y.J. Chabal, in *Proceedings of Les Houches Winter School on Semiconductor Interfaces, Formation and Properties*, G. Le Lay, J. Derrien and N. Boccara, eds. (Springer Verlag, Berlin, 1987) pp.301-327.

LOCAL PHOTOCURRENT AND HIGH POWER DENSITY INVESTIGATIONS ON OXIDE FILMS OF VALVE METALS WITH A FOCUSSED LASER BEAM

J. Thietke, K. Bade, J.W. Schultze
Institut für Physikalische Chemie und Elektrochemie, Universität Düsseldorf, Universitätsstr. 1, 4000 Düsseldorf, Fed. Republic of Germany

1. Problem

Photoelectrochemical experiments are usually carried out on macroscopic surfaces with low power densities PD ≈ 10 mW/cm². The electrodes are treated as homogeneous surfaces, and the processes are analysed perpendicular to the interface. With a focussed laser beam, on the other hand, lateral inhomogenities can be resolved for microprobe analysis /1, 2/. Laser radiation can be used for microscopic marking of the surface /2/ but lateral problems arise at high PD. Moreover, the oxide growth overlaps the effects. Hence, the present study was carried to investigate the lateral effects which depend on the PD and the transients which also depend on PD and the oxide growth. In previous experiments Ti-electrodes were used exclusively due to the high quantum efficiency of TiO_2. We therefore tried to apply this method to other metals.

2. Local Resolution

In order to demonstrate the ability of the method, various laser scans, taken on Ti-electrodes, are given in Fig. 1.

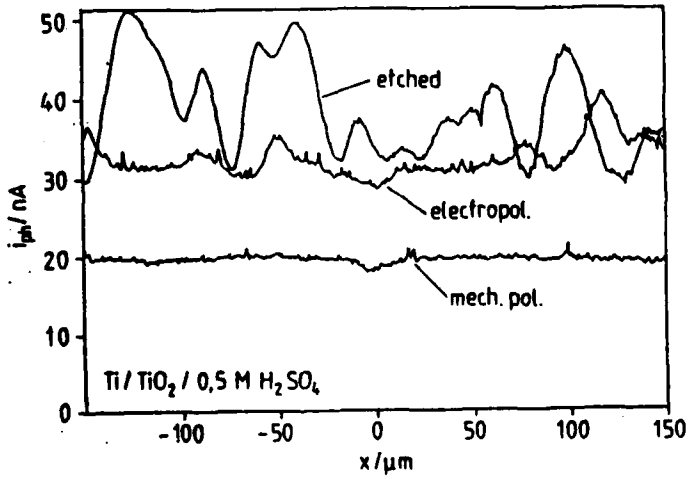


Fig. 1: Local photocurrent measurements of Ti-electrodes after different pretreatment (mechanical-, electropolishing and etching) and following passivation ϵ_{ox} = 5 V; ϵ = 1.5 V; P = 10 µW

The pretreatment of the surface has a strong influence on the scans: while the mechanical polishing yields a homogeneous surface, strong local

differences are observed on the etched electrodes. The lateral resolution is about 5 μm which allows the distinction of various grains corresponding to microscopic pictures.

3. Transients

The laser induced formation of electron-hole pairs causes oxide growth and oxygen evolution. Both increase with the illumination time t, potential ϵ and the light power P.

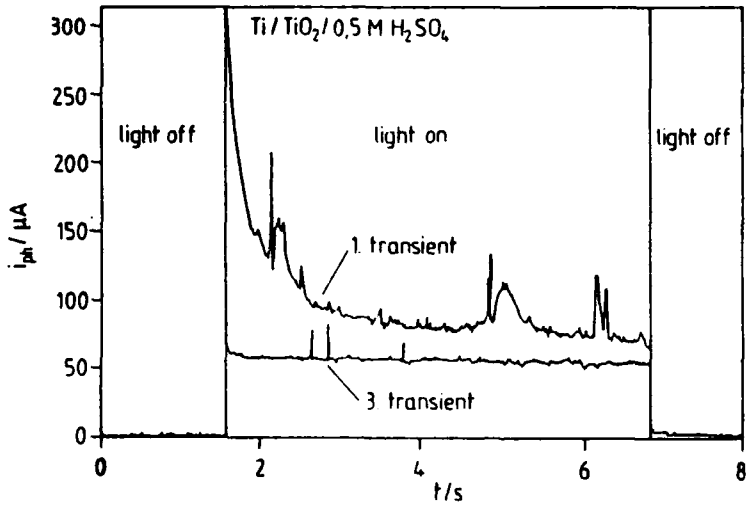


Fig. 2: Photocurrent transients for a 1st and 3rd run, ϵ_{ox}=5 V, ϵ=1.6 V. power density PD=40 kW/cm^2.

Fig. 2 shows the 1st and 3rd photocurrent transient on titanium as an example. After a sharp maximum (i_{max}) the current decreases rapidly to a final value (i_{fin}). In repeated experiments the photocurrent decreases further and finally remains constant. Microscopic pictures show that the colour of the oxide changes corresponding to the growth of the oxide. Further crystallisation indicates an inhomogeneous oxide growth on different grains. Moreover, all transients show peaks or sparks which are due to a local breakdown of the oxide. The quantum efficiency of the photoprocess decreases with increasing oxide thickness d, which corresponds well with the microscopic observation that the radiation damage of the oxide film decreases.

4. The influence of power density

The power of light could be changed from 10^{-5} to 10^{-1} W which corresponds to PD from 10 to 10^5 W/cm^2. Electrochemical and microscopic results of such experiments are given in Fig. 3 in a double logarithmic plot. The current of the transients i_{max} and i_{fin} as well as the charge Q increase almost linearly, but the slope of the line is about 0.65. This means that the quantum yield decreases with increasing PD. Since holes will be accumulated at the surface of the oxide, the rate of recombination will increase even

faster. Since the local current density at high PD will be in the range of A/cm², even the potentiostatic condition for the laser spot may be insufficient, but the band bending within the oxide will probably be maintained. Hence, only photoholes have the possibility to diffuse laterally to the surface. This effect can be derived from the laser induced oxide growth taken from microscopic pictures. The radius of the damaged area increases by a factor of 10, and the corresponding area $A \approx r^2$ increases by 2 orders of magnitude. This is also shown in Fig. 3. This lateral extension increases with the quantum efficiency, i.e. with ϵ and decreasing d.

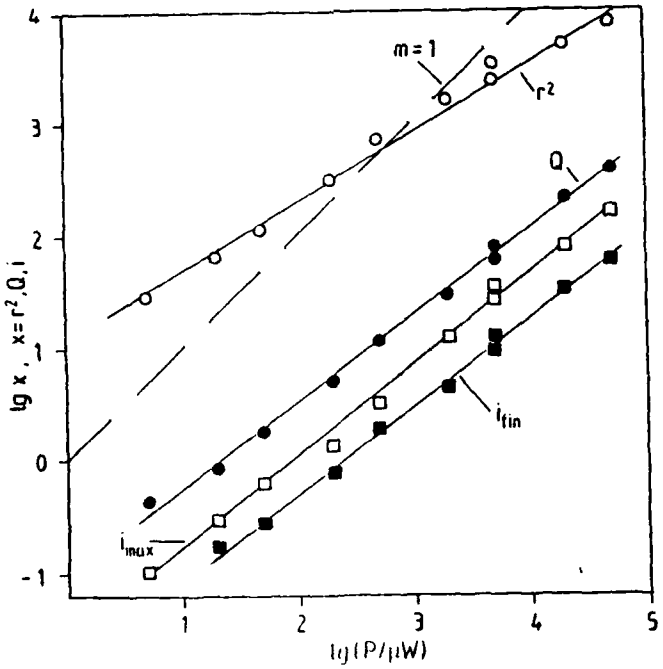


Fig. 3: Intensity P (μW) dependence of i_{max}, i_{fin} (μA); charge Q (μC); A ~ r^2 (μm^2) in a double logarithmic scale

5. Other metals

Similar measurements were carried out with other metals. The effects depend strongly on ϵ, d and t, but the most important influence has the quantum yield, which decreases in the order Ti > Nb > Ta > Zr > Hf.

/1/ M.A. Butler: J. Electrochem. Soc., 130, p.2358 (1983), and 131, p.2185 (1984)

/2/ K. Leitner, J.W. Schultze: Ber. Bunsenges. 92, 181 (1988)

PROFILE OF THE ELECTRICAL POTENTIAL IN AN ELECTROLYTE-INSULATOR-SEMICONDUCTOR SYSTEM

M.Grattarola, A.Morro, F.Conzi, A.Cambiaso, M.Parodi(*)
Biophysical and Electronic Engineering Department
Via all'Opera Pia 11a, 16145, Genova, Italy
(*)Institute of Electrical Engineering, Piazza d'armi
09100, Cagliari, Italy

1. INTRODUCTION

The study of electrolyte-insulator-semiconductor (EIS) systems is a basic step toward the understanding of the behaviour of ion- sensitive field effect transistors (ISFETs). In fact, the EIS system is a simpler configuration as compared to the ISFET, and, at the same time, it represents the operational entity in any ISFET structure that has the insulating layer exposed directly to the electrolyte. The EIS considered in the present work is characterized as follows:

i) the surface of the insulating layer presents two binding sites, for H^+ and OH^- groups only (that is, it is an ideal SiO_2 insulator);

ii) the electrolyte is a water solution of an ideal $z:z$ salt;

iii) the distance d between the surface of the insulating layer and the diffusion plane, which is reached by the cations and anions of the salt, is viewed as a parameter. Next, the profile of the electrical potential inside the electrolyte is modelled by a Poisson- Boltzmann-type equation. Our EIS system is sketched in Fig. 1 (left), together with the spatial compartments adopted in this work (right).

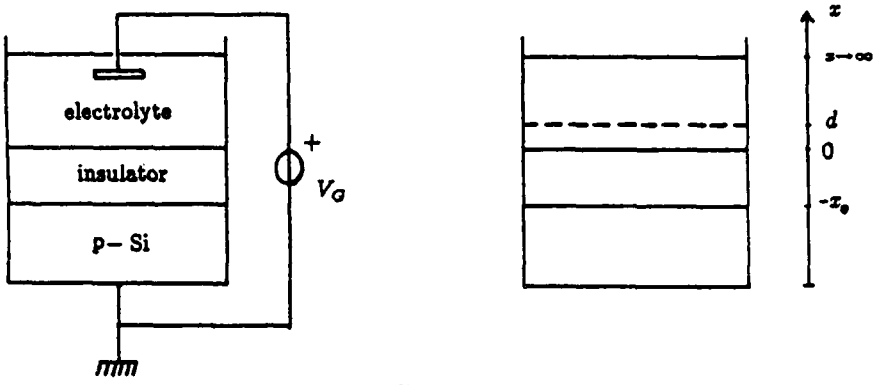


Fig. 1

2. Modelling of the electrical parameters in the electrolyte solution

We consider a one-dimensional model, and the origin of the coordinate x is at the diffusion plane. As far as variations of the dielectric permittivity ϵ have been observed in liquid dielectrics for field intensities of 10^7 V/m or less [1], the Poisson-Boltzmann equation can be written as

$$\frac{d}{dx}\left(\epsilon \frac{d\phi}{dx}\right) + \sum_{i=1}^{2} q\, z_i\, c_i(\infty) \exp\left[-\frac{q\, z_i(\phi - \phi_\infty)}{kT}\right] = 0 \qquad (1)$$

where $\phi_\infty = \phi(\infty)$. Here ϕ is the unknown electric potential, and q, z_i, k and T have the usual meaning. The non linearity of the electrolyte is described as

$$\epsilon = \epsilon(|\frac{d\phi}{dx}|^2). \tag{2}$$

For the sake of mathematical convenience, we consider $\psi = \phi - V_G$ and write the boundary conditions

$$\psi(\infty) = 0, \qquad \frac{d\psi}{dx}|_{x=-\infty} = 0. \tag{3}$$

There results a useful relation between ψ and $d\psi/dx$, namely

$$|\frac{d\psi}{dx}|^2\ \epsilon(|\frac{d\psi}{dx}|^2) - \frac{1}{2}\int_0^{|\frac{d\psi}{dx}|^2} \epsilon(y)dy = kT\{c_1(\infty)[\exp(-\frac{qz\psi}{kT}) - 1] + c_2(\infty)[\exp(\frac{qz\psi}{kT}) - 1]\}. \tag{4}$$

Since the differential permittivity has to be positive, we have

$$\epsilon + 2\epsilon E^2 \geq 0. \tag{5}$$

A solution to the constraint (5) is

$$\epsilon = \epsilon(\infty) + [\epsilon(0) - \epsilon(\infty)]\exp(-\alpha|\frac{d\phi}{dx}|^{\frac{1}{2}}), \qquad \alpha > 0. \tag{6}$$

The permittivity functions (6), parameterized by $\epsilon(0)$, $\epsilon(\infty)$ and α, satisfy (5) and are likely to constitute a realistic model of non-linear dielectrics. Correspondingly, if we let $c_1(\infty) = c_2(\infty) = c_\infty$, we have

$$\phi = -\frac{2kT}{qz}\sinh^{-1}\{\frac{\frac{d\phi}{dx}}{|\frac{d\phi}{dx}|}[\frac{1}{4kTc_\infty}(\frac{1}{2}\epsilon(\infty)|\frac{d\phi}{dx}|^2 + \Delta\exp(-\alpha|\frac{d\phi}{dx}|^{\frac{1}{2}})\Gamma(|\frac{d\phi}{dx}|) - \frac{12\Delta}{\alpha^4})]^{\frac{1}{2}}\} + V_G \tag{7}$$

$$\text{where}\quad \Gamma(|\frac{d\phi}{dx}|) = |\frac{d\phi}{dx}|^2 + \frac{2}{\alpha}|\frac{d\phi}{dx}|^{\frac{3}{2}} + \frac{6}{\alpha^2}|\frac{d\phi}{dx}| + \frac{12}{\alpha^3}|\frac{d\phi}{dx}|^{\frac{1}{2}} + \frac{12}{\alpha^4}, \qquad \Delta = \epsilon(0) - \epsilon(\infty). \tag{8}$$

In order to compare the solution (7) with the analogous one calculated with ϵ equal to its bulk value, the mathematical procedure can easily be repeated, giving the following expression

$$\phi_{\epsilon(0)} = -\frac{2kT}{qz}\sinh^{-1}[(\frac{\epsilon(0)}{8kTc_\infty})^{\frac{1}{2}}\frac{d\phi}{dx}] + V_G. \tag{9}$$

By comparing (7) with (9) we can get remarkable results for the two cases. Fig.2 shows that, with the same potential, the electric field is higher in the non linear case. Moreover, the non-linearity is strongly influenced by the parameter α.

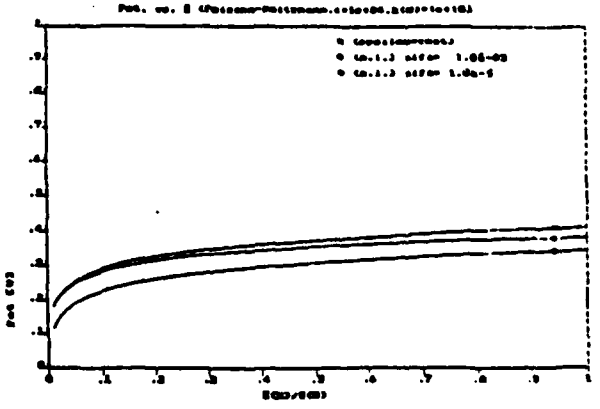


Fig.2

A more detailed investigation for the case when ϵ depends on the electric field is performed with variational procedures.

The relationship between the electrical parameters of the solid phase and the pH of the solution is obtained by following the approach of Fung et al. [2]. A pH-induced drift in the C-V curves is shown in Fig.3 .

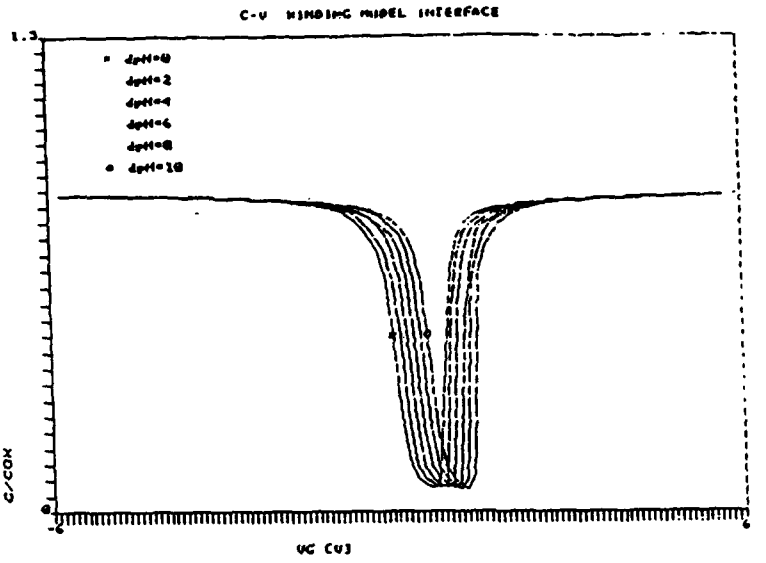


Fig.3

3. Conclusions

This paper represents a preliminary step toward the physico- mathematical characterization of (bio)chemically sensitive FET. Future work will be devoted to the variational approach to the solution of the Poisson-Boltzmann equation (1). The existence of multiple binding sites, simulating the presence of biological material which adheres to the insulating layer will be also considered.

References

[1] A.Morro, M.Parodi: " Variational approach to non-linear dielectrics: application to polielectrolytes." J.Electrostatics 20, Pg.219 (1988).

[2] C.Fung, P.Cheung, W.Ko: "Generalized theory of an Electrolyte Insulator Semiconductor Field Effect Transistor" IEEE Transactions on Electron Devices, Vol.ED 33,Pg 8,(1986).

Work supported by the National Research Council of Italy (CNR), PF MADESS.

MULTILAYER-MULTIJUNCTION PHOTOELECTRODES

W.M. Ayers
Electron Transfer Technologies
PO Box 160 Princeton, NJ 08542

Photoelectrochemical energy conversion and chemical synthesis processes based on single layer (single crystal, polycrystalline, and thin film) liquid junction semiconductors have a major limitation in that they cannot produce sufficient photovoltage to carry out water photolysis or other equally energetic reactions with the visible spectrum of sunlight.

The hope that liquid junction photoelectrodes would provide a low cost means for solar energy conversion due to elimination of expensive diffused dopant junctions (e.g. pn junctions) and the fact that liquid junction could be used with lower cost polycrystalline semiconductors did not compensate for the problems of utilizing small band gap, single junction materials.

To overcome the limitations of liquid junction photoelectrodes multilayer thin film, multijunction photoelectrodes (MJPE) were developed (1,2,3). These devices cascade PIN layers layers in a single structure to form a majority carrier photocathode.

The primary advantages of MJPE's are; they haveopen circuit photovoltages greater than 1.4 volts in visible light, are photocathodes and hence do no experience photocorrosion reactions, utilize the metal substrate of the MJPE as a stable anode, and have low fabrication costs Furthermore, since light only passes through the front surface of the MJPE in contact with the electrolyte (the metal substrate anode is in darkness) engineering of the photoelectrochemical cell is greatly simplified.

MJPE's also have the advantage of inherently greater efficiency than is possible with single layer photoelectrodes due to the adsorption and coupling of the energies of several photons of equal or different energies in one structure. For example, a photovoltaic a-SiH PIN structure has an open circuit photovoltage of about 0.7 volts. Photovoltages in multiples of 0.7 volts are obtained in the multijunction configurations e.g. 1.4 volts for PINPIN and over 2 volts for PINPINPIN.

Figure 1. illustrates the open circuit photovoltage dependence of an a-SiHx PINPIN structure in the electrolytes

listed in Table 1. Note the photovoltage is a linear function of the redox potential in contact with metal substrate and hence rear P layer. In these experiments the front N layer was only in contact with 0.1 M HClO4 for the hydrogen evolution reaction. The redox electrolyte was separated from the N layer with a Nafion membrane. What this data suggests is that depending on the redox electrolyte, there is an optimum rear P thickness to maintain the maximum photovoltage.

To date we have succeeded with a simple model of the open circuit photovoltage dependence on redox potential, E', short circuit current, Isc, maximum P layer/I layer barrier height, Ob, and a constant, A, that depends on intrinsic region carrier density, diffusivity and diffusion lengths in the dark. This equation is:

$$Voc = nkT/e\ [Ln(Isc) - Ln(A) + e(Ob - E')/kt]$$

A value of A = 1.05e-8 and Ob=0.6 fits the data in Figure 1.

We are now developing a comprehensive model which will acount for short circuit current and maxiumum power photcurrent behavior. The model must incorporate interaction of the internal electric field of the PIN junctions with the electrolyte contacts to the front N layer and rear metal contact, majority carrier injection from the N layer/electrolyte contact, and surface recombination/reactions rates for reactions of interest.

1. Ayers, W. US Patent 4,466,869 (1984).

2. Matsumura, M. Sakai, Y. Sugahara, S., Solar Energy Materials, 5, 10 (1985).

3. Ueda,K., Saki,Y., Matsumura, Y. "Photoelectrochemical Solar to Chemical Conversion by Use of Amorphous Silicon Electrodes", Extended Abst. 891, Vol 87-2, Electrochemical Soc. Honolulu (1987).

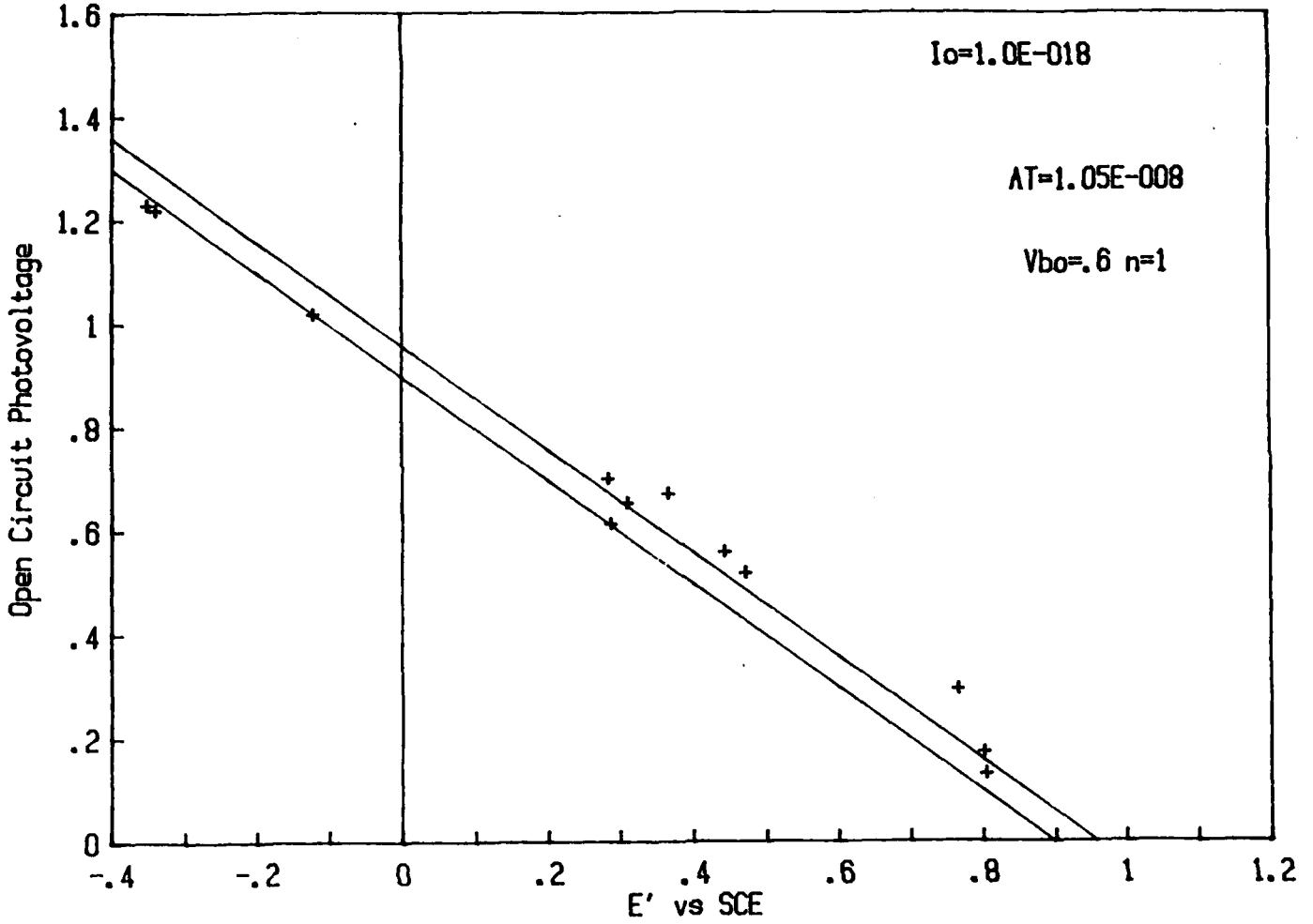

Io=1.0E-018
AT=1.05E-008
Vbo=.6 n=1
Open Circuit Photovoltage
E' vs SCE
1.6
1.4
1.2
1
.8
.6
.4
.2
0
-.4
-.2
0
.2
.4
.6
.8
1
1.2

TABLE 1

Redox couple	E'	Epsc	Epoc	Voc(V)	Isc(uA/cm^2)
NaI	0.283	0.289	0.980	0.702	330
Fe	0.355	0.412	1.022	0.673	110
NaBr	0.765	0.770	1.050	0.295	100
NaI	0.310	0.344	0.970	0.655	
Fe	0.471	0.462	0.980	0.520	
NaBr	0.801	0.800	0.970	0.173	
NaBr	0.804	0.805	0.935	0.130	28.5
NaI	0.287	0.345	0.960	0.615	370
PdHx	-0.297	-0.297	0.9	1.02	250
Iron chloride at N layer					
Fe/I	0.340	0.340	0.9	0.56	150
Fe/Fe	0.422	0.470	0.9	0.430	47
Fe/PdHx	0.079	0.079	0.9	1.02	240
Platinized N surface					
PdHx	-0.34	-0.34	0.9	1.22	300
NaBr	0.336	0.336	0.9	0.564	160

0.1 M NaX, 0.1 M Hclo4 supporting electrolyte. Light intensity, 0.104 W/cm^2.

REDUCTION OF $V(OH)_4^+$ ON PASSIVE TITANIUM

Werner Wilhelmsen
Department of Chemistry, University of Oslo,
P.O.Box 1033, Blindern, N-0315 Oslo 3, Norway

Previous investigations on ETR at passive titanium have revealed pronounced asymmetrical current potential curves. The two transfer coefficients α_- and α_- have been found to be about 0.1 and 0.9, respectively—thus indicating that the electron exchange mainly occurs with the conduction band in the passive film. As opposed to charge transfer polarization, concentration polarization (either pure diffusion limitation or slow chemical reaction to the electroactive reactant species as the rate determining step) has, hitherto, been believed to be of little importance for ETR at passive electrodes. However, the present chronopotentiometric data indicate that a chemical reaction to an electroactive vanadium (V) species precedes the electron transfer and eventually limits the cathodic reduction rate.

The measurements were carried out in 0.5 M H_2SO_4 + x M VO^{2+} + y M $V(OH)_4^+$ (x and y = 0 to 0.4) at 25 °C. The test solutions were deoxygenated by nitrogen bubbling and kept under nitrogen atmosphere during the measurements. The cell was shielded from light and stray fields by a surrounding aluminium foil. The potentials given here refer to *sce*.

Initial polarization data

In order to determine the net rates of the electron transfer reactions, current transients from potentiostatic pulses were recorded both in the presence and in the absence of the redox system. Figure 1 gives an example of initial polarization data thus obtained from potentiostatic transients.

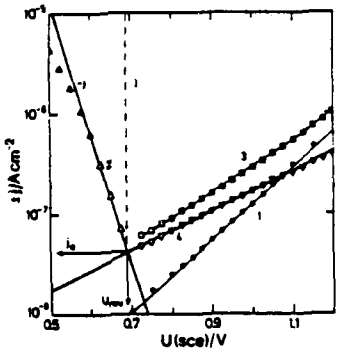


Fig.1. Initial polarization data for titanium electrode stabilized (20 h) at 0.9 V(sce) in 0.5 M H_2SO_4. The curves 1,2 and 3 represent measurements in 0.5 M H_2SO_4, in 0.5 M H_2SO_4 − 0.009 M $V(OH)_4^+$ and in 0.5 M H_2SO_4 + 0.1 M VO^{2+} + 0.009 M $V(OH)_4^+$, respectively. Curve 4 is the difference between the curves 3 and 1. Open symbols apply to Wagner-Traud corrected data.

The curves 2 and 4 in Fig.1 represent the net rates of reduction of $V(OH)_4^+$ and of oxidation of VO^{2+}, respectively. The oxidation of VO^{2+} gave a straight Tafel line (with α_- about 0.1). Near the reversible vanadium (IV)/(V) potential, the reduction of $V(OH)_4^+$ also gave a straight Tafel line (with α_- about 0.9). However, below 0.6 V(sce) this reduction gave a non linear Tafel curve—*ie* α_- was found to decrease with decreasing potential.

The rate of reduction of $V(OH)_4^+$ was found to increase linearly with increasing $[V(OH)_4^+]$ and to be independent of the presence of VO^{2+}. The rates of the redox reactions (reduction of $V(OH)_4^+$ and oxidation of VO^{2+}) were found to decrease a little with increasing film thickness.

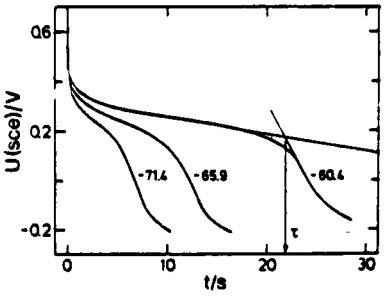
Under the present experimental conditions, electron exchange with the underlying metal seems little probable, even with resonance tunneling, since:

1. The passive films of the present work, which give tunneling barriers with high thickness (3 – 5 nm) and height (> 1 eV), have a tunneling probability which is almost vanishing and cannot explain the observed electronic current densities ($> 10^{-8} A cm^{-2}$).
2. In the case of electron exchange with the underlying metal, the exchange current (j_o) has been found to decrease exponentially with increasing film thickness. This is not at all compatible with the present observed small decrease of j_o with increasing film thickness.

Accordingly, the electron exchange must be with one of the bands (CB or VB) of the passive film. The present measurements clearly support a CB mechanism by the anodic and cathodic transfer coefficients being about 0.1 and 0.9, respectively.

Chronopotentiometric data

Figure 2 shows examples of chronopotentiometric curves. From these curves, the transition time (τ) was determined as shown for one of the curves in Fig.2. Figure 3 shows the observed dependence of $j\tau^{\frac{1}{2}}$ on j for the titanium electrode. The $j\tau^{\frac{1}{2}}$ curve exhibits a current independent range at $|j| > 80\ \mu A\, cm^{-2}$ where $|j\tau^{\frac{1}{2}}|$ is about 110 $\mu A\, cm^{-2} s^{\frac{1}{2}}$. At lower current densities, $|j\tau^{\frac{1}{2}}|$ decreases with increasing $|j|$— the slope $\frac{\partial(j\tau^{\frac{1}{2}})}{\partial j}$ was found to be $-32.5\ s^{\frac{1}{2}}$.



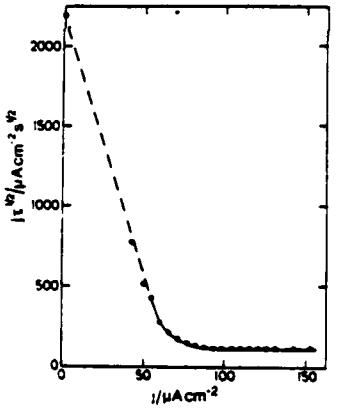


Fig.2. Chronopotentiometric curves for reduction of $V(OH)_4^+$ on titanium electrode stabilized (20 h) at open circuit in 0.5 M H_2SO_4 + 0.01 M $V(OH)_4^+$. Values of the imposed current density (in $\mu A cm^{-2}$) are given at the curves.

Fig.3. A $j\tau^{\frac{1}{2}}$ *vs* j plot for reduction of $V(OH)_4^+$ on titanium electrode.

These observations have been interpreted by means of a CE (Chemical/Electrochemical) mech-

anism, which can be written as follows:

$$Y \underset{k_{-1}}{\overset{k_1}{\rightleftharpoons}} O \tag{1}$$

$$O + ne^- \rightarrow R \tag{2}$$

where only O is considered to be electroactive. This CE mechanism gives the following equation for $j\tau^{\frac{1}{2}}$:

$$|j\tau^{\frac{1}{2}}| = \frac{1}{2}nF\left(C_O^b + C_Y^b\right)(\pi D)^{\frac{1}{2}} - \left(\frac{\pi^{\frac{1}{2}} erf[(k_1 + k_{-1})^{\frac{1}{2}}\tau^{\frac{1}{2}}]}{2K(k_1 + k_{-1})^{\frac{1}{2}}}\right)|j| \tag{3}$$

provided $D_Y = D_O = D$. The rate constants k_1 and k_{-1}, and the equilibrium constant $K = \frac{k_1}{k_{-1}}$ have been calculated to be 0.013 s^{-1}, 0.24 s^{-1} and 0.054, respectively. Use has then been made of Equation (3) and the present $j\tau^{\frac{1}{2}}$ data.

Even though our chronopotentiometric measurements clearly support a CE mechanism, they do not necessarily exclude all other possibilities. Perhaps a slow adsorption of $V(OH)_4^-$ on the oxide surface, preceding the charge transfer step, may explain the bend of the cathodic polarization curve. However, our polarization measurements are insufficient to establish this explanation.

The Role of Redox-Ion Migration in Electrochemical Processes on Polymer-Coated Electrodes

Karl Doblhofer and Jianhui Ye[1]
Fritz-Haber-Institut der Max-Planck-Gesellschaft
Faradayweg 4-6, D-1000 Berlin 33, Germany(West)

Electrodes coated with permeable polymer films are the subject of considerable current interest. We consider coatings of negligible electronic conductivity, i.e., the charge is transported by ions partitioned into the film from the electrolyte. Electrochemical analyses of such systems lead to new quantitative insights into membrane phenomena [cf. K. Doblhofer and R. D. Armstrong, Electrochim. Acta *93*, 453 (1988)]. Additionally, the results are relevant in a number of fields ranging from electropolymerisation and charging/dischargig of redox polymers to corrosion protection by organic coatings.

Calculations, as well as experiments with [coated disk]/[uncoated ring] electrodes demonstrate that in many systems of practical relevance the transference number of redox ions in the film is considerably larger than zero. This means, migration of the redox ions contributes to the charge transport across the coating. The standard electrochemical methods are based on diffusion as the only mechanism of of redox-ion transport associated with the interfacial charge-transfer processes. These techniques are thus not straightforwardly applicable in presence of the membrane-type coatings.

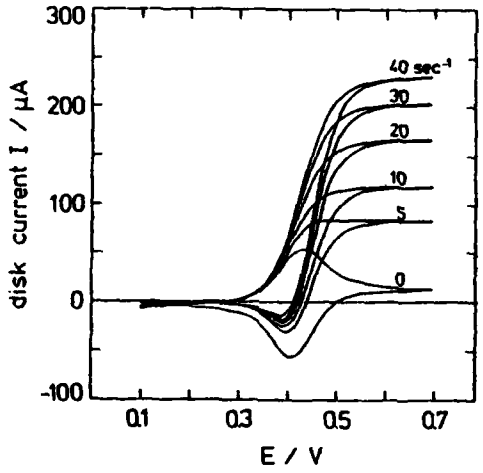


Figure 1: Pseudo-stationary Fe^{2+} oxidation at a rotated disk electrode coated with a 1.2 μm "Nafion" film. Electrolyte: 1 mM $FeSO_4$ + 0.1 M H_2SO_4. Electrode area: 0.27 cm^2. The rotation rates are given in sec^{-1}. The electrode potential (E) is reported with respect to the SCE.

[1] Permanent address: Dep. of Chemistry, Xiamen University,Xiamen, China

We present experimental results obtained with platinum electrodes coated with perfluorosulfonate polymer ("Nafion") films. The electrochemical behaviour is studied with the redox system $Fe^{2+/3+}$ in various concentrations of H_2SO_4. In particular, results on the anodic Fe^{2+} oxidation are presented. In Figure 1 the stationary anodic currents in case of 0.1 M H_2SO_4 as the background electrolyte are represented. The system follows the two-phase diffusion model. A plot of the reciprocal limiting diffusion current *vs.* $\omega^{-1/2}$, ($\omega = 2\pi\nu$, ν is the rotation frequency) leads to a value for the dynamic diffusion coefficient of Fe^{2+} in the coating: $D^{M}_{red} = 4\times10^{-7} cm^2 s^{-1}$.

However, the behaviour of the system changes as the coating is allowed to equilibrate with the redox ions. Probably, the redox ions form cross links in the organic matrix by association with the $-SO_3^-$ groups. The system is characterized by large-amplitude chronoamperometric experiments, as represented in the Figures 2 and 3. Only in the case of 0.5 M H_2SO_4 the system response at the longer times agrees with the anticipated Cottrell behaviour (with the deviations caused by the "thin layer cell" properties introduced by the coating). Yet, even in this case the diffusion coefficient is smaller by a factor of 4 ($1.5 \times10^{-7}\ cm^2 s^{-1}$) than determined in the dynamic diffusion case (in experiments as in Figure 1).

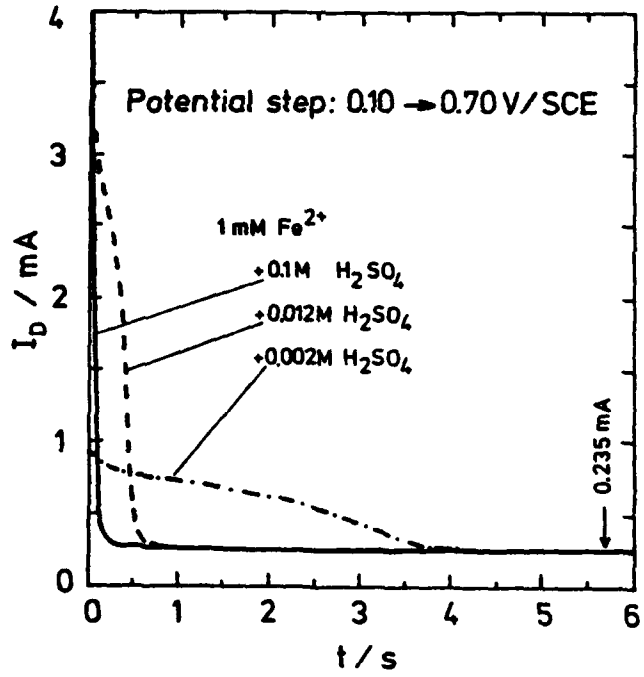


Figure 2: Current (I_D) transients observed with the rotated "Nafion"-coated platinum electrode in electrolytes of 1 mM Fe^{2+} in various concentrations of H_2SO_4. Electrode area 0.27 cm^2 .

As the H_2SO_4 concentration is reduced, the mobility of the redox ions in the film becomes smaller and the effect of their migration becomes significant. The Nernst-Planck equation is solved with the appropriate boundary conditions by digital simulation techniques (cf. R. Lange and K. Doblhofer, J. Electroanal. Chem. *237*, 13 (1987); and Ber. Bunsenges. Phys. Chem., in press). The experimental findings can be understood on the basis of these model calculations.

Secondly, the response of the system to small amplitude potential steps is recorded. The digital Laplace-transformation technique yields the system's frequency dependent complex-plane impedance. This analysis gives further valuable information elucidating the behaviour of the "Nafion"-coated electrodes.

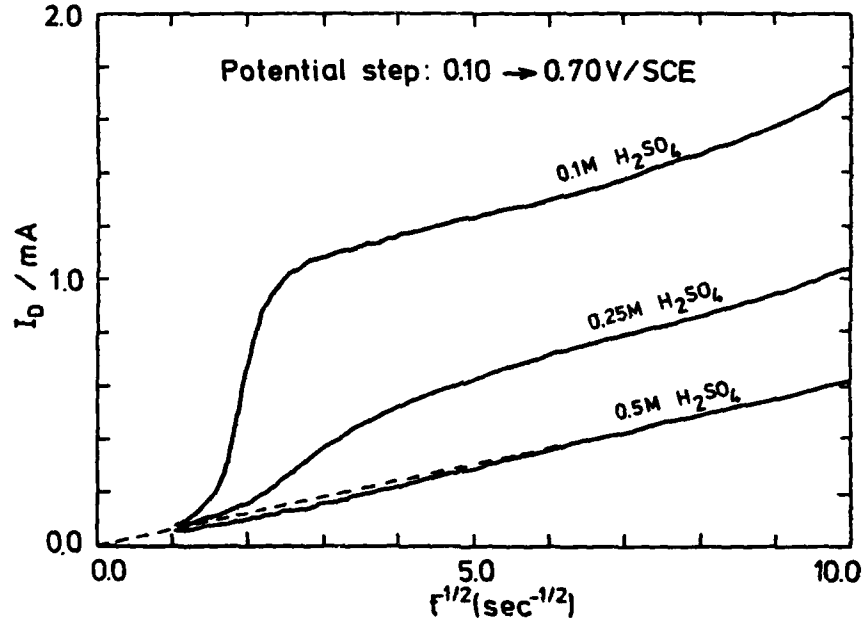


Figure 3: Cottrell-type representation of chronoamperometric current (I_D) transients observed with electrolytes of indicated H_2SO_4 concentration and 1 mM Fe^{2+}. Electrode area 0.27 cm^2.

THE ELECTROCHEMISTRY OF GRAPHITE AND MODIFIED GRAPHITE SURFACES

S. Hossain, D. Tryk and E. Yeager
Case Center for Electrochemical Sciences
and the Department of Chemistry
Case Western Reserve University
Cleveland, Ohio 44106

Introduction

The basal plane of highly oriented pyrolytic graphite (HOPG), which approximates the behavior of single crystal graphite, is unusual in that all of the valencies are satisfied in the plane of the surface [1,2]. A. c. impedance measurements show abnormally low capacitance (3.6 $\mu F\ cm^{-2}$), which has been explained by Randin and Yeager [1] in terms of the penetration of the electric field into the graphite material. Recently, McIntyre et al.[3] also obtained a value of 3.0 $\mu F\ cm^{-2}$ for the basal plane of HOPG in CH_3CN (0.2 M tetrapropylammoniumtetrafluoroborate) using voltammetry. The capacity-potential curve, however, is essentially parabolic rather than hyperbolic [1], with the potential dependence smaller than normally expected for a semiconductor. Gerischer [4] interpreted this low capacitance value as due to a low density of electronic states near the Fermi level of graphite. The capacitance value is also the same in acid and base [2] and is not perturbed by the addition of iodide to the electrolyte, in contrast to the behavior exhibited by most metal and semiconductor electrodes. The lack of sensitivity to pH and I^- reflects the fact that the surface is free of functional groups that interact specifically with the ions of the electrolyte.

The capacitance has also been examined for the basal plane of ordinary pyrolytic graphite and the edge orientation of HOPG both after mechanical polishing with alumina [5]. The capacitance values for the polished basal plane of pyrolytic graphite are 25% of the values for the edge orientation of HOPG. Randin and Yeager [5] have proposed that the higher capacitance on the polished edge orientation is due in good part to higher surface area associated with fissures in the surface. The capacitance curves and voltammograms both are strongly dependent on the potential range, the sweep direction and the electrolyte. The behavior clearly indicates the presence of functional groups that strongly influence the electrochemical properties.

The behavior of redox couples has been examined on the basal and edge planes of HOPG [6]. The kinetics of the ferri-ferrocyanide couple are under predominantly pure diffusion control on the edge plane and under combined kinetic and diffusion control on the basal plane. This difference is explained on the basis of the surface area differences but is moderated by double layer effects arising from charged surface groups and the large charge on the redox species. Intrinsic electronic differences between the basal and edge planes, however, are also likely to be involved and must be considered.

The electroreduction behavior of O_2 has also been examined on the graphite surfaces. Ordinary pyrolytic graphite (OPG) shows catalytic activity for O_2 reduction to HO_2^- in alkaline solution, whereas on the basal plane of HOPG this reaction is greatly suppressed [6]. This difference in O_2 reduction behavior may be attributed to the presence of surface functional groups on OPG and the lack of these groups on HOPG. A variety of surface functional groups, e. g., carboxyl, phenolic hydroxyl, quinone-type

carbonyl and normal lactones, are present on carbon surfaces. The question is which type of functionality is responsible for O_2 electrocatalysis. There are indications that surface oxidative treatments of carbon that tend to increase the coverage of quinoid-type functional groups also make the surface more active for O_2 reduction in alkaline solution [7].

The role of the electrode material in the cathodic reduction of O_2 to $O_2^{\cdot}$ in aprotic nonaqueous solvents has been extensively studied [see e.g. Ref. 8]. In both aprotic and concentrated aqueous alkaline solutions the O_2 reduction to $O_2^{\cdot}$ appears to occur by an outer sphere electron transfer mechanism on the basal plane [9].

The objectives of the present studies are :

(i) to examine the effects of electronic and surface properties of graphite on the kinetics of O_2 reduction to $O_2^{\cdot}$ in acetonitrile using cyclic voltammetry and rotating disk electrodes;

(ii) to establish the type and role of surface functional groups responsible for O_2 reduction to HO_2^{-} in alkaline solutions by adsorptive and covalent attachment of the functional groups on the graphite surfaces.

The experimental procedures and results will be presented in the poster paper. Only the overall observations and conclusions are summarized in this abstract.

Results and Conclusions

Cyclic voltammetry and rotating disk electrode techniques have been used to examine O_2 reduction to $O_2^{\cdot}$ on OPG and the basal plane of HOPG in acetonitrile with 0.1 M tetraethylammonium perchlorate (TEAP) as the supporting electrolyte. The voltammetry curves for OPG and HOPG were fitted with theoretical curves calculated on the basis of a generalized treatment in which the rate constants and transfer coefficients of both the anodic and cathodic processes are considered [10] (see Fig. 1). The standard rate constants (k^o) for the electrode reaction $O_2 + e^- \rightarrow O_2^{\cdot}$ are 5×10^{-3} cm s^{-1} and 5×10^{-4} cm s^{-1} for OPG and HOPG, respectively. The transfer coefficients (α_c) are -0.45 for OPG and -0.35 for HOPG. The relatively low α_c for HOPG may be attributed to its semiconductor properties.

The rate of reduction of O_2 to $O_2^{\cdot}$ on the basal plane of HOPG was determined in aqueous concentrated NaOH using a flow cell and ESR techniques to evaluate the $O_2^{\cdot}$ concentration in samples cooled to 77 K. The O_2 reduction to $O_2^{\cdot}$ in alkaline aqueous solution was found to have a standard rate constant of $\sim 2.5 \times 10^{-5}$ cm s^{-1} with a transfer coefficient of -0.30 (11, 12). The much lower rate constant in aqueous solution as compared with non-aqueous solution probably results from an inner sphere reorganizational free energy of activation in aqueous solutions with hydrogen bonding of H_2O to the $O_2^{\cdot}$ involved.

O_2 reduction also has been examined in alkaline aqueous solutions on HOPG and OPG surfaces with adsorptively attached and chemically attached quinones, respectively. The reduction behavior is very similar to that observed on unmodified OPG in alkaline solution (see Fig. 2).

Acknowledgement

This research has been supported by the U.S. Department of Energy through a subcontract with the Lawrence Berkeley Laboratory.

References

1. J. P. Randin and E. Yeager, J. Electroanal. Chem., 36, 257 (1972).
2. J. P. Randin and E. Yeager, J. Electrochem. Soc., 118, 711 (1971).
3. R. McIntyre, D. Scherson, W. Storch and H. Gerischer, Electrochim. Acta, 32, 51 (1987).
4. H. Gerischer, J. Phys. Chem., 89, 4249 (1985).
5. J. P. Randin and E. Yeager, J. Electroanal. Chem., 58, 313 (1975).
6. I. Morcos and E. Yeager, Electrochim. Acta, 15, 953 (1970).
7. Z. W. Zhang, D. A. Tryk and E. B. Yeager, in "The Electrochemistry of Carbon," S. Sarangapani, J. R. Akridge and B. Schumm, Editors, The Electrochemical Society Proceedings, Vol. 84-5, Pennington, NJ, 1984, pp. 158-178.
8. P. Cofre and D. T. Sawyer, Anal. Chem., 58, 1057 (1986).
9. M. S. Hossain, Ph. D. Thesis, Case Western Reserve University, 1986.
10. H. Matsuda and Y. Ayabe, Z. Elektrochem., 59, 494 (1955)
11. J. T. Lu, D. Tryk and E. Yeager, in "Extended Abstracts," Vol. 82-2, The Electrochemical Society, Pennington, NJ, pp. 520-521.
12. E. Yeager, J. A. Molla and S. Gupta, in Ref. 7, pp. 123-157.

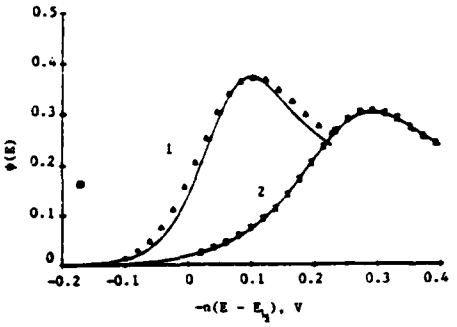


Fig. 1. Variation of current function, $\psi(E)$ with potential for OPG (A) and uncycled HOPG (X) in O_2 - saturated CH_3CN (0.1 M TEAP). Scan rate: 500 mV s^{-1}. Solid lines are theoretical curves for ideal quasi-reversible behavior.

1 - for $\alpha = 0.52$ and $k^o = 5.0 \times 10^{-3}$;
2 - for $\alpha = 0.37$ and $k^o = 5.0 \times 10^{-4}$.
$\psi(E) = I/[nFA(c_{ox})_{bulk}D_{ox}^{1/2}(nF/RT)^{1/2}v^{1/2}]$

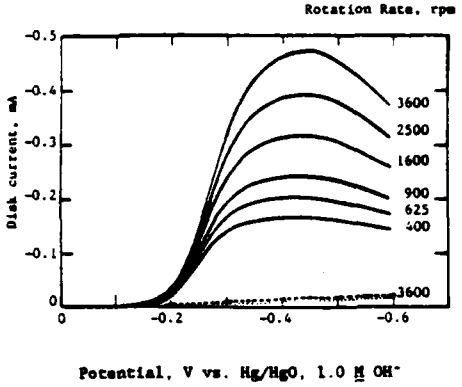


Fig. 2. Disk currents for O_2 reduction on HOPG with adsorbed 9, 10-phenanthrenequinone in O_2-saturated 1.0 M NaOH at 22°C. Scan rate: 20 mV s^{-1}; electrode area: 0.169 cm^2; basal plane without quinone (· · ·).

PHOTOLUMINESCENCE AND MOLECULAR ORBITAL THEORY IN ANODIC OXIDE FILMS FORMED ON Al_2O_3

Jovanic B.[1],Zekovic Lj.[1,2],Urosevic V.[1],Radenkovic B.[3]

The samples were prepared by anodic oxidation Al in different aquious electrolyte solutions (H_2SO_4; H_3PO_4; H_2CrO_4; Na_2CO_3; $H_2C_2O_4$; HCOOH). Forming conditions are same for all samples (j=10mA/cm; T= 295 K). Thicknes of samples were about 3μm. Calculation was perfomed at the PC-XT compatibile computer.

We used clasical LCAO method to construct MO's for the complex.These orbitals are at the form:

$$\psi_{mol} = \Psi(\Gamma) \sum_i a_i \Psi_i$$

were $\Psi(\Gamma)$ is a wave function of the central atom transformed in the molecular point group as irreducibile representation Γ. $\sum a_i \Psi_i$ is linear combination of ligand wave functions transforming as the same irreducibile representation Γ. The radial part of wave function we describe by Slater functions as:

$$R(r) = \left[\frac{[2*\alpha]^7}{6!}\right]^{1/2} * r^{n-1} * e^{-\alpha * r}$$

were $\alpha = Zeff/n$.

The energy of the lowest energy level we found by:

$$E_n = \frac{\int \Psi^*_{mol} H \Psi_{mol} 4\Pi r^2 dr}{\int \Psi^*_{mol} \Psi_{mol} 4\Pi r^2 dr}$$

1

(1) Instityte of Physic,11001 Beograd, POBox 57 Zemun, M.Gorkog 118
(2) Faculty of Physical Science, POBox 550, 11000 Beograd,YU
(3) Faculty of Org. Sciences, 11000 Beograd, Jove Ilica 154, YU

The energy difference between (e_g) and (t_{2g}) orbitals is taken as 10Dq, which is equal to:

$$(10Dq) = e_g - t_{2g}$$

The first step in construction MO's for Al^{3+}- Ligands, was construction of valenc MO's for Ligands, which are the complex ions too. Ligands as (SO_4^{2-} ; PO_4^{3-} ; CrO_4^{2-}) belong to the T_d group of symetry. CO_3^{2-} and $COOH^-$ belong to the D_{3h} and $C_2O_4^{2-}$ to the D_{2h} group of symetry. In the case of SO and PO ions, for construction valenc MO's we used (3s),(3p),(3d) atomic orbitals for sulphor and Phosphor atoms, also (2s)and (2p) orbitals for oxigen. For CrO_4 ions we used (3p)(3d)(4s) chromium orbital and (2s)(2p) for oxigen. MO's for carbonate, carboxylate and oxalate anions we constrycted using (2s) (2p) orbitals for C and O atoms, and expecealy (1s) for H atoms.

Validity for this choice of atomics orbitals one can see by analysing electronics spectra for announce anions. Finely,for Al-Ligand complex we used, below taken MO's and "outher" (3d) Al^3 orbitals. Calculation "ionicity of bonding" we found that in all cases the bonding have covalent character.For this reason in our calculation we supposing that all used orbitals are Pauling's covalent orbitals.

Excitation Photoluminescence Spectars, for samples formed in Sulphoric,Phosphoric and Oxalic acid have two maxima. First, shorter wavelenght, we connected with $(e_g) \Rightarrow (t_{2g})$ transition in complex ions which were formed by incorporation announced anions in oxide replacing O^{2-} ions. Coordinat number are different N(SO)=6 and N(PO_4)= 4. In another words, in samples formed in Sulphoric and Phosphoric acid Al^{3+} ion formed Octahedron and Tetrahedron complex ions, respctively. When spaces incorporated deeper than 10 nm, they pull down and formation of new type of complex ions occure. Oxigen ions were replacing with S and P ions, insted Suplhate and Phosphate anions, without changing environment symetry. This, new, complex ions shaw new maxima in PL excitation spectar. Comparing calculated and experimental value of maxima one can see good agreement between them.

In the case of Oxalic acid, existence the maxima at shorter wavelenght,we conected with forming Octahedron complex ions betwen Al^{3+} and oxalate anions. This anions are placed in outermost oxide layer. In deeper part of oxides, separat carboxilate ions are present and Al^{3+} ions formed another complex. Consequence of this is new position of maxima in PL excitation spectra.

In the smples formed in Chromic acid ,Formic acid and Sodium carbonate, excitation PL spectra have one maxima . In this case incorporated anions are anchanged and in that form replacing oxigen ions. Consequence is formation Tetrahedron complex ions. Calculated and experimental wavelenght of excitation maxima are in good agreement.

CONCLUSION

In all cases of complex ions there are good agreement between calculated and experimental wavelenght in excitation PL spectra (Tab.1). This agreement is proof of validity in our assumptions for stryctyral changing in formed complex ions. Also, it is proof that luminescence centres in formed oxides are not pure incorporated electrolyte anions but these are complex ions.

TABELA 1

ANIONS	λ_{nm} (exp)	λ_{nm} (calc)	ENVIRONMENT SYMETRY
SO_4^{2-}	340	338	O_h
S^{2-}	265	265	O_h
PO_4^{3-}	340	337	T_d
P^{2-}	270	279	T_d
CrO_4^{2-}	325	344	T_d
CO_3^{2-}	360	379	T_d
$COOH^-$	370	373	T_d
$C_2O_4^{2-}$	250	250	O_h
COO^-	305	305	Oh

REFERENCE

1. V.Urosevic,B.Jovanic,Lj.Zekovic, Proc.Itner.Conf.Elec. Quantym Phenom.Interface.,Telavi (1984),USSR
2. T.Sasaki and H.Adachi,J.Electron.Spectr.Related Phenom.,19 (1980) 261
3. S.Sugano,Y.Tanabe,H.Kamimura,Multiples of Transition-Metal Ions in Crystal, Acad.Press, London (1968)
4. D.P.Graddon, J.Inorg.Nucl.Chem.,3 (1956) 308
5. S.J.H.Shute,The Wave Mechanics of Atoms,Molecuis and Ions,E.Arnold Press,London (1968)

Photoelectrochemically Synthesized Interfacial Oxides on Silicon: Composition and Electronic Properties

J. Stumper , C. Pettenkofer, R. Greef [+)]
and H. J. Lewerenz
Hahn-Meitner Institut Berlin GmbH
Bereich Strahlenchemie
Glienicker Str. 100
Federal Republic of Germany

In-situ photoelectrochemical synthesis of interfacial films can improve the electronic properties of electrochemical devices such as photoelectrochemical and photovoltaic solar cells. The formation and dissolution of oxides is particularly interesting for multicomponent structures. Examples of those structures are electrolyte-oxide- semiconductor (EOS) junctions and MOS-structures. For silicon, oxide formation and process control are of substantial technological importance and in-situ interface conditioning has been carried out for single crystalline and amorphous material. The main issues associated with in-situ photoassisted synthesis refer to the correlation of composition, structure and electronic properties. Surface recombination velocity and surface state density can be influenced greatly by interface conditioning. In the present work, the formation and dissolution behavior of oxides on silicon will be presented and the composition will be analyzed by ellipsometry and X-ray photoelectron spectroscopy (XPS). Surface and interface electronic properties are discussed using a modified Sze-Cowley model (1).

In the experiments single crystalline as well as amorphous hydrogenated silicon (a-Si:H) films have been investigated. Standard electrochemical instrumentation was used for sample preparation. An automatic nulling ellipsometer at $\lambda = 632.8$ nm was used for in-situ ellipsometric studies. Surface analysis was performed in a commercial ESCA system (Escalab MKII, Vacuum Generators) with a base pressure in the 10^{-11} Torr range using Mg Kα radiation.The typical electrochemical behavior of n-type silicon in aqueous electrolytes is shown in Fig. 1. In fluorine free solution the sample rapidly passivates upon anodic polarization and illumination whereas after addition of fluorine an increased photocurrent and no passivation are observed. Depending on the presence of F^- anions in solution photogeneration of holes leads to formation of an oxidic layer or oxide dissolution (depassivation) and

[+)] Department of Chemistry, University of Southampton, Southampton SO9 5NH, England

subsequent silicon dissolution forming SiF_6^{2-} complexes (2,3). From the insert in Fig. 2 a change of composition with thickness can be deduced showing a lower optical thickness for thin passivating layers. This may be due to a higher void fraction (water content) near the Si/SiO_2 interface.The peak positions in Fig. 3 can be attributed to SiO_2 (Fig. 3a) and to an oxidic layer containing water or hydroxyl groups (Fig. 3b) (4). This indicates, that incorporation of H_2O takes place to compensate the lattice mismatch between Si and SiO_2.

The electronic characterization follows a model wich correlates the change of photovoltage with redox potential with the respective surface state density D_{ss}. Fig. 4 shows a superior behavior for the reduced sample with $D_{ss} = 4 \cdot 10^{13}\ eV^{-1}cm^{-2}$ and $D_{ss} = 3 \cdot 10^{14}\ eV^{-1}cm^{-2}$ for the untreated sample . For the passivated sample scattering of data points is too large for reliable analysis.

Surface passivation by fluoride has been shown to be very effective on crystalline silicon (5) and our results show that interface electronic properties can be improved also on high bulk defect density materials.

References

(1) Lewerenz, H. J.; Goslowsky, H. ; J. Appl. Phys. 63 2420 (1988)
(2) Gerischer, H.; Lübke, M.; Ber. Bunsenges. Phys. Chem. 91 394 (1987)
(3) Lewerenz, H. J.; Stumper, J.; J. Electrochem. Soc. 134 1877 (1987)
(4) Grunthaner, F. J.; Grunthaner, P. J.; Mat. Sci. Rep. 1 65 (1986)
(5) Yablonowitch, E.; Allara, D. L.; Chang, C. C.; Gmitter, T.; Bright, T. B.; Phys. Rev. Lett. 57 249 (1986)

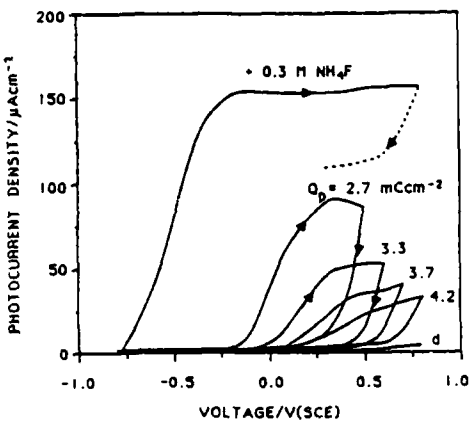


Fig. 1: Cyclic voltamogram of an untreated intrinsic a-Si:H layer deposited on stainless steel under white illumination (20 $mWcm^{-2}$). Lower curves: in phtalate buffer ph 4.5, the integrated charge Q_p is given for successive cycles. Upper curve: after addition of 0.3M NH_4F. Scan velocity : 20 mVs^{-1}.

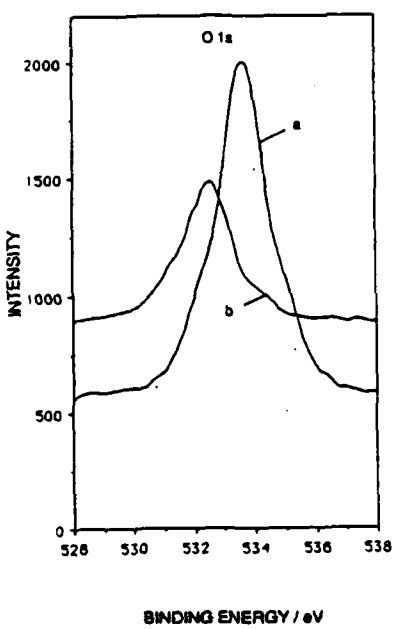


Fig. 3: XPS data for the O 1s line for a) a thick and b) a thin passivating layer on a-Si:H with Mg Kα radiation at normal emission. The thickness for a) is about 10 times higher than for b).

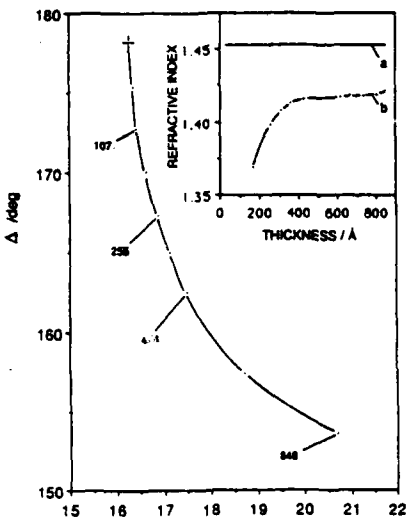


Fig. 2: Ellipsometric Profile during formation of an electrochemical oxide on p-Si <111> $N_A = 1.5 \cdot 10^{16}$ cm^{-3} in Phtalate buffer at $\phi = 60°$, $\lambda = 632.8$ nm. Numbers at the graph denote thickness in Å. Insert: Comparison of the calculated refractive index vs. thickness for the b) electrochemical oxide and a) thermal oxide.

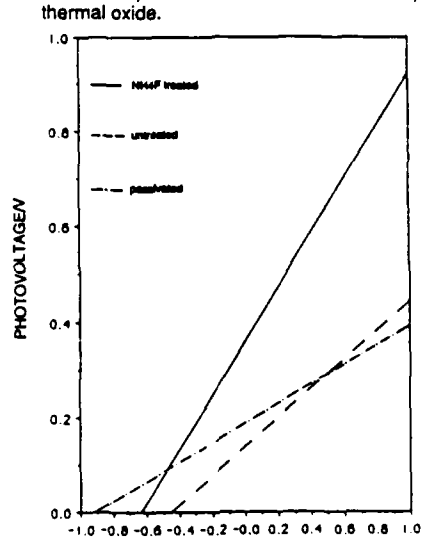


Fig. 4: Dependence of photopotential for a-Si:H/redox electroyte junctions on redox potential for differently prepared surfaces. Redox couples: $Ce^{3+/4+}$, $Fe^{2+/3+}$, $Fe(CN)^{3-/4-}$, I/I_3^-, $V^{2+/3+}$. Where photovoltages were not constant, initial values are plotted in the figure.

STUDY OF THE ANODIC DECOMPOSITION OF III-V SEMICONDUCTOR ELECTRODES INDUCED BY HOLE INJECTION

D. Vanmaekelbergh and J.J. Kelly
Fysisch Laboratorium, Rijksuniversiteit Utrecht
P.O. Box 80.000, 3508 TA Utrecht, The Netherlands

Stabilization results obtained with rotating ring-disc voltammetry have been widely used to elucidate the mechanism of anodic decomposition of semiconductors [1]. In this work we describe an alternative approach: holes are generated in an n-type electrode by injection from an oxidizing agent in solution and the rate of thermal excitation of electrons into the conduction band from intermediates of the dissolution reaction is then studied as a function of the hole injection rate. Results for GaP [2] and GaAs [3] are compared.

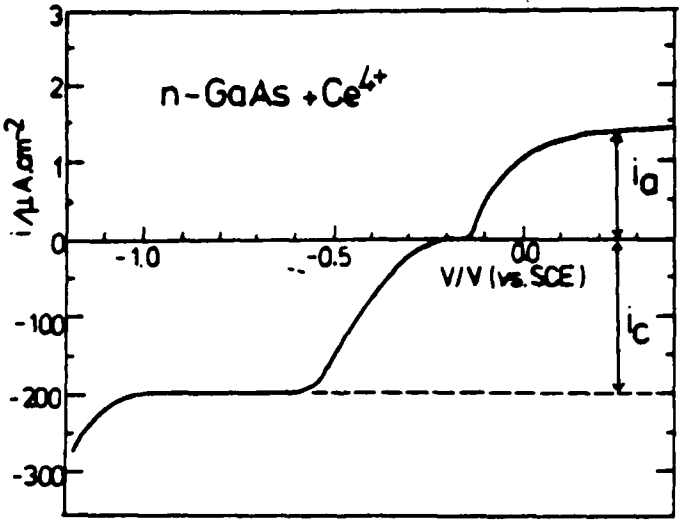


Fig.1. Current-potential curve measured at an n-GaAs rotating disk electrode in aqueous 2 mol.dm^{-3} H_2SO_4 + 10^{-2} mol.dm^{-3} $Ce(SO_4)_2$; rotation rate 17 s^{-1}; T = 298 K.

In fig.1 the current-potential curve is shown for an n-GaAs electrode in a solution of pH = 0 containing Ce^{4+} ions. Reduction of Ce^{4+} occurs via the valence band and the limiting current density i_c is diffusion controlled in the entire potential range shown [4]. At potentials positive with respect to the rest potential an anodic current is observed. The limiting anodic current density (i_a), which is the difference between the anodic decomposition current density and the

cathodic (hole-injection) current density (i_c), must be attributed to thermal excitation of electrons from decomposition intermediates into the conduction band:

$$Ce^{4+} \rightarrow Ce^{3+} + h^+ \qquad (1)$$

$$GaAs + (6 - n)h^+ \rightarrow Ga^{III} + As^{III} + ne^- \qquad (2)$$

The current-potential curve for the GaP/Ce^{4+} system shows almost the same features as that for the GaAs/Ce^{4+} system.

The relationship between i_a and $-i_c$ for the GaP (fig.2) and GaAs (fig.3) systems at pH = 0 are obviously quite different. In the case of GaP the results conform to:

$$i_a = \frac{-i_c}{A + B.(-i_c)} \qquad (3)$$

where A is a constant close to 5 and B is a strongly temperature dependent constant. At higher hole injection rates ($-i_c$ > 1 mA cm^{-2}), i_a measured at GaAs is a linear function of $-i_c$

$$i_a = K + L.(-i_c) \qquad (4)$$

where K is a small constant and L is a constant slightly dependent on temperature

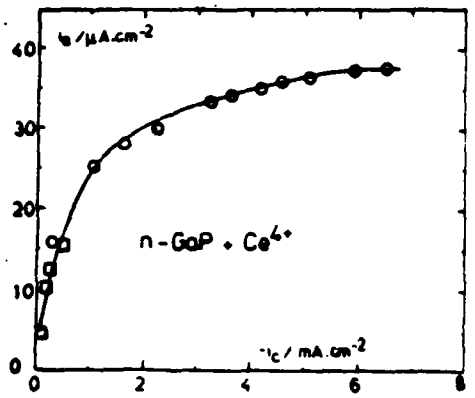


Fig.2. Plot of the anodic limiting current density i_a as a function of the cathodic current density i_c measured at an n-GaP rotating disk electrode in 2 mol.dm^{-3} H_2SO_4 + $Ce(SO_4)_2$; T = 298 K. Ce^{4+} concentration: (□) 1 × 10^{-2} mol.dm^{-3}, (○) 2.5 × 10^{-2} mol.dm^{-3}.

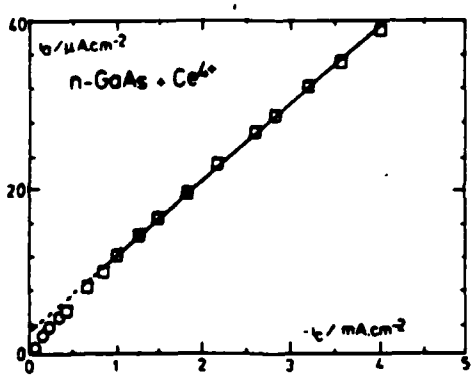


Fig.3. Plot of i_a as a function of i_c measured at an n-GaAs rotating disk electrode in 2 mol.dm^{-3} H_2SO_4 + $Ce(SO_4)_2$; T = 298 K. Ce^{4+} concentration: (○) 5 × 10^{-3} mol.dm^{-3}, (□) 10^{-2} mol.dm^{-3}.

In refs. 2 and 3 it was shown analytically that the different i_a vs. i_c relationships for GaP and GaAs anodes correspond to different mechanisms of anodic decomposition. The results can also be understood intuitively. The anodic decomposition mechanism for GaP is schematized below:

$$(GaP)_{surf} \xrightarrow{h^+} X_1 \xrightarrow{h^+} X_2 \cdots$$
$$\qquad\qquad\qquad\qquad\quad \searrow e^- \nearrow$$

The electron excitation step competes with a hole step of a higher order in holes; hence electron excitation becomes suppressed by the hole step as the hole injection rate is increased [see eq.(3)]. The linear relationship between i_a and $-i_c$ observed at the GaAs/Ce^{4+} system is the result of a competition between an electron excitation step and a chemical step [3]:

$$(GaAs)_{surf} \xrightarrow{h^+} X_1 \xrightarrow{H_2O} X_1OH \xrightarrow{X_1} X_2 \cdots$$
$$\qquad\qquad\qquad\qquad\quad \searrow e^- \nearrow$$

At sufficiently high hole injection rates, the chemical step becomes irreversible because of the fast following electrochemical step. Both the electron excitation and the chemical steps are then first order in X_1 leading to a linear relationship between i_a and $-i_c$ [see eq.(4)].

It can be concluded that study of the relationship between the rates of electron excitation and hole injection provides a useful method to investigate the anodic decomposition mechanism of III-V semiconductor materials, including chemical as well as electron excitation steps.

References

1. B. Miller, J. Electroanal. Chem., 168, 91 (1984)
2. D. Vanmaekelbergh and J.J. Kelly, submitted to J. Electrochem. Soc.
3. D. Vanmaekelbergh, J.J. Kelly, S. Lingier and W.P. Gomes, submitted to Ber. Bunsenges. Phys. Chem.
4. F. Decker, B. Pettinger and H. Gerischer, J. Electrochem. Soc., 130, 1335 (1983).

SEMICONDUCTING METAL OXIDE PHOTOANODES
THEIR CHARACTERISTICS AND IMPLICATIONS (XXI)

Sardar K. Bahador

Department of industrial chemistry, Faculty of engineering
Kyoto university
P.O. Box 51, Sakyoku Kyoto 606 Japan

It is for more than a century that a great deal of some exploratory efforts primarily concerned with the essential requirements for finding a durable energy resource, that has consequently become characteristics of our critical era, have been directed towards a significant branch of scientific research aiming at the effective utilization of solar power; say an eternally available extremely clean and embargo-proof energy source. In particular, conversion of solar radiant energy via photosynthetic procedures and photo-(assisted-)electrolysis of water for the production of power and useful chemicals through some novel techniques is a well established concept today. Purely solid state (p-n junction) and semiconductor based photoelectrochemical cells (s-l junctions),PEC, are the well known devices designed for such performances.

In accord with these facts and as part of a research project concerned with the science and technology of some model metallic oxides, chalcogenides including other lamellar compounds and conducting polymeric materials crucial for scientific research and technological processes of the advanced energy conversion and storage devices; a series of photosensitive oxides and chalcogenides have been systematically investigated for the sake of their photocatalytic activity and possible use as photoelectrodes in solar driven devices. Typical oxides such as TiO_2, PbO_2, SnO_2, MnO_2, ZnO, WO_3, $SrTiO_3$, Fe_2O_3,...., were evaluated either in the single crystal or polycrystalline forms. Thin films of the polycrystalline materials were prepared via several methods, depending on the kind of the material investigated, such as thermal oxidation, anodic growth, chemical vapor deposition, plasma spraying and r.f. sputtering; while pressed and sintered powders were provided from either of the commercially available chemicals or have been synthesized through some appropriate methods. Studies have also been conducted on optical and photoelectrochemical behaviors of colloidal suspensions of some oxides and sulfides of interest.

Of various materials investigated, we will take into account here Ti-O system as an example. The systematic study carried out on preparation and characterization of TiO_2 single crystals, poly crystalline thin films, pressed and sintered powders with various preparative nature as well as the colloidal suspensions have yeilded very exciting and promissing results. The afore-mentioned techniques of film deposition including plasma enhanced CVD and screen printing, with the exception of sputtering, these methods do not offer much versitallity in selecting and controlling film structures. In the case of TiO_2 for example, oxidation requiers high temperature ($>500\ ^oC$) and well surface treated Ti substrate, and CVD necessitates temperatures $> 500\ ^oC$ $TiCl_4$ and O_2 are to be reacted at a reasonable rate.

Sputtering process in general, an accepted and fast growing method for production-line deposition of thin films today, appears to offer excellent control over film properties such as adhesion, degree of crystallinity, density and chemical compositions. The reactive sputtering process in particular and in the case of TiO_2 is a potentially valuable method for producing suboxide films (especially the Magneli phases) with controled stoichiometry and chemical compositions. It was shown that the chemical composition of TiO_2 film, with the dark blue-greyish color for example, prepared by reactive sputtering in pure O_2 or in an O_2-Ar mixture were changed by ca. 0.1 O/Ti ratio. This will be a documentation for our ability to establish a relationship between the photocatalytic activity and the electrical characteristics of semiconductor .

Thin films of TiO_2 served the experimental purposes were deposited on several substrates including glass and Au,...., by r.f. sputtering techniques. Beside the ease of thin film preparation compared to crystal growth, various experiments such as possibility of separating the bulk transport vs. interfacial transfer process by varying the film thickness etc., can be conducted with thin films that are not feasible on thick crystals. Obviously, film thickness which is an essential parameter in regard with the electrode photoresponse can be easily controlled via adjusting the film deposition time. A much important advantage of using thin films as photoelectrodes is that for thin enough films of the order of the thickness of the depletion layer for a doped sample, there is no doping requirements inorder to increase the electrical conductivity of the electrode materials. Since efficiency and stability of the defect doped metal oxides emerges as significant problems, thus the properties of undoped oxide films should be carefully taken into considerations.

All the reactively sputtered TiO_2 films on glass s/

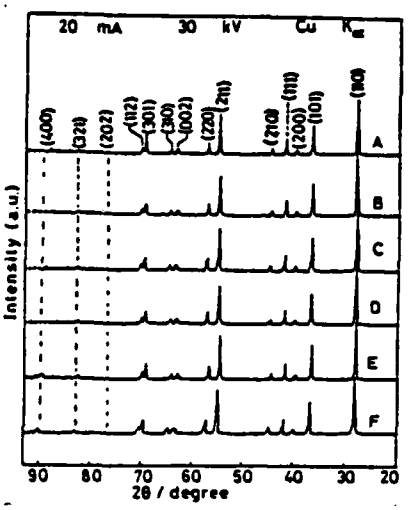


Fig.1. X-ray diffractograms of the sintered TiO_2 specimens. The powders were heated prior to compressing, in an electrical furnace under static air for 5hr at 1000 °C. The compressed pellets labled as A-F, all were sintered at temperatures between 800 to 1500 °C, for different time intervals ranged between 2 to 20 hr at each experimental temperature; where all other conditions were the same as for heating the original powders.

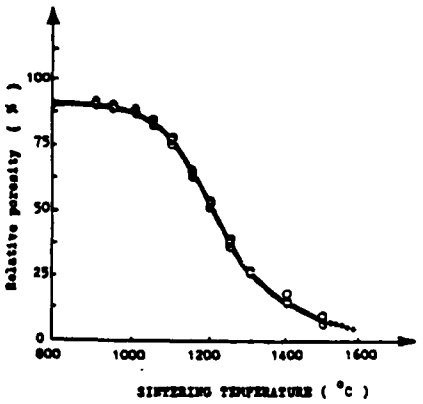


Fig.2. Relationship between sintering temperature and the porosity variation of the TiO_2 specimens.

or Au substrates in O_2 and O_2/Ar mixtures using a r.f. diode type instrument was prepared through employing a 99.9 % in purity, 20 mesh Aldrich fine chemicals compressed Ti target, while the product films were a mixture of amorphous, anatase and rutile modifications as detected by XRD measurements on RIGAKU DENKI RAD IIIA instrument. Amorphous TiO_x phases were obtained for the oxygen mole fraction in the range $0 > x > 2$ by changing the oxygen mole fraction in the argon plasma in the range $0 > y > 0.15$. The photosensitivity of these films (i_{ph}/i_d ratio) were critically a function of the deposition parameters such as composition of the O_2-Ar mixture, the input r.f. power, the residual pressure in the vacuum chamber etc. The feasibility of H_2 production utilizing these electrodes in a photoelectrolysis cell were considered. The photoresponse of each electrode, i.e. freshly prepared and/or catodically treated thereafter were monitored using cyclic voltammetry and via measurement of i_{ph}/i_d vs. Ag/AgCl reference electrode. In this conference, results obtained through XRD, SEM, ESR, AES, Laser Raman and standard photoelectrochemical measurements employing TiO_2 specimens will be discussed in some detail.

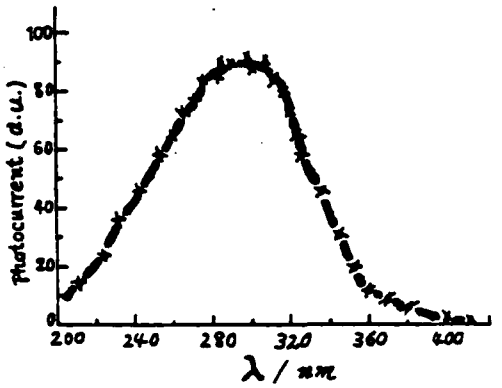


Fig. 3, The photoresponse vs. wave length for a r.f. sputtered TiO_2 (rutile) anode in 1M NaOH electrolyte.

ACKNOWLEDGEMENTS: The work in this series have been conducted entirely on private expenses and self scientific responsibilities in a uniquely dark, racially discriminative and criminally interruptive environment. Regardless of all... !, I wish to thank all those colleagues from several institutions and manufacturing companies who let me use their facilities in the course of this work. As a well documented oppressed foreign researcher and as powerful as avalanche," TOWARDS A HISTORICALLY REFULGENT TOMORROW ! ".

REFERENCES:

1) S.K. Bahador, in "Ext.Abst., 38th I.S.E. meeting, Vol. II, P.607-609 and references cited therein" Sept. 1987 Maastricht The Netherlands.
2) S.K. Bahador, in "proc. VII th Australian Electrochem. Conf." Feb. 1988, Sydeny Australia.
3) S.K. Bahador, in " Proc. 1986 Inter.Congr.Renew.Energ.Sourc., Vol. II, P. 968-977, S. Terol editor, C.S.I.C., 1987 " Madrid Spain.
4) S.K. Bahador, in " Proc.Symp.Photoelectrochem.Electrosynth.Semicon.Mater., E.C.S. soft bound proc. vol., 1988, D.S. Ginley etal. editors" E.C.S. fall meet. Oct. 1987 Honolulu Howaii U.S.A.
5) S.K. Bahador, " Semiconducting metal oxide photoelectrodes-Their characteristics and implications " Submitted to J.E.C.S. 1988.
6) S.K. Bahador, in "Ext.Abs., 39th I.S.E. Meet." Sep. 1988, U.K.
7) S.K. Bahador, in "Ext.Abs., 6th Inter.Conf.Surf.Colloid Sci." June 5-10, Hakone Japan.
8) S.K. Bahador, in "Ext.Abs., XII th I.U.P.A.C. Symp.Photochem." July 1988 Bologna Italy.
9) S.K. Bahador, in "Ext.Abs., VII th Intern.Conf.Photochem.Conver. Stor.Solar Energ." Jul-Aug. Argonne IL. U.S.A. 1988.

STUDY OF THE IONIC ADSORPTION ON EOS STRUCTURES BY COUPLING ELECTROREFLECTANCE, PHOTOCURRENT AND CAPACITANCE MEASUREMENTS

N. Jaffrezic-Renault*, H. Perrot*, C. Nguyen van Huong **

* Laboratoire de Physicochimie des Interfaces,
Ecole Centrale de Lyon -B.P. 163, 69131 Ecully Cédex, France

** Laboratoire d'Electrochimie Interfaciale du CNRS
1, Place Aristide Briand, 92195 Meudon Principal Cédex,France

The origin of the pH response of the silica gate ISFET is the adsorption of the H^+ ions on the surface of the silica in contact with the electrolyte solution. The site-binding theory, based on the acid/base behavior of hydroxyl groups on the surface,allows to fit the ISFET's response (1,2). New ion-sensitivity has been confered to silica ISFET by chemical grafting of ion-sensitive groups on silica [3].

The Si/modified SiO_2/electrolyte structure is a very important tool for studying the ionic adsorption at the modified SiO_2/electrolyte interface. Capacitance measurements have been performed on these structures [4]. Flat band potential shift has been observed with H^+ adsorption on bare SiO_2 surface [4] and with Ag^+ adsorption on cyanografted SiO_2 surface [5].

In this paper is reported, for the first time, a study on the influence of the ionic adsorption on the electroreflectance, photocurrent and capacitance responses of Si/SiO_2 and Si/modified SiO_2/electrolyte structures.

Experimental

The Si/SiO_2 structures were provided by LETI (CEN, Grenoble France). Substrates were p-type silicon wafers of low doping density (about $10^{21} m^{-3}$) with (100) crystal orientation. The thickness of the thermic SiO_2 layer originally 900 A° ± 100 A° was reduced to 350 A° by etching with 1% HF aqueous solutions. The electrochemical cell was a classical three-electrode type. The counter electrode was a glassy carbon plate, a saturated sulfate mercury electrode served as a reference electrode.

The experimental arrangement allowing capacitance and electroreflectance measurements was described elsewhere [6]. Photocurrent potential characteristics were obtained with monochromatic chopped light.

Results and discussion

In the dark, no observable d.c. current flows through the electrolyte/ SiO_2/Si junction.

Characteristic electroreflectance (ER) spectra measured at the direct absorption edge of silicon for different hole-accumulation fields are shown in fig. 1. The lineshape of the spectra is very similar to that is reported in the literature [7,8]. The energy of the critical point corresponding to the transition $\Lambda_3 - \Lambda_1$, calculated by the ASPNES' three point method [9] is 3.42 eV, the broadening parameter about 130 meV. These values agree fairly well with those reported previously [7,8].

As it can be seen in fig.1, the amplitude of the ER signal is field dependent, as expected by the following expression relating the variation of reflectivity $\Delta R/R$ with the modulating electric field E :

$$\Delta R/R = E^2 L(h\omega)$$

where $L(h\omega)$ is the lineshape function of the field induced change in the dielectric function.

The ER signal disappears at a potential slightly different from the flatband potential deduced from capacitance measurements analogous to that is already observed in MOS structure [8,10].

Under illumination, in the depletion region (negative potentials) a photocurrent i_{ph} can be observed, corresponding to the hydrogen evolution. The flatband potential deduced from i_{ph}-potential characteristics agrees rather well with that is given by ER responses.

All the measured parameters depend on the pH of the solution. In fig. 2, 3 and 4 are represented capacitance, electroreflectance and photocurrent responses as a function of potential for different pH values. The curves shift towards more negative potentials with increasing. In table 1 are reported for comparison the potential shifts of the three measured parameters

Table 1 - Potential shifts as a function of pH of photocurrent electroreflectance and capacitance

pH	photocurrent	electroreflectance	capacitance
11.2			
	110	70	100
5.7			
	170	220	180
0.8			

The results obtained by photocurrent and capacitance measurements are similar. Discrepancies observed with electroreflectance measurements are due to the shape of the curves and to experimental difficulties.

These results show that as capacitance, photocurrent and electroreflectance are very sensitive to ionic adsorption and appear to be very promising for the study of adsorption phenomena in EOS structure.

References

1. W.H. SIV, R.S.C. COBBOLD, IEEE Trans. Electron Devices, Vol. ED 26 (1979) 1805.
2. L.J. BOUSSE, N.F. ROOIJ, P. BERGVELD, Surf. Sci. 135 (1983) 479.
3. P. BATAILLARD,P.CLECHET,N.JAFFREZIC-RENAULT,C.MARTELET, N.F. DE ROOIJ, H.van DEN VLEKKERT, Digest of Technical Papers.4th Int.Conf. on Solid State Sensors and Actuators, Institute of Electrical Engineers of Japan, Tokyo (1987) 772.
4. J.L. DIOT, J. JOSEPH, J.R. MARTIN, P. CLECHET, J. Electroanal. Chem. 193 (1985) 75.
5. P. BATAILLARD, P. CLECHET, N. JAFFREZIC-RENAULT, X.G. KONG, C. MARTELET, Sensors and Actuators 12 (1987) 245.
6. C. HINNEN, C. NGUYEN van HUONG, A. ROUSSEAU and J.P. DALBERA, J.Electroanal.Chem. 95 (1979) 131.
7. V.A. TYAGAI, A.M. EVSTIGNEEV and O.V. SNITKO, Soviet Physics-Semiconductors 6 (1973) 1968.
8. K. MISAWA, A. MORITANI and J. NAKAI, Jap. J. Appl. Phys. 15 (1976) 1309.
9. D.E. ASPNES and R.E. ROWE, Phy. Rev. Lett. 27 (1971) 188.
10. F. HOLTZ, Phys. Stat. Solidi A 21 (1974) 469.

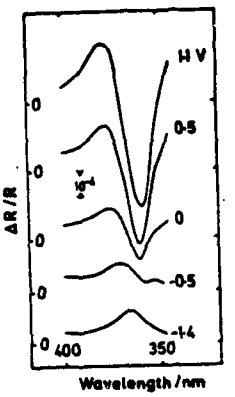


Fig.1 - Electroreflectance spectra of the electrolyte-SiO2/Si structure for different applied dc voltages.

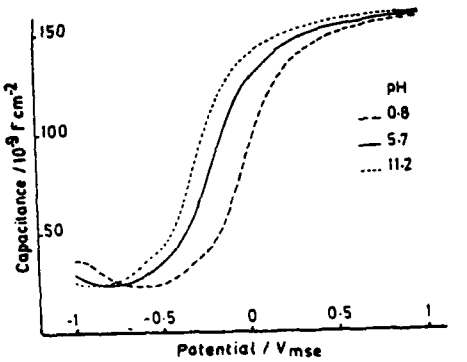


Fig.2 - Influence of the pH on the capacity-potential characteristics of the electrolyte - SiO2/Si junction.

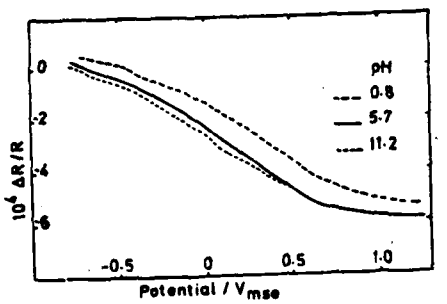


Fig.3 - Electroreflectance-potential curves for different pH.

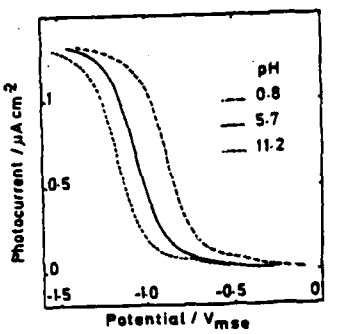


Fig.4 - Photocurrent-potential curves for different pH.

$La_{0.175}WO_3$ - Perowskite: Chemical Characterisation of the Single Crystal (111)/Aqueous Solution Interface by XPS/UPS

H. Kohler[o+], W. Neu[+], K.-D. Kreuer[o*], D. Schmeisser[+] and W. Göpel[+]
[o] CONDUCTA GmbH+Co., Dieselstr. 24, 7016 Gerlingen (FRG)
[+] Institut für Physikalische und Theoretische Chemie, Auf der Morgenstelle 8, 7400 Tübingen (FRG)
[*] Max-Planck-Institut für Festkörperforschung, Heisenbergstr. 1, 7000 Stuttgart 80

1. INTRODUCTION

EMF measurements on electron conducting transition metal oxides (La_xWO_3 ($0.06 \leq x \leq 0.25$), $W_{18}O_{49}$, NbO_x x=2.47, 2.49) in aqueous solutions yielded constant but low pH sensitivity (~10mV/dec) in the regime $4 \leq pH \leq 8$ and significantly higher sensitivities beyond (1).

In explanation of this behaviour we expect to get insight into the potential generating processes on the La_xWO_3 (111)/aqueous solution interface from combined electrochemical and XPS/UPS surface analytical studies. The application of UHV surface analytical methods on emersed surfaces as "quasi in-situ methods" is still a topic of discussion. Investigations on emersed Au, Pt and Ag electrodes however, yielded a linear correlation with a slope close to unity between the EMF and the work function measured with UPS (2,3). These remarkable results demonstrate the preservation of the electrode/electrolyte double layer even after transfer to an UHV chamber.

2. EXPERIMENTAL

A La_xWO_3 crystal was cut parallel (111) and contacted on a steel stic for mechanical fixation and potential recording. The immersions were done in a gas tight electrochemical cell operated in a catalytically purified N_2 atmosphere within a glove box. As electrolytes 0.1N KOH/0.1N HCl mixtures were used in equilibrium with pure N_2 as well as with synthetic air. Before each surface analysis the sample was handled in the following manner: (1) polishing (0.3µm final grading) in N_2 atmosphere, (2) immersion and potential recording (fig. 1), (3) special emersion procedure for repelling the electrolyte and keeping the surface contamination as low as possible, (4) mounting on the manipulator of an UHV transport box, (5) connection of the transport box with the XPS/UPS analysis chamber and transfer after evacuating below $1*10^{-6}$mbar (4).

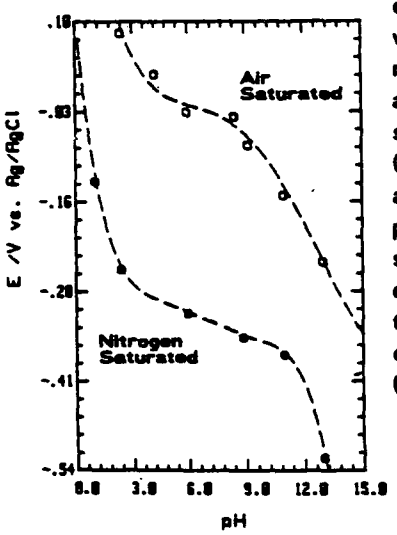


Fig. 1
EMF (vs. Ag/AgCl/sat. KCl sol.) after 14h immersion.

All surface analytical experiments (Leyboldt-Heraeus system: XPS spectra with MgK_α radiation, UPS with HeI radiation) were carried out immediately after the sample transfer.

The W^{4f} spectra of the surfaces emersed from N_2 saturated electrolytes are shown in fig. 2. They indicate different integrated intensities and peak profiles depending on pH. The comparison with the W^{4f} spectrum of the completely oxidized surface (WO_3 formed by heating in air at T=573K) revealed these spectra as a superposition of three LS-doublets for W^{6+}, W^{5+} and W^{4+}. All spectra were deconvoluted to determine the mean tungsten surface oxidation state $n_{ox}=\sum I^{W^{n+}}n / \sum I^{W^{n+}}$, where $I^{W^{n+}}$ is the intensity of the LS-doublett for W^{n+}. In addition, the deconvolution was proven on the W^{4f} spectrum of the freshly polished unimmersed surface. From the fitted ratio $I^{W^{6+}} / I^{W^{5+}} / I^{W^{4+}}$ the crystal composition $La_{0.174}WO_3$ was deduced which agrees quite well with the ICP analysis ($La_{0.175(13)}WO_3$) of the identical crystal.

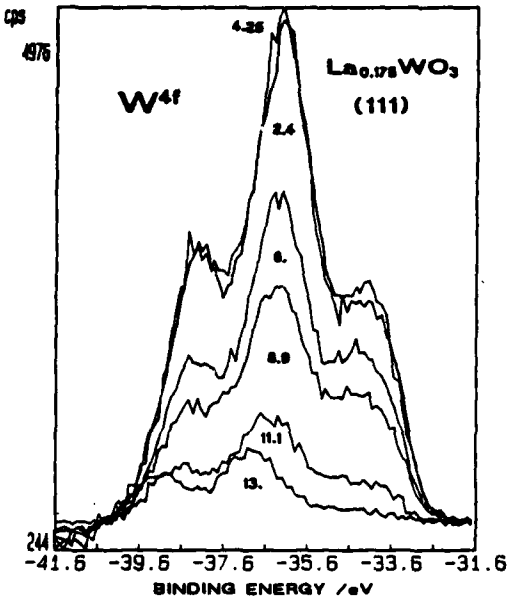


Fig. 2
W^{4f} spectra of emersed surfaces at different pH values of the electrolyte.

3. RESULTS AND DISCUSSION

The interpretation of the surface analytical spectra yielded three main features of the interface:

The integrated intensity ratio La^{3d}/W^{4f} is considerably increased with decreasing solution acidity. This indicates a decrease of the La concentration in acidic solutions and a decrease of W concentration in basic solutions on account of stationary corrosion processes. After emersion from strongly alcaline solutions (e.g. 0.1N KOH) an aqueous corrosion layer was observed by SEM. A hydrated oxide/hydroxide layer (e.g. $La_2O_3/LaO(OH)/La(OH)_3{*}xH_2O$) is formed as indicated by the high La^{3d}/W^{4f} ratio and the distinct hydroxide signal of the O^{1s} spectrum.

The mean tungsten surface oxidation state n_{ox}, i.e. the surface acidity decreases with increasing pH value (fig. 3) on account of increasing corrosion of WO_3 (5). This behaviour is reversed in the regime pH>9. In this pH regime the corrosion layer (see above) begins to grow and therefore n_{ox} is progressively determined by the signal of the corrosion products (WO_4^{2-}).

This interpretation is confirmed by the UPS valence band spectrum recorded at pH 11.1. The density of state (N(E)) near E_F (fig. 4) is significantly lower compared with N(E)

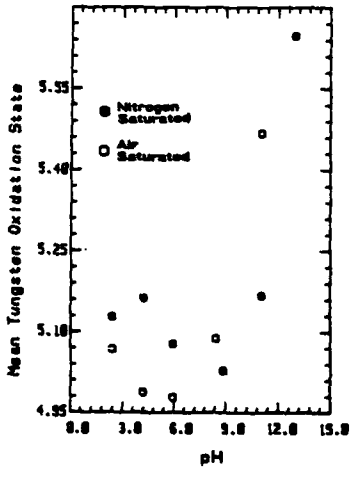
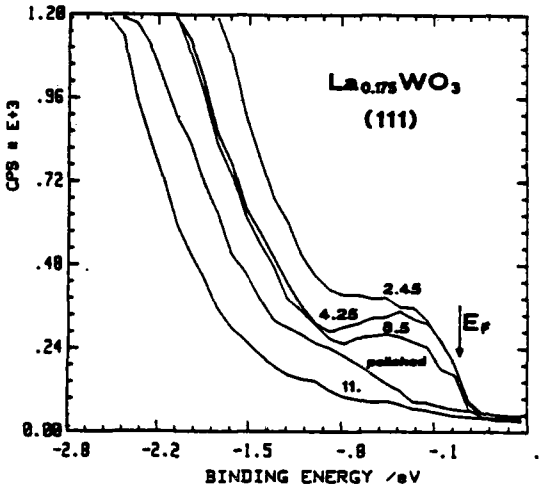


Fig. 3
Mean tungsten oxidation state n_{ox} dependent on the solution acidity.



of the polished surface. With increasing acitity of the solutions, however, N(E) increases and exceeds even N(E) of the polished surface. This behaviour indicates the formation of H_xWO_3 (6) e.g. by cation exchange $3H^+ \leftrightarrow La^{3+}$.

Fig. 4
UPS valence band spectrum of the unimmersed and emersed surface from air saturated electrolyte at different pH values.

Based on the surface analytical data presented above and some additional electrochemical measurements (7) the following qualitative model for the potential generation can be given:

Fig. 1 demonstrates the considerable dependency of E on p_{O_2} in the whole pH regime. This is confirmed by exchange current density (I_o) measurements which yielded I_o at air saturated electrolytes more than a decade higher than at low p_{O_2} (7). For the explanation of the E versus pH curve three pH regimes have to be discussed separately:

In the regime $3 \leq pH \leq 11$ (N_2 saturated solution) the small increase of E with solution acidity is due to the increase of the surface oxidation n_{ox} on account of stationary corrosion processes as described above. Below this regime I_o is considerably increased probably with the increasing formation of H_xWO_3. Here E is a mixed potential dependent on p_{O_2} and pH. Beyond pH 9 no surface analytical data of the locus of potential generation are available because of the corrosion layer. However, a mixed potential generated by p_{O_2} and corrosion reactions as e.g. $WO_3 + 2OH^- \leftrightarrow WO_4^{2-} + H_2O$ (3) is assumed.

4. CONCLUSIONS

With combined electrochemical and surface analytical studies the potential generating processes on the $La_{0.175}WO_3$ (111)/aqueous solution interface were revealed. The surface analytical data explain quite well the non Nernstian behaviour of the EMF in the regime $1 \leq pH \leq 13$.

REFERENCES

(1) H. Kohler, K.-D. Kreuer; GBF Monographs 10, 297 (1987)
(2) E.R. Kötz, H. Neff, K. Müller; J. Electroanal. Chem. 215, (1986) 331
(3) D.M. Kolb; Zeitschrift für Physikalische Chemie 154, (1987) 179
(4) W. Neu, H.-D. Wiemhöfer, D. Schmeisser, W. Göpel; Surface and Interface Analysis, submitted
(5) M. Pourbaix; Atlas of Electrochem. Equilibria in Aqueous Solutions, Pergamon Press 1966
(6) G.K. Wertheim, M. Campagna, J.-N. Chazalviel, D.N.E. Buchanan; Appl. Phys. 13, (1977) 225
(7) K.-D. Kreuer, H. Kohler; to be published

IN VITRO PHOTOELECTROCHEMICAL MODEL OF THE Z SCHEME IN PLANT PHOTOSYNTHESIS

A. Agostiano, M. Della Monica, °F.K.Fong

*Dipartimento di Chimica, Università degli Studi, Bari, (Italy)
°Department of Chemistry, Purdue University, West Lafayette, Indiana (USA).

Recently,several research groups have been involved in work on the developement of photogalvanic cells whith electrodes coated with chlorophyll in attempt to reconstitute photosynthetic reactions Water photoelectrolysis using Chl a aggregates on platinum electrodes was reported by Fong and co-workers[2]. Photogeneration of current and potential between electrodes covered with PSI and PSII particles has been described by Agostiano and al.[3]In the present investigation we develop the construction of an in vitro photoelectrochemical model of the Z scheme.

The in vitro apparatus makes use of the oxygen evolving apparatus of PS II in spitting water and the platinum metal in mediating the electrons from water to reduce the $NADP^+$. In this model PS I and PS II enriched particles from spinach chloroplasts are used in a three-compartment photoelectrochemical cell (Fig.1).

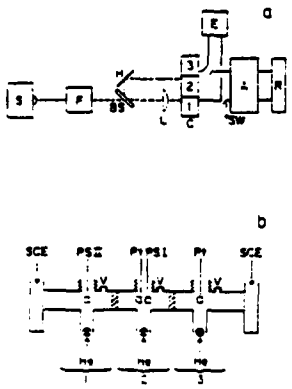


Fig. 1. Experimental apparatus for photogalvanic measurements: S = source; F = water filter; BS = beam splitter; L = lens; C = cell; A = current amplifier; R = recorder; E = electrometer. (b) Details of three-compartment photoelectrochemical cell.

[2]M.S. Showell and F.K. Fong,J.Amer. Chem. Soc., 104,(1982), 2773
[3]A.agostiano, A.Ceglie, M.Della Monica,Bioelectrochem. Bioenerg. 12,(1984),499

Specific acceptors and donors for the two photosystems are employed in this cell in order to reproduce in each compartment the reactions occurring in the different branches of the Z scheme The three-cell compartment respectively correspond to the branches:

(1) the dark oxidation of water by $P680^+$ to evolve oxygen

(2a) the photoreductio of an electron acceptor by the P680 light reaction

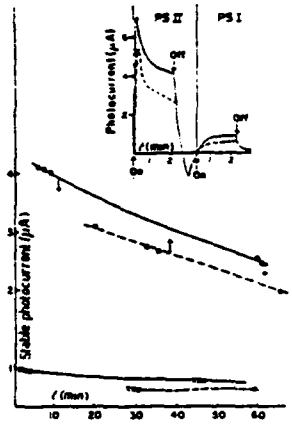
(2b) the dark oxidation of an electron donor by the $P700^+$ light reaction

(3) the photoreduction of $NADP^+$ by the P700 light reaction.

The light reaction of PS I particles leads to $NADP^+$ reduction in the presence of specific donor such as $DCPIH_2$.The light reaction of PS II particles results in the oxygen evolution from water splitting and the reduction of an electron acceptor such as ferricyanide.The rate of the PS II light reaction was found greater than that of PSI.

From a comparison of the photolytic rates of O_2 evolution and $NADP^+$ reduction with the corresponding photocurrents ,average current yields of 78% for O_2 evolution and 82% for $NADP^+$ are obtained.

This study demostrate that the reaction sequences 1-2a and 2b-3 can occur independently in the presence of suitable donors and acceptors (Fig.2)



Steady photocurrent–time runs for PS II (○) and PS I (×) covered electrodes. (——) Both electrodes illuminated; (— — —) only one electrode illuminated. Compartment (1) contains pH 7 buffer phosphate solution; compartment (2) contains 1.0×10^{-4} M 1:1 $[Fe(CN)_6]^{3-}/[Fe(CN)_6]^{4-}$ in pH 7 phosphate buffer solution; compartment (3) contains 1.2×10^{-3} M $NADP^+$ in pH 7 phosphate buffer solution. The on and off arrows indicate the turning on and off of illumination of the second photochemical system, later. Photocurrent–time behavior for PS II and PS I-covered electrodes with both electrodes (——) or only one (— — —) illuminated electrode. Arrows indicate the turning on and off of the light.

Significantly ,the photochemical yields are improved when the two light reactions are allowed to operate in series in which the acceptors and donors are continuously regenerated.

PHOTOANODIC BEHAVIOUR OF CUPROUS OXIDE LAYERS ON COPPER ELECTRODES IN AQUEOUS ELECTROLYTES

A. Aruchamy and A. Fujishima
Department of Synthetic Chemistry
Faculty of Engineering
University of Tokyo
Tokyo-113, Japan

Studies at illuminated semiconductor/electrolyte interfaces provide valuable information about the optical and electronic characteristics of the solid phase. In the study of surface films on metals, photoelectrochemical (PEC) measurements have been successfully applied as an in situ method of characterization[1]. The passive films can be significantly different from their bulk solid phases in their crystallographic defects, stoichiometry and electronic conductivity. The advantage of the PEC method over other in situ optical techniques is in the determination of the electronic properties of these films.

The photoelectrochemical behaviour of oxide layers on copper electrodes have been studied in considerable detail [1-8]. Most studies refer to the p-type Cu_2O and CuO phases. However, there are observations made from PEC measurements that suggest the formation of n-Cu_2O especially under certain corrosion conditions. Bertocci[4] and Di Quarto et al.[7] have noticed anodic photobehaviour of corrosion films in near neutral electrolytes. Wilhelm et al.[5] also observed anodic photocurrents for Cu_2O films on copper in sodium hydroxide electrolyte but, interpreted them to arise from surface states of p-type Cu_2O. Photoanodic behaviour of copper electrodes due to a very thin Cu_2O film under electropolishing conditions in highly acidic electrolytes is also known[9]. The electronic characteristics of such films have not been studied. In the present work, the anodic photoeffects of cuprous oxide layers formed on copper electrodes have been studied in alkaline electrolytes.

The corrosion of copper electrodes in water or in aqueous cupric salt solution results in cuprous oxide layers. The formation of cuprous oxide in Cu solution is well known [10]. Cu O is formed by the reaction of copper as $Cu+Cu^{2+} \dashrightarrow 2Cu^{+}$. Electropolished or mechanically polished electrodes etched in dil. HNO_3 are used. The electrodes are immersed in 0.1M $CuSO_4$ (aqueous) solution for 5-7 days to obtain a thick layer appearing either reddish-yellow or brown. 0.1M NaOH is used as the electrolyte. A standard three electrode system with a potentiostat and potential programmer are used for electrochemical characterization. A 1000W Xe lamp is used as the light source. Electrodes are characterized by photopotenital, current-voltage(i-v), capacitance and spectral response measurements. Surfaces are observed using SEM.

Under white light, the photopotentials (V_{ph}) are found to be negative with magnitudes as high as 550mV for thick films. The current-voltage(i-v) curves (Figs. 1a and 1b) show that the Cu/Cu_2O electrodes exhibit both anodic and cathodic photocurrents. The magnitudes of anodic photocurrents and photovoltages are large for films appearing reddish-yellow and having smooth surface structure with very small grains. The potential of anodic photocurrent on-set (or that of photocurrent inversion, V_{on}) is $\sim$ -0.75V vs SCE. This potential is more positive for films formed on rough surfaces having large crystallites (grains). Thinner corrosion films of Cu_2O formed on Cu in water (no added Cu^{2+}) show large photocurrent transients. Spectral response of electrodes polarized in the region of anodic photocurrents show that at longer wave lengths ($\lambda > 630$nm) some cathodic photocurrents flow. At $\lambda < 630$nm, anodic photocurrents appear and increase sharply. The capacitance measurements are in apparent agreement with the i-v behaviour (Fig. 2).

The energy band model of cuprous oxide would predict a very negative flatband potential (V_{fb} =-2.5V vs SCE) for n-Cu_2O. But, the V_{ph} and V_{on} (-0.75V vs SCE) are not so negative but are closer to the flatband potential of p-Cu_2O which is $\sim$ -0.52V vs SCE [5,8]. One possible interpretation is that the film is a mixture of both n- and p-type Cu_2O in which the n-type behaviour is dominant. The spectral response seems to suggest that a deep lying p-type layer may be responsible for the long wavelength response giving cathodic photocurrents. On the otherhand, a high density of interband gap states and surface states can also cause similar effects. The n-type conductivity of Cu_2O of a corrosion layer is important from the defect chemistry point of view. In the usual solid state preparations carried out at elevated temperatures only oxygen excess phase giving p-Cu_2O is known[11]. The photoeffects of the corrosion layers which are prepared at room temperature seem to indicate that copper excess Cu_2O phases are possible. However, identification of the n-type defects and possible p-Cu_2O/n-Cu_2O junction effects are necessary for a complete electronic characterization of these layers.

Acknowledgements: Acknowledgements are due to the Ministry of Education, Culture and Science, Japan and Tokyo Ohka Science Foundation for support of this research. The authors thank Dr. K. Itoh for helpful duscussions.

References:

1. U. Stimming, Electrochim. Acta, 31, 425(1986).
2. K.L. Hardee and A.J. Bard, J. Electrochem. Soc., 124, 215(1977).
3. W. Paatsch, Ber. Bunsenges. Phys. Chem., 81, 645(1977).
4. U. Bertocchi, J. Electrochem. Soc., 125, 1598(1978).
5. S.M. Wilhelm, Y. Tanizawa, Chiang-Li Liu, and N. Hackerman, Corrosiion Science, 22, 791(1982).
6. L.M. Abrantes, L.M. Castillo, and L.M. Peter,

J. Electroanal. Chem., 163, 209(1984).
7. F. Di Quarto, S. Piazza, and C. Sunseri, Electrochim. Acta, 30, 315(1985).
8. U. Collisi and H.-H. Strehblow, J. Electroanal. Chem., 210, 213(1985).
9. B. Pointu, M. Braizaz, P. Poncet, and J. Rousseau, J. Electroanal. Chem., 163, 209(1984).
10. G.T. Miller, Jr., and K.R. Lawless, J. Electrochem. Soc., 106, 854(1959).
11. Yu. D. Tretyakov, V.F. Komarov, N.A. Prosvirnina, and I.B. Kutsenok, J. Solid State Chem., 5, 157(1972).

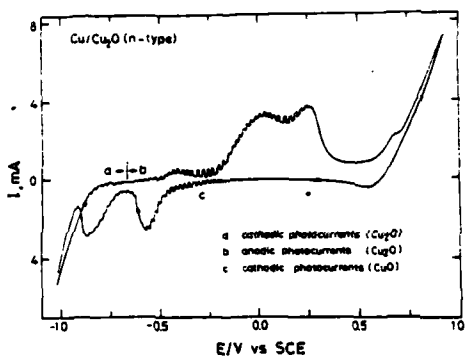


Fig. 1a



Fig. 1b

Figure 1: i-v curves of Cu O electrode in).1M NaOH (chopped white light illumination; scan rate: 10 mV/sec)
a) scan range from -1.0V to +0.9V vs SCE
b) photocurrents about the inversion potential (i_{pa}-anodic photocurrent, i_{pc}-cathodic photocurrent).

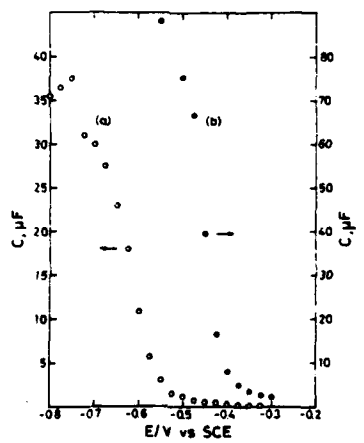


Fig. 2

Figure 2: Capacitance-voltage behaviour of Cu/Cu O electrode in 0.1M NaOH for potential scan
a) towards negative potentials and
b) towards positive potentials.

PHOTOCATALYTIC DEPOSITION OF URANYL ONTO SEMICONDUCTOR SUSPENSIONS.

Amadelli R., Maldotti A., Carassiti V.

Centro di Studio sulla Fotochimica e Reattività degli Stati Eccitati dei Composti di Coordinazione, C.N.R.
via L. Borsari,46 - 44100 Ferrara, Italy.

Introduction

Photodeposition of metals on semiconductor powders or electrodes constitutes an important part of the fast developing field of photoassisted reactions on semiconductors. The interest, in this case, lies on both the need to modify the semiconductor surfaces in order to improve their catalytic activity (1) and on the recovery of precious or environmentally hazardous metals from wastes (2).
In this work, we examine the photodeposition of uranyl from solutions of different composition.

Experimental

Uranyl nitrate (Strem), sodium acetate (Fluka), sodium formate (Fluka) and 2-propanol (Fluka, HPLC grade) and titanium dioxide (Degussa P25) were used as received. Irradiation was performed with a Hanau Q400 medium pressure lamp using a 360 nm filter.
Polycrystalline TiO_2 electrodes were prepared as described by Frank and Bard (3). Electrochemical measurements were performed with a conventional equipment (Amel). Decrease of uranium species in solution was monitored through a decrease in the absorbance at five different wavelengths in the UV range.

Results

Figure 1 shows the results of photoelectrochemical measurements on a TiO_2 polycrystalline electrode in 0.1M $NaClO_4$ in the absence and in the presence of $UO_2(NO_3)_2$. Comparison of curves B and D shows that a relatively large cathodic current is observed in the presence of the uranyl salt, indicating that this species undergoes photoreduction. It is interesting to note that the anodic photocurrent onset is shifted to more positive potentials. This usually indicates competition of surface recombination with the charge transfer (4). In this particular case, the cathodic deposit may be in part reoxidized during the anodic scan.

Curve E was obtained in the presence of 2-propanol as a hole scavenger. In this case, within the time of few scans from the beginning of the experiment, there is no shift in the anodic photocurrent onset; it is apparent, instead, the current doubling process, as is expected from the oxidation of alcohols on TiO_2. For continuous scanning, however, the pattern approaches that observed for curve D, even in the presence of a high alcohol concentration in well stirred solutions. This can be explained by the formation and thickening of a cathodic deposit. Its

reoxidation competes with charge transfer for holes.

The deposition of uranyl was also studied on powdered TiO_2 suspended in aqueous solutions containing $UO_2(NO_3)_2$ in the absence of air. Initial rates of deposition in the presence of three different hole acceptors are reported in the following table.

TABLE I : Initial rates of photodeposition of UO_2^{2+} on a TiO_2 suspension.[a]

rate, μm/min	hole acceptor
0.35	2-propanol[b]
2	sodium formate[c]
2.75	sodium acetate[c]

a- 3 μm $UO_2(NO_3)_2$

b - 2 mole/l

c - 0.1 mole/l

Light intensity: 8.5 mW/cm^2

The large difference in the initial rate between 2-propanol(and alcohols in general) on the one side and the organic acid salts on the other side is to be attributed to the recognized better hole scavenger properties of the latter.

Another factor which needs to be taken into account in our system is that UO_2^{2+} tends to form strong complexes with both acetate and formate, as reported in the literature (5). We observed that the formation of these complexes has a strong influence on the adsorption of uranyl species on TiO_2 in the dark; the amount adsorbed increases in the presence of the added species in the order: alcohol < formate < acetate.

We did some attempts to identify the nature of the deposit obtained upon photoreduction of the uranyl species. Attempt to establish the nature of the deposit by X-ray analysis proved unfruitful; the only information obtained was that it probably corresponds to some form of non-stoichiometric uranium oxide. On the other hand, if this powder is left in the air its color changes from grey to yellow. The IR spectrum of this yellow powder corresponds to that of UO_3 (5).

It is unlikely that the deposit is UO_2 since this oxide is stable in air (6). It is more probable that it is uranium in the V valence state (UO_2OH) or, in any case, a non- stoichiometric oxide with a valence state intermediate between V and VI.

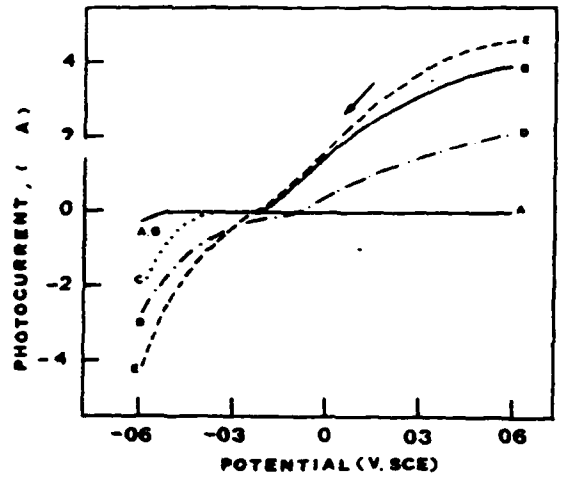


Fig. 1 . Current -potential curves for polycrystalline TiO_2 in 0.1 M $NaClO_4$, A) in the dark, B) Illumination, C) with $5x10^{-3}$ M uranyl nitrate in the dark, D) with uranyl nitrate and illumination, E) with uranyl nitrate and 1M 2- propanol during illumination. $\lambda > 360$ nm. Scan rate: 50 mV/s.

References

1) B. Kreutler and A.J. Bard, J. Amer. Chem. Soc., 100, 4317 (1978)
2) E. Pelizzetti, C.Minero, M.Barbeni, E.Borgarello and N. Serpone, Abstracts, Sixth International Conference on Photochemical Conversion and Storage of Solar Energy, July 1986, Paris.
3) S.N.Frank and A.J. Bard, J.Amer. Chem.Soc., 99, 4667 (1977)
4) H.Gerischer, J.Electroanal.Chem., 150, 553 (1983)
5) E. Rabinowitch and L.Belford, Spectroscopy and Photochemistry of Uranyl Compounds, Pergamon Press, 1964.
6) S. Kihara, Z. Yoshida, H. Muto, H.Aoyagi, Y.Baba and H.Hashitani, Anal. Chem., 52, 1601 (1980).

DIRECT MEASUREMENTS OF SEMICONDUCTOR BANDS UNPINNING UNDER ILLUMINATION BY ELECTROLYTE ELECTROREFLECTANCE

D. Tafalla, M. Pujadas and P. Salvador

Instituto de Catálisis y Petroleoquímica (C.S.I.C.)
Serrano, 119, 28006-Madrid, Spain.

An important source of efficiency loss in photoelectrochemical devices is semiconductor bands unpinning produced by illumination of the semiconductor-electrolyte interface. Shifts of the semiconductor bandedges upon illumination can be brought about by trapping of photogenerated carriers at surface states and/or by changes in the concentration of dissolved flatband potential determining species (e.g., H^+ and OH^- in the case of semiconducting oxides). Several techniques, including impedance measurements and photocurrent transient behaviour analysis, are able to provide indirect experimental evidence of the band unpinning phenomenon. However, none of them allows a direct measurement of the semiconductor flatband potential (V_{fb}) photoinduced shifts. We have shown recently that electrolyte electroreflectance (EER) permits easy and reliable measurements of V_{fb} under illumination of the semiconductor-electrolyte interface (1). Taking advantage of this fact, we present here some examples of V_{fb} shifts, measured with EER on a n-TiO_2 electrode, as a function of the intensity and time of illumination, electrolyte pH and V_{dc} applied bias.

A 2 mm-thick TiO_2 (rutile) slice, (001) oriented, was used as photoelectrode. After being reduced in pure H_2 (1 atm) at 400°C for 30 min its donor concentration from impedance measurements was estimated to be of the order of 10^{17} cm^{-3}. The experimental set-up for EER measurements has been already described (1). In EER experiments for V_{fb} determination, the V_{dc} potential was swept at constant speed (v = 10 mV/s), while measuring the in-phase and -quadrature components of the EER signal ($\Delta R/R$) at λ = 330 nm, corresponding to the TiO_2 direct transition at $\vec{k} = 0$, for constant V_{ac} = 200 mV (r.m.s.) and frequency f = 180 Hz. The V_{dc} value at which both components of $\Delta R/R$ change sign simultaneously constitutes a reliable measurement of V_{fb}(1).

Figure 1 shows a plot of $\Delta R/R$ *vs.* V_{dc} for different electrolyte pH values. The fact that the different curves are parallel to each other and shifted by about 60 mV per pH unit, as corresponds to the well known Nerstian behaviour of TiO_2, indicates that the observed dependence of $\Delta R/R$ on $(V_{dc}-V_{fb})$ is an intrinsic property of the semiconducting electrode. Photocurrent (I_{ph}) *vs.* V_{dc} curves are also included in Fig. 1. Low illumination intensities were used in order to have a small I_{ph} in the V_{dc} range where $\Delta R/R$ depends on the bandbending. The effect of illumination intensity, and so I_{ph}, on the $\Delta R/R$ *vs.* V_{dc} plots is shown in Fig. 2. The experimental curves for pH 13 and 3 coincide with those of Fig. 1 obtained at low illumination intensity. However, those curves for 13 > pH > 5 drastically deviate from the behaviour observed in Fig. 1 in the high band-

bending region (high I_{ph}), and approach that curve corresponding to pH 4. In the low bandbending region (small I_{ph}) no deviation from the "theoretical" curves of Fig. 1 is observed. At pH values 9 and 10 the curves also appear shifted towards anodic values in the high bandbending region, and a plateau is observed in the small bandbending region. Similar effects are observed in Fig. 3 at pH 10, where the illumination intensity is progresively increased and the corresponding $\Delta R/R$ vs. V_{dc} curves also appear anodically shifted in the high bandbending region.

Figures 2 and 3 clearly show anodic shifts of the TiO_2 bandedges when the photocurrent exceeds a critical value, which depends on the electrolyte pH. Two mechanisms can account for the observed V_{fb} shifts: 1) The accumulation of photogenerated holes at surface states. This is for instance, at basic pH, the photogeneration of surface OH°_s radicals from chemisorbed OH^-_s groups (2):

$$Ti\text{-}OH^-_s + h^+ \longrightarrow Ti\text{-}OH^{\circ}_s \qquad [1]$$

The situation is different at acidic pH, since in this case OH°_s radicals are mainly generated from chemisorbed H_2O molecules and there is not surface accumulation of positive charge:

$$Ti\text{-}H_2O_s + h^+ \longrightarrow Ti\text{-}OH^{\circ}_s + H^+ \qquad [2]$$

2) The decrease of the local pH at the TiO_2-electrolyte interface occurring during photooxidation of water:

$$2OH^- + 4h^+ \longrightarrow O_2\uparrow + 2H^+ \qquad [3]$$

V_{fb} shifts due to local pH changes, according to [3], explain the behaviour observed in Fig. 2. In fact, at pH 13 ($[OH^-] = 10^{-1}$ M) is $I_{ph} \ll I_{Lim}$ (limiting diffusion current of electrolyte OH^- and H^+ species), even at high bandbending, and the local pH can hardly change. By contrast, at pH 10 is $I_{ph} > I_{Lim}$ at high bandbending, so that the local pH decreases until a value near 4 is reached where $I_{ph} < I_{Lim}$. Again, at pH 3 is $I_{ph} < I_{Lim}$ and, therefore, no shift with respect to the theoretical curve of Fig. 1 can be observed. The effect of illumination intensity observed in Fig. 3 at pH 10 is also consistent with this model. Only at high enough bandbending, where $I_{ph} > I_{Lim}$, the local pH decreases up to a value about 4 and a corresponding shift of the $\Delta R/R$ vs. V_{dc} curve is observed.

V_{fb} shifts due to hole trapping at surface states (reaction [1]) can be seen in Fig. 4 at pH 13. In this case is $I_{ph} \ll I_{Lim}$ and no local pH changes are expected. Therefore, the observed changes of $\Delta R/R$ for constant V_{dc}, under variable light intensity, must be associated with accumulation of holes at the TiO_2 surface. By contrast, at pH 2, reaction [2] takes place instead of [1], and positive charge does not accumulate at the TiO_2 surface. Consequently, V_{fb} must not shift, as it is in fact observed in Fig. 4.

(1) J.Gandia, M.Pujadas and P.Salvador.J.Electroanal.Chem.(in press).
(2) P.Salvador. Nouv. J. Chim. 12, 35 (1988).

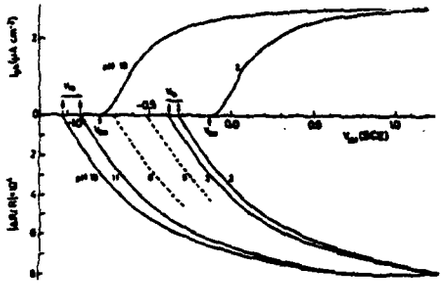


Figure 1

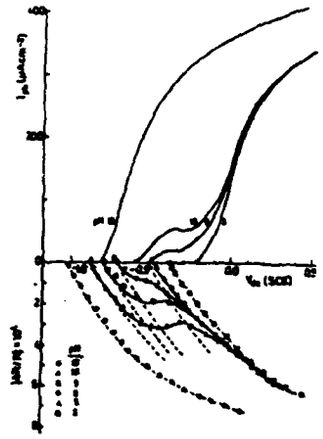


Figure 2

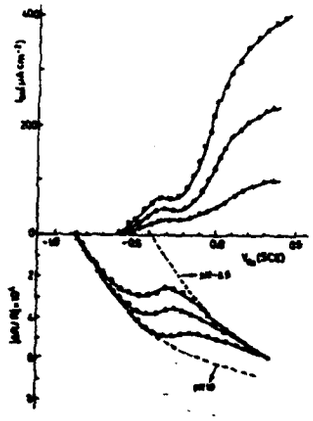


Figure 3

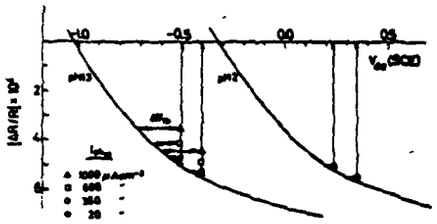


Figure 4

This work was supported by the "Comité Conjunto Hispano-Norteamericano para la Investigación Científica y Tecnológica" (Project Nº CCA 83/038).

ELECTROCHEMICAL BEHAVIOUR OF THE CELL Pb/PEO $_n$.Pb(ClO$_4$)$_2$/Pb

A. K. Saraswat, A. Magistris, G. Chiodelli and P. Ferloni

Centro di Studio per la Termodinamica ed Elettrochimica dei sistemi salini fusi e solidi del C. N. R. e Dipartimento di Chimica Fisica della Universita', Viale Taramelli 16, 27100 Pavia (Italy)

Several studies have reported that poly(ethylene oxide), PEO, dissolves inorganic salts to form polymeric electrolytes with ionic conductivities significantly high for potential use in solid state batteries (1). Recently, a growing interest has been shown in systems of PEO with salts of divalent metals (2-5), which might conduct both cations and anions with a predominant possibility of anion transport (6). We prepared several compositions of a new polymeric electrolyte system, PEO-Pb(ClO$_4$)$_2$ (7). Here we present the results on the electrochemical behaviour of the cell Pb/(PEO)$_n$.Pb(ClO$_4$)$_2$/Pb (where n = O/Pb is 40 and 20) ; results for additional compositions will be presented later.

The polymeric films, 100 - 200 μm thickness, were prepared as follows: Pb(ClO$_4$)$_2$.3H$_2$O (Aldrich and K & K) was dissolved in acetonitrile (C. Erba, RPE) and added to a solution of PEO (BDH, 4M) in the same solvent. After casting on teflon plates, the films were thoroughly dried under vacuum at about 50° C. No evidence of the presence of water or solvent was observed by DSC and thermogravimetric analysis of these films.

AC conductivity measurements with Pb electrodes (12 mm in diameter) were carried out by means of a Solartron 1255 frequency response analyzer in the frequency range 10^{-2} - 10^{6} Hz. DC measurements were performed using an EG & G potentiostat - galvanostat PARR model 273. The investigated temperature range was 20 - 160 ° C. The samples were held under vacuum during measurements.

Investigations on these films by means of DSC, hot stage microscopy and X-ray diffraction (7) have revealed the existence, at room temperature, of a crystalline phase mainly constituted of pure PEO.

Usually the following thermal cycle of conductivity was performed. Starting from a low value at ambient temperature (~10^{-9} ohm^{-1} cm^{-1}), a sharp increase is recorded up to a discontinuity at about 65 °C corresponding to the melting of the crystalline PEO. In the higher temperature regime rearrangement phenomena take place within the elastomeric phase leading to changes in conductivity with time up to a constant value. At 160 °C, a costant value of about 10^{-3} ohm^{-1} cm^{-1} was reached in nearly one hour. The subsequent measurements on step cooling were carried out after attaining an equilibrium value of the conductivity. Crystallization occured at ~50 °C with a steep fall in conductivity down to the previously observed room temperature value.

In fig. 1, we report typical complex impedance plots at different temperatures for the cell Pb/(PEO)$_{40}$.Pb(ClO$_4$)$_2$/Pb: only one fully defined semicircle is apparent. It is assumed that the Z' values at high and low frequency intercepts of a semicircle on the real axis coincide with the bulk resistance, R_b, and the sum of bulk and charge transfer resistance, R_b +

R_{ct}, respectively. Since it was very difficult to obtain the diffusion impedance , $Z_d(0)$, from low frequency AC data, these values were determined by means of the DC polarization methods as described elsewhere (8,9). Double layer capacity ranging between 6 and 11 $\mu F\ cm^{-2}$ was calculated from the frequency corresponding to the maximum of each semicircle over the whole temperature range.

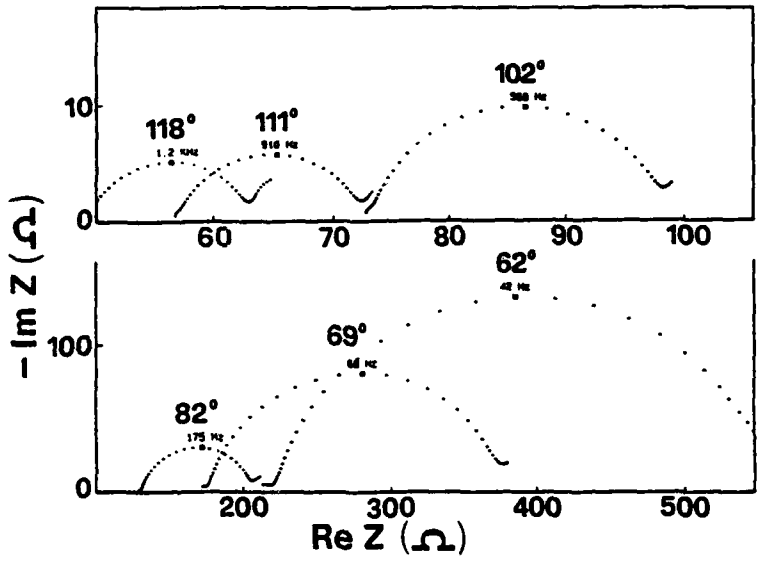


Fig.1 . Complex impedance plots for the cell $Pb/(PEO)_{40}.Pb(ClO_4)_2/Pb$ at the indicated temperatures.

Fig. 2 shows the temperature dependence of the different resistance contributions to the total resistivity of the cell. All the three parameters display a linear trend in a plot with logarithmic ordinates. An activation energy of ~ 0.3 eV was calculated for the bulk conductivity, which is close to those previously reported for lead halides in the same temperature range (4). The activation energy for the charge transfer process is 1.3 eV. In the analogous system of PEO with $LiClO_4$, a similar trend was found with an activation energy of 0.9 eV (8). Work on the determination of transport numbers as a function of temperature is in progress.

This work has been supported by P. F. Energetica II, CNR - ENEA.
One of the authors, A. K. Saraswat, acknowledges the support of the "ICTP Programme for Training and Research in Italian Laboratories", Trieste, Italy.

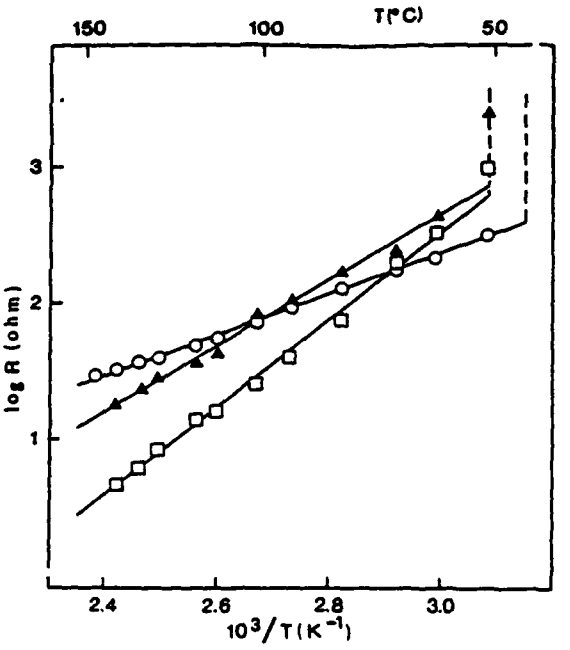


Fig. 2. Bulk resistance R_b (○), charge transfer resistance R_{ct} (□) and diffusion impedance Z_d (0) (▲) as a function of $10^3/T$.

REFERENCES

1. J. R. MacCallum and C. A. Vincent, Eds., Polymer Electrolyte Reviews - 1, Elsevier Applied Science, London, 1987
2. A. Moryoussef, M. Bonnat, M. Fouletier and P. Hicter, in F. W. Poulsen et al., Eds., Transport-Structure Relations in Fast Ion and Mixed Conductors, Risø National Lab., Roskilde 1985, pp. 335-340
3. A. Patrick, M. Glasse, R. Latham and R. Linford, Solid State Ionics 18/19, 1063 (1986)
4. R. Huq, G. Chiodelli, P. Ferloni, A. Magistris, and G. C. Farrington, J. Electrochem. Soc. 134, 364 (1987)
5. P. G. Bruce, F. Krok, J. Evans, and C. A. Vincent, I Int. Symp. on Polymer Electrolytes, St. Andrews 1987, pp. 12.1-12.3
6. R. Huq and G. C. Farrington, VI Int. Conf. on Solid State Ionics, Garmisch 1987, pp. 311-312
7. A. K. Saraswat, P. Ferloni, A. Magistris and G. Chiodelli, to be published
8. P. Ferloni, G. Chiodelli, A. Magistris, and M. Sanesi, Solid State Ionics 18/19, 265 (1986)
9. G. Chiodelli, P. Ferloni, A. Magistris and M. Sanesi, VI Int. Conf. on Solid State Ionics, Garmisch 1987, p. 318

ENTRAPMENT OF ENZYMES IN ELECTROCHEMICALLY POLYMERISED ORGANIC FILMS

Philip N. Bartlett and Richard G. Whitaker

Department of Chemistry, University of Warwick, Coventry, CV4 7AL, England

The use of electrochemical polymerisation to entrap enzymes at electrode surfaces is attractive for a number of reasons. First, the procedure is simple to perform and can be achieved in one step. Second, the thickness of the layer can be controlled to some degree by varying the charge passed. Third, the technique allows the precise localisation of the enzyme at the electrode surface - this can be important in the development of micro-scale devices. Finally the technique is flexible, for example multiple layers can be built up in by successive polymerisation steps in suitable cases.

In order to immobilise enzymes in general it is necessary to carry out the polymerisation of the monomer from buffered aqueous solution. This restricts the choice of monomer but pyrrole[1,2] and aniline[3] have both been used for this purpose. We have investigated the use of N-methylpyrrole[4], aniline and phenol[5] for the immobilisation of glucose oxidase.

Studies of the mechanism for the oxidation of glucose at electrodes coated with N-methylpyrrole films containing immobilised glucose oxidase show that the reaction proceeds within the film with the generation of hydrogen peroxide which is then detected at the underlying platinum electrode [4,6]. There is no evidence for either direct oxidation of the reduced enzyme by the poly-N-methylpyrrole or for oxidation of the hydrogen peroxide on the polymer. The reaction can be written:

in the film:

$$GOD(FAD) + \text{glucose} \rightarrow GOD(FADH_2) + \text{gluconolactame}$$

$$GOD(FADH_2) + O_2 \rightarrow GOD(FAD) + H_2O_2$$

at the platinum electrode:

$$H_2O_2 \rightarrow 2H^+ + 2e + O_2$$

Homogeneous mediators, such as ferrocene derivatives, have been used very successfully to mediate the oxidation of glucose oxidase in homogeneous solution[7]. They can also be used with our immobilised systems. In the presence of an added mediator, such as ferrocene monocarboxylic acid, the role of oxygen in the process can be taken by the oxidised form of the mediator:

in the film:

$$GOD(FADH_2) + 2\ Fc' \rightarrow GOD(FAD) + 2\ Fc$$

at the electrode:

$Fc \rightarrow Fc^{+} + e$

Investigations of the mediated system show that the mediator can react on the poly-N-methylpyrrole.

Systems of this type are of interest for applications in amperometric biosensors, in the of bioelectronics, and in studies of the effects of immobilisation on enzyme activity.

Acknowledgements. This work was supported by the SERC and by a research studentship for R.G.W. from MediCerse Ltd.

References

1) M. C. Poulds and C. R. Lowe, J. Chem. Soc. Faraday Trans. 1, 82 (1986) 1257.
2) M. Umana and J. Waller, Anal. Chem., 58 (1986) 2979.
3) M. Chineharm, T. Chiba and M. Aizawa, Sensors and Actuators, 13 (1988) 87.
4) P. M. Bartlett and R. G. Whitaker, J. Electroanal. Chem., 224 (1987) 37.
5) P. M. Bartlett and R. G. Whitaker, J. Electroanal. Chem., 224 (1987) 27.
6) P. M. Bartlett and R. G. Whitaker, Biosensors, in press.
7) A. E. G. Cass, G. Davis, G. D. Francis, H. A. O. Hill, W. J. Aston, I. J. Higgins, C. V. Plotkin, D. I. Scott and A. P. F. Turner, Anal. Chem., 56 (1984) 667.

CHEMICO-PHYSICAL CHARACTERIZATION OF AMORPHOUS ANODIC FILMS ON NIOBIUM BY PHOTOCURRENT SPECTROSCOPY.

F. Di Quarto, S. Piazza, R. D'Agostino and C. Sunseri

Dipartimento di Ingegneria Chimica dei Processi e dei Materiali, Università di Palermo, Viale delle Scienze, 90128 Palermo (Italy).

In previous papers (1,2) we have studied the influence of the amorphous nature of passive films on niobium (a-Nb_2O_5) on the mechanism of generation and transport of photoinjected carriers at the a-Nb_2O_5/aqueous electrolyte junction.

In this work we will present a quantitative analysis of the photocharacteristics of such junction performed both during the growth of the films as well as at constant band bending for different film thicknesses.

The experimental results pertaining films grown tensiodynamically, potentiodynamically or galvanostatically at different growth rates have shown that clear interference effects on the measured photocurrent can be detected at low voltages by varying the thickness ($20 \leqslant d_{ox} \leqslant 250$ nm) as well as during the growth of the films. Such effects are visible at wavelengths well below the absorption edge of the films and tend to vanish only at the shortest wavelengths (λ=230 nm).

Fig.1 shows the photocurrent vs. film thickness plots obtained at constant band bendings for films formed galvanostatically at 10 mA cm^{-2}, together with the theoretical fitting curves. The fitting of the experimental plots was performed on the basis of a theoretical model, previously suggested for the a-Nb_2O_5/electrolyte junction (2,3). The model, which modifies the Goodman-Rose theory (4) of photocurrent at non-injecting contacts by taking into account the efficiency of generation of electron-hole pairs, is based on the following assumptions:

a) existence of geminate recombination of the photogenerated carriers;
b) trapping of the photoinjected carriers for relatively low electric fields inside the oxide;
c) negligible diffusive contribution to the photocurrent;
d) absence of kinetic control at the oxide/electrolyte interface.

From the fitting of the experimental curves the mobility times lifetime product (drift range) of the slow photocarriers at low band bendings has been estimated ($\sim 2\ 10^{-13}$ $cm^2\ V^{-1}$ for the holes). The potential distribution inside the oxide film

is in agreement with that expected on the basis of the impedance analysis of the a-Nb_2O_5/electrolyte junction (5).

On the other hand, the fitting of the photocurrent vs. anodization voltage plots for films growing at constant rate (see Fig.2) allows to estimate both the drift range of the photocarriers at high electric field and the anodizing ratio (and hence the average electric field inside the growing film). A shift in the maxima and minima of the curves is evident in Fig.2 due to the change of the anodizing ratio with the growth rate, according to the theories of film growth. The anodizing ratio values are in good agreement with those obtained by other methods for a-Nb_2O_5 anodic films and reported in the literature (6).

In this last case the experimental results suggest that trapping of photocarriers is negligible in the explored thickness range due to the very high electric fields existing inside the oxide film during the anodization.

The fitting of the experimental curves at different wavelengths has been performed on the basis of previous models for the photocurrent generation in insulators (7,8) and by taking into account the optical properties of the metal/oxide/electrolyte interface.

Evidence of surface recombination effects will be presented for the photocurrent generated at the shortest wavelengths.

References

1 - F. Di Quarto, S. Piazza and C. Sunseri, Ber. Bunsenges. Phys. Chem. 91 , 437 (1987).

2 - F. Di Quarto, S. Piazza, R. D'Agostino and C. Sunseri, J. Electroanal. Chem. 228 , 119 (1987).

3 - F. Di Quarto, S. Piazza, R. D'Agostino and C. Sunseri, submitted for publication.

4 - A.M. Goodman and A. Rose, J. Appl. Phys. 42 , 2823 (1971).

5 - F. Di Quarto, C. Sunseri and S. Piazza, Ber. Bunsenges. Phys. Chem. 90 , 549 (1986).

6 - L. Young, "Anodic Oxide Films", chap.15 , Academic Press (1961); L. Young, Trans. Faraday Soc. 52 , 502 (1956).

7 - N.F. Mott and R.W. Gurney, "Electronic Processes in Ionic Crystals", p.122, Dover Publications Inc., 2nd ed., N.Y. (1964).

8 - A. Many, J. Phys. Chem. Solids 26 , 575 (1964).

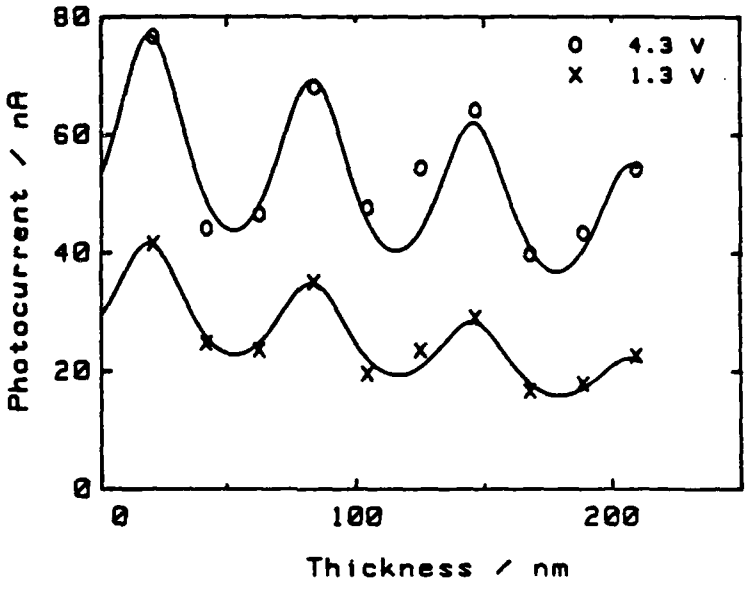


FIGURE 1

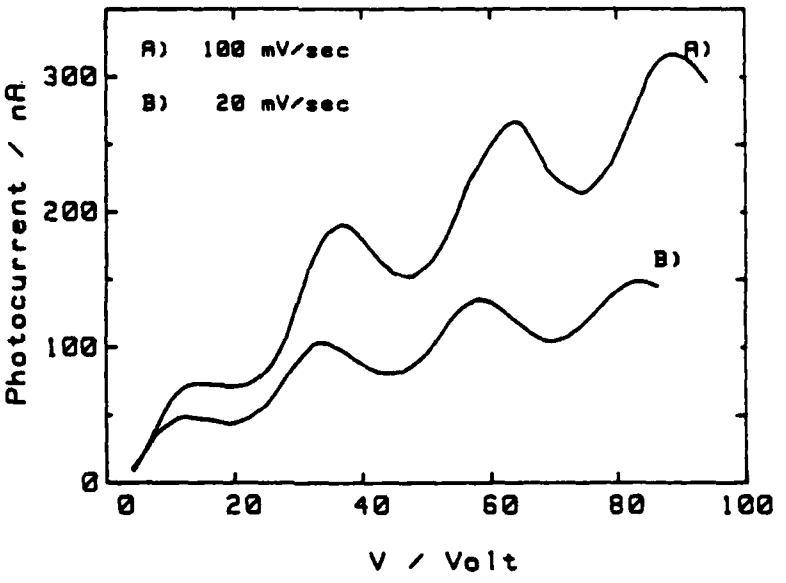


FIGURE 2

Electrochemical and Photoelectrochemical Study of Passivated Ti and Nb Electrodes in Nitric Acid Solutions

W.A. Badawy*, A. Felske, and W.J. Plieth
Institut für Physikalische Chemie der Freien Universität
Berlin, Takustr. 3, D-1000 Berlin 33 (Germany)

The electrochemical and photoelectrochemical behaviour of passivated Ti and Nb electrodes in nitric acid solutions was studied and compared with the behaviour of the electrodes passivated in sulphuric acid. The technique of pulsed laser used in this work allows simultaneous recording of the cell current and the photocurrent with the applied potential /1/. The semiconductor parameters of the passive film, e.g., flatband potential, U_{fb}, donor concentration, N_D, etc., were measured using a commercial impedance spectrometer. Capacitance measurements were carried out by means of the lock-in technique at a frequency of 1330 Hz. The metals were passivated galvanostatically to the desired formation potential. The rate of oxide film formation was about 2.5 nm V^{-1} /2/. The varying behaviour of the passivated Ti electrode in 1 N H_2SO_4 and 1 N HNO_3 is presented in Fig. 1. The electrode passivated and investigated in H_2SO_4 gave a linear increase of the photocharge with the potential during anodic polarization at potentials more positive than 1.84 V. The electrode passivated in HNO_3 under the same conditions showed at high anodic potentials (2.5 V) a large, non-linear increase of the photocharge with the potential. On the cathodic side of that potential, the photocharge shows a flat minimum at a potential range of 1.5 to 0.8 V. At more cathodic potentials, Q_{ph} increased again and passed through a maximum at a potential of 0.250 ± 0.100 V (NHE). The difference in behaviour of the two electrodes is confirmed by the Mott-Schottky plots shown in Fig. 2. The passive layer formed in 1 N

* Permanent address: University of Cairo, Faculty of Science, Dept. of Chemistry, Giza, Egypt

H_2SO_4 solution (Fig. 2-1) gave a donor concentration of 4.23×10^{19} cm^{-3}. For the passive film formed in 1 N HNO_3 solution (Fig. 2-3), a donor concentration of about 5 times of that of the above value was calculated (2.85×10^{20} cm^{-3}). When the oxide film is formed in H_2SO_4 and the capacity is measured in HNO_3 (Fig. 2-2), a value of the donor density lying between the above two values was obtained (6.66×10^{19} cm^{-3}). This value is in consistence with the incorporation of donors (nitrate ions) from the electrolyte into the bulk of the passive film. In the case of passivated Nb electrodes the difference in behaviour is not so remarkable as with the passivated titanium. Fig. 3 shows that the passivation of Nb in nitric acid decreases the concentration of donors in the passive film. The anomalous behaviour of the photocurrent of the titanium electrodes passivated in nitric acid is explained by the different structure of the oxide film, corresponding to the presence of NO_3^- and the reduction product NO_2^- in parts of the film. NO_3^-/NO_2^- can either form an impurity band in the band gap of the TiO_x layer or, when built in higher concentrations, change the structure of the oxide layer, especially at the interface oxide/electrolyte to a porous, "spongy" nature /3/. The band structure of the oxide film in this case can be represented by Fig. 4. The film consists actually of three different zones. the first zone (I) is characterized by a zero electric field (flat energy levels), and hence a high rate of electron-hole recombination is expected. The second zone (II) represents the space charge region of the close-packed TiO_x layer. The separation of electron-hole pairs occurs by the electric field across this layer. The third zone (III) is the porous, "spongy" layer which can be considered as accumulation of surface states. The potential dependence of the photocurrent, the intensity dependence, the frequency dependence, showing the changing ratio between surface state/conduction band excitation and band/band excitation and thickness and pretreatment dependence could be well explained using the model shown in

Fig. 4. The effect of the surface states is suppressed by longer hydrogen evolution.

References

/1/ A. Felske and W.J. Plieth, J. Opt. Soc. Am. B, 3 (1986) 815.

/2/ J.W. Schultze, U. Stimming, and J. Weise, Ber. Bunsenges. Phys. Chem. 86 (1982) 276.

/3/ A. Felske, W.A. Badawy, and W.J. Plieth, J. Electrochem. Soc., submitted.

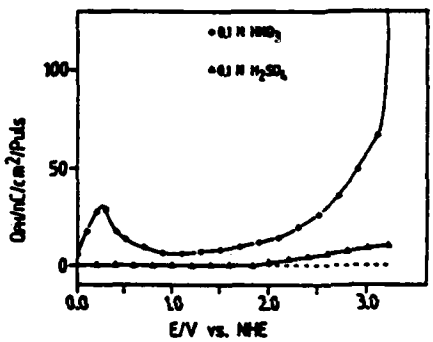


Fig. 1
Photocharge-potential dependence of passivated Ti electrode (3.2 V TiO_2 layer); light intensity I = 0.33 mJ/pulse; λ = 500 nm. ● 0.1 N NH_4Br. ▲ 0.1 N H_2SO_4.

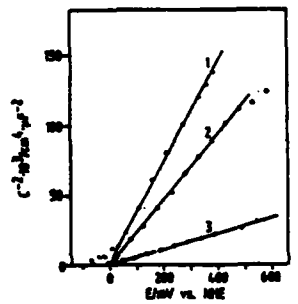


Fig. 2
Mott-Schottky behaviour of anodic oxide films on Ti: 1. formed and measured in H_2SO_4. 2. formed in H_2SO_4 and measured in NH_4Br. 3. formed and measured in NH_4Br.

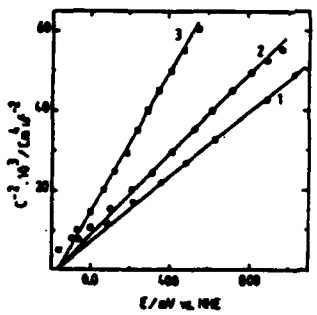


Fig. 3
Mott-Schottky plots of passivated niobium: 1. formed and measured in H_2SO_4. 2. formed in H_2SO_4 and measured in NH_4Br. 3. formed and measured in nitric acid.

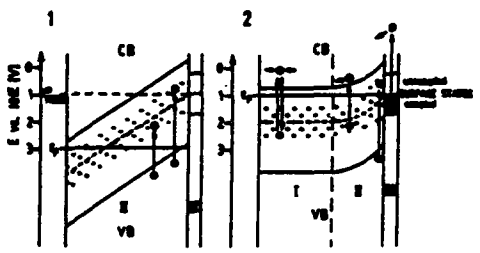


Fig. 4
Schematic model of the band structure of TiO_2 formed on Ti in 1 N NH_4Br solution.
1. Polarization potential E = 2.95 V;
2. Polarization potential E = 0.95 V.
E_F = Fermi niveau, --- = unoccupied impurities in the band gap, ... = occupied impurities in the band gap.

AN IMPEDANCE STUDY OF POLYANILINE AND POLYPYRROLE FILMS IN NON AQUEOUS SOLUTIONS

G. Pistoia

Centro di Studio per la Elettrochimica e la Chimica Fisica delle Interfasi, C.N.R., Via Castro Laurenziano, Rome, Italy.

S. Panero and B. Scrosati

Dipartimento di Chimica, Universita' di Roma-La Sapienza, Rome, Italy

Relevant interfacial characteristics of Polyaniline (PAn) and Polypyrrole (PPy) films, electrochemically grown on Pt electrodes, have been measured in organic solutions by Impedance Spectroscopy. Charge transfer resistance (R_{ct}), double layer capacitance (C_{dl}) and limiting capacitance (C_L) in $LiClO_4$-containing organic solutions have been derived as a function of the oxidation level of the films.

Both PAn and PPy show a transition in conductivity when approaching the fully reduced state, i.e. the resistivity markedly increases at potentials below ~3.1 V vs Li/Li^+. This change is reflected in the R_{ct} values (as shown in the Table). For PAn, in agreement with independent conductivity measurements, R_{ct} has minimum values at intermediate oxidation levels, whilst for PPy a monotonous decrease is observed.

An important characteristics of these films is represented by the high limiting (at low frequencies) capacitance, 10^{-1} - 10^{-2} F/cm^2. Therefore, due to the simultaneous occurrence of a quite reduced R_{ct} and of a high C_L since the early oxidation stages, thin PAn films tend to behave as almost pure capacitors in series with the electrolyte

resistance. Thin PPy films, instead, always show the semicircle due to the parallel connection of C_{dl} and R_{ct}, followed by a Warburg straight line which converts to an almost vertical spike at low frequencies, from which C_L may be calculated.

Limiting capacitances for both films are in agreement with those obtained from cyclic voltammetry tests by the relation C=I/V (V is the scan rate). More precisely, C_L from impedance data are somewhat inferior to those corresponding to the current plateaus observed in the CV curves after the major anodic peak at 3.1-3.4 V vs Li/Li^+. The last piece of evidence points to the fact that the plateaus are only partially capacitive in nature, being composed of a faradaic, I_F, and a capacitive, I_C, component. By using C_L from impedance experiments, the extent of the faradaic current may be calculated.

Both PAn and PPy show asymmetric CV curves with a broad cathodic peak markedly shifted with respect to the anodic one. Due to the substantial symmetry of the anodic and cathodic capacitive currents, as evidenced by impedance tests, the asymmetry may be reconducted to the faradaic component, I_F. This is to be connected, for both films, to the electronic transition occurring at low oxidation levels.

The tendency of PAn and PPy films to act like capacitors has relevance in their use for nonaqueous reversible Li cells. The coulombic efficiency of such electrodes has always been reported to be less than 100%. This may be attributed to a non completely reversible charging of the polymeric capacitor.

Table. Impedance data for polymer films in organic solutions.

V (Volts vs. Li/Li^+)	R_{ct} (Ohm)	I_o (mA/cm^2)	C_L (F/cm^2)
PAn in $LiClO_4$-PC/DME			
3.1	54	0.5	
3.5	12	2.2	0.094
3.7	7	3.6	0.094
3.9	5	5.2	0. 11
4.1	10	2.5	
PPy in $LiClO_4$-PC			
2.7	545	0.06	0.023
2.9	275	0.12	0.022
3.1	50	0.63	0.018
3.3	20	1.6	0.016
3.5	14	2.2	0.016

pH EFFECTS ON THE PHOTOOXIDATION OF D-SORBITOL AT TiO_2 SURFACES

O. ENEA, J.P. ANGO and D. DUPREZ
UA au CNRS 350, Université de Poitiers,
40, Avenue du Recteur Pineau
86022 POITIERS (France)

INTRODUCTION

Recently, we brought some evidence on the relation between the number of OH groups, n_{OH}, contained by polyols and their efficiency in consuming the photoproduced holes on the surface of the illuminated TiO_2 particles in suspension [1], [2], [3], [4]. For a given pH value, the rate of the increase of photocurrent with time, $\Delta i/\Delta t$, depends on n_{OH} for TiO_2 - polyol suspensions [1], [2], [3], and so is the case for the rate of production of hydrogen with the illumination time, r_H, measured for Pt/TiO_2 or TiO_2 + Pt/SiO_2 suspensions [4].

Hole consumption and hydrogen evolution processes are both governed by the concentration of OH^- (or H^+) ions in the bulk : $\Delta i/\Delta t$ and r_H values are function of the initial pH.

Conversely, the anodic currents recorded for the electrooxidation of C_2-C_6 polyols on small Pt or Au electrodes were found to be more related to the number of the adjacent OH groups than to that of the total number [5].

The adsorption of polyols on semiconductor (TiO_2) or metallic (Pt, Au) surfaces, and their subsequent photo- or electro-oxidation, depends not only on the molecular structure of these molecules but also on their concentration at metal (or semiconductor)/electrolyte interfaces, i.e. on the surface area of electrodes or particles in suspension.

The purpose of this study is to examine the influence of pH on the behaviour of D-sorbitol in the photooxidation processes occuring at small ($\sim 1 cm^2$) TiO_2/Ti or $Pt/TiO_2/Ti$ electrodes, comparatively to the high surface area ($\sim 5 m^2$) Pt/TiO_2 photocatalysts in suspension.

EXPERIMENTAL

Pro analysis compounds (K_2SO_4, H_2SO_4, KOH, D-sorbitol) were dissolved in deionized "Milipore Q" quality water to prepare all solutions and suspensions.

TiO_2 (anatase) films having a high surface roughness, were prepared as previously described [6], [7], by thermal decomposition (at 450°C) of titanium ethoxide spread on the surface of Ti sheets (1 cm^2). TiO_2/Ti electrodes having numerous pores and crevices in the anatase film, were doped with Ti by annealing at 550°C under pure Ar flow.

$Pt/TiO_2/Ti$ electrodes were prepared by the photodeposition of Pt particles from $8. 10^{-3}$ M K_2PtCl_6 solutions at pH 2.4 [7].

Pt/TiO_2 photocatalysts were prepared as described [8], by loading TiO_2 (P 25 Degussa) particles with 0.6% wt. of Pt.

All photocurrents were measured in a two-compartment cell having a large area counter electrode (a platinized platinum foil) in one of the compartments, the reference (SCE) and the working (TiO_2/Ti) and glass electrodes being in the second compartment equipped with a flat window. A 150 W Xenon lamp, equipped with a water filter, was used in the photoelectrochemical measurements, performed under continuous stirring and N_2 bubbling.

Photocurrents were recorded with a conventional electronic equipment (PAR 362 potentiostat-galvanostat, Kipp-Zonen X-Y recorder).

A square quartz tube (1x1 cm) was used to realise the small cell necessary to follow the production of hydrogen during the illumination of $Pt/TiO_2/Ti$ electrodes at open circuit. In a typical experiment, a volume of 5 ml of 0.1M sorbitol at a given (adjusted) pH is introduced into the cell, the purified N_2 is bubbled during 30 minutes, the stopcock is closed and then, aliquots of 100 µl are sampled through a septum during the illumination time.

A 80 ml Pyrex flask, equipped with a flat window and a septum was used in the photocatalytic experiments with Pt/TiO_2 particles. Typically, 50 ml of suspension (containing 0.1g Pt/TiO_2 and 0.1 M sorbitol) whose pH is initially adjusted to the desired value, are introduced into the flask, pure N_2 is bubbled during 30 minutes, the vial is closed and the sample stirred at constant speed (200 rpm) and irradiated at $350 < \lambda < 420$ nm with a 900 W Xenon lamp. Gas aliquots are analysed by means of a 5 m Porapak column under N_2 flow and a GIRA gas chromatograph.

RESULTS AND DISCUSSION

The introduction of 0.02 M sorbitol in the supporting electrolyte (0.0325 M K_2SO_4) increases the photocurrents recorded with TiO_2/Ti electrodes at various pH values (ranging from 2 to 13) and produces a significant shift (by 3-400 mV) of the onset values of I - E curves towards more negative potentials. Clearly, the presence of a polyol having 6 OH groups, like sorbitol, enhances the consumption of the photoproduced holes at TiO_2 surfaces; this effect is comparatively more pronounced in acidic (pH from 2 to 5) than in alkaline (pH from 10 to 13) media.

The amounts of H_2 photoproduced at the illuminated $Pt/TiO_2/Ti$ electrodes at open circuit generally increase with the initial concentration of OH^- ions in the bulk. Noticeably, almost no hydrogen was produced in blank tests performed in acidic or alkaline solutions without sorbitol. The evolution of hydrogen becomes energetically possible due to the potential shift (into the cathodic direction) of I - E curves, produced by the adsorption and the subsequent photooxidation of sorbitol molecules.

r_H vs. pH_i dependence is plotted (Figure) for Pt/TiO_2 suspensions containing 0.1 M sorbitol : a maximum value is observed in the neutral range (pH 7 to 10) and quite high r_H values in the acidic media. Sorbitol molecules appear to be less efficient to compete with the adsorption of OH^- ions on the surface of Pt/TiO_2 particles comparatively to that of $Pt/TiO_2/Ti$ electrodes.

The effects of changes in surface area of the semiconductor on the reactions can also play an important role on the mechanism and control of the majority carrier current flow [9].

All these features are comparatively discussed for Pt/TiO_2 particles considered as microelectrodes, and for $Pt/TiO_2/Ti$ electrodes visualised as big particles, in relation with the problems concerning the conversion of light (solar) and chemical (biomass) energies into electricity and/or convenient fuels.

REFERENCES

1) O. ENEA, 166th Meeting of the Electrochemical Society, October 1984.
2) O. ENEA and A.J. BARD, ISE Extended Abstracts, 36, 7100 (1985).
3) O. ENEA, Electrochim. Acta, 31, 405 (1986).
4) O. ENEA, 6th International Conference on Photochemical Conversion and Storage of Solar Energy, Paris, July 1986.
5) J.P. ANGO, O. ENEA and C. LAMY, ISE Extended Abstracts, 38, 505 (1987).

6) C. STADLER and J. AUGUSTYNSKI, J. Electrochem. Soc., 126, 2007 (1979).
7) O. ENEA and M. GRATZEL, ISE Extended Abstracts, 36, 7090 (1985).
8) O. ENEA, A. ALI and D. DUPREZ, New. J. Chem., 12, 27 (1988).

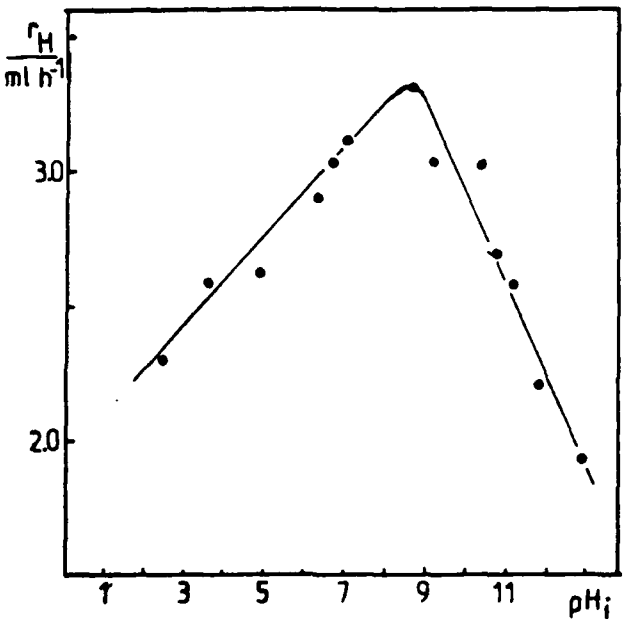


Figure r_H vs. pH_i for Pt/TiO_2 suspensions in 0.1 M sorbitol solution at 25°C.

INDIUM/III/-HEXACYANOFERRATE/II,III/ AS A NOVEL POLYNUCLEAR MIXED-VALENT INORGANIC MATERIAL FOR MODIFICATION OF ELECTRODE SURFACES

Pawel J. Kulesza* **and Mariola Krzowska**

Department of Chemistry, University of Warsaw, Pasteura 1, 02-093 Warsaw, Poland

There is a considerable interest in the preparation, characterization, and application of the mixed-valence compounds, including the transition metal hexacyanometallates. The latter systems constitute an important class of insoluble mixed-valent compounds of the general formula $M^A_x[M^B/CN/_6]_y$ where M^A and M^B stand for transition metals with different oxidation states x and y are stoichiometric subscripts. Of the systems under discussion, the most important so far are Prussian Blue, iron/III/-hexacyanoferrate/II/, and its analogs, e.g. Ruthenium Purple, ferric ruthenocyanide. The intensive development of research into this type of polynuclear transition metal cyanides undoubtedly results from the growing interest in materials for modified electrode surfaces. Indeed, thin films of these complexes on conducting substrates have features in common with redox organic polymer modified electrodes.

In the present study, we propose a novel system which is composed of In/III/ and hexacyanoferrates. The respective films were grown on conducting substrates by cycling the potential between 0.85 and 0 V /vs. SCE/ for 1-120 min in 0.5 mM $InCl_3$, 0.5 mM $K_3Fe/CN/_6$, 0.5 M KCl solution at pH 2. During the negative scans, the cationic In^{3+} species interacted with the simultaneously formed anionic $Fe/CN/_6^{4-}$ to yield sparingly soluble deposits on the electrode surfaces. Different thicknesses could be obtained by varying the cycling times. The absorption spectra of the coatings obtained at SnO_2-covered glass electrodes were dependent on the applied potential: the system exhibited electrochromic behavior. IR spectroscopic measurements confirmed the presence of a CN group in the deposit, as well as showing

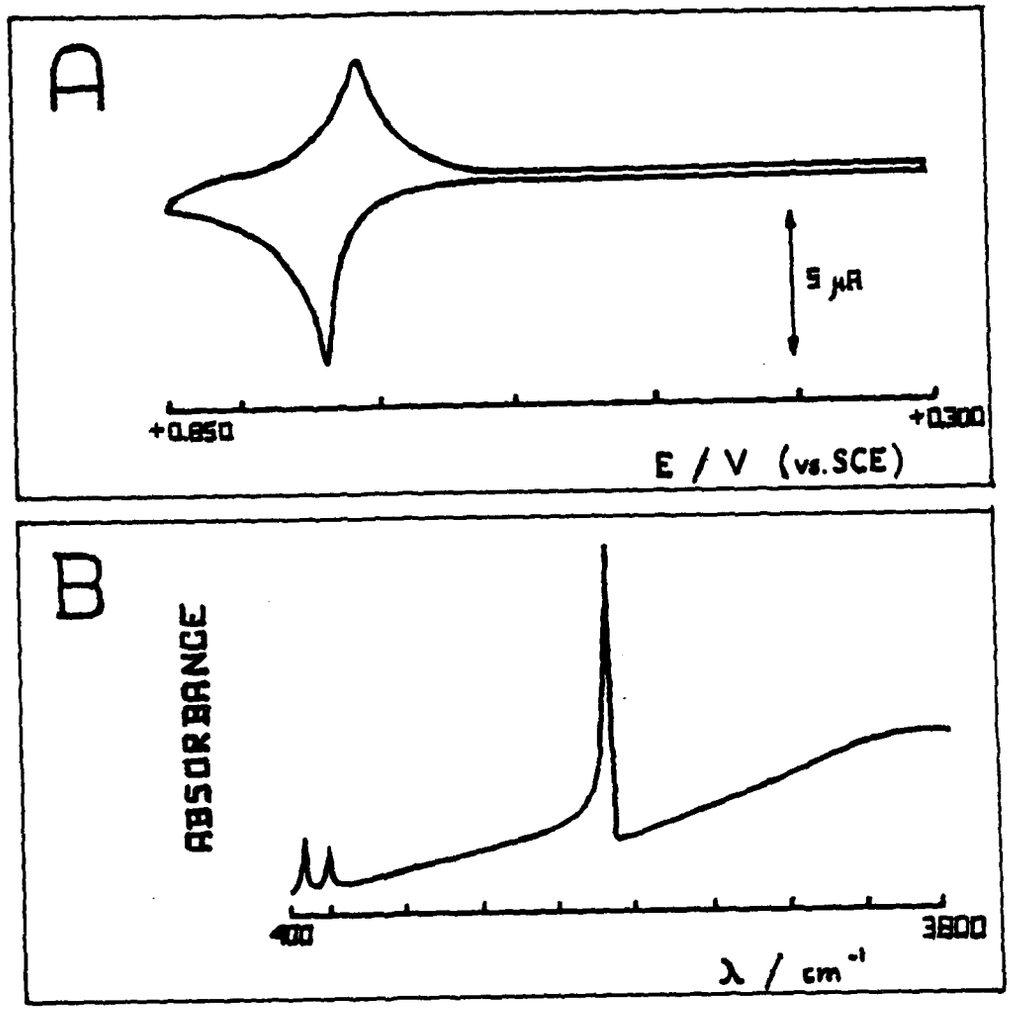
significant aquation of the entire coating; here both reflectance /Figure 1, curve B/ and conventional, i.e. on the deposits scraped from electrode surfaces, approaches were considered. Stoichiometry of the system was determined from voltammetric experiments in which charges under hexacyanoferrate peaks as well as under the oxidation In-to-In^{3+} peak /that was recorded after reductive destruction of the film/ were estimated.

The film electrochemistry and stability are significantly enhanced in K^+-containing supporting electrolytes; a typical and durable response is shown in Figure 1, curve A. Mechanistically hexacyanoferrate portions of the film are electroactive; it is shown that potassium ion migrates into or out of the film active during the electrolysis. One of the most unique aspects associated with the solid-state nature of these surfaces is that the surface voltammetric peaks are sensitive in terms of height and position to the alkali metal ions present in the supporting electrolyte; for example largely different responses have been observed for K^+ and NH_4^+. In conclusion, the systems are zeolitic in nature.

Figure Captions

Figure 1. Curve A; Steady state cyclic voltammogram of the indium/III/-hexacyanoferrate/II,III/ film on glassy carbon in 0.5 M KCl at pH 2. Scan rate, 50 mV s^{-1}; electrode area, 7.1 mm^2.

Curve B; IR spectrum of the indium/III/-hexacyanoferrate/III/ film on glassy carbon slide; in the experiment reflectance technique was employed.


A
5 μA
+0.850
+0.300
E / V (vs.SCE)
B
ABSORBANCE
400
3800
λ / cm⁻¹

ON THE CAPACITY BEHAVIOR OF INHOMOGENEOUS AND AMORPHOUS SEMICONDUCTOR ELECTRODES

Mary Helen Dean and Ulrich Stimming
Department of Chemical Engineering and Applied Chemistry
Columbia University
New York, NY 10027

A common technique for determining the electronic properties of semiconductor electrodes is to measure the capacitance as a function of electrode potential. In general, data have been analyzed using the Mott-Schottky equation according to which the donor or acceptor concentration and the flatband potential can be evaluated from the slope and intercept, respectively, of a linear C^{-2} vs potential plot (1-3). However, numerous reports of experimental results that yield non-linear Mott-Schottky plots have appeared in the literature (4-9). An investigation was undertaken to quantitatively determine how localized states alter the charge/potential relationship under depletion conditions in a semiconductor. Calculations have shown that the capacitance is affected by the distribution of states and experimental capacitance data have been analyzed within the framework of this model to recover approximations of the density of states.

Beginning with the Poisson equation, a general expression for the dimensionless space charge capacitance, C'_{sc}, can be derived as a function of the potential difference across the space layer, $\Delta\phi_{sc}$ (10) :

$$C'_{sc} = \rho(\Delta\phi_{sc}) \Big/ \left[\frac{e}{kT} \int_0^{\Delta\phi_{sc}} \rho(\Delta\phi)\, d\Delta\phi \right]^{1/2} \qquad [1]$$

The dimensionless charge density, ρ', is defined as ρ/eN_C where N_C is the effective density of states at the conduction band edge and $C'_{sc} = C_{sc}/(\epsilon\epsilon_0\, e^2N_C/2kT)^{1/2}$ where ϵ is the relative dielectric constant and ϵ_0 is the permittivity of space. Potential-dependent functions that represent the contribution of localized states to the stored charge may be substituted for ρ'.

By differentiating C'^{-2}_{sc} with respect to $\Delta\phi_{sc}$, a linear first order ordinary differential equation for ρ' can be obtained:

$$\frac{d\rho'}{d\Delta\phi_{sc}} + \frac{C'^{2}_{sc}}{2} \frac{d\,C'^{-2}_{sc}}{d\Delta\phi_{sc}} = \frac{e}{2kT} C'^{2}_{sc} \qquad [2]$$

It is possible to solve this equation for $\rho'(\Delta\phi_{sc})$ when C'_{sc} is known as a function of $\Delta\phi_{sc}$. Furthermore, the approximation

$$D'(E_F - e\Delta\phi_{sc}) = (kT/e)\, d\rho'/d\Delta\phi_{sc} \qquad [3]$$

may be introduced to approximate the dimensionless density of states, D', at the energy $E_F - e\Delta\phi_{SC}$.

In crystalline semiconductors, bulk localized states due to impurities may exist at well-defined energy levels in the band gap. Calculations have been performed using a charge density function for a finite number of discrete donor levels in an n-type material. The example of two donor types was studied in detail. It was assumed that one donor species at energy E_{D1} was close to the conduction band edge and ionized at $\Delta\phi_{SC} = 0$ while the other donor at a lower energy, E_{D2}, was not ionized. With increasing $\Delta\phi_{SC}$, the capacitance decreases in a manner similar to Mott-Schottky behavior. When $\Delta\phi_{SC}$ approaches $(E_F - E_{D2})/e$, where E_F is the Fermi level, the deep donors are ionized and the capacitance increases due to the activation of new sources of charge. At higher values of $\Delta\phi_{SC}$, C_{SC} again decreases with potential. Mott-Schottky plots show linear regions at high and low values of $\Delta\phi_{SC}$ although the behavior is highly non-linear at potentials near $\Delta\phi_{SC} = (E_F - e\Delta\phi_{SC})/e$. The intercept of the linear region at low potentials yields the correct flatband potential while the extrapolation of the linear portion at higher potentials does not.

The electronic structure of semiconductors that lack long-range structural order can be described using density of states functions that extend into the band gap. Expressions for the charge density incorporating continuous functions for D(E) were used to calculate C_{SC}. By combining an exponentially decaying conduction band tail and a constant density of states at lower energies, Mott-Schottky plots were calculated which display continuous curvature and are similar in appearance to examples in the literature. The slopes of these $C'_{SC}{}^{-2}$ vs $\Delta\phi_{SC}$ plots decrease with $\Delta\phi_{SC}$ and it is incorrect to use the slope in the Mott-Schottky equation to calculate a donor density. The flatband potential can not be obtained by extrapolating these curves through the potential axis. Also, it is shown that linear $C'_{SC}{}^{-2}$ vs $\Delta\phi_{SC}$ plots may result for certain distributions of localized states although the condition for the valid application of the Mott-Schottky equation, that is, all donors are ionized at $\Delta\phi_{SC} = 0$, is not satisfied.

Since the Mott-Schottky equation is not generally valid, an alternate technique is proposed for the analysis of capacitance-potential data. Eq.[2] can be solved for the charge density and, subject to the approximation in Eq.[3], the density of states function may be estimated. This procedure has been applied to capacitance data for Fe-Ti oxides with varying compositions and the estimated density of states functions display differences that are indicative of the changes in iron content. Capacitance data for iron passive films of different thicknesses, d, have also been treated according to Eq.[2]. Results show that the onset of additional sources of charge occurs at different $\Delta\phi_{SC}$'s depending on d. This behavior may be explained by either of two models: (i) the density of states, N(E), is dependent on film thickness or (ii) the density of states, N(d), varies spatially

within the film, which could be rationalized by assuming a two layer film with the outer layer growing with film thickness and $N_{outer} < N_{inner}$. These examples illustrate that capacitance-potential data can be interpreted using a model which includes the effect of localized states and, furthermore, the data may be processed to recover information regarding the distribution of electronic states in the material.

References

1) K. Bohnenkamp and H.J. Engell, Z. Elektrochem. 61(1957) 1184.

2) J.F. Dewald, Bell Syst. Tech. J. 39(1960) 615.

3) H. Gerischer in P. Delahay (Ed.), Advances in Electrochemisrty and Electrochemical Engineering, Vol. 1 Interscience Publishers, New York (1961), p.139.

4) F. Moellers, H.J. Tolle and R. Memming, J. Electrochem. Soc. 122(1974) 1160.

5) U. Stimming and J.W. Schultze, Ber. Bunsenges. Phys. Chem. 80(1976) 1297.

6) W. Gissler and R. Memming, J. Electrochem. Soc. 124(1977) 1710.

7) J.H. Kennedy and K.W. Frese, J. Electrochem. Soc. 125(1978) 723.

8) F. DiQuarto, A. DiPaola and C. Sunseri, Electrochim. Acta 26(1981) 1177.

9) B. Danzfuss and U. Stimming, J. Electroanal. Chem. 164(1984) 89.

10) M.H. Dean and U. Stimming, J. Electroanal. Chem. 228(1987) 135.

USE OF SEMICONDUCTOR ELECTROCHEMISTRY TECHNIQUES FOR THE CHARACTERIZATION OF ANTICORROSIVE COATINGS

L. Giorgi
Centro Sviluppo Materiali SpA
C.P. 10747 Roma EUR
Italy

EXTENDED ABSTRACT

The behaviour of materials as regard of corrosion is influenced and determined by the presence of surface layers, due to corrosion and/or oxidation processes, which prevent or reduce the contact between the beneath metal and the agressive environment (1).

The physical and morphologycal properties (thickness, continuity, insolubility and permeability) of the barrier layers alone are not able to explain completely the passive state (2).

Recently, starting from the investigations about the behaviuor of oxides with semiconducting properties (3), it was shown the specific role of the surface compounds on the corrosion reactions (4); the theory of double activation barrier (5) and electronic tunneling through thin films in electrochemical reactions (6) were developed.

The aim of the present paper is to show some examples of application of semiconductor electrochemistry in order to understand the practical behaviour of anticorrosive inorganic coatings.

The semiconducting properties of the oxides present on the surface of material employed in aggressive environment are very important, because the characteristics of these compounds control corrosion rate and adhesion between substrate and lacquers (8). That is particularly true in the case of steel coated with inorganic conversion/barrier layers. In fact the corrosionistic behaviour of these coatings is a function of non-stoichiometry of surface oxides with anionic or cationic vacancies (9). Moreover, the adhesion phenomena between lacquer and metallic substrate is a consequence of the saturation of surface energies both of substrate and organic film; therefore the solid state characteristics of substrate, i.e., the semiconducting properties are fundamental factors in realizing a good adhesion with the polymeric film.

These properties are well measured by means of electrochemical techniques such as cyclic voltammetry (CV) (10), space charge capacitance (SCC) (7) and photoeffects (PE) (11) measurements. In fact it is possible to achieve information about the type of defectiveness of the surface compounds and their changes during anodic and/or cathodic reactions.

The instrumentation to perform photoeffect measurements was built up using pre-existent and home made devices (12) and it is constituted by: a) radiation source, b) monochromator, c) mechanical chopper to obtain an impulsive light, d) signal amplifier, e) low noise electrochemical instrumentation, f) data management system. The electrochemical cell is situated in a

Faraday's cage to avoid external noise.

Some examples of measurements performed on different inorganic coatings are described.

The tinplate, used in the packing industry, constituted by a low carbon steel electrocoated with tin, shows a CV plot as in fig. 1, in which it is possible to locate the different species of tin oxides both during oxidation and reduction.

The proceedings of tin coatings oxidation was also followed by means of a galvanostatic polarization with a parallel photopotential recording (fig. 2). The apparence of an easy measurable photoresponse corresponds to the Sn(IV) formation by means of an oxidation of the original film formed by oxide or hydroxide of Sn(II).

The negative photoresponse is present in the whole range of formation and growth of SnOx, according to the n-type semiconduction properties of the massive tin dioxide (16).

During galvanostatic polarization, in a few range of electrodic potential, a very small positive photoresponse, is present denoting a partyally p-type semiconduction.

The PHES spectrum (11) of the SnOx obtained at the end of the anodic oxidation, shows an energetic gap of 3.1 eV (fig. 3), while the values reported in literature is 3.6 eV for the monoxide and 4.1 eV for the dioxide (7). Such a discrepancy can be explained considering the literature data refering to massive electrodes, while the experimental results are relative to SnOx surface films and therefore they have different chemical composition and defectiveness.

The double semiconduction nature of tin oxides obtained by controlled oxidation is also evident from Mott-Schotttky plot (8), from which it is possible to obtain the charge carrier concentration (17).

The presence of mixed tin oxides leads to a "hoctron" structure (hole + electron) in which the lower conduction band edge of an oxide is situated below the upper valence band of the other oxide (8); therefore there are energy levels in which the coexistence of holes and electrons is possible.

At the end of industrial process for tinplate production, a passivating film of Cr+CrOx is electrodeposited on the surface (13). Such a film, in reality, is formed by a mixture of tin and chromium oxides with different hydratation grade (14).

Thanks to the presence of these surface compounds it is possible to perform photopotential measurements in phosfate buffer (pH=7.4) from which it was resulting both p and n-type semiconduction (fig.4).

From the galvanostatic plot it is possible to obtain the total amount of chromium (5.5 mg/m^2) in the passivation film (15) and to give an interpretation of photopotential progress. In fact by the comparison of the two plots is possible to point out a parallelism between electrodic potential and photoeffect. The later is constant up to -0.3 Vsce, with a very small amplitude; then it grows and stabilizes in the range 0.0-0.7 Vsce, which corresponds to the oxidation of surface chromic compounds. For higher electrodic potential, it is evident an exponential growth of the PE which can be interpreted considering that at these

electrodic potential values the chromic film is no more present; therefore the passivated tinplate shows the same behaviour of tinned steel.

The electrolytic zinc coated steel for automotive application shows CV plots like that in fig. 5. Such plots were obtained after an anodic oxidation in boric buffer at 0.8 Vsce for 2 min. In dark conditions the anodic current is very small and it depends on the rate of chemical dissolution of ZnOx and on anionic vacancy concentration. The cathodic current is relative to the discharge of hydrogen, with a little influence of oxide reduction, and it is independent by irradiation.

In the anodic region the oxide is decomposed under light, giving zinc ions and oxygen, as the following reaction:

$$2\ ZnO + 4\ h\nu \longrightarrow 2\ Zn^{2+}_{acq} + O_2 + 4e^-$$

Such a reaction agrees with the n-type semiconduction pointed out by SCC measurements (Mott-Schottky plot) (12).

Since the zinc oxide is n-type the reduction of hydrogen ions is easily performed by electronic transfer mechanism from conduction band. In fact due to the amplitude of forbidden band (3.2 eV) (7) it is impossible an interaction in the field of the valency band, because an energetic level in this region will correspond to a redox couple with a very high electrochemical standard potential.

The corrosionistic behaviour of the stainless steels is affect by the solid state characteristics of the defective passivation films (3) constituted by few molecular layers. In fact there is a strict correlation between pitting susceptibility and semiconducting properties (20).

The changes of solid state characteristics can be pointed out by means of thermal treatments at low temperature (100-300 °C) or anodic oxidation in boric buffer (12). For example fig. 6 shows the photoresponse of an AISI 304 steel before and after
a treatment at 200 °C for 2 hours. In the natural passive film the anionic vacancies are predominant while after the thermal treatment there is an inversion of tendency.

Acknowledgements

The author thanks Mr. B. Ferri for the technical assistance.

REFERENCES

1) U.R. Evans, Electrochim. Acta, 16 (1971) 1825
2) R. Memming, F. Moellers, Ber. Busenges. Physik Chem., 76 (1972) 469
3) S.R. Morrison, in Passivity of Metals and Semiconductors, M. Froment ed., Elsevier Science Pub., B.V. Amsterdam
4) U. Stimming, ibidem
5) R.E. Meyer, J. Electrochem. Soc., 107 (1970) 847
6) J.W. Schultze, J.K. Vetter, Electrochim. Acta, 18 (1973) 889
7) S.R. Morrison, Electrochemistry at Semiconductor and Oxidized

Metal Electrodes, Plenum Press, N.Y. 1980
8) L. Giorgi, N. Azzerri, G.M. Ingo, Giornate dell'Elettrochimica Italiana 1986, Bologna 28-30 October 1986
9) L. Giorgi, B. Ferri, CSM Report n. 5503R, December 1986
10) A.J. Bard, L.R. Faulkner, Electrochemical Methods Wiley, N.Y., 1980
11) E.K. Oshe, I.L. Rozenfeld, V.G. Doroshenko, Zasch. Met., 13 (1977) 410
12) L. Giorgi, CSM Report n. 5671R, July 1987
13) E. Morgan, Tinplate and Moder Canmaking Technology,Pergamon Press, 1985
14) N. Azzerri, U. Cerboncini, 3rd Int. Tinplate Conf., London, 15-19 October, 1984
15) P.J. Aubrun, G.A. Pennera, Revue de Metallurgie, (1976) 745
16) S. Kapusta, N. Hackermann, Electrochim. Acta, 25 (1980),100
17) V.A. Myalmin, Yu.V. Pleskov, Electrochemistry of Semiconductors, Plenum Press, N.Y. 1967
18) H. Gerischer, J. Electrochem. Soc, 113 (1966) 1174
19) E.K. Oshe,I.L. Rozenfeld, 6° I.C.M.C., Sydney, 1975
20) G. Bianchi, C. Cerquetti, F. Mazza, S. Torchio, Corrosion Science,12 (1972) 495

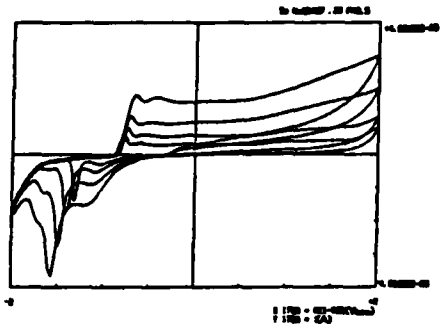


Fig.1 - Cyclic voltammetry related to tinplate in boric buffer at pH=8.5.

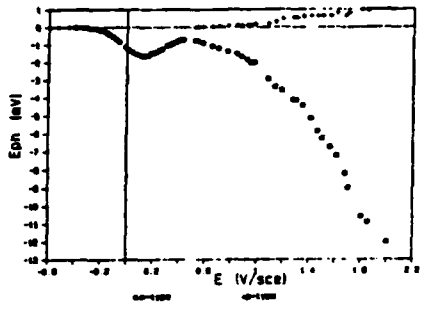


Fig.2 - Photopotentials recordered during galvanostatic oxidation (200 nA/cm²) of tinplate in boric buffer.

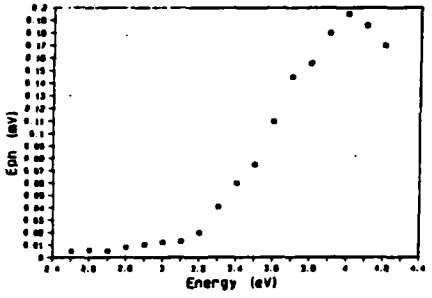


Fig.3 - PHES spectrum of electrotinned steel.

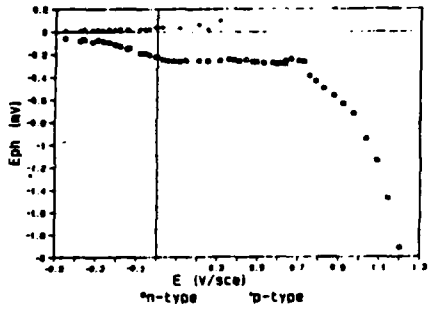


Fig.4 - Galvanostatic oxidation and photopotentials of passivated tinplate.

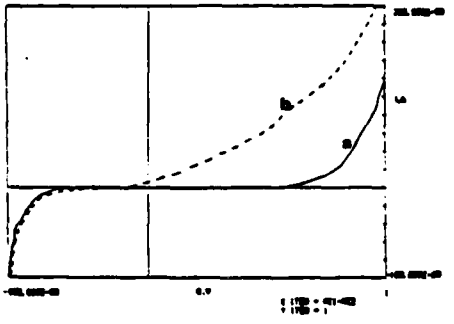


Fig.5 - Voltammetry of electrolytic zinc coated steel in dark (a) and light (b) conditions.

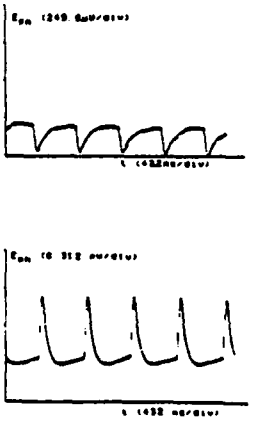


Fig.6 - Photopotentials of stainless steel before (a) and after (b) treatment at 200 °C.

Oxidation Behaviour of Chevrel Type Oxygen Reduction Catalysts

W. Jaegermann, C. Pettenkofer, B. Schubert,
N. Alonso-Vante, E. Gocke*, and H. Tributsch

Hahn-Meitner-Institut, Bereich S
Glienicker Str. 100, 1000 Berlin 39, West Germany
*Technische Universität Berlin, Fachbereich Chemie

Chevrel type chalcogenides of stoichiometry $Mo_{6-n}MSe_8$ (M=Ru, n=2; M=Re, n= 4) are very active electrocatalysts for the reduction of molecular oxygen in acid medium [1,2,3]. Their catalytic ability is found to be dependent on composition with $Mo_4Ru_2Se_8$ being the most efficient and Mo_6Se_8 the less active electrocatalyst. The catalytic properties and electrochemically observed stability have been related to the electronic structure which based on theoretical calculations should be characterized by high contributions of metal d-states around the Fermi level [4]. In this paper the combination of UHV surface spectroscopies (XPS and UPS) with electrochemical techniques is used to elucidate the surface oxidation properties after different sequences of (electro)chemical treatments. The electronic structure (DOS) of the compounds is discussed based on valence band photoemission spectra obtained with different excitation wavelenghts.

Only small amounts of oxidation products are found in XPS for samples exposed to air. The surface stoichiometry of long term air stored samples of the different compounds are shown in fig 1. In all cases the formation of MoO_3 is evident from the spectra. Whereas for $Mo_2Re_4Se_8$ the oxidation of Re to ReO_3 is observed no clear evidence for Ru oxidation products are detected $Mo_4Ru_2Se_8$. In the range of the oxygen reduction potential the most active compound $Mo_4Ru_2Se_8$ also prove to be rather inert towards oxidation. Mechanically cleaned electrodes show after extensive reduction time ($0.04 < U < 0.84$) no changes of their XP-spectra. At more positive potentials, however, anodic corrosion currents are observed which are partly due to the observable formation of oxidative

corrosion in correspondence to the oxidation products formed in air. This is considered to be the reason for the poor catalytic properties of the Chevrel compounds for oxidation processes.

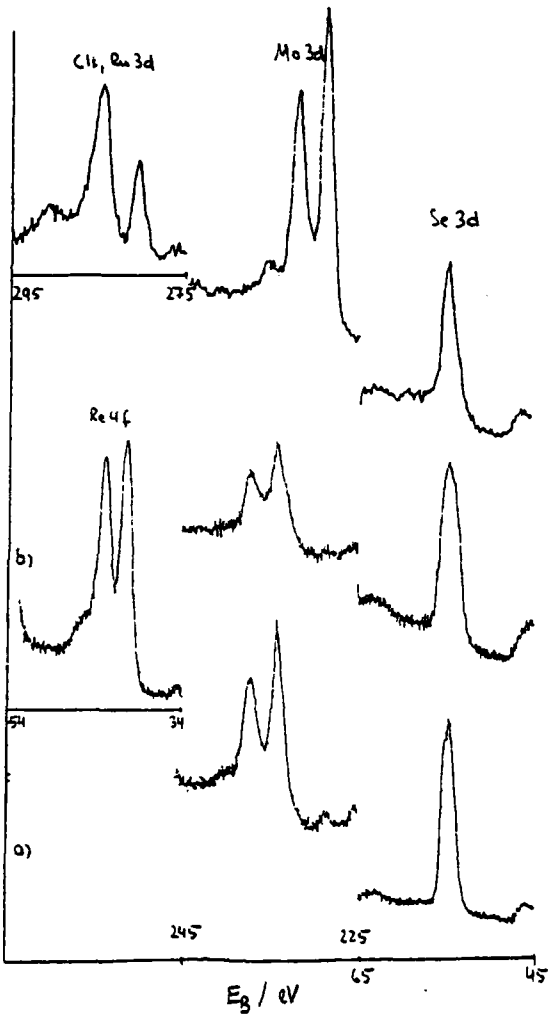


Fig 1. XP spectra of the main peaks of air oxidized Chevrel type cluster compounds. a)$Ru_2Mo_4Se_8$, b)$Re_4Mo_2Se_8$, c)Mo_6Se_8

The density of states distribution for the different compounds are analyzed based on XPS and UPS (HeI and HeII) data and theoretical electronic structure calculations. In fig 2. the valence band spectra

of $Ru_2Mo_4Se_8$ are shown as an example. No pronounced differences are observed.for the different compounds In all cases a strong metal d state contribution (about 2.5 eV wide) is found below the Fermi level which is considered to be the reason for the observed catalytic ability. A broad band of Se 4p character is obtained between 2.5 and 6 eV. In all cases the metal d-states are strongly hybridized with chalcogenide p-states.

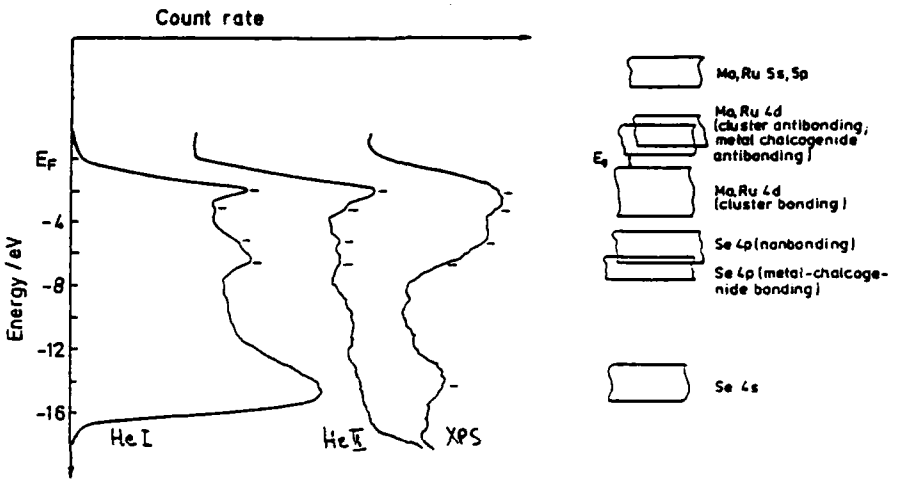


Fig. 2 Valence spectra of $Ru_2Mo_4Se_8$ and schematic density of state distribution

The catalytic activity is discussed in terms of possible surface interactions (different surface coordination complexes) which are determined by the electronic nature of the band edge states. The difference in reactivity is related to the different chemical nature of the involved metal sites.

1. N. Alonso Vante and H. Tributsch, Nature 323 (1986) 431
2. N. Alonso Vante, W. Jaegermann, H. Tributsch, W. Hönle, and K. Yvon, J. Am Chem. Soc., 109 (1987) 3251
3. N. Alonso Vante, B. Schubert, H. Tributsch, and A. Perrin, J. Catal., 112 (1988) 000
4. N. Alonso Vante, B. Schubert, H. Tributsch, in Materials Chemistry and Physics "*Materials Research in Electrocatalysis*", S. Trassatti (ed.), submitted

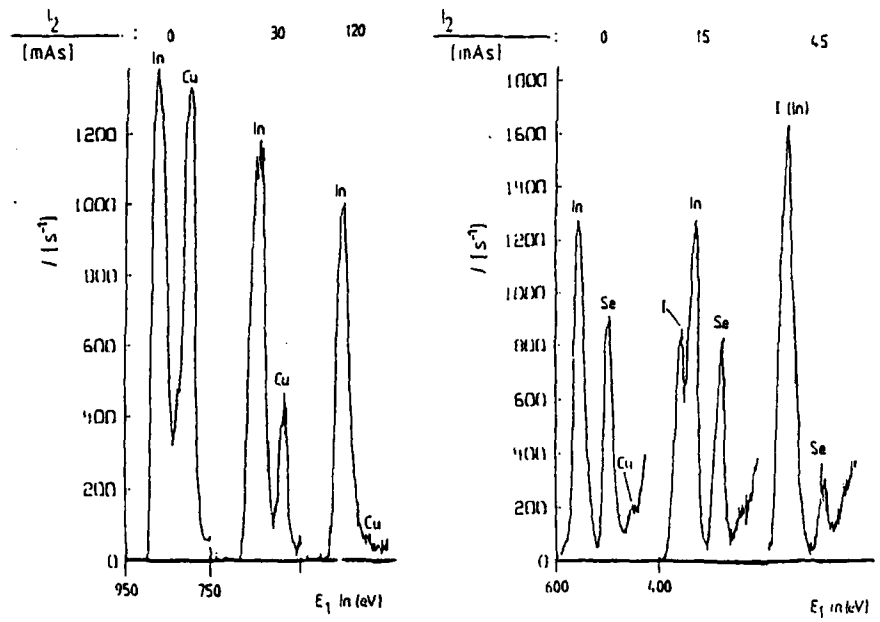
Site Specific Surface Interaction of I_2 on $CuInSe_2(112)$ In Relation to Photoelectrochemical Phase Transformation

M. Sander, W. Jaegermann, and H. J. Lewerenz
Hahn-Meitner-Institut, Bereich S
Glienicker Str. 100, 1000 Berlin 39, West Germany

n-$CuInSe_2$ is a promising material for solar cells with achieved efficiencies of 12 % in photoelectrochemical cells [1]. The active interface forms a heterojunction with an in-situ (I_2/HI/Cu^+ electrolyte) formed p-type $CuISe_3$-Se contacting phase. In this paper the microscopic details of the surface transformation are analyzed in model experiments of surface interaction. For this purpose the adsorption of I_2 onto UHV cleaved $CuInSe_2$ surfaces is investigated by XPS, UPS, LEISS and LEED measurements.

LEED data of the UHV cleaved surfaces indicate the existence of (112) cleavage planes. In this plane Cu and In are equivalently exposed. For small dosage the LEISS data indicate an initial site specific interaction of I_2 with Cu surface sites (fig 1). A preferential discrimination of the Cu backscatter signal is observed due to the shadowing effect of the adsorbed I_2.

Fig 1. LEISS data (He and Ne) of $CuInSe_2/I_2$ interfaces



The UPS and XPS spectra indicate that I_2 is dissociatively adsorbed at low coverages. At higher dosage molecular adsorption is observed (figs 2,3). The work function increases during adsorption contineously to a saturation value of 1.4 eV partly due to a bend bending of 0.4 eV. After annealing to room temperature the molecular adsorbed I_2 desorbs whereas the I^- remains on the surface possibly still bound to Cu as extra In peaks are not observed in the XP-spectrum.

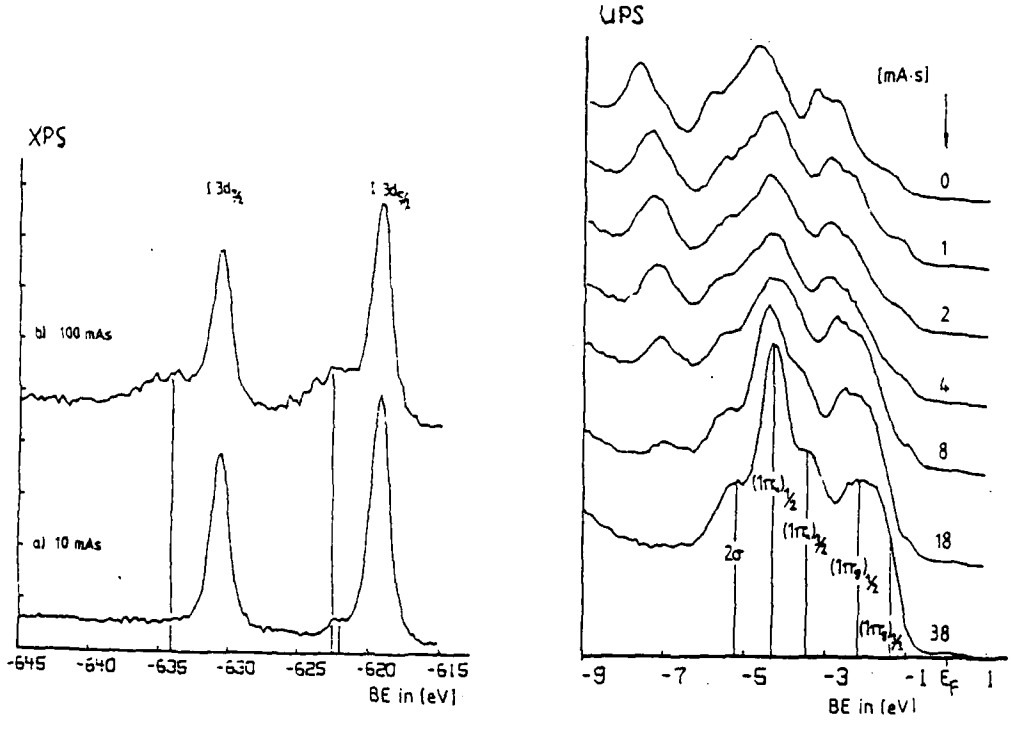


Fig. 2. XP-spectra of $CuInSe_2/I_2$ interfaces for different doses of I_2

Fig. 3 UP-spectra (HeI) of $CuInSe_2/I_2$ interfaces for different doses of I_2

The obtained results are compared to recently obtained data on Cl_2 and H_2O adsoption [2] and are discussed in relation to the photoelectrochemically induced surface transformation.

1. S. Menezes, Appl. Phys. Lett., 45 (1984) 148
2. M. Sander, H. J. Lewerenz, W. Jaegermann, and D. Schmeißer, Ber. Bunsenges. Phys. Chem., 91 (1987) 416

INCORPORATION OF ELECTROACTIVE SPECIES IN SELF-ASSEMBLING MONOLAYERS ON GOLD ELECTRODES

Kathryn A. Bunding Lee

S. C. Johnson & Son
M.S. 056, 1525 Howe St., Racine, WI 53403, USA

Certain molecules will self-organize into compact monomolecular films. These films can be specifically constructed for applications including catalysis, energy transfer, insulators, lubricants, and membrane models. One method to construct monomolecular films on substrates is called "self-assembly." The self-assembling method consists of immersing a substrate into a solution of molecules which then assemble into an organized monolayer due to surface, van der Waals and solution interactions[1-3]. Self-assembling films can be made in a few minutes, are monolayers, and require only small amounts of solvent. In many cases, the molecules bond to the substrate, making the film very adherent and able to completely cover the surface.

Alkyl mercaptans and disulfides with tails containing 12 or more carbons spontaneously self-assemble to form well-oriented, strongly adherent, completely covering and passivating films on Au electrodes[4-8]. To further understand self-assembling films and electron transfer into self-assembling films, we incorporated molecules with electroactive groups into mercaptan films on Au electrodes. We studied six molecules: N-octadecyl-4,4'-dipyridinium bromide (C_{18}bipy), N-hexadecyl-4,4'-dipyridinium bromide (C_{16}bipy), N-dodecyl-4,4'-dipyridinium bromide (C_{12}bipy) and their hydrobromide derivatives: C_{18}bipyHBr, C_{16}bipyHBr, and C_{12}bipyHBr respectiviely. These molecules co-assemble with hexadecyl mercaptan to yield adherent, electroactive monolayer films. These films were analyzed by cyclic voltammetry, ellipsometry, Fourier Transform Infrared (FTIR) spectroscopy, and surface-enhanced Raman spectroscopy (SERS).

The electrodes were 100nm Au evaporated onto 10nm of TiO_2 on glass, about 6 cm^2, and were cleaned by an oxidation-reduction step cycle in 0.5mol/L sulfuric acid; this changed the electrodes from hydrophobic to hydrophillic. They were then rinsed and dried and immersed in a 2:1 $CHCl_3$:methanol solution with 5 mmol/L bipyridinium and 10 mmol/L hexadecyl mercaptan. The electrodes were removed after 8 minutes, rinsed with methanol, and then immersed in the phosphate buffer for electrochemical analysis. Electrodes emersed from the mixed bipyridinium/mercaptan deposition solution are not wetted by water, chloroform or methanol, indicating that the surface coating has a low critical surface tension and that the layer is organized with the chains extending from the surface.

Cyclic voltammetry was used to study the electrochemical characteristics of these films. The cyclic voltammograms generally all show a small (10-30mV) redox peak separation and nearly linear i_p vs. scan rate dependence for the range 50-500mV/sec. The charging current at constant sweep rate decreased by a factor of 20 or more. This is consistent with a

non-conductive compact organic coating which does not desorb in aqueous electrolyte. The redox potentials for C_{18}bipy, C_{18}bipyHBr, C_{16}bipyHBr, and C_{12}bipyHBr are around -700 to -900 mV, which is near the H_2 reduction wave in these solutions. When the potential was scanned more negative of -1.0 V, the cyclic voltammograms became less reproducible. When the potential was kept positive of -1.0 V, multiple scans showed good, though not exact, reproducibility. The redox waves are attributed to the one electron reduction and oxidation of the bipyridyl group. Though the reduction of bipyridyl molecules in solution is often accompanied by a purple color, no color was observed. For comparison to the organized monolayer, a film of C_{18}bipyHBr was "cast" onto the electrode by putting a drop of the C_{18}bipyHBr in methanol on the electrode and evaporating the solvent. The redox potential of this cast, and presumably random, film had a redox potention around −800 mV, 100 mV shifted from the self-assembled film, and did not reduce the charging current.

The C_{16}bipy and the C_{12}bipy films have redox potentials more positive of the other compounds. The C_{12}bipy has two pairs of redox peaks, one pair about -0.5 V and the other about -0.9 V. This may be due to the existence of protonated and non-protonated species.

Though the films are made from a solution of 2:1 ratio of hexadecylmercaptan to bipyridinium compounds, that ratio did not dictate the proportion of those compounds in the film. The coverage of electroactive species can be calculated by counting the electrons transferred. If we assume 50 $Å^2$/molecule, the percent coverage for the films ranges from 7-29%. If all the bipy coumpounds undergo electron transfer, the coverage is less than the 1/3 coverage expected if the molecules assemble in proportion to their solution concentrations. However, only compounds that are electroactive can be detected. If the bipy groups are oriented away from the electrode, they may not be electroactive. Since bipyridyl groups can exchange electrons with the electrode surface at close to reversible rates, it seems that the active centers are close to the electrode and not at the exterior of the monolayer.

The surface redox wave is very sensitive to the presence of dissolved oxygen. If the Ar purge is stopped for a few minutes, the cathodic peak increases dramatically and the anodic peak disappears. After prolonged Ar bubbling and reapeated potential cycles, the syummetrical surface wave is restored. Oxygen reduction on an electrode coated with a pure hexadecylmercaptan monolayer appears as a low plateau current at ca. -0.6 V. We interpret these results as electrocatalytic reduction of oxdygen by the bipy radical.

The film thicknesses in Å calculated from the ellipsometric results were as follows: C_{12}bipy 24.2, C_{16}bipy 9.2, C_{18}bipy 21.0, C_{12}bipyHBr 11.7, C_{16}bipyHBr 19.3, and C_{18}bipyHBr 20.8. Though these results are low compared to theoretical thicknesses for the molecules oriented with their chains perpendicular to the electrode, they do indicate coverage of not more than one monolayer.

The grazing angle infrared reflection spectrum of a self-assembled film of hexadecyl mercaptan and N-Octadecyl-4,4'-dipyridyl hydrobromide has bands at 2965 ($\nu_a CH_3$), 2937, 2029 ($\nu_a CH_2$), 2879 ($\nu_s CH_3$), 2851 ($\nu_s CH_2$), 1634 (pyridinium CH in-plane bending), 1503 (ring stretching), and 1463 cm^{-1} (CH_2 scissors mode). The band positions and relative intensities of the CH stretching region are consistent with a

well-ordered monolayer oriented with the alkyl tails nearly perpendicular to the electrode surface[6-7]. Of particular note in these self-assembled film spectra is the greatly increased relative intensity of the CH_3 vibrations compared to the CH_2 vibrations. Since the ratio of CH_3 bonds to the CH_2 bonds is small, it is expected, and seen, that the CH_3 vibrations are relatively weak in the spectra of bulk materials. The dramatic change in these relative intensities for the monolayer films has been interpreted as resulting from the alkyl C-C chains being organized nearly perpendicular to the substrate. The CH_2 vibrations are then more nearly parallel to the substrate and are weak due to the infrared selection rules of grazing incidence light with polarization parallel to the light plane of incidence. The vibrations assigned to the pyridinium ring breathing are also observed, reaffirming their incorporation into the film, and suggesting that the rings are also organized, more nearly perpendicular than parallel to the surface.

The incorporation of electroactive species into self-assembling monolayers on gold electrodes yields sturdy, adherent, monolayer electroactive films. The electroactive groups resist solvent removal from the film presumably due to van der Waals forces with the anchored mercaptan molecules. The molecules are oriented nearly perpendicular to the gold surface. The films are catalytic to oxygen reduction, but their oleo- and hydrophobicity indicate good surface coverage.

References:

1. W. C. Bigelow, D. L. Pickett and W. A. Zisman, J. Colloid Sci., 1 (1946) 513.

2. L. Netzer, R. Iscovici and J. Sagiv, Thin Solid Films, 99 (1983) 235-241.

3. J. Gun, R. Iscovici and J. Sagiv, J. Col. and Interfac. Sci., 101 (1984) 201-213.

4. H. O. Finklea, S. Avery, M. Lynch and T. Furtsch, Langmuir, 3 (1987) 409.

5. R. G. Nuzzo and D. L. Allara, J. Am. Chem. Soc., 105 (1983) 4481.

6. R. G. Nuzzo, F. A. Fusco and D. L. Allara, J. Am. Chem. Soc., 109 (1987) 2358.

7. M. D. Porter, T. B. Bright, D. Allara and C. E. D. Chidsey, J. Am. Chem. Soc., 109 (1987) 3559.

8. E. Sabatini, I. Rubinstein, R. Maoz and J. Sagiv, J. Electroanal. Chem., 219 (1987) 365.

PHOTOELECTROCHEMICAL MICROSCOPY OF THIN TiO_2 FILMS

M. R. Kozlowski, C.-H. Paik, P.S. Tyler, and W. H. Smyrl
Corrosion Research Center and Dept. of Chemical Engineering and Materials Science
University of Minnesota
Minneapolis, MN 55455
and
R. T. Atanasoski
Institute of Electrochemistry, ICTM, University of Belgrade, Belgrade, Yugoslavia

An understanding of the local properties of thin semiconducting oxide films is important in the areas of microelectronics, corrosion, catalysis, and solar energy conversion. We report here the results of a study of the local photoelectrochemical and structural properties of thin (<20 nm) TiO_2 films grown by anodic polarization of polycrystalline titanium substrates. The principal technique used in the investigation was photoelectrochemical microscopy (PEM). PEM is a quantitative in-situ technique which utilizes a focussed laser beam to measure local photocurrents in semiconducting films [1,2].

The photoelectrochemical properties of thin anodic TiO_2 films grown on polycrystalline titanium substrates have been shown to be heterogeneous and dependent on the oxide growth rate and the crystallography of the underlying titanium substrate [1-3]. By combining PEM data with that of structural studies and local metal photo-deposition studies on these same films, a model is evolved which attributes the heterogeneous photoelectrochemical properties of the oxide to variations in the oxide defect structure.

Experimental:

The thin films of TiO_2 (1-20 nm) were grown by anodic polarization in 0.05 M H_2SO_4.

PEM data was obtained by rastering a focussed laser beam (λ=351 nm, spot size ~ 5 μm) across the biased oxide at a scan rate of 60 mm/s. The data was stored digitally in a 250 x 200 array and displayed in the form of a gray-scale image on a video screen.

The solution used for metal deposition was 30 mM $PdCl_2$ dissolved in an aqueous methanol/HCl mixture. The sample was illuminated while at open circuit potential using the PEM apparatus. Pd deposition was analyzed using scanning electron microscopy and scanning Auger spectroscopy.

Results:

For oxides grown slowly (~1 nm/h), by ramping the potential of the metal substrate at 0.1 mV/s, the oxide photoresponse was found to map the grain structure of the underlying titanium substrate. As the oxide growth rate was increased the photoresponse became more homogeneous and the average photocurrent decreased. Electron diffraction studies of the oxides showed that the oxide structure was also dependent on the oxide growth rate and the substrate crystallography [2]. The slowly grown films had an ordered rutile structure with a preferred growth direction evident on some substrate grains. As the oxide growth rate was increased the oxide structure became more homogeneous and the oxide crystallite size decreased. The decrease in oxide crystallinity with increase in oxide growth rate was also observed in photospectroscopy measurements as a loss of the 3.7 eV direct bandgap.

Studies of local photodeposition of Pd on these same oxides has shown that the metal deposition was also dependent on the oxide growth rate and the crystallography of the underlying titanium substrate [4]. The morphology of the metal deposition pattern changed abruptly at the grain boundaries of the substrate. The correlation of the metal deposition morphology with the

local photocurrents measured on these areas using PEM showed that the heaviest deposition occurred on the oxide areas with the lowest photocurrents.

We propose that the local variations in the photoelectrochemical properties of the oxide films are due to variations in the density of defects in the oxide. These defects, such as oxygen vacancies or titanium interstitials, generate sub-bandgap electronic states in the bulk and at the oxide surface. The sub-bandgap states act as recombination centers producing low photocurrents in areas of high defect density. These same defects produce surface states which increase the density of electrons available for the reduction of metal ions at the oxide surface. The same defects may therefore lead to low photocurrents and high rates of Pd deposition. The density of the defects is controlled by the structure of the oxide film and is therefore dependent on the oxide growth rate and the crystallography of the titanium substrate.

In order to identify the energy levels of the defects, the oxides were characterized by photoelectrochemical spectroscopy and photoacoustic spectroscopy.

The influence of metal photodeposition on the photoresponse of the semiconducting films is also considered. This includes the influence of the Pd/TiO_2 interface and photo-assisted electromigration of defects [5] in the oxide as a result of extended focussed laser illumination.

Acknowledgement. This work was supported by DOE Agreement No. DOE/DE-FG02-84ER45173. R.A. would like to thank the support of the Yugoslav-American Fund for Scientific Cooperation, DOE Grant No. 675.

References.

1. M.A. Butler, J. Electrochem. Soc., 131 (1984) 2185.
2. M.R. Kozlowski, P.S. Tyler, W.H. Smyrl, and R.T. Atanasoski, Surface Science, 194 (1988) 505.
3. P.S. Tyler, M.R. Kozlowski, W.H. Smyrl, and R.T. Atanasoski, J. Electroanal. Chem., 237 (1987) 295.
4. C.H. Paik, M.R. Kozlowski, P.S. Tyler, W.H. Smyrl, submitted to J. Electrochem. Soc.
5. M.R. Kozlowski, P.S. Tyler, W.H. Smyrl, and R.T. Atanasoski, presented at the 172nd Meeting of the Electrochem. Soc., Honolulu, Oct. 18-23, 1987; proceedings in press.

IMPEDANCE RESPONSE OF PYRITE PHOTOANODE/REDOX ELECTROLYTE INTERFACE

N. Alonso Vante, X.-P. Li, and H. Tributsch

Hahn-Meitner-Institut
Bereich Strahlenchemie
Glienicker Strasse 100
1000 Berlin 39, F.R.G.

The pyrite (FeS_2) photoanode can be stabilized efficiently by reducing agents, e.g., I^-, Br^- [1]. Recently, we have shown that positive iron complexes can also mediate such a stabilization through a bridge formed with Cl^- [2]. Furthermore, it was demonstrated that this stabilization is carried out through a chemical coordination electron transfer on the pyrite surface [2]. The response of such an interface measured with the impedance technique is of interest since it provides kinetic information about the interaction between the reacting species with the pyrite semiconductor surface.

The interfacial behaviour of the pyrite/electrolyte system containing the reducing species was analysed in darkness and under illumination. To get a more representative and intuitively accesible view of our experimental data, obtained in a large frequency range (0.044 to 80 kHz (14 points per decade)) and polarization bias (-0.65 to 0.8V/Hg_2SO_4), we depicted the surface resulting from the joining of the experimental curves in a three dimensional plot. The impedance diagram used was the Bode plot (log |Z| *vs* log f) and the phase angle plot (phi *vs* log f). Figures 1 and 2 show this interfacial behaviour of the pyrite semiconductor electrode in presence of Br^- in darkness and under illumination, respectively. Complicated features result as a function of the applied polarization. Typical wave shaped Bode and phase angle surfaces were obtained in darkness and under illumination at 0.4V/Hg_2SO_4. At this polarization the shift of the energy bands, due to the Fermi level pinning, ceases simultaneously with an increase of the anodic photocurrent. The reaction kinetic improves (charge transfer resistance decreases) at the same time to an extent as to generate difussion controlled processes. This is indicated by the phase angle approaching zero at 0.4V/Hg_2SO_4 in figures 1b and 2b, respectively. The interfacial capacity deduced from the Bode curves, after correction of series resistance, turned out to be enhanced at polarization near the redox potential of the reducing species.

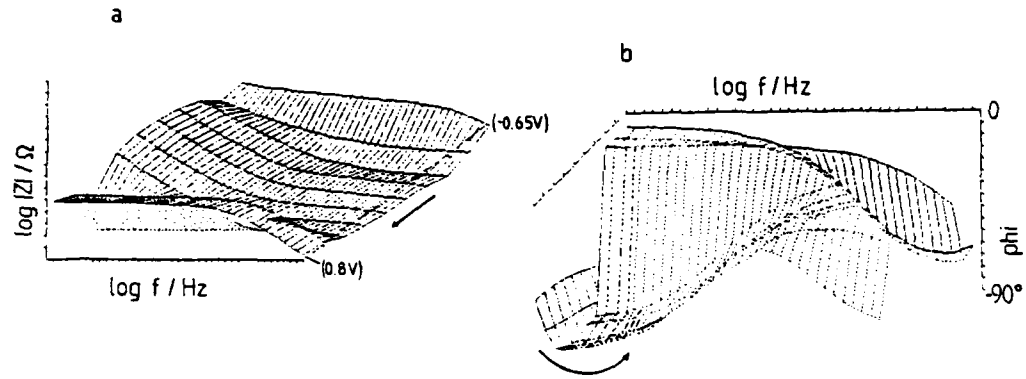


Figure 1. (a) Bode plot and (b) phase angle surface of the system n-FeS_2/0.5M H_2SO_4 + 0.1M Br^- in darkness. Geometric electrode area is 0.029 cm^2. The polarization (*vs* $HgSO_4$) of the curves is related to the drawn lines (1-10) as follows: (1) -0.65; (2) -0.5; (3) -0.35; (4) -0.2; (5) -0.05; (6) 0.1; (7) 0.2; (8) 0.4; (9) 0.6; (10) 0.8V. Arrows indicate the anodic direction.

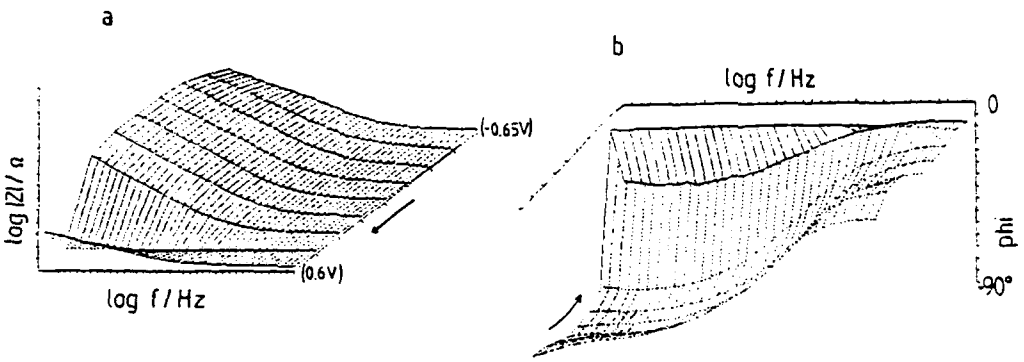


Figure 2. (a) Bode plot and (b) phase surface of the system n-FeS_2/0.5M H_2SO_4 + 0.1M Br^- under illumination using RG-645 cut-off filter. Geometric electrode area is 0.029 cm^2. The polarization (*vs* $HgSO_4$) of the curves is related to the drawn lines (1-9) as follows: (1) -0.65; (2) -0.5; (3) -0.35; (4) -0.2; (5) -0.05; (6) 0.1; (7) 0.2; (8) 0.4; (9) 0.6V. Arrows indicate the anodic direction.

Other experiments carried out on the same system with $Fe(phen)^{2+}$ + Cl^--containing electrolyte [3] showed similar behaviour to that obtained with bromine. This fact demonstrates again that the stabilization of the pyrite/electrolyte interface [2] is due to a coordination chemistry *via* Cl^- at the iron surface states. This is not the case when only the $Fe(phen)^{2+}$-containing electrolyte is present, in spite of it having a similar redox potential ($0.43V/Hg_2SO_4$) with Br^- ($0.46V/Hg_2SO_4$).

Acknowledgement
The authors thank Mr. L. Cramer (Algorithmus) for the development of the surface three dimensional programm.

References:

1. A. Ennaoui, H. Tributsch, J. Electroanal. Chem., **204**(1986)185.
2. X.-P. Li, N. Alonso Vante, H. Tributsch, J. Electroanal. Chem., **242** (1988)255.
3. N. Alonso Vante, X.-P. Li, H. Tributsch, in preparation.

Morphology and Reactivity of Semiconductor Electrode Surfaces Studied by Laser Spot Scanning Technique.

Carlsson[1], P., Holmström[1], B., Uosaki[2], K. and Kita[2], H.

[1]Department of Physical Chemistry,
University of Göteborg,
S–412 96 Göteborg, SWEDEN

[2]Department of Chemistry,
Faculty of Science, Hokkaido University,
Sapporo 060, JAPAN

ABSTRACT

Introduction. The photoelectrochemical properties of semiconductor materials are to a large extent determined by the surface properties of the material. It is well known that scratches, grain boundaries and, in layered compounds, steps between adjacent layers reduce the photocurrent. The reason for this behaviour is that these defects introduce surface states which promote recombination. With the laser spot scanning (LSS) technique it is possible to make laterally resolved studies of the photoelectrochemical properties of semiconductor surfaces. The laser spot generates a photocurrent the magnitude of which is determined by the local properties making it possible to visualize the effect on the photocurrent of grain boundaries and steps (1)–(6).

In this paper we have studied the effect of steps and of Pt treatment of p–InSe in 0.1M K_2SO_4. InSe is a layered compound with layers held together by Van der Waals forces. The most characteristic feature of the surface morphology is steps between adjacent layers. By lifting off layers with adhesive tape it is to prepare a well ordered surface with few steps, making it to correlate surface structure with photoelectrochemical properties.

Experimental. The experimental equipment used, showed in figure 1, is based on a new optical concept. The optical system consists of a step index single mode optical fibre and a Selfoc micro lens. Around the central emitting fibre a bundle of optical fibres is arranged in such a way that they can pick up reflected light. It can also be used for illumination of the electrode with a second light source. With this system a very compact and flexible instrument can be constructed. The minimal spot size which can be obtained with this system is determined by the core diameter of the optical fibre and by the wavelength of the light. In our case we use a HeNe laser (λ = 632 nm) and a corresponding fibre with a fibre core diameter of 4.0 μm. The smallest spot diameter obtained is 4.15 μm. The x–y scan is accomplished with a x–y coordinate table equipped with step motors. The step motor control and the data acquisition are handled by a NEC PC 8801 MR personal computer.

Result and Discussion. The lower part of figure 2 shows the laser spot photocurrent observed then the spot was scanned over a step at the InSe surface. The photocurrent drop at the step also influences the photocurrent over a much larger distance compared to the physical dimension of the step. The reason for this that the laser spot creates a charged semisphere (or semiellipsoid) which moves along with the laser spot. When this sphere reaches the step recombination starts and the

photocurrent decreases. The dimensions of this region is given by the lateral diffusion and the electrochemical reaction rate. In a layered compound there is a two dimensional electronic structure and the diffusion coefficient for minority carriers parallel to the planes is very large compared to the perpendicular one. The dimension of the sphere becomes much larger than laser spot.

In the upper curves in figure 2 the electrode was dip treated for 5 minutes in 20 mM H_2PtCl_4 solution and rinsed with water. In this case the drop in photocurrent is more localized to the step and the resolution is apparently better. Pt treatment of p–semiconductors is known to improve the cathodic photocurrent as it catalyses the hydrogen evolution reaction. The diameter of the charged sphere created by the laser spot is hereby reduced as the electrochemical reaction rate increases.

The effect of Pt treatment can also be seen in figure 3. The electrode was Pt treated by putting a drop of the Pt solution on the electrode and the laser spot was scanned over the treated and the untreated area. A reference point was made by putting a drop of epoxy on the electrode so the Pt treated area could be found. In the area which had been Pt treated the photocurrent is much higher (central parts in figure 3) and in the untreated area the photocurrent is much lower (outer parts in figure 3).

With the laser spot probe used it is possible to pick up the light reflected from the electrode surface. In figure 4 the laser spot was scanned and the photocurrent and intensity of the reflected light were recorded simultaneously. The light intensity increases as the photocurrent increases, a result which was not expected. The reason for this behaviour might be that the platinum is unevenly distributed. This assumption is supported by the observation in figure 3 which shows the effect of Pt treatment on the photocurrent.

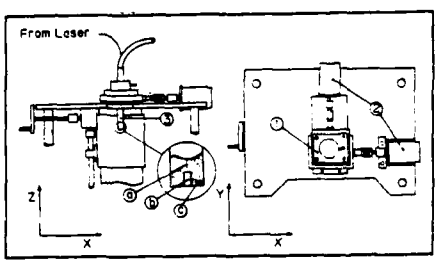


Fig. 1 The experimental equipment used for the LSS experiment. (1) x–y coordinate table. (2) Step motors. (3) Laser spot probe with (a) single mode optical fibre, (b) Selfoc microlens and (c) assembly of optical fibres.

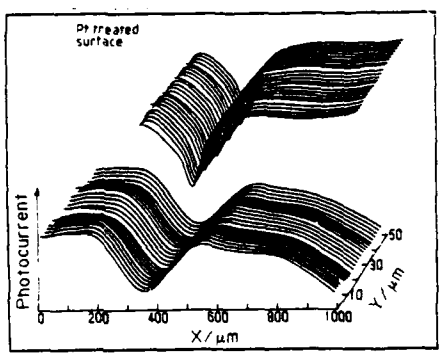


Fig. 2 Line images of the cathodic laser spot photocurrent in 0.1M K_2SO_4 at an InSe surface. The decrease in photocurrent is due to recombination at a step between adjacent layers. The upper curves show the effect of Pt treatment on the cathodic laser spot photocurrent.

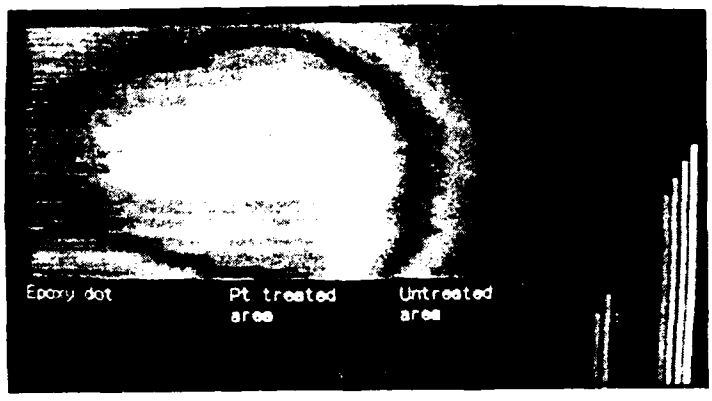


Fig. 3 A computer generated picture showing the effect of Pt treatment on the photocurrent. A drop of 20 mM H_2PtCl_4 was applied onto the electrode for 5 min, which was then rinsed with water. The photocurrent is much higher at the area which was covered with the Pt solutution compared to the untreated area. The scanned area is 400 μm in Y–direction and 1000 μm in X–direction.

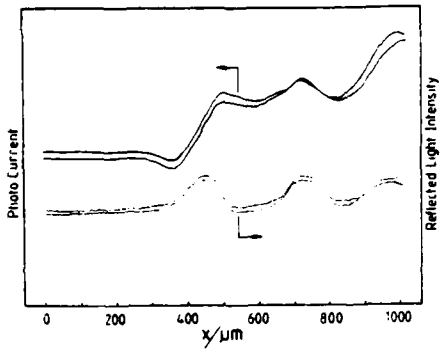


Fig. 4 A line scan showing the reflected light intensity and the cathodic laser spot photocurrent from the same area.

References

(1) F.E. Furtak, D. C. Canfield and B. A. Parkinson
J. Appl. Phys., 51, 6018 , (1980)
(2) M. A. Butler
J. Electrochem. Soc., 130, 2358 , (1983)
(3) M. A. Butler
J. Electrochem. Soc., 131, 2158 , (1984)
(4) C. A. Kavassalis, D. H. Longendorfer, R. A. Le Lievre and R. D. Rauh
Mat. Res. Soc. Symp. Proc., 29, 151 , (1984)
(5) P. S. Tyler, M. R. Kozlowski, W. H. Smyrl and R. T. Atanasoki
J. Electroanal. Chem., 237, 295 , (1987)
(6) D. Shukla, T. Wines and U. Stimming
J. Electrochem. Soc., 134, 2086 , (1987)

3. Microscopic Aspects

THE ADSORPTION OF WATER ON SURFACES: BASIC ASPECTS

Theodore E. Madey
National Bureau of Standards
Gaithersburg, Maryland 20899, USA

This paper addresses recent experimental and theoretical results relating to the interaction of water with clean and additive-dosed single crystal surfaces of metals, semiconductors, and insulating oxides [1]. The experimental results, which are obtained under ultrahigh vacuum conditions, include bonding modes and binding energies of adsorbed H_2O, the molecular vibrational characteristics of adsorbed H_2O, long range and short range order in the adsorbed layer, and information about the local bonding geometry. The theoretical results include cluster calculations of the structure and energetics of H_2O monomers on clean and impurity-dosed surfaces, and molecular dynamics simulations of H_2O on idealized electrodes.

H_2O adsorbed in molecular form is generally bonded to substrates via the oxygen atom. Water is mobile on surfaces, and tends to form hydrogen bonded clusters (even at fractional monolayer coverages), because the strength of the attractive interaction between two molecules is comparable to that of the substrate-H_2O bond.

Specific recent examples to be discussed include evidence for the formation of the smallest adsorbed water cluster, the $(H_2O)_2$ dimer adsorbed on two-fold symmetric Ni(110) and Cu(110) surfaces [2,3]. Larger, ordered clusters are formed on several surfaces having hexagonal symmetry. The influence of impurity adatoms and molecules (e.g., O, Br, HF and CO) on the structure and chemistry of H_2O will be discussed [4-7]. The dissociative adsorption of H_2O on Si(100) [8] and the influence of surface defects on the interaction of H_2O with TiO_2 [9] will also be presented. Finally, there will be a brief discussion of relevant recent theoretical results including ab initio calculations on a Pt_{10}-K-H_2O cluster [10] and Monte Carlo calculations of water adjacent to surfaces [11].

1. For a recent review, see P.A. Thiel and T.E. Madey, Surface Sci. Reports 7, 211 (1987)

2. C. Benndorf and T.E. Madey, Surface Sci. 194, 63 (1988); C Nöbl, C. Benndorf and T.E. Madey, Surface Sci. 157, 29 (1985).

3. M. Polak and T.E. Madey, Surface Sci., in press.

4. K. Bange, T.E. Madey, J.K. Sass and E.M. Stuve, Surface Sci. 183, 334 (1987).

5. K. Bange, T.E. Madey and J.K. Sass, Surface Sci. 152/153, 550 (1985).

6. F.T. Wagner, T.E. Moylan and S.J. Schmieg, Surface Sci. 195, 403 (1988).

7. F.T. Wagner and T.E. Moylan, Surface Sci. 182, 125 (1987).

8. C.U.S. Larsson, A.L. Johnson, A. Flodström and T.E. Madey, J. Vac. Sci. Technol. A5, 842 (1987).

9. E. Roman, R.L. Kurtz, R. Stockbauer, J.L. de Segovia and T.E. Madey, in preparation.

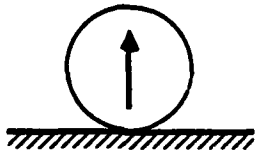
10. H.P. Bonzel, G. Pirug, and J.E. Müller, Phys. Rev. Lett. 58, 2138 (1987).

11. J.P. Valleau and A.A. Gardner, J. Chem. Phys. 86, 4162 (1987).

THE INTERACTION OF DIPOLES WITH METAL SURFACES: BEYOND THE ARROWED CIRCLE?

Stephen Holloway
The Surface Science Research Centre
The University of Liverpool
P.O. Box 147 Grove Street
Liverpool L69 3BX
U.K.

In most elementary electrochemistry textbooks, one often encounters diagrams which portray the interaction of dipoles (i.e. water molecules) with metal surfaces thus:



the aim of the work presented here was an attempt to extend our understanding of the microscopic interaction between a dipole and a "real" metal surface.

I will begin with a brief introduction which will set the conventional picture of image interactions. Following this, I will sketch out an ab initio method for calculating the electronic structure of a metal surface in the presence of a single adsorbate. This technique, based on the density functional formalism, exploits the local nature of adsorption interactions which arises from the efficient nature by which metallic systems screen impurities. We have calculated the self-consistent electronic structure of a dipole with a jellium surface. Unlike the classical counterpart, we find significant assymetries in the behaviour of the binding energy and the dipole moment. Further, it will be shown that using the effective medium approximation, the electrostatic potentials around the adsorbed dipole may be used as an input to more complex calculations concerning the interaction of many dipoles or dipoles interacting with coadsorbed species (e.g. Na or Cl).

Abstract for The International conference on "Chemistry and Physics of Electrified Interfaces", Bologna 29 August-2 September 1988.

Extended Abstract

Individual Ionic Hydration Properties in Relation to Ion Adsorption at Electrodes and the Transition from "Molten - Salt to "Hydrated-Ion" Behaviour at Interfaces

B.E. Conway

Chemistry Department, University of Ottawa,
32 George Glinski Street,
Ottawa, Canada

Evaluation of hydration (solvation) properties of individual types of ions in solution is essential for several aspects of physical electrochemistry: (a) structure of, and interaction in, the double-layer at electrode interfaces; (b) adsorption of ions at electrodes, with and without charge-transfer; (c) discharge of ions, a process that necessarily involves *individual* ions of one sign or the other, and depends in its rate on the reorganization energy of the ion that is intimately determined by the ion's solvation shell or ligand coordination structure and (d) such matters as specificity of ion association at colloids and polyelectrolytes.

The current status of evaluation of several principal thermodynamic properties of individual cations or anions in solution is briefly reviewed.[1]

In electrode processes and electrode interfacial studies, specific anion or cation adsorption is of major significance. When ion adsorption occurs, account must be taken of changes of the ion's solvation in relation to solvation of the charged electrode interface itself (solvent dipole orientation at the electrode and local electrostriction effects). The polarization state of solvent water dipoles at electrodes bearing various charge-densities, q_M, is compared with that at individual ions of various charge-to-radius ratios (ctr).

Current theories of solvent dipole orientation polarization at electrodes deal only with the inner-region monolayer of solvent molecules in which saturation

orientation polarization can be shown to be expected at sufficiently large ± q_M. However, at ions of increasing ctr, no such orientation-polarization saturation is indicated, e.g., by the continuity of the plot of (negative) entropy of hydration *vs* dipole polarization energy, over a wide range of the latter. Hence, by analogy, it seems that a similar situation will obtain at electrode interfaces with increasing ± q_M, so that solvent dipole orientation polarization will not be restricted to the inner-region monolayer except at low ± q_M values. This corresponds to a substantial revision of ideas on the structure of the double-layer at electrode-solution interfaces, as required also by T-dependence of β.

An additional problem regarding solvent orientation is that arising from ion adsorption: At appreciable ± q_M (especially with anions at + q_M), there is a sufficient 2-dimensional density of ions in the double-layer that solvation co-sphere lateral interactions must begin to play a major role in determining both the structure and energy of the interface, because appreciable surface fractions of solvent dipoles are orientationally influenced both by the surface charge-density q_M and by the adsorbed ions' fields in cases where the extent of charge-transfer-to-metal is not large.

Results of new experiments on the transition from "molten-salt" to "hydrated ion" behaviour in the interphasial capacitance at Au and Hg, using $H_3O^+.CF_3SO_3^-$ (molten salt), $H_5O_2^+.CF_3SO_3^-$ and $H_9O_4^+.CF_3SO_3^-$ will be presented[2] that add new insights regarding the structure of the double-layer and the role of solvent in concentrated solutions or a molten salt. Correspondingly, individual anion adsorption is shown to play a major and surface-specific role in the initial stages of noble-metal oxidation[3] [e.g., at the (111), (100) and (110) single-crystal surfaces of Au, and at polycrystalline Au and Pt].

References

1. B.E. Conway, J. Solution Chem., 7, 721 (1978).
2. B.E. Conway and J. Qian, in course of publication.
3. H.A. Kozlowska, B.E. Conway, A. Hamelin and L. Stoicoviciu, J. Electroanal. Chem. 228, 429 (1987); see also Electrochim. Acta, 31, 1051 (1986).

OPTICAL PROPERTIES OF ROUGH METAL SURFACES

M.I.URBAKH

The A.N.Frumkin Institute of Electrochemistry, Academy of Sciences of the U.S.S.R., 117071, Moscow, Leninsky prospect, 31

Real interfaces are always characterized by certain roughness whose degree depends on the actual material, method of surface treatment, presence of adsorbed particles on the surface. The influence of roughnesses on the optical properties of metal surfaces has been studied in numerous experimental and theoretical works. In recent years the interest in this problem has greatly increased. It has been stimulated not only by practical needs, but olso by the discovery of new phenomena associated with the field enhancement near a rough surface, such as an surface enhanced Raman scattering, enhancement of the second harmonic generation and photoemission. Though these phenomena themselves are not completely understood as yet, ample experimental data on the optical properties of rough interface have accumulated.

The aim of the present report is to discuss in a unifide and accesible manner the latest achievements in the optics of rough metal-medium interface and to point out vital problems. The follows topics will be considered:

1.Slightly rough surfaces (the characteristic size of inhomogenities in the direction normal to the surface is less than that in the direction along the surface).
   a.Perturbation theory on the interaction of light with roughnesses.
   b.Resonance interaction of light with surface plasmons.
   c.Localization effects in optics of rough metal surfaces.
   d.Field enhancement.
   e.Main experimental results, diagnostic possibilities of optical methods.

2. Very rough metal surfaces (the characteristic sizes of inhomogenities in all directions are the same order).
   a.Model theories of optical response.
   b.Localized electromagnetic modes, interactions of localized modes with light, with surface plasmons and with one another.
   c.The dependence of the frequences of localized modes on potential drop.
   d.The expression for observable quantities; field enhancement.

3.Optical diagnostics of phase transitions in adsorbed layers and adsorbtion on inhomogeneous electrodes.
   a.Electroreflectance and diffuse light scattering at the point of second order phase transitions.
   b.Potential dependence of the diffuse light scattering due to the adsorbtion on the inhomogeneous electrodes.

4. Biological Systems

EXPERIMENTAL TESTS OF THE GOUY-CHAPMAN THEORY USING PHOSPHOLIPID BILAYERS

Stuart McLaughlin, Marek Langner & Robert McDaniel
Department of Physiology & Biophysics
Health Sciences Center
SUNY, Stony Brook, NY, 11794
USA

Phospholipid bilayers and monolayers have been used to test the Gouy-Chapman theory of the diffuse double layer. This theory predicts how the potential in the aqueous phase at the surface of a bilayer membrane depends on the surface charge density and monovalent salt concentration. Several different experimental techniques demonstrate the Gouy-Chapman theory, as modified by Stern to include ion adsorption, describes adequately the dependence of surface potential on charge density and salt concentration (e.g. McLaughlin, 1977; Eisenberg et al., 1979; Cafiso & Hubbell, 1981; Hartsel & Cafiso, 1986; Winiski et al., 1986). The Gouy-Chapman theory also predicts how the potential should fall with distance from the surface; we have examined experimentally the profile of the potential. The theory assumes the charges on the surface are uniformly smeared over the interface; we examined experimentally the discreteness-of-charge effect on the adsorption of ions to charged membranes.

Profile of the Potential. The Gouy-Chapman theory predicts the potential falls in an approximately exponential manner with distance from the surface. Two techniques have been used recently to provide definitive tests of this prediction. Measurements of the force and distance between bilayer surfaces (Marra & Israelachvili, 1985; Marra, 1986; Pashley et al., 1986) and X-ray diffraction estimates of the distance between bilayers when the force is known (Loosley-Millman et al., 1982; Evans & Parsegian, 1986) both demonstrate that for separation distances greater than 2 nm the Gouy-Chapman theory describes the potential very accurately. Unfortunately, these techniques cannot be used to measure the dependence of potential on distance from a phospholipid bilayer for distances less than 2 nm from the surface: the large forces tend to warp the mica sheets used as substrates for the bilayer in the Israelachvili apparatus (Marra, 1986) and, more importantly, a force of unknown origin, the "hydration force", overwhelms the electrostatic repulsion for distances less than 2 nm from most surfaces (e.g. Loosley-Millman et al., 1982; Israelachvili, 1985). Thus, there is a gap in our knowledge of how the potential adjacent to a phospholipid membrane varies with distance.

Hentschel et al. (1985) approached the problem by making neutron diffraction measurements of the concentration profile of deuterated tetramethylammonium ions between negatively charged phosphatidylglycerol bilayer membranes. Their approach was direct, and the experimentally measured profiles agreed with the values predicted by the Gouy-Chapman theory, but the resolution of this technique is poor.

We approached the problem by making fluorescence measurments (Winiski et al., 1988). We placed a fluorescent probe at a known distance from the membrane-solution interface and quenched its fluorescence with monovalent

cations. The quenching is proportional to the concentration of charged quencher adjacent to the fluorophore. The Boltzmann equation relates this concentration to the electrostatic potential at the location of the fluorophore. Specifically, we attached fluorescent probes to the sialic acid residue of the ganglioside G_{M1}. The sialic acid residue is about 1 nm from the surface of a membrane formed from a mixture of phosphatidylcholine and G_{M1} on the basis of X-ray diffraction experiments (McDaniel & McIntosh, 1986). We incorporated trace concentrations of the fluorescent gangliosides into neutral and charged phospholipid bilayers and quenched the fluorescence with the cations thallium and tempamine. The average potential 1 nm from a negative phosphatidylserine membrane was -30 mV in 0.1 M salt solutions. We also used this technique to measure the surface potential of charged phospholipid bilayers by employing fluorophores that are known to be located at the membrane-solution interface. The average surface potential was -80 mV, which agrees with other measurements. The Gouy-Chapman theory predicts that the potential 1 nm from a membrane with a surface potential of -80 mV is -24 mV; this prediction agrees qualitatively with the experimental results obtained with fluorescent gangliosides.

When the fixed charges are located 1 nm from the surface, the profile of the potential cannot be described by Gouy-Chapman theory but can be adequately described by the more general Poisson-Boltzmann equation (Langner et al., 1988).

Discreteness-of-charge effects. The electrostatic properties of charged bilayers and the bilayer component of biological membranes are often described theoretically by assuming the charge is smeared uniformly over the surface. This is one of the fundamental assumptions in the Gouy-Chapman-Stern theory. However, the average distance between the charged phospholipids in a typical biological membrane is 2-3 nm, which is 2-3 times the Debye length in a 0.1 M salt solution. Most discreteness-of-charge theories predict significant deviations from the Gouy-Chapman-Stern theory for the adsorption of ions to such membranes. We considered the predictions of the simplest discreteness-of-charge theory (Nelson & McQuarrie, 1975), in which the charges are assumed to be fixed in a square lattice and the potential is described by the linearized Poisson-Boltzmann relation. This theory predicts deviations that are larger for counterions than for co-ions and much larger for divalent than for monovalent counterions. We tested these predictions by measuring the adsorption of a fluorescent monovalent anion and a paramagnetic divalent cation to both positive and negative membranes formed from mixtures of monovalent anionic or cationic lipids with the zwitterionic lipid phosphatidylcholine. We demonstrated experimentally that these positive and negative membranes had the same average surface potential by making electrophoretic mobility and conductance measurements. All the experimental results with fluorescent, NMR and ESR probes agreed with the predictions of the Gouy-Chapman-Stern theory rather than with the Nelson and McQuarrie discreteness-of-charge theory (Winiski et al., 1986; Hartsel & Cafiso, 1986). However, a more sophisticated mobile discrete-charge theory, based on the outline of Kjellander and Marcelja (1986), makes predictions that agree with both the experimental results and the Gouy-Chapman-Stern theory (S. Marcelja, personal communication).

In summary, we do not observe discreteness-of-charge effects with monovalent phospholipids such as phosphatidylinositol, phosphatidylserine or phosphatidylglycerol. However, we do observe significant discreteness-of-charge effects with the trivalent lipid phosphatidylinositol 4,5-bisphosphate. This lipid is important because it is the source of two second messengers in many cells.

REFERENCES

Cafiso, D.S., Hubbell, W.L. (1981) Annu. Rev. Biophys. Bioeng. 10, 217-244

Eisenberg, M., Gresalfi, T., Riccio, T., McLaughlin, S. (1979) Biochemistry 18, 5213-5223

Evans, E. A., Parsegian, V. A. (1986) Proc. Natl. Acad. Sci. USA 83, 7132-7136

Hartsel, S.C., Cafiso, D.S. (1986) Biochemistry 25, 8214-8219

Hentschel, M.P., Mischel, M., Oberthur, R.C. Buldt, G. (1985) FEBS Lett. 193, 236-238

Israelachvili, J.N. (1985) Intermolecular and Surface Forces, Academic Press, New York

Kjellander, R., Marcelja, S. (1986) Chem. Phys. Lett. 127, 402-407

Langner, M., Winiski, A., Eisenberg, M., McLaughlin, A., McLaughlin, S. (1988) New Trends in Ganglioside Research (Ledeen, R., Tettamanti, G., Yu, R., Hogan, E., Yates, A., eds), Springer Verlag, New York

Loosley-Millman, M.E., Rand, R.P., Parsegian, V.A. (1982) Biophys. J. 40, 221-232

Marra, J. (1986) Biophys. J. 50, 815-825

Marra, J., Israelachvili, J.N. (1985) Biochemistry 24, 4608-4618

McDaniel, R. V., McIntosh, T. J. (1986) Biophys. J. 49, 94-96

McLaughlin, S. (1977) Current Topics in Membranes and Transport 6, 71-144

Nelson, A.P., McQuarrie, D.A. (1975) J. Theor. Biol. 55, 13-27

Pashley, R.M., McGuiggan, P.M., Ninham, B.W., Brady, J., Evans, D.F. (1986) J. Phys. Chem. 90, 1637-1642.

Nelson, A. P., McQuarrie, D. A. (1975) J. Theor. Biol. 55, 13-27

Winiski, A., Eisenberg, M., Langner, M., McLaughlin, S. (1988) Biochemistry 27, 386-392

Winiski, A., McLaughlin, A., McDaniel, R., Eisenberg, M., McLaughlin, S. (1986) Biochemistry 25, 8206-8214

STRUCTURAL REARRANGEMENTS IN BIOMEMBRANE ELECTRIC FIELDS

Eberhard Neumann and Kinko Tsuji*
Faculty of Chemistry, University of Bielefeld, D-4800 Bielefeld 1,
*Max-Planck-Institut für Ernährungsphysiologie, D-4600 Dortmund,
F.R.Germany

Structure and function of biological membranes are vitally dependent on the electric membrane polarization; prolonged depolarization of the plasma membrane causes cell death.
The natural cross-membrane electric fields affecting the protein/lipid dielectrics are on the order of 100 kV/cm. The inhomogeneous fields originating from ionic groups and adsorbed small ions are of the same order of magnitude; these fields are restricted to the interfacial compartments adjacent to the membrane surface. Externally applied electromagnetic fields which are strong enough to compete with the intrinsic membrane fields, cause structural rearrangements in the proteins and in the lipid bilayer parts.

For example, electro-optic data of aqueous suspensions of purple membranes indicate that bacteriorhodopsin exhibits conformational flexibility in electric field pulses (1-30 kV/cm, 1-100 μs). The electric dischroism shows two kinetically different structural transitions within the protein molecule. The electrically induced rearrangements comprise a rapid ($\approx$ 1 μs), however concerted change in the orientation of both retinal and tyrosine and /or tryptophan side chains. These angular positon changes are accompanied by changes in the local protein environment of the chromophores. A slower relaxation mode ($\approx$ 100 μs) involves alterations in the microenvironment of aromatic amino acid residues and is accompayied by pK-changes of at least two types of proton binding sites, leading to a sequential uptake and release of protons.

Light scattering data are consistent with the maintenance of the random distribution of the membrane discs within the short duration of the applied electric fields.

The kinetics of the electro-optic signals and the steep dependence of the relaxation amplitudes on the electric field strength suggest a saturable induced-dipole mechanism and a rather large reaction dipole moment of $\Delta m = 1.1 \times 10^{-25}$ C m ($= 3.3 \times 10^{4}$ debye) per cooperative unit at $E = 1.3 \times 10^{5}$ V/m. The large reaction dipole moment $\Delta M = N_A \cdot \Delta m = 6.62 \times 10^{-2}$ C m/mol is indicative of appreciable cooperativity in the probably unidirectional transversal displacement of ionic groups on the surfaces of, and within, the bacteriorhodopsin proteins of the membrane lattice.

The numerical value of ΔM thus reflects ionic polarization involving ion pairs of the protein inclusively the intrinsic Ca/Mg-ions and the ionic atmosphere of the entire membrane disc.

The data of detergent treated purple membranes suggest that detergent binding interferes with the protein/protein lattice interactions. At low concentrations of Triton X-100 the detergent appears to loosen the crystalline-like bacteriorhodopsin lattice structure. At higher detergent content, however, the protein/protein contacts seem to be strengthened, facilitating long-range interactions. Finally, at very high detergent concentration the protein lattice is dissolved.

Photobleaching disrupts the retinal Schiff's base bond. Thereby the internal fluidity of the protein increases as well as the internal flexibility of the neighbouring unbleached proteins. The bleaching experiments suggest that the protein polarization in external electric fields is independent of wether the retinal is covalently bound or not. Furtheron, the field-induced uptake and the release of protons are not affected by the state of the neighbouring proteins. The proton transfer is directly coupled to the existence of the intact Schiff's base.

Adressing the functional aspect of field-induced structural rearrangements in bacteriorhodopsin there are some similarities between the photocycle and the electro-optic cycle of rotational chromophore displacements and conformational transitions in the protein part. In particular, there is a hyperpolarizing increase in the absolute value of the electric membrane potential difference during light-induced proton pumping. This increase in the membrane field is concomitant with a decrease in the proton transport.

The temporal coincidence and the opposite sequence of field-induced pH-changes compared with the light-induced pH-changes suggest a direct functional role of the electric field changes. The increase in the electric membrane field resulting from proton pumping may exert a negative feed-back (reducing proton transport) via an electric field effect directly on the structure of bacteriorhodopsin, switching off pump activity.

A further functional aspect of the bacteriorhodopsin data may be of general fundamental importance. Compared with the rapid induction of the electric field-mediated structural changes (μs range), annealing of the changes after the electric impulse is very slow (ms). The field-induced conformational transitions therefore exhibit memory properties.

It may be recalled that electric field-induced, long-lived structural changes have been suggested as a mechanism for the initial, physical step of biological memory recording.

Besides the field-induced conformational changes in membrane proteins the phenomena of electroporation and electrofusion are impressive examples for electrically induced structural rearrangements most probably in the lipid part of biomembranes. Both electroporative gene transfer and electrofusion are of great importance in cell biology and biotechnology.

Support by DFG (grant Ne 227/4) ist greatfully acknowledged.

Ref.:

1. K.Tsuji, E.Neumann, Biophys.Chem. 17, 153-163 (1983); FEBS Lett. 128, 265-268 (1981).
2. E.Neumann, Bioelectrochem.Bioenerg. 13, 419-428 (1984).
3. E.Neumann, Prog.Biophys.Mol.Biol. 47, 197-231 (1986); Comments Mol.Cell.Biophys. 4,121-141 (1987)
4. I.Sugar, E.Neumann, Biophys.Chem. 19, 211-225 (1984); Biophys.Chem. 26, 321-335 (1987).
5. K.Tsuji, E.Neumann (1988), in prep.

THE APPLICATION OF THE LASER INDUCED PROTON PULSE FOR MEASURING CHARGE TRANSLOCATION ACROSS BIOMEMBRANES

Menachem Gutman and Esther Nachliel

Laser Laboratory for Fast Reactions in Biology, Dept. of Biochemistry, The George S. Wise Faculty of Life Sciences, Tel Aviv University, Israel

---

Bioenergetic processes are driven by a proton potential gradient built across the membrane of specialized subcellular organelles. In our lecture we shall demonstrate how the combination of the laser induced proton pulse and time resolved current measurements can be instrumental in the study of reactions coupled with this gradient.

The laser induced proton pulse is a fast perturbation method. The basic event is the pK shift of aromatic alcohols when photoexcited to their first electronic singlet state. In the excited state the hydroxyl proton dissociates and diffuses out of the Coulomb cage. When the excited anion relaxes to the ground state, the system is poised in an acid-base disequilibrium. The discharged protons are usually detected by their diffusion controlled reaction with pH indicators (1,2). In the present case we monitored them by electric current measurements (3).

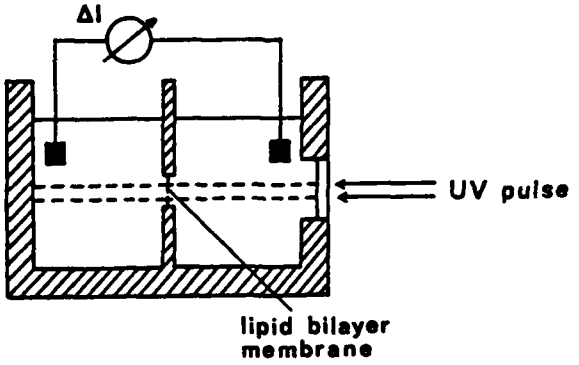


Fig. 1. Schematic presentation of the observation cell.

The observation cell (Fig. 1) contains a small phospholipid black lipid membranem (1 mm in diameters) separating two cells filled with 0.1M cholin chloride as conductive electrolyte. On one side a proton emitter (8 hydroxy pyrene 1,3,6 trisulfonate) is present. When excited by laser pulse, the dye emits a proton which reacts with one side of the membranes, i.e. charging the membrane capacitor. As the resistance of the membrane to protons is very high, the voltage is discharged through the external measuring circuit.

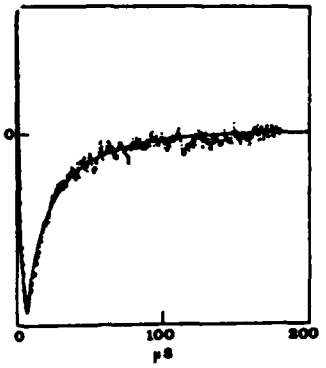
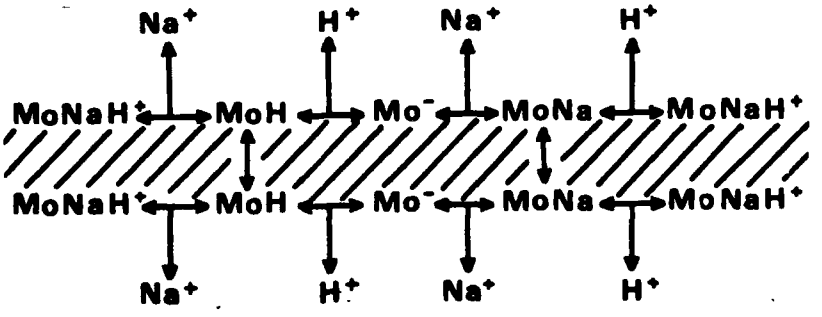


Fig. 2. Transient current measured during pulse protonation of a black lipid membrane made of phosphatidyl cholin (PC) and phosphatidyl serin (PS) at 6-4 molar ratio. The continuous line is reconstruction of the current curve by numerical solution of differential equation.

Fig. 2 depicts a current transient corresponding with reversible protonation of phosphatidyl-serine headgroups (PS) on a black lipid membrane. This tracing is essentially identical with the first time derivative of the compound's state of protonation (d(PSH)/dt). The dynamics of phosphatidyl-serine protonation has been studied on micellar surface and reconstructed by numerical solution of coupled, non linear differential equations. As seen in Fig. 2, the rate constants deduced from chemical kinetic measurements reconstruct the electric transient of the membrane charging. Consequently we can utilize current measurements for identification of chemical events associated with pulse protonation of one face of a membrane.

We applied this method for investigating the mechanism of ion translocation by monensin. This ionophore (4) forms hydrophobic, uncharged complexes with proton H^+, Na^+ or K^+. Due to this property monensin carries an electroneutral exchange of these ions across biomembranes.



Scheme I. The reaction steps involved in pulse protonation of a membrane impregnated with monensin.

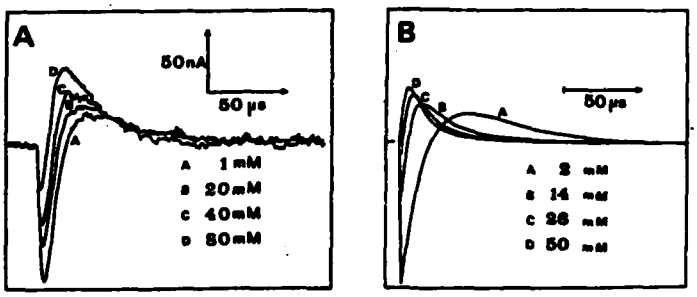


Fig. 3. A - current transient recorded after proton pulsing of a PC+PS black lipid membrane in presence of monensin and increasing K^+ concentrations. B - Simulation of the current transient by numerical solution of differential equation pertinent to the system described in scheme I.

Studying the mechanism of ion transport by monensin is restricted by two inherent limitations: (A) the diffusing carrier-cation complex is uncharged and (B) monitoring of ion concentration in the bulk phase can reveal only the slowest, rate limiting, step of the whole process.These limitations are circumvented by application of the laser induced proton pulse. The large perturbation synchronizes a massive protonation of the membrane bound carrier, which charges the membrane capacitor. The relaxation of this charge is modulated by all chemical steps defined in Scheme I. It is the combination of all charge producing reactions on the two sides of the membrane which produce the current signal shown in Fig. 3A. The deduction of the dynamics of the individual chemical reactions must rely on global analysis, where all reactions defined in Scheme I are combined into a set of coupled nonlinear parametric differential equations and solved by numeric integration. Fig. 3B depicts the current signal reconstructed by such procedure. It reproduces both shape of signal and its dependence on the metal ion concentration.

In our lecture we shall consider the magnitude of the various rate constants and their effect on the overall observed dynamics.

References

1. M. Gutman, Methods in Enzymology 127: 522-538, 1986.

2. M. Gutman, Methods Biochem. Anal. 30: 1 - 103, 1984.

3. M. Gutman, E. Nachliel, E. Bamberg and B. Christensen, Biochim. Biophys. Acta 905: 390-398, 1987.

4. B. G. Cox, P. Firma and H. Schneider, J. Am. Chem. Soc. 107: 4297-4300, 1985.

"A Gradient of the Electrochemical Potential of the Proton, Driving Force and Modulator of Proton Transfer at the Biological Membrane/Water Interface"

R. Naumann, E. Merck, Postfach 4119, D-6100 Darmstadt, FRG

Proton transfer at the biological membrane/water interface is assumed to occur due to the imbalance or protonation equilibria of chemical reactions taking place mostly within the membrane phase. This assumption is in agreement with experimental findings, e.g. K. Matsushita and H.R. Kaback, Biochemistry 25 (1986), 2321. Free protons thus obtained exchange with the aqueous phases via charged protein macromolecules embedded in the membrane. The double layer at the interface is seen as a accumulation of (or depletion from) protons released from or consumed by the above mentioned chemical reactions. Due to the proton profile (experimental evidence of it was given by A.G. Volkov, J. Electroanal. Chem. 205 (1986), 245 and R. Kraayenhof, F.A. de Wolf, H.S. van Walraven and K. Krab, Bioelectrochem. Bioenerg. 16 (1986), 273) in the immediate vicinity the interface, the kinetics of proton transfer is taken to be controlled by a $\Delta\mu_{H+}$ rather than a $\Delta\psi$ alone. The Butler-Volmer equation is modified in terms of an electrochemical overpotential of the proton which is regarded to overcome the activation barrier of proton transfer at the membrane/water interface (L.I. Krishtallik, J. Electroanal. Chem. 204 (1986) 245). This is shown to be formally equivalent to an approach brought forward by Y.Y. Gurevich and Y.I. Kharkats, J. Electroanal. Chem. 200 (1986), 3, to the transfer of heavy particles (ions) under the influence of an electric field and with the concentration of the ions at the interface not at equilibrium with the bulk phase. Furthermore self-induced oscillations of the interfacial $\Delta\mu_{H+}$ are discussed in terms of their rectifying properties for transmembrane proton transport. This is explained on the basis of the theory of metastable states and hysteries of polyelectrolytes by A. Katchalsky and R. Spangler, Quarterly Review of Biophysics 1 (1968), 127.

PHOTO INDUCED TRANSMEMBRANE ELECTRON TRANSFER IN MODEL SYSTEMS FOR PHOTOSYNTHESIS

+SETA P., +BIENVENUE E., ++MOORE T.A., ++MOORE A., ++GUST D.

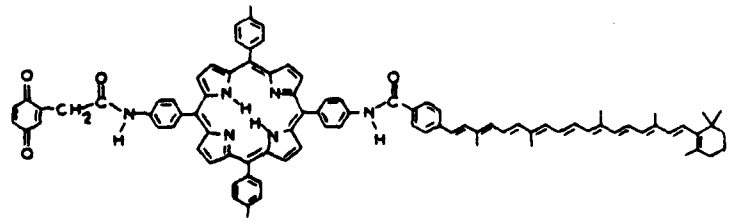
+ Laboratoire de Physico-Chimie des Systèmes Polyphasés - UA 330 - CNRS - Route de Mende -BP 5051 - 34033 Montpellier - France

++ Department of Chemistry - Arizona State University - TEMPE - Arizona 85287 - USA

In natural photosynthetic membranes light is absorbed and converted into electrochemical energy in the form of charge separated species belonging to the reaction center. The latter is composed of pigments (chlorophylls) and other redox components acting as electron donors and acceptors, embedded in a protein matrix. The entities have intramembrane positions and orientations which seem to be crucial for the efficiency. The fact that the primary electron phototransfer is followed by fast secondary electron transfers is the basis of the energy conversion process. The stabilization of the charge separation is sufficient for the corresponding energy to be utilized for various chemical processes, the kinetics of which covering much longer time scales as the primary events.

Many attempts of mimicking the charge separation across membranes have been achieved with compounds such as porphyrin-quinone molecules, called "diads", in which the charge separation occurs between an electron donor D and an electron acceptor A, giving rise to a radical pair D^+A^-. Unfortunately the lifetime of the charge separated state never lasted longer than a few tenths of a picosecond, which is too short a duration to allow subsequent reactions. As in natural systems the problem was solved by the design of superstructured molecules called "triads" or "tetrads" built of three or four centers along which a multistep electron transfer occurs. We report the energy conversion obtained at the membrane level with a carotenoporphyrin-quinone I (See Figure) The primary donor -a porphyrin is covalently linked to the acceptor a quinone-, and to the secondary donor -a carotenoid. Optical and electrochemical experiments have been performed to confirm the intramolecular and transmembrane charge separation.

Triad : Q-P-C



a) Spectroscopic experiments

A solution of the triad I in methylene chloride showed under visible light illumination a transient absorption with λ_{max} = 970 nm and τ = 400 ns which is assigned to the formation of the carotenoid radical cation C^+ : Under light excitation, the singlet excited state of the porphyrin is depleted, giving rise first to the transient species $C\text{-}P^{+}\cdot\text{-}Q^{-}\cdot$; then, $C^{+}\cdot\text{-}P\text{-}Q^{-}\cdot$ is formed by a second electron transfer step which competes with the back reaction. The potential energy stored in the photoseparated biradical ion-pair is more than 1 eV. When the triad was incorporated into liposomes, a transient absorption due to the formation of the $C^{+}\cdot\text{-}P\text{-}Q^{-}\cdot$ state was also observed. When a reducing agent (ascorbic acid) was added outside the liposomes a 50 % decrease of the initial absorption was measured, due to the formation of only a half of the $C^{+}\cdot\text{-}P\text{-}Q^{-}\cdot$ intermediates. The quinone groups facing the external aqueous solution are reduced by the ascorbic acid. The species $CPQH_2$ formed cannot undergo charge separation because the QH_2 moiety is already reduced. Furthermore, the ascorbic acid quenches the decay of the biradical transient signal, indicating that the electron depleted carotenoid groups facing the external solution are reduced. These results are consistent with a structural arrangement in which the triads span the membrane, and only the molecules having their quinone group facing the internal solution participate in charge separation.

b) Electrical experiments

Planar bimolecular lipid membranes (BLM) have been formed from lipid solutions in hydrocarbon solvents interposed between two redox phases, a reducing one (ascorbic acid) and an oxidizing one (potassium ferricyanide). After incorporation of the triad I into the membrane forming solution, photocurrents were recorded between two silver, silver chloride electrodes dipped in the aqueous phases on each side of the membrane (the membrane was light excited in the absorption spectrum of the porphyrin moiety). Excitation of the porphyrin generates by successive electron transfers the biradical $C^{+}\cdot\text{-}P\text{-}Q^{-}\cdot$. The quinone radical anion on the side of the membrane facing the potassium ferricyanide solution is oxidized to regenerate the neutral quinone ; and the carotenoid radical cation facing the ascorbic acid solution accepts an electron to regenerate the neutral carotenoid. The result of these electron transfer steps is the net transfer of an electron from one side of the membrane to the other side, and regeneration of the photocatalyst. If either the extrinsic electron donor or acceptor is omitted, no steady state photocurrent is observed.

A characteristic feature of the photocurrent is its very fast risetime (< 1ms), faster than that of the shutter used to generate light pulses, revealing a very fast electron transfer rate. The linearity of the current to voltage relationship obtained under light excitation points to a transfer process that cannot be considered as dependent of a single activation barrier. The process could be either tunelling, or a through bong mechanism composed of several intramolecular electron transfer

steps, each step depending on a small fraction of the external applied membrane potential. The understanding of unimolecular electron transfer processes between fixed acceptor and donor centers is the basis of the progress in biomimetic energy conversion systems.

THE HELMHOLTZ FORMULA AND THE MEMBRANE POTENTIAL

Daniel SCHUHMANN

Laboratoire de Physicochimie des Systèmes Polyphasés
UA 330 - Route de Mende - BP 5051 - 34033 Montpellier Cedex
France

INTRODUCTION

Since Helmholtz, the surface potential ΔE_{dip} due to a distribution of dipoles on an infinite plane is usually expressed as :

$$\Delta E_{dip} = M_{\perp} N / \epsilon_v \qquad (1)$$

where ϵ_v is the permittivity of vacuum, $M_{\perp}$ the perpendicular component of the dipole moment and N the surface density. Using the Coulomb's law for dipoles and neglecting the size of the species bearing the dipoles, it may be shown that this expression is valid when the latter are localized in vacuum only. If the medium around them has a permittivity ϵ, it has been shown that ϵ_v in eq. 1 should be replaced by ϵ [1].

However, in general and especially in the case of membranes, the thickness of the plate bearing the dipoles cannot be neglected and its permittivity is different from those of the media of each side of the plate. The potential distribution is thus affected by imaging effects. With at least two mirrors, the number of images becomes infinite. However, the calculation can be simplified even for a foliated system containing layers with different permittivities using a method proposed by Smythe [2] using the Fourier-Bessel transform for calculating the potential due to a point charge in the vacuum near a dielectric film. This method is here generalized for several films in contact containing uniform distribution of dipoles.

THE TREATMENT

Details on the calculation are given for one film (Fig. 1). In a first step, the potential created by a point charge q at the origin of the z axis is calculated. If this charge was in the infinite medium 2, it would create the potential $V_0(q)$:

$$4\pi \epsilon_2 V_0(q)/q = 1/r = \int_0^{\infty} J_0(k\rho) e^{-k|z|} dk \qquad (2)$$

J_0 being the Bessel function of zero order. The presence of other dielectrics leads to other components in the phases i such as :

$$4\pi\varepsilon_2 V_i(q)/q = \int_0^\infty F_i(k)\, J_0(k\rho) e^{-kz} dk + \int_0^\infty G_i(k)\, J_0(k\rho) e^{kz} dk \qquad (3)$$

with $F_1 = G_3 = 0$. These functions are determined by equating the functions V_i and $\varepsilon_i \partial V_i/\partial z$ for two adjoining phases at their boundaries. As shown by Smythe, the boundary conditions are satisfied if the equalities are written for the integrands. F_i and G_i are thus derived from a system of first order algebraic equations :

$$G_1 - F_2/A - G_2 = 1 \; ; \; G_1 + KF_2/A - KG_2 = K \; ; \; F_2 + G_2/B - F_3 = 1 \; ;$$

$$- LF_2 + LG_2/B + F_3 = L \qquad (4)$$

with

$K = \varepsilon_2/\varepsilon_1$, $L = \varepsilon_2/\varepsilon_3$, $A = \exp(-2ka)$, $B = \exp(-2kb)$, $C = \exp(-2kc)$

and one finds :

$$(1+K)\, G_1/2K = (1-fB)/(1-dfC) \; ; \; (1+L)\, F_3/2L = (1-dA)/(1-dfC) \qquad (5)$$

with $d = (1-K)/(1+K)$ and $f = (1-L)/(1+L)$.

A component such as $u \int_0^\infty J_0(k\rho)\, e^{k(pz-s)} dk$ obtained in expanding the above expressions is equivalent to the potential due to the charge u at $z = s/p$.

In a second step, a charge-q is placed at another origin distant from 1 of the former, creating a dipole of moment $\mu = lq$. The images due to G_1 are to the right of the film. Those due to $1/(a-dfC)$ and $V/(1-dfC)$ may be easily shown to have different signs. In an infinite medium (ε) the potential at each side of a plane distribution is $\pm \mu N/(2\varepsilon)$. Finaly the potentials $V_i(M)$ in phases i may be obtained without expanding the equations 5 in infinite image components and one finds :

$$V_1(M) - V_3(M) = \mu N/\varepsilon_2 \qquad (6)$$

while separately V_1 and V_3 depend also on ε_1 and ε_3.

In the case of membranes (see Fig. 2), it may be assumed that the permittivities of the surface regions bearing the polar heads are different from that of the inner paraffinic part and the system is now characterized by five permittivities. The same method of calculation was used with now eight unknown properties F_i or G_i instead of four. Whatever the

region i where point dipoles are localized, one finds :

$$V_1(M_i) - V_5(M_i) = M_i N_i / \varepsilon_i \qquad (7)$$

Similar expressions may be obtained for foliated systems containing more than three films. In the case of membranes, taking into account dipoles in both surface regions, the potential distribution is obtained by summing the contributions of both faces. If the membrane is symmetrical ($M_2 = M_4$) $\varepsilon_2 = \varepsilon_4$, $N_2 = N_4$, $V_1 = V_5$; in other words, the dipoles bear no contribution to the membrane potential. In contrast any asymmetry due to dipole orientation ($M_2 \neq M_4$) or variation of their surface density due for example to uniform implanting of solutes ($N_2 \neq N_4$) eventually acting also on ε can lead to a finite surface potential V_m. The distribution in the different phases may be calculated and assuming now that the size l of the dipoles is pratically equal to the thickness of phases 2 and 4, this distribution is represented in Fig. 3. The value of V_m deriving from such an assymmetry could be non negligible. The dielectric constant of the polar regions is unknown but is probably between 1 and 10. Taking 5, 0.5 nm for the charge separation and a density corresponding to an area of 0.4 nm^2, each face leads to a potential equal approximately to 0.5 V and an asymmetry of 10 % to a value of V_m equal to 50 mV.

REFERENCES

1 - D. Schuhmann, J. Electroanal. Chem., 201, 247 (1986).

2 - W.R. SMYTHE, Static and Dynamic Electricity, 2nd Ed., Mc Graw Hill, New York, 1950, p. 182.

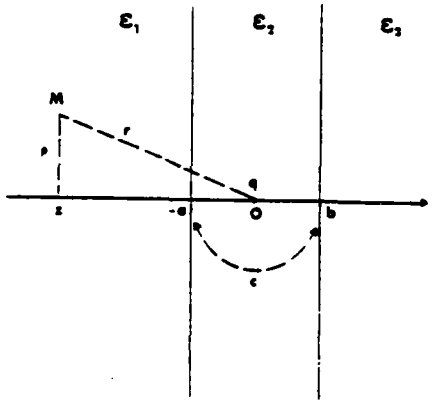


Fig. 1

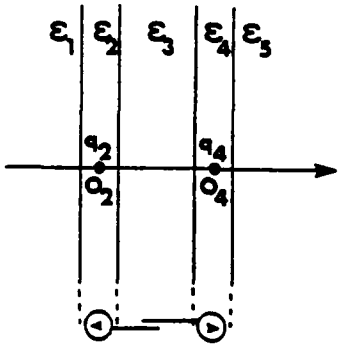


Fig. 2.

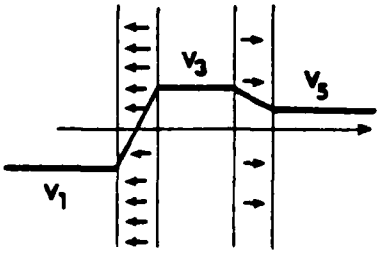


Fig. 3

PHASE TRANSITIONS INDUCED BY AN ELECTRIC FIELD IN BLACK LIPID MEMBRANES.

M.Robello and A.Gliozzi

Dipartimento di Fisica dell'Universita' di Genova
16146 Genova-Italy

In the past years only a limited number of works had appeared on phase transitions of black lipid membranes. These transitions are induced by changes in temperature and consist of the so called liquid crystal-gel main transition, essentially related to the melting of the hydrophobic chains. It has been shown that this transition is characterized by steep changes in electrical parameters such as conductance and capacitance. Besides the main transition, other structural changes have been observed especially in black membranes made from bipolar lipids. The main role of these changes seems to be played by the polar head groups of neutral lipids, which can be regarded as an ordered bidimensional system of electrical dipoles. Such a system can undergo ferroelectric or antiferroelectric phase transitions at a critical temperature, whose value can be affected by the presence of an external electric field. However it is well known that applying a potential of the order of few hundred millivolts the membrane breaks and the possibility of observing the effect of an electric fields is limited by such a value. We have therefore performed current-voltage measurements under current clamp conditions rather than in voltage-clamp conditions. At a certain critical value of the potential the membranes displayed a sharp transition to a higher con-

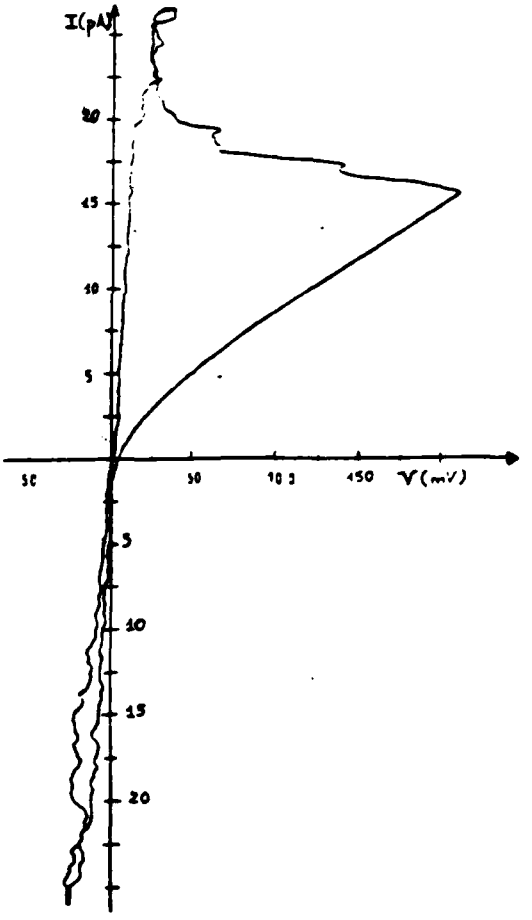


Fig.1 I-V curve of a membrane in current-clamp condition.

ductance, as indicated in Fig.1. Correspondingly the capacitance of the membrane was increased. Results refer to membranes made of egg lecithin, diphytanoyl lecithin, cholesterol-lecithin mixtures and some other lipid systems in which such a transition is not observed. The discontinuity in conductance and capacitance is qualitatively interpreted, in terms of a simple electrostatic model, as a structural change of the dipole structure induced by the electric field.

SOME PROBLEMS IN ELECTROARTERIOGRAPHY

ANTON, C.G., VAZQUEZ, J.L., MEDRANO, J. * FELIU, J.M., * ALDAZ, A.

Departamentos de Cirugia y * Quimica Fisica, Universidad de Alicante
Apartado 99, 03080 Alicante, SPAIN.

INTRODUCTION:

The earlier works of Sawyer et al (1) have shown the existence of a potential drop through bood vessel, variable and proportional to the blood flow. The experimental technique, involved to micropipetes crossing the vessel wall. By using this invasive technique it was demonstrated that the best recording conditions where when the interelectrode distance was a ten fold the arterial diameter under study.

Findl et al (2) have shown that this potential drop can be measured by using a non invasive technique, by means the direct contact between the electrode and the skin over the arterial vessel. The technique uses two Ag-AgCl electrodes separated ten fold the arterial studied diameter. Both electrodes are conected to an electrometer input, and the common mode electrode was placed near of the active ones, this metode was called "Electroarteriography".

EXPERIMENTAL:

We have obtained similar responses by using a modification of this method which can be called "Monopolar Electroarteriography".

In this method a single active electrode was put in contact with the femoral arteria of an anaesthesiated dog. The active electrodes, 2x5 mm in lengt, were directly put in contact with the blood vessel and connected to the positive input of the electrometer, whereas the negative one was located in a place out of the chirurgical field.

The technique can also be used in human studies in a non invasive manner, as in the Findl method (2). The electrode had a size of 2x5 mm for the pedia and radial arteries, and 10-20 mm for the femoral and carotid arteries and was placed in the maximal pulsatile zone. The common mode electrode had 30x40 mm size and was placed on the ankle for pedia and femoral arteries, on the anterior fore-arm for the radial artery and on the front for the carotid.

With this experimental arrangement, the interference of the electrocardiographic (ECG) signals were minimized.

It was built an amplifier with selected qualiti components. The input impedance was 10^{12} ohms, common mode rechace 120 dB, passing 0,5-20 Hz. Curves were recorded with a battery suplied apparatus in order to avoid any external periodical signals.

RESULTS:

We have verified the following statements:

1) The electroarteriographic wave shapes obtained by our method have the same characteristic features as those obtained with another flow measurement methods (3). In figure 1, it can be seen: (a) a fast forward flow due to cardiac systole reaching a peak velocity, (b) a back flow phase following inmediately afterwards reaching a more rounded peak velocity and falling off more gradually than the systolic phase, (c) a

forward flow following the back flow, and (d) a short and small back flow inmediately preceding systole.

2) In the electroarteriogram the flow from the heart to the active electrode gives negative potential values, and the flow to reverse side gives a positive ones. In some cases it has been observed a inversion of this response, both in the dogs femoral artery, when the external pressure on the electrode increased, the same fact was obtained in the human pedia artery, but this later case it was probably due to the faillure of the vessel (figure 2).

3) The intensities of the electroarteriographic waves changes both, whith the external pressure exerced on the electrode as by modifications in the electrolite composition between electrode-skin; i.e the dog femoral electroarteriogram diminishes when physiological solution is added to the experimental arrangement. (figure 3).

CONCLUSION:

The main conclusion is that the registred curves seem to be a response to a gret numbers of variables. However, this technique may be useful for the systolic interval times measurement, i.e. the report between the electroarteriogram and the peripheral arteries flow wave. It must be pointed out that there is not yet a well-defined method to quantify the absolute value of the blood flow from the electroarteriographic measurement.

REFERENCES:

1) Sawyer, P.N; Himmelfarb, E; Lustrin, I and Ziskind, H. Biophysical Journal 6 (1966) 641-651

2) Findl, E; Conti, J.C; Strope, E.R; Milch, P.O; Griffiths, C.L and Kurtz, R.J. Bioelectrochemistry and Bioenergetics, 12 (1984) 3-14.

3) McDonald, D.A; J. Physiol, 127 (1955) 533-552.

CAPTIONS:

Figure 1: Simultaneous recording of the electrocardiogram (ECG) and the electroarteriogram (EAG) obtained at the pedia human arteria. The different parts of the EAG are shown (see text)

Fifure 2: Progressive change in the EAG shape recorded in the same conditions as in figure 1.

Figure 3: EAG voltage response to the external pressure change over the indicator electrode. Human femoral artery.

Figure 1

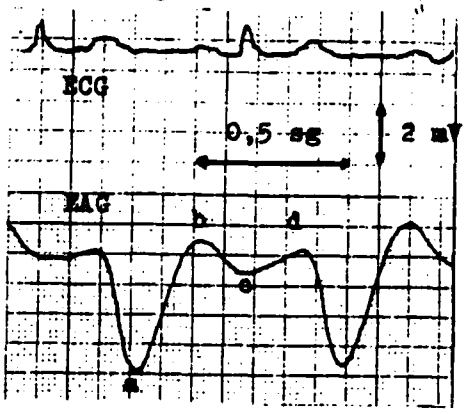
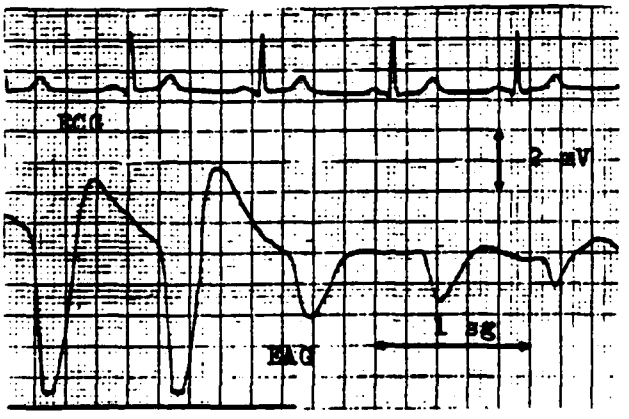


Figure 2



Figure 3



High Pressure

LATERAL PROTON CONDUCTION ALONG LIPID MONOLAYERS AT THE AIR/WATER INTERFACE

Prats M., Tocanne J.F. and Teissié J.
Centre de Biochimie et de Génétique cellulaires du CNRS, Toulouse,FRANCE

Experimental evidences have been gathering which suggest that lateral proton conduction may occur along restricted domains in biological membranes. A "microlocalized" pathway would then link the proton pump and the proton sink in a coupling unit and the exchanged proton would not need to be delocalized in the bulk water phase (1).

Results

In order to provide a direct experimental evidence to the "localized" proton transfer, we developped an approach using a fluorescence assay on lipid monolayers spread at the air/water interface (2). A pH sensitive chromophore was covalently bound to the polar group of a phospholipid and provided a reliable probe of the proton concentration in the interface region when embedded at a low concentration in the host lipid matrix (3). Following a pH jump close to the interface, transfer of proton was observed specifically along the interface (2, 4) and the thickness of the proton conductive pathway was estimated by surface potential measurements (5). The transfer occured along the polar headgroups when the film was organized (2). It was modulated by the nature of the polar head groups and was observed only in the liquid expanded (LE) state of the film (6). No conduction was detected when the film was compressed to the liquid condensed (LC) and solid condensed (SC) states (6). Ca^{++} inhibited the transfer specifically in the case of phosphatidylethanolamine (PE)(6).

Discussion

From what is known on proton transfer in solution (7), we proposed that our experimental observations were linked to a network of hydrogen bonds at the level of the polar head groups(6). Any theoretical attempt to describe chemical reactions such as proton transfer at the membrane/water interface must take into account the peculiarities of the system.

Reduction in dimensions As nicely told in "Flatland" (8), processes in a bimensional array (R^2) are different from what occurs in a tridimensional volume (R^3). The bulk aqueous phase belongs to R^3 but the membrane is a bidimensional network with a given thickness and must be pictured as R^2+P. The polar headgroup region is conveniently described by P^2. Classical diffusion processes as described by the Fick laws are no more valid at the level of charged interfaces. Indeed very little work has been devoted to the analysis of ion diffusion in the double layer. As shown in (9), the ion dynamics should be described by the Smoluchowski diffusion equation and the average electrostatic field. The electrostatic interactions present in the electrically perturbed layer adjacent to the membrane may enhance reencounter effects.

Water at charged interfaces Computer simulations of liquid water between walls showed that the water structure near the wall tends to be more ice like (10). This was described in a more thermodynamical way by taking into account the spatially varying electric field expected to be present in the vicinity of a charged surface (11). In the case of phosphatidylcholine (PC), one of the most abundant lipid in biological membranes, the electric field space dependence was very complex. The molecular structure of the polar head region is now rather well known (12). The tilt of the phosphocholine residue with respect to the membrane surface, assumed to be flat, induced a small dipolar field of opposite direction with the one originating from the ester group region. As a

consequence, a strong dielectric anisotropy is present in the interface region (13). Another feature of this organisation is that the electric field reverses twice in the interface layer. An important property of the polar head region is its ordered organization with the occurence of hydrogen bonding. Hydrogen bonding and steric restrictions limit the orientation of water molecules at the interface giving rise to a polarization in the aqueous phase. Close to the surface, water molecules will be preferentially oriented with both hydrogen atoms pointing towards the water phase (14).

Localization	Dimension
Hydrophobic core, fatty acid chains	R^2+R
Charged interface layer:	
-ester linkage	R^2
-polar head group	
Electrically perturbed layer:	
- oriented water molecules	R^2
- double layer	R^2+R
Bulk water phase	R^3

Fig. 1: Organization of the water/phospholipid interface layer

Conclusions Reduction of dimensions, organization of adjacent water molecules, electric field inversion and hydrogen bonding should be taken into account when trying to describe proton transfer at the lipid/water interface. This was not the case in studies concluding to a delocalized pathway either from a theoretical point of view but by use of Fick laws (15) or from experiments on micellar systems where the interface organization is far from what occurs in pure phospholipid models (16).
As a general conclusion, description of the exchange steps involved in the lateral proton conduction we observed is still lacking at the present stage of investigations. The complexity of the processes favors the experimental approaches as developped in our laboratory and by others (17) which both conclude on repeating hopping of protons along the surface. Furthermore our observations that this translocation is controlled by the organization of the matrix suggest that its occurence in biological membranes may be restricted to specific domains and can be hindered by protein networks in agreement with the results on appressed thylakoids (18).

References:
1- Kell D.B. (1979) Biochim.Biophys.Acta 549, 55
2- Teissié J., Prats M., Soucaille P. and Tocanne J.F. (1985) Proc. Natl. Acad. Sci. USA, 82, 3217
3- Soucaille P., Prats M. Tocanne J.F. and Teissié J. (1988) Biochim. Biophys. Acta, 939, 289
4- Prats M., Tocanne J.F. and Teissié J. (1985) Eur. J. Biochem., 149, 663
5- Prats M., Teissié J. and Tocanne J.F. (1986) Nature, 322, 756
6- Prats M., Tocanne J.F. and Teissié J. (1987) Eur. J. Biochem., 162,379
7- Onsagers L. (1969) Science, 166, 1359

8- Abbott E.A. in "Flatland" (1952), Dover Publ., New York
9- Chan D.Y.C. and Halle B. (1984) Biophys. J., 46, 387
10- Spohr E. and Heinzinger K. 51986) J. Chem. Phys., 84, 2304
11- Gruen D.W.R. and Marcelja S. (1983) J. Chem. Soc., Farad. trans. 2, 79, 211
12- Hauser H., Pascher I., Pearson R.H. and Sundell S. (1981) Biochim. Biophys. Acta, 650, 21
13- Raudino A. and Mauzerall D. (1986) Biophys. J., 50, 441
14- Luzar A., S. Svetina and B. Zeks (1984) Bioelectrochem. Bioenerg., 13, 473
15- Junge W. and McLaughlin S. (1987) Biochim. Biophys. Acta, 890, 1
16- Gutman M., Nachliel E., Bamberg. E. and Christensen B. (1987) Biochim. Biophys. Acta, 907, 390
17- Nachliel E. and Gutman M. (1988) J.A.C.S., 110, 2629
18- Polle A. and Junge W. (1986) Biochim. Biophys. Acta, 848, 257

THE ELECTRIC STATE OF ION-EXCHANGE MEMBRANE SURFACES EMERSED FROM ELECTROLYTES

Marcella Cappadonia and Karl Doblhofer

Fritz-Haber-Institut der Max-Planck-Gesellschaft
Faradayweg 4-6, D - 1000 Berlin.33

The electronic work function of fixed-charge polymer films deposited on gold electrodes has been determined after emersion from aqueous solutions. The investigation was conducted in order to obtain informations about the electric state of solvated ion-exchange membranes.

The emersion occured under potentiostatic control after polarization of the polymer coated electrode in absence of faradaic processes. After emersion the work function of the solvated polymer has been measured by Kelvin's method of the vibrating capacitor plate. A previous calibration of Kelvin's vibrating surface has been performed as described in a recent paper (K. Doblhofer and M. Cappadonia, J. Electroanal. Chem., 243 (1988) 337). It allowed to determine the true work function in a humid atmosphere.

The work function of the emersed polymer films, Φ^{M}_{ex}, has been found to be directly proportional to the electrode potential, independent of ion-exchanger type, charge of the exchanged ion and solution concentration. In this respect, the coated electrodes behave in the same fashion as uncoated metal electrodes.
Yet, parallel shifts of the work function-electrode potential lines have been observed with changes of the solution concentrations. A linear correlation between the work function at constant emersion potential and the logarithm of the solution concentration has been found (Fig.1).
It is proposed that this concentration dependence of the work function is directely related to the equilibrium potential drop across the polymer electrolyte interface, i.e. it is a measure of the Donnan potential. In fact as table 1 shows, the slopes depend on the sign and on the charge number of the exchanged ion as aspected for the Donnan-potential - log[C] correlation.

The determined values of Φ^{M}_{ex}, are compared with the work function of the elecrolyte, Φ_{S}, at the same electrode potential (Fig.1). It is concluded that a surface dipole potential exists at the emersed polymer surface. Its sign and magnitude depend on the type of fixed-charge polymer and on the electrolyte.
Apparently, during the emersion a charge segregation occurs at the membrane surface (Fig.2), an excess of fixed polymer charges on the membrane surface developes a positive dipole potential on the surface of emersed cation-exchanger, a negative dipole potential on emersed anion-exchanger.

TABLE 1

Polymer	Ion	$\delta\Phi$ / δlog[C]
PVP	ClO4-	0.054 eV
PVP	SO4--	0.031 eV
Nafion	Na+	-0.067 eV
Nafion	Mn++	-0.035 eV

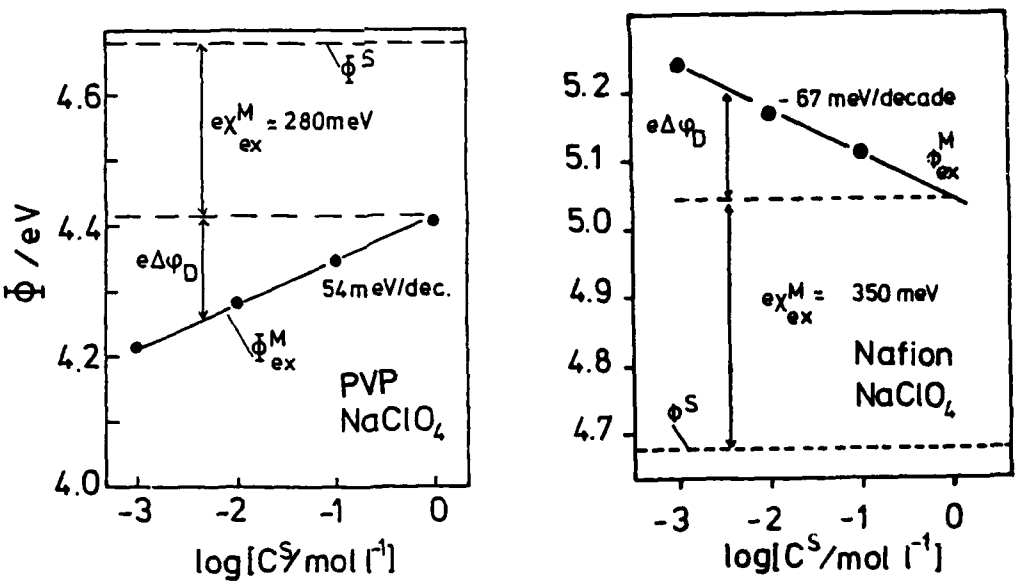


Fig.1 The work funcion of the electrolyte, Φ_S , at E=0.0 V/SCE, and of the coated electrodes emersed at the same E, Φ^M_{ex}

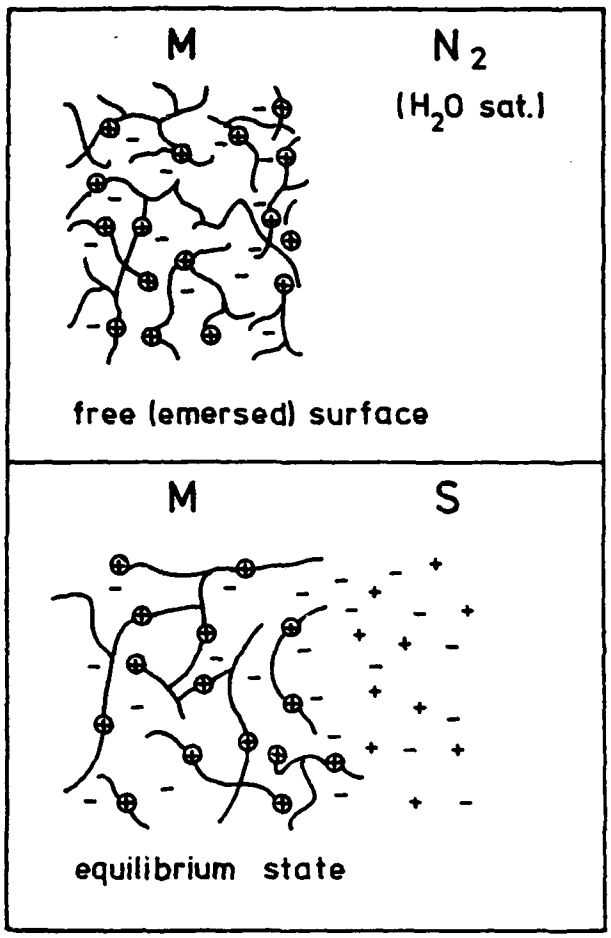


Fig.2 The surface dipole layer generated upon emersion of a anion-exchange membrane.

SOME ELECTROCHEMICAL BEHAVIOUR OF BILAYER LIPID MEMBRANES MODIFIED WITH PORPHIRYNES.

Paweł Krysiński
Laboratory of Electrochemistry, Dept. of Chemistry, Warsaw University, 02-093 Warsaw, Poland.

ABSTRACT

Negatively charged and neutral bilayer lipid membranes (BLM) modified with metal porphirynes with different central metal ions were studied by means of cyclic voltammetry in dark. Such modified BLMs were placed in redox gradients originated from redox couples present on both sides of the membrane.

Obtained results show the screening effect of fixed charges of membrane surface against the action of redox ions on metal porphirynes incorporated into the BLMs.

Spectral data testifying for the redox reaction of metal porphirynes across the liquid/liquid interface were also obtained.

INTRODUCTION

In recent years there has been an increasing interest in application of electroanalytical techniques to problems of biological importance. Biochemists are now rather successful in their electroanalytical studies of biomolecules (c. ref. 1), while electrochemists are involved in development of fuel cells basing on the properties of biological membranes and interfaces. It is an attractive notion that a combination of techniques from membrane science and electrochemistry be applied to the study of properties of biomolecules in their native or pseudonative state. The planar, bilayer lipid membrane is one of the most suitable models for the studies of electrical behaviour of membrane bound molecules found in various types of biomembranes. The membrane, which is formed in a controlled manner, can function as the sole conductor of charges between two compartments partitioned by this membrane. This feature makes the BLM very useful for the studies of electrochemical phenomena associated with membrane itself and the membrane bound molecules (2,3).

It has been firmly established that in photosynthetic, visual and water splitting processes, lipid bilayers containing photoactive compounds such as chlorophylls, retinals, porphyrines and dyes are involved (4,5). The primary phenomenon in these processes is the light induced electronic excitation of the involved pigments followed by the photovoltaic effects originated from the charge separation caused by light induced redox reactions taking place at the membrane interfaces. Most investigations in this area however, ignore the possible screening effect of fixed charges of membrane surface against the interfacial redox reaction of membrane bound pigment molecules placed in redox gradient. The aim of present

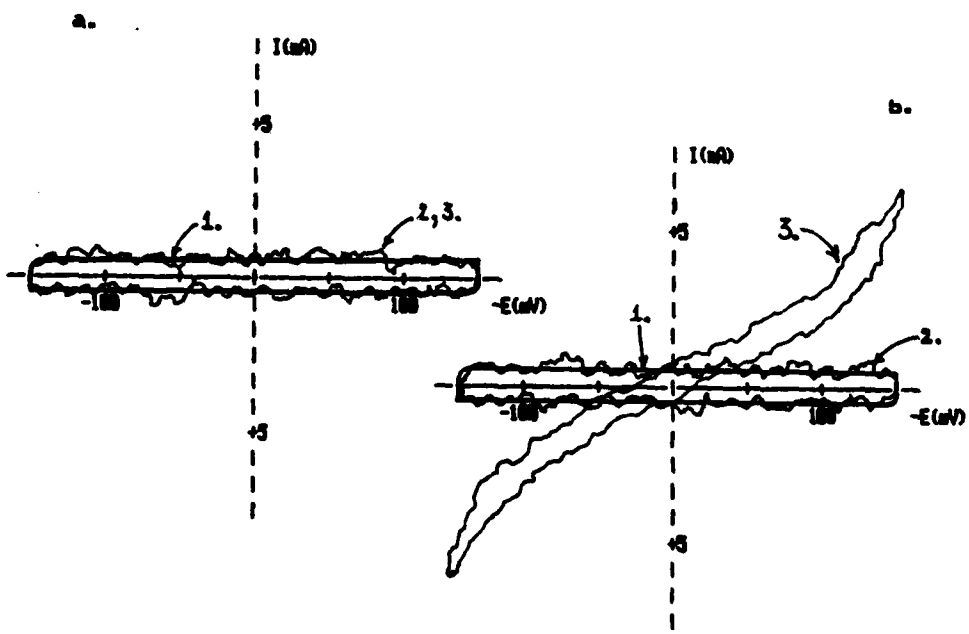
work was to demonstrate this effect for the case of Fe(III)- and Mn(III)-tetraphenyl porphine chloride (Fe(III)TPP-Cl or Mn(III)TPP-Cl) modified BLMs made from the neutral or negatively charged phospholipids.

EXPERIMENTAL

The BLMs were formed from negatively charged (phosphatidylserine - PS) or neutral (dipalmitoyl phosphatidylcholine/cholesterol - PC/Chol) phospholipids using micropipette technique according to the published methods (c.ref.2,3). To endow the BLM with desired properties, the membrane forming solution was saturated with Fe(III)TPP-Cl or Mn(III)TPP-Cl. Such modified BLMs were studied by means of cyclic voltammetry in dark with or without the redox gradients originated from the redox couple ($K_3Fe(CN)_6$ /$K_4Fe(CN)_6$) present in different concentration ratios on both sides of the membrane. In our experiments, the typical three electrode system was used in the following configuration: one saturated calomel electrode (SCE) was placed on one side of the BLM, whereas the other two SCEs (treated as reference and auxilliary) were on the other side. This provided a potentiostatically controlled polarization of one side of the BLM (solution iR drop is neglisible due to the BLM resistance of ab. 10^{10} ohm).

RESULTS AND DISCUSSION

The obtained voltammograms are shown in Fig.1.



They were recorded for: 1 - unmodified PS (Fig.1a) and PC/Chol (Fig.1b) BLMs in the absence of redox couple in bathing solution; the presence of redox couple in bathing solution does not affect the shape of voltammogram; 2 - Fe(III)TPP-Cl or Mn(III)TPP-Cl modified BLMs in the absence of redox couple; noticeable are minutessimal transient current changes probably due to the BLM structural disturbances caused by porphine molecules; 3 - observed only for the neutral, Fe(III)TPP-Cl modified BLM placed in redox gradient.

The latter curve is of particular interest, since it presents the typical behaviour of BLM with ionic type of conductance. Moreover, it is almost symmetrical (only up to 20mV of open circuit potential, donor side positive), suggesting that the observed current increase is neither due to the diffusion of aqueous phase components nor the result of conjugated interfacial redox reactions of the BLM working as a "bipolar" electrode. These results suggest the interfacial reduction of Fe(III)TPP-Cl to Fe(II)TPP by $Fe(CN)_6^{4-}$ present in bathing solution producing an excess of Cl^- anions within the membrane phase and thus decreasing the membrane resistance. As is evident from Fig.1a, this interfacial reaction is inhibited by the electrical screening effect if the BLM is negatively charged (PS). The question remained why such an effect was not observed for the case of Mn(III)TPP-Cl modified BLMs. For this purpose the experiments with ITIES (interface between two immiscible electrolyte solutions) as the BLM model systems were carried out, with water phase containing $K_4Fe(CN)_6$ as the reductor, Fe(III)- or Mn(III)TPPCl as the substrate was present in n-decane phase. By means of spectral analysis the course of interfacial redox reaction was followed. As was expected, only the optical spectrum of Fe(III)TPP-Cl was changed, the spectrum of Mn(III)TPP-Cl remained unchanged, probably due to the more negative value of its formal potential (6). The reduction of Fe(III)TPP-Cl was reversible. If the ITIES system after reduction was left in contact with atmosphere, the spectral signal of Fe(II)TPP disappeared.

ACKNOWLEDGEMENTS

This work was started in the Universität Tübingen, GFR, Institut für Chemische Pflanzenphysiologie headed by Prof. Dr. H. Metzner within the framework of exchange program between our Universities.

REFERENCES

1. E. Pungor, ed., BIOELECTROANALYSIS, 1, 1st Symposium, Akadémiai Kiadó, Budapest, Hungary, 1985.
2. H.T. Tien, Planar bilayer lipid membranes, in: Progress in Surface Sci., vol.13, Pergamon Press, N.Y., 1983.
3. P. Krysiński, H.T. Tien, Membrane electrochemistry, in: Progress in Surface Sci., vol.23, Pergamon Press, N.Y., 1986.
4. J.Barber, ed., Topics in Photosynthesis, vol.3, Elsevier, 1979.
5. R.Antolini, A. Bliozzi, A. Gorio, eds., TRANSPORT IN MEMBRANES, Raven Press, N.Y., 1982.
6. J.-H. Fuhrhop, The oxidation states and reversible redox reactions of metalloporphyrins, in: Structure and Bonding, vol.18, Springer-Verlag, N.Y., 1974.

BIOELECTROCHEMICAL ACTIVITY ON THE SURFACE OF INERT METALS ELECTRODES IMPLANTED INTO THE BRAIN TISSUE

Shvets-Teneta-Guriy T.B.,* Dubinin A.G.**

*Institute of Higher Nervous Activity and Neurophysiology, USSR Academy of Sciences, Moscow; **Mendeleev Chemical Technological Institute, Moscow

This study is dedicated to the problem of application of inert metals electrodes as selective sensors which allow to record changes of own electrochemical brain activity (bioelectrochemical activity) in neurophysiological studies.

The work was carried out on rabbits, active electrodes (gold, platinum) were implanted up to dura and pia matters and in the cortical thickness. Reference electrode of the same metal was implanted in the skull bone. Thanks to the peculiarities of this method (Shvets-Teneta-Guriy, 1980) slow electrical brain activity was eliminated from the brain slow bioelectrochemical activity - BEChA.

By means of sensors some complicated processes were revealed in the brain BEChA, consisting of a number of superposed components: prolonged BEChA changes (from one to several days) with the amplitude up to $\pm$ 50 mV and rhythmical oscillations with the periods from several seconds up to several minutes and the amplitude - up to 3-5 mV.

It is found that formation of rhythmic oscillations in the brain BEChA is due to an increase of the brain functional loads on the brain having both unspecific character - reaction to electrodes implantation depending on the number of electrodes and the character of their implantation, reaction to the pressure on the brain surface, - and specific character - various forms of the brain integrative activity (habituation to the new situation, elabora-

tion of conditioned defensive reflex, formation of defensive dominant).

The presence in the total brain BEChA of the oscillations with different parameters testifies that at tension of metabolism in the brain tissue a number of biochemical oscillators appears. It is suggested that their formation is based on the ability of certain electrochemical systems providing for various manifestation of cortical metabolism, to synchronize their internal oscillations (biochemical synergetics). The problem is discussed about the nature of the factors which simultaneously synchronize oscillations in the electrochemical systems with various oscillations periods.

Dynamics of Lateral Charge Transport in Amphiphilic Monolayer and Bilayer Assemblies

Cindra A. Widrig and Marcin Majda
Department of Chemistry
University of California
Berkeley, California 94720
U.S.A.

Charge transport in organized monolayer and bilayer assemblies is a key issue in biomembrane research and bioelectrochemistry. Our approach involves two novel experiments in which classical electrochemical techniques are used to investigate the kinetics of translational diffusion of amphiphilic components of bilayer assemblies and the kinetics of lateral electron hopping in well ordered Langmuir monolayers at the water/air interface.

In the first experimental approach, porous aluminum oxide films are used to synthesize bilayers via spontaneous self-assembly. The oxide films contain parallel, cylindrical pores typically 1000 A in diameter incorporated in a dense array in the rigid film structure. The internal surfaces of the aluminum oxide films serve as a template for the assembly of bilayers. The perpendicular orientation of the oxide pores with respect to the electrode surface constitutes bases for the electrochemical measurements of the dynamics of the lateral charge transport. Bilayers consist of an octadecyltrichlorosilane (OTS) monolayer and a monolayer of an electrochemically active surfactant assuming the characteristic tail-to-tail conformation with the OTS layer. In the cases involving viologen, ferrocene or naphthoquinone amphiphiles, voltammetric and chronocoulometric experiments combined with fluorescence probe investigations and temperature studies provided detail kinetic data demonstrating that the translational diffusion is the mechanism of the lateral charge propagation.

The involvement and dominance of lateral electron hopping was observed in the second experimental approach where the kinetics of charge transport was investigated in Langmuir monolayers at the water/air interface under controlled surface pressure conditions. In these experiments, the 500 A wide micro-band electrodes floated at the water surface are fabricated by creating an edge in a layered assembly consisting of glass slide (1 mm), gold (500 A) and polystyrene (2000 A). The observed increase in voltammetric current with surface pressure provides evidence that the electron hopping and not translational diffusion is a mechanism of lateral charge propagation. These experiments open a possibility of measuring the rate of electron transfer between molecules at known distances and in known orientations.

OSCILLATIONS IN IRON-BROMATE SYSTEMS

F. D'Alba ♦, S. Di Lorenzo ♦ and C. Lucarini ♦♦

♦ Dipartimento di Ingegneria Chimica dei Processi e dei Materiali, Università di Palermo, Viale delle Scienze, 90128 Palermo, Italy

♦♦ Dipartimento di Studi di Chimica e Tecnologia delle Sostanze Biologicamente Attive, Università di Roma, Piazza Aldo Moro 5, 00185 Roma, Italy

The occurrence of electrochemical oscillations in electrode processes and the occurrence of electrophysiological oscillations in nerve, muscle and sensory organ cells of living systems are both linked to the interfacial structure of the electrode and the membrane respectively.
Frank (1) has considered the interfacial phenomena as the determining step for the occurrence of periodicity in such systems. Ostwald (2,3) has studied oscillations in the corrosion of chromium in hydrochloric acid and of iron in nitric acid and has claimed an analogy between the kinetics in the electrochemical oscillations and the electrophysiological ones .

As it is too complicated to study in vivo the influence of the chemical-physical and the electrochemical parameters on the oscillations in living systems, in our previous papers (4-9) we have studied oscillatory phenomena in chemical systems from both the theoretical and the experimental points of view, in order to set up models suitable for the interpretation of the more complex phenomena occurring in biological systems.
The purpose of the present work is to study the oscillatory behaviour of iron corrosion by bromate in sulphuric acid .

Tests were performed in a batch reactor containing 75 cm^3 of solution composed as follows : $KBrO_3$ 0.45 mol/dm^3 ; H_2SO_4 0.5 mol/dm^3 . The potential of an iron wire electrode put in the solution, measured with respect to a reference saturated calomel electrode, was recorded during the oscillatory corrosion phenomenon in open electrical circuit conditions, by means of a potentiometric recorder. The temperature was controlled by an air thermostat $\pm$ 0.5 ° C .

A blank test carried out without bromate does not show oscillatory behaviour and the potential value of iron electrode is lower than that in the analogous oscillatory test with bromate . During the periodic phenomenon in the system with bromate, visible liquid bromine forms on the iron electrode and falls to the bottom of the reactor while the iron electrode consumption is easily detectable . Stable oscillations 300-500 mV wide are obtained in an unstirred system, but oscillations of 1000 mV amplitude are obtained by a 1.5 cm^2 plate iron electrode measured with respect to a platinum one in an unstirred system. Stirring interrupts the oscillatory phenomenon while the potential falls to the minimum value of the oscillations . An increase in temperature from 25 ° C to 55 ° C leads to an

increase in the frequency , and a threshold value around 60 ° C exists above which frequency decreases . The potential of an indicator wire platinum electrode put in the bulk of the solution , measured with respect to a reference saturated calomel electrode , does not show oscillatory behaviour , so that it is demonstrated that the periodic phenomenon is localized at the iron/solution interface. The abovementioned blank test also showed that the presence of bromate in solution is essential to the occurrence of oscillations .

References

1 - U. F. Franck, Angew. Chem. Int. Ed. Engl., 17, 1 (1978)

2 - Wi. Ostwald, Phy. Z., 8, 87 (1899)

3 - Wi. Ostwald, Z. Phys. Chem. 35, 33, 204 (1900)

4 - C. Botrè, C. Lucarini, A. Memoli and M. Mascini, Bioelectrochem. Bioenerg., 4, 54 (1977)

5 - C. Botrè, C. Lucarini and A. Memoli, Bioelectrochem. Bioenerg., 6, 451 (1979)

6 - F. Botré, E. D'Ascenzo, C. Lucarini, A. Memoli and R. Bianchi , Bioelectrochem. Bioenerg., 11, 89 (1983)

7 - F. D'Alba and S. Di Lorenzo, J. Chem. Soc., Faraday Trans. 1, 79, 39 (1983)

8 - S. Di Lorenzo and F. D'Alba , J. Chem. Soc., Faraday Trans. 1, 81, 421 (1985)

9 - F. D'Alba and S. Di Lorenzo, Bioelectrochem. Bioenerg. ,15, 505 (1986)

DYNAMIC CHANGES OF BACTERIORHODOPSIN RECONSTITUTED IN DMPC-BILAYERS DURING PROTON PUMPING

A. Böttcher*, N. Dencher+, R. Groll*, F. Meyer* and J. F. Holzwarth*
+ FB Physik, Abt. Biophysik, Freie Universität Berlin, D-1000 Berlin 33
* Fritz-Haber-Institut der Max-Planck-Gesellschaft, Faradayweg 4-6, D-1000 Berlin 33, West Germany

Integral membrane proteins, like the light driven proton pump bacteriorhodopsin (bR), span the lipid bilayer matrices of biological membranes because they possess highly hydrophobic surfaces which are in contact with the alkane chains of anular lipids and hydrophilic areas exposed to the aqueous phases on both sides of the membrane. To study the biological activity of such membrane proteins in detail, it is suitable to separate the proteins from other components of the natural membrane, and to reconstitute the selected proteins in a functionally active state in lipid bilayers.

We prepared reconstituted bR in unilamellar dimyristoylphosphatidylcholine (DMPC) vesicles as a model system to investigate the dynamics of the interaction of the anular lipids with the hydrophobic surface of bR. The functional protein is either in an active state, pumping protons, or passive. The related interactions can best be studied in the temperature range of the main phase transition of DMPC around 23 °C because the biological activity of bR is strongly influenced by passing from the liquid crystalline to the fluid state of the DMPC bilayer.

The iodine-laser temperature-jump (ILTJ) technique with a time resolution from 10^{-9} s to 10 °s offers a unique tool for such kinetic experiments. We studied the dynamics of pure DMPC bilayers and compared these results with analogous bilayers containing increasing amounts of functionally active bR. As a result we could define the range of interaction between the protein bR and the anular lipids reaching as far as three lipid layers. Furthermore we could observe that the two relaxation processes around 0.5 ms and 5 ms, which are very important in pure lipid bilayers, are negligible in DMPC/bR systems containing 1 mole % of bR. The relaxation process in the time range of 10 µs was strengthened.

bR pumps protons through the bilayer if its chromophore retinal is excited by photons of 560 nm. In the time range of 10^{-3} s strong spectral changes either at 412 nm or 560 nm can be monitored being due to the biological activity of bR

(fig. 1). At 360 nm the turbidity changes due to the increasing mobility of the lipid molecules can be observed.

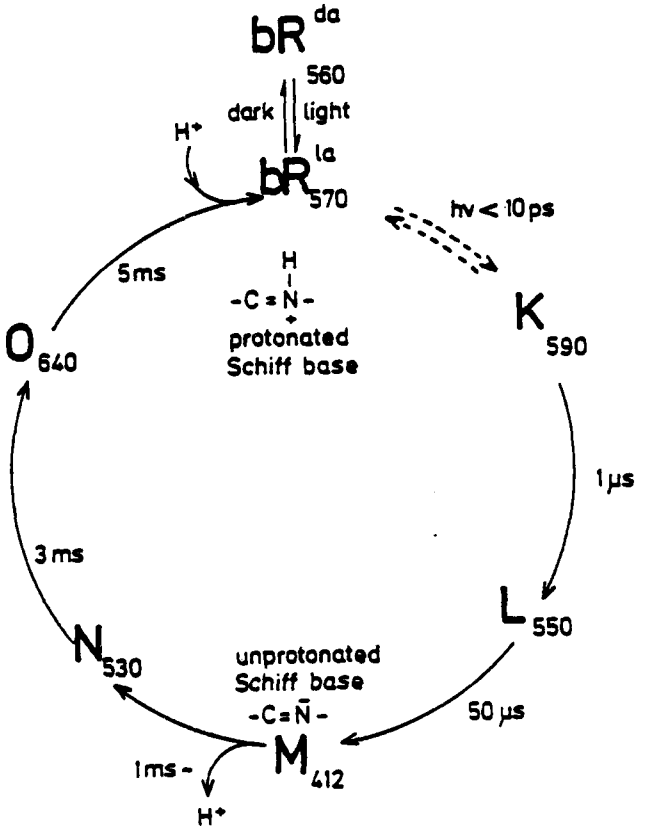


Fig. 1: Schematic Photocycle of Bacteriorhodopsin (bR) including averages of absorption maxima and lifetimes of intermediate states

By monitoring spectral changes at 560 nm or 430 nm and 360 nm simultaneously after a temperature jump we can separate dynamic changes due to the activity of bR from kinetic processes resulting from the lipid molecules. By comparing the bR and the lipid relaxations we observed that the lipid motions around 10 µs and the functional activity of bR are strongly coupled. We conclude that the surface of bR undergoes a funcitonally important movement (after Frauenfelder) during its biological activity in the microsecond time range (fig. 2).

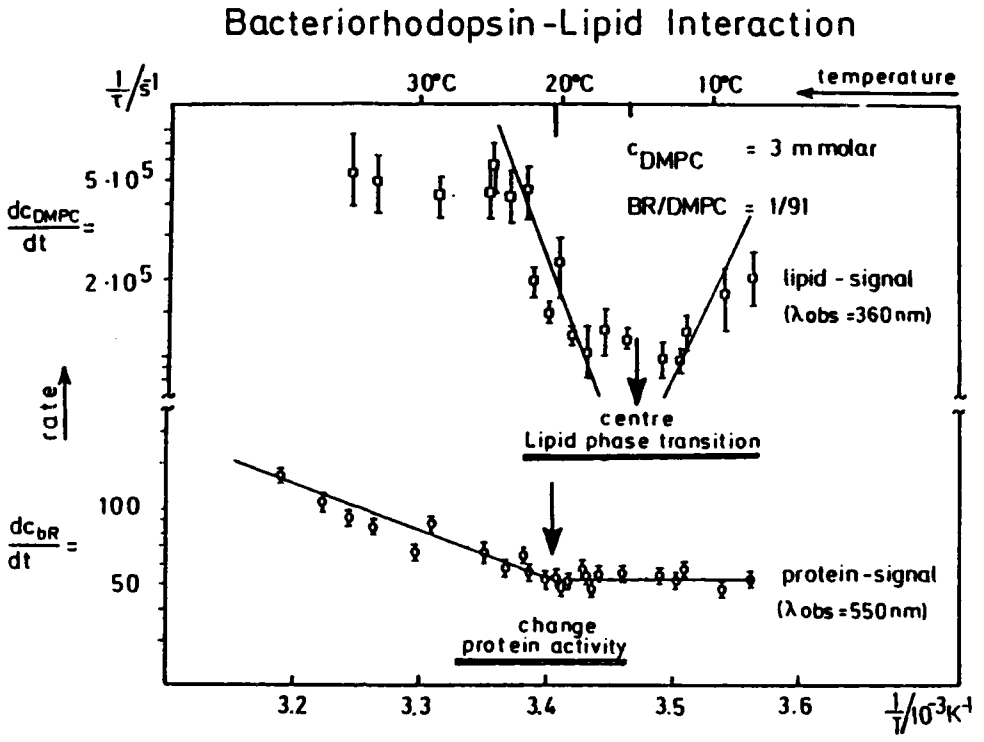


Fig. 2: Arrhenius dependence of the lipid relaxation τ_{DMPC} and the bR relaxation τ_{bR}

Literature

/1/ J. F. Holzwarth, in: Faraday Discussion No. 81 (1986) "Lipid Vesicles and Membranes", pp. 74-79, 340-342, 353-367

/2/ J. F. Holzwarth, V. Eck and A. Genz, in: Spectroscopy and Dynamics of Molecular Biological Systems, eds. P. Bayley and R. E. Dale, Academic Press (1985) pp. 351-377

/3/ J. F. Holzwarth, A. Schmidt, H. Wolff and R. Volk, J. Phys. Chem. 81, 2300 (1977)

Charge Injection via Light-induced Picosecond Charge Separation in an Artifical Molecular Membrane

R. Eichberger, F. Willig, W. Storck and *W. S. Durfee*

Fritz-Haber-Institut der Max-Planck-Gesellschaft,
Faradayweg 4-6, D-1000 Berlin 33, West Germany

It is established now that the reaction center of photosynthesis is a molecular photovoltaic machine. This and other biological structures continue to inspire the search for photoactive charge separating supermolecules that can be aligned in a suitable membrane.

We have built a molecular structure that functions with some of the desired properties. A compound molecule was synthesized that comprises one hydrophilic and two consecutive hydrophobic chromphores to facilitate two-step down-hill charge transfer. A high concentration of these tri-chomophoric molecules was aligned in an LB film. Excitation of the strong optical charge transfer transition between the first hydrophilic and the second hydrophobic chromophore is accompanied by a corresponding hole transfer. Further transfer to the third choromophore moves the hole in total across the diameter of the LB film. This last step was detected as shortening of the charge transfer fluorescence decay when the third chromophore was attached (Fig. 1). The charge transfer transition was excited with a pulse train, 4-5 ps width, from a cavity dumped synchronously pumped dye laser and the fluorescence was measured with a syncroscan streak camera. The actual hole transfer rate was inferred from the dramatic shortening and the by a factor of 50 decreased signal height in the presence of the third chromophore. The time dependence of the decay was simulated with a simple rate constants model indicating a time constant of 500 fs for the last step, identical at room temperature and at 4 K.

The long small tail which is hard to recognize in Fig. 1 (lower curve) has been measured with time resolved single photon counting. It is attributed to slow back transfer of the hole from the third to the second chromophore. There was a drastic change in the rate constant for the last step when the chemical environment was exchanged in the LB film with an accompanying shift in the electronic level.

The photoactive film was deposited onto the surface of an organic insulator crystal serving as collector electrode and the system mounted on a microstrip. The current loop through the external circuit was closed by applying an aqueous contact solution. In this configuration the excitation spectrum of the photocurrent was measured for hole generation in the photoactive LB film (Fig. 2). The photocurrent transient was measured with 100 ps time resolution.

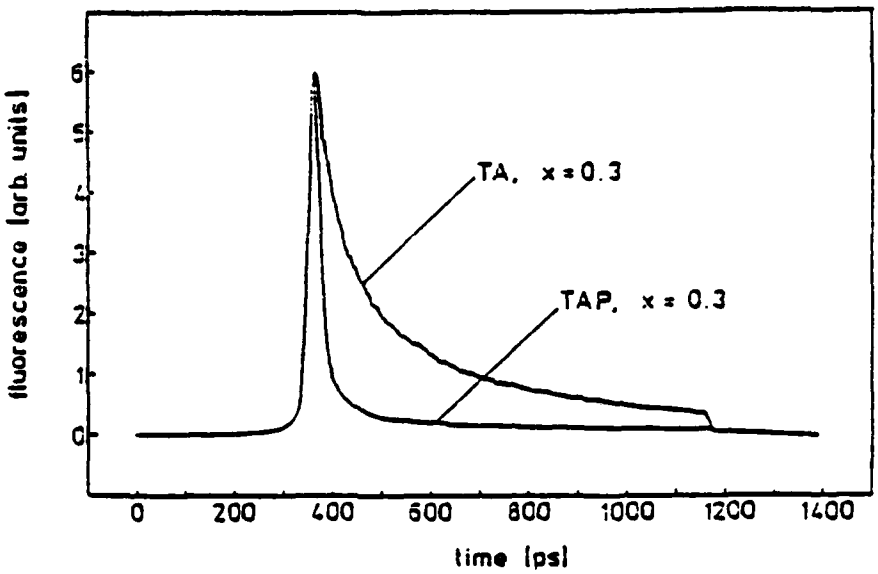


Fig. 1: Charge transfer fluorescence decay in the LB film in the presence (TAP) (lower curve) and in the absence (TA) (upper curve) of the third chromophore (normalized). *x is the molar ratio of* photoactive to inert supporting molecules.

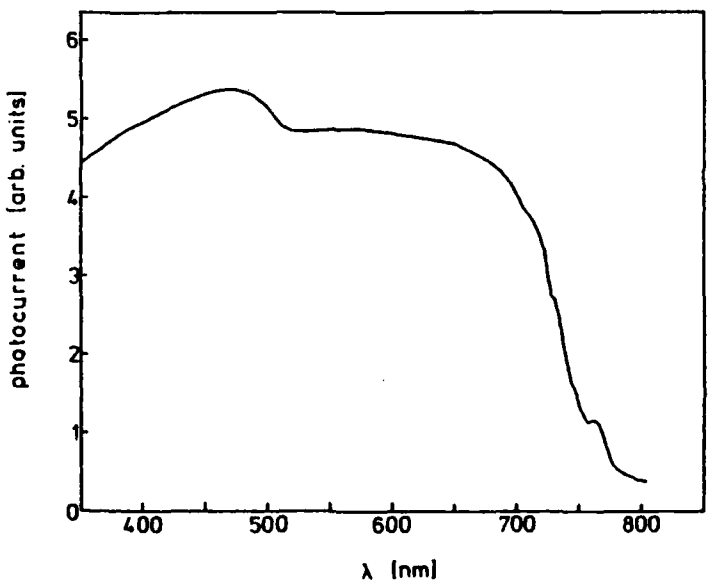


Fig. 2: Excitation spectrum of the hole photocurrent originating in the functionalized Langmuir Blodgett film (uncorrected).

MICROELECTROPHORETIC INVESTIGATIONS OF LIPOPHILIC ANIONS TRANSPORT KINETICS ACROSS THE MEMBRANE OF HUMAN ERYTHROCYTES in vitro.

S. Kalinowski, P. Krysiński, S. Minc
Laboratory of Electrochemistry, Dept. of Chemistry,
Warsaw University, 02-093 Warsaw, Pasteura 1, Poland.

SUMMARY

Under the influence of picrate and tetraphenylborate anions the electrophoretic mobility of human erythrocytes undergoes time-dependent changes. This transient response was related to the adsorption and transport processes within the membrane phase. Obtained results were compared with the kinetic model of quaternary ammonia transport proposed earlier.

INTRODUCTION

With rapid development of membrane biophysics coupled with the advances in electrochemical techniques in the last two decades (1) new opportunities exist to apply electrochemistry for the in vitro studies of cell membrane and the electrical double layer structure at the cell membrane - electrolyte solution interface. In our laboratory this type of approach is based on the microelectrophoresis, and as a model system for the investigations of cell membrane/electrolyte solution interfacial region we use the human red blood cells due to their availability and relatively simple structure as compared to the other mammalian cells. Their surface is negatively charged due to the membrane structural components and any change in this charge can be detected microelectrophoretically in proper conditions.

In our previous studies (2-4) we presented some results regarding the adsorption and permeation phenomena occuring at the membrane/solution interface for quaternary ammonia symmetrical cations. They were interpreted in terms of the two-step transport process with adsorption within the membrane phase (4). The aim of this work is to verify the applicability of proposed model for the case of lipophilic anions influence on the cell membrane intefacial region.

MATERIALS

Human erythrocytes were separated, as described earlier (2-4), from ACD (acid-citrate-dextrose) preserved blood obtained from the Department of Blood Storage and Preparation, Haematological Inst., Warsaw. The blood samples were stored at 4 °C no longer than 2 days. Solutions containing picrate (Pi^-) or tetraphenylborate ($TPhB^-$) anions (sodium salts) in the concentration range of 0.5 - 10 mM were obtained by replacing the equimolar amount of NaCl in the standard buffer. For microelectrophoretic measurements, freshly prepared cells were

suspended in the solution of a given concentration of investigated anions and the data were taken with use of microelectrophoretic setup.

APPARATUS

The microelectrophoretic apparatus constructed in our Laboratory, was described in details in our previous work (2-4). However, the major change in optics was introduced - the phase contrast, which amplifies the small difference in the phase of light wave passing through the membrane and surrounding solution. The other change was that the microscope screen was replaced by TV-camera with monitor, giving the system which is more convenient and of higher resolution. Improved was also the power supply for microelectrophoresis, which is now potentiostatically controlled by two sampling electrode probes R_1, R_2, with feed-back, maintaining the constant electric field gradient across the measuring cuvette. The block diagram of the electrical part of our setup is shown in Fig.1.

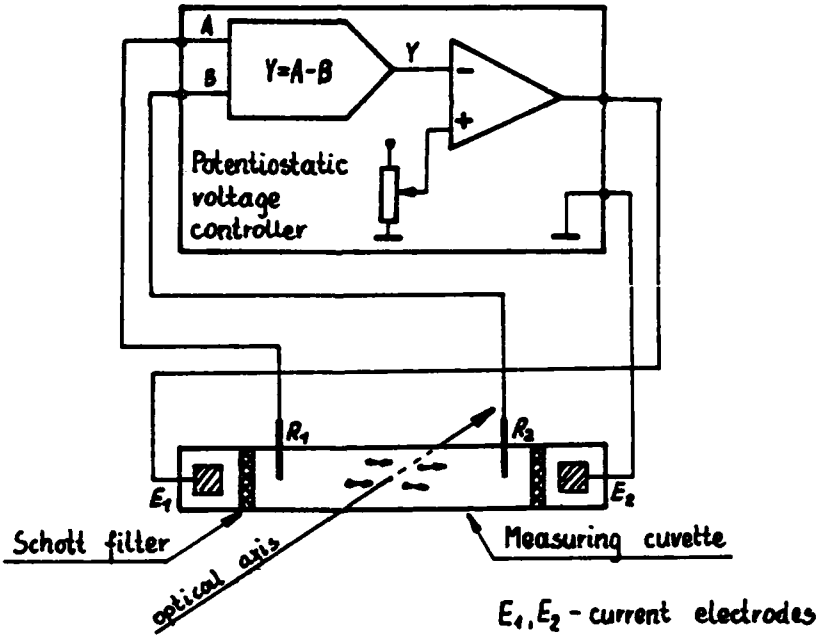


Fig.1. The block diagram of microelectrophoretic setup.

RESULTS AND DISCUSSION

As was discussed in our previous work (4) the transient change of human erythrocytes mobility $\Delta u(t)$ under the influence of quaternary ammonia can be described by two

exponentials, with four parameters - A_1, A_2, r_1, r_2, relating the kinetic and adsorption processes (see Fig.2, inset) to the surface charge density change of cell membrane:

$$\Delta u(t) = A_1 \exp(-r_1 \cdot t) - A_2 \exp(-r_2 \cdot t) + A_2 - A_1,$$

In present work the same equation was fitted for parameters A_1, A_2, r_1, r_2 in the case of investigated anions. The results of computer operations compared with the experimental data are shown in Fig.2 for Pi^- anions of concentration 2.5 mM.

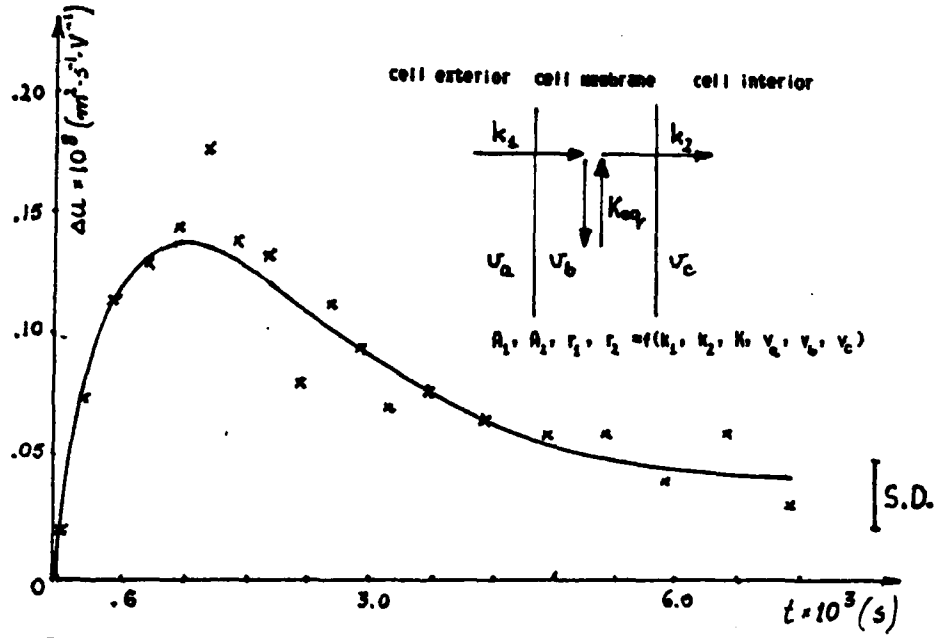


Fig.2. Changes in the electrophoretic mobility of human red blood cells influenced by Pi^- anions; solid line represents the calculated curve. S.D. - standard deviation.

There is a satisfactory good agreement between the experimental and calculated curves $\Delta u(t)$ obtained from the model. The values of discussed parameters were subsequently used to calculate the two rate constants of transport process - k_1 and k_2 and the other parameters of assumed model.

REFERENCES

1. G. Milazzo (ed), Topics in Bioelectrochemistry and Bioenergetics, Wiley, 1983
2. P. Krysinski, S. Minc, Bioelectrochem. Bioenerg., 10, 261, 1983.
3. P. Krysinski, E. Herzyk, S. Minc, Bioelectrochem. Bioenerg., 12, 367, 1984.
4. P. Krysinski, Z. Fiszszewski, Kinetic Model of Quaternary Ammonium Cations Transport through the Human Red Blood Cell Membrane in vitro - Electrolyte Solution Interface, in press.

COMPOSITE FILMS OF COBALT TETRA/p-TOLYL/PORPHYRIN IMMOBILIZED IN ZEOLITIC RUTHENIUM-OXIDE/CYANORUTHENATE MICROSTRUCTURES AS CYTOCHROME P_{450} LIKE MODELS FOR ANODIC ELECTROCATALYSIS

Pawel J. Kulesza*

University of Warsaw, Department of Chemistry, Pasteura 1, 02-093 Warsaw, Poland

Teresa Mlodnicka and Jerzy Haber

Institute of Catalysis and Surface Chemistry, Polish Academy of Sciences, Niezapominajek 1, 30-239 Cracow, Poland

Metalloporphyrins are interesting as potential modification agents for electrode surfaces, because they are electroactive and undergo fast redox transitions, as well as offer versatile catalytic reactivities while being chemically fairly stable. These macrocycle species can be effective electron transfer agents due to the extended porphyrin system; further, they also possess axial ligation sites that are available for stabilization of such reactive entities as H and O atoms /1/. Finally, not only oxygen but also other species such as alcohols, aldehydes, hexacyclodiene, CO, N_2H_4, NO and many others have been found to form adducts with metalloporphyrins or related phtalocyanines /2/.

The promise of metalloporphyrin films for electrocatalytic oxidations rests on the system ability to form, upon oxidation of porphyrin ring, radical cations as active intermediates /1/. A number of homogeneous studies have been made using cobalt tetra/p-tolyl/porphyrin, Co/II/TTP, which, under oxidative conditions, forms reactive dication $Co/III/TTP^{2+\bullet}$ radical capable of abstracting hydrogen from the substrate molecule and inducing the actual oxygen transfer in the course of aldehyde oxidations. This communication concerns the way in which the radical is stabilized in order

to prevent its deactivation and dissolution of the metalloporphyrin film on an electrode. Optimum matrix for the Co-porphyrin centers would also distribute electrons rapidly to the immobilized catalytic sites as well transport readily the oxidizing equivalents of oxygen to the reactants.

A structured modified electrode based on a composite film, consisting of zeolitic ruthenium-oxide/cyanoruthenate /3/ matrix and Co-porphyrin species, is proposed here. In the modification procedure, the simultaneous oxidative codeposition of both components is explored; further fixation of the Co-porphyrin centers is apparently achieved in a manner analogous to ion exchange attraction by zeolites. Infrared spectroscopy showed the presence of a CN-group, H_2O and characteristic metalloporphyrin peaks in the deposit, and suggested that the system was not a simple mixture of the components. Further information about the chemical composition was gained from absorption spectra of the coatings prepared at SnO_2-covered glass slide electrodes. Cyclic voltammetric studies of the composite film on glassy carbon are consistent with the observation that the formation of Ru/IV/-oxo species in the system induces oxidation of the coexisting Co-porphyrin species. The Co-porphyrin dication radicals seem to be both stabilized and activated by ruthenium/oxide cyanoruthenate portions of the film. The composite system exhibits a notable electrocatalytic oxidation of otherwise highly irreversible propionaldehyde. The catalytic effect is related to the primary action of of the Co-porphyrin radical, leading to the H-abstraction from the aldehyde group, and the secondary action of Ru-oxo species, providing O-transfer pathways. The latter implies some analogy to the action of the iron porphyrin /heme/ based oxo-species in cytochrome P_{450} monooxygenase enzymes.

References

1. T. Mlodnicka, J. Mol. Catal., 36 /1986/ 205.

2. D. K. Kyriacou and D. A. Jannakoudakis, Electrocatalysis for Organic Synthesis, Wiley, New York, 1986, pp 29-31.

3. P. J. Kulesza, J. Electroanal. Chem., 220 /1986/295.

LIQUID JUNCTION POTENTIALS BETWEEN pH BUFFER SOLUTIONS

M.J.F. REBELO

(INIC) - CECUL - R. Escola Politécnica, 58, 1294 LISBOA CODEX, PORTUGAL

The determination of pH is a matter of prime importance in many fields, including physiology. However, the assignement of a pH value to a reference solution is still a matter of controversy.

The operational definition of pH includes a residual liquid junction potential.(1)

Measurements of the e.m.f. of cells

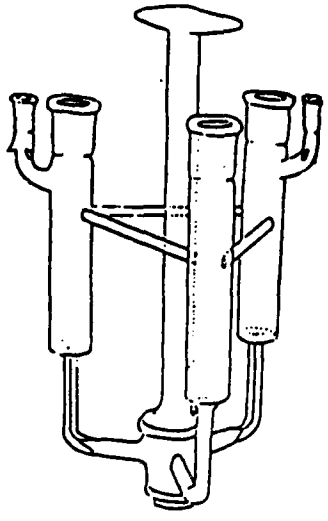
Na glass electrode	Na containing buffer solution X	Na containing buffer solution Y	Na glass electrode

and

Na glass electrode	Na containing buffer solution X	Bridge solution	Na containing buffer solution Y	Na glass electrode

were made, in order to get a better knowledge of the liquid junction potential contribution to the operational pH value.

The liquid junction is formed within a capillary tube of cylindrical



symmetry in a cell vessel, shown in the figure, whose design was developed by the author[2] and proved to give reproducible and stable pH values when used with $Pt|H_2$ electrodes[3].

(1) A.K. Covington, Anal. Chim. Acta, 127 (1981) 1-21.

(2) M.J.F. Rebelo, Ph.D. Thesis, Newcastle-upon-Tyne, 1981.

(3) A.K. Covington, M.J.F. Rebelo, Anal. Chim. Acta, 200(1) (1987), 245.

THE EFFECT OF TRANSMEMBRANE ELECTRICAL FIELDS ON THE KINETICS OF ELECTRON TRANSFER REACTIONS

G.Venturoli, M.T. Scupoli and B.A.Melandri

Dipartimento di Biologia. Universita' di Bologna.

Photosynthetic or respiratory electron transfer complexes are thought to catalyze charge separating processes across biomembranes. These electrogenic events can be considered to sustain a transmembrane electrochemical potential difference for protons which acts as a form of free energy storage in energy transducing organelles (1). The rate of such electron transfer reactions must be influenced by the onset of a transmembrane electrical potential difference in a way dependent on the distance between the electron donating and acceptor groups, the potential profile within the membrane and the orientation with respect to the membrane plane of the dipole resulting from the electron transfer process. Studies on these effects are therefore of considerable interest in relation to the topology of the functional groups and the basic mechanisms in electron transfer. These studies are best performed in photosynthetic systems, where, by means of spectroscopic techniques, a better time resolution of the redox events can be obtained. We present examples of such studies in chromatophores from the photosynthetic bacterium Rhodobacter capsulatus. In this system the membrane potential can be monitored in real time following electrochromic changes in the spectrum of endogenous pigments. The same spectral changes, however, interfere with the absorbance changes produced by the redox reactions in the spectra of redox components involved in electron transfer. A deconvolution procedure for obtaining pure electrochromic and redox signals from composite spectroscopic traces has been developped (2). This method is based on the numerical re-construction of the electrochromic trace at any given wavelenght on the basis of a reference trace at 505 nm and a correlation function determined independently. This procedure allows the study of the rates of electron transfer in the presence of large transmembrane electrical potentials. An example of this correction is presented in Fig.1. The photooxidation of the photosynthetic reaction center (RC) by a train of 8 flashes has been recorded at 542 and 605 nm, wavelenght at which the ox-red difference spectrum is opposite in sign and the

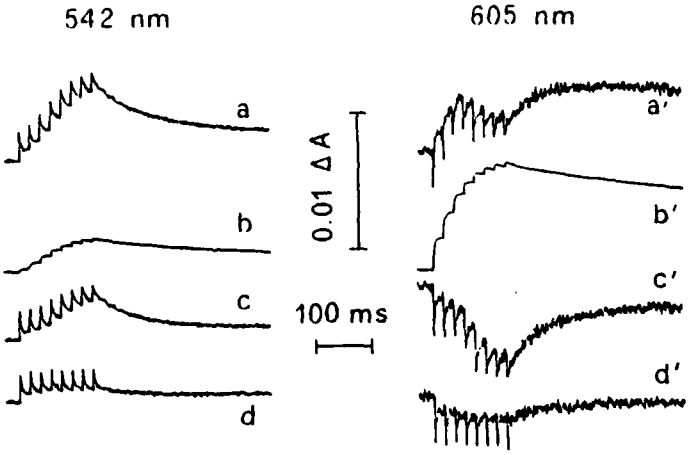
electrochromic interferences markedly different. The original traces (a and a'),manifestly distorted, have been corrected by subtracting traces b and b'(the electrochromic contribution evaluated from the signal at 505 elicited by the same train of 8 flashes). The corrected traces (c and c') are very similar, taking into account the different extinction coefficients, and show a progressive accumulation of oxidized RC parallel to the onset of a transmembrane electric field. These effects are absent when the electric field is abolished by uncouplers (d and d').

These phenomena are totally consistent with the topology of the prostetic groups within the RC, as established by X-ray crystallography (3). The structure in fact shows the primary electron donor, whose oxidation is measured, placed about 10 A inside the membrane dielectric. Electron transfer from cyt c_2 in the aqueous phase therefore is electrogenic, and the rate is expected to be lower in the presence of a transmembrane electric fields.

(1) Crofts,A.R. and Wraight,C.A. (1983) Biochim. Biophys. Acta 726, 149-185

(2) Venturoli,G., Virgili,M., Melandri,B.A. and Crofts,A.R. (1987) FEBS Lett. 219,477-484

(3) Allen,J.P., Feher,G.,Yeates,T.O.,Komiya,H. and Rees,D.C. (1987) Proc. Natl. Acad. Sci. USA 84, 5730-5734.



5. Double Layer Structure: Theory and Modeling

Effects of Ion Pair Correlations in Electric Double Layers

S. Marčelja
Department of Applied Mathematics
Research School of Physical Sciences
The Australian National University
Canberra, Australia

The problem of diffuse ion layers near charged surfaces immersed in electrolyte solutions can be analysed with a number of increasingly elaborate physical models. Since the statistical mechanics equations of these models cannot be solved exactly, they are treated at different levels of analytical approximation or numerical simulation. In the simplest model, ions are replaced by point charges and the solvent is a dielectric continuum. The appropriate mean field theory dates back to the work of Gouy and Chapman. With a more elaborate "primitive" model, ions are represented as charged hard spheres with a given radius.

We are now able to evaluate the behaviour of the primitive model of the double layer with great accuracy. At that level, even such a simple model presents many surprises. The collective behaviour of ions in the electrolyte, most easily described via ion-ion pair correlation functions, modifies mean field results and leads to interesting effects. While the most dramatic changes from the expected behaviour are found in the evaluated surface-surface interaction, other quantities like the ion density or the electrostatic potential are also affected. Experimental data obtained in direct measurements with the surface forces apparatus in Canberra support our conclusions.

The theoretical advances have been made via two major routes. In the first case one considers two surfaces at a separation relatively large compared to the Debye screening length. By approximating the long range behaviour of the direct pair correlation function with its asymptotic limit, $c(\mathbf{r},\mathbf{r}') \sim - U(\mathbf{r},\mathbf{r}')/k_BT$, one can derive different limiting laws for the surface-surface interaction. This work has re-emphasised the intrinsic link between the Van der Waals forces and the double layer interaction. The temperature-dependent zero-frequency term in the dispersion force calculations is screened by the fluctuation of the ionic cloud. The effect has been described in a classical book on the dispersion forces[1], and some of the formulas derived earlier for the simpler cases work remarkably well. New

results have extended this work to a more difficult case of charged[2,3] and dipolar[2,4] surfaces.

The second theoretical method involves solving the standard integral equations of liquid-state physics for the inhomogeneous ionic fluid between two surfaces. In planar geometry, we consider such fluid as consisting of many layers of uniform density, which are then equivalent to a multi-species two-dimensional fluid. With this method, we have achieved[5] the long-standing goal of treating the inhomogenous ionic fluid near a charged surface as accurately as if it were a bulk fluid.

The results of our calculations of the ion correlation effects depends on the strength of the coupling in the system. For low surface charges (when area/unit charge is above about 5 nm^2) and low monovalent electrolyte concentrations (up to about 0.1 M) the mean field theory results are only slightly changed. For higher charges, one can often very accurately fit the surface-surface interaction data to the mean field theory calculations, but only if one assumes a surface charge which is substantially smaller than the real surface charge. This effect is particulary dramatic in the presence of divalent ions. Finally, when counterions are divalent and surface charge rather high (below about 2 nm^2/unit charge) surface interaction at moderately small separations changes sign and becomes attractive[6,7]. This attractive well has now been observed in surface force apparatus experiments and shown to explain the stability of calcium clay dispersion[8].

1. J. Mahanty and B. W. Ninham, Dispersion Forces, Academic Press, New York 1976.
2. P. Attard, R. Kjellander, D. J. Mitchell and B. Jönsson J. Chem. Phys. (in press).
3. P. Attard, D. J. Mitchell and B.W. Ninham, J. Chem. Phys. (in press).
4. P. Attard, D. J. Mitchell and B.W. Ninham, Biophysical J. 53, 457 (1988).
5. R. Kjellander and S. Marčelja, J. Chem. Phys. 82, 2122 (1985).
6. L. Guldbrand, B. Jönsson, H. Wennerström and P. Linse, J. Chem. Phys. 80, 2122, (1985); D. Bratko, B. Jönsson and H. Wennerström, Chem. Phys. Letters 128, 449 (1986).
7. R. Kjellander and S. Marčelja, J. Phys. Chem. 90, 1230 (1986); J. Physique (in press).
8. R. Kjellander, S. Marčelja, R. M. Pashley and J. P. Quirk (preprint). R. Kjellander, S. Marčelja and J. P. Quirk, J. Coll. Interface Sci. (in press).

MOLECULAR DYNAMICS SIMULATION OF WATER AT INTERFACES

K. Heinzinger and E. Spohr
Max Planck-Institut für Chemie (Otto-Hahn-Institut)
D-6500 Mainz, Federal Republic of Germany

Recent computer simulation studies were concerned with the behaviour of water in inhomogeneous and anisotropic systems. Several models to describe the interactions between liquid water and solids have been used (cf. [1] and references therein). Most of them treat the solid phase as an uncorrugated wall. In this paper we want to discuss Molecular Dynamics simulation results obtained with a flexible water model in contact with a model platinum surface.

Figure 1 shows a sketch of the basic simulation cell employed. The water phase is located in the central part of the rectangular box and the metal atoms are represented by circles. Thus two interfaces between water and the (100) lattice plane of the face centered cubic platinum lattice are simulated simultaneously. The distance between the two interfaces depends on the number of water molecules and the desired density of the liquid phase. The numbers given in Fig. 1 are for 216 water molecules and an average density of 1 g/cm^3. Standard periodic boundary conditions have been employed in the x- and y-direction and in addition for the platinum atoms in the z-direction.

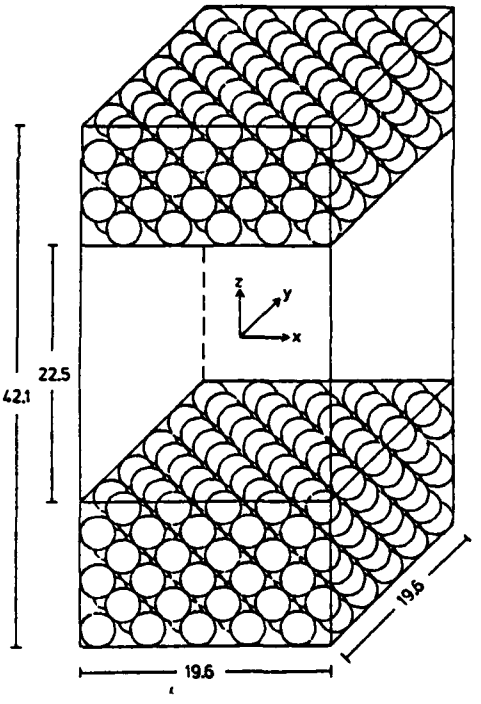


Figure 1: Sketch of the basic tetragonal simulation cell. The water molecules are located in the center of the box and the platinum atoms are represented by the circles. All distances are in Å.

The water water interactions are described by a modified central force potential [2] which has been well tested in simulations of bulk water and aqueous electrolyte solutions. The water metal interactions are described by a set of pair potentials between oxygen (hydrogen) and platinum atoms such that the adsorption site of a water molecule is preferentially on top of a surface platinum atom and the most favourable orientation is that with the water dipole vector pointing away from the metal surface. The potential parameters have been fixed in order to obtain an adsorption energy

(potential minimum) of 41.3 kJ/mol and considerable barriers for surface diffusion (21.5 kJ/mol) and water reorientation (27.4 kJ/mol for a rotation about the axis perpendicular to the molecular plane). They have been chosen in rough agreement with experimental data of water adsorption energies on transition metal surfaces [3] and extended Hückel-MO calculations of $H_2O(Pt)_5$ clusters, respectively [4]. The metal metal interactions have been modelled by a harmonic nearest-neighbour pair potential which gives an adequate description of the vibrational motions of bulk platinum.

The strong water metal interactions result in an inhomogeneous atomic density distribution perpendicular to the interface. Figure 2 shows the oxygen and hydrogen density profiles obtained from a simulation of a lamina of 305 water molecules at a temperature of 274 K. Both density profiles exhibit a pronounced first and a weaker second maximum, similar to ion-water radial distribution functions in bulk electrolyte solutions [5]. Contrary to the hydration shell of cations the hydrogen atom peak is not shifted towards larger distances than the oxygen peak. This shows the weak orientational preference given by the water metal interaction model. It indicates that the water water interactions force the dipole vectors into an orientation with only a small residual dipole moment perpendicular to the interface. Nevertheless there is a considerable charge inhomogeneity in the interfacial region (see shaded areas in Fig. 2) which leads to a non-vanishing electrical field perpendicular to the interface which, in turn, results in an electrical potential drop across the interface, usually referred to as the dipole or surface potential χ. Additional orientational distribution functions obtained from the MD trajectories will be discussed.

The corrugation of the metal surface leads to a strong density inhomogeneity parallel to the interface. A strong preference exists for the water molecules to occupy adsorption sites on top of surface metal atoms. Figure 3 shows the density distribution in the xy-plane for the first (see Fig. 2; $0 < \Delta z \leq 4.2$Å) and second layer of oxygen atoms ($4.2 < \Delta z \leq 6.7$Å). It is evident from these two figures that the strong localization of the particles on top of the platinum atoms does not persist into the second layer. However, some kind of staggered arrangement of the second layer relative to the first one can be inferred from Fig. 3. Statistically more reliable pair correlation and other distribution functions related to hydrogen bond properties will be discussed

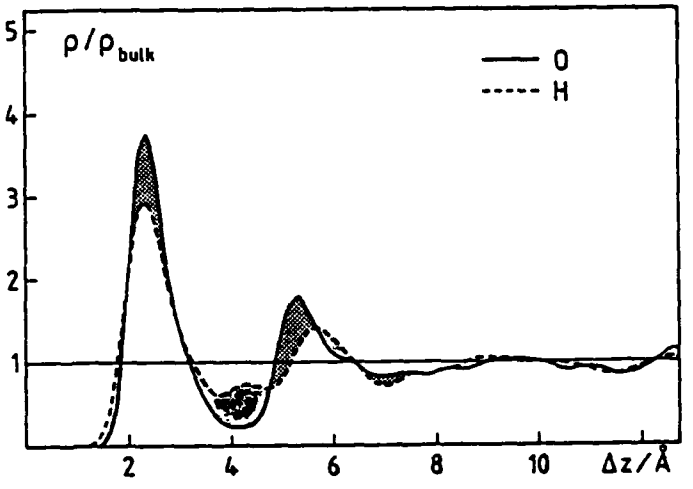


Figure 2: Normalized oxygen and hydrogen density profiles $\rho^{(1)}(z)/\rho_{bulk}$ for a simulation of 305 water molecules between two (100) faces of a face centered cubic platinum crystal.

leading to a microscopically complete picture of the interfacial water structure. Figure 3 also shows drastic changes in the dynamical behaviour of adsorbed water molecules. These will be further discussed in the framework of autocorrelation functions of velocities and molecule fixed vectors.

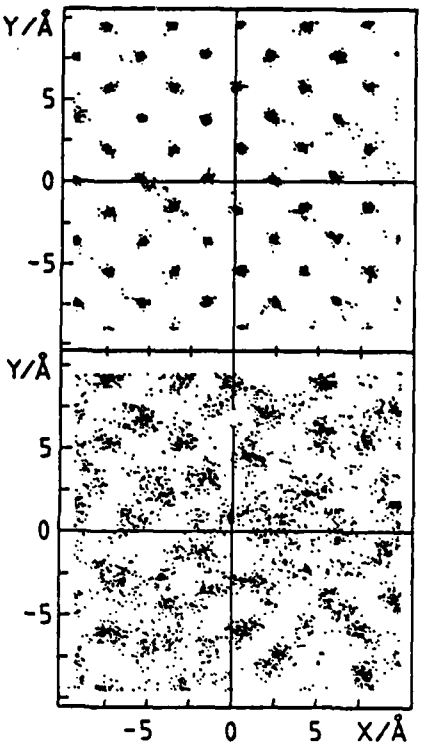


Figure 3: Density distribution in the xy-plane for the first (top) and second (bottom) layer of oxygen atoms (see text for exact definition). A dot is made every 0.15 ps at the (x,y)-position of oxygen atoms which are located in the corresponding layer at that time.

[1] E. Spohr and K. Heinzinger, submitted to *Electrochim. Acta.*

[2] P. Bopp, G. Jancsó and K. Heinzinger, *Chem. Phys. Lett.* **98**, 129 (1983).

[3] e. g. Th. E. Madey and J. T. Yates jr., *Chem. Phys. Lett.* **51**, 77 (1977); G. B. Fisher and J. L. Gland, *Surface Sci.* **94**, 446 (1980); C. Benndorf, C. Nöbl, and F. Thieme, *Surface Sci.* **121**, 249 (1982).

[4] S. Holloway and K. H. Bennemann, *Surface Sci.* **101**, 327 (1980).

[5] K. Heinzinger, *Physica* **131B**, 196 (1985).

WATER ADSORPTION. QUANTUM CHEMICAL APPROACH

An.M.Kuznetsov,* R.R.Nazmutdinov, M.S.Shapnik

Chemical Technological Institute, KAZAN (USSR)

The solvent structure at the electrode/solution interface is one of the fundamental problems in electrochemistry. Adsorption energy, partial charge transfer, molecular orientation and geometrical parameters of the molecule are of great interest for the double-layer theory. At the present time there is no accurate microscopic theory of the molecular adsorption. In this contribution, the chemisorption of a single water molecule on the Cu, Ag, Au and Zn, Cd, Hg surfaces has been investigated by means of the standard spin-polarized CNDO/2 program together with the geometrical optimization of atom positions. The d orbitals have not been taken into account, since these orbitals should give only small contribution to the bonding. The bonding parameters and the orbital exponents for the s and p orbitals have been looked for which fit the interatomic distances in the Me_2 dimers. For the metal surfaces the cluster model was used. The computations yield the following results.

On all the metals under consideration the water chemisorption in the hollow position via the oxygen atom is most favoured. On the mercury surface the water molecule lies relatively flat, with the bent angle α of 26°. For the (111) face of Cu, Ag and Au and also for the (0001) face of Zn and Cd there are two energetical minima: at the orientation of the molecule normal to the surface ($\alpha = 90^{\circ}$) and under the angle α of $55\text{-}75^{\circ}$. The first minimum is energetically more favoured. The change of the molecular geometry under the effect of chemisorption in the most stable position is negligible small. However, at the orientation of the molecule normal to the surface via the hydrogen atoms an increase of the bond angle (within ca. 10°) takes place.

*Some of these results were obtained in collaboration with Dr. J.Reinhold and Prof. W.Lorenz (KMU, Leipzig, GDR)

Reorientation energies of a single water molecular dipole and with inclusion of the lateral interactions in the first monolayer, have been also calculated using the mean field approximation for the three-positional model. Based on the obtained values of the adsorption energy, the partial charge transfer to the metal and the work function change (higher occupied molecular orbital) a new "microscopic" sequence of metal hydrophilicity was established:

$$Hg < Ag(111) < Ag(100) \approx Zn(0001) \approx Cu(111) \approx$$
$$Zn(1100) < Au(111) < Cu(100) < Ag(110) < Cd(1100) <$$
$$Cd(0001) < Au(100) < Cu(110) \approx Au(110)$$

Calculations are critically discussed in the light of experimental and other quantum chemical data.

As a next step, the structure of some molecular associates on the close-packed mercury surface and on the (111) face of silver has been investigated. Linear, cyclic and bifurcated dimers, cyclic and open trimers and also tetra- and pentamers of water have been considered. It was shown that on both metals the associates with two and three molecules (excl. the cyclic and linear dimers on Ag) are relatively stable, the hydrogen bonds between molecules being weakened. The analysis of the hydrogen bonding in the adsorbed tetra- and pentamers show a more pronounced structuring of the second water monolayer on silver in comparison with mercury.

Water structuring on the electrode surface has been also studied by using the Metropolis Monte Carlo procedure. Computation was carried out for mercury only, because the quantum chemical results on the water adsorption on this metal are in a good agreement with available experimental data. A (N,V,T) ensemble containing of 64 water molecules have been considered, the 37 molecules being in contact with metal. For the water molecules the close-packed structure with fixed centres was adopted. For discription of the pair intermolecular interactions the Bjerrum tetrahedron model for the neighbouring molecules and atom-atom potential $U = A/r^6 + B \cdot \exp(C \cdot r)$ were used. The interaction of the water molecular array with its arrangement was not taken into account. However, for the first monolayer, the dipole-

dipole interaction of each molecule with its 12 neighbours of the second shell has been included using the mean field approximation for the three-positional model. For a water molecule contacting with metal the adsorption energy profile as a function of the bent angle was obtained by means of CNDO method.

Association of water on mercury is noticeable. For instance, at 293 K, the number of molecules with three and four hydrogen bonds is maximum. The existence of dimers is possible too. The number of molecules with the maximum possible number of hydrogen bonds increases with increasing of the temperature.

The distribution function of the dipole moment component normal to the surface has three pronounced peaks. The first one is attributed to preferable orientation via the positive end of the dipole to metal, the second most pronounced peak - to the flat orientations and the third peak - to the orientation of dipoles by means of the oxygen atoms. These results reflect qualitatively the main assumption of the three-positional model of the double-layer. The most contribution to the first and the third peaks is determined by the water molecules contacting with metal. For the molecules of the second monolayer the orientations with zero dipole z-component are predominant.

METAL ELECTRONS IN THE DOUBLE LAYER MODELLING

Alexei A. KORNYSHEV

The A.N.Frumkin Institute of Electrochemistry of the Academy of Sciences of the U.S.S.R., 117071 Moscow, Leninskii prosp.31

Present status of electron density functional theory of the metal/electrolyte interface is discussed with emphasis on the predicted shape of the compact layer differential capacity dependence upon charge ($C_H(\delta)$-curves) and results on the electromodulation of optical response.

1. Brief review of recent "jellium" models, particularly of -
   * BRG /1/
   * SH /2/
   * FKP /3/
   * HP /4/
2. Modulation of the surface electronic profile, interfacial relaxation and the compact layer capacity
   * Expectations of "soft" behaviour /5-7/
   * Anomalies and catastrophes; electromechanical analogy: divergence and negative $C_H(\delta)$ values /8/ Arrival of $C_H(\delta)$ anomalies in SH, FKP, and HP models /9/
   * A search for singular behaviour in experiment (data by Hamelin et al /10/ for silver and gold (111) surfaces)
3. Electromodulation of optical response
   * Interfacial relaxation via s-polarized electroreflectance /11/

* The form of the surface electronic profile and p-polarized optical phenomena /12/

* Surface electronic profile and the electromodulation of surface plasmon dispersion relation: the role of adsorption of anions /13/

5. Modern status of the first principle calculations

* Discrete pseudopotential Kohn-Sham calculations for the periodical film model with vacuum intervals /14,15/

* How to extend them on the in situ interfaces? - The role of electrolyte solution

6. Metal nature in the double layer properties

* Electronic and ionic structure of the metal surface

* Where do we stand: can we predict variation of p.z.c., $C_H(6)$, and optical response in a series of metals or single -crystal faces?

REFERENCES

1. J.-P.Badiali, M.-L.Rosinberg and J.Goodisman, J.Electroanal. Chem. 143(1983)73
2. W.Schmickler and D.Henderson, J.Chem.Phys. 85(1986)1650
3. V.I.Feldman, A.A.Kornyshev and M.B.Partenskiĭ, Solid State Commun. 53(1985)157
4. J.W.Halley, B.Johnson, D.Price and M.Schwalm, Phys.Rev.B 31(1985)7695; J.W.Halley and D.Price, ibid. 35(1987)9095
5. D.Price and J.W.Halley, J.Electroanal.Chem.150(1983)347
6. A.A.Kornyshev and M.A.Vorotyntsev, J.Electroanal.Chem. 167(1984)1
7. A.A.Kornyshev in The Chemical Physics of Solvation (R.R.Dogonadze, E.Kálmán, A.A.Kornyshev and J.Ulstrup, eds.), part C, Chapter 6; Amsterdam: Elsevier, 1988
8. V.I.Feldman, A.A.Kornyshev and M.B.Partenskiĭ, J.Electroanal. Chem. 237(1987)1
9. Z.B.Kim, A.A.Kornyshev and M.B.Partenskiĭ, J.Electroanal. Chem., submitted(1988)
10. A.Hamelin and L.Stoicoviciu, J.Electroanal.Chem. 236 (1987)267; A.Hamelin, L.Doubova, L.Stoicoviciu and S.Trasatti, ibid., in Press(1988)
11. A.A.Kornyshev and M.I.Urbakh, J.Electroanal. Chem. 235 (1987) 11.

12. A.M.Brodsky and M.I.Urbakh, Usp.Fiz.Nauk 138(1982)413; Prog.Surf.Sci. 15(1984)121

13. P.G.Dzhavakhidze, A.A.Kornyshev, A.Tadjeddine and M.I.Urbakh, this conference.

14. S.H.Liu, C.Hinnen, G.Nguen Van Hong, N.R.Tacconi and K.-M.Ho, J.Electroanal.Chem.176(1984)225

15. E.V.Chulkov, V.M.Silkin, A.G.Lipnitskii, V.E.Panin, in the Proc.Intern.Conf. "Electrodynamics and Quantum Phenomena at Interfaces" (Telavi,1984), Tbilisi: Mezniereba, 1986, p.6

MOLECULAR MODELS OF WATER AND NEUTRAL SOLUTES AGAINST A CHARGED WALL

Rolando Guidelli and Giovanni Aloisi

Dipartimento di Chimica dell'Università di Firenze

Via G.Capponi,9 50121 FIRENZE

A lattice model of water molecules against a charged wall, with the lattice extending into the bulk, is developed. The statistical mechanical treatment of the model is carried out on the basis of the Barker's self consistent approximation (which is equivalent to the quasi-chemical approximation). Water-water interactions are accounted for via the TIP4P point-charge intermolecular potential. The only adjustable parameter in the model is the distance of closest approach of the water molecules to the charged wall. The model does not include ions, so that the electric field created by the charged wall penetrates into the bulk solvent. The surface excess of the potential difference across the interphase, of electric polarization and of entropy are estimated as a function of the charge density on the wall. It is shown that these surface excesses can be directly compared with the corresponding experimental quantities corrected for "diffuse layer effects" on the basis of the Gouy-Chapman theory, provided ionic specific adsorption is absent. The model predicts (i) a net water orientation with the negative end of the dipole pointing towards the metal at zero charge, (ii) a capacity maximum at positive charges, and (iii) a maximum of the entropy surface excess at negative charges. All these three features are actually observed experimentally at the mercury/water interphase in the presence of the nonspecifically adsorbed NaF salt. The choice of the lattice geometry does not affect the above quantitative conclusions. The model is extended in order to include the presence of a solute molecule both in the bulk and in direct contact with the charged wall. Adsorption isotherms at different charges and applied potentials are calculated and compared with experiment.

CONTRIBUTION OF THE METAL TO THE SILVER-WATER INTERFACIAL CAPACITANCE

Georges VALETTE

(L.E.I. du C.N.R.S., 1 place Aristide Briand, 92195 Meudon, France)

Specific metal-water interactions at the potential of zero charge are expressed by the modification of the surface potential of the metal $\delta\chi^{M}_{\sigma=0}$ and the surface potential of the water molecules $g^{H_2O}_{\sigma=0}$. In the case of the three low-index faces of silver, $\delta\chi^{M}_{\sigma=0}$ was determined from theoretical calculations [1], and $g^{H_2O}_{\sigma=0}$ was deduced from capacitance data by assuming a metal capacity C^{M} independent of the electrode charge σ [2]. Recommended values of the work function Φ were proposed in ref.2.

Table I. $\delta\chi^{M}$, g^{H_2O} and C^{M} at the pzc, and Φ for silver.

face	$-\delta\chi^{M}_{\sigma=0}$ / V	$g^{H_2O}_{\sigma=0}$ / V	$C^{M}_{\sigma=0}$ / $\mu F.cm^{-2}$	Φ / eV
(111)	0.39	0.21	17.0	4.47
(100)	0.32	0.19	15.1	4.21
(110)	0.29	0.18	11.7	4.04

Although a quasi σ independence of C^{M} was proposed for mercury and gallium [3], it was of interest to simulate different linear variations of C^{M} between $\sigma=0$ and $\sigma \ll 0$ for which C^{i} begins to be constant, for silver, mercury and gallium. The following relations have been used:

$$\begin{cases} 1/C^{i}_{\sigma} = 1/C(\text{ion}) - 1/C^{M}_{\sigma} - 1/C^{H_2O}_{\sigma} & (1) \\ 1/C^{i}_{\sigma \ll 0} = 1/C(\text{ion}) - 1/C^{M}_{\sigma \ll 0} & (2) \end{cases}$$

and

$$E_{\sigma} = \Phi + \left[\delta\chi^{M}_{\sigma=0} - 2\sigma/(C^{M}_{\sigma=0} + C^{M}_{\sigma})\right] - g^{H_2O}_{\sigma} + \sigma/C(\text{ion}) - 4.31 \quad (3)$$

C(ion) due to free charges is considered as constant.

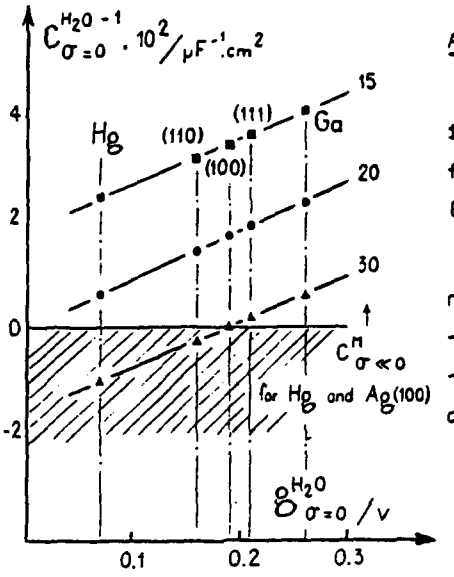


Fig.1. $(C^{H_2O}_{\sigma=0})^{-1}$ as a function of $g^{H_2O}_{\sigma=0}$ for different $C^M_{\sigma \ll 0}$.

A. C^M increase.

$(C^{H_2O}_{\sigma=0})^{-1}$, from eqns (1) and (2), is plotted as a function of $g^{H_2O}_{\sigma=0}$ in fig.1 for three values of $C^M_{\sigma \ll 0}$ for Hg and the (100) face of silver taken as references.

$C^M_{\sigma \ll 0} \geq 30\ \mu F.cm^{-2}$ leads to negative values of $C^{H_2O}_{\sigma=0}$ which would correspond to an increase of g^{H_2O} for a decrease of the electrode charge. This contingency is more than improbable.

B. C^M decrease.

C(ion) being determined from eqn.(2) for a value of $C^M_{\sigma \ll 0}$, $g^{H_2O}_{\sigma \ll 0}$ can then be deduced from eqn.(3). The g^{H_2O} dependence on σ is represented in fig.2 for different $C^M_{\sigma \ll 0}$. $g^{H_2O}_{\sigma \ll 0} = -1.9V$, for $C^M_{\sigma \ll 0} = 5\ \mu F$, is undoubtedly much too high with regard to that expected for the possible maximum orientation of the water dipoles compatible with the hydrogen bond formation. Besides, the dielectric constant in C(ion) would have a value, equal to 2, which would not be significant. These arguments would be probably applicable to data for $C^M_{\sigma \ll 0} = 10\ \mu F.cm^{-2}$.

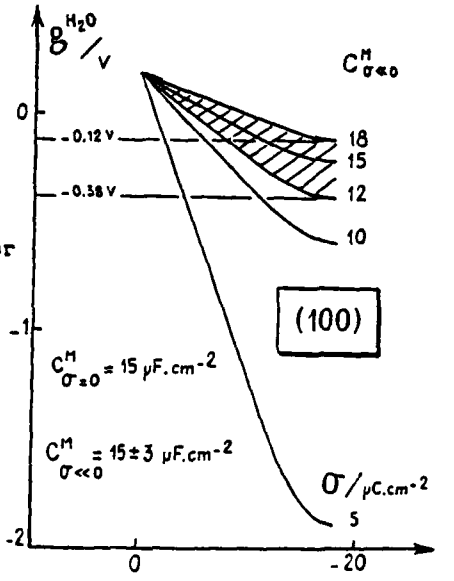


Fig. 2. g^{H_2O} as a function of σ.

It appears therefore likely that the maximum variation of C^M, in the range of negative σ, compatible with the $\delta\chi^M_{\sigma=0}$ and $C^M_{\sigma=0}$ theoretical estimates and the σ dependence of the experimental C^i would be about $\pm$ 20 % for every face of silver.

The asymmetry of the $C^i(\sigma)$ curves, with respect to the pzc, for the (100) and (111) faces of silver [4][5] could be interpreted from actual variations of C^M in the range of positive electrode charges. In contrast, the symmetry of the $C^i(\sigma)$ for the (110) face [6] would correspond to equivalent electrode charge dependences of C^M for positive and negative σ. These proposi-tions are illustrated in fig.3.

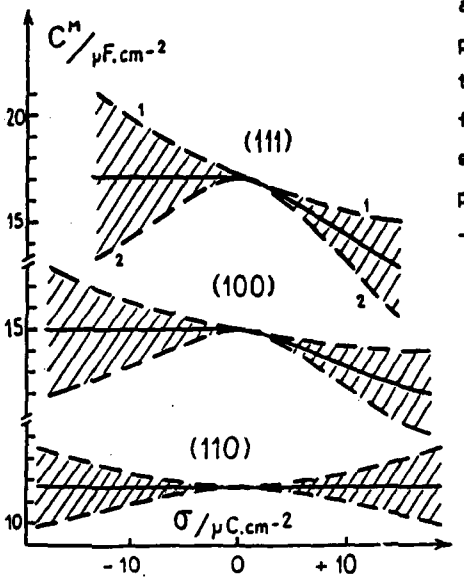


Fig. 3. Proposed electrode charge dependences of C^M for the (111), (100) and (110) faces of silver.

References.

1. V. Russier, Thèse, Paris, 1986, and private communication.
2. G. Valette, J. Electroanal. Chem., to be published.
   10^{th} European Conf., Chemistry of interfaces, San Benedetto del Tronto, Italy, 1988.
3. J.P. Badiali, M.L. Rosinberg and J. Goodisman, J. Electroanal. Chem., 143 (1983) 73.
4. G. Valette, J. Electroanal. Chem., 138 (1982) 37.
5. G. Valette, J. Electroanal. Chem., to be published.
6. G. Valette, J. Electroanal. Chem., 122 (1981) 285.

ADSORPTION FROM DILUTE SOLUTIONS OF SOLVENTS WITH ASYMMETRIC MOLECULES

P. Nikitas and A. Pappa - Louisi

Laboratory of Physical Chemistry, Department of Chemistry,
University of Thessaloniki, 54006 Thessaloniki, Greece.

Introduction: The study of the electrical double layer properties in solvents with asymmetric molecules, from a geometrical point of view, has not attracted enough attention up to now. At such interfaces differentiations in the adsorption features which can imorove our knowledge on the relevant phenomenon may be expected. For this re son, we have started in our laboratory an attempt to examine the properties of electrified interfaces formed in solvents with asymmetric molecules. Here we present the results, theoretical and experimental, concerning the interface Hg/0.1M LiCl in pentanol in the presence of triphenylphosphine oxide (TPO) and tri-n-octylphosphine oxide (TOPO).

Theoretical part: The available literature[1] shows that the molecules of alcohols are adsorbed perpendicular to a mercury electrode. In this case their dipole moment is directed almost parallel ($\rightarrow$) to the adsorbing surface. Therefore, at extreme polarizations it is very likely for the molecules to undergo a reorientation oriented with their dipole moments normal to the electrode in up ($\uparrow$) or down ($\downarrow$) positions. We have adopted this model to examine the properties of the interface under consideration. Its equilibrium properties in the presence of adsorbate (A) and solvent (S) molecules may be described by the following set of equations:

$$\mu_A(\text{ads}) - n_{\downarrow}\mu_{\downarrow} = \mu_A(\text{bulk}) - n_{\downarrow}\mu_S(\text{bulk}) \qquad (1)$$

$$n_{\rightarrow}\mu_{\rightarrow} - n_{\downarrow}\mu_{\downarrow} = (n_{\rightarrow} - n_{\downarrow})\mu_S(\text{bulk}) \qquad (2)$$

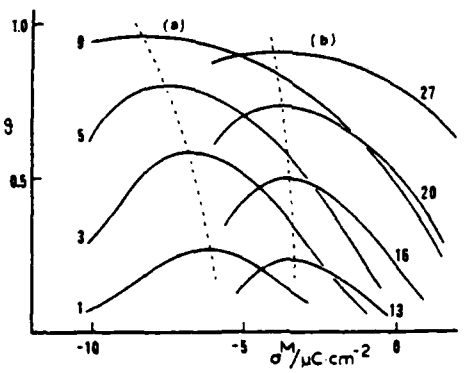


Fig.1 Plots of θ vs σ^M calculated at various $\ln(\beta c)$ values indicated by the lines for (a) r=3, $\alpha_A=7\cdot10^{-29}$ m^3 and (b) r=7, $\alpha_A=1.2\cdot10^{-28}$ m^3. Other molecular parameters: $P_A=1.4\cdot10^{-29}$ Cm, $P_S=6\cdot10^{-30}$Cm, $\alpha_{\uparrow}=\alpha_{\downarrow}=1\cdot10^{-28}$m^3, $\alpha_{\rightarrow}=\alpha_{\downarrow}/2$, $d=5.2\cdot10^{-10}$m, $z_e=10.6$, $n_{\rightarrow}=r$, $n_{\uparrow}=n_{\downarrow}=n_{\rightarrow}/2$, $\Delta U=0$, $\beta'=100$, $A^{AS}=0$. The meaning of symbols is given in ref.2.

$$\mu_{\uparrow} = \mu_{\downarrow} \qquad (3)$$

Here, $n_{\downarrow}, n_{\uparrow}, n_{\rightarrow}$ are the number of solvent molecules in $\downarrow$, $\uparrow$, $\rightarrow$ positions replaced by one adsorbate molecule and μ_i is the chemical potential of i. When the lattice model is adopted, μ_i may be calculated from eqs.18,25,29,30 of ref.2. Equations 1-3 can be used for the calculation of the adsorption isotherm. The surface pressure of the adsorbed film at dilute solutions is given by[3]

$$-\Phi/n_{\downarrow}\Gamma_m = \mu_{\downarrow} - \mu_{\downarrow}(\theta_A=0) \qquad (4)$$

where Γ_m is the saturation surface excess of A and θ_A its surface coverage. Finally, the potential drop across the monolayer may be calculated from

$$\varphi^{M-2} = 4\pi\sigma^{M}1 + 4\pi M\{P_A^t\theta_A + P_{\uparrow}^t\theta_{\uparrow}n_{\uparrow} + P_{\downarrow}^t\theta_{\downarrow}n_{\downarrow} + P_{\rightarrow}^t\theta_{\rightarrow}n_{\rightarrow}\}/n_{\rightarrow} \qquad (5)$$

where the meaning of the symbols is given in ref.2.

In order to illustrate the properties of the model eqs.1-3 were solved numerically using a large number of values for the molecular parameters. It was found that in all cases we studied the model predicts a non-congruent adsorption behaviour, which fades as the adsorbate dimensions increase. In addition, the adsorption maximum is concentration dependent (fig.1) provided that at the interface the solvent exists with at least two geometrically different states. Since a non-congruent behaviour is also predicted by models in which the solvent has spherical molecules[3], we have to conclude that from a modelistic point of view the notable differentiation in the adsorption characteristics due to the presence of geometrically different solvent states is the concentration dependence of the adsorption maximum.

Experimental part: The electrosorption of TPO and TOPO on mercury from 1-pentanol solutions of 0.1M LiCl was studied by means of electrocapillary measurements. The results obtained are in qualitative agreement with the theoretical predictions. Thus, the isotherms of TPO are non-congruent with respect to both electrical variables (fig.2). Also the plots of the inner potential against the adsorbate surface concentration are non-linear. On the contrary, within the experimental error, the adsorption behaviour of TOPO appears to be congruent. This may due to the fact that the dimensions of TOPO molecules are much larger than those of solvent. Moreover, the high solubility of TOPO in 1-pentanol did not allow us to study thoroughly this substance. It was also found that TPO appears to have a concentration dependent adsorption maximum (fig.3) which ranges from -6.8 to $-7.5\,\mu C\cdot cm^{-2}$, whereas the adsorption maximum of TOPO is located at $-4.7\,\mu C\cdot cm^{-2}$ inde-

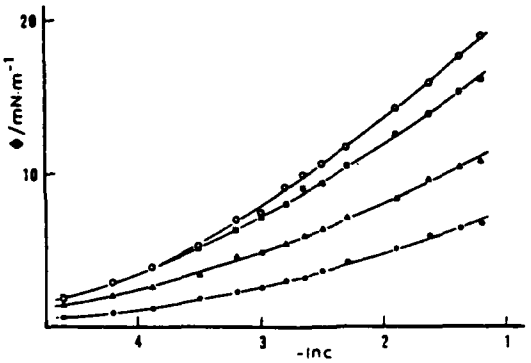


Fig.2 Surface pressure against lnc for TPO adsorption at the following surface charge densities (o)-7.5; (□) - 6; (Δ) - 4; (●) - 2 μC·cm^{-2}.

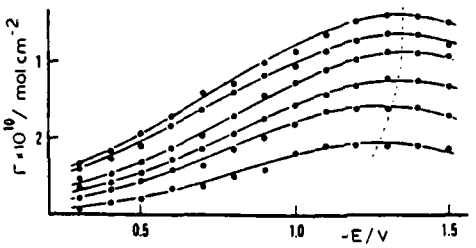


Fig.3 Surface excess of TPO vs potential with respect to a 0.1M LiCl/H_2O calomel electrode at the following concentrations of TPO: 0.2; 0.1; 0.05; 0.03; 0.02; 0.01 mol·dm^{-3}.

pendent of its concentration. Since phosphinoxides have a high dipole moment (~4.3D) the above values show that at least at polarizations negatively to -5 μC·cm^{-2} the molecules of pentanol should lie flat on the electrode. The same orientation arises from capacitance data which we have obtained for the interface Hg/LiCl in various alcohols. In what concerns the normal orientation, which is supposed in literature[1], our present results do not give any clear indication for its presence simultaneously at the interface we study. The adsorption maximum of TOPO is concentration independent, but the range of concentrations studied is rather limited. On the other hand, the dependence of the adsorption maximum of TPO appears only at its lower concentrations. The work in this direction is still in progress.

References:

1. R.Payne, Advances in Electrochemistry and Electrochemical Engineering (Edited by P.Delahay), V.7, Interscience Publishers, N.Y. 1970 ; R. Salem, Zh. Fiz. Chem.,43(1969)1839.
2. P.Nikitas, J. Chem. Soc.,Faraday Trans.1, 82 (1986) 977.
3. P.Nikitas, Electrochim. Acta, 32 (1987) 1279.
4. P.Nikitas, Electrochim. Acta, 32 (1987) 205.

POISSON-BOLTZMANN EQUATION FOR HIGHLY CHARGED POLYELECTROLYTE SYSTEMS

F. Bordi - C. Cametti - A. Di Biasio
Dipartimento di Fisica - Università di Roma "La Sapienza"
Roma - Italy

Owing to long-range electrostatic interactions, polyelectrolyte aqueous solutions, composed of polyions, counterions and simple salt exhibit unexpected behaviour, different from that of charged colloidal particles and that of uncharged polymer solutions 1).

Different transport and colligative properties 2), such as osmotic pressure, ion activity, electrical conductivity and dielectric permittivity at radiowave frequencies are determined, in a more or less extent, by the distribution of small ions in the neighbourhood of the charged polyion. To this end, the Manning counterion condensation theory 3)4) has been of continuing interest in the study of polyelectrolyte solutions. This theory predicts that for a uniformly charged line of infinite length, in the limit of infinite dilution, counterions condense on the polyion to reduce the charge density parameter $\xi = l_B/l_\sigma$ to the critical value $\xi_c = |z_1 z_2|^{-1}$.

Here l_B is the Bjerrum length, l_σ the charge spacing on the polyion chain in the full stretched configuration and z_1 and z_2 are the valences of the fixed charges on the polyion and counterions respectively. If ξ is initially less than ξ_c, no counterion condensation occurs and the counterion concentration equals its stoichiometric value in the whole solution.

The Manning condensation theory, that has been originally proposed to avoid the divergence of the partition function for an infinite-charged line at large values of the charge density parameter, in the limit of ionic strength and polyion radius tending to zero, continues to attract attention owing to its simple formulation and ability to describe qualitatively well some physico-chemical aspects of ionic aqueous solutions.

Although successful in many applications, this theory is only partially satisfactory at high salt concentration, confirming the characteristic of a limiting-law behaviour.

On the other hand, the nonlinear Poisson-Boltzmann equation 5) (PB equation) in connection with the cell model 6) gives a fairly accurate picture in modeling these systems, particularly in the ion distribution in vicinity of the polyion even at moderate dilution of the added simple electrolyte.

The solution of the PB equation for a free-salt solution furnishes, as ξ aproaches to ξ_c, a critical behaviour for the radius of the cylinder which exactly contains the fraction f of counterions that is assumed to condense in the Manning theory.

In this way 7), a well-motivated relationship is established between the PB equation and the condensation model for dilute solution in absence of added salt.

Since the full non-linear PB equation cannot be solved in closed form for polyelectrolytes in presence of simple salt, it is no possible to describe analytically the amount of the condensed charge as a function of distance from the polyion or of

the bulk concentration of the added ions.

We present here some numerical calculations for a cylindrical polyion in a symmetric uni-univalent and di-univalent electrolytes which extend previous results 8) towards higher values of the charge density parameter.

In the polyelectrolyte cell model, for a cylindrical polyion of radius a and length L, bearing N fixed charges of valence z_i, with a degree of ionization α, the PB mean-field equation, neglecting ion correlation, takes the form

$$d^2\Psi/d\rho^2 = e^{2\rho}\left\{\sum_j (K_{nj}a)^2 f_j z_j e^{z_j\Psi}\right\} \qquad j = 0,1,2. \qquad [1]$$

where $\rho = l_B r/a$; $-e/k_BT$ is the scale factor for the potential and $K_{nj} = 4\pi l_B n_j$, with n_j the bulk average concentration of counterions and simple ions from the added salt respectively. The boundary conditions

$$\Psi|_{l_B R/a} = 0$$

$$d\Psi/d\rho\,|_0 = -2|z_i|\xi\alpha$$

express a natural origin of the potential and the Gauss law respectively.

The electroneutrality of the cell implies

$$f_j = \frac{1}{2}\left(\frac{R^2}{a^2} - 1\right) \Big/ \int_0^{l_B R/a} e^{z_j\Psi + 2\rho}\, d\rho \qquad j = 0,1,2.$$

Eq. [1] was solved by a traditional *fourth-order Runge-Kutta* method to a precision of better than 1% which requires for convergence about 100 steps.

Calculations for systems corresponding to polyelectrolyte model in 1:1 and 2:1 valent electrolyte solutions have been performed for various values of the polyion radius, concentration, charge density and different degrees of ionization.

Some typical results are shown in figs. 1 and 2.

In fig. 1, the fraction of the total "condensed" charge contained within an anular region of increasing radius is plotted as a function of its radius Rf for 10^{-3} Mol/l, 1:1 valent electrolyte solution, $\xi = 1.42$, and different values of the degree of ionization α.

As α increases, and the ionic character of the solution is enhanced, the ion condensation implies that approximately the total charge is confined in regions of very small radius compared with that of the cell.

Fig. 2. shows the average concentration of cations with $z_i = 2$ confined within an anular region of thickness a, as a function of the bulk concentration of the 2:1 valent added salt, for different values of the charge density parameter ξ. As can be seen, as ξ increases the cations are condensed in the immediate vicinity of the polyion, so that the ion distribution consists approximately of two independent regions, an inner region with

high ion concentration, insensitive to salt concentration which screens the effective polyion charge density and an outer region whose ion concentration is largely independent of the polyion charge. This peculiar selective feature can assume relevance in polyions of biological interest. The results presented here indicate that the PB equation generalizes the condensation hypothesis of the Manning limiting laws to systems with added salt.

The detailed distribution of mobile ions near a charged polyelectrolyte molecule can provide an useful theoretical background in problems where the ion condensation affects the functionality of important biopolymers such as DNA or other highly charged polyions.

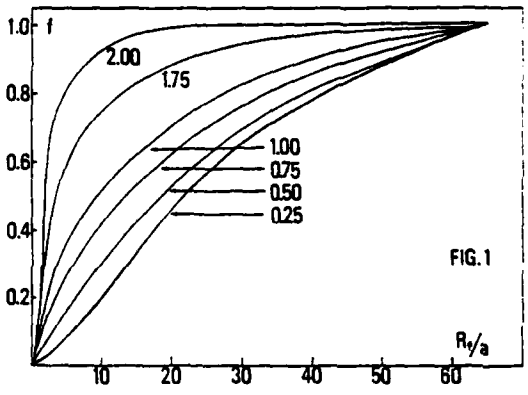


FIG.1

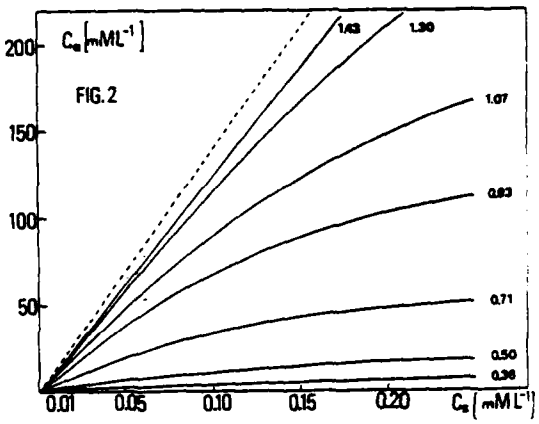


FIG.2

1) G. Jannink - "Experiments on polyelectrolyte solutions" in "The Physics and Chemistry of Aqueous ionic solutions" Edited by M.C. Bellisent-Funet and G.W. Neilson-Nato ASI Series C vol. 205 (1986).
2) C.F. Anderson - M.T. Record Jr. - Annu. Rev. Phys. Chem. 33, 191, (1981).
3) G.S. Manning - J. Chem. Phys. 51, 924, (1969); 51, 3249, (1969).
4) G.S. Manning - Q. Rev. Biophys. 11, 179, (1978).
5) D. Stigter - J. Colloid Interface Sci. 53, 296, (1975).
6) A. Katchalsky - Pure Appl. Phys. 26, 327, (1971). R.M. Fuoss - A. Katchalsky - S. Lifson - Proc. Nat. Acad. Sci. 37, 579, (1951).
7) M. Le Bret - B.H. Zimm - Biopolymers 23, (287), (1984).
8) A.R. Bizzarri - C. Cametti - A. Di Biasio - Ber. Bunsenges. Phys. Chem., 92, 17, (1988).

A variational calculation of the static image plane position at a charged jellium surface.

M.L. Rosinberg
Laboratoire de Structure et Réactivité aux Interfaces,Université P.et M. Curie, 4 place Jussieu , 75230 Paris Cedex 05, France.
V.Russier
L.E.I. , CNRS,1 place Aristide Briand,92195,Meudon Cedex,France

It is now widely recognized that the metal plays an important role in the electrical properties of the metal/electrolyte interface due to the spillover of the electrons into the solution. In the recent years several authors[1-7] have proposed to calculate this contribution by modelling the metallic surface by a semi-infinite jellium and by using the density functional formalism [8] for the conduction electrons. In the case of the metal/vacuum interface this method provides simple variational expressions for some important surface properties (work function, surface energy, image plane position), avoiding the heavy computations involved at the Schrodinger equation level. The need for a simplified treatment is especially important in the more complicated case of the metal/solution interface where one would like to interpret the experimental data which are now available from electrical (differential capacitance) or optical (ellipsometry, surface plasmons) measurements. The theoretical interpretation of these experiments is difficult because one needs to separate the different phenomena which occur at the interface.

An important quantity which governs the electrical response of the metal to an external charge and therefore its contribution to the capacitance is the centroid $z_0(\sigma)$ of the induced electronic charge density at the surface. This quantity is defined by

$$z_0(\sigma) = \frac{1}{\sigma}\int z\, n_{ind}(z)\, dz \qquad (1)$$

where $n_{ind}(z) = n_0(z) - n_\sigma(z)$ is the charge density induced by a plane with charge $-\sigma$ (atomic units are used) located at $z = d$ far away from the jellium edge (the metal occupies the $z < 0$ half space). If $n_\sigma(z)$ is the self-consistent solution of the Schrodinger equation this expression can be used safely [4,5,7] . However, when one uses a trial density profile which is obtained by minimization of the surface energy $E_s(\sigma)$ as proposed originally by Smith [9], expression (1) depends strongly on the shape of the trial function.

We have shown that it is possible to get another variational expression of $z_0(\sigma)$ which is much less sensitive to the details of the electronic density profile. By using the properties of the density functional formalism we first derive an expression which we call $z_0^{\Delta SCF}(\sigma)$

$$z_0^{\Delta SCF}(\sigma) = d - \frac{1}{4\pi\sigma}\left(\frac{dE_s}{d\sigma} - \frac{dE_s}{d\sigma}\Big|_{\sigma=0}\right) \qquad (2)$$

This is an extension of the well known ΔSCF ("change- in -self- consistent- field") expression for the work function [10]

$$\Phi^{\Delta SCF} = \left.\frac{dE_s}{d\sigma}\right|_{\sigma=0} \qquad (3)$$

The advantage of the ΔSCF expression is that it is second order in any deviation Δn in the electronic density and thus gives much better results than (1) for a variational profile which is not the exact one. Moreover, when the class of variational density profiles admits a rigid displacement with respect to the positive background, we have

$$n_{\sigma+d\sigma}(z) = n_\sigma(z+d\sigma/n) \qquad (4)$$

and we get a "displaced-profile-ΔSCF" (DPΔSCF) expression for $z_0(\sigma)$

$$z_0^{DP\Delta SCF}(\sigma) = -\frac{\sigma}{2n} + \frac{1}{\sigma}\int_0^\infty z n_{ind}(z)\, dz \qquad (5)$$

In the special case when the profile satisfies the Budd and Vannimenus sum-rule [11] the expression (5) can be also derived from (1) by transforming the $z<0$ part of the integral [3,4].

As an illustration, we present the results obtained with a simple two-parameters monotonic profile which as been used previously in the study of the metal/electrolyte interface [2]

$$n_\sigma(z) = n \begin{cases} 1 - A\, e^{\alpha(z-z_1)} & z<z_1 \\ B e^{-\beta(z-z_1)} & z>z_1 \end{cases} \qquad (6)$$

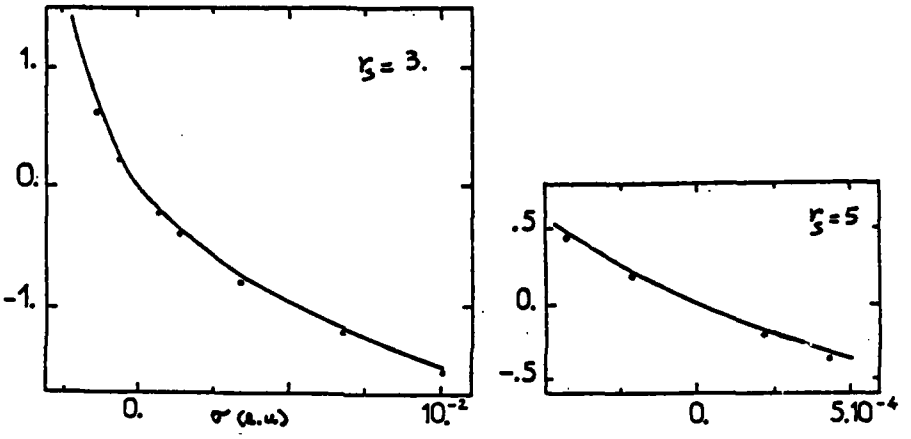
There are indeed only two free parameters for the minimization because of the continuity conditions of $n_\sigma(z)$ and $dn_\sigma(z)/dz$ at z_1 and the charge neutrality condition. In the energy functional we use the LDA for the exchange-correlation energy and include the second order gradient term for the kinetic energy. The results for Φ and z_0 at zero charge are listed in the Table for different bulk densities and compared to the corresponding results of self-consistent calculations. We see that the DPΔSCF expression for z_0 represents a considerable improvement at low electron density and that the agreement with the "exact" self-consistent results is quite satisfactory. The variation of $z_0^{DP\Delta SCF}(\sigma) - z_0^{DP\Delta SCF}(0)$ with the charge is given in the Figure for two densities. Again excellent agreement with "exact" results is observed. Note that the profile (6) does *not* verify the Budd-Vannimenus sum-rule and that the long range Friedel oscillations, which are a significant feature of the exact profile at low density are *not* included. Indeed, this is not possible in this type of approach since Friedel oscillations are a consequence of the sharpness of the Fermi surface, an effect which can be described only at the Schrodinger's equation level [8].

We thus conclude that, in the range of density and charge considered here, these restrictions have no serious consequences on the numerical value of $z_0^{DP\Delta SCF}(\sigma)$ and that the two-parameter class (6) can be used successfully in more complicated situations.

r_s	$\Phi^{\Delta SCF}$	$\Phi^{(a)}$	z_0	$z_0^{DP\Delta SCF}$	$z_0^{(b)}$
2	3,85	3,89	1,64	1,68	1,58
3	3,41	3,5	1,15	1,36	1,35
4	3	3,06	0,85	1,14	1,24
5	2,67	2,73	0,65	1,08	1,16

Table

Work function and image plane position at zero charge: $\Phi^{\Delta SCF}$ (in e.v.) is calculated from Eq (3), z_0 (in a.u.) in the 4th column is calculated from Eq (1). (a):Lang (8), (b):Schreier and Rebentrost (7).



Figure

Variation of $z_0^{DP\Delta SCF}(\sigma) - z_0^{DP\Delta SCF}(0)$ with the surface charge σ (in a.u.) for $r_s = 3$ and 5. Points: self-consistent calculation of Gies and Gerhardts (4).

References

1. Partenskii M and Smorodinskii Y 1974 Sov. Phys. Solid State 16 423
2. Badiali J P, Rosinberg ML and Goodisman J 1983 J. Electroanal. Chem. 143 73
3. Schmickler W and Henderson D 1984 Phys. Rev. B 30 3081; 1986 Prog. Surf. Sci. 22 323
4. Gies P and Gerhardts R R 1985 Phys. Rev. B 31 6843; 1986 Phys. Rev. B 33 982
5. Liebsch A 1985 Phys.Rev. B 32 625
6. Holmstrom S and Apell P 1986 Surf. Sci. 165 337
7. Schreier F and Rebentrost F 1987 J. Phys. C : Solid State Phys. 20 2609
8. Lang N D 1973 Solid State Phys. 28 225
9. Smith J R 1969 Phys. Rev. 181 522
10. Monnier R, Perdew J P, Langreth D C and Wilkins J W 1978 Phys. Rev. B 18 656
11. Budd H F and Vannimenus J 1973 Phys. Rev. Lett. 31 1218

IMPROVEMENTS IN THE TWO-PARALLEL CONDENSER MODEL OF THE DOUBLE LAYER IN THE PRESENCE OF ORGANIC ADSRORPTION

Daniel SCHUHMANN

Laboratoire de Physicochimie des Systèmes Polyphasés
UA 330 - Route de Mende - BP 5051 - 34033 Montpellier Cedex
France

The Frumkin's theory [1] for the influence of an electric fielf on organic adsorption at metals is of widespread use. It is based on the linear coverage dependence of the surface charge density σ at a given rational potential E expressed in the form :

$$\sigma = C^0 E(1 - \theta) + C^1 (E - E_N) \theta \qquad (1)$$

where C^0 and C^1 are the capacities of the water-filled and organic- filled condensers and E_N the shift of the potential of zero charge between $\theta = 0$ and 1. If the adsorption is congruent with respect to potential (Bc = f(θ) with $\partial B/\partial\theta = 0$), Frumkin derived :

$$- A \, d\ln B/dE = (\partial\sigma/\partial\theta)_E \qquad (2)$$

with $A = RT \Gamma_m$ and integrated in the form :

$$\sigma = \sigma_0 (1 - \theta) + \sigma_1 \theta \qquad (3)$$

with $\sigma_0 = C^0 E$ and $\sigma_1 = C^1 (E - E_N)$.

These equations have allowed to relate B to the electrode capacity but lead to the puzzling consequence that at zero net charge the nude and covered parts bear finite and opposite charges. This unconsistency disappears is the Frumkin's model is modified using a new expression of the surface potential E_{dip} instead of the Helmholtz formula.

In another communication, it is shown that for a film between two semi-infinite media E_{dip} is equal to $\mu N/\epsilon$ where μ is the normal component of the dipole moment, N the dipole surface density and ϵ the permittivity of the film. This expression being independent on the permittivity of the surrounding media can also be applied to an adsorbed layer. Assuming that the permittivity ϵ of the film is equal to $\epsilon_w (1 - \theta) + \epsilon_1 \theta$ where ϵ_w is the permittivity of water remaining in the film and ϵ_1 the permittivity at $\theta = 1$, that the capacity is equal to ϵ/δ, δ being the film thickness and that the total potential E is $\sigma/C + E_{dip}$, an equation analogous to eq. 1 is found but with $C'_0 = \epsilon_w/\delta$ instead of C^0 [2]. With the separation of charge and dipole potentials, integration of eq. 3 does not lead to eq. 3 and its puzzling consequence disappears but one can write [3] :

$$- A \, d\ln B/dE = (C'_0 - C_1)E + C_1 E_N \qquad (4)$$

E_N being equal to E_{dip} ($\theta = 1$).

At the isotherm plateau, for polar molecules such as alcohols adsorbed from aqueous solutions, the adsorbed film still contains water, in an amount depending on the chain length. Analysing literature data in the light of the modified model, the linear variation of ϵ with Γ_m led to affect a value of 6 to the dielectric constant of the residual water [2], probably influenced by the contact to the hydrophobic chains.

If ϵ_w and or $1/\delta$ are assumed to be linearly coverage dependent, it is easy by thermodynamic calculation analogous to those carried by the Frumkin to show that adsorption may still be described with the Frumkin isotherm but with an interaction parameter varying as E^2. If this is μ which is assumed to be linearly θ dependent, a varies in proportion with E [3].

The most recent treatments of the double layer without any organic adsorption show that the part of its capacity independent of electrolyte concentration contains a contribution due to the electronic distribution near the metal surface and another one without any determined localization but deriving from the diffuse layer. It is reasonable to think that these components remain eventually perturbated in the presence of an organic film.
On the other hand, anions [4] or cations [5] may be fixed by neutral polar species and layers of adsorbed ionic surfactants are partially neutralized by counter ions [6]. Taking into account both effects and assuming a great excess of supporting electrolyte, a further modification of eq. 1 may be proposed :

$$E = \sigma/C + (\sigma + z\alpha F\Gamma)C^0 + \beta F h/C \qquad (5)$$

where Γ is the surface excess of the surfactant, z the number of elementary charges $\pm$ e borne by its heads, α ($= 1 - \beta$) the degree of neutralization and $h = \mu/(\delta e)$, the dipoles for ionic surfactants being due to their partial neutralization. It turns our that this equation is equivalent to the "Generalized Surface Layer" (GSL) equation formaly proposed by Damaskin et al [7] as a formal generalization of the Frumkin's, Parsons' and Hansen's models :

$$\sigma = \frac{[C_0^G (1 - \theta) + n^G C_1^G \theta] E + n^G C_1^G E_N^G [1-\theta) k^G + \theta]\theta}{1 + n^G \theta - \theta} \qquad (6)$$

with : $1/C_0^G = 1/C_0 + 1/C_w$; $1/C_1^G = 1/C_0 + 1/C_1$; $n^G = (C_0 + C_1)/(C_0 + C_w)$;

$k^G = [\beta h (C_0 + C_w) + z\alpha C_w]/[\beta h (C_0 + C_w) + z\alpha C_1]$;

$$E_N^G = F\Gamma_m [\beta h (C_0 + C_w) + z\alpha C_1]/C_0 C_1 \qquad (7)$$

The GSL equation (GSLE) could be alternatively found in assuming that δ and μ are linearly θ dependent. The GSLE in particular predicts that the variation of the potential of zero charge with θ is non monotonous, behaviour observed with the adsorption of alkylbetaine [8]. I was also shown by Damaskin et al, that GSLE is not consistent with the Frumkin isotherm, save perhaps at E = 0. The thermodynamic relation between the electrostatic properties of the surface layer and the isotherm show in addition that non congruent adsorption is rather due to deviations of the former from the simplest model than to variations of intrinsic activity coefficients of the components in the surface layer.

The model for variations of μ was applied [9] to literature data on the adsorption from ethylene glycol solutions of alcohols [10] which seem to be adsorbed in a parallel orientation. The decrease of μ deduced from this analysis seems to be due to interactions between neighbouring dipoles favoured by attraction between the aliphatic chains.

The works reviewed in the present communication show the importance of the variations in the state of the surface layer. It is thus difficult to derive definitive conclusions from adsorption data for one compound only. The study of several species differing in one molecular property only (chain length, dipole...) is an useful test. Accurate derivations of molecular properties cannot be derived but at least it seems possible to evaluate some of them.

REFERENCES

1 - A.N. Frumkin, E. Phys. Chem., 116, 466 (1925) ; Z. Phys., 35, 792 (1926).

2 - D. Schuhmann, J. Electroanal. Chem., 201, 247 (1986).

3 - D. Schuhmann, Electrochim. Acta, 32, 1331 (1987).

4 - P. Vanel, D. Schuhmann and M. Guettala, J. Colloid Interface Sci., 115, 299 (1987).

5 - A. Maestre-Alvarez, N. Morel-Desrosiers and J.P. Morel, Can. J. Chem., 65, 2656 (1987).

6 - D. Schuhmann, J. Surface Sc. Technol., in press.

7 - B.B. Damaskin, A.N. Frumkin and A.V. Chizov, J. Electroanal. Chem., 28, 93 (1970).

8 - N.O. Belambri, impublished results.

9 - D. Schuhmann and P. Vanel, Electrochim. Acta, 33, 425 (1988).

10 - J.I. Japaridze, N.N. Abuladze, Sh.S. Japaridze, A. de Battisti and S. Trassati, Electrochim. Acta, 31, 261 (1986).

DETERMINATION OF THE DISTANCE OF CLOSEST APPROACH FOR SOLVENT MOLECULES TO A METAL SURFACE.

V. Russier, L.E.I. , 1 place Aristide Briand , Meudon Cedex, France.

S. Amokrane, J.P. Badiali, S.R.I., Université P.M. Curie, Bt F(74) 75230 Paris cedex

Recent models of the ideally polarized electrode have emphasized the importance of parallel progress in the description of both the metal and the solution sides of the interface and also of their coupling (1-3). Because of the complexity of a microscopic description of this system, different approximations are introduced. An important simplification is to consider that the density profiles vary only in the direction normal to the interface thus leading to one dimensional models. Another important weakness of the models is the introduction of unknown parameters such as the strength Vo of the interaction between the solvent molecules and the metal electrons and their distance of closest approach d to the metal surface. These parameters are found to be of crucial importance in the determination of properties such as the differential capacitance. Because of these restrictions, these models are too simple in order to provide quantitative informations. However, they may be used for the investigation of qualitative trends. A model which determines the distance d as a function of Vo has been recently proposed (4). In this work the initial results obtained at the potential of zero charge (P.Z.C.) are generalized to the case where the metal bears a charge σ per unit area.

For the total free energy of the metal- solution interface per unit area we use a special case of the weak coupling approximation, which has been discussed in (4). We have

$$\text{I-}\quad F = Es + Fref + \int_d^\infty \rho(z-d)\, U(z)\, dz$$

where Es is the surface energy of the metal , Fref the free energy of the solution in the vicinity of a srtuctureless hard wall located at a distance d from the metal surface and the last term represents the metal solvent interaction. Here, we assume that the ions are solvated and thus do not come in contact with the wall; therefore, the ionic distribution is ignored and replaced by a charged plane when the charge is non zero. Then $\rho(z-d)$ is the density profile of the solvent molecules. In eq.I, U(z) is the effective interaction potential of a solvent molecule with the metal and includes both an attractive and repulsive term:

$$\text{II-}\quad U(z) = Uvdw(z) + Vo \int n(z1,\sigma)\, W(\vec{r}-\vec{r1})\, dz1$$

where Uvdw(z) is the Van der Waals potential which we evaluate following (5) with the input parameters of the water molecule and n(z1, σ) is the metal electronic density. n(z1, σ) is determined by minimizing Es. The effective interaction $W(\vec{r}-\vec{r1})$ is also the same as in our previous work, the only unknown parameter being Vo. Then d is obtained from an optimisation condition of the solution free energy based on the Gibbs Bogolioubov inequality (6) wich reads:

$$\text{III -}\quad Pref + \vec{E}(0)/8\pi + \int_d^\infty \rho(z-d)\, \frac{\partial U(z)}{\partial z}\, dz = 0$$

where Pref is bulk pressure of the solution. In eq.III, E(0) is the total electrical field felt by the molecules at contact with the wall and includes the direct contribution $4\pi\sigma$ of the surface charge and the contribution due to the solvent polarization. The distribution function $\rho(z\text{-}d)$ depends only weakly on the charge and is known to be at least in σ^2 near the potential of zero charge, while U(z) is strongly dependent on σ because of the response of the electronic density to the charge. In principle, the contribution in eq.-III of terms in σ^2 can be written explicitly. However, its precise evaluation is not an easy task. In this work, we simply introduce a new parameter εeff to be understood as an effective dielectric constant in the first layer of solvent molecules adjacent to the metal. Then eq.III is written as :

$$\text{IV-}\quad \text{Pref} + 2\pi\sigma^2/\varepsilon\text{eff} + \int_d^\infty \rho_0(z\text{-}d)\,\frac{\partial U(z)}{\partial z}\,dz = 0$$

where $\rho_0(z\text{-}d)$ is the distribution of the solvent at zero charge. The determination of d and the electronic density profile then proceeds as in the case of zero charge. Because the electronic density profile obtained by minimizing Es depends on the value of d, the process must be iterated to self consistency. We now have two unknown parameters, εeff and Vo. We finally mention that the distance d is introduced only because we approximate the true potential U(z) by a hard wall. We illustrate the method on the direct contribution of the metal to the (inverse) differential capacitance:

$$\text{V-}\quad 1/\text{Cm} = d/d\sigma\,(\,\delta\chi + 4\pi\sigma\,(\,d(\sigma) - \text{Ro})\,) = 4\pi\,Y(\sigma)$$

where $\delta\chi$ is the change of the metal potential drop due to the solution and Ro the molecular radius. We give the results obtained from a jellium-like model of the metal where the ionic lattice is represented by the Aschcroft pseudo-potential. The input parameters are chosen in order to roughly simulate a Silver electrode (rs =2.64 and rc =.85 a.u.). The distance $d(\sigma)$ is shown in fig. 1 for εeff =1 and different values of Vo. In fig.2 we show $Y(\sigma)$ for different values of εeff. Both figures are for the (1 1 0) cristallographic orientation. As we can see, $d(\sigma)$ depends rather strongly on Vo but its variation with σ is nearly independent on Vo. The potential drop is also nearly independent on Vo at the P.Z.C. Indeed, we find $\delta\chi$ =.46 Volts for Vo= .45 a. u. and the same value, .42 Volts, for Vo= .6, .9 and 1.2 a.u. This must be understood as a consequence of the force balance included in eq III when d is allowed to relax in the iterative process. We also observe that the qualitative behaviour of $Y(\sigma) - Y(0)$ is not modified when the value of εeff is changed: we find a parabolic curve with a maximum at a slightly negative charge: $\sigma_o \sim -5$ μCb/cm^2.

In this work, we have calculated 1/Cm which is a contribution to the total capacitance with no classical analog. We find that it depends on the charge but its qualitative behaviour is not sensitive to the value of the parameters used in the model.

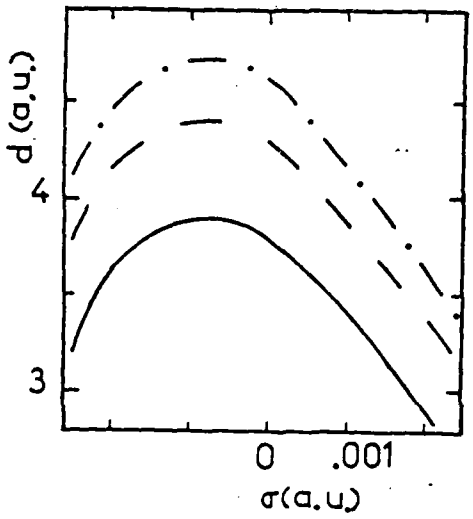


Fig.1

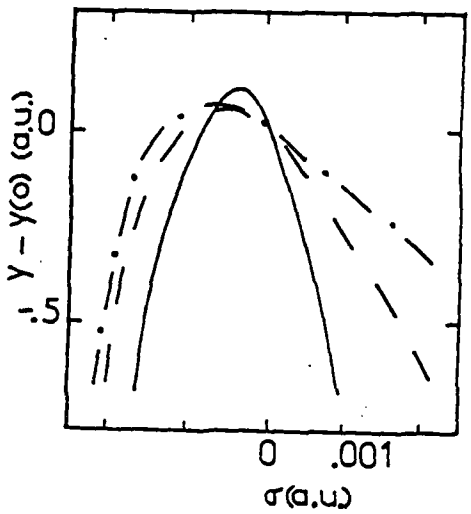


Fig.2

Fig.1 Variation of the wall position d with the charge:

————: Vo=0.6 a.u. , — — — : Vo= 0.9 a.u. , — · — · —: Vo=1.2 a.u.

Fig.2 Variation with the charge of Y defined by eq. V.

(.001 a.u. = 5.72 μCb/cm^2)

———— : εeff = 1, — — — : εeff = 6 , · — · — : εeff = oo

References

1. J.P. Badiali, M.L. Rosinberg, F. Vericat and L. Blum, J. Electroanal. Chem., 158, 253, (1983)
2. W. Schmickler and D. Henderson, J. Chem. Phys. 80, 3381, (1984)
3. J.W. Halley, B. Johson, M. Shwalm and D. Price Phys. Rev. B 31, 7695, (1985)
4. S . Amokrane and J.P. Badiali . Electrochimica Acta. (In press)
5. J. P Annett and P.M. Echenique, Phys. Rev. B32,1430, (1985)
6. J.P. Badiali and M.E. Boudh- Hir, Mol. Phys. 53, 1399, (1984)

ELECTRICAL DOUBLE LAYER INTERACTIONS BETWEEN IONIZED INVERTED MICELLES IN MICROEMULSIONS

D. Bratko[1], A. Luzar[2] and S. H. Chen[3]

Department of Chemistry, Faculty of Natural Sciences and Technology[1] and Institute of Microbiology, Medical Faculty[2], University E. Kardelj, Ljubljana, Yugoslavia[1,2], and Department of Nuclear Engineering, Massachusetts Institute of Technology, Cambridge, MA, USA[3]

The electrostatic contribution to the interaction between inverted micelles in water in oil microemulsions formed in the presence of ionizing surfactant is studied by means of Monte Carlo simulation. The inverted micelles are treated as monodisperse spherical entities consisting of the charged surfactant shell and aqueous core with neutralizing counterions (1,2). The dispersion force due to the fluctuations in the ionic distributions (3) within electroneutral micelles is considered. A comparison of the results of the simulation with recent measurements of intermicellar correlations by small angle neutron diffraction (SANS) in water in oil microemulsion is made.

References:

(1) R. Kubik, H. F. Eicke and B. Jönsson, Helv. Chim. Acta 65, 170 (1982).

(2) D. Bratko, A. Luzar and S. H. Chen, J. Chem. Phys. 89, (1988), in press.

(3) L. Guldbrand, B. Jönsson, H. Wennerström and P. Linse, J. Chem. Phys. 80, 2221 (1984).

ELECTRICAL RESPONSE OF FRACTAL AND POROUS ELECTRODES

J.-N. Chazalviel, B. Sapoval
Laboratoire de Physique de la Matière Condensée*, Ecole Polytechnique, F-91128 Palaiseau

and

J. Peyrière
Centre de Mathématiques, Université Paris-Sud, F-91405 Orsay, France

The electric impedance of rough and porous electrodes has long been known to exhibit a high-frequency behavior known as"constant-phase-angle" (CPA) behavior, i.e., $Z \propto (j\omega)^{-\eta}$ with $0<\eta<1$. A recent renewal of interest for this poorly understood problem has followed the proposal by Le Méhauté and Crépy [1] that such electrodes might be described as fractal objects and the CPA exponent η be simply related to the fractal dimension D of the electrode. There has been however several conflicting papers about this proposal, on one hand because it is experimentally difficult to determine the fractal dimension D of real objects embedded in three-dimensional space, and on the other hand because several different relationships between η and D have been derived by various authors on purely theoretical grounds (see refs. in [2]). We here consider the problem of calculating the impedance of a fractal electrode for various model geometries, in the blocking and non-blocking case, including the role of diffusion. The systematic use of Bode diagrams has been found to be of invaluable help for such calculations. We first outline the principle of this useful method, illustrated on the case of the "parallel spherical pore" electrode, then we will present some other interesting electrode geometries that we have considered, then give our results and conclusions.

The Bode diagrams as a straightforward way to get the impedance of hierarchical structures. Let us consider an electrical system consisting of many "similar" elements connected in parallel. Here "similar" means that the admittance of a given element at frequency $\omega/2\pi$ is of the form

$$y_n(\omega) = \lambda'^{\,n}\, y_0\,(\lambda^n \omega)$$

where n is an index referring to the type (size) of the element, and λ and λ' are two dimensionless scaling constants. We further assume that the number of elements of type n scales as N^n, where N is another constant. Such a situation occurs for example for the "parallel spherical pore" (PSP) electrode, shown in Fig.1(a). Each element consists in a spherical cavity of radius $b_n=b/\alpha^n$, connected to the electrode outer surface through a small aperture whose diameter also scales as $1/\alpha^n$. The admittance of such a single element in the blocking case is equivalent to that of a simple resistor-capacitor serial circuit, with $R_n \sim (\rho/b) \times \alpha^n$ and $C_n \sim (\gamma b^2) \times \alpha^{-2n}$; (here ρ is electrolyte resistivity and γ surface capacitance). This gives

$$y_n(\omega) = (R_n - j/C_n\omega)^{-1} = \alpha^{-n}\,(R_0 - j/C_0\omega\alpha^{-n})^{-1}$$

hence here $\lambda = \lambda' = 1/\alpha$. The Bode diagrams of y_0, y_1 and y_2 are shown in Fig. 1(b). The Bode diagrams of $N^n y_n(\omega)$ (n=0,1,2,....) follow by translating the $y_n(\omega)$ curves by an amount n logN along the vertical axis . The

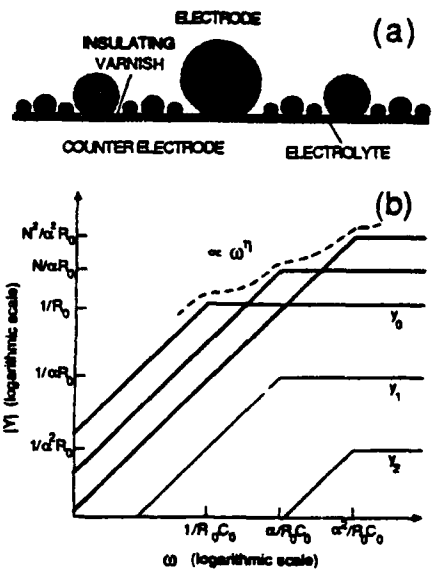


Fig.1. Illustration of the use of the Bode plot for finding a CPA exponent. Case of the "parallel spherical pore" electrode (shown in (a)) with N=2 and α =1.6 .

admittance of the electrode is obtained by summing the contributions $N^n y_n(\omega)$ over n. Due to the logarithmic structure of the Bode diagram, such a summation is obtained with a good approximation by taking *the upper envelope* of all these curves, thus yielding the dashed line of Fig. 1(b). Except for a small unessential oscillation, this is just a straight line of slope $\eta = -\ln(N\lambda')/\ln\lambda$ (here $= (\ln N/\ln\alpha) - 1$). The CPA behavior of the total admittance $Y \propto (j\omega)^\eta$ results by virtue of the analyticity of $Y(\omega)$. A rigorous justification of this procedure will be given elsewhere [2]. This example shows how simply the Bode diagram construction leads to CPA exponents for parallel-branched hierarchical structures. The case of series-parallel branching, though not so readily tractable, may also be solved by using the same kind of arguments [2].

Some interesting electrodes: geometry and impedance in the blocking case. Besides the PSP electrode, we consider here the two kinds of electrodes shown in Fig.2 : the "Mickey-mouse electrode" (ME) where now the spherical cavities are connected one upon another, each cavity of rank n giving access to N cavities of rank (n+1); and the "Super-Mickey-mouse electrode" (SME) where now each cavity of rank n gives access to N cavities of rank (n+1), N^2 cavities of rank (n+2),....., N^k cavities of rank (n+k),..... All these surfaces are self-similar, and can be fractal under certain conditions for N and α. Constructibility problems may arise for large values of N. This is not a real problem if we restrict our scope to "physical fractals", i.e., if we stop the decimation to some maximum order μ.

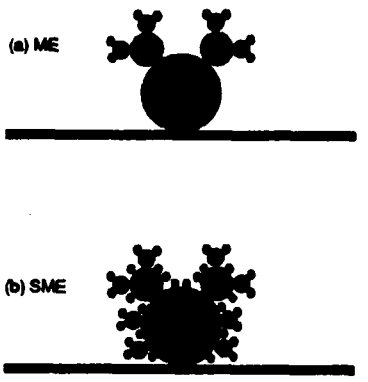


Fig.2. (a) "Mickey-mouse electrode" and (b) "Super Mickey-mouse electrode" as described in the text (here N=2, α=2, μ=3). Electrolyte in dark.

The geometrical properties of these electrodes are summarized in the first two columns of Table I. The impedance behavior for the blocking electrode, obtained with the help of the Bode diagram construction, is shown as the last two columns. CPA behavior is found for the PSP electrode *only when non-fractal*. It is *never* found for the ME (even after subtraction of the trivial series resistance R_0). It does occur for the SME, though not through the whole fractal range, but it is clear from the expressions of η and D as a function of N and α that η *cannot be simply given as a function of* D. This clearly dismisses early claims [1] regarding the connection of CPA

Table I. Summary of the properties of various electrodes.

Geometrical situation		Dimension	Impedance behavior**	
		D	Z	η
PSP	$N < \alpha$	2	$(R_0 - j/C_0\omega)$ (largest cavity dominant)	not CPA
	$\alpha < N < \alpha^2$	2	$R_0 \times (j\omega R_0 C_0)^{-\eta}$	$\ln N/\ln\alpha - 1$
	$N > \alpha^2$	$\ln N/\ln\alpha$	$(R_\mu - j/C_\mu\omega)N^{-\mu}$ (smallest cavities dominant)	not CPA
ME	$N < \alpha^2$	2	$R_0 - j/C_0\omega$	not CPA
	$N > \alpha^2$	$\ln N/\ln\alpha$	$R_0 + [jC_0\omega + J(1/R_1)]^{-1}$	not CPA
SME	$N < \alpha^2/2$	2	$R_0 - j/C_0\omega$	not CPA
	$\alpha^2/2 < N < \alpha$	$\ln 2N/\ln\alpha$	$R_0 + [jC_0\omega + \vartheta(1/R_1)]^{-1}$	not CPA
	$\alpha, \alpha^2/2 < N$	$\ln 2N/\ln\alpha$	$R_0[1 + (j\omega R_0 (2N)^\mu C_\mu)^{-\eta}]$	$\ln(N/\alpha)/\ln(2N/\alpha)$

** μ is the maximum decimation order.

behavior with fractal electrode geometry. We rather conclude that two most important points are i) parallel character of the branching: parallel branching easily yields CPA behavior, whereas serial branching can only do so under very special circumstances (such as long pores, see [2]); ii) at a given frequency, the structures contributing to energy dissipation have a characteristic size $b/\alpha^n \sim b/R_0C_0\omega \sim (\rho\gamma\omega)^{-1}$.

Faradaic and diffusive impedance. Inclusion of a Faradaic specific resistance r in parallel with the specific capacitance γ is straightforward from the formulas obtained in the blocking result, by replacing ω by $(\omega - j/\gamma r)$. An important result is that, in those cases where CPA behavior has been obtained, the Faradaic admittance is now proportional to $(1/r)^\eta$ and not simply to $(1/r)$ as naively expected. Also, the electrode admittance is *not* an extensive quantity (i.e., it is *not* proportional to the square of electrode dimensions).

More subtle is the case of diffusive impedance. Fig.3 shows the Bode plot of the Faradaic admittance of a single spherical cavity of radius b, including diffusion. At the larger frequencies the constant value b^3/r is obtained, whereas at the lowest frequencies (diffusion length much smaller than cavity radius) an ω regime is found. An intermediate $\omega^{1/2}$ regime only exists for sufficiently large cavities. When electrodes such as those of Figs.1-2 are considered, and if the resistivity of the electrolyte is neglected, the Faradaic impedances of the various cavities must be linked in parallel. This leads to a behavior such as shown in Fig.4: two CPA regimes are obtained for fractal electrodes, with a low-frequency exponent (D-1)/2 [3] and a high-frequency exponent (D-2) (which would not exist for zero r [2]). Here the CPA exponents are *truly related to fractal dimension* D. The low-frequency exponent can be understood as follows: the volume of solution undergoing electrochemical reaction at frequency $\omega/2\pi$ is just a coating of the electrode surface, of characteristic thickness the diffusion length $\Lambda_D \sim (D/\omega)^{1/2}$ (here D is diffusion coefficient). The variation of this volume Ω_D with frequency is given by the Minkowski-Bouligand definition [2] of the fractal dimension, i.e., $\Omega_D \propto \Lambda_D^{3-D}$, hence the admittance $Y \propto \omega\Omega_D \propto \omega^{(D-1)/2}$, which justifies the generality of this result. The high-frequency exponent (D-2) is also fairly general, though its validity might be limited to hollow electrode surfaces [2]. The generality of the exponents found in the diffusion case are due to the *local character* of the diffusive response. In the case where the resistivity of the electrolyte is incorporated, an exponent $\eta/2$, which is not related to D, may also appear [2].

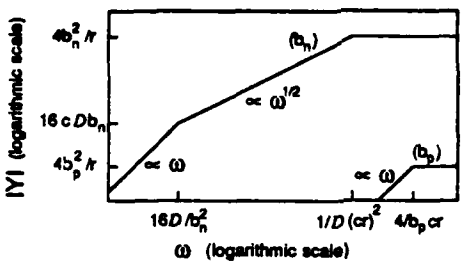


Fig.3. Faradaic impedance of a spherical pore of radius b in the presence of diffusion. Two different cases for b are shown ($b_n >> Dcr >> b_p$). Here c stands for $(z^2e^2/kT)\, c_{red}c_{ox}/(c_{red}+c_{ox})$.

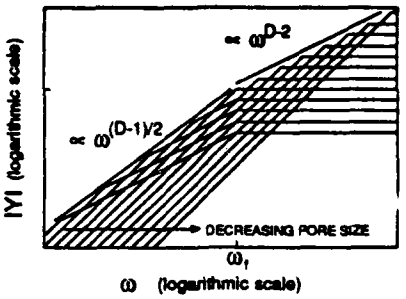


Fig.4. Typical behavior for the Faradaic impedance of a fractal electrode in the presence of diffusion: the characteristic frequency ω_f is of the order of $1/D(cr)^2$ with $c=(z^2e^2/kT)\, c_{red}c_{ox}/(c_{red}+c_{ox})$.

*URA N° 04 1254 du Centre National de la Recherche Scientifique.

References.

[1] A. Le Méhauté and G. Crépy, Solid State Ionics 9&10,17 (1983).
[2] B.Sapoval, J.-N. Chazalviel and J. Peyrière, Phys. Rev.A (in print).
[3] L. Nyikos and T. Pajkossy, Electrochim. Acta 31, 1347 (1986).

WHAT CAN BE INFERRED ABOUT THE STRUCTURE OF THE METAL SOLUTION INTERFACE FROM THE ELECTROCHEMICAL EXPERIMENT

Janusz Stafiej and Zofia Borkowska
Institute of Physical Chemistry, Polish Academy of Sciences,
ul. Kasprzaka 44/52, 01-224 Warszawa, POLAND

In the recent development of the double layer modelling the attention is focused on the approximate theories of the electron gas and/or of the solution in the interfacial region [1]. These theories are far from being complete and still too complicated to consider the question put in the title. Therefore we feel there is a need for a simple but rigorous statistico mechanical formalism providing a useful common language to describe the experimental data and set criteria for the models. The lack of such a language is the cause to the series of misunderstandings of the Cooper - Harrison catastrophe [2].

Two aproaches to the double layer modelling can be distinguished with regard to the choice of the electrical variable. In the potential drop ensemble the interfacial region is characterized by the grand canonical partition function Ξ_ϕ and $\Xi_\phi = pV^\pi - \gamma A$, where p is the pressure, V^π is the volume, A is the surface area and γ is the interfacial tension. The interfacial capacity can be expressed by the fluctuation in charge on the metal, $D^2(Q^M)$:

$$C = D^2(Q^M)/(Ak_BT) \qquad 1.$$

where k_BT is the thermal energy and T is the temperature. It is worth noting that the interfacial capacity calculated from eq. 1 is always positive. In the uniform field ensemble only negative contributions to the overall reciprocal capacity can be calculated on the basis of statistico mechanical considerations.

$$1/C_{int} = -D^2(P)/(\epsilon_o^2 Ak_BT) \qquad 2.$$

where P is the overall dipole moment of the system considered and ϵ_o is the vacuum permittivity. It is assumed that the source capacitor of the uniform external field is large enough to contain the system considered and its contribution, $1/C_{ext}$, makes the overall reciprocal capacity positive. We express it as:

$$1/C_{ext} = d/\epsilon_o + 1/C_M + 1/C_D \qquad 3.$$

where $d = V^\pi/A$ is the thickness of the interfacial region, $1/C_M$ and $1/C_D$ are determined by the theories describing the screening of the external field by the both conducting phases. Selecting the value of d large enough it is always possible to obtain negative $1/C_{int} = 1/C_{exp} - 1/C_{ext}$, where C_{exp} is the experimental value of the interfacial capacity. Note that the shape of the of $1/C_{int}$ vs charge density (σ) curve is independent of the value assumed for d. It seems reasonable to assume that it is due to the dipolar fluctuations resulting from dipolar transitions not included in the theories from which to calculate C_M and C_D. The origin of these transitions could be either the solvent dipole reorientation and/or the ionic and electronic motions. Let us consider a model in which the 'inner layer' is represented by a system of surface area, A, large enough to neglect the edge effects. The system can be found in a number of states labelled i, i=1,n. Each state is characterized by its dipole moment P_i, residual energy U_i,

weight w_i. The states in this model are also characterized by the same surface area A, and the same thickness, d. The formulae for $1/C_{int}$ and $\delta\Phi S_{int}/\delta\sigma$ are as follows

$$1/C_{int} = -\Sigma_{i,j} f_i f_j (p_i - p_j)^2 / (\epsilon_o^2 A k_B T) \qquad 4.$$

$$\delta\Phi S_{int}/\delta\sigma = -\Sigma_{i,j} f_i f_j (p_i - p_j)(H_i - H_j) / (\epsilon_o A k_B T^2) \qquad 5.$$

where $H_i = -Ep_i + U_i$, $f_i = \exp(-H_i/k_BT)/(\Sigma_j \exp(-H_j/k_BT))$ and Σ_i and $\Sigma_{i,j}$ denote summing over all states and pairs of states (transitions). $f_i f_j$ is just the probability of transition from i-th to j-th state at a thermodynamic equilibrium. It is fairly simple to obtain the predictions of this model in the low temperature limit, as shown in fig. 1a,b,c,d.

Fig.1a

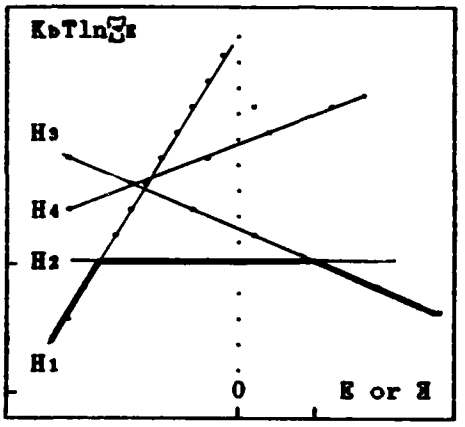


Fig.1b

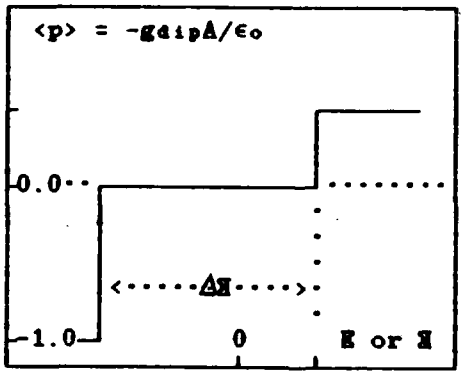


Fig.1c

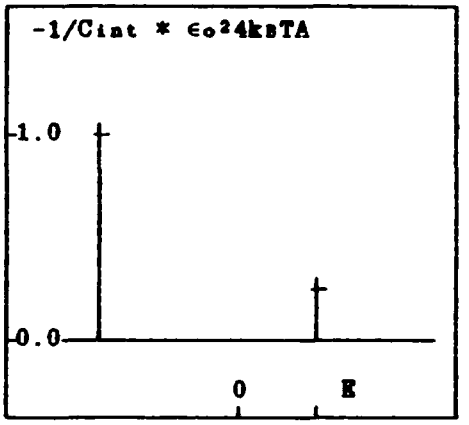
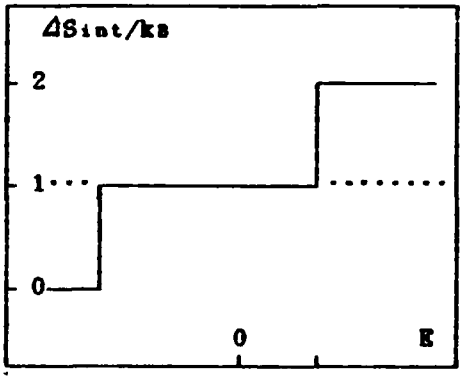


Fig.1d



In fig.1a the energies of states H_i are plotted as functions of the field $E=\sigma/\epsilon_o$ for a hypothetical 4-state model with p1=-1, p2 = 0, p3= 0.5, p4=-0.5 (slopes of the straight lines) in arbitrary units. U_i's are intercepts of these lines with the axis E = 0. The behaviour of the system at T ≈ 0K is given by the polygonal figure for the ground state energy dependence on E. $k_BT\ln\Xi_E = pV^\pi - \xi_{dip}A$, where ξ_{dip} is defined like Parsons function $\xi_{dip} = \gamma + \sigma g_{dip}$. For T ≈ 0 $k_BT\ln\Xi_E$ is just the ground state energy. Its derivative - the average dipole moment - displays step function behaviour (see fig.1b) and the

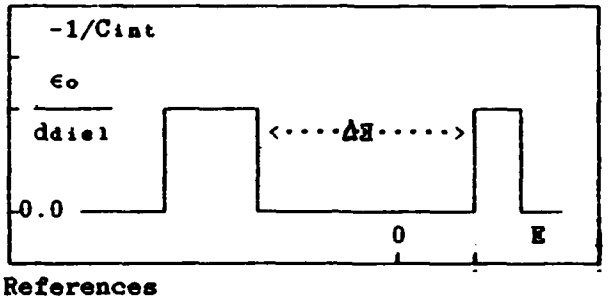
second derivative - $1/C_{int}$ - is composed of δ function sharp peaks corresponding to the vertices of the polygon (fig.1c). The energy of the state no.4 is too high to influence low temperature behaviour of the system. It is worth noting that the capacity peaks in fig. 1c are finite due to the scaling with k_BT. For any inner layer thickness, d, the model predicts negative capacities at sufficiently low temperatures. This is not surprising if we recall that the interaction energy of the system with its exterior may be of the order of k_BT at a very low temperature and the assumption that the considered area is sufficiently large to neglect the edge effects may not be valid. The dependence of $\mathcal{S}_{int}$ on σ is obtained assuming the weights $w_1 = 1$, $w_2 = e$, $w_3 = e^2$. In the points of reorientation the values $k_B\ln(w_1+w_2)$ and $k_B\ln(w_2+w_3)$ should be assumed. From the above figures and from eqs 5 and 6 it is clear that both the capacity and entropy curves are invariant with respect to the choice of the reference state. We can only learn about dipolar transitions, not the values of the dipole moments from an electrochemical experiment.

Let us assume that the area considered corresponds to one molecule of solvent, $A = \sqrt{3}a^2/2$, where a is the solvent diameter, and the interactions with the exterior of such a system are accounted for substituting the field E with the field $\mathcal{E}$. The second is the function of the first. It is clear that all formulae given above hold if the factor $\partial\mathcal{E}/\partial E$ is supplied. In the mean field approximation the relation of E with $\mathcal{E}$ is $\mathcal{E} = E + X$, where $X = (-C_e/4\pi\epsilon_o a^3\langle P\rangle)$ as it is usually written[3]. We shall write it in the form :

$$E = \mathcal{E} + \langle P\rangle/(\epsilon_o V_{diel}) \qquad 6.$$

where $V_{diel} = 4\pi a^3/C_e$ is the volume of the dielectric in the equation relating the Maxwell field (here denoted by $\mathcal{E}$ while in the textbooks by E), the displacement (here E, in the textbooks D), and the dipole moment of the considered piece of a dielectric $\langle P\rangle$ (likewise in the textbooks). The obvious requirement that the piece of the dielectric representing the inner layer should be placed in it, $V_{diel} \le V^*$ is the condition for the non occurence of the Cooper-Harrison catastrophe.

Fig.2



Inner layer capacity obtained for parameters as in fig.1a,b,c, d in mean field approximation, $d_{diel}=V_{diel}/A$ in low temperature limit. $\Delta\mathcal{E}$ is defined in fig.1b

References
1.J.P. Badiali, Ber. Bunsenges. Phys. Chem.,91(1987),270, D. Henderson, E. Leiva, W.Schmickler, Ibid. p.280.
2. J. R. Macdonald, J. Electroanal. Chem.,223(1987)1
3. W.R. Fawcett, R.M. de Nobriga, J. Phys. Chem.,86(1982)371
4.Z. Borkowska i J. Stafiej, J. Electroanal. Chem., 182(1985)253

ELECTROCHEMICAL WORK FUNCTION APPROACH TO THE KINETICS ALONG SIMPLE RATE-DETERMINING STEPS: EXAMPLE OF OXYGEN REDUCTION AT PLATINUM ELECTRODES.

A. Damjanovic
Allied-Signal Inc., Corporate Technology Center
Morristown, New Jersey 07960

Although no effect is expected of electrode material, specifically of work function, Φ, on the rates of simple electrochemical reactions when reactants and reaction products in the rate determining step (rds) interact negligibly with the electrode surface [1-4], it has been demonstrated that the rates of some simple reactions with a single electron transfer step, such as Fe^{3+}/Fe^{2+}, increase exponentially with Φ (cf. [2-5]). Here, it is reported that even the rates of a complex reaction such as oxygen reduction (OR) involving four electron transfers and multiple reaction steps and reaction intermediates, depend strongly on Φ.

From the published data for OR at Pt, Pd, Rh, Ir and Au electrodes in acid solutions, it is seen that there is a nearly linear E-logi section at all these electrodes with the Tafel slopes close to -120 mV at room temperature [7-11]. As illustrated in Fig. 1, the catalytic activity in this section, expressed as the electrode potential, E, at a constant current density, i, markedly decreases in the order $i_{Pt} > i_{Pd} > i_{Rh} > i_{Ir} > i_{Au}$. This shows that for the OR also, as for simple redox systems, the rates are strongly affected by electrode material. In Fig. 2, E vs. RHE at 5×10^{-4} Amp cm^{-2} are plotted against Φ. The preferred values of Φ's, as suggested by Trasatti [4], are used in this plot. In addition, from the published data for the OR at Pd-Au alloys [12], the potentials at the same i for these alloys at different compositions (10, 25 and 50 at.% Au) are included in the figure. For the alloys, it is assumed that Φ changes linearly with the alloy composition between Pd and Au.

It is clear from Fig. 2 that an excellent linearity exists between E_i and Φ for Pt, Pd, Pd-Au, Rh, and Au electrodes suggesting that the work function is the predominant factor controlling the rates of the OR at these electrodes. The potential for irridium electrodes significantly departs from the established dependence for the former electrodes. Since the rds at Ir electrodes is different than at Pt, Pd, Pd-Au and Rh electrodes, such digression may be associated with this difference. However, the rds at gold electrodes [11] is the same as at irridium electrodes [10]. The alignment of the potential at Au electrodes with those at Pt, Pd, Pd-Au and Rh electrodes would not then be expected. Rather, the activities at Ir and Au electrodes should follow the same dependence on Φ. This is sketched in Fig. 2 by a broken line.

The observed linear dependence for oxygen reduction is compared with the linear dependence for the Fe^{3+}/Fe^{2+} reaction at Pt, Pd, Rh, Ir, Au, Ru and Ni electrodes shown in Fig. 3 (cf. [2-4]). For the former reaction $dE/d\Phi$ ($\sim$2.1 e^{-1}) is more than three times higher than for the latter reaction ($\sim$0.59 e^{-1}). In Table 1, data are summarized for these and some other reactions.

A qualitative analysis is made of the effect of the diffuse double layer potential difference, ϕ_2, on the kinetics of the OR. It is estimated that in the potential region in which OR occurs, e.g., 500 mV positive to the potential of zero charge,

$$\frac{\Delta E_{M-2}}{\Delta \Phi} = - \frac{\Delta \Phi_2}{\Delta \Phi} = - 0.06 \text{ e-1} \qquad (1)$$

For Pt and Rh, $\Delta \Phi \approx 0.07$ eV and $\Delta E_{M-2} = 0.004$V, i.e., the change in the potential difference between the metal electrode and the outer Helmholtz plane, E_{M-2}, in going from Pt to Rh, and which difference arises from the change in ϕ_2 at these electrodes, is only 0.004V. Thus, E_{M-2} is practically independent of the diffuse double layer, and the observed effect of Φ on the catalytic activity cannot be accounted for in terms of the diffuse double layer effects.

The reversible potential for the Fe^{++}/Fe^{+++} reactions at Pt, Pd and Rh electrodes are at least 200-300 mV closer to the respective potentials of zero charge than is the potential (~0.8 V vs, RHE) at which the rates of oxygen reduction at different metals are compared, and therefore the $dE/d\Phi$ should be larger for the Fe^{++}/Fe^{+++} than for the OR reaction. This is, however, contrary to the experimental observations.

The effect of Φ on the rates of OR is further discussed in terms of a model in which Gibbs activation energy is related to the ground state energy of the species reacting in the rds.

References

1. R. Parsons, Surface Sci., 2, 418(1964).
2. J.O'M. Bockris, R.J. Mannan and A. Damjanovic, J. Chem. Phys., 48 1898(1968).
3. D. Galizzioli and S. Trasatti, J. Electroanal. Chem., 44, 367(1973).
4. S. Trasatti, in Advances in Electrochemistry and Electrochemical Engineering (H. Gerischer and Ch.W. Tobias, eds.). John Wiley and Sons, N.Y. 1977, Vol. 10, p. 213.
5. M.V. Vojnovic and D.B. Sepa, J. Chem. Phys., 51, 5344(1969).
6. A.N. Frumkin, N.V. Fedorovich and S.I. Kulakovskaya, Elektrokhimiya, 10, 330(1974).
7. D.B. Sepa, M.V. Vojnovic and A. Damjanovic, Electrochim. Acta, 26, 781(1980).
8. Lj.M. Vracar, D.B. Sepa and A. Damjanovic, J. Electrochem. Soc., 133, 1835(1986).
9. J.M. Martinovic, D.B. Sepa, M.V. Vojnovic and A. Damjanovic, Electrochim. Acta, in press.
10. D.B. Sepa, M.V. Vojnovic, M. Stojanovic and A. Damjanovic, J. Electroanal. Chem., 218, 265(1987).
11. A. Damjanovic, D.B. Sepa, Lj.M. Vracar and M.V. Vojnovic, Ber. Bunsenges. Phys. Chem., 90, 1231(1986).
12. A. Damjanovic and V. Brusic, Electrochim. Acta, 12, 1171(1967).

Legends to Figures

Fig. 1 Representation of E-logi for OR and different electrodes.
Fig. 2 Potentials at 5×10^{-4} A cm^{-2} against Φ.
Fig. 3 Φ-$\log i_o$ relation for Fe^{2+}/Fe^{3+} ammonium sulfate solution.

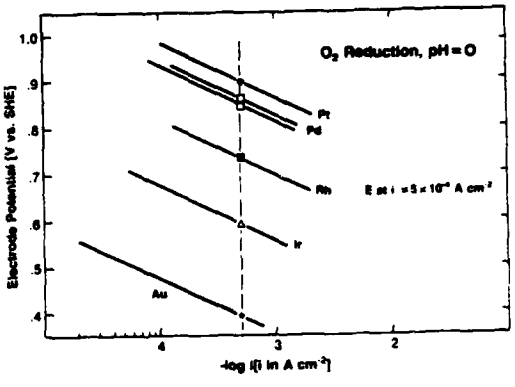


Fig. 1

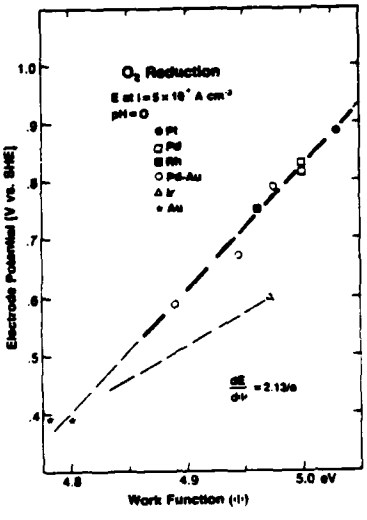


Fig. 2

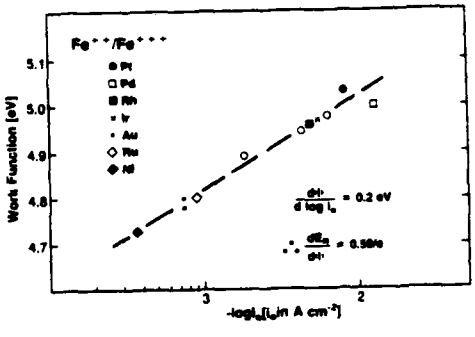


Fig. 3

An Overview of the Change of Rates and Electrode Potentials With Work Function

	$\left(\frac{d\log i}{d\phi}\right)_E$	$\left(\frac{dE}{d\phi}\right)_i$
O_2 reduction at Pt, Pd, Rh and Pd-Au	17.75	2.13
O_2 reduction at Au and Ir	(9.1)	(1.1)
Fe^{++}/Fe^{+++} (ammonium sulfate)	5	0.59
$Fe(C_2O_4)_3^{2-}/Fe(C_2O_4)_3^{3-}$	1.3	0.16
$Fe(CN)_6^{3-}/Fe(CN)_6^{4-}$ at Au and Pt	0(<0)	0(<0)
H^+/H_2	5	0.6(0.3)

UNDERPOTENTIAL DEPOSITION OF JELLIUM ON JELLIUM

E. Leiva
Departomento Fisico-Quimica, Universidad Nacional de Cordoba, Argentina

W. Schmickler
Institut of Physical Chemistry, University of Bonn
Wegelerstr.12, 5300 Bonn, FRG

Recently, the jellium model for metals has been successfully applied to the problem of the double layer between a metal and an electrolyte solution. In particular, for simple metals this model gives the correct correlation between the electronic density and the capacity at the p.z.c.. Encouraged by this relative success, we have explored the possibility to apply a similar model to the problem of the specific adsorption of metal ions on a foreign metal substrate.

We consider the adsorption of an ion of unit charge on a metal electrode:

$$M^+(sol) + e^-(metal) \longrightarrow M_{ad}$$

in the case, where the coverage with the adsorbate is near unity. Our model is an extension of the corresponding work of Lang [1] for adsorption from the vacuum. The metal substrate is represented as *jellium*: the electrons of the metal are considered to be a quantum mechanical plasma, the metal ions are represented by a positive background charge of constant density, which drops abruptly to zero at the metal surface. The adsorbate layer is represented by a thin slab of jellium with a different electronic density situated on top of the substrate (see fig.1). The electronic density is calculated self-consistently by minimizing the energy of the system within a suitably chosen set of trial functions.

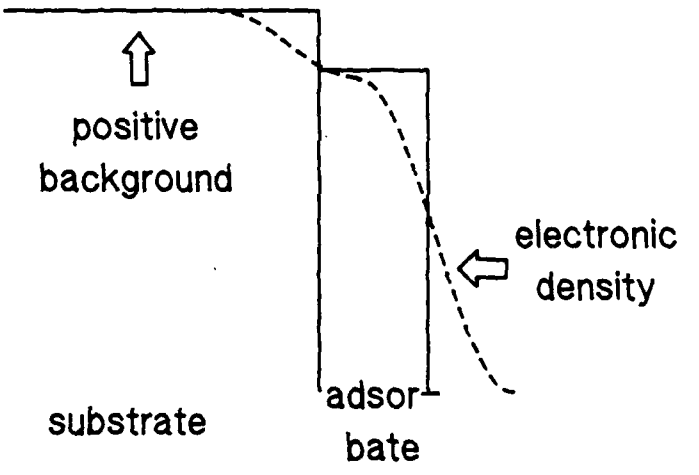
Calculations are performed twice: for the case where the metal substrate and the adsorbate have the same electronic density, and for the case where they differ. The difference in the free energy of adsorption for the two cases is calculated from the variation

of the energy of the system with the density of the adsorbate layer, and from the work functions. The energy of solvation of the metal ion is not required, since it drops out when taking the difference. Results of preliminary calculations give a correlation between the work function and the difference in the free energy of adsorption which is similar to the Kolb, Przasnyki, Gerischer relation [2].

References:

1) N.D. Lang, Phys. Rev. B12 (1971) 4234

2) D. Kolb, M. Przasnyki, and H. Gerischer, J. Electroanal. Chem. 54 (1974) 25



Pair Correlation Functions and the Structure of the Electric Double Layer

Michael Plischke
Physics Department
Simon Fraser University
Burnaby, B.C., Canada V5A-1S6

Douglas Henderson
IBM Almaden Research Center
650 Harry Road
San Jose, CA 95120, USA

A long standing problem in electrochemistry is the theory of the electric double layer - the layer of electrolyte near a charged surface. The classical theory of the double layer is due to Gouy and Chapman[1] and many authors have addressed this problem since then. The double layer problem falls into the category of inhomogeneous liquids, a subject which has been extensively studied in recent years. In contrast to the adsorbtion of simple liquids on surfaces, the theory of the double layer is complicated by the existence of long range correlations[2] parallel to the surface of a charged electrode. These long range correlations cause difficulties in both computer simulations and in integral equation based theories. Thus despite its long history, the problem is not yet solved and well worthy of further study.

In a series of articles[3], we have developed numerical techniques for the solution of the inhomogeneous Ornstein -Zernike equation with various closures. We have applied these methods to hard sphere and Lennard-Jones fluids near impenetrable plane surfaces with good results and, in a recent article[4] have solved the inhomogeneous Ornstein-Zernike equation for the electric double layer in the hypernetted chain (HNC) approximation for a range of parameters. Similar calculations have also been carried out by Kjelländer and Marcelja[5]. In these calculations we used the so called primitive model of the electric double layer, i.e., the ions are modeled by charged hard spheres; the role of the solvent is simply to modify the dielectric constant of the half space to which the charged particles are confined. Moreover, we have taken the dielectric constant of the electrode to be the same as that of the solvent. This last approximation removes the complication of image charges and also allows comparison of the results with the extensive Monte Carlo data of Torrie and Valleau[6]. It is clear from the above description that the primitive model is far too simple to allow comparison with experiment. Nevertheless, it serves as a useful testing ground for approximate theories. The hypernetted chain approximation to the Ornstein-Zernike equation indeed provides a very good approximation to the computer results, at least as far as the density profile and diffuse layer potential are concerned. As a byproduct of our calculations we also obtain the pair correlation functions in the inhomogeneous region. To date there are no simulation results to which these correlation functions can be compared.

In this article we report results obtained with the mean spherical approximation (MSA) for the same model of the double

layer. The MSA is technically easier to handle than the HNC because the direct correlation function is explicitly known in the region oputside the hard core[7]. As we shall see below, the results obtained from the MSA are comparable in quality to those obtained from the HNC as far as the density profiles and diffuse layer potential are concerned even for unphysically high electrode charge.

The inhomogeneous Ornstein-Zernike equation for a mixture of two species is

$$h_{ij}(x_1,x_2,r_{12}) = c_{ij}(x_1,x_2,r_{12}) + \sum_{m=1}^{2}\int_0^\infty dx_3 \int d^2r_3\, n_m(x_3) \times c_{im}(x_1,x_3,r_{13})\, h_{mj}(x_3,x_2,r_{32}) \quad (1)$$

where h_{ij}, c_{ij} are the total and direct correlation functions for particles of species i and j respectively and where x_j is the distance of particle j from the charged plane located at x=-d/2. The vector r_{ij} is the projection of the position vector between particles i and j onto the plane of the charged surface. Equation (1) is solved together with the Lovett-Mou-Buff-Wertheim equation[8] for the density profile $n_j(x)$:

$$\frac{\partial}{\partial x_1} \ln n_i(x_1) = \beta \frac{\partial U_{w,i}(x_1)}{\partial x_1} + \sum_{j=1}^{2}\int_0^\infty dx_2 \frac{\partial n_j(x_2)}{\partial x_2}\int d^2r_{12}\, c_{ij}(x_1,x_2,r_{12}) \quad (2)$$

where $U_{w,i}(x)$ is the potential energy of a particle of species i a distance x from the charged surface. In the primitive model we take $U_{w,i}(x) = \infty$ for $x < 0$ and $U_{w,i}(x) = 2\pi\sigma e z_i x/\varepsilon$ for $x \geq 0$. Here z_i is the valence of species i, e the electronic charge, σ the surface charge density and ε the dielectric constant of the solvent. Equations (1) and (2) can be solved self consistently once a particular closure of equation (1) has been specified. The methods are described in detail in references 3 and 4. In this article we report results for symmetric electrolytes ($z_1=-z_2=1$) at a bulk concentration of 1M with dimensionless ($\sigma^*=\sigma d^2/e$) charge density σ^* of the electrode in the range $0.1 \leq \sigma^* \leq 0.7$. The hard sphere diameter d is taken to be 4.25A in order to compare with the data of Torrie and Valleau[6]. The MSA closure of the Ornstein- Zernike equation is given by $c_{ij}(R_{12})=-\beta U_{ij}(R_{12})$ for $R_{12}>d$ and $h_{ij}(R_{12})=-1$ for $R_{12} < d$. Here $U_{ij}(R_{12}) = z_i z_j e^2/\varepsilon|R_1-R_2|$ is the Coulomb potential between particles of species i and j at positions R_1 and R_2, $\beta = 1/k_BT$ with T = 298K and ε=78.35.

In figure 1 we plot the density profiles for σ^*=0.7 obtained from both the HNC and MSA approximations. At this very high electrode charge density the counterions display layering which

is due to the hard core and which is not obtained in the Gouy-Chapman theory. As mentioned above, the two approximations are in striking agreement with each other and in reasonable agreement with the computer simulations of Torrie and Valleau.

In figure 2 we plot the diffuse layer potential $\Psi(0)$ as function of the surface charge density. Once again, we see that the two approximations are in very good agreement with other. From this we conclude that the MSA is certainly an acceptable substitute for the more complicated HNC as far as the single particle distribution functions are concerned. The pair correlation functions resulting from the MSA, on the other hand, can be unphysical, i.e. in some cases $g_{ij}(R)$ can be negative. It seems that this does not prevent the LMBW equation (2) from providing good results for the singlet functions.

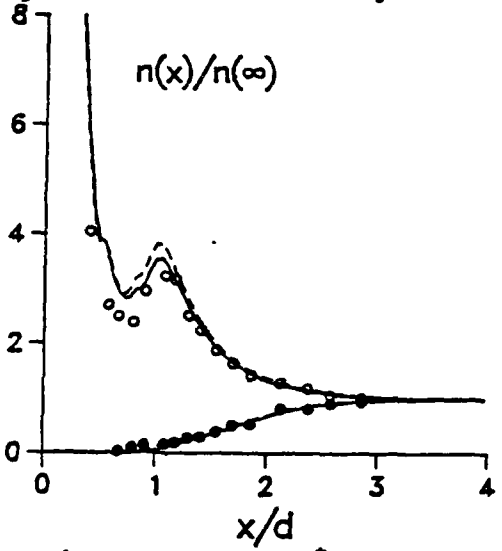


Figure 1: n(x) for σ^*=0.7. Solid line:MSA, dashed line:HNC, points: data of reference 6

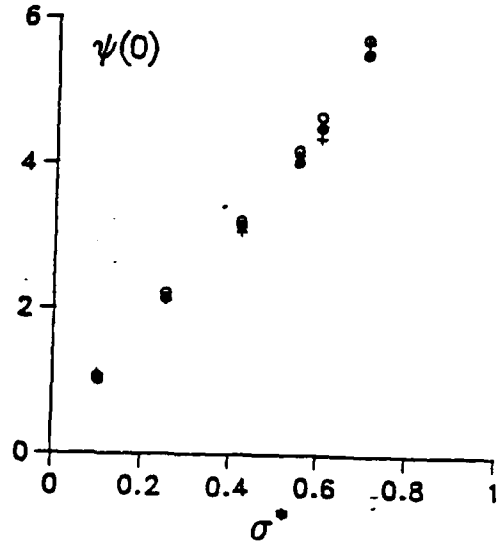


Figure 2: $\Psi(0)$ as function of σ^*. Filled circles:MSA, open circles:HNC, crosses: data of reference 6.

1. G. Gouy, J.Phys. 9, 451, (1910), D.L. Chapman, Phil. Mag. 25, 475 (1913)
2. B. Jancovici, J. Stat. Phys. 28, 43 (1982)
3. M. Plischke and D. Henderson, J. Phys. Chem. 88, 6544 (1984), Proc. Roy. Soc. (London), A404, 323 (1986), J. Chem. Phys. 84, 2846 (1986)
4. M. Plischke and D. Henderson, J. Chem. Phys. 88, 2712 (1988)
5. R. Kjelländer and S. Marcelja, J. Chem. Phys. 82, 2122 (1985), Chem. Phys. Lett. 112, 49 (1986), 127, 462 (1986)
6. G.M. Torrie and J.P. Valleau, J. Chem. Phys. 73, 5807 (1980)
7. See for example J. Barker and D. Henderson, Rev. Mod. Phys. 48, 587 (1976) for a discussion of the MSA.
8. R. Lovett, C.Y. Mou and F.P. Buff, J. Chem. Phys. 65, 570 (1976); M. Wertheim, J. Chem. Phys. 65, 2377 (1976).

THE DIFFERENCES OF SURFACE POTENTIALS BETWEEN WATER AND SOME ORGANIC SOLVENTS

Z. KOCZOROWSKI, I. ZAGÓRSKA and A. KALIŃSKA
Department of Chemistry, Warsaw University,
Pasteura 1, 02-093 Warsaw, Poland

Surface potential of a liquid solvent s, χ^s, arising from a preferred orientation of the solvent dipoles in the surface zone, is not a measurable property. χ^s and differences of the surface potentials of two solvents, $\Delta^{s_1}_{s_2}\chi$, can be estimated from:

- the differences of real and chemical energies of solvation of ions,
- the Volta potentials and components of mercury solvents interfaces at zero charge potential,
- concentration dependence of electrolyte solutions.

We proposed a method of the $\Delta^{s_1}_{s_2}\chi$ measurement * using the following voltaic cell, e.g. for water (w) organic solvent (s) system:

$$\text{SCE} \;\Big\|\; \begin{matrix} s \\ MX \end{matrix} \;\Big|\; N_2 \;\Big|\; \begin{matrix} w \\ MX \end{matrix} \;\Big\|\; \text{SCE},\ E_1 \qquad \text{(I)}$$

If liquid junction potentials are eliminated ($\|$) and MX are supporting electrolytes not changing the surface potentials of w and s, then the compensation voltage (E), measured by dynamic

* J.Electroanal.Chem., 159 (1983) 183; 193 (1985) 113 and 37th Meeting ISE, Vilnius (1986); 10th Europ. Conf. "Chemistry of Interfaces", San Benedetto del Tronto (1988).

condenser method, is equal to $\Delta^{w}_{s}\chi$. Further, in above cell N_2 represents an inert gas, e.g. nitrogen and SCE - a saturated calomel electrode.

The value of $\Delta^{s_1}_{s_2}\chi$, in the case of the cell (I), may be measured by the jet method or, as it was done by us, using the dynamic condenser method, namely from the difference between compensating voltages of the following two cells that are shown below, for example, for the water/nitrobenzene system:

$$M \left| \text{vibrating plate} \right| N_2 \left| \begin{matrix} w \\ NaCl \end{matrix} \right\| SCE \left| M,\ E_2 \right. \qquad \text{(II)}$$

and

$$M \left| \text{vibrating plate} \right| N_2 \left| \begin{matrix} n \\ TEACl \end{matrix} \right\| \begin{matrix} ns \\ TEAPi \end{matrix} \left| \begin{matrix} wn \\ TEAPi \end{matrix} \right\| SCE \left| M,\ E_3 \right. \qquad \text{(III)}$$

$$E_2 - E_3 = \Delta^{w}_{n}\chi$$

Cell (III) contains the water nitrobenzene interface with tetraethylammonium picrate (TEAPi) in a partition equilibrium. Either Galvani potential of that interface, as well as the diffusion potentials on the aqueous phase side and at the nitrobenzene the studied solvent contact, are close to zero.

The results of the $\Delta^{s}_{w}\chi$ measurements for the various, immiscible and miscible with water, solvents that have been investigated by us are collected in Tables 1 and 2. The experimental $\Delta^{w}_{s}\chi$ data are compared with $\Delta^{w}_{s}\chi$ values calculated from primitive model i.e. from Helmholtz equation.

Table 1

Solvent	$\Delta^{s}_{w}\chi / v$
Nitrobenzene	- 0.24
Nitrobenzene satd. with Water	- 0.23
Water satd. with Nitrobenzene	- 0.13
1,2 - Dichloroethane	- 0.08
Water satd. with Dichloroethane	- 0.01
Izobuthyl Methyl Ketone	- 0.17
Izobuthyl Methyl Ketone satd. with Water	- 0.17
Water satd. with Izobuthyl Methyl Ketone	- 0.33

Table 2

Solvent	$\Delta^{s}_{w}\chi / v$
Methanol	- 0.30
Ethanol	- 0.31
Ethane-1.2-diol	- 0.21
Propan-1.2-diol	- 0.24
Propan-1.3-diol	- 0.22
Methoxyethanol	- 0.33
Buthoxyethanol	- 0.31
Acetonitrile	- 0.19
Propionitrile	- 0.18
Butyronitrile	- 0.21
γ- Butyrolactone	- 0.26

U.H.V. SIMULATION OF THE DOUBLE LAYER STRUCTURE AT THE AU(100)-(5x20)/CH_3CN AND ϕ-CN INTERFACES

T. Solomun, K. Christmann and H. Baumgärtel
Institut für Physikalische und Theoretische Chemie,
Freie Universität Berlin, 1000 Berlin 33, FRG.

Electrochemical concepts have a precise significance only for structurally and compositionally well-defined interfaces. Surface-science methods and concepts are, therefore, playing an increasing role in electrochemistry. Furthermore, in order to benefit fully from experimental/theoretical feed-back it is necessary at present, to study simple interfaces.

We have chosen to study the Au (100)-(reconstructed)/acetonitrile (AN), and benzonitrile (BN) interface. The rational for the experiment was as follows. The theoretical treatment of the interfacial properties of the solvent layer is easier in the case of simple, non-associating aprotic solvents than in the case of water, due to the absence of H-bonding and therefore a reduced number of internal degrees of freedom. In addition, use of common aprotic solvents, such as AN and BN, provides access to a larger potential range over which the electrode is ideally polarizable. The geometrical parameters of the reconstructed Au(100) surface are well-established /1/. It has also been reported /2/ that the (1x1)-(5x20) reconstruction is stable, and can be irreversibly lifted in-situ, under certain electrochemical conditions.

We have therefore, firstly, undertaken a LEED, Auger, High-resolution electron-energy loss spectroscopy (HREELS), Temperature-programed thermal desorption (TDS) and work function ($\Delta\Phi$) study of the interaction of AN and BN with the clean, reconstructed Au(100) surface, under UHV conditions. Acetonitrile: On the clean gold surface AN was reversibly adsorbed, desorbing with an activation energy of about 11 kcal/mol^{-1} at 175 K from a monolayer state and at 150K from a multilayer state. The associated work-function changes were -650 mV and -50 mV for the monolayer and multilayer states, respectively. The EELS frequencies of sub-monolayer, monolayer and multilayer CH_3CN are in excellent agreement with the gas phase infrared spectrum /3/, indicating a rather weak interaction with the surface. In particular, at monolayer coverages the C≡N stretch was observed at 2277 cm^{-1} versus 2268 cm^{-1} for gas phase AN. Irrespective of AN surface coverage, no other long-range order except that of the '5x20' reconstructed substrate could be detected by LEED. Thus, the surface reconstruction is not lifted by the presence of AN on the surface. Benzonitrile: In contrast to AN, BN interacts significantly stronger with the surface although again, the reconstruction of the surface is not lifted. It adsorbs reversibly with TDS revealing two monolayer states (β_1 and β_2) and a multilayer state, with desorption temperatures (binding energies) of 286 K (17 kcal/m l^{-1}), 233 K (14 kcal/mol^{-1}) and 190 K, respectively. The associated work-function changes for the monolayer β_1 and β_2 states and multilayer state were -550 mV, -175 mV and -125 mV, respectively. The EELS modes were assigned on the basis of BN infrared and Raman spectra /4/. The most important aspect of the

spectra, at sub-monolayer and monolayer surface concentrations is the lack of the dipolar C≡N stretching mode; in most cases, a stretching frequency typical of a CN triple bond was seen in the spectra of multilayers. The spectra are indicative of molecularly adsorbed BN species with the ring-plane and the CN group parallel to the surface. A similar conclusion was reached in the case of BN adsorbed on Cu(111) /5/.

Coadsorption of AN and BN with K. Of particular interest in the context of this study is the orientation of AN and BN on the electrode surface as a function of potential. In principle, the potential at the solid/vacuum interface can be varied by coadsorbing electropositive or electronegative species /6/. In the case of alkali metals 'cathodic' conditions are simulated. An increase of K coverage up to about 20% of the maximum K-monolayer coverage results in a linear decrease of the surface work-function by 3V without lifting of the reconstruction of the surface /7/. Thus, the precise potential can be adjusted by a choice of an appropriate coverage of K on the surface. In the case of both, AN and BN coadsorption with small amounts of K on the surface produce up to three additional monolayer states in the TDS spectra, corresponding to increase in the binding energy of about 6 kcal/mol^{-1}. They were assigned to direct electrostatic and through-metal K/AN,BN interactions. The most interesting aspect of the study is the K_{ads} induced reorientation of benzonitrile species, whereby the molecular plane is normal to the surface and the C≡N stretch is significantly red shifted.

We have also obtained the double layer capacities for the Au(100) surface in contact with AN,BN/$LiClO_4$ electrolytes, and discussed

them in terms of the double layer structure as derived from the UHV data.

References:

1) G.K. Binnig, H. Rohrer, Ch. Gerber and E. Stoll, Surf. Sci., 144 (1984) 321.

2) D.M. Kolb and J. Schneider, Electrochim. Acta, 31 (1986) 929.

3) J. E. Davies, J. Mol. Struct., 9 (1971) 483.

4) J. H. S. Green and D.J. Harrison, Spectrochim. Acta, 32A (1976) 1279.

5) M. E. Kordesch, W. Feng, W. Stenzel, M. Weaver and H. Conrad, J. Elect. Spect. Rel. Phenom., 44 (1987) 149.

6) J. K. Sass, Vacuum, 33 (1983) 741.

7) T. Solomun, H. Baumgärtel and K. Christmann, to be published.

INFLUENCE OF SURFACE CRYSTALLOGRAPHY ON MOLECULAR ADSORPTION AT THE GOLD-SOLUTION INTERFACE

J. Richer[1], A. Iannelli[1], L. Stolberg[1], D.E. Irish[2] and J. Lipkowski[1]

Guelph-Waterloo Center for Graduate Work in Chemistry
[1] University of Guelph, Guelph, Ontario, N1G 2W1
[2] University of Waterloo, Waterloo, Ontario. N3L 3G1

Adsorption of neutral organic compounds such as t-amyl alcohol, pyrazine and pyridine at the low index and high index (stepped) single crystal surfaces of gold has been investigated.

Auger electron spectroscopy (AES) and low energy electron diffraction (LEED) have been employed to control the purity and to characterize the structure of the surface investigated. Chronocoulometry has been used to measure the electrode charge densities. Classical thermodynamic analysis has been applied to obtain adsorption isotherms, free energies of adsorption and electrosorption valencies. The calculation was performed with both potential and charge density as the independent electrical variable. The orientation of the adsorbed molecules has been determined from the dependence of the potential drop across the interface on the amount of adsorbed species. In addition, IR electroreflectance experiments (SNFTiRS) have been performed to obtain additional information about surface orientations of the molecules.

All molecules investigated interact specifically with the gold surfaces. In the case of t-amyl alcohol, these interactions orient the adsorbed molecules with the hydroxyl group facing the metal and hydrocarbon tail toward the solution indicating that the energy of interaction is greater than the energy of hydration for the alcohol functional group.

Pyrazine has no net permanent dipole moment. It has a tendency to adsorb flat at the metal surface. Overlap of the bonding π orbitals of the molecule with the empty states in the metal band structure is thought to be involved in the formation of the chemisorption bond.

Pyridine assumes two orientations; flat with the aromatic ring to the metal at a negatively charged surface and vertical with the nitrogen atom directed toward the metal at a positively charged surface. At the low index planes, (111) and (100), the reorientation of the molecules take the form of a phase transition.

The adsorption of all compounds investigated is strongly influenced by the surface crystallography. The free energy of adsorption becomes more negative by going from the smooth (low index) to the stepped (high index) planes. At the same time the potential range in which adsorption takes place decreased as the roughness (on an atomic scale) of the surface increases. For pyridine adsorption, a tendency towards preferential adsorption in the vertical orientation is observed at stepped surfaces. Molecular models which explain the above results are presented and discussed.

ADSORPTION OF β-CYCLODEXTRIN ON THE MERCURY ELECTRODE FROM WATER AND WATER + ETHANOL MIXTURE

J. Taraszewska and J. Śledzik
Institute of Physical Chemistry, Polish Academy of Sciences, 01-224 Warsaw, Poland

The growing interest in the study of electrochemical properties of cyclodextrins (cycloamyloses) is due to their ability to form inclusion complexes with a variety of electroactive species. Cyclodextrins (CDs) are adsorbed on the Hg electrode (1,2) and can influence the course of the electrode reactions.

Inclusion processes are often studied in the presence of an organic solvent which is usually adsorbed also on the electrode surface and can have a pronounced effect on the adsorption of CD. However, there is a lack of information on this subject in the literature.

The aim of our work was to study the adsorption of β-CD from aqueous solutions of 0.1M Na_2SO_4 and 0.1M and 0.5M phosphate buffer (pH=7) as well as from water + ethanol (EtOH) mixture containing 20 vol.% EtOH. We hope that in connection with increasing interest in electrochemistry of CDs our studies may be also usefull for further comparison of β-CD adsorption on other electrode materials.

Experiments were performed using the impedance bridge method.

The C-E curves for 0.1M Na_2SO_4 are shown in Fig. 1. Curves in 0.1 and 0.5M phosphate buffer were similar. The shape of the curves is different from that observed for simple sugars (3). A lowering of the capacitance in the potential range 0-100 mV indicates that β-CD is adsorbed in this region. One cannot also exclude simultaneous complexation by β-CD of anions of the supporting electrolyte. The subsequently recorded peak at about -220 mV, which upon increasing the β-CD concentration moves towards more positive potentials, seems to be associated with the reorientation of β-CD on the Hg surface. In the potential range -300 to -800 mV the C-E curves show a broad minimum with an adsorption maximum near the potential of zero charge (pzc). As in the case of simple sugars, the pzcs were almost independent of the β-CD concentration. At potentials more negative than -900 mV, β-CD starts to desorb.

In solutions of β-CD in 0.1M Na_2SO_4 the C-E curves were integrated twice using as the second integration constant the values of the surface tension at the pzc determined by Borkowska (4). The electrocapillary curves obtained by double integration were consistent with the electrocapillary curves determined by the drop time method, except in the most negative potential range.

The degree of surface coverage Θ by β-CD was calculated on the basis of our previous studies (5) concerning the influence of very low concentrations of β-CD on the electroreduction of isomeric chloronitrobenzenes (ClNB) on the hanging Hg drop electrode.

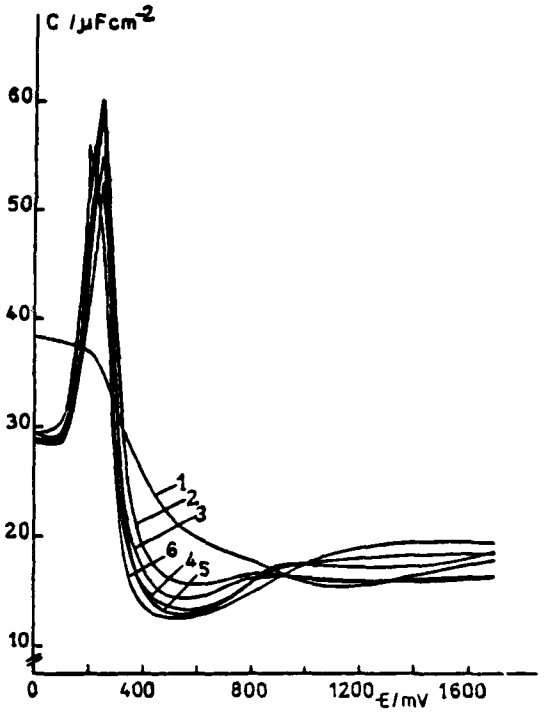


Fig.1. Double layer capacity curves for aqueous 0.1M Na_2SO_4 containing β-CD at the following concentrations: (1) 0, (2) 0.02, (3) 0.05 (4) 0.314, (5) 0.785, (6) 3.14 mmol·l^{-1}

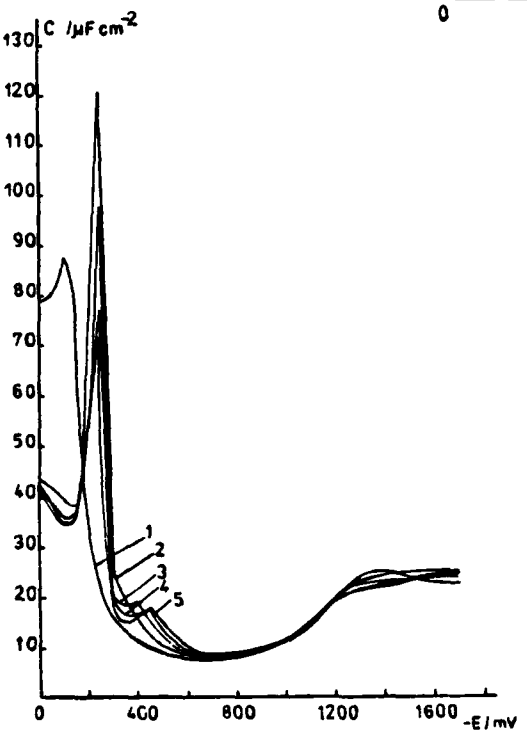


Fig.2. Double layer capacity curves for 0.1M phosphate buffer in H_2O + 20% vol.EtOH containing β-CD at the following concentrations: (1) 0, (2) 3.14, (3) 6.28, (4) 9.41, (5) 12.5 mmol·l^{-1}

$$\Theta = i_o - i/i_o - i_\infty \quad (1)$$

where i_o, i and i_∞ - denote the peak current of ClNB reduction in the absence of β-CD, at a given analytical concentration of β-CD, and at the maximum electrode surface coverage by CD, respectively.

Assuming that $i_\infty = 0$ and the adsorption of β-CD follows the Langmuir isotherm we evaluated the adsorption coefficient from the relation

$$i_o/i - 1 = \beta C_{\beta\text{-CD}} \quad (2)$$

A value of $\beta = 7 \times 10^4 M^{-1}$ was obtained, which is in good agreement with the literature data (1,2).

The presence of EtOH can influence the adsorption of β-CD significantly.

The C-E curves in the presence of 20 vol.% EtOH are shown in Fig. 2. In the potential region 0-100 mV adsorption of β-CD is similar to that from pure aqueous solutions, however the nature of the peak at -250 mV may be different. We suppose that it is connected with the simultaneous adsorption of EtOH, which may cause a partial desorption of β-CD due to its limited solubility (6) in EtOH rich mixtures.

In the presence of 20 vol.% EtOH the pzc shifts towards more negative values with increasing β-CD concentration, which is indicative for the removal of EtOH from the electrode surface. The removal of EtOH may be connected with formation of the inclusion complex of EtOH with β-CD (7). This complex may then be desorbed from the electrode surface at potentials corresponding to the peak of rather unusal shape whose potential moves with increasing in β-CD concentration from -360 mV to -450 mV.

REFERENCES

1. Y. Matsui, H. Sawada, K. Mochida and Y. Date, Bull. Chem. Soc. Japan, 48 (1975) 2446
2. L. Daruhazi, J. Szejtli and L. Barcza, Acta Chim. Acad. Sci. Hungaricae, 110 (1982) 127
3. R. Parsons and R. Peat, J. Electroanal. Chem., 122 (1981) 299
4. Z. Borkowska, J. Electroanal. Chem., in press
5. J. Taraszewska and A.K. Piasecki, J. Electroanal. Chem., 226 (1987) 137
6. W. Schlenk and D.M. Sand, J. Am. Chem. Soc., 83 (1961) 2312
7. Y. Matsui and K. Mochida, Bull. Chem. Soc. Japan, 52 (1979) 2808

LOCAL INTERACTIONS IN THE DOUBLE LAYER AND ORIENTATION OF ADSORBATE MOLECULES

A. Daghetti, S. Trasatti

Department of Physical Chemistry and Electrochemistry
University of Milan, Via Venezian 21, 20133 Milan, Italy

G. Rocchini

ENEL-CRTN, Via Rubattino 54, 20134 Milan, Italy

I. Zagorska and Z. Koczorowski

Department of Chemistry, University of Warsaw
ul. Pasteura 1, 02-093 Warsaw, Poland

The orientation of neutral adsorbate molecules at solid/liquid interfaces is determined by a number of factors which, in a simplified picture, may be described by pair-wise interactions: solid-adsorbate, adsorbate-adsorbate and adsorbate-solvent. In addition, an electric field may be operative if the solid surface is electrified. Thus, chemical and electrostatic terms sum up to determine the actual situation.

Experimental separation of the various factors to make an approach to the understanding of the local situation possible, is very hard since the factors are intimately interrelated. A first-approximation, possible way out is to keep one of the variables alternatively constant. Thus, the electric field is cancelled out by operating under zero charge conditions (uncharged solid surface), while the role of the solid-adsorbate interaction may be explored by varying the nature of the interface (which however results in also varying the solid/solvent interactions).

The design of the above approach is not recent: it was pioneered by late Prof. Frumkin in early 1930's. Nevertheless, it still proves useful. In particular, the role of metal-adsorbate interactions can be inferred by comparing the adsorption behaviour of the same substance at an electrode interface and at the free surface of the solution.

Following previous studies with nitriles and ethers of ethylene glycol which have proved the practical usefulness of these studies, in this work the adsorption behaviour of propargyl alcohol has been investigated at the Hg/solution interface and the free surface of water. The use of Hg as a reference material is well established due to the possibility of carrying out surface tension measurements enabling a rigorous thermodynamic analysis to be performed.

Propargyl alcohol is a substance used in technology as a corrosion inhibitor for iron, whose mechanism of action is to be elucidated. The first step has thus been to investigate the adsorption behaviour at an uncharged solid surface. Interfacial

tension measurements have been performed by means of a classical Lippman electrometer and have been supplemented by capacitance measurements by means of a Wien-type impedance bridge. Twice integrated capacity data give the interfacial tension so that cross-checking of the reliability of experiments carried out with the two techniques is possible. The surface tension of water was measured by the maximum bubble pressure method. In addition, surface potential variations due to adsorption were measured by the streaming Hg technique for the metal/solution interface and by the vibrating condenser method at the free surface of the solution.

Experimental data have shown that the adsorbability of propargyl alcohol is the same at the two interfaces. This rules out any specific interaction of the polar head or of the triple bond of the adsorbate with the electron gas of the metal surface. The value of the electrical capacity and of the surface concentration at saturation suggest that the adsorbate is very likely to lie with its major molecular axis parallel to the metal surface. It is reasonable to envisage a molecule with the OH group, which is not in line with the molecular axis, turned towards the liquid phase as a consequence of local hydrogen bonding to the solvent. The hydrocarbon tail is not strongly hydrophobic because of the presence of the trible bond. This favours the planar configuration since squeezing out effects are presumably reduced.

The absolute adsorbability of propargyl alcohol is modeste so that it alone cannot explain its corrosion inhibiting properties. Higher adsorbability is exhibited by the technical-grade product as normally available commercially, probably on account of the tendency of this molecule to polimerize because of the reactivity of the triple bond (it is also reduced in the most negative range of the usually explored potential range, i.e. 0 to -1.6 V *vs* SCE). The specific activity for inhibiting the corrosion of iron may perhaps be explained in terms of strong interaction of the triple bond with the partly empty d-bonds of the transition metal. Experiments with solid electrodes are in progress.

The financial support to this work by ENEL is gratefully acknowledged.

DIFFUSION KINETICS AT FRACTAL INTERFACES

Lajos NYIKOS and Tamás PAJKOSSY

CENTRAL RESEARCH INSTITUTE FOR PHYSICS
H-1525 Budapest, P.O. Box 49, Hungary

The effect of surface irregularities on diffusion kinetics is studied by using the fractal description of the irregular interface. We treat both small and large signal response including the diffusion impedance, the Cottrell response and linear sweep or cyclic voltammetry.

The decay of the diffusion-controlled current of particles diffusing from an initially homogeneous medium to a completely absorbing fractal boundary was previously shown to exhibit $t^{-\alpha}$ time-dependence instead of the conventional $t^{-1/2}$ one with the exponent α being determined by the fractal dimension, D_f, of the interface as $\alpha=(D_f-1)/2$. In electrochemical terms this corresponds to a generalized Cottrell equation (or Warburg impedance) and can be used to describe the frequency dispersion caused by surface roughness effects. We verify the predicted behaviour for fractal surfaces with $D_f>2$ (rough interface), and $D_f<2$ (partially blocked surface or active islands on inactive support). In addition, the fractal decay kinetics is shown to be valid for both contiguous and non-contiguous surfaces.

Computer simulation, a mathematical model, and direct experiments on well-defined fractal electrodes were the tools for verifying the fractal decay law for the different surfaces. The predicted power-law behaviour was in fact observed in each case, and the predicted $\alpha(D_f)$ relationship was seen to prevail in each case.

The expressions describing the shape of voltammograms of reversible redox couples were generalized for a fractal boundary. It was shown that they are analogous to the conventional ones except for the need to use a Riemann-Liouville transformation of order $q=-\alpha$ instead of $q=-1/2$ to bring the fractal voltammogram to the same simple and perturbation-invariant form. The order $-\alpha$, determined by the fractal dimension, D_f, of the interface as $\alpha=(D_f-1)/2$, is the same fractional value which appears in the fractal Cottrell expression and the fractal Warburg impedance.

A computer simulation technique was developed for approximately calculating the voltammograms for arbitrary potential sweeps and different interface geometries. The simulated fractal voltammograms (using a self-affine interface with $D_f>2$) were shown to be in agreement with the theoretical prediction: the RLT of the predicted order brings them to the neopolarographic form, and the difference in relation to the conventional semiintegrated curves is quite pronounced.

Experiments were done on partially covered gold electrodes having a well-defined fractal dimension by construction. These experimental voltammograms, similarly to the simulated ones, agreed with our theoretical predictions.

Consequently, the fractal generalization of the conventional voltammetry equations was seen to be valid for both $D_f>2$ and $D_f<2$ surfaces. The generalized model was shown to be valid for non-linear potential sweeps as well.

Since voltammetry is a widely used technique, and many solid surfaces show fractal behaviour, we expect the generalized model, developed and verified in the present work, to be useful in many branches of electrochemistry, including possible applications in electroanalysis.

Furthermore, since many real surfaces can very effectively be modelled as fractals, we expect the presently verified fractal Cottrell, Warburg, and voltammetry models to be generally useful in diffusion-related problems connected with irregular interfaces. When studying complex systems, the present model can offer valuable help by which the dispersion caused by geometrical irregularities can be separated from complex system behaviour caused by other factors. If it is only the geometry which is complicated, the results described in the present work allow the approximate determination of the same relevant chemical parameters as in the conventional case.

The presently verified fractal diffusion model has an additional feature which deserves some emphasis: this being its generality. It is based on a very general assumption - *ie* self- similarity of the irregular interface - and nothing specific concerning the electrode material, diffusing substance, etc is assumed. As we have seen, it is equally valid for contiguous or non-contiguous, rough or partially active surfaces.

ANALYSIS OF CONCENTRATION, ELECTRIC POTENTIAL AND CHARGE DENSITY PROFILES IN INTERFACIAL REGION OF AN AQUEOUS ELECTROLYTE, NEAR A CHARGED SURFACE.

V.S.Vaidhyanathan
Department of Biophysical Sciences, School of Medicine,
State University of New York at Buffalo, Buffalo, New York, 14214.

Extended Abstract.

Certain fundamental questions, regarding the nature of ion distribution, electric and charge density profiles in interfacial region near a charged surface, are addressed. In the classical Gouy-Chapman-Stern theory as well as in many of the so-called modifications, the mass conservation conditions seem to have been completely ignored. The influence of ions of electrolyte on the electric potential profile, arising from charged surface also appear to have been neglected. The concentration profiles of anions and cations of a univalent electrolyte, would be similar in the absence of a charged surface. In the presence of a charged surface, these concentration profiles are disturbed, with unlikely charged ions enjoy being in the neighborhood of ions localized on the surface. It should be evident that the integral over the extent of inhomogeneous region of say, the concentration profiles of a univalent anion should equal the value of similar integral over the univalent cation. This result obviously requires that there should be at least two extrema values in the concentration profiles of positive and negative ions, as schematically shown in Figure 1, near a surface containing an excess of negative ions. Clearly, the Poisson-Boltzmann equation of classical physical chemistry, or one of its modified forms, which predict essentially monotonic behavior, at least in the dilute solution limit, is inconsistant with the above conclusion.

The classical Gouy-Chapman approach to the electric double layer is very unsatisfactory on many points, when one critically examines it. Blum (1) has presented the thesis that statistical mechanical considerations indicate that charge oscillations should occur at the higher concentrations, while the classical theory predicts that the net charge density in the diffuse layer decays exponentially with distance from the interface. Levine and Outhwaite (2) have expressed displeasure with Blum's point of view. They claim that the Poisson-Boltzmann equation, significantly modified in the form of an integro-differential-difference equation, and the theory of Buff and Stillinger (3) inherently predict charge oscillations for higher concentrations. The classical theory also requires that the signs of charge density and electric potential in interfacial region should be opposite.

In the absence of any chemical reaction, including ion-pair formation, above mentioned mass conservation conditions, require an oscillatory behavior in charge density profile, even in dilute solutions, near a charged surface. The inclusion of ion-ion interaction energy terms to the limiting expression for the chemical potential of ions in solution, have been shown by me to lead for such behavior, and to the unexpected conclusion that the signs of electric potential and charge density should be the same in interfacial region for significant concentrations as seen in biological systems. One suspects also, that the electric potential profile should also exhibit oscillations, depicting essentially a quasi-lattice structure for ions near the interface. It also follows that the assumption of constant dielectric coefficient can never be valid.

It is our belief, that however much it is appealing, the separation of two phases of differing constant dielectric coefficients, with the presence of a mathematical discontinuity in dielectric profile with the resultant, fictituous image charge effects, except in clearly defined phases, should be discarded. The presence of localized charge density perturbs the concentration profiles of charged species, and affect the force experienced by such ions in transit, (gradients of chemical potential under stationary state conditions). The validity of the limiting expression for chemical potential of ions in solution, leading to Nernst distribution, for inhomogeneous interfacial region should be questioned. It is worth stating that the logarithmic dependence on concentration of chemical potential arises from the entropy of mixing of ideal solutions, in which the mole fractions have been replaced by concentration terms valid for extremely dilute solutions, and to which the influence of external electric field has been phenomenologically added. Ideal solution expression arise for systems containing molecules with no interactions. Ion-ion interactions are long range coulombic, and such interactions lead to some structure, such as ion atmosphere. Thus, the limiting expression can never be valid, and one must include, ion-ion and ion-dipole interaction terms.

The fundamental definitions of electric potential at an arbitrary location in the inhomogeneous system, includes contributions from all charges present in the system. Thus, one cannot assign special role for charges of the surface and minority role if any for charges present in aqueous phase. Similarly, the charge density at an arbitrary location is the algebraic sum of all charges present in this location. Since both sums involve terms of both positive and negative signs, with unknown magnitudes, one cannot apriori, assume that the signs of electric potential and charge density should be similar or opposite. Classical theory assumes that if the surface contains an excess of say, negative charges, the potential at the surface is negative. However, it assumes that the potential in electrolyte adjacent to surface is negative while the charge density is positive. The conclusions arrived in a previous publication (4), using an approximation to denote the integral contribution to chemical potential arising from ion-ion interaction terms is in disagreement and states that the signs of charge density and electric potential should be similar.

In order to examine the validity and correctness of these two divergent conclusions, the electric potential profile arising from the presence of a finite number of discrete charges, on a square lattice, normal to the plane of the lattice is computed and results are presented in figure 2. This profile depicts the influence of fixed charges on the surface, and is monotonic, decaying to null value at large distance. However, the presence of other charges in solution, perturbing this profile, is examined by placement of additional grids of charges of opposite kind, at specified distance from the original grids. These and other results present elsewhere, reiterate the nonvalidity of concepts of classical double layer theory. The need for reexamination of the problem is emphasized. A schematic representation of charge density profiles suggested by our analysis is presented in figure 1. In figure 3, are presented the results of our computation from grids with various fixed discrete charges.

REFERENCES. 1. L. Blum, J. Phys.Chem. 81,(1977) 136.
2. S.Levine & C.W.Outhwaite, J.Chem.Soc. Faraday Trans.74(1978)1670.
3. F.P.Buff & F.H.Stillinger, J. Chem.Phys.,39(1963)1911.
4. V.S.Vaidhyanathan, in 'Electric Double Layers in Biology' M.Blank, editor, Plenum Press, (1986) p.31-51.

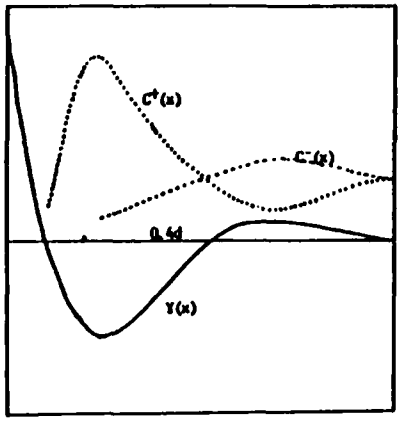


FIGURE 1. Schematic representation of the concentration profiles of anions and cations and charge density profiles - Y(x) , obtained, when mass conservation relations (5b) are imposed.

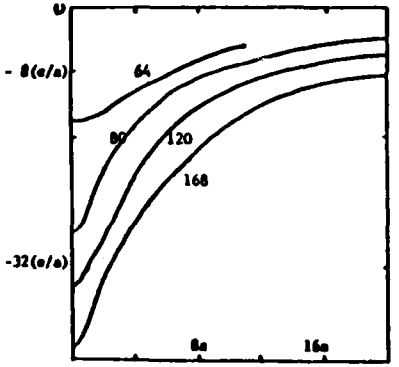


FIGURE 2. Plots of electric potential profiles, along direction normal to grids of charges, on a plane square lattice. The number of charges, on the grids causing the profiles, are presented adjacent to plots.

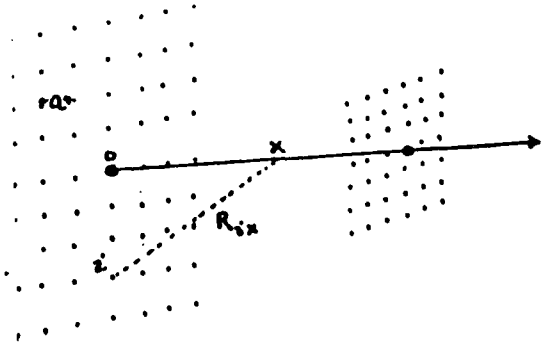


FIGURE 2a. Grids of charge locations utilized in computations of electric otential profiles presented in figures 2 and 3. No charge is present t origin, in order to avoid singularity.

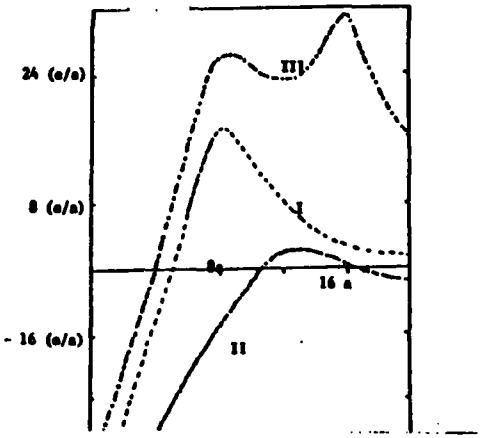


FIGURE 3. Computed values of the electric potential profiles, obtained when grids of different number of charges are placed parallel to each other, at specified locations. Plot I is obtained when two grids with 168 negative charges at x = 0, and another with 120 positive charges at x = 8a. Plot II is obtained when a grid with 168 negative charges is at x = 0, and a second grid with 64 positive charges is placed at x = 12a. Plot III is obtained by placement of 3 grids, 168 at x = 0, 120 at x = 8a and 80 at x = 16a.

THE FRACTAL STRUCTURE OF SURFACE INHOMOGENEITY AS THE ORIGIN OF CPE-BEHAVIOUR IN THE FARADAIC AND NON-FARADAIC REGIONS.

W.H. MULDER, M. SLUYTERS-REHBACH and J.H. SLUYTERS, Van 't Hoff Laboratory, University of Utrecht, Padualaan 8, 3584 CH Utrecht, The Netherlands.

The usual representation of the impedance of an electrochemical cell in performing a.c. impedance measurements with an indicator electrode very small in comparison with the counter electrode and with a d.c. potential in the ideally polarizable region is usually taken as an equivalent circuit consisting of the solution resistance R_Ω in series with the double layer capacitance of the indicator electrode, C_d (fig. 1(a)). When the potential is changed to a value where a slow electrode process starts to proceed, the equivalent circuit must be extended with a charge transfer resistance R_{ct}, parallel to the capacitance C_d (fig. 1(c)). When we plot the cell impedance as a function of frequency ω of the applied a.c.-voltage in the complex impedance plane $Z'-iZ''(i=\sqrt{-1})$, the plot for the circuit of fig. 1(a) is a vertical line (fig. 1(b)) and for the circuit of fig. 1(c) it is a semi-circle with its center on the real axis and a diameter equal to R_{ct} (fig. 1(d)).

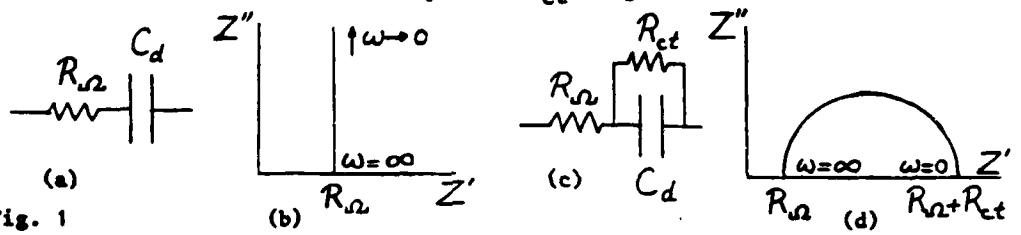


Fig. 1

With mercury as the electrode material this all works well. However, at a solid electrode (e.g. Au), a marked deviation with respect to the impedance behaviour just described, is frequently observed. This deviation consists of the clockwise rotation of the diagram of fig. 1(b) around the point $(R_\Omega,0)$ (and a subsequent re-parametrization of the line in terms of ω)(fig. 2(a)). This so-called CPE-behaviour (from Constant Phase Element, so called because it effects a frequency-independent phase-shift between the applied a.c.-voltage and its current response) extends from the mHz-up to the MHz-region, outside of which the behaviour is again capacitive. The phenomenological description of the frequency dependence of this impedance is given as:

$$Z_{CPE}(\omega) \sim (i\omega)^{-\alpha} \quad (0 < \alpha < 1)$$

The CPE angle φ is related to α by

$$\varphi = \frac{\pi}{2}(1-\alpha)$$

Obviously $\alpha = 1$ corresponds to normal capacitive behaviour. Values for φ up to $\sim 15°$ have been observed with Au [1].

In the case of a slow faradaic process occurring at the electrode surface, a similar effect is observed, showing a Depressed Semi-circular Arc (DSA) in the first quadrant as the complex plane-impedance plot. (Fig. 2b)
For a long time these effects were left unexplained, and were only described in a phenomenological way.

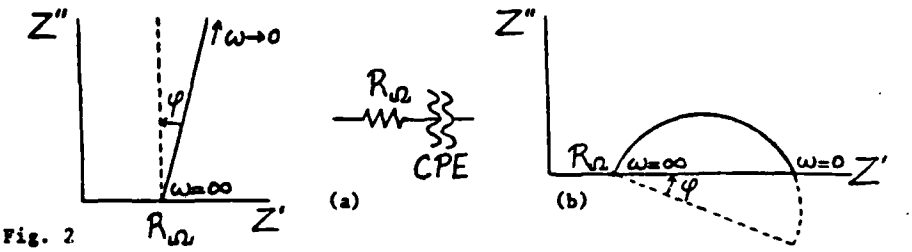


Fig. 2

Recently, new ideas have been put forward ([2], [3], [4]) in order to explain the CPE in a satisfactory way. The central idea is that the deviations from ideal behaviour are caused by surface roughness of a special kind, namely roughness showing scaling properties over a wide range of length scales, a behaviour nowadays commonly denoted by the term "fractal" [5]. The expectation that the scaling property of surface roughness is responsible for the maintenance of rectilinear impedance plots in the ideally polarizable potential region has been justified by a number of authors ([2], [3], [4]). Here it is shown that CPE-behaviour, as well as DSA-behaviour, can be deduced in a rather general way, without specifying the exact morphology of the surface, but only characterising it by a single number, the so-called fractal dimension, D. This is a formal quantity, introduced by Mandelbrot [5], which attains a value between 2 and 3 for a fractal surface, and reduces to 2 when the surface is flat. It appears that there is a unique relation between the phenomenological exponent α in the CPE-equation, and this dimension D of the interface. The way to arrive at the form of this relationship is to describe the rough electrode and the adjacent solution layer in terms of a boundary value problem for the potential $\phi(\vec{r},t)$ in that region, which determines the total current response to some applied signal (e.g. a transient potential step). The form of this (mixed) boundary value problem is as follows:

$\Delta\phi = 0$ (Δ is the Laplace operator)

for the solution adjacent to the electrode; this is the equation of continuity of current).

At the electrode surface we have the current density balance equation

$$-\sigma \frac{\partial\phi}{\partial\nu} = C_d \frac{\partial}{\partial t}(\phi-\phi_{el}) + \sigma'_{ct}(\phi-\phi_{el})$$

l.h.s. = normal component of the current density flowing to the surface (σ = solution conductivity, $\partial/\partial\nu$ = normal derivative at the surface)
r.h.s. = the sum of the charging and faradaic current densities, respectively (C_d = double layer capacity cm^{-2}, $\partial/\partial t$ = time derivative, ϕ_{el} = applied potential, σ'_{ct} = faradaic admittance cm^{-2}).

Finally

$\phi = 0$

at a surface near the electrode, bounding the inhomogeneous current region. Making use of the general properties of the solution ϕ of this problem, in combination with the scaling properties of the surface only, it appears that the general form of the impedance spectrum is given as:

$$Z_{DSA}(\omega) = \sigma' A_2^{-1}\, \sigma^{(D-2)/(D-1)} (\sigma'_{ct})^{-1/(D-1)} [1+\sigma''(\frac{i\omega C_d}{\sigma'_{ct}})^{1/(D-1)}]^{-1}$$

where A_2 = apparent (2-dimensional) surface area of the electrode and σ'

and σ'' are two geometry-dependent constants.
The complex plane representation of this equation is indeed of DSA-form, and in addition, in the ideally polarizable case ($\sigma'_{ct} = 0$) it reduces to a CPE with a CPE-angle $\varphi = \frac{\pi}{2}\left(\frac{D-2}{D-1}\right)$ (in accordance with refs. [2] and [4]), which embodies the relation between the impedance behaviour and surface geometry.

References

[1] G.J. Brug, A.L.G. van den Eeden, M. Sluyters-Rehbach and J.H. Sluyters, J. Electroanal. Chem. 176 (1984) 275.
[2] A. Le Méhauté and G. Crepy, Solid State Ionics, 9-10 (1983) 17.
[3] S.H. Liu, Phys. Rev. Lett., 55 (1985) 529.
[4] L. Nyikos and T. Pajkossy, Electrochim. Acta, 30 (1985) 1533.
[5] B.B. Mandelbrot, The Fractal Geometry of Nature, Freeman, San Francisco (1977).

ADIABATIC CHARGE TRANSFER ACROSS A CHARGED METAL/ELECTROLYTE INTERFACE

A.V. Gorodyskii, A.I. Karasevskii and D.V. Matyushov
Institute of General and Inorganic Chemistry, Kiev, USSR

Electrochemical processes activated by thermal motion in the medium, viz by fluctuations of static solvent-polarization and release of ion from the solvated state to the electrode surface have been studied theoretically [1]. Charge transfer in an electrochemical system is considered in terms of adiabatic electron-exchange between the electrode and the reactant when the coupling between the electronic states of the metal and reactant is considerable, and the population of the electronic reactant-states follows adiabatically the dynamic fluctuations of the medium. The type of the potential energy surface, which depends on overpotential and on the two reaction coordinates corresponding with two independent stochastic processes leading to a dynamic shift of the electronic levels of reactants - static-polarization fluctuations and desolvation of the discharging species -, has been determined by the functional integral method. The rate constant of the electrochemical process is found from the corresponding Focker-Plank equation.

It has been found that the behaviour of an electrochemical system under adiabatic conditions differs from the Tafel behaviour, and that three characteristic overvoltage-regions can be discerned. Stable reaction products are formed only at overpotentials above the threshold value, which may lie, in the general case, in the anodic region for the cathodic process. The polarization curves have in this case a Tafel shape. As overpotential increases and reaches its limiting value, the reactant states lose their stability, and the reactants pass continuously into reaction products. A further increase in the polarization of the region at the electrode is impossible [2]. In this overpotential range, the polarization curve rises steeply parallel to the current axis [2, 3].

Expressions have been obtained for polarization curves which describe the behaviour of an electrochemical system in the entire electrode polarization region.

References

1. A.V. Gorodyskii, A.I. Karasevskii and E.V. Panov, Ukr. Khim. Zhurn., vol 53, no 1, p 32 (1987).
2. A.V. Gorodyskii, Ukr. Khim. Zhurn., vol 31, p 1263 (1965).
3. A.V. Gorodyskii, T.A. Karasyova, A.M. Matiyasevich and V.G. Oreshnikov, DAN SSSR, vol 295, p 846 (1987).

SELF-ORGANIZATION PHENOMENON IN MULTISTAGE METAL ELECTROREDUCTION PROCESS. THEORY AND EXPERIMENT

I.N. Karnaukhov, A.I. Karasevskii, N.D. Ivanova and Y.I. Boldyrev
Institute of General and Inorganic Chemistry, Kiev, USSR

The electroreduction of polyvalent metal-ions such as Cu^{2+}, Cr^{3+}, Cr^{6+}, Mo^{6+} and others involves formation of a cathode film from incomplete metal ion reduction products at the electrode/electrolyte interface in the first reduction stage. The subsequent reduction stages occur in the bulk of the film, which safeguards the low-valency metal-ions against oxidation by the electrolyte and makes it possible to shift the electrode potential towards more negative values and to attain potential values at which a complete electroreduction of metal ions such as molybdenum and tungsten ions is achieved. The formation of a cathode film consisting of incomplete metal ion reduction products gives rise to current or potential oscillations. The period of oscillations and their amplitude depend on the applied potential and current.

The semiconductor film that is formed on the cathode is an example of dissipative structures, whose dynamic functioning is due to an inhomogeneous electric field that is induced in the bulk of the film. This field produces a positive feedback, which ensures the dynamic functioning of the complex electrochemical system: cathode-film-electrolyte. A characteristic internal parameter reflecting the behaviour of the system is the size of Schottky layer, L 10^{-5}-10^{-4} cm, at a film thickness of ca 10^{-4}-10^{-3} cm and at a thickness of the compact layer in the film of 10^{-5}-10^{-4} cm.

It has been shown that interfaces are formed in the bulk charge region. The phases consist mainly of products of incomplete lower oxidation state metal ion reduction. This makes it possible to propose a set of kinetic equations describing the time dependence of the fine film-structure thickness. The nonlinearity of the equations is determined by the dependence of electrochemical reaction rate constants, estimated according to the Tafel law, on the strength of inhomogeneous field in the Schottky layer.

A set of equations describing the dynamic behaviour of the fine structure of a film composed of layers rich in Cr^{3+} and Cr^{2+} ions has been examined for the three-stage ion discharge: Cr^{6+} Cr^{3+} Cr^{2+} Cr^{0}. This set of equations has, along with stationary solution, an instability region with solutions varying periodically with time. The bifurcation point and the oscilation frequency characterizing the periodic solutions have been calculated.

The transition from the stationary state to the vibrational conditions is determined by the current or potential value. Small film thicknesses correspond with vibrational conditions since the size of the compact layer must not exceed the L value.

The results of the calculations correlate with the experimental data for the dependence of critical metal deposition current density on ligand concentration in the electrolyte, temperature and cathode potential oscillation frequency.

References

1. N.D. Ivanova, S.V. Ivanov and Y.I. Boldyrev, Fluorine compounds in electroplating, Naukova Dumka, Kiev, 1988, 235 p.

DETERMINATION OF THE COMPOSITION OF ELECTROCHEMICALLY ACTIVE IONS ON AN ELECTRODE

V.S. Kublanovskii and A.V. Gorodyskii
Institute of General and Inorganic Chemistry, 252142 Kiev, USSR

One of the most important problems of modern electrochemistry is the elucidation of the mechanism of electrode processes and chemical stages which accompany the formation of electrochemically active complexes on an electrode. The usual methods for determining the composition of electrochemically active complexes are based on the fact that only one complex in equilibrium with the complex that is dominant in the bulk of the electrolyte is discharged on the electrode. It is evident that the overwhelming mejority of electrochemical systems are characterized by quite a number of complex compounds in the bulk of the electrolyte and in the electrode layer. It is also quite logical to think that metal ions are discharged from all or several ionic species that are present in the bulk of the electrolyte or are formed in the cathode layer and on the electrode surface; in a particular case, a single species may be such an electroactive species.

We have developed methods for determining electroactive ionic species on the basis of the method developed earlier for determining all concentrations on the electrode surface. New electrochemical functions are proposed: "discharging ions complexity", which relates formation constants to electrode reaction parameters, and "average coordination number of discharging ion", which indicates the composition of discharging complexes.

Methods for determining electrochemically active and electrochemically inactive ions are shown for the discharge of cadmium, zinc and copper coordination compounds with complexones and halide ions.

THEORETICAL CONSIDERATIONS ON THE ADSORPTION ISOTHERM FOR IONIC SYSTEMS AT ELECTRODE INTERPHASES

BY

Ramon GONZALEZ and Fausto SANZ
Departament de Química Física. Universitat de Barcelona
Martí i Franqués 1. 08028-Barcelona (Spain)

Many theoretical attempts have been made in order to describe the adsorption process of inorganic anions. Thus, the Stern-Grahame-Devanathan theory of the electrochemical double layer was modified by introducing the so-called discreteness of charge effect. Levine and others proposed an expression in terms of cavity potential in the inner layer and selfatmosphere potential in the inner and diffuse layer. Their model led to a calculation of the free energy of adsorption and to propose later a modified Frumkin adsorption isotherm including a Boltzmann term Φ_2. This term is able to do with the large value of the adsorbed charge at low salt activities.

Nevertheless, Levine's isotherm or other adsorption isotherms including a Boltzmann term in Φ_2 have not been proved to follow a thermodynamic treatment and consistent standard states have not been defined for the isotherm. We endeavour in this work to deal with the system of anion specific adsorption by means a thermodynamic treatment based on the Guggenheim model of the interphase.

THEORETICAL TREATMENT

Let us assume that the adsorbed ion and the solvent have the same size and that the adsorption layer can be treated as a separate phase. The adsorption process can be

equated. then:

$$B(sln) + S(ads) \rightleftharpoons B(ads) + S(sln)$$

where B is the adsorbing anion ans S is the solvent. The equilibrium constant. β . is said to be the adsorption coefficient.

The consideration of the total Gibbs energy of the system at constant temperature and pressure as made in ref.[1], gives us the following equations. known as Randless relationships:

$$\bar{\mu}_B^{ads} - \bar{\mu}_B^{sln} = \frac{\gamma}{\Gamma_{max}}$$

$$\bar{\mu}_S^{ads} - \bar{\mu}_S^{sln} = \frac{\gamma}{\Gamma_{max}}$$

where γ is the interfacial tension and Γ_{max} the maximum surface concentration excess of specifically adsorbed anion. Also. from the foregoing equations we obtain the equilibrium condition:

$$\mu_B^{ads} - \mu_B^{sln} - \mu_S^{ads} + \mu_S^{sln} = 0$$

These equations are true for systems at constant ionic stregth. and also for systems of pure binary electrolytes having variable ionic stregth. If Randless relationships are integrated taking account of the electrocapillar equation as deduced by Parsons and Dutkiewicz [2] and using Levine adsorption isotherm:

$$\frac{\theta}{1-\theta} \exp(-B\theta) = \beta a_B \exp\left(\gamma\sigma^M + \frac{F\Phi_2}{RT}\right)$$

we obtain the interphase electrochemical potentials of both the solvent and the specifically adsorbed anion:

$$\frac{\bar{\mu}_s^{ads}}{RT} = IC + \ln(1-\theta) + \frac{B\theta^2}{2} + \frac{2\sqrt{1+x^2}}{l} + \gamma\sigma^M\theta$$

$$\frac{\bar{\mu}_B^{ads}}{RT} = IC + \ln\theta - B\theta + \frac{B\theta^2}{2} + \frac{2\sqrt{1+x^2}}{l} + \gamma\sigma^M(\theta-1) - 2\,\mathrm{arg\,sh}\,x$$

Here, IC is an integration constant dependent on σ^M. θ is the coverage, B is the Frumkin interaction parameter. γ is a constant related to the isotherm. x and l are:

$$x = \frac{\sigma^M + \sigma^1}{(8RT\varepsilon C_T)^{1/2}} \qquad l = \frac{\sigma^1_{max}}{(8RT\varepsilon C_T)^{1/2}}$$

In order to obtain invariant standard states, a value of the metall charge equal to minus the charge of an adsorbed monolayer seems the most plausible for the electrochemical potential of adsorbed anion. Levine isotherm must be only corrected for the B/2 factor as deduced in the case of neutral molecules [1].

[1] R. Gonzalez,J. Torrent and F. Sanz,J. Electroanal. Chem. in press.

[2] E. Dutkiewicz and R. Parsons, J. Electroanal. Chem. 11 (1966)100.

THE PROTON DISCHARGE REACTION ON GOLD AND SILVER

U. Frese and W.Schmickler
Insitute of Physical Chemistry, University of Bonn
Wegelerstr.12, D-5300 Bonn, F.R. Germany

Recently, there has been considerable interest in the temperature dependence of the transfer coefficient α. In a number of reactions, the apparent value of α, as obtained from the slope of Tafel plots, depends markedly on temperature, and can often be described by a linear law: $\alpha = \alpha_H + \alpha_S T$ [1]. So far, this effect has remained unexplained.

This temperature dependence has been observed for *inner sphere* electron and proton tranfer reactions only. Most experimental data are for the formal transfer coefficient of the overall reaction, so that the relation to the elementary steps is not clear. We therefore thought it desirable, to measure the potential - current characteristics of an elementary step of an inner sphere reaction, and to attempt an interpretation in terms of a microscopic model.

We have measured the discharge of the first proton in the hydrogen evolution reaction on gold and silver by pulse techniques. We took $HClO_4 \times 5.5\ H_2O$ for the electrolyte solution; this mixture freezes at 228 K. The same system has previously been investigated by Frese and Stimming [3], but since potentiodynamic sweeps were used by these authors, the tranfer coefficients measured are not characteristic for any elementary step.

To obtain reproducible results, the working electrodes were subjected to a flame treatment before each measuring cycle. After further pretreatment, the electrode potential was kept at a value in the double layer region. Then, a potentiostatic pulse was applied to a potential in the hydrogen evolution region. The current transients were recorded and extrapolated to the time t=0 by the procedure described in ref. [4], and the current for the discharge of the first proton was obtained. The corresponding Tafel plots gave straight lines, from which the transfer coefficients were determined. Fig. 1 shows the results for Au and Ag; in both cases, the tranfer coefficients for the proton dicharge reaction decreases markedly with temperature in the

liquid state, but seems to tend to a constant value below 200 K. The energy of activation and the preexpontential factor were also evaluated. The latter shows a strong increase with cathodic overpotential, while the activation energy depends less strongly on the potential, and, surprizingly, shows a small *increase* with increasing cathodic overpotential.

An interpretation of these results must take account of the following facts: 1) The reacting proton (or H_3O^+ ion) sits immediately in front of the metal surface; hence, when the potential difference between the metal and the bulk of the solution is varied by an amount $\Delta\phi$, the potential drop between the reactant and the metal varies only by a fraction $\gamma \cdot \Delta\phi$. 2) The proton is subject to a very high electric field, which varies strongly with the electrode potential. 3) The interfacial capacity is fairly constant in the relevant potential region; hence, the concentration of the reactants varies only weakly with the potential.

As a result, the variation $\Delta\phi$ of the electrode potential leads not only to a change in the energy minimum of the potential energy surface for the proton, but also to a shift in the equilibrium position, since this is influenced by the magnitude of the electric field at the interface. In contrast, the potential energy curve for the reduced state, the adsorbed hydrogen atom, is not affected (see fig.2). As a consequence, the part λ_{in} of the energy of reorganization corresponding to the motion of the proton depends on the electrode potential. Since the proton is expected to tunnel through the potential energy barrier, this leads to a strongly potential dependent preexponential factor, and hence to a temperature dependence of the transfer coefficient. Numerical estimates show, that the expected order of magnitude of this effect compares well with the experimental observations.

1) J.N. Agar, Disc. Farad. Soc. 1 (1947) 81
2) U. Stimming and W. Schmickler, J. Electroanal. Chem. 150 (1983) 125
3) U. Frese and U. Stimming, J. Electroanal. Chem. 198 (1986) 409
4) H. Gerischer and W. Mehl, Z. Elektrochemie 59 (1955) 1049

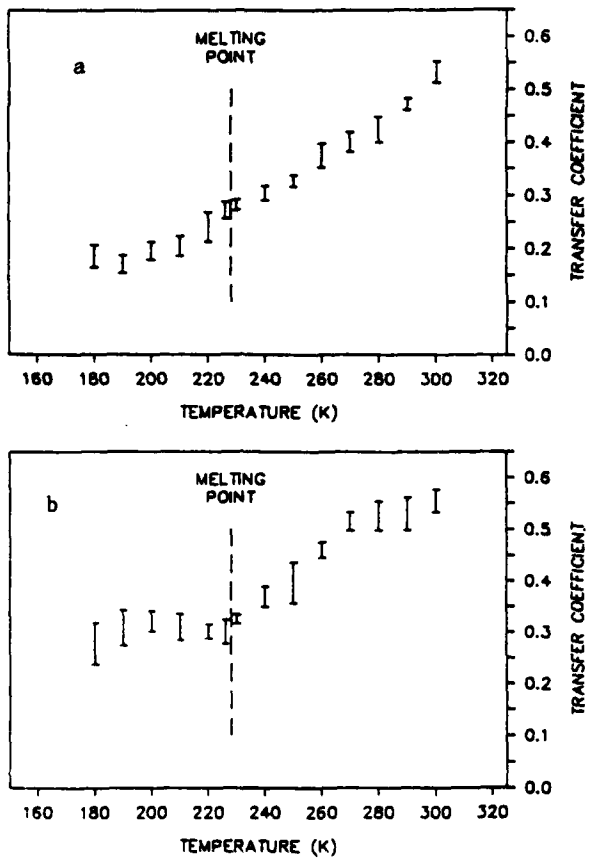


fig. 1: transfer coefficient for the proton discharge as a function of temperature
a: gold electrodes
b: silver electrodes

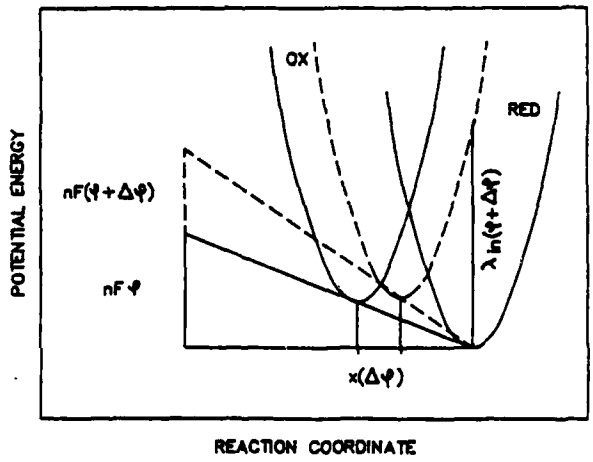


fig. 2: effect of electric field on the potential energy curve of the oxidized state

ADSORPTION BEHAVIOUR OF 2-PROPANOL AND OF HEXAFLUORO-2-PROPANOL.

M.R.MONCELLI and R.GUIDELLI
Dipartimento di Chimica
Universita' di Firenze

The adsorption behaviour of 2-propanol (P) on mercury from an aqueous solution of 0.1 M NaF is compared with that of the corresponding perfluorated compound, 1,1,1,3,3,3-hexafluoro-2-propanol (HFP), by using a computerized chronocoulometric technique for the measurement of the capacitive charge.

In the case of P adsorption, the charge σ_{max} of maximum adsorption shifts from -3 to -2 $\mu C\ cm^{-2}$ with an increase in the surfactant concentration; whereas the potential E_{max} of maximum adsorption shifts from -0.60 to -0.55 V/SCE. P adsorption at constant potential satisfies the Frumkin isotherm $\theta \exp[(a\theta)/(1-\theta)] = c \exp(-\Delta G_{ads}/RT)$, with a negative (i.e.attractive) interaction factor which becomes progressively more negative with an increase in the applied potential. The adsorption behaviour of P at constant charge shows greater deviations from the Frumkin isotherm. Thus, the $\ln [c(1-\theta)/\theta]$ vs θ plots exhibit appreciable curvatures at positive and far negative charges. The interaction factor a at constant charge attains a minimum negative value in the proximity of σ_{max}.

In the case of HFP adsorption, a gradual increase in the surfactant concentration causes a pronounced shift of σ_{max} from +2 to +5 $\mu C\ cm^{-2}$ and a corresponding shift of E_{max} from -0.35 to -0.15 V/SCE. The curve of the standard Gibbs energy of adsorption ΔG°_{ads} at zero coverage vs the charge density σ shows a minimum at +2 $\mu C\ cm^{-2}$, and hence decreases monotonically up to this value when proceeding towards less negative charges. In this respect this curve resembles that observed in thiourea adsorption from NaF aqueous solutions [1], where the range of positive charges is experimentally inaccessible due to an oxidation process. The notable positive shift in σ_{max} when passing from P to HFP can be explained by noting that, for a given orientation of the adsorbed molecule, the replacement of H atoms by F atoms produces a reversal in the direction of the dipole moment of the whole molecule (the $C^{\ominus}$-$^{\oplus}H$ bond moment equals -0.4 D whereas the $C^{\oplus}$-$^{\ominus}F$ bond moment equals +1.4 D). In particular, if the adsorbed HFP molecule has a $-CF_3$ group directed towards the metal, the negative end of its overall dipole moment will also be almost certainly directed towards the metal. This will produce a positive shift in σ_{max} when passing from P to HFP adsorption, as actually observed experimentally.

[1] R. Parsons, Proc.Roy.Soc., 261A (1961)79.

ADSORPTION OF AROMATIC AMINOACIDS AND RELATED COMPOUNDS IN RELATION TO CALCULATED MOLECULAR STRUCTURAL INDEXES

C. Fontanesi, A. Barbieri, R. Andreoli, L. Benedetti and G. Gavioli
Department of Chemistry, University of Modena, Via Campi 183, 4110 Modena (ITALY)

The adsorption of N-Dansylglycine (5-dimethylamino naphtalene-1-sulphanylglycine) in monoanionic and dianionic forms has been characterised in aqueous solution at the mercury electrode. The technique used to measure the differential capacitance is the "ac" phase selective polarography and the thermodynamic treatment has been performed in the concentration range $10^{-4} \div 3 \cdot 10^{-3}$ M at pH=6 and in the range $10^{-4} \div 10^{-2}$ M at pH=12. At pH=6 (only monoanionic form present in the bulk) N-Dansylglycine is arranged on the metal surface in a perpendicular way through the naphtyl moisty, and an attractive interaction factor among the adsorbed molecules is observed (the interfacial behaviour is well represented by a Frumkin type isotherm). At pH=12 (dianionic form) the molecules still arranged in a perpendicular way show a greater hindrance and no interaction factor is revealed. Moreover, the adsorption Gibbs energy ΔG°_{ADS} at the two pH values has been obtained as a function of the potential.

The main adsorption parameters are reported in Table I together with those regarding, other N-substitued aminoacids [1,2], other compounds in some way structurally related [3,4] and a series of aromatic compounds studied by Bockris [5]; they show a variation in the ΔG°_{ads} values, suggest two different dispositions of the aromatic moisty of the adsorbate on the surface (planar or perpendicular) and reveal an interaction factor, A, attractive or repulsive (or even zero) independently on the net charge of the adsorbed molecular species. So, a tentative generalisation of the interfacial behaviour in the whole series on a structural ground can be pursued on the basis of comprehensive molecular parameters like the energy values of HOMO (Highest Occupied Molecular Orbital) and LUMO (Lowest Unoccupied Molecular Orbital). Calculations to obtain LCAO-MO data were performed at the CICAIA, University of Modena, by a CNDO/2 standard program (hybrid basis). Experimental geometries when available or standard bond lengths and angles optimised according to the maximum localisation criterion were used.

TABLE I

compound	species	$^{a}\Delta G^{\circ}_{ads}$ kJ mol^{-1}	Disposition on the Hg surface	A	E_{LUMO} Hartree	E_{HOMO} Hartree	Q^{π}_{par} (e)	$Q^{(COO^-)}_{O_2}$ (e)	$Q^{(SO_2)}_{O_2}$ (e)
(1) *N-Dansylglycine*	monoanion	20.6	perpendicular	−2.8	+.1665	−.1548	−.0508	−1.1323	−1.0621
(2) N-Dansylglycine	dianion	21.3	perpendicular	0.0	+.3164	+.0349	−.0637	−1.2218	−1.1987
(3) *N-Bensoylglycine*	monoanion	20.0	planar	+2.1	+.2077	−.1386	+.0099	−1.2218	−
(4) N-Tosylglycine	neutral	16.0	planar	−0.7	+.0661	−.4227	−.0280	−0.5527	−1.0139
(5) N-Tosylglycine	monoanion	16.8	planar	+2.6	+.2013	−.1593	−.0295	−1.1073	−1.0703
(6) p-Amino Bensoic Acid	monoanion	16.3	planar	+0.8	+.3034	−.1361	−.0378	−1.1392	−
(7) Bensoic Acid	monoanion	15.0	planar	+1.7	+.3042	−.1375	+.0017	−1.1338	−
(8) Sulphanylamide	monoanion	20.4	planar	+3.9	+.2900	−.1764	−.0698	−	−1.1691
(9) Bensaldehyde	neutral	27.6	planar	-	+.0805	−.4729	+.0431	−	−
(10)Phenol	neutral	23.4	planar	-	+.1408	−.4570	−.0652	−	−
(11)Bensoic Acid	neutral	28.0	planar	-	+.0835	−.4703	+.0409	−	−
(12)α-Naphtaldehyde	neutral	37.6	planar	-	+.0488	−.4236	+.0463	−	−
(13)α-Naphtol	neutral	36.8	planar	-	+.0825	−.4035	−.0591	−	−
(14)α-Naphtoic Acid	neutral	35.9	-	-	+.0509	−.4218	+.0491	−	−

a= ΔG°_{ads} are referred to −0.6 V (SCE) and $\theta \rightarrow 0$ for compounds 1-8; for compounds 9-14, the adsorption parameters are obtained from reference [5].

So, while the relation between oxidation/reduction potentials and HOMO/LUMO energies respectively are realiable for an electron transfer process, in the case of an adsorption process some features of the interaction between the molecule and mercury may be explained with the model of a partially discharged sorbate within the double layer involving a partial charge transfer [6].

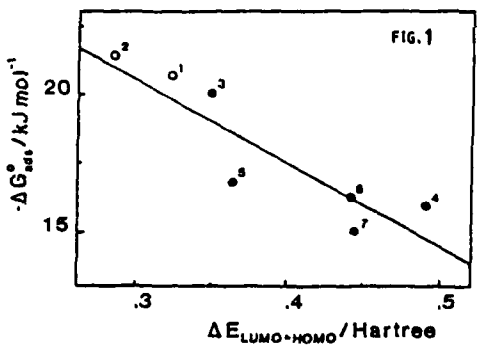
In fact, poor relations are obtained when E_{HOMO} and E_{LUMO} are individually considered with respect to ΔG°_{ads}, while a rather good linear correlation is shown in the plot of ΔE_{L-H} vs. ΔG°_{ads} (Fig.1): the lower the energy gap ΔE_{L-H} the higher the adsorption Gibbs energy. Then, the difference in energy LUMO-HOMO, should not be considered directly representative of the promotion of an electron from a double occupied MO up to a higher in energy, free one, but rather regarded as an indirect probe of the interaction of the frontier molecular orbitals HOMO and LUMO of the sorbate with the electronic energy bands in the metal [7].

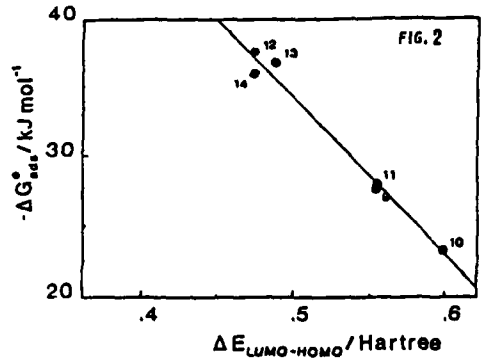
In this view, the ΔE_{L-H} value reveals to be an index related to the formation of a "feeble covalent bond" between the organic molecule and the metal surface.

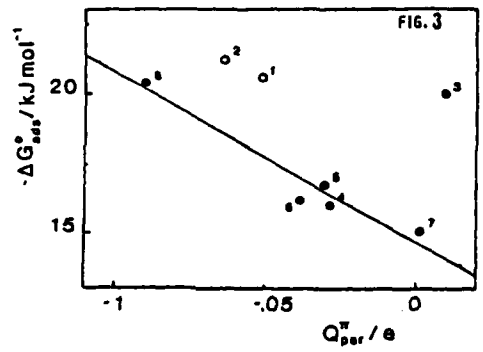
The relatively high dispersion of the data in Fig.1 is related to the fact that differently charged molecular species are considered, neutral, monoanionic, dianionic, and that the compounds are only partially structurally related

Then, it is resonable that a pure electrostatic factor affects in a specific way for any charged species the feeble covalent interaction, and when a group of phenyl and naphtyl derivatives studied by Bockris [5] in neutral form is analysed using the same parameters, the corresponding plot (Fig.2) shows a better linear relation. It is worth mentioning that the slope in Bockris relation is higher than that concerning our data, so that the intervention of ΔE_{L-H} in determining ΔG°_{ads} is prominent and cleaner in the first case. Taking into account that a recent study on the interfacial behaviour of phenol on mercury showed the possibility to define a coefficient of partial electron transfer, λ, when the interaction occurs via the aromatic system of the surfactant [8], it becomes well founded to consider that a pseudo oxidation potential, related to the energy gap between occupied and unoccupied molecular levels, governs the adsorption Gibbs energy

Finally, when the direct intervention in the adsorption process of particular atoms or groups of atoms is intended to be found out, the specific features of local calculated structural parameters have to be considered: in this case, apart from the two molecular species of N-Dansylglycine, all the other







compounds are adsorbed flat with their aromatic moiety on mercury, so that a good index is represented by the net π charge of the phenyl or naphtyl system. Fig.3 shows a good relation between this index and ΔG°_{ads}: the higher the adsorption Gibbs energy, the higher the partial net π charge and monoanionic and dianionic N-Dansylglycine species, adsorbed in a perpendicular disposition as calculated by the Γ_{max} values, do not fulfill the relation. Also Bensoylglycine (compound nr.3) does not fit this linear relation: in this case an anomalous value of the hindrance on the electrode surface with respect to the other parent compounds was already found [1], but, most important, the group $\phi - CO - NH -$ is planar and a direct intervention of the lone pair of the N atom on the surface is justified, giving rise to a more extended π system than that taken into account on the basis of the π charge of the phenyl ring only. In fact, the value of ΔG°_{ads} for Bensoylglycine should correspond, from the relation in Fig.3, to a higher partial net π charge than the calculated one.

REFERENCES

[1] C. Fontanesi, G. Battistussi Gavioli, R. Andreoli and L. Benedetti, *J. Electroanal. Chem.*, **210** (1986) 181.

[2] R. Andreoli, A. Barbieri, L. Benedetti, G. Borghesani and G. Battistussi Gavioli, *Electrochim. Acta*, **32** (1987) 325.

[3] R. Andreoli, G. Battistussi Gavioli, G. Grandi and L. Benedetti, *J. Electroanal. Chem.*, **157** (1983) 369.

[4] L. Benedetti and R. Andreoli, *Bioelectrochem. Bioenerg.*, **9** (1982) 541.

[5] E. Blomgren, J. O'M. Bockris and C.Jesch, *J. Phys. Chem.*, **65** (1961) 2000.

[6] F. D. Koppitz, J. W. Schultze and D. Rolle, *J. Electroanal. Chem.*, **170** (1984) 5.

[7] D. Döhnert, J. Koutecký and J. W. Schultze, *J. Electroanal. Chem.*, **82** (1977) 81.

[8] D. Rolle and J. W. Schultze, *Electrochim. Acta*, **31** (1986) 991.

POLYCRYSTALLINE EFFECTS IN THE DOUBLE LAYER STRUCTURE AND ADSORPTION ON SOLID ELECTRODES

U.Palm, E.Lust, K.Lust, M.Salve

Tartu State University, Laboratory of Electrochemistry
Tartu, 202400 Estonian S.S.R. (U.S.S.R.)

It is commonly accepted that the electrochemical properties of a solid metal surface significantly depend not only on the chemical composition but also on the crystallographic structure and electronic properties of the surface of the metal studied. The term "surface crystallographic structure" reflects a surface orientation of the various single crystal planes, their distribution and geometrical dimensions as well as the boundaries between them and the defects of various origin on the elctrode surface. The first experimental evidence of the influence of the polycrystalline electrode surface on the electrochemical results was discovered in the form of splitting of the adsorption-desorption maxima of pyridine on the bismuth drop electrode /1, 2/, due to the presence of various single crystal planes on the surface of the solid drop electrode. The splitting effect was highly sensitive to the polycrystalline nature of the surface, to the character of the particle adsorbed, of the solvent and also to the electrode surface charge q. In some systems the effect of the adsorption-desorption maxima splitting can be used for the crystallographic analysis of the structure of the solid polycrystalline surface and for the verification of the electrochemical theories of polycrystalline surfaces /2/.

On the basis of the considerable experimental material presumably two kinds of the theories simulating the structure of different types of polycrystalline surfaces have been developed: the earlier theory of the independent diffuse layers, developed in the years 1970-77 /3, 4/, and the theory with the common diffuse layer /5, 6/. According to these conceptions, on the polycrystalline surface various single crystal faces i are exposed and since their zero charge potentials $E^{i}_{q=0}$ and hydrophilities, inner layer capacities C^{i}_{H} and other properties are

different, the different regions of the polycrystalline surface are always electrically charged. For instance, if the $E_{q=o}$ of the two crystal planes on polycrystalline surface is about 100 mV (typical for bismuth) and the fractions of the both planes X_i in the surface are the same ($X_1 = X_2 = 0.5$) the charges of the corresponding regions are $q_1 = 0.6$ and $q_2 = -0.6$ $\mu C\ cm^{-2}$ at the total charge of the polycrystalline surface $q_{pc} = 0$. If $\Delta E_{q=o} = 0.3$ (type of silver), the corresponding values are $q_1 = 2.0$ and $q_2 = -2.0$ $\mu C\ cm^{-2}$. Therefore, at E = const the electrical conditions of various points of the polycrystalline surface are different and the characteristics of the electrochemical processes may considerably differ, the choice of the adequate electrical parameter in the equations is an unambiguous problem foer the polycrystalline surfaces /2/.

In the contemporary theories a common feature is a simulation of the polycrystalline surface by a set of capacitors corresponding to the single crystal planes on the electrode surface and considering a fraction of one or another face of the surface of the polycrystalline electrode. In one of these conceptions a polycrystalline surface is regarded as consisting of relatively large single crystal areas (so-called macropolycrystallinity), where the diffuse layers on the various single crystal planes at the polycrystalline surface can be considered independent of one another /1, 2, 4/. In the second theory the polycrystalline surface consists of a number of comparatively small monocrystalline regions (crystallites), the dimensions of which are comparable with the thickness of the electrical double layer and the diffuse layers on different single crystal areas can be regarded as collectivized (so called macropolycrystallinity). For the both cases the equivalent electrical models are developed, including an influence of the role of the boundaries between the different crystallites /2/.

As found, the capacity curves of the polycrystalline electrodes $C_{pc}(E)$, both in the solutions of the indifferent electrolyte and in the presence of organic compounds, can be obtained with the accuracy of $\pm$1-2% by superposition of the partial capacity curves of the corresponding single crystals $C_i(E)$ with consideration of their surface fraction X_i

$$C_{pc}(E) = \sum_i f_i X_i C_i(E) \quad , \qquad (1)$$

where f_i is surface roughness factor /2/.

An experimental verification of the both models was made using the two-plane model polycrystalline electrodes with the modified nature and fraction of the single crystal planes. Considering Grahame's relation

$$1/C = 1/C_H + 1/C_D \qquad (2)$$

valuable, a following formula for the theoretical calculation of the capacity of the model polycrystalline electrode can be obtained

$$C_{pc} = \frac{X_1 f_1 C_{1H} C_{1D}}{C_{1H} + C_{1D}} + \frac{X_2 f_2 C_{2H}}{C_{2H} + C_{2D}} \quad , \qquad (3)$$

where indexes 1 and 2 denote the various crystal planes.

The calculated C,E-curves coincided with the experimental ones in the all range of potentials for the KF concentration interval 10^{-3} - 10^{-1} M with the accuracy of 2-3%.

The solution of the problem of the theoretical description of the experimental C - E plots becomes more complicated for the solid drop bismuth electrode, where the number of various single crystal areas is somewhat higher. As shown by X-ray investigations, simultaneously with the comparatively large single crystal areas on the surface of the bismuth drop electrode exist areas of crystallites, consisting of a number of variously oriented small crystals with polycrystalline structure. In the first approximation such a surface can be described by the formula

$$C_{pc} = \sum_{i=1}^{n} \frac{X_i C_{iH} C_{iD}}{C_{iH} + C_{iD}} + X_{m+1} \left\{ C_D(\bar{q}) \sum_{i=n+1}^{m} X_i C_{iH}/C_D(\bar{q}) + \sum_{i=n+1}^{m} X_i C_{iH} \right\}, \qquad (4)$$

where $X_{m+1} + \sum_{i=1}^{n} X_i = 1$; $\sum_{i=n+1}^{m} X_i = 1$ $(m > n)$; n and $(m-n)$ are the numbers of large and small crystal areas. Selecting a suitable value of X_{m+1} (area with the collectivized diffuse layer) a rather good coincidence between an experiment and calculation was obtained in the KF solutions.

An additional analysis showed that the Parsons-Zobel plot does not become in the case of polycrystalline surfaces unambiguous criterion of applicability of the classical Gouy-Chapman diffuse layer theory. The difficulties arise also in application of the formula (3) and (4) for the description of the ad-

sorption of organic molecules on the polycrystalline electrodes in the region of the adsorption-desorption maxima. All the set of these problems obviously need a further theoretical and experimental investigation.

References

1. U.Palm, Trans Tartu State Univ., 757 (1986) 3.
2. U.Palm, Acta Polytechnica Scand., 178 (1987) 9.
3. G.Valette, J.Hamelin, J.Electroanal. Chem., 45 (1973) 301.
4. U.V.Palm, M.P.Pärnoya, N.B.Grigoryev, Elektrokhimiya, 13 (1977) 1074.
5. I.A.Bagotskaya, B.B.Damaskin, M.D.Levi, J.Electroanal.Chem., 115 (1980) 189.
6. M.A.Vorotyntsev, Elektrokhimiya, 17 (1981) 197, 576, 1018.

Study of Electrochemical Kinetics Using the "FREECE" Technique

U.Stimming

Department of Chemical Engineering and Applied Chemistry
Columbia University,New York, New York 10027

and
J.K.Sass and J.Schott

Fritz-Haber-Institut der Max-Planck-Gesellschaft
Faradayweg 4-6, D-1000 Berlin 33, FRG

The recent observation by Frese and Stimming /1/ that the transfer coefficient α of the hydrogen evolution reaction on Ag and Cu electrodes is proportional to temperature, with $\alpha \rightarrow 0$ for $T \rightarrow 0$, is discussed. This surprising result implies that the electrode potential influences only the entropic part of the Gibbs free energy of activation, and not the enthalpic part as is commonly assumed in standard models of electrochemical kinetics. Conway /2/ has recently reviewed some of the mechanisms that may give rise to an electrode-potential dependent entropy of activation.

It is argued that the results found by Frese and Stimming /1/ can be explained in terms of a simple model suggested by Bockris and Matthews /3,4/ for proton tunneling through a one-dimensional Eckart barrier. Model calculations based on this concept have been performed for a range of barrier parameters. The results show that, in principle, the transfer coefficient can become proportional to temperature for reasonable barrier conditions.

It is pointed out, however, that the concept of a one-dimensional barrier for proton tunneling from a molecular aggregate even as simple as H_3O^+ is probably somewhat questionable and that it would be desirable to construct three-dimensional potential energy surfaces for interfacial proton tunneling.

References

1. U.Frese and U.Stimming, J.Electroanal.Chem. 198(1986)409

2. B.E.Conway, in B.E.Conway, R.E.White and J.O'M.Bockris (eds.) "Modern Aspects of Electrochemistry" Vol. 16, Plenum Press, 1986, p. 103.

3. J.O'M.Bockris and D.B.Matthews, J.Chem.Phys. 44(1965)298.

4. J.O'M.Bockris and D.B.Matthews, Electrochim.Acta 11(1966)143.

SURFACE POTENTIAL AT LIQUID-LIQUID INTERFACE CALCULATED ON THE BASIS OF POTENTIAL VOLTA DIFFERENCES METHOD

V.I.Parfenyuk, G.A.Krestov

Nonaqueous Solutions Chemistry Institute, USSR Ac.Sci., Ivanovo.

The problem of definition of the thermodynamic characteristics of solvation of individual ions is one of the classic but still unsolved problems of the physical chemistry of electrolyte solutions. In this connection, of special interest is the method of potential Volta differences allowing to define experimentally a strict thermodynamic value - real activity coefficient of an individual ion [1]. Possibility of calculating the surface potential ($\Delta\chi^{S}_{W}$, V) at water/air/nonaqueous solvent interface is not less important peculiarity of this method.

By the method of vertical jet (Kenrick's method [2]) the compensating tensions ($\mathcal{E}$, V) of Volta-chain were defined at 298 K:

$$Ag,AgCl \mid NaCl(m),S(X) \mid air \mid 0.05mHCl,H_2O \mid AgCl,Ag$$

where m is molality; S is a mixed water-ethyl alcohol, water-i-propyl alcohol, water-acetone solvent; X is the mole fraction of the nonaqueous component.

On the base of the compensating values of the corresponding Volta-chains, the values of the surface potentials $-\Delta\chi^{S}_{W}$ were calculated, where W is water, S is ethyl, i-propyl alcohols, acetone. These values appeared equal to 0.371 V, 0.386 V, 0.448 V respectively. The basis for calculating $\Delta\chi^{S}_{W}$ is the assumption of the constancy of the surface potential of the mixed solvent beginning with the certain concentration of the nonaqueous component which is confirmed by the results of [3,4]. Comparison of the values obtained with the literature data was carried out, which in some cases yields not satisfactory enough results.

Using a fixed value of the surface potential of water and knowing $\Delta\chi^{S}_{W}$ value, one can calculate χ^{S} - the surface potential of nonaqueous solvents. Proceeding from the analysis of the literature data we assume χ^{W} value equal 0.100 V. This results in the negative values of the surface potentials of ethyl, i-propyl alcohols, acetone. We consider the molecules of the organic solvents investigated to be oriented toward the gas phase by their positive side.

References

1. Rabinovich V.A. Thermochemical activity of ions in electrolyte solutions. L.: Khimiya, 1985, 176 p.
2. Kenrick F.B. Z. phys. Chem., 1986, Bd 19, S.625.
3. Iakuszewski B., Partyka S., Prsasuyski M. Roczuiki chemi ann. soc. chim. polonorum, 1972, v.46, p.921.
4. Semenchenko V.K., Israilov I.U. Zhurn. fiz. khimii, 1974, v.48, No. 12, p. 3082-3083.

ADSORPTION OF ORGANIC SUBSTANCES AT THE MERCURY/ETHYLENE GLYCOL INTERFACE AND AIR/ETHYLENGLYCOL INTERFACE: Lauronitryle in 0.5M $NaClO_4$

Borghesani G.,De Battisti A.
Department of Chemistry,University of Ferrara,Via Borsari 46
44100 Ferrara,Italy.

Japaridze J.I.
Institute of Inorganic Chemistry and Electrochemistry,
Georgian Academy of Science,ul.Djikiya 7,380086
Tbilisi,USSR

S.Trasatti
Department of Physical Chemistry end Electrochemistry,
University of Milan,Via Venezian 21,20133 Milano,Italy.

Double layer studies in non aqueous solutions are one of the actual problems in electrochemistry. Three main aspects are of interest:i)the knowledge of the structure of the solvent at the interface,ii)the adsorption of ions,iii)the adsorption of non electrolytes.

The present work has been undertaken to go deep into the knowledge of the role of the solvent in the surface behaviour of non ionic surfactants. Here the adsorption of lauronytrile (LN) is studied both at the Hg/ethylenglicol (Hg/EG) and at the air/EG (A/EG)interfaces.

Data on a polarized Hg electrode have been obtained by capacity measurements in 0.5M $NaClO_4$.EG solutions at various LN concentration (Fig.1).

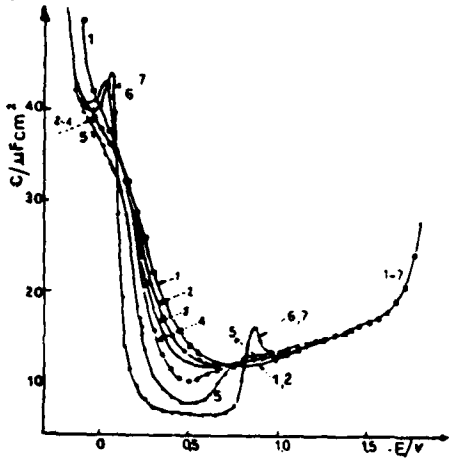


Fig.1-Differential capacity curves of a Hg electrode in 0.5M $NaClO_4$ in EG solutions at various LN concentrations:(1) 0; (2)0.0005;(3)0.0010;(4)0.0025;(5)0.0050;(6) 0.0075;(7)0.010M.

the Frumkin-Damaskin theory(2).
The surface tension at the air/0.5M $NaClO_4$ EG solution interface has been determined by the maximum bubble pressure method (Fig.2). The temperature of the solution was kept at 20°C.

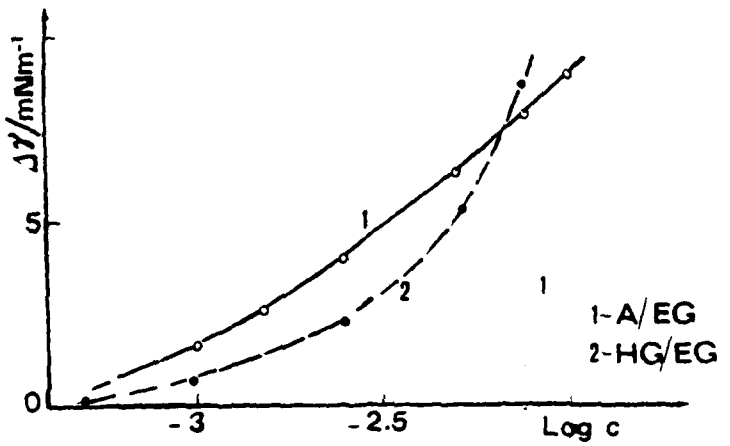


Fig.2-Surface pressure curves of LN at the A/EG (1) and at the HG/EG interface (2).

The adsorption isotherm of LN on mercury has been determined at the potential of maximum adsorption, E_m (≈-0.5 V), at which the experimental capacity, C, is related to the coverage, ϑ, by the equation:

$$C = C_0(1-\vartheta) + C_1\vartheta$$

where C_0 is the capacity of the electrode when $\vartheta \approx 0$ and C_1 is the capacity of the electrode at full coverage. C_1 value of about 6 $\mu F cm^{-2}$ has been estimatyed by extrapolation of 1/C vs 1/c to $1/c \to 0$, at E_m.
The adsorption isotherm of LN at A/EG interface, obtained with the aid of *Gibbs equation*, is reported in Fig.3.
Results have shown that the adsorption of LN conforms to a Frumkin isotherm with particle-particle interaction corresponding to attraction at both interfaces. The derived parameters have been compared to those for adsorption of aliphatic nitriles from aqueous solutions (3). A structural picture of the adsorption layer is discussed.

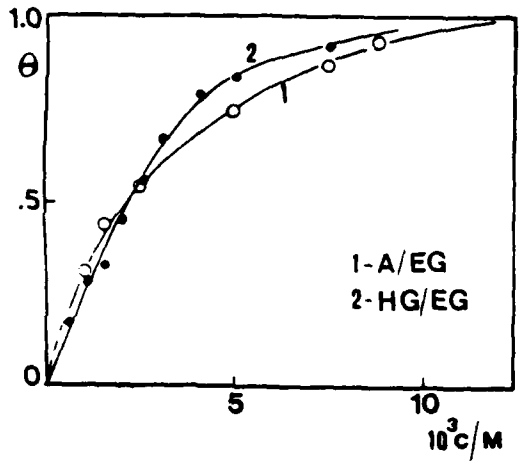


Fig.3-Adsorption isotherm of LN at the A/EG (O) and HG/EG (●) interface from 0.5M $NaClO_4$ solutions.

1-J.I.Japaridze,N.A.Abuladze,S.H.Japaridze,A.De Battisti and S.Trasatti, Electrochimica Acta,31,621(1986)
2-B.B Damaskin,O.A.Petrii and V.V. Batrakov,Adsorption of Organic Compounds on Electrodes,Nauka,Moscow(1968)(Plenum, New York,1971).
3-G.Borghesani,A.De Battisti,R.Pedriali and F.Pulidori,Annali Chim.,74.269(1984).

ELECTRICAL DOUBLE LAYER BETWEEN MERCURY AND ALIPHATIC DIOLS

Borghesani G.,De Battisti A.,Locatelli C.
Department of Chemistry,University of Ferrara
Via Borsari 46 ,44100 Ferrara,Italy.

Japaridze J.I.
Institute of Inorganic Chemistry and Electrochemistry,
Georgian Academy of Science,ul.Djikiya 7,380086
Tbilisi,USSR

S.Trasatti
Department of Physical Chemistry end Electrochemistry,
University of Milan,Via Venezian 21,20133 Milano,Italy.

The problem of understanding of the relationship between bulk and interfacial properties of polar solvents is still open, despite the large volume of experimental data thus far published Changing the solvent as a rule involves the modification of a number of factors hard to be disentangled. Considerable semplification is expected to ensue from choosing classes of isomer solvents where the main molecular skeleton remains the same. In view of the interesting interfacial behaviour exhibited by diols in previous studies , in this work the interfacial properties of isomer butanediols have been investigated and compared to those of isomers propanediols yet described(1,2).

The main objective has been to verify the applicability of the Gouy-Chapman-Stern-Grahame (GCSG) model of the electrical double layer to these Hg/non-aqueous solvent interfaces. As a corollary,the possible existence of a non specifically adsorbed electrolyte has been explored.

The interfacial behaviour of the solvents 1,2-butanediol (1,2-BD), 2,3-butanediol (2,3-BD) and 1,4-butanediol (1,4-BD) was investigated as a function of potential and electrolyte concentration (KF and $LiClO_4$ in the concentration range $5x10^{-3}$ to 0.2 mol dm^{-3}) by measuring the differential capacity of a polarized HME with a low-frequency impedence bridge working at 7 Hz (Figs.1a and 1b). The curves exhibit the typical features of class III polar solvents (according to Parsons'classification(3). The deepness of the minimum visible close to -0.5 V(vs.aq.SCE) in the capacity curves,increases with decreasing electrolyte concentration. Its potential,practically independent of electrolyte concentration,can be regarded,to a first approximation,as the potential of zero charge ($E_{p.z.c.}$)of Hg in the given solvents.$E_{p.z.c}$ values have been summarized in Table1 which also includes data for propanediols. Table 1 reports also capacity values (C_i) corresponding to the shallow minimum observed in the experimental curves at negative rational potentials for the highest concentration (Fig.1) The values of capacitance at the far negative end of the potential range are higher and more concentration-dependent in KF than in $LiClO_4$ solutions. The applicability of the Gouy-Chapman theory has been tested by means of plots of 1/C vs

1/√c at constant charge (fig.2).c=electrolyte concentration) The charge and concentration dependence of the inner layer capacitance, C_i has also been investigated.

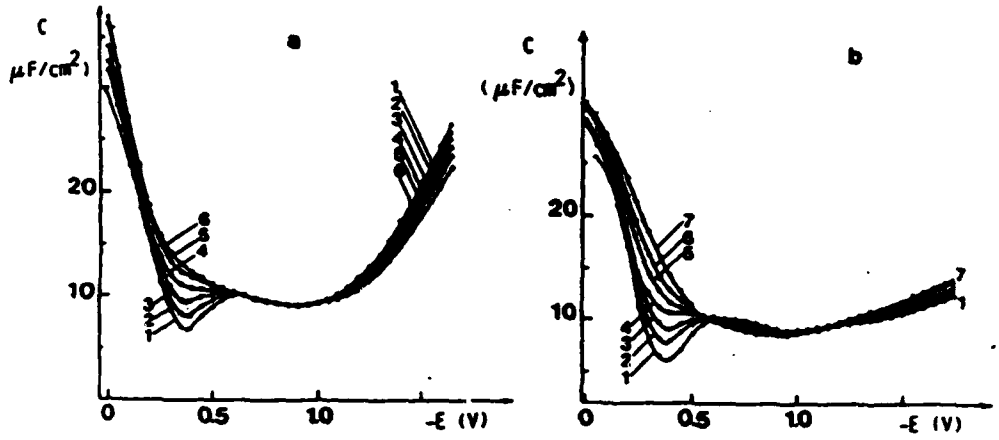


Fig.1. Differential capacity curves of a Hg electrode in contact with KF solutions in 1,4-BD (a) and $LiClO_4$ solutions in 1,4-BD (b) at different concentrations: (1) 0.005; (2) 0.01; (3) 0.02; (4) 0.05; (5) 0.1; (6) 0.2; (7) 0.5.

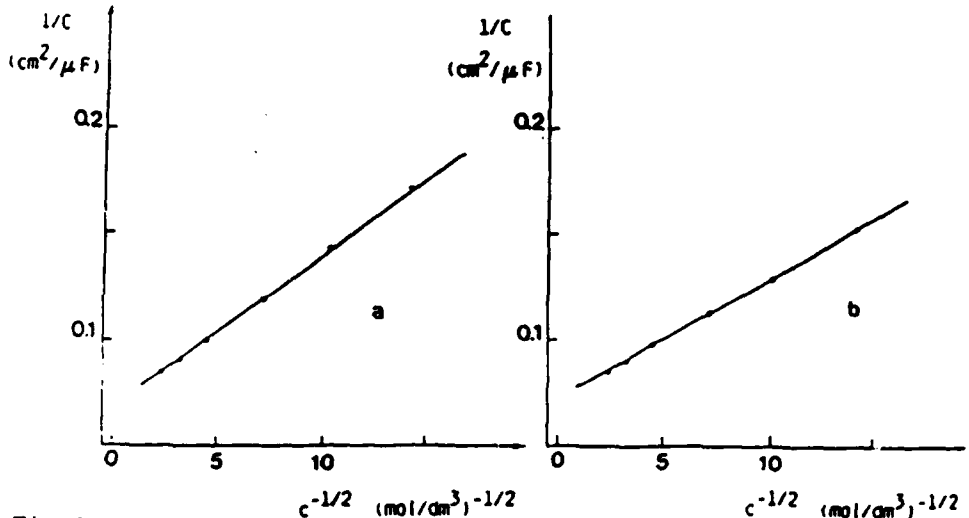


Fig.2. Dependence of 1/C on 1/√c of a Hg electrode in contact with KF solutions in 1,4-BD (a) and $LiClO_4$ solutions in 1,2-BD(b).

TABLE 1

GROUP	SOLVENT	ELECTROLYTE	E (p.z.c.)/mV	C_1 ($\mu F cm^{-2}$)
I	ED	$LiClO_4$ KF	-330 ± 5	10.6 ± 0.1
	1.2 PD	$LiClO_4$ KF	-325 ± 5	9.4 ± 0.1
	1.2 BD	$LiClO_4$ KF	-335 ± 5	8.4 ± 0.1
	2.3BD	$LiClO_4$ KF	-330 ± 5	8.8 ± 0.1
II	1.3PD	$LiClO_4$ KF	-395 ± 5	10.3 ± 0.1
	1.3BD	$LiClO_4$ KF	-370 ± 5	8.6 ± 0.1
	1.4 BD	$LiClO_4$ KF	-385 ± 5	9.2 ± 0.1
	H_2O	KF	-625 ± 5	16

On the basis of the interfacial behaviour,diols have been divided in two groups(I,II) differing by the presence or absence of intramolecular hydrogen bonds (Table 1)

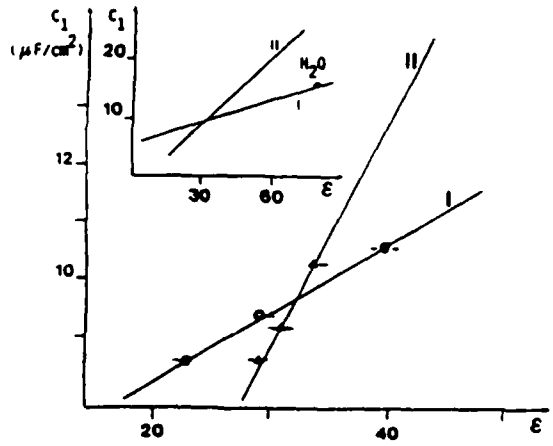


Fig.3-Dependence of C_1 on solvent bulk permittivity,ε.

The dependence of capacitance on bulk permittivity ε is different within the two groups(Fig.3).The same is the case of specific adsorption of anions and cations.
It is concluded that the relative structural features of the two groups of solvents(4) are retained also at the electrode interface.

1-J.I.Djaparidze,V.A.Chagelishvili,Zh.A.Khutzishvili,Elektrokhim. 23,1342 (1987).
2-J.I.Japaridze,Elektrokhim.,13,668 (1977).
3-R.Parsons,Electrochim.Acta,29, 1563(1984).
4-G.Borghesani,R.Pedriali,F.Pulidori,J.Solution Chem.15, 397 (1986);ibid. (1988) in press.

ELECTROCHEMICAL INTERCALATION INTO GRAPHITE SEEN AS AN ELECTROCAPILLARY PROCESS.

André METROT and Ahmed HARRACH
Laboratoire d'Electrochimie et Chimie du Solide
Université de Reims Champagne Ardenne
BP 347 - 51062 REIMS CEDEX - FRANCE

The electrochemical anodization of graphite in various acids HA such as H_2SO_4, HF, $HClO_4$... leads to well-known graphite salts of the formula $C_n^+A^-$, xHA via the "staging process" i.e. c-axis ordering of intercalated layers.

The striking features of the quasi-equilibrium potential-charge E(Q) curves obtained for slow galvanostatic intercalation (fig.1) led us some years ago to propose an electrocapillary model involving two serial capacitances, one of which, stage-dependent, being attributed to the interfacial capacitance between graphite and intercalated layers and the other, stage-independent, to the Fermi level lowering in bulk graphite [1,2].

Quantitative interfacial values derived from this model are discussed here in relation with other differential capacitance studies of Highly Oriented Pyrographite (HOPG) [3,4].

Electrocapillary modelling of intercalation

Going apart from the PZC (point Ω on fig.1) the surface charge σ of the external double layer between HOPG and H_2SO_4 increases with subsequent decrease of the interfacial tension γ, according to

$$\partial\gamma / \partial E = - \sigma$$

We consider that intercalation occurs when γ is sufficiently negative in order to equilibrate the separation work of graphite layers. The corresponding threshold value σ_t explains the proportionality of the massic charge Q_{ts} to the stage number s at the beginning of each stage domain (σ_t = 11 μCcm^{-2} corresponding to the charge values C^+_{28s} as the developped area of graphite is 2600 m^2g^{-1}). Furthemore for each stage a quite linear E(Q) capacitive law is observed, the slope of which decreases with s as the interfacial area increases.

Less clear is the regular increase of potential from stage to stage, which needs modelling with the second serial capacitance C_F.

Calculated interfacial capacitances between graphite and intercalated layers

According to our model the E(Q) relation for a stage s is governed by the capacitive law

$$dE/dQ = C_s^{-1} \text{ with } C_s^{-1} = sC_A^{-1} + C_F^{-1}$$

We obtain $C_A \simeq 240$ F/g of graphite (or 9 μFcm^{-2}) and $C_F \simeq 500$ F/g of graphite.

Impedance spectroscopy confirms those results [5].

The C_F value in relation with Fermi Level lowering

In situ reflectance measurements have allowed us the determination of Fermi level during intercalation as a function of the charge Q [6], using the rigid band model of BLINOWSKI-RIGAUX [7] : some results are reported on Table I.

Table I **Fermi level determined at various charges by means of near I-R/visible reflectance spectroscopy [6].**

Carbon charge	Graphite	C^+_{56}	C^+_{48}	C^+_{28}	C^+_{24}
E_F (eV)	0	0.87	0.93	1.17	1.24

Noteworthy is that the Fermi level variation (ΔE_F = 300 mV) calculated between C^+_{56} and C^+_{28} at the beginning of the 2nd and 1st stages corresponds roughly to the observed electrochemical potential shift (DG - BE on fig.1), suggesting us to identify those two quantities. Moreover, considering the Helmhotz capacity of intercalated H_2SO_4 as constant leads to the interfacial energetics diagram of fig.1b, assuming a constant potential drop in graphite (600 mV).

This phenomena can be seen as a **Fermi Level pinning** effect [8], due to screening of the space charge by a highly conductive surface layer : graphite intercalation compounds are indeed well known as good 2-D synthetic metals.

The C_A value in relation with external capacitance measurements

Our attempts to measure the external capacitance of HOPG in contact with H_2SO_4 18M have been untill now unsuccessfull, even using the teflon hood technique described by the YEAGER's group [3] in order to isolate the sample edges from the electrolyte. Measurements performed on more dilute H_2SO_4 (in the range 0.1 M to 10 M) are on the contrary in relative agreement with previous results [3,4], showing very low capacitances near the PZC (2.1 μFcm^{-2} for H_2SO_4 0.1 M at - 0.5 V/Hg/Hg_2SO_4 and 2.5 μFcm^{-2} for H_2SO_4 5 M at - 0.7 V). The PZC is no more attainable for H_2SO_4 10 M, being under the cathodic limit. Our conclusion is that the PZC of HOPG is indeed well under the cathodic limit of H_2SO_4 18 M (at - 1.75 V/Hg/Hg_2SO_4 according to the diagram of fig.1b). Spontaneous charging of the double layer occurs when contacting HOPG with H_2SO_4 18 M, explaining a very negative γ value : in those "pre-intercalation" conditions spreading of H_2SO_4 to the edges of the sample, or into tiny craks, cannot be avoided, explaining too high and irreproducible capacitance results.

Nevertheless the assumed values at the intercalation threshold (C_s = 9μFcm^{-2}, σ_s = 11 μCcm^{-2}, E = 1.8 V/PZC with 0.6 volt in graphite) do not appear as unrealistic.

Apparent disagreements with other group's measurements appear for the PZC value, which is claimed near 0 V/NHE for aqueous solutions [3], in agreement with our results for dilute H_2SO_4, at - 0.3 V/Ag/Ag^+ in acetonitrile [4] and here at - 1.75 V/Hg/Hg_2SO_4 in the H_2SO_4 18 M : shifts of the reference systems from one solvent to another may explain those differences

Fermi level pinning has not been considered in a recent study [4] : we consider it as a matter of debate which needs perhaps further experimental results i.e. actual surface tension values.

References

[1] A. METROT, Synth. Metals 7 (1983) 177

[2] A. METROT, M. TIHLI. Synth. Metals 12 (1985) 517

[3] J.P. RANDIN, E. YEAGER. J. Electroanal. Chem. 36 (1972) 257

[4] M. GERISCHER, R. McINTYRE, D. SCHERSON, W. STORCK, J. Phys. Chem. 91 n°7 (1987) 1930

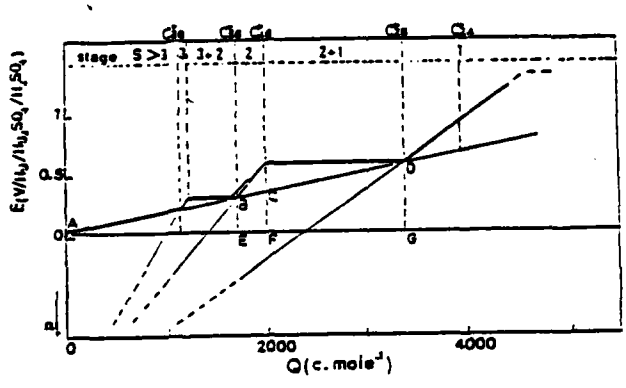
[5] A. METROT, A. OLIVIER, M. TIHLI. Proceed. Carbon 86, Baden-Baden, FRG (1986) p.482

[6] M. SAINT-JEAN, M. MENANT, NGUYEN HY HAU, C. RIGAUX, A. METROT, Synth. Metals 7 (1983) 189

[7] J. BLINOWSKI, C. RIGAUX, Journal de Physique 41 (1980) 667

[8] A.J. BARD, A.B. BOCARSLY, F.R.F. FAN, E.G. WALTON, M.S. WRIGHTON, J. Am. Chem. Soc. 102, n°11 (1980) 3671

(a)



(b)

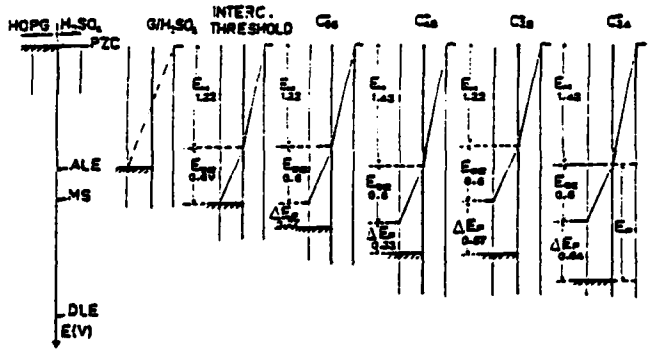


Fig.1(a) Potential charge E(Q) curve for slow intercalation of H_2SO_4 18 M into HOPG : Potential plateaus correspond to two-phases domains, while slopes correspond to pure stage domains except for the mixtures of high-stage compounds.

(b) Presumed interfacial energetic diagrams at various charge levels. At the PZC (flatband potential) the Fermi level of graphite is situated at the top of the valence band. ALE and DLE are the approximate positions of the acceptor and donor levels in H_2SO_4 and MS the Mercurous Sulfate reference.

Specific Adsorption of Halides on Ag(110): Surface Science Model Studies of the Inner Layer Structure

B. Straehler, J.K. Sass, K. Bange and J. Schott

Fritz-Haber-Institut der Max-Planck-Gesellschaft
Faradayweg 4-6, D-1000 Berlin 33

The coadsorption of halogens (chlorine, bromine) and water on Ag(110) has been studied in ultrahigh vacuum using TDS, LEED and a Kelvin probe for work function measurements. The major purpose of the study has been the determination of the electrostatic potential drop in the inner layer (first monolayer) of the simulated interfacial region and the comparison between these data and equivalent data derived from in situ capacity measurements for zero diffuse layer charge /1/.

For both specifically adsorbed ions the results show very satisfactory agreement between the gas phase adsorption data and the electrochemical data. This finding confirms for the first time the relevance of the detailed structural information which may be obtained in simulation experiments in ultrahigh vacuum by the extensive arsenal of surface science techniques.

Microscopic models of the inner layer structure and an analysis of the different components of the double layer (ions and two types of solvent molecules) contributing to the electrostatic potential drop across the interface will be presented. An earlier study using ESDIAD for determining the orientation of water molecules coadsorbed with bromine on Ag(110) /1/ will be critically reviewed in the light of the results of this study.

/1/ K. Bange, B. Straehler, J.K. Sass and R. Parsons, J. Electronal.Chem., 229 (1987) 87.
/2/ K. Bange, T. E. Madey and J.K. Sass, Surface Sci. 162 (1985) 252.

Author Index

AUTHOR INDEX

Aberdam D. 1-2 (14)
Adžić R. R. 1-17 (57), 1-18 (60)
Agostiano A. 1-21 (70), 2-27 (199)
Aldaz A. 1-11 (39), 1-15 (51), 1-16 (54), 4-5 (283)
Allongue P. 2-5 (134), 2-6 (136)
Aloisi G. 5-L26 (328)
Alonso-Vante N. 2-40 (238), 2-44 (249)
Amadelli R. 2-29 (204)
Amokrane S. 5-6 (344)
Anastasijević N. 1-17 (57)
Andreoli R. 5-27 (394)
Ango J. P. 2-36 (224)
Anton C. G. 4-5 (283)
Aruchamy A. 2-28 (201)
Arvia A. J. 1-13 (45)
Atanasoski R. T. 2-43 (247)
Ayers W. M. 2-17 (168)
Badawy W. A. 2-34 (218)
Bade K. 2-15 (162)
Badiali J. P. 5-6 (344)
Bahador S. K. 2-24 (190)
Baker S. H. 2-L7 (115)
Bange K. 5-34 (413)
Barbieri A. 5-27 (394)
Bartlett Ph. N. 2-32 (213)
Baumgärtel H. 5-14 (365)
Beden B. 1-16 (54)
Behm R. J. 1-7 (27)
Beley M. 2-12 (153)
Bellier J. P. 1-L2 (1)
Benedetti L. 5-27 (394)
Bienvenue E. 4-2 (275)
Birkle S. 1-10 (36)
Blonkowski S. 2-6 (136)
Böttcher A. 4-12 (300)
Boldyrev Y. I. 5-22 (384)
Bordi F. 1-5 (21), 5-3 (335)
Borghesani G. 5-31 (404), 5-32 (407)
Borkowska Z. 5-9 (351)
Bratko D. 5-7 (347)
Brunoro G. 1-6 (24)
Bukowska J. 1-14 (48)
Bunding Lee K. A. 2-42 (244)
Burke L. D. 1-26 (83)
Cachet H. 2-6 (136)
Cambiaso A. 2-16 (165)
Cametti C. 5-3 (335)
Cappadonia M. 4-7 (289)
Carassiti V. 2-29 (204)
Carlá M. 1-5 (21)
Carlsson P. 2-45 (252)
Caselli M. 1-21 (70)
Castillo R. 1-30 (93)
Cecchini R. 1-5 (21)
Cella N. 2-4 (131)
Chao F. 1-L2 (1)
Chartier P. 2-12 (153)
Chazalviel J. -N. 2-14 (159), 5-8 (348)

Chen S. H. 5-7 (347)
Chiodelli G. 2-31 (210)
Christensen P. A. 1-6 (30)
Christmann K. 5-14 (365)
Clavilier J. 1-11 (39)
Conway B. E. 3-L14 (260)
Conzi F. 2-16 (165)
Costa M. 1-L2 (1), 1-23 (75)
Cowen S. 1-3 (17)
D'Agostino R. 2-33 (215)
D'Alba F. 4-11 (298)
Daghetti A. 5-17 (373)
Damjanovic A. 5-10 (354)
De Battisti A. 5-31 (404), 5-32 (407)
Dean M. H. 1-35 (106), 2-38 (230)
Decker F. 2-4 (131)
Della Monica M. 1-21 (70), 2-27 (199)
Denker H. 4-12 (300)
Desilvestro J. 1-4 (18)
Deville J. -P. 2-12 (153)
Di Biasio A. 5-3 (335)
Di Lorenzo S. 4-11 (298)
Di Quarto F. 2-33 (215)
Doblhofer K. 2-19 (175), 4-7 (289)
Dong S. 1-27 (86)
Dubinin A. G. 4-9 (295)
Duprez D. 2-36 (224)
Durand R. 1-2 (14)
Durfee W. S. 4-13 (303)
Dzhavakhidze P. G. 1-32 (97)
Eichberger R. 4-13 (303)
Enea O. 1-12 (42), 2-36 (224)
Faulkner L. R. 2-L10 (120)
Faure R. 1-2 (14)
Feliu J. M. 1-11 (39), 4-5 (283)
Felske A. 2-34 (218)
Ferina S. 2-3 (128)
Ferloni P. 2-31 (210)
Fernández-Vega A. 1-11 (39)
Fichou D. 2-2 (125)
Fong F. K. 1-21 (70), 2-27 (199)
Fontanesi C. 5-27 (394)
Fracastoro-Decker M. 2-4 (131)
Franke C. 1-20 (66)
Frese U. 5-25 (390)
Frignani A. 1-6 (24)
Fujishima A. 2-28 (201)
Funtikov A. M. 1-33 (101)
Garnier F. 2-2 (125)
Gavioli G. 5-27 (394)
Giorgi L. 2-39 (233)
Gliozzi A. 4-4 (281)
Göpel W. 2-26 (196)
Gocke E. 2-40 (238)
Gomes W. P. 2-8 (141)
Gonzalez R. 5-24 (387)
Goossens H. 2-8 (141)
Gorodyskii A. V. 5-21 (383), 5-23 (386)
Grattarola M. 2-16 (165)
Greef R. 2-22 (184)

Groll R. 4-12 (300)
Grozdić T. 2-9 (144)
Guidelli R. 5-L26 (328), 5-26 (393)
Gust D. 4-2 (275)
Gutman M. 4-L20 (271)
Haber J. 4-15 (308)
Hamelin A. 1-29 (89)
Hamnett A. 1-8 (30)
Harrach A. 5-33 (410)
Heinzinger K. 5-L23 (319)
Henderson D. 5-12 (359)
Holloway S. 3-L13 (259)
Holmström B. 2-45 (252)
Holzwarth J. F. 4-12 (300)
Horowitz G. 2-2 (125)
Hossain S. 2-20 (178)
Hurlen T. 1-22 (72)
Iannelli A. 5-15 (369)
Irish D. E. 5-15 (369)
Ivanova N. D. 5-22 (384)
Jackowska K. 1-14 (46)
Jaegermann W. 2-40 (236), 2-41 (241)
Jaffrezic-Renault N. 2-25 (193)
Japaridze J. I. 5-31 (404), 5-32 (407)
Jaszczynski K. 1-14 (46)
Jovanić B. R. 2-21 (181)
Kalińska A. 5-13 (362)
Kalinowski S. 4-14 (305)
Karasevskii A. I. 5-21 (383), 5-22 (384)
Karnaukhov I. N. 5-22 (384)
Kautek W. 1-10 (36)
Kazarinov V. E. 1-33 (101)
Kelly J. J. 2-23 (187)
Kita H. 2-45 (252)
Koczorowski Z. 5-13 (362), 5-17 (373)
Kohler H. 2-26 (196)
Kokkinidis G. 1-19 (63)
Kolb D. M. 1-7 (27), 1-20 (66)
Kornyshev A. A. 1-32 (97), 5-L25 (325)
Kozlowski M. R. 2-43 (247)
Krestov G. A. 5-30 (402)
Kreuer K. -D. 2-26 (196)
Krysiński P. 4-8 (292), 4-14 (305)
Krzowska M. 2-37 (227)
Kublanovskii V. S. 5-23 (386)
Kulesza P. J. 2-37 (227), 4-15 (308)
Kumar A. 2-L6 (113)
Kuznetsov An. M. 5-L24 (322)
Lackey D. 1-37 (110)
Lamy C. 1-15 (51), 1-16 (54)
Langner M. 4-L16 (265)
Lecoeur J. 1-L2 (1)
Leger J. -M. 1-15 (51), 1-16 (54)
Leiva E. 5-11 (357)
Lemasson P. 2-13 (156)
Lewerenz H. J. 2-22 (184), 2-41 (241)
Lewis N. S. 2-L6 (113)
Li X. -P. 2-44 (249)
Liebeskind D. 1-35 (106)
Lipkowski J. 5-15 (369)

Liszi J. 1-31 (96)
Locatelli C. 5-32 (407)
Lucarini C. 4-11 (298)
Lunt S. R. 2-L6 (113)
Lust E. 5-28 (397)
Lust K. 5-28 (397)
Luzar A. 5-7 (347)
Madey Th. E. 3-L12 (257)
Magistris A. 2-31 (210)
Majda M. 4-10 (297)
Maldotti A. 2-29 (204)
Marcelja S. 5-L22 (317)
Marinković N. S. 1-18 (60)
Marković N. M. 1-18 (60)
Matyushov D. V. 5-21 (383)
McDaniel R. 4-L16 (265)
McLaughlin S. 4-L16 (265)
Medrano J. 4-5 (283)
Melandri B. A. 4-17 (312)
Melroy O. R. 1-L5 (10)
Memming R. 2-11 (150)
Metikoš-Huković M. 2-3 (128)
Metrot A. 5-33 (410)
Meyer F. 4-12 (300)
Minc S. 4-14 (305)
Miodnicka T. 4-15 (308)
Moncelli M. R. 5-26 (393)
Monticelli C. 1-6 (24)
Moore A. 4-2 (275)
Moore T. A. 4-2 (275)
Morin M. -C. 1-15 (51)
Morro A. 2-16 (165)
Mouhandess T. 2-7 (138)
Moura C. 1-29 (89)
Muir A. V. G. 1-8 (30)
Mulder W. H. 5-20 (380)
Nachliel E. 4-L20 (271)
Naumann R. 4-1 (274)
Nazmutdinov R. R. 5-L24 (322)
Ndzebet E. 2-10 (147)
Neu W. 2-26 (196)
Neumann E. 4-L17 (268)
Nguyen van Huong C. 2-25 (193)
Nikitas P. 5-2 (332)
Nishikitani Y. 2-2 (125)
Nowak J. F. 2-7 (138)
Nyikos L. 5-18 (375)
O'Dwyer K. J. 1-26 (83)
O'Leary W. A. 1-26 (83)
Ozanam F. 2-14 (159)
Paik C. -H. 2-43 (247)
Pajkossy T. 5-18 (375)
Palm U. 1-34 (103), 5-28 (397)
Panero S. 2-35 (221)
Papanastasiou G. 1-19 (63)
Pappa-Louisi A. 5-2 (332)
Parfenyuk V. I. 5-30 (402)
Parodi M. 2-16 (165)
Peraldo Bicelli L. 2-1 (122)
Perdriel C. L. 1-13 (45)

Perez J. -M. 1-16 (54)
Perrot H. 2-25 (193)
Petit J. -P. 2-12 (153)
Pettenkofer C. 2-22 (184), 2-40 (238)
Pettinger B. 1-26 (66)
Peyrière J. 5-8 (348)
Piazza G. 1-20 (66), 1-23 (75)
Piazza S. 2-33 (215)
Picq G. 2-7 (138)
Pistoia G. 2-35 (221)
Plieth W. J. 1-30 (93), 2-34 (218)
Plischke M. 5-12 (359)
Pons S. 1-4 (18)
Posadas D. 1-24 (78), 1-25 (80)
Prats M. 4-6 (266)
Pujadas M. 2-30 (207)
Radenkovic B. 2-21 (181)
Rahmani A. 1-23 (75)
Raud T. 1-34 (103)
Razzini G. 2-1 (122)
Rebelo M. J. F. 4-16 (310)
Reineke R. 2-11 (150)
Richer J. 5-15 (369)
Richmond G. L. 1-L4 (7)
Robello M. 4-4 (261)
Rocchini G. 5-17 (373)
Romeo F. M. 1-25 (80)
Rosinberg M. L. 5-4 (338)
Ross P. N. 1-L3 (4)
Rouina F. 2-7 (138)
Russier V. 1-L2 (1), 5-4 (338), 5-6 (344)
Šeruga M. 2-3 (128)
Salvador P. 2-30 (207)
Salve M. 5-28 (397)
Sambles J. R. 1-3 (17)
Sander M. 2-41 (241)
Santangelo P. G. 2-L6 (113)
Sanz F. 5-24 (387)
Sapoval B. 5-8 (348)
Saraswat A. K. 2-31 (210)
Sass J. K. 1-36 (107), 1-37 (110), 5-29 (401), 5-34 (413)
Schmeisser D. 2-26 (196)
Schmickler W. 5-11 (357), 5-25 (390)
Schott J. 1-37 (110), 5-29 (401), 5-34 (413)
Schubert B. 2-40 (238)
Schuhmann D. 2-10 (147), 4-3 (278), 5-5 (341)
Schultze J. W. 2-15 (162)
Scrosati B. 2-35 (221)
Scupoli M. T. 4-17 (312)
Seta P. 4-2 (275)
Shapnik M. S. 5-L24 (322)
Shvets-Teneta-Guriy T. B. 4-9 (295)
Silk T. 1-34 (103)
Silva F. 1-29 (89)
Sledzik J. 5-16 (370)
Sluyters J. H. 5-20 (380)
Sluyters-Rehbach M. 5-20 (380)
Smyrl W. H. 2-43 (247)
Solomun T. 1-9 (33), 5-14 (365)
Song S. 1-27 (86)

Souteyrand E. 2-5 (134)
Spear W. E. 2-L7 (115)
Spohr E. 5-L23 (319)
Stafiej J. 5-9 (351)
Stimming U. 1-35 (106), 1-36 (107), 2-38 (230), 5-29 (401)
Stolberg L. 5-15 (369)
Storck W. 4-13 (303)
Straehler B. 5-34 (413)
Strbac S. 1-17 (57)
Stumper J. 2-22 (184)
Stupnisek-Lisac E. 1-1 (11)
Sunseri C. 2-33 (215)
Tadjeddine A. 1-23 (75), 1-32 (97)
Tafalla D. 2-30 (207)
Takenouti H. 1-1 (11)
Taraszewska J. 5-13 (370)
Tassinari H. 1-6 (24)
Teissié J. 4-6 (286)
Tellefsen K. 1-36 (107)
Thietke J. 2-15 (162)
Tiedemann U. 1-28 (88)
Tocanne J. F. 4-6 (286)
Trabanelli G. 1-6 (24)
Traore S. 1-2 (14)
Trasatti S. 5-17 (373), 5-31 (404), 5-32 (407)
Tributsch H. 2-L9 (118), 2-40 (238), 2-44 (249)
Tryk D. 2-20 (178)
Tsirlina G. A. 1-33 (101)
Tsuji K. 4-L17 (268)
Tucceri R. I. 1-24 (78), 1-25 (80)
Tufts B. J. 2-L6 (113)
Twomey T. 1-7 (27)
Tyler P. S. 2-43 (247)
Uosaki K. 2-45 (252)
Urbakh M. I. 1-32 (97), 3-L15 (262)
Urošević V. V. 2-21 (181)
Vaidhyanathan V. S. 5-19 (377)
Valette G. 5-1 (329)
Vanden Kerchove F. 2-8 (141)
Vanel P. 2-10 (147)
Vanmaekelbergh D. 2-23 (187)
Vargas H. 2-4 (131)
Vazquez J. -L. 1-15 (51), 4-5 (283)
Vennereau P. 2-7 (138)
Venturoli G. 4-17 (312)
Whitaker R. G. 2-32 (213)
Widrig C. A. 4-10 (297)
Wiechers J. 1-7 (27)
Wilhelmsen W. 1-22 (72), 2-18 (172)
Willig F. 2-L8 (116), 4-13 (303)
Ye J. 2-19 (175)
Yeager E. 2-20 (178)
Zagórska I. 5-13 (362), 5-17 (373)
Zeković Lj. D. 2-21 (181)
Zerbino J. O. 1-13 (45)